NIST Technical Note
NIST TN 2282

The Impact of Material Composition on Ignitability and Fire Growth. Volume 1: Full-Scale Burning Behavior of Combustible Solids Commonly Found in Nuclear Power Plants

Isaac T. Leventon
Michael V. Heck
Kevin B. McGrattan
Matthew F. Bundy
Rick D. Davis

This publication is available free of charge from:
https://doi.org/10.6028/NIST.TN.2282

NATIONAL INSTITUTE OF STANDARDS AND TECHNOLOGY
U.S. DEPARTMENT OF COMMERCE

NIST Technical Note
NIST TN 2282

The Impact of Material Composition on Ignitability and Fire Growth. Volume 1: Full-Scale Burning Behavior of Combustible Solids Commonly Found in Nuclear Power Plants

Isaac T. Leventon
Michael V. Heck
Kevin B. McGrattan
Matthew F. Bundy
Rick D. Davis
Fire Research Division
Engineering Laboratory

This publication is available free of charge from:
https://doi.org/10.6028/NIST.TN.2282

February 2024

U.S. Department of Commerce
Gina M. Raimondo, Secretary

National Institute of Standards and Technology
Laurie E. Locascio, NIST Director and Under Secretary of Commerce for Standards and Technology

Certain equipment, instruments, software, or materials, commercial or non-commercial, are identified in this paper in order to specify the experimental procedure adequately. Such identification does not imply recommendation or endorsement of any product or service by NIST, nor does it imply that the materials or equipment identified are necessarily the best available for the purpose.

Publication History
Approved by the NIST Editorial Review Board on 2024-02-02

How to cite this NIST Technical Series Publication:
Leventon IT, Heck MV, McGrattan KB, Bundy MF, Davis RD (2024) The Impact of Material Composition on Ignitability and Fire Growth. Volume 1: Full-Scale Burning Behavior of Combustible Solids Commonly Found in Nuclear Power Plants. (National Institute of Standards and Technology, Gaithersburg, MD), NIST TN 2282. https://doi.org/10.6028/NIST.TN.2282

Author ORCID iDs
Isaac T. Leventon: 0000-0002-8835-8087
Michael V. Heck: 0000-0002-6279-5908
Kevin B. McGrattan: 0000-0002-1135-1274
Matthew F. Bundy: 0000-0002-1138-0307
Rick D. Davis: 0000-0003-2264-0490

Abstract

Primary Audience

Fire protection engineers (FPEs) conducting or reviewing fire modeling that supports fire probabilistic risk assessments (PRAs) related to predictions of fire growth and peak heat release rate of combustible solids (e.g., circuit boards or wiring in electrical enclosure fires). Extensive detail is provided to quantify the impact of material properties on observed burning behavior of combustible solids at full scale.

Key Research Question

How does material composition affect ignition, fire growth rate, and peak fire size in large-scale fire experiments designed to represent an electrical enclosure with a simplified fuel-loading configuration.

Research Overview

This report provides an overview of measurements (e.g., heat release rate, gaseous species production, and flame-to-surface heat transfer) and visual observations obtained from a series of 66 full-scale fire growth experiments conducted on 18 unique combustible solids including: natural and synthetic polymers, copolymers, fiberglass-reinforced composite materials, porous polymer foams, and electrical cables. Some of these materials were selected because they can be found in electrical cabinets and circuit boards. Others were selected in order to provide a wide range of material compositions (i.e., chemistries) and burning behaviors: physical deformation (e.g, swelling, charring collapse, dripping, and/or melt flow), heavy or light soot formation, and varied ignitability and fire growth rate.

In a typical electrical enclosure, combustible solids (e.g., wiring or circuit boards) are most often found attached to the inside walls. A test setup was thus selected to represent this configuration: two parallel panels (2.44 m tall by 0.61 m wide) were assembled such that they could support combustible solids of varying thicknesses (each spaced 0.30 m apart), which were then ignited at their base. This simplified configuration ensured (1) the production of a large-scale burning scenario representative of typical fuel loading in an electrical enclosure, and (2) that the experiments could be repeated to highlight the impact of material composition on observed burning behavior (e.g., ignitability, fire growth rate, and peak fire size) while minimizing test sensitivity to variations in other factors such as fuel loading (e.g., wire packing density), configuration, or orientation.

Key measurement devices were incorporated into this test apparatus in order to measure the primary mechanism controlling fire growth (flame-to-surface heat transfer during upward flame spread over the surface of the combustible solids) and to measure global quantities characterizing fire behavior and development: heat release rate (HRR), soot

and gaseous species (i.e., CO and CO_2) yields. Additionally, video of each experiment was recorded by at least two video cameras and photographs were taken throughout each experiment. Selected measurement data is presented and analyzed in this report; a complete set of all measurement data and videos recorded during these experiments is available online on the NIST Fire Calorimetry Database [1]: https://www.nist.gov/el/fcd/vertical-upward-flamespread-on-parallel-panels.

Qualitatively, the burning behavior of each of the materials tested in this work could be separated into three broad groups: (1) materials that ignite but do not support upward flame spread, (2) materials that ignite and support flame spread as long as an external ignition source is present, and (3) materials that support self-sustained flaming and fire growth without an external ignition source.

A brief summary of quantitative measurements obtained during these experiments highlights the diverse range of burning behaviors supported by each of the materials tested in this study:

Fire Size (Heat Release Rate, HRR)

- Peak Heat Release Rate (Peak HRR): 110 kW to 4186 kW
- Time to Peak HRR: 16 s to 1022 s after burner exposure
- Total Heat Release: 16 MJ to 566 MJ
- Heat of Combustion: 9.6 kJ/g to 39.9 kJ/g (energy release per gram of fuel *burned*)

Heat Transfer

- Peak, total flame-to-surface heat transfer: 71 kW/m^2 to 254 kW/m^2
- Fraction of total wall flame heat flux attributed to radiation: 11 % to 69 %
- Peak radiation heat flux at a distance (3.6 m from panels): 0.02 kW/m^2 to 7.72 kW/m^2

Species Yields

- Soot yield [g/g]: Below Detectable Limits to 0.21
- CO yield [g/g]: 0.004 to 0.42
- CO_2 yield [g/g]: 0.62 to 3.6

Summary

The information provided in this report will support a more realistic assessment of fires in electrical enclosures and the overall impact of material composition on key burning behaviors of interest to fire safety scientists and engineers. Beyond the direct observations and experimental measurements obtained for this specific test configuration, this study also offers a comprehensive set of validation data for computational fluid dynamics (CFD) simulations of large scale fire growth due to flame spread over the surface of combustible solids. The design and expected impact of the next phase of this study (including how it integrates with these full-scale measurements) is concisely summarized in the Future Work section, below.

Future Work

Additional volumes of this report will include bench-scale measurements conducted on all 18 materials presented in this work, including (1) thermogravimetric analysis (TGA), (2) differential scanning calorimetry (DSC), (3) microscale combustion calorimetry (MCC), and (4) pyrolysis of coupon sized slabs in an anaerobic (nitrogen) environment when exposed to well-characterized radiant heating. The data will be used to derive material properties controlling heating, decomposition, and production of gaseous volatiles.

Collectively, the measurement data obtained from each of these experiments (from bench- to full-scale) will provide a comprehensive set of measurement data needed to calibrate pyrolysis models for combustible solids (i.e., determine relevant material properties), use these material property sets for quantitative prediction of fire growth using CFD tools, and validate the simulation results.

Keywords

Electrical Enclosures; Fire Model Validation; Flame Heat Flux; Flame Spread; Heat Release Rate; Ignitability; Material Flammability; Nuclear Power Plant (NPP); Oxygen Consumption Calorimetry

Acknowledgments

This work was supported by the Office of Nuclear Regulatory Research (RES) of the US Nuclear Regulatory Commission (US NRC). This program was directed by Mark Henry Salley with support from Kenneth Hamburger, Nicholas Melly, Gabriel Taylor, and David Stroup.

The large scale experiments described in this report were conducted at the National Fire Research Laboratory (NFRL) at NIST. This facility is directed by Matt Bundy. Marco Fernandez supervised the construction and maintenance of the NIST/NRC parallel panel apparatus. Technical support for the experiments was provided by NFRL staff members

Laurean DeLauter, Anthony Chakalis, Philip Deardorff, Marco Fernandez, and Artur Chernovsky; their efforts and expertise made these experiments possible.

Table of Contents

List of Tables

List of Figures

Glossary

General

CFR	Code of Federal Regulation
ECS	Emissions Control System
EPRI	Electric Power Research Institute
FPE	Fire Protection Engineer
GDC	General Design Criterion
HEAF	High Energy Arc Fault
NFPA	National Fire Protection Association
NFRL	National Fire Research Laboratory
NIST	National Institute of Standards and Technology
NPP	Nuclear Power Plant
NRC	U.S. Nuclear Regulatory Commission
PRA	Probabilistic Risk Assessment

Experimental Tools

CAPA	Controlled Atmosphere Pyrolysis Apparatus
DSC	Differential Scanning Calorimetry
MCC	Microscale Combustion Calorimetry
TGA	Thermogravimetric Analysis

Materials

ABS	Acrylonitrile Butadiene Styrene
GPO-1	Fiberglass-Reinforced Polyester laminate (limited arc- and flame-resistance)
GPO-3	Fiberglass-Reinforced Polyester laminate (improved arc- and flame-resistance)
HDPE	High Density Polyethylene
HIPS	High Impact Polystyrene
OSB	Oriented Strand Board
PBT	Poly(butylene terepthalate)
PMMA	Poly(methyl methacrylate)
Polyiso	Polyisocyanurate
POM-GF	Poly(oxymethylene) reinforced with chopped Glass Fibers
PVC	Poly(vinyl chloride)
SIS Wire	Switchboard Wire
XLPE	Cross-linked Polyethylene
XPS	Extruded Polystyrene

1. Introduction

Electrical enclosures (e.g., switchgears, relay cabinets, control and switch panels, and motor control centers) present a fire risk in nuclear power plants (NPPs) because they contain both combustible materials and energized electrical circuits. Unwanted fires in these systems are particularly dangerous in NPPs because they can disrupt power, instrumentation, and control in the facility. In an analysis of global fire events in NPPs [2] it has been noted that electrical cabinets (i.e., electrical enclosures) and transformers are the components that provide the highest share of fire initiations (approximately 12 % each). In a recent review of all fire events reported[1] in US NPPs between 1990 and 2011 [5], it was found that 13.5 % (269 out of 1998) occurred in electrical enclosures. Of these fires, 8.2 % and 39.4 % were reported as "Challenging" or "Potentially Challenging," respectively. In this reporting system, "Challenging" fire events are those that had "an observable and substantive effect on the environment outside the initiating source;" "Potentially Challenging" events "were not judged to be [challenging] events, but ... could have led to fire growth, fire spread, equipment damage or cable damage beyond the fire ignition source had the circumstances of the fire event been different" [4]. Collectively, these results demonstrate why electrical cabinets (and medium voltage switchgear [600 V to 69 kV]) are "commonly identified in fire PRAs [probabilistic risk assessments] as one of the important sources of fire ignition in nuclear power plants" [6].

Electrical fires can be caused by: poor connections (e.g., due to aging and deterioration or due to personnel error such as improper alterations or installation), overheating (typically due to abuse, damage, environmental effects, or manufacturing, installation, and/or design defects), arcing (in air or across carbonized paths; including high energy arc fault, HEAF, and non-HEAF events), overload, excessive thermal insulation, and external heating (e.g., due to direct flame impingement or external heating or simple product failure) [4, 7, 8]. Many ignition phenomena have a strong probabilistic aspect to them [9] and, in the case of common faults such as poor connections or arcing, "ignition usually takes a long time after the initial conditions were established for the fault" [8]. A wide range of bench- and full-scale experimental studies and standard test methods have thus been developed to assess the fire performance of electrical components; however, as noted in thorough reviews of such works [10–12], no single test criteria has evolved by which the response of electrical components to fire is evaluated. Instead, multiple criteria are considered: electrical continuity, ease of ignition and extinction, critical times or temperatures (e.g., time to failure, to ignition, or of self-sustained burning), mass loss rate, heat release rate, damage (e.g., char) length, and smoke generation and/or obscuration.

While it is known that fires occur in electrical enclosures in NPPs, for the reasons described above, it is difficult to predict ignition in these fire events. Further, it has been

[1] All events were reported in the Fire Events Database (FEDB), which was developed by the Electric Power Research Institute (EPRI). The FEDB was first published in the early 2000s [3], updated in 2013 [4], and it is intended to be "the most comprehensive and consolidated source of fire incident information available for nuclear power plants operating in the United States" [4].

reported that many investigators still question the degree to which small-scale test results reflect full-scale fire behavior, especially for plastic materials, and until small-scale test results are fully evaluated through larger-scale experiments, "caution must be exercised in the use of small-scale test results in the prediction of full-scale fire behavior." [13]. Those performing PRAs rely on recommended peak HRRs that are based on distributions of likely worst-case fire scenarios [14].

The primary regulation governing fire protection in nuclear power plants is Title 10, Section 50.48, of the Code of Federal Regulations [15], which requires that each license holder have a fire protection plan that satisfies "General Design Criterion 3" (GDC 3) of Appendix A to 10 CFR Part 50. Of note, GDC 3 requires that "structures, systems, and components important to safety shall be designed and located to minimize, consistent with other safety requirements, the probability and effect of fires and explosions. Noncombustible and heat resistant materials shall be used wherever practical throughout the unit, particularly in locations such as the containment and control room."

The term "noncombustible" is not well defined; it implies that materials are either combustible or noncombustible when, in fact, most materials display varying degrees of combustibility and a wide spectrum of burning characteristics. The term "noncombustible" was later clarified in Generic Letter 86-10 [16] as material "with a surfacing not over 1/8-inch thick that has a flame spread rating not higher than 50 when measured using ASTM E-84 Test [17]: Surface Burning Characteristics of Building Materials." When fire protection requirements were purely prescriptive, this pass/fail criterion was sufficient to demonstrate regulatory compliance.

During the 1990s, the nuclear power industry began a considerable shift from prescriptive rules and practices towards broadened use of risk information to supplement decision-making. Around the same time, the fire protection industry was undergoing similar changes, and more sophisticated methods for modeling fires and evaluating their impact were beginning to mature. In 2001, the National Fire Protection Association (NFPA) issued the first edition of NFPA 805 [18] (Performance-Based Standard for Fire Protection for Light-Water Reactor Electrical Generating Plants). On July 16, 2004, the U.S. Nuclear Regulatory Commission (NRC) amended its regulations in 10 CFR 50.48, to allow U.S. utilities to adopt and maintain risk-informed, performance-based fire protection programs. Paragraph (c) of 10 CFR 50.48 endorses, with exceptions, the NFPA 805 Standard (2001 Edition), as a voluntary alternative for demonstrating compliance with the deterministic programs given in Appendix R to 10 CFR 50 in accordance with Paragraph (b) of 10 CFR 50.48 or the plant-specific fire protection license conditions.

In 2005, the Electric Power Research Institute (EPRI) and the NRC's Office of Nuclear Regulatory Research (RES) issued a joint technical report titled EPRI/NRC-RES Fire PRA Methodology for Nuclear Power Facilities, EPRI 1011989, NUREG/CR-6850 [14], presenting methods and data for conducting a fire probabilistic risk assessment (fire PRA). NUREG/CR-6850 covered a wide range of fire hazards, including electrical enclosures.

NUREG/CR-6850 was a landmark publication and represented the state of the art in the mid-2000s. It was the first fire PRA methodology to use probability distributions for

heat release rate values, as opposed to the point values of existing PRA methodologies[2]. However, as plants began to implement probabilistic, risk-informed fire protection programs, two trends became apparent: (1) the predicted risk from electrical enclosure fires exceeded that suggested by commercial operating experience, indicating conservatisms in the methodology, and (2) electrical enclosures represented the largest contributor to the plants' fire-induced risk by a wide margin. Accordingly, during the intervening years, significant effort and resources have been dedicated to refining the methods, tools, and data used to model electrical enclosure fires in fire PRA:

- In 2013, a series of experiments were sponsored by the Nuclear Regulatory Commission's Office of Nuclear Regulatory Research (NRC-RES) and conducted by the National Institute of Standards and Technology (NIST) at the Chesapeake Bay Fire Test Detachment (CBD) of the Naval Research Laboratory to obtain additional data to support re-quantification of HRR estimates for electrical enclosures. This testing effort used electrical enclosures removed from a nuclear facility, and electrical cables and panel wiring representative of those commonly found in U.S. nuclear power plants (NPPs). In total, 112 individual fire tests were conducted, and the result of this effort is documented in NUREG/CR-7197, "Heat Release Rates of Electrical Enclosure Fires (HELEN-FIRE)" [20].

- In 2014, NRC and EPRI published NUREG-2169 (EPRI 3002002936), "Nuclear Power Plant Fire Ignition Frequencies and Non-Suppression Probability Estimation Using the Updated Fire Events Database"[21]. This report provides fire ignition frequencies and non-suppression probability estimates through the year 2009 using EPRI's updated fire events database.

- In 2016, a joint NRC/EPRI working group devised an enhanced methodology for modeling electrical enclosure fires, which included classification of electrical enclosures in terms of function, size, contents, and ventilation; determination of peak heat release rate (HRR) probability distributions considering specific electrical enclosure characteristics; and development of a method to account for the impact of the enclosure on the vertical thermal zone of influence (ZOI) above the enclosure during fire. This enhanced methodology is documented in NUREG-2178 Vol. 1 (EPRI 3002005578), "Refining and Characterizing Heat Release Rates From Electrical Enclosures During Fire (RACHELLE-FIRE)" [22].

- In 2020, a joint NRC/EPRI publication (NUREG-2230//EPRI 3002016051 [19]) provided a revised set of parameters to address both the fire growth and the suppression response. Here, electrical cabinet fire events were classified into one of two fire categories: (1) growing or (2) interruptible. Interruptible fires are those that, "have

[2]Current guidance[14] when defining time-resolved HRR curves for PRAs assumes that the fire grows exponentially as a function of time, $\dot{Q} \propto t^2$, reaching its peak HRR in approximately 12 minutes and burning at that peak HRR for approximately 8 minutes. Revised timing is suggested in NUREG-2230 [19] for 'interruptible' fire events: i.e., events in which plant personnel could detect and perform early suppression activities.

observed ignition but no significant growth for a period of time". Growing fires, "experience growth immediately after ignition". In NUREG-2230 [19], the detection-suppression event tree was also updated to better allow for early plant personnel suppression actions and additional manual non-suppression bins were added to better reflect the scenario characteristics.

- In 2023, an experimental campaign was conducted (a NIST/NRC collaboration) to measure the HRR of fires burning in steel enclosures with limited ventilation (Oxygen-Limited Fires Inside Under-Ventilated Enclosures, OLIVE-FIRE [23]). The objective of this study was to validate a simple empirical model that predicts the maximum heat release rate of a fire within a closed compartment as a function of its ventilation openings.

Although the enhanced methodology described in NUREG-2178 Vol.1 provides more specificity in terms of the enclosure's function, size, contents, and ventilation, the evaluation of the enclosure's contents is still limited to its overall level of fuel loading (default, low, very low) and whether the fuel is thermoset or thermoplastic. It does not distinguish between specific fuel types and their burning characteristics.

As the nuclear [18] and general fire protection [24, 25] industries continue to expand their use of risk-informed, performance-based design principles, simple pass/fail criteria of standard fire tests are no longer sufficient to provide the granular level of risk information needed to support effective decision making. There is a growing need for verified and validated design tools (i.e., fire models) that can predict relevant fire behavior and its consequences. This report represents the first step towards gathering the data needed to provide additional refinements based on an enclosure's specific fuel content and accurate inputs for fire models of increasing complexity.

NUREG-1824 [26] documents the verification and validation of five fire models that are commonly used in NPP applications (e.g., the NIST Fire Dynamics Simulator, FDS, and Consolidated Fire Growth and Smoke Transport Model, CFAST). Fire protection engineers (FPEs) conducting or reviewing PRAs related to electrical enclosure fires in NPPs could be aided by the development, verification, and validation of a design tool that allows for accurate, efficient, and reliable prediction of fire development in electrical enclosures based on knowledge of the materials contained within and simulation of the relevant condensed- and gas-phase processes controlling their burning behavior. A brief summary of the controlling mechanisms of early fire growth is thus provided as follows.

When a combustible solid (e.g., cable jacketing/insulation or circuit board material) is heated, it can degrade and produce flammable gases. If sufficient heat is continuously provided to the solid, flammable gases will be produced at such a rate that, in the presence of a local ignition source (e.g., an arc, spark, or hot surface), they can react with the ambient oxidizer to form a premixed flame. In the presence of a steady flow of flammable gases and oxidizer, this premixed flame quickly transforms into a diffusion flame. A fraction of the energy released in this flame is transferred back to the solid; if this heat transfer (plus any externally applied heating) is sufficient, sustained degradation of the combustible solid,

production of flammable gases, and flaming is observed. When combustible solids are supported in a vertical configuration in normal gravity (e.g., vertical wall fires or discrete fuels spaced above one another), this process has the potential for rapid growth because flammable gases move upward (driven by buoyancy) and burn downstream from where they were created, thus heating a region of the solid that is not yet degrading. Resulting expansion of the pyrolysis region (i.e., the region of the combustible solid undergoing thermal decomposition) increases the gaseous fuel production, which, in turn increases the heating. Thorough reviews regarding the fundamentals of flame spread dynamics are provided elsewhere [27, 28].

Because of this positive feedback, fire development due to upward flame spread is non-linear and highly sensitive to initial conditions [29, 30]. Further, fire growth rate and peak fire size can be affected by numerous factors including: material composition and thermophysical properties [31–33]; initial conditions (i.e., ambient conditions and/or type, strength, size, and duration of ignition source) [20, 29, 30, 34, 35]; configuration (e.g., fuel orientation or geometry [32, 36–41]; fuel, loading, spacing or packing density [13, 22, 31, 32, 39, 42–46]; and air entrainment and oxygen availability [31, 32, 39, 40, 47–54].

This study represents a first step in a combined experimental and modeling effort to develop the tools and techniques (experimental and analytical) needed to quantitatively predict fire growth rate and peak size of fires due to flame spread over combustible solids found in NPPs. A careful focus is maintained on the impact of material composition because it has been noted [5] that the combustible initiating group in more than 95 $\%$ of electrical enclosure fires reported in the Fire Events Database (FEDB) was some sort of solid (in-situ) material or cable jacketing/insulation material. Advancement of computational models to allow for the quantitative prediction of flame spread represents significant progress in how FPEs can use these fire modeling tools: no longer would a design fire have to be prescribed a priori (which can often require costly, full-scale experiments or simplifying assumptions to select a suitable, potentially over-conservative, design fire) but this fire growth could be *predicted* in response to a range of likely ignition conditions based on the material properties and fuel loading of the combustible solid(s) of interest.

The experiments conducted for this study are designed to provide the following short and long term impacts:

- Large scale tests are conducted in this work (Vol. 1) with sufficiently severe exposures to qualitatively identify materials that will: (a) not burn, (b) only burn with a sustained ignition source, or (c) ignite and support self-sustained flaming. This information can be used to improve the analysis and determination of fuel loading [22] in electrical enclosures, which in turn can be used to define peak fire size (HRR) for use in PRAs.

- Previous reviews of the fire behavior of combustible materials found in NPPs highlight the need for well-instrumented experiments, conducted across a range of scales, that enable the simulation of large-scale fire behavior “based on fuel parameter val-

ues obtained primarily from small-scale tests" [55]. Large-scale experiments conducted in this work (Vol. 1) are therefore carefully designed and instrumented to provide critical measurement data needed for validation [56] of numerical models that can predict ignitability, fire growth rate, and peak fire size of combustible solids (e.g., materials found in electrical enclosures). Bench scale experiments (Vol. 2) are designed to quantify the material properties controlling this behavior.

A summary of the measurement data to be collected at each scale is provided below:

Volume 1 (large scale experiments): Measurement data for model validation

Controlling mechanisms of fire growth

- Flame spread over the surface of combustible solids occurs due to positive feedback between gas-phase energy release (flame-to-surface heat transfer) and condensed-phase pyrolysis (thermal degradation and generation of gaseous volatiles). Spatially-resolved measurements of flame-to-surface heat transfer are thus obtained during upward flame spread over 10 of the 18 materials tested in this work, with at least 2 replicate measurements obtained at each measurement location of interest (i.e., height, z) in repeated tests on each material.
- For small, laminar wall flames, flame-to-surface heat transfer occurs primarily by convection [35, 57, 58]. For large, turbulent wall flames, flame heat transfer is reported to be dominated by radiation [59, 60]. Correspondingly, peak heat flux from these large wall flames is noted to increase with fuel sooting tendency [61]. It has been shown that, when simulating wall flame spread over 1.5 m tall panels in a corner configuration, representing the flame heat flux as purely convective or radiative has a substantial impact on the simulation results (factor of 2x difference in predicted flame spread rate) [62]. Thus, for six of the materials tested here (and in repeated experiments), the fraction of total flame heat flux attributed to radiation was calculated by measuring both total, $\dot{q}''_{\text{total}}$, and purely radiative, $\dot{q}''_{\text{rad}}$, components of flame heat flux using multiple measurement devices positioned at the same height in the sample.

Global quantities characterizing fire behavior

- Initial and final sample mass;
- Time-resolved measurements of fire size (i.e., HRR), soot generation, and gaseous species (CO and CO_2) production;
- Ignition time (s) and fire growth rate (in response to a well-characterized ignition source);

- Peak heat release rate (kW) and total heat released (MJ);
- Radiative heat flux at a distance (kW/m^2);
- Heat of combustion, ΔH_c (kJ/g);
- Species yields, Y_{CO} and Y_{soot} (g/g);
- Photographs and video of material ignition and fire growth behavior

Volume 2 (bench scale experiments): Measurement data for model calibration (i.e., material property determination)
This dataset includes results from (a) mg-scale experiments — themogravimetric analysis (TGA), differential scanning calorimetry (DSC), and microscale combustion calorimetry (MCC) — that can be used, among other things, to determine decomposition reaction mechanisms tested in this work as well as associated kinetics, thermodynamics, and heats of combustion of the gaseous volatiles that they produce and (b) g-scale controlled atmosphere gasification experiments that can be used to determine material properties controlling heat and mass transport through the solid and to validate numerical predictions of material decomposition under well-characterized heating conditions [63–65].

Future work can consider the impact of key secondary factors that affect fire growth rate: e.g., type and strength of ignition source, aging of fuels, ventilation conditions, physical phenomena (e.g., melt flow and dripping), and configuration factors such as panel spacing or fuel packing density, orientation, and geometry. These configuration factors may be of great interest as previous cable fire research has demonstrated that, “the parameter that has the most effect on the test results [i.e., the fire response of cables in real-scale tests] is the method of mounting the tested cables” [43].

2. Experimental

2.1. Test Configuration/Apparatus

A representative selection of electrical enclosures found in Nuclear Power Plants (NPPs) — which shows typical combustible loading, configuration, and ventilation conditions — is presented in NUREG/CR-7197 [20]. Although not intended to be a comprehensive survey of all possible enclosure designs or fuel-loading configurations, these images demonstrate that electrical enclosures contain a range of wiring and electrical equipment (e.g., circuit boards, circuit breakers, relays) with a variety of loadings (i.e., packing densities of combustible components within the enclosures). Pictures of two electrical enclosures originally shown in NUREG/CR-7197 [20], are reproduced in this work as Fig. 1. Figure 2 shows a representative row of open electrical enclosures that could be found in and around the main control room in a NPP. As seen in each of these images, the combustible solid components (e.g., wires or circuit boards) found within these systems are typically attached to the interior walls of the enclosures.

Fig. 1. Photographs of electrical enclosures typically found near the main control room in a Nuclear Power Plant.

In this study, a test assembly was thus developed that could (a) represent the fuel loading of a typical electrical enclosure and (b) allow for the quantitative study of ignitability,

Fig. 2. Photograph of a series of electrical enclosures in a Nuclear Power Plant.

fire growth rate, and peak fire size of enclosure fires in which the impact of material composition was highlighted while de-emphasizing potential variations due to physical configuration factors (e.g., fuel packing density, orientation, or spacing). Future tests that consider the impact of such key factors are important, but beyond the scope of this work. The reader is refered to NIST Technical Note 2232 (OLIVE FIRE) [23] for a recent study on the impact of ventilation on peak fire size (i.e., peak HRR) in electrical enclosure fires and modeling guidelines for growing vs. interruptible fires (i.e., fires that grow immediately after ignition or show no significant growth for a period of time after ignition) [19].

Figure 3 provides a schematic of the test apparatus used for each of the full scale experiments conducted in this work. The design of this apparatus was based on an assembly originally developed at FM Global for experiments that measured fire propagation and smoke development behavior of polymeric materials [66]; this test method has been standardized as FM 4910 [67]. Here, combustible solids are mounted (facing one another) onto two inert parallel walls and ignited at their base using a 60 kW propane burner.

As seen in Fig. 3, in this work, a steel frame was constructed to support two parallel panels, each 2.44 m tall by 0.61 m wide (nominally 8 ft. tall by 2 ft. wide). The panel walls were each constructed by a 0.025 m thick layer Marinite Board attached to a 0.013 m thick layer of plywood, both of which are mounted to the vertical metal frame. At the base of these walls is a rectangular propane burner used for sample ignition. The metal support frame for the NIST/NRC Parallel Panel Apparatus was constructed in two parts, each positioned on a sliding track. This track allowed for the testing of combustible solids (samples) with varying initial thickness: at the start of each test, the panels were positioned such that the front surface of each sample aligned with the outer edge of the propane burner below (i.e., 30 cm apart). Depending on the sample's thickness (up to 0.05 m), a strip of flexible Kaowool insulation blanket was supported by a metal plate at the base of the assembly, as needed, to seal the gap between the base of the sample (and the Marinite board) and the outer edge of the propane burner [3].

In tests conducted in this work, most samples were attached to the parallel panel walls by a series of bolts (twelve bolts per panel, evenly distributed at six heights, z, across the height of each sample). Each bolt was drilled approximately 10 cm away from the center-line of the panels (i.e., at y = - 10 cm or y = 10 cm; see Fig. 3 for relevant coordinate system). A steel washer, approximately 2.5 cm in diameter, was used to distribute the load held by the bolt at each attachment point at the sample's front surface. Additionally, multiple steel brackets were used to secure the top, bottom, and outer edges of each sample to the panel walls. For porous polymer foams tested in this work, steel bolts were not used; instead, 12 gauge steel wire was placed across the front of the sample and threaded through each bolt location, to affix samples to the wall. At up to four additional locations across the height of foam samples, horizontal strips of this same wire were wrapped around the entire front surface of samples and affixed to the back of the panel. Representative images of each test conducted in this work (which depict sample mounting conditions) are available in Appendix C.

The entire parallel panel test assembly was positioned beneath the 6.1 m by 6.1 m exhaust hood at the National Fire Research Laboratory (NFRL) at NIST, which is instrumented and capable of performing heat release rate measurements by oxygen consumption calorimetry for fires up to 3 MW [68], with an average combined uncertainty for generic combustible fuels of 6.8 %. Additionally, for tests on ten of the materials tested in this work — i.e., ABS, HIPS, GPO-1, GPO-3, SIS wire, OSB, PMMA, POM-GF, PVC, and Western Red Cedar (these material designations are clarified in Table 1) — flame-to-surface heat flux measurements were obtained by a series of up to 14 water-cooled heat flux gauges positioned flush with the the front surface of the wall lining materials. More details about these measurement devices and techniques as well as their respective capabilities and uncertainties are provided in Sec. 2.3.

[3]The identification of any commercial product or trade name does not imply endorsement or recommendation by NIST (or any other contributing institution).

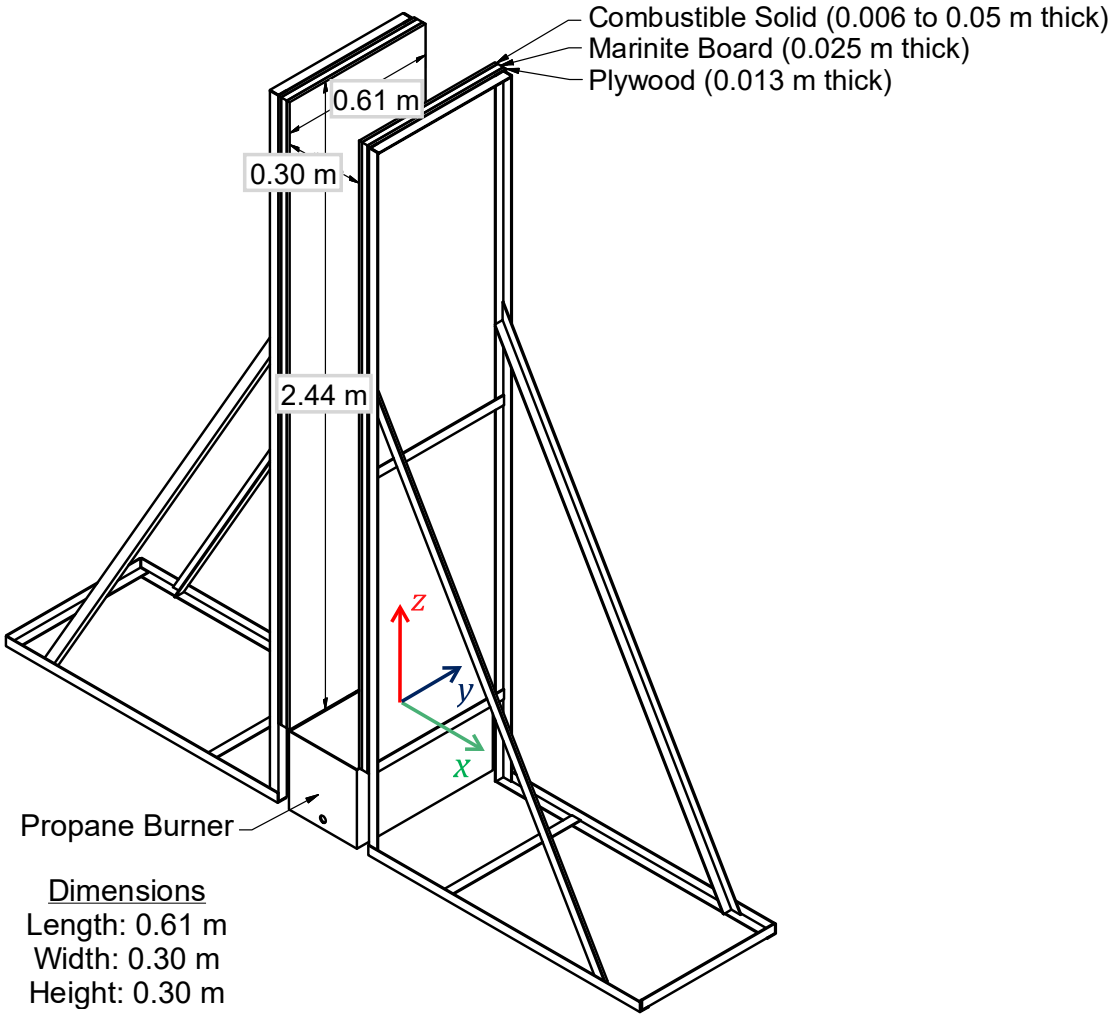

Fig. 3. Schematic of the NIST/NRC Parallel Panel Apparatus. Origin of coordinate system is located at the center of the top of the propane burner.

2.2. Materials

Table 1 provides an overview of each of the 18 combustible solids tested in this work. A wide range of combustible solids was tested, including: natural and synthetic polymers, copolymers (alloys), fiberglass-reinforced composite materials, porous polymer foams, and electrical cables. Some of these materials were selected because they can expected to be found in electrical cabinets and circuit boards (e.g., SIS Wire, GPO-1 and GPO-3, and PBT). Other materials, several of which were chosen due to their involvement in previously reported fire events in NPPs [69–72], were selected in order to observe a wide range of burning behaviors: charring and non-charring materials; physical deformation (e.g, swelling, collapse, dripping, and/or melt flow); heavy or light soot formation; and ease of ignitability.

Previous experiments studying laminar flame spread (samples less than 20 cm tall) over the surface of multiple polymeric materials [73] were used to guide this material selection. Figure 4, which was reproduced from a recent work [73], demonstrates some of these burning behaviors (including polymer melt flow, heavy soot formation and deposition, and sample burnout) during flame spread over six unique materials, each of which was also tested at the full scale in this test series. The blue flame (second image from left in Fig. 4) is supported by poly(oxymethylene) (POM), which is a highly-oxygenated (more than 50 wt.% oxygen), non-sooting fuel. Additionally, to explore the parameter space of material properties controlling flammability behavior, for some selected polymers, the same material (nominally) was procured from two different sources or in multiple densities or thicknesses (which could each vary, in these tests, by up to a factor of 3 or 4, respectively).

Fig. 4. Representative behavior of laminar wall flames supported by six common commodity plastics: (from left to right) PMMA, POM-GF, HIPS, ABS, PBT (reinforcecd with 20 wt. % chopped glass fibers), and fiberglass-reinforced polyester.

Table 1. Materials Tested

Material	Trade Name	Thickness (mm)	Color	Description
'Pure' Synthetic Polymers				
High Density Polyethylene (HDPE)	Polystone G Natural HDPE	6.15 - 6.30	White	Smooth finish
High Impact Polystyrene (HIPS)	HIPS	6.5 - 6.7	White	Matte Finish
Polybutylene Terepthalate (PBT)	HYDEX 4101 PBT	6.4 - 6.6	Color	Description
Poly(methyl methacrylate) (PMMA)	Acrylite 9H01 GT	5.3 - 6.25	Black	Cell-cast, smooth finish
Poly(vinyl chloride) (PVC)	Type I PVC Sheet	6.15 - 6.30	Black	Smooth Finish
Copolymers				
Poly(Acrylonitrile Butadiene Styrene) (ABS)	King KPC ABS	6.1 - 6.3	Natural, beige	Smooth Finish
PMMA-PVC alloy (Kydex)	Kydex 100	6.4 - 7.0	Pinstripe Gray	Haircell texture on backside (P3)
Porous Polymer Foams				
Cross Linked Polyethylene (XLPE 2#)	SOLU-CELL-P2000	23.4 - 23.7	Black	Closed-cell Foam
Cross Linked Polyethylene (XLPE 4#)	SOLU-CELL-P4000	24.4 - 26.0	Black	Closed-cell Foam
Cross Linked Polyethylene XLPE 6#	SOLU-CELL-P6000	24.3 - 24.6	Black	Closed-cell Foam
Poly(Isocyanurate) (PolyIso)	Thermasheath	23.9 - 26.9; 50.5 - 51.7	Light Yellow	Foil wrapped on both sides
Extruded Polystyrene (XPS)	GreenGuard XPS Insulation Board	18 - 24.9	Green	Smooth, rigid foam board
Extruded Polystyrene (XPS)	FOAMULAR 150 & FOAMULAR 250 Foam	24.8 - 26.0 , 49 - 51	Pink	Smooth, rigid foam board
Composite Materials				
GPO-1	Glastic, GPO-1	6.2 - 6.6	Tan	Matte finish
GPO-3	Redboard	6.1 - 6.4	Red	Matte finish
Poly(oxymethylene) (POM-GF)	Delrin 570	6.9 - 7.1 (and 9.5 mm, Test R3)	Natural, white	Smooth finish
Other Materials				
SIS Wire	12 AWG RSCC FIREWALL® TYPE XHHW-2 ORSIS 600V (UL) VY-1 NU-CLEAR Gray 2017	3.8	Gray	0.76 mm cable jacket over 2.3 mm copper wire. Wire insulation: flame retardant cross-linked polyolefin
Oriented Strand Board (OSB)	OSB Sheating	10.7 - 12.5	Natural	Textured
Western Red Cedar	Western Red Cedar	21.1 - 21.5	Natural	Sound Tight Knot Grade

Additional material information (including manufacturer and distributor) is provided in Appendix A

2.3. Instrumentation

2.3.1. Video and Photographs

Two digital cameras were used to record video of material burning behavior throughout each experiment. A digital single-lens reflex camera (Canon EOS 5D Mark IV) was positioned to view the two panels from a large stand-off distance (i.e., at approximately $x = 0$ m, $y = -8$ m, and $z = 1$ m). A custom script was written to analyze recordings from this camera to quantify uniformity of flame length development along either wall during experiments. This script extracts still frames (at 3 Hz) from video recordings, converts the images to gray scale, and determines flame length (z_f) along either wall based on critical average brightness (light intensity of 75 % of the maximum pixel brightness) and whether the light intensity criteria is continuous over 3 vertical pixels. This analysis helped to inform understanding of flame uniformity (from wall-to-wall) during experiments; however, script outputs (e.g., time-resolved plots of flame height along either panel wall are not presented in this manuscript).

One or two hi-definition, wide-angle camera(s) (GoPro Hero 4 or Logitech HD Pro C920 Webcam), were also placed near the base[4] of the parallel panel assembly to provide a close up view of the surface of one (or both) of the panel wall(s) as it burned. Videos recorded during each test are available online on the NIST Fire Calorimetry Database [1]. Photographs were also taken prior to ignition (setup) and throughout each experiment using a SONY Model Number SLT-A55V camera.

Still photographs were taken prior to ignition (test setup) and throughout each experiment using a SONY Model Number SLT-A55V camera. This camera was moved throughout each test, as needed, to provide additional perspective on burning phenomena representative of the specific material being tested. Four representative images of material burning behavior (pre-test, ignition, peak HRR, end of test) are provided for each experiment in Appendix C.

2.3.2. Heat Release Rate and Species Yields

All experiments were conducted underneath the 6.1 m by 6.1 m exhaust hood at the National Fire Research Laboratory (NFRL) at NIST. The base of this hood is positioned approximately 6.4 m above the test floor and is capable of performing heat release rate measurements by oxygen consumption calorimetry with a nominal capacity of 3 MW. Reported uncertainty in measured heat release rates in this system averages 6.5 % across the range of fire sizes observed in this test series (0.1 MW to 4.2 MW) [68]. Previous experiments indicate that this calorimeter can resolve fire events with HRR peaks lasting at least 15 s.

This system is instrumented to measure gaseous species concentrations (i.e., O_2, CO, and CO_2); smoke particulate generated by the fire is also measured via the light extinction of a HeNe laser beam across the center of the exhaust duct. This mesaurment method

[4]These cameras were positioned at approximately $x = \pm 2.0$ m to 2.5 m, $y = \pm -2.0$ m to 2.5 m, and $z = -0.15$ m to view opposite panel walls).

follows the optical design and implementation described elsewhere [74][5]. These measurements were used to calculate soot and gaseous species yields (Y_i [g/g]) for each of the materials tested in this work (when total sample mass loss data was available).

For most experiments conducted in this work, an exhaust flow rate of 16 kg/s was used to minimize the influence of induced air flow on fire behavior and on the resolution of HRR measurements, while maintaining adequate ventilation of combustion products. For highly sooting materials (e.g., ABS or HIPS) or those which produced more hazardous gaseous volatiles or combustion products during pyrolysis and/or burning (e.g., POM-GF or PVC) this exhaust flow rate was increased to 20 kg/s. When these highly-sooting or more toxic materials were tested, gaseous combustion products and smoke particules were treated prior to release into the atmosphere using an emissions control system (ECS) to comply with local environmental requirements. The ECS is positioned downstream in the exhaust duct from all measurement devices used in this system (i.e., gas volume fraction, temperature, and velocity).

2.3.3. Heat Flux

For all experiments, a Schmidt-Boelter heat flux gauge (2.54 cm diameter), with a response time of less than 100 ms, was positioned approximately 4.25 m away from the parallel panel assembly, approximately 45 degrees away from the gap between the two panels (i.e., at x = -3 m or -1 m, y = -3 m, z = 0.9 m)[6]. This gauge was used to identify the timing of fire events at the test floor and to provide a measurement of radiation heat transfer at a distance from the fire for model validation.

For experiments involving ABS, HIPS, GPO-1, GPO-3, SIS wire, OSB, PMMA, POM-GF, PVC, and Western Red Cedar, flame-to-surface heat flux measurements were obtained by an array of up to 14 water-cooled Schmidt-Boelter heat flux gauges, each positioned flush with the front surface of the samples. An additional series of experiments was also conducted in which heat flux from the propane burner flames to inert panel walls (i.e., Marinite panels) was measured. These tests quantified the spatial uniformity and time-dependent nature of the heat feedback profile of this ignition source as well as its repeatability from test to test. Burner characterization experiments were repeated several times throughout the test series, to ensure reproducibility of this ignition source. Across each of these experiments, heat flux gauges could be located along the centerline of panels (y = 0 cm) at nine unique heights (z = 10, 20, 30, 50, 75, 100, 140, 180, and 220 cm). At five of these heights (z = 20, 50, 75, 100, and 180 cm) heat flux gauges could also be distributed across the width of the panels (i.e., at y = -25, -15, 0, 15, and 25 cm).

At each of the measurement locations, a 2.54 cm (1 in) diameter hole was first drilled through the Marinite and plywood layers of the parallel panel assembly; for a given test,

[5] From Mulholland and Croarkin [75], the recommended value and standard uncertainty for the specific extinction coeffcient of flame generated smoke are 8.71 $m^2/g \pm 0.47$ m^2/g.

[6] The location of the heat flux gauge used to measure radiation heat transfer at a distance away from the parallel panel walls may vary between tests; test-specific location of this heat flux gauge is provided in Appendix C.

when gauges were not positioned at these locations, these holes were filled with ceramic fiber insulation. After the samples were mounted to the panel walls, a hole was then drilled with a diameter matching that of the heat flux gauge to be used.

All heat flux gauges used in this work varied between 0.64 cm and 1.59 cm in diameter (nominally between 1/4 in and 5/8 in). For the majority of tests only 0.95 cm and 1.59 cm gauges were used. In repeated experiments in which differently-sized-gauges were positioned at the same location, no statistically significant difference is heat flux was measured. This suggests that, for this system, the presence of the heat flux gauge did not strongly impact material burning behavior or flame structure (e.g., due to blowing [76] or quenching effects [77]). Each gauge was inserted through the back of the panel (and sample) and positioned such that its front surface was flush with that of the test sample. Behind the sample, the body of each gauge was protected by an insulation collar: a cylindrical bushing, 2 cm to 3 cm long, with an outer diameter of 2.54 cm and an inner diameter matching that of the gauge. Gauges were held in place throughout each experiment using a clamp or a length of 12 gauge wire that firmly attached gauge water cooling lines to horizontal lengths of wood (i.e., a shelf) affixed to the back of the parallel panel assembly.

When using water-cooled heat flux gauges to measure wall flame heat flux, their surface temperature is typically lower than that of the surrounding pyrolyzing material, in which case the measured rate of heat transfer from flame to burning surface is overestimated. To correct for this, up to six of the water-cooled heat flux gauges had embedded k-type thermocouples; the starting locations of these gauges were therefore carefully selected to provide optimal spatial resolution of gauge temperature data (e.g., if two gauges of the same size were placed at the same height, and thus likely to observe similar time-resolved heating, temperature readings from one gauge could provide a reasonable estimate for the other).

The radiative ($\dot{q}''_{\text{rad}}$) and total ($\dot{q}''_{\text{total}}$) heat flux from flames can be measured using multiple devices [78, 79]. Multiple experiments were conducted in which the total and radiative heat flux was measured by a pair of water-cooled heat flux gauges located at the same height. To protect the gauges' surface from deposits, both gauges were shielded during the initial stages of the experiments by small, custom fitted pieces of insulation. Once steady flaming conditions were observed, the shields were removed and a "clean gauge" measurement of incident heat flux was recorded.

Heat flux gauge insulation shields were formed from a 0.6 cm-thick disc of Kaowool PM board (a rigid, ceramic fiber insulation) that measured 2.5 cm in diameter. As shown in Fig. 5 these shields (four white discs on the left panel) were held in place during testing by 0.6 cm diameter metal rods that were compressed between the two panels, acting as springs that pressed the insulation shields towards the front surface of either heat flux gauge as needed. Attached to each rod was a length of thin wire that was used to pull the rods (with shields attached) out from the panel walls. In separate tests, shields were removed at different times based on the time needed for continuous flaming to be observed at the gauge location of interest. For a given test, shield removal time could vary

with height. However, at the same height, shields were always removed simultaneously to expose both the total heat flux gauge and the radiometer to flames at the same time.

Fig. 5. Photograph of GPO-1 prior to testing showing mounting, support, and shielded of heat flux gauges. Here, each panel wall is instrumented with heat flux gauges; on the left wall, two gauges at each height $z = 100$ cm and $z = 180$ cm are shielded by 2.54 cm diameter insulation discs to ensure clean gauge readings of $\dot{q}''_{\text{rad}}$ and $\dot{q}''_{\text{total}}$.

Prior to each test, total heat flux gauges were cleaned, repainted with an optical black coating supplied by the gauge manufacturer (listed average absorptance of 0.95 from 0.3 μm to 15 μm), and calibrated using a secondary standard gauge in a well-characterized calibration facility[80]. Repeated refinishing of the heat flux gauge ensured the accuracy of recorded measurements, despite potential accumulation of deposits on its surface by the conclusion of each test.

For the first series of experiments in which heat flux gauges were used (12 total experiments: PMMA, R1-R6; GPO-3, R1-R3; SIS Wire/GPO-3, R2; PVC R1 and R2)[7] this calibration was performed as follows. First, the supply voltage and current to a 2000 W tungsten–

[7]Here, 'R#' indicates test repetition number.

halogen filament lamp (used as a heat source) was set and allowed to stabilize for 20 minutes. A reference water-cooled Schmidt-Boelter heat flux gauge (SN124421, a secondary standard), originally calibrated by the Radiometric Physics Division of the National Bureau of Standards (now NIST), is then positioned at a reproducible location (in a water-cooled mount) in front of this heat source and the voltage generated by this gauge is recorded. The reference gauge is removed, replaced by the gauge being calibrated, and its voltage signal is recorded. Up to 12 heat flux gauges were calibrated at a time (in series) in this manner; after the readings from four different gauges were recorded, the voltage signal produced by the reference gauge is remeasured to ensure that the applied radiant heat flux remains constant.

Once a calibration is complete at a given heat flux, the power to the lamp is adjusted to the next flux level, and the measurement procedure is repeated. In total, three heat flux levels are chosen (between 3.5 kW/m^2 and 15 kW/m^2). After measurements are obtained by all gauges at each of these three flux values, the incident heat flux [kW/m^2] measured by the reference gauge is plotted versus measured response [mV] of the gauge being calibrated; a linear least-squares fit of this data is calculated and gauge sensitivity is then reported in terms of (kW/m^2)/mV. Further details regarding this calibration procedure are provided elsewhere [80, 81].

The sensitivity coefficient calculated for each heat flux gauge used in this test series was logged after each calibration. After an initial series of experiments and gauge calibrations (Tests 1-14), calibration logs were reviewed for each of these gauges (145 total gauge uses across repeated tests; gauge diameters of 0.64 cm, 0.95 cm, and 1.59 cm). This review demonstrated that the repeated use (direct flame exposure in parallel panel experiments), cleaning, repainting, and recalibration of each of these gauges did not significantly affect their measured sensitivities. That is, throughout these use, cleaning, repainting, and recalibration cycles, measured sensitivity of each gauge varied by (on average) less than 1 % and this value showed no systematic dependence on time, gauge exposure, or gauge size.

To limit the time needed for recalibration of gauges used later in this test series — for all gauges used in a single experiment (on average, 12 gauges), calibration requires approximately 4 hours when two trained laboratory technicians are available (neglecting the time required for their cleaning and repainting) — an expedited calibration procedure was thus developed as follows (and used for Tests 15 - 66). At the *start of* a new round of testing (two weeks of continuous testing, conducting up to five experiments recording heat flux measurements during this time) heat flux gauges were cleaned, repainted, and recalibrated as described above. However, *during* this test series, after gauges were cleaned and repainted, an average sensitivity coefficient was prescribed as the calculated mean value of all recent calibration results. For each gauge, prior to testing, this average calibration was spot checked by placing the heat flux gauge of interest side by side with a reference gauge, such that they were both positioned 2.54 cm below the center of the radiant heater of a cone calorimeter [82]. The cone heater was set to approximately 800 °C to provide an incident radiant heat flux of approximately 50 kW m^{-2} and the response of the freshly painted gauge was recorded. On average (236 total spot checks), measured

gauge response matched the reference value within 1 %, thus confirming the accuracy of this calibration approach.

A detailed uncertainty analysis of this calibration technique is provided in Appendix B.4.

The sensitivity coefficient calculated for each heat flux gauge was logged after each calibration. After an initial series of experiments and gauge calibrations, a review of these logs (145 separate measurements, including 1/4 in., 3/8 in., and 5/8 in. diameter gauges; between 0.64 cm and 1.59 cm in diameter) demonstrated that the repeated use (direct flame exposure in parallel panel experiments), cleaning, repainting, and recalibration of each of these gauges did not significantly affect their measured sensitivities. That is, throughout 14 use, cleaning, repainting, and recalibration cycles, measured sensitivity of each gauge varied by (on average) less than 1 % and this value showed no systematic dependence on time/gauge use. Thus, to limit the time needed for recalibration of gauges for experiments conducted later in the test series — for all gauges used in a single experiment (on average, 12 gauges), calibration requires approximately 4 hours when two trained laboratory technicians are available (neglecting the time required for their cleaning and repainting) — an expedited calibration procedure was used as follows.

Measurements of $\dot{q}''_{\text{rad}}$ were obtained using a 0.95 cm diameter water-cooled Schmidt-Boelter heat flux gauge that had been fitted at their front surface with a 1 mm thick ZnSe window, of viewing angle 150°. ZnSe windows were selected due to their near constant transmitance ($\tau \simeq 0.7$) between 1 μm and 17 μm; this corresponds to a near constant fractional transmission of electromagnetic radiation for blackbody temperatures between 500°C and 2000°C [83], which spans the range of expected wall and flame temperatures observed in these experiments. Prior to each test, after cleaning and repainting of gauges, ZnSe windows were cleaned (soaked in an acetone solution and gently wiped with an acetone-soaked cotton cloth), reattached to a total heat flux gauge, and then calibrated beneath the heater of a cone calorimeter as described above. This calibration approach accounted for reductions in measured radiation heat flux to the gauge sensor due to the reduced transmissivity of the ZnSe window and its limited viewing angle. When exposed to the harsh conditions of direct flame impingement, the transmissivities of these windows would decrease over time. Consequently, ZnSe windows were replaced when their calibrated transmissivities decreased below (approximately) 30% of their original values.

During parallel panel experiments, heat flux (and heat flux gauge temperature) measurements were recorded using National Instruments (NI) data acquisition (DAQ) modules (NI-9213I/O-Modules) connected to a cDAQ-9184 chassis. Data signals were acquired and recorded using a custom program called MIDAS (Modular In-situ Data Acquisition System), which was developed in LabVIEW. Each channel (i.e., each thermocouple and heat flux gauge signal) was sampled at 90 Hz; mean values were then recorded at 1 Hz as the numerical mean of measured values obtained across a 1 s time interval. The NI-9213 modules have a typical gain error 0.04 % (percentage of voltage reading) and 0.017 mV typical offset error under the operating conditions in these experiments. Ultimately, the uncertainties from the DAQ system were orders of magnitude lower than those of the measurements

devices and/or systems used in these experiments. Detailed calculations of measurement uncertainties are provided in AppendixB.4.

At the conclusion of this test series, a recalibration and validation exercise was conducted with the support of the Optical Radiation Group of the NIST Physical Measurement Laboratory. This exercise identified a calibration issue with the reference heat flux gauge (SN124421) that was used as the secondary standard (in the tungsten lamp calibration apparatus [80]) to calibrate all heat flux gauges used in this parallel panel test series: specifically, when calibrated against a blackbody [84], SN124421 produced a non-linear response that yielded a bias (4.3 % overestimate of measured heat fluxes) in the tungsten lamp calibration apparatus. A means to correct this bias (4.3 % error) in measurements was developed and validated through a test series that included repeated calibrations of seven Schmidt-Boelter heat flux gauges in the tungsten lamp calibration apparatus [80] and the calibration of three of these gauges against a blackbody [84] (one of which now serves as the new reference heat flux gauge for calibrations performed in the NIST Fire Research Division). Details of this gauge calibration and validation exercise will be provided in an upcoming report [85].

A detailed uncertainty analysis of this calibration technique (as applied in this study) is provided in Appendix B.4. The major sources of uncertainty for these calibration techniques include:

- The combined standard uncertainty of calibrations performed in the blackbody apparatus of the NIST Optical Radiation Group (1.5 %).
- The repeatability of calibrations made in the tungsten lamp calibration apparatus [80] or beneath the cone calorimeter (estimated as 0.5 %; type B uncertainty).
- Measured average drift (decrease in sensitivity from the beginning to the end of the parallel panel test series) in the calibration coefficients of each of the heat flux gauges used in this test series (1.3 %). This uncertainty component is included as it is not possible to determine if this represents a real, measurable decrease in gauge sensitivity that arises as a result of their repeated use during multiple years of testing in harsh conditions, or because of deterioration of the previous reference gauge (SN124421) that had been used as the secondary standard in the tungsten lamp calibration apparatus [80].

2.4. Ignition Source

Previous studies have reported that predicting electrical fires is challenging because they have a particularly low failure rate and many ignition phenomena have a strong probabilistic aspect to them [9]. Further, it has been reported that it is difficult for an electric arc to start a fire, even under better-than-average conditions [86]. Nevertheless, fires are known to start in electrical enclosures: Ref. [5] provides an overview of the ignition sources of 269 electrical enclosure fires that were reported in US NPPs between 1990 and 2011. In this work, it is noted that the majority (approximately 85 %) of these fires were “initiated

by some kind of electrical failure: arcing, sparks, or overheating (both [High Energy Arc Fault] (HEAF) and non-HEAF)". Further, when fires in these electrical enclosures do occur, statistics indicate that nearly half of reported [5] events are 'Challenging' or 'Potentially-Challenging', which means that they had "an observable and substantive effect on the environment outside the initiating source" or "could have led to fire growth, fire spread, equipment damage or cable damage beyond the fire ignition source had the circumstances of the fire event been different" [4].

In this study, the key research question was not to determine whether or not a specific electrical discharge (e.g., voltage, current, and/or duration) could ignite a specific fuel type and configuration of interest. Rather, this study seeks to quantify how material composition affects ignitability, fire growth rate, and peak fire size in large-scale experiments designed to represent electrical enclosure fires. A representative ignition source was thus designed that was sufficiently severe to ignite the variety of combustible solids that are found in electrical enclosures in NPPs but still small enough such that fire growth during experiments was controlled by flame spread over the surface of the combustible solids (i.e., burner HRR was selected to emphasize flame-spread-driven fire growth). A brief summary of how this ignition source was designed and characterized is provided:

- A rectangular propane burner (nominal heat release rate: 63 kW) positioned at the base of the parallel panel assembly was used as the ignition source for all samples. Two burner configurations were considered:
  - Preliminary burner configuration (Tests 1-6) - the burner chamber was filled by a single layer of pea gravel resting on top of a steel mesh that maintained a 0.05 m plenum at the base of the burner.
  - Final burner configuration (Tests 7-66) - multiple layers (from bottom to top: pea gravel, sand, and a Kaowool insulation blanket) rest on top of the steel mesh inside of the burner chamber.
- A series of "Burner Shakedown" experiments was conducted in which time-resolved measurements of burner heat release rate and flame heat flux (to inert panel walls) was measured. Burner Shakedown tests were repeated throughout the experimental series to confirm repeatability of its performance.
- The final burner configuration was selected based on its improved repeatability from test to test, and a dataset characterizing burner performance is provided for model validation when simulating these parallel panel experiments.

As seen in Fig. 3, a rectangular propane burner was placed at the base of the parallel panel assembly to ignite samples. A mass flow controller was used to feed chemically pure (CP grade) propane to the burner at a rate that would support, nominally, a 63 kW fire. Because the main focus of this series of experiments was to determine the influence of material composition on early fire growth, an attempt was made to turn off the propane burner as soon as possible in order to minimize its impact on flame spread over the surface

of each combustible solid. Thus, once (if at all) sustained, uniform ignition was observed across the base of both parallel panel walls, gas flow to the burner was turned off[8]. Due to variations in the decomposition reaction mechanism and thermophysical properties of each material tested in this work, burner application time (and sample ignition time) varied for each material tested. In many cases, after ignition was observed and the burner was turned off, flames continued to spread upwards across the length of each panel. In some cases (e.g., OSB or Western Red Cedar) flames were observed to spread upwards while the burner flame was still on but they were not self-sustaining after the burner was turned off. In these tests, the burner flame was thus reignited and gas flow was subsequently maintained throughout the duration of the test; repeated experiments on the same material were then conducted with the burner flame turned on throughout the duration of testing. Burner application time was recorded in each test and is reported in Section 3 and in Appendix C.

In a separate series of "Burner Shakedown" tests, burner flame heat flux (to inert panel walls) was measured using an array of up to 12 water-cooled Schmidt-Boelter heat flux gauges that were positioned across each panel wall, at multiple heights and widths (z- and y-locations, respectively), such that they were flush with the front surface of either panel. Gauges were cooled with water from the main building supply line, with an average initial temperature of 15 °C. Approximately half of the heat flux gauges used in each experiment had embedded K-type thermocouples, which continuously monitored temperature throughout the duration of experiments.

Burner Shakedown tests were repeated multiple times in order to improve the spatial resolution of heat flux measurements, to quantify measurement variability, and to ensure reproducibility of the burner throughout the test series. Prior to further analysis, noise in measured burner HRR and total flame-to-surface heat flux was reduced by applying a Savitzky-Golay filter (4^{th} order, 39 frames). As seen in Fig. 6, applying this filter removes random noise in the HRR and $\dot{q}''$ signals without over-smoothing or loss of resolution in meaningful data (here, filtered and unfiltered HRR and $\dot{q}''$ data are plotted as thick and thin lines, respectively). Thus, all further burner measurements presented throughout this section represent filtered data.

[8]Because of the rapid flame spread supported by samples of PolyIso and XPS foam, a discrete sample ignition time could not be reliably defined in real time (i.e., as experiments were conducted) and so, to improve test to test repeatability, the propane burner was left on throughout the duration of these experiments. Further details are provided in Secs. 3.1.10 and 3.1.16.

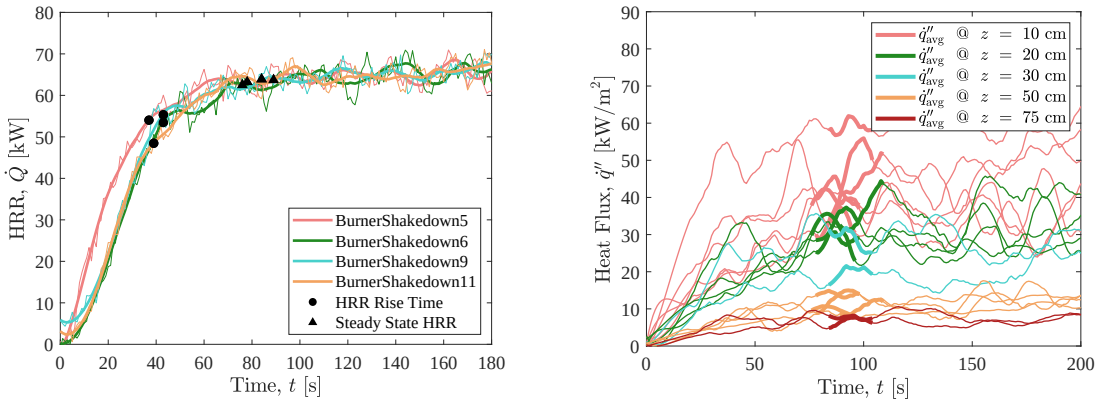

(a)

Fig. 6. Measurements of (a) burner heat release rate and (b) total heat flux from the burner flame to water-cooled Schmidt-Boelter heat flux gauges positioned along the centerline of panel walls during Burner Shakedowns 5, 6, 9, and 11. Thin lines represent smoothed data using a Savitzky-Golay filter, while thick lines represent the average of the data at that particular height across Shakedowns.

Preliminary Burner Configuration

At the start of this test series (i.e., Burner Shakedowns 1-11 and Material Tests 1-6: PMMA R1-R5 and Redboard R1), the propane burner was filled with a 0.25 m thick layer of pea gravel that rested on top of a steel mesh that maintained a 0.05 m plenum at the base of the burner. As seen in Fig. 6a, measured heat release rate in these tests was highly repeatable (i.e., at the same time in different test repetitions, approximately the same HRR was measured) thus allowing for a straightforward, unified analysis of wall flame heat flux measured at different locations across the panel walls in repeated tests.

In each of these Burner Shakedown tests, after burner ignition at time, $t = 0$, flames grow as measured HRR quickly increases to approximately 52 kW by $t = 40$ s. This 'Burner Rise Time', t_{rise}, was defined as the first time at which the rate of change of burner HRR (i.e., $d\dot{Q}/dt$, calculated as the numerical derivative, 1 s time step, of filtered HRR with $\pm$20 s running average smoothing applied remained below 0.75 kW s^{-1} (i.e., $\overline{d\dot{Q}/dt}$ <0.75 kW s^{-1}) for a minimum of 5 s. From $t = 40$ s to $t = 80$ s, burner HRR continues increasing (at a slower rate) before finally reaching a relatively steady value of 64 kW. Steady flaming is observed at time t_{steady}, which was defined as the first time at which the average rate of change of HRR (i.e., $\pm$20 s running average of $d\dot{Q}/dt$) remained below 0.10 kW s^{-1} (i.e., $\overline{d\dot{Q}/dt}$ <0.10 kW s^{-1}) for a minimum of 10 s. The critical times t_{rise} and t_{steady} are identified in Fig. 6a as solid black circles and triangles, respectively.

A similar trend in heat flux is observed, as seen in Fig. 7a, which plots filtered, time-resolved measurements of burner flame heat flux, $\dot{q}''$ (obtained at the centerline of panels, $y = 0$, and at five different heights, z). As seen here, following burner ignition, measured flame heat flux quickly increases at each location until t_{rise} and then continues increasing more gradually (by approximately 35 %) until t_{steady}, at which point a relatively steady value heat flux, $\dot{q}''_{\text{steady}}$, is measured[9]. Note: for this original burner configuration, reproducibility of time-resolved $\dot{q}''$ measurements is lower than that of HRR data.

The average heat flux recorded during the 20 s period after t_{steady} (shown in Fig. 7a as the bolded segments of $\dot{q}''$ curves) defines $\dot{q}''_{\text{steady}}$ for that test at a given measurement location of interest. Along the centerline of panels, $\dot{q}''_{\text{steady}}$ was found to decrease with height, z, above the burner as shown in Fig. 7b. Here, colored circles represent values of $\dot{q}''_{\text{steady}}$ measured in individual burner shakedown tests; solid vs. open symbols indicate whether this value was measured on the left or right wall (i.e., at $x = -15$ cm or $x = 15$ cm). Solid black circles represent the average of repeated measurements obtained at the same height, z, when uniform flaming was observed (see discussion below); error bars indicate the expanded uncertainty (U_c; 95 % confidence interval, coverage factor = 2). The primary sources of uncertainty in this measurement include fluctuations in repeated measurements and the uncertainty in the calibration of the heat flux gauges; details of this uncertainty calculation are provided in Appendix B.4. Also plotted in this figure is

[9] After steady flaming is observed, although HRR remains constant, a slight increase in $\dot{q}''$ is measured, likely due to further increases in temperature at the base of the assembly (which would result in greater reradiation from the parallel panel walls and the top surface of the burner).

previously-measured heat flux data (gray crosses [87] and gray diamonds [88]) obtained from burner characterization tests conducted in this same configuration in two previous studies.

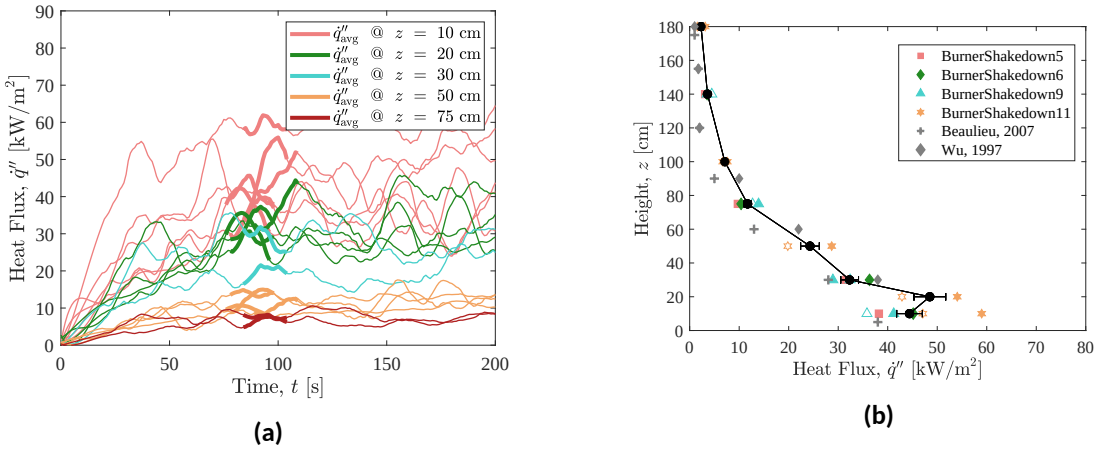

Fig. 7. Measurements of (a) time-resolved total heat flux, $\dot{q}''$, from the burner flame to water-cooled Schmidt-Boelter heat flux gauges positioned along the centerline of panel walls during Burner Shakedowns 5, 6, 9, and 11 ('Preliminary Configuration') and (b) steady state heat flux, $\dot{q}''_{\text{steady}}$, to the centerline of panel walls as a function of height, z above the burner. Solid vs. open symbols indicate whether $\dot{q}''_{\text{steady}}$ was measured on the left or right wall, respectively. Error bars indicate expanded uncertainty of the heat flux measurements (U_c; 95% confidence interval, coverage factor = 2), as described in Appendix B.2.

Collectively, the results shown in Fig. 7 demonstrate that burner flame heat feedback is fairly repeatable between tests. However, for a given test there can be notable wall-to-wall variability. Wall flame heat flux measurements and video recordings of burner flame behavior were analyzed to quantify (and determine the source of) potential variations in burner heat feedback between repeated experiments. The results of this analysis indicate that the primary source of these variations was stochastic flame attachment to a single panel wall (as opposed to uniform flame exposure to both panel walls). This is demonstrated in Fig. 8, which shows that measured flame heat feedback (Fig. 8b) is the same to both panel walls in a single experiment when uniform flaming is observed (Fig. 8a). However, as seen in Fig. 9, measured flame heat flux and flame height (i.e., the length scale, z, over which elevated heat fluxes were measured) were substantially higher or lower dependending on the presence or absence of flames along that wall. In Section 3 the impact of this variability on measured ignition of (and fire growth across) combustible solids is discussed. It was observed that the addition of a 0.075 m layer of sand and a 0.025 m thick Kaowool Blanket at the top of the burner chamber reduced, but did not completely eliminate, variability in propane burner flame structure (and thus variability in flame heat feedback and sample ignition behavior), therefore this burner configuration was used for the majority of experiments.

(a) Burner flame structure during during uniform flaming

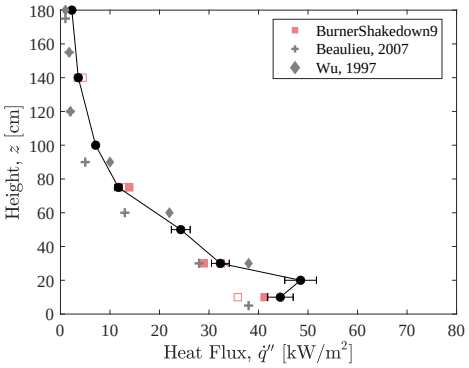

(b) Measured $\dot{q}''_{\text{steady}}$ during uniform flaming for Burner Shakedown 9, compared to the average steady state heat flux. Error bars indicate expanded uncertainty of the heat flux measurements (U_c; 95% confidence interval, coverage factor = 2), as described in Appendix B.2.

Fig. 8. Impact of flame attachment to panel walls on measured flame heat flux. Here, uniform flame heat flux is measured along either panel wall, consistent with observed flame structure.

(a) Burner flame structure with preferential flame attachment on left wall (Shakedown 11, green symbols at right)

(b) Burner flame structure with preferential flame attachment on right wall (Shakedown 5, red symbols at right)

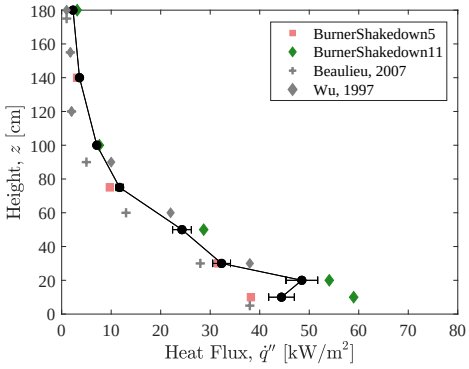

(c) Measured $\dot{q}''_{\text{steady}}$ along the left panel wall with preferential flame attachment. Error bars indicate expanded uncertainty of the heat flux measurements (U_c; 95% confidence interval, coverage factor = 2), as described in Appendix B.2.

Fig. 9. Impact of flame attachment to panel walls on measured flame heat flux. Here, images (a) and (b) demonstrate preferential flame attachment to the left or right panel walls (at $x = -15$ cm or $x = 15$ cm, respectively). Image (c) demonstrates that, consistent with flame structure, measured flame heat flux along the left wall is correspondingly higher or lower in these cases as compared to the average values measured during uniform flaming.

Final Burner Configuration

For the majority of the experiments conducted in this work (i.e., Burner Shakedowns 12-27 and Material Tests 7-66, including PMMA R6) the burner was filled with a 0.15 m deep layer of pea gravel, topped by 0.075 m layer of sand, and a 0.025 m thick sheet of porous, flexible insulation (Kaowool Blanket). This final configuration was selected because it supported more uniform flaming across the burner's surface and, between repeated tests, greater reproducibility of flame structure along either panel wall.

Figure 10a plots the HRR measured in each burner shakedown test that was conducted using the final burner configuration. As seen here, in each of these tests, HRR rises to a steady state value after ignition (quickly at first, until t_{rise} and then more gradually until t_{steady}) but two distinct groups of HRR profiles are observed: (1) those that reach t_{steady} within approximately 80 s (as observed in shakedown tests of the burner in its preliminary configuration) and (2) those that reach steady HRR within approximately 45 s [10].

Analysis of these results revealed that the more rapid observation of steady state behavior (i.e., $t_{\text{steady}} = 45$ s) occurred only in test repetitions that were conducted within approximately 30 minutes of one another (likely as a result of the gas transfer line and lower plenum of the propane burner having been recently filled in the prior experiment). However, both of these groups of tests (fast and slow) reach a steady state HRR of approximately 63 kW and, at this HRR, measured $\dot{q}''_{\text{steady}}$ is approximately equal. Further analysis demonstrated that wall flame heat fluxes measured at the same location along the panel wall throughout the duration of Burner Shakedown tests (both fast and slow) were highly repeatable when compared at the same HRR. Consequently, $\dot{q}''$ measurements from all Burner Shakedown tests conducted using the final burner configuration could be analyzed together (for enhanced statistics and greater spatial resolution in measurements) when these measurements were unified as a function of burner HRR rather than time. Final reported time-resolved HRR values (e.g., HRR at 20 s, 40 s, 60 s, or 80 s) are thus defined based only on Burner Shakedown tests in which $t_{\text{steady}} = 80$ s, as this matches the time response observed during parallel panel tests with combustible solids.

Fig. 10b, plots time-resolved measurements of burner flame heat flux, $\dot{q}''$ obtained at the centerline of panels, $y = 0$, and at four different heights, z (note: test data shown here is taken only from Burner Shakedown tests in which $t_{\text{steady}} = 45$ s). As seen here, following burner ignition, measured flame heat flux quickly increases at each location before reaching a relatively steady value, $\dot{q}''_{\text{steady}}$. With this new burner configuration, time-resolved measurements of $\dot{q}''$ (at the same height, z) show greater reproducibility from test to test (compare to $\dot{q}''$ shown in Fig. 7a). The average heat flux recorded during a 20 s period after t_{steady} (shown in Fig. 10b as the bolded segments of $\dot{q}''$ curves) is then used to define $\dot{q}''_{\text{steady}}$ for that test. Fig. 10c.

[10] Note: t_{rise} and t_{steady} are defined identically for both the Preliminary and Final Burner Configurations. t_{rise} is defined as the first time that a $\pm$20 s running average of $d\dot{Q}/dt$ remained below 0.75 kW s^{-1} for 5 seconds. t_{steady} is defined as the first time a $\pm$20 s running average of $d\dot{Q}/dt$ remained below 0.10 kW s^{-1} for 10 seconds.

Figure 10c plots $\dot{q}''_{\text{steady}}$ along the centerline of panel wall with the burner in its final configuration. This includes data from Burner Shakedown tests in which $t_{\text{steady}} = 45\ s$ and $t_{\text{steady}} = 80\ s$. Here, colored circles represent values of $\dot{q}''_{\text{steady}}$ measured in individual burner shakedown tests; solid vs. open symbols indicate whether this value was measured on the left or right wall (i.e., at $x = -15$ cm or $x = 15$ cm). Solid black circles represent the average of repeated measurements obtained at the same height, z. Error bars indicate an expanded uncertainty (U_c; 95 % confidence interval, coverage factor = 2); details of this uncertainty calculation are provided in Appendix B.4. Also plotted in this figure (as gray crosses [87] and gray diamonds [88]) is previously-measured heat flux data obtained from burner characterization tests conducted in this same configuration (a parallel panel assembly with the same burner dimensions, HRR, and fuel type).

As seen here, flame heat flux measured in the current study (final burner configuration) is generally consistent with previous measurements: $\dot{q}''_{\text{steady}}$ was found to decrease with height, z (slightly higher than 2007 data, gray crosses [87]; approximately equal to 1997 data, gray diamonds [88]). These two reference datasets were obtained in the same laboratory under nominally the same conditions and burner configuration; though tests were ten years apart, the latter study notes that, "the reason for this difference [in measured flame heat flux profiles] is unknown" [87].

Wall flame heat flux measurements and video recordings of burner flame behavior were further analyzed to characterize the uniformity of burner flame structure across the width of the panel (y-dimension), and from left wall to right wall ($x = -15$ cm or $x = 15$ cm). This analysis revealed that, during these burner shakedown experiments, flame structure and heat feedback were similar between either panel wall. Thus, measurements of flame heat flux taken from opposite panel walls (i.e., at $x = -15$ cm and $x = 15$ cm) were averaged together (at the same y and z) such that spatially-resolved measurements of the average total burner flame heat flux across the panel walls could be calculated. Figure 11 provides representative profiles of these average measurements at four different heat release rates: $\dot{Q} =$ 20 kW, 35 kW, 50 kW, and 63 kW. Recall: the y and z dimensions identify location across the panel width and above the base of the panel walls, respectively). Note: isocontours are interpolated between individual measurement locations, which are identified in Fig. 11 by solid black symbols. At each of these locations, $\dot{q}''$ measurements shown here represent average values obtained from least 3 unique heat flux gauges in different tests (up to 12 for measurements along the centerline, $y = 0$).

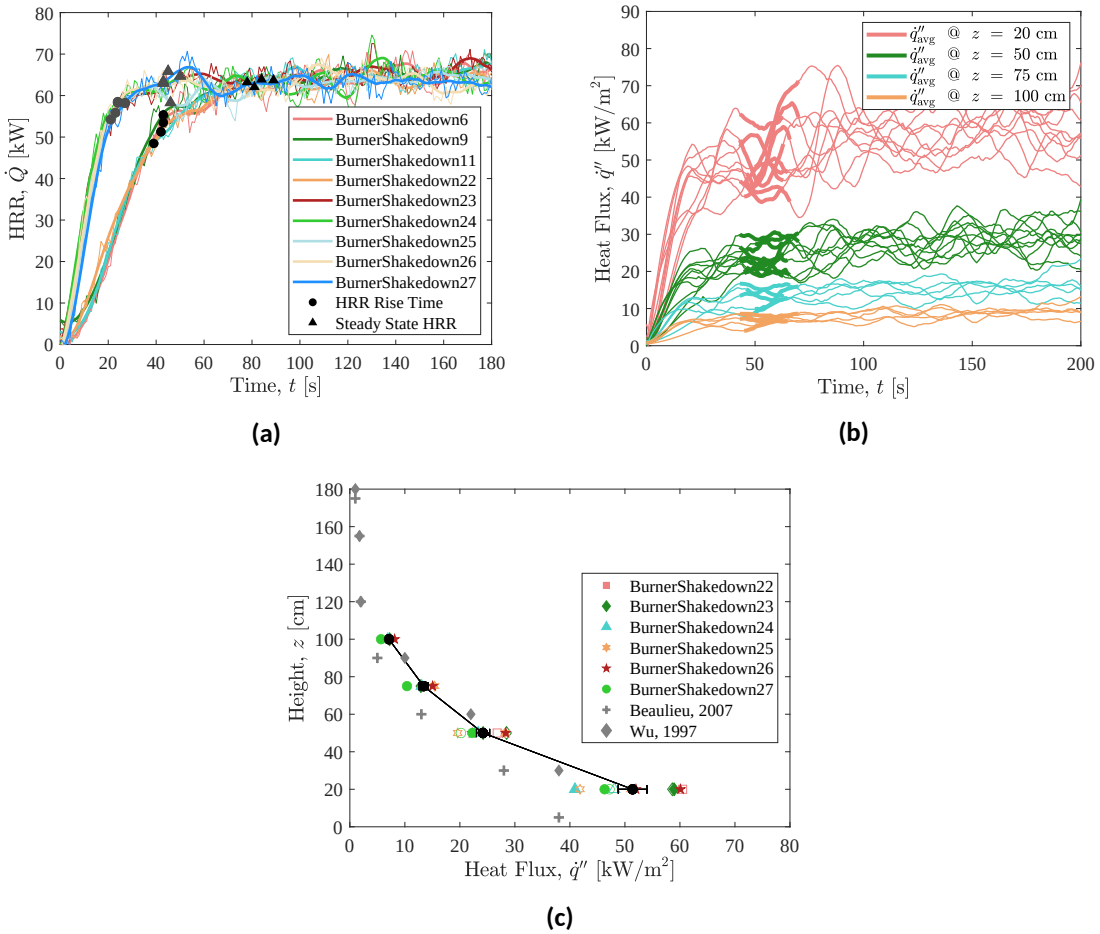

Fig. 10. Propane burner behavior in its final configuration measured during Burner Shakedowns 23 through 27: (a) burner heat release rate; (b) time-resolved total heat flux , $\dot{q}''$, from the burner flame to water-cooled Schmidt-Boelter heat flux gauges positioned along the centerline of panel walls during Burner Shakedowns 23 through 27; and (c) steady state heat flux, $\dot{q}''_{\text{steady}}$, to the centerline of panel walls as a function of height, z above the burner. Bolded segments of $\dot{q}''$ curves highlighted in (b) are used to define $\dot{q}''_{\text{steady}}$ measurements plotted in (c). Error bars in (c) indicate expanded uncertainty of the heat flux measurements (U_c; 95% confidence interval, coverage factor = 2), as described in Appendix B.2.

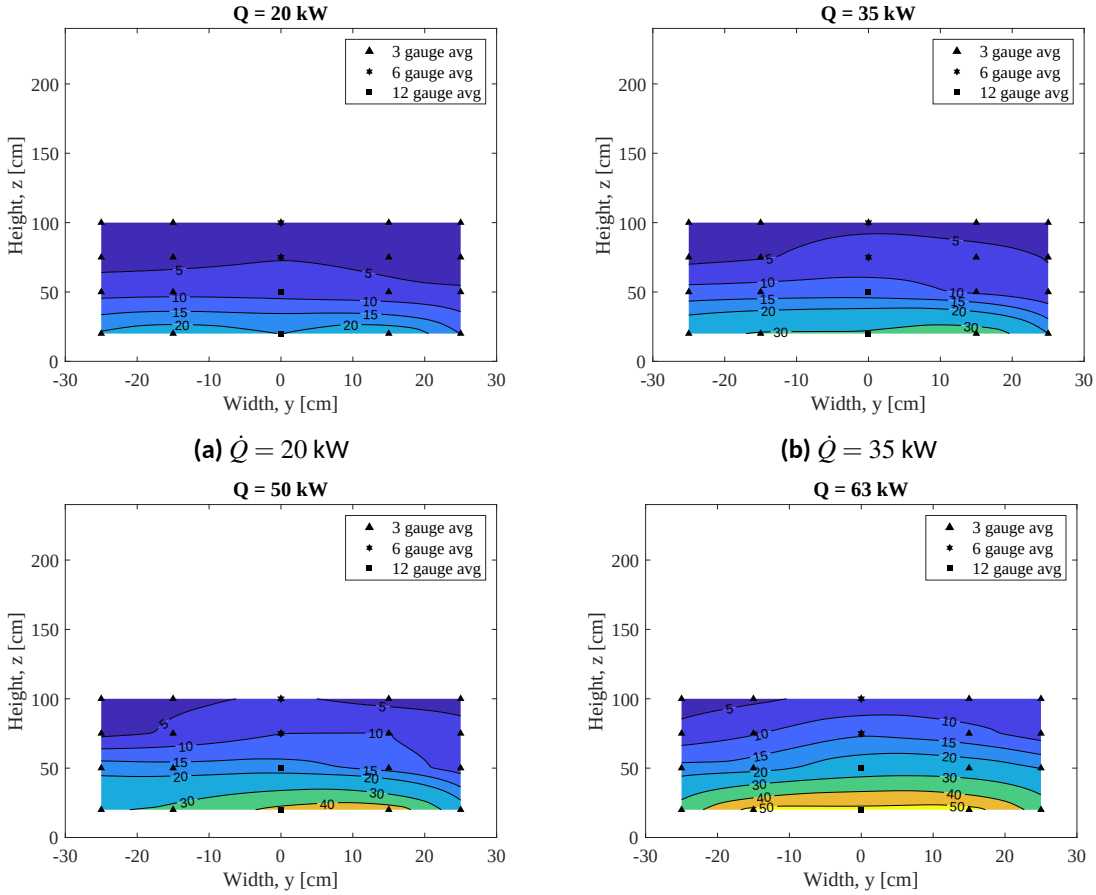

(a) $\dot{Q} = 20$ kW **(b)** $\dot{Q} = 35$ kW

(c) $\dot{Q} = 50$ kW **(d)** $\dot{Q} = 63$ kW (i.e., at steady state)

Fig. 11. Spatially-resolved measurements of burner flame heat flux.

Summary of Burner Setup for Fire Modeling

As seen in Fig. 3, a rectangular propane burner was placed at the base of the parallel panel assembly to ignite samples. A mass flow controller was used to feed propane (CP grade, 99 % purity) to the burner at a rate that would support, nominally, a 63 kW fire. For the the first six experiments (PMMA R1-R5 and GPO-3 R1), the burner was filled only with pea gravel (see Fig. 12c). For Test PMMA R6 (and all further experiments in this test series; i.e., Tests 7 - 66), this burner was filled with a 0.15 m deep layer of pea gravel, topped by 0.075 m layer of sand, and a 0.025 m thick sheet of porous, flexible insulation (Kaowool Blanket). This multi-layered-fill design (see Fig. 12d) supported more uniform flaming across the burner's surface. In both cases, the pea gravel in the burner chamber rested on top of a steel mesh that maintained a 0.05 m plenum at the base of the burner.

For both burner configurations, measured burner heat release rate (HRR) quickly increases (i.e., at $t = 40$ s after burner ignition) to 52 kW (pea gravel fill) or to 50 kW (multi-layer fill); a steady state HRR of 64 kW (pea gravel) or 63 kW (multi-layer) is achieved by $t = 80$ s. In a series of repeated experiments, burner flame heat flux (to inert Marinite walls) was measured at multiple locations across the lower half of the panel walls. Time-resolved measurements of flame heat flux demonstrate similar behavior to HRR: a quick rise within the first 40 s of burner ignition, followed by a more gradual increase to quasi-steady values by $t = 80$ s.

Figs. 12a and 12b plot total burner flame heat flux measured by water-cooled Schmidt-Boelter gauges positioned along the centerline of panels, at multiple heights, z above the base of the panel walls. Tabulated values of burner HRR and centerline burner flame heat flux (average of repeated measurements obtained 20 s, 40 s, 60 s, and 80 s after burner ignition) are provided in Table 2 for the preliminary burner configuration (Tests PMMA R1-R5 and GPO-3 R1), and in Table 3 for the final burner configuration (Tests 7-66, including PMMA R6). Table 4 provides spatially-resolved measurements (across the width and height of panel walls; y- and z-dimensions, respectively) of burner flame heat flux (final configuration, multi-layer-fill) obtained during steady flaming (i.e., 20 s average of $\dot{q}''_{\text{burner}}$ measurements obtained after HRR = 63 kW); this measurement data is also plotted in Fig. 11d. In each of these tables and figures, error bars indicate an expanded uncertainty ($u_{\text{exp}}(\dot{q}''_{\text{burner}})$) [see Appendix B.4].

Table 2. Burner flame heat flux along the centerline ($y = 0$) of panel walls, 20 s, 40 s, 60 s, and 80 s after burner ignition; Preliminary Burner Configuration, Tests 1-6

		Total Heat flux, q''_{burner} [kW m^{-2}]							
Time [s]	**HRR [kW]**	z = 10 cm	z = 20 cm	z = 30 cm	z = 50 cm	z = 75 cm	z = 100 cm	z = 140 cm	z = 180 cm
20	25±3.8	19.4±2.7	24.0±3.2	10.9±1.4	9.8±1.1	3.6±0.3	3.1±0.3	1.5±0.1	1.3±0.2
40	52±5.3	28.3±3.4	38.2±4.7	19.5±3.1	19.7±2.1	7.2±0.7	5.9±0.8	2.3±0.2	2 ±0.5
60	60±6.1	34.8±3.5	39.5±4.0	22.5±1.3	20.1±2.3	8.7±1.0	5.6±0.5	2.7±0.4	2.1±0.6
80	64±6.4	43.1±2.4	47.4±4.3	32.4±1.9	25.1±2.6	11.8±0.7	7.3±0.6	3.7±0.2	2.4±0.3

Error bars indicate an expanded uncertainty ($u_{\text{exp}}(\dot{q}''_{\text{burner}})$)

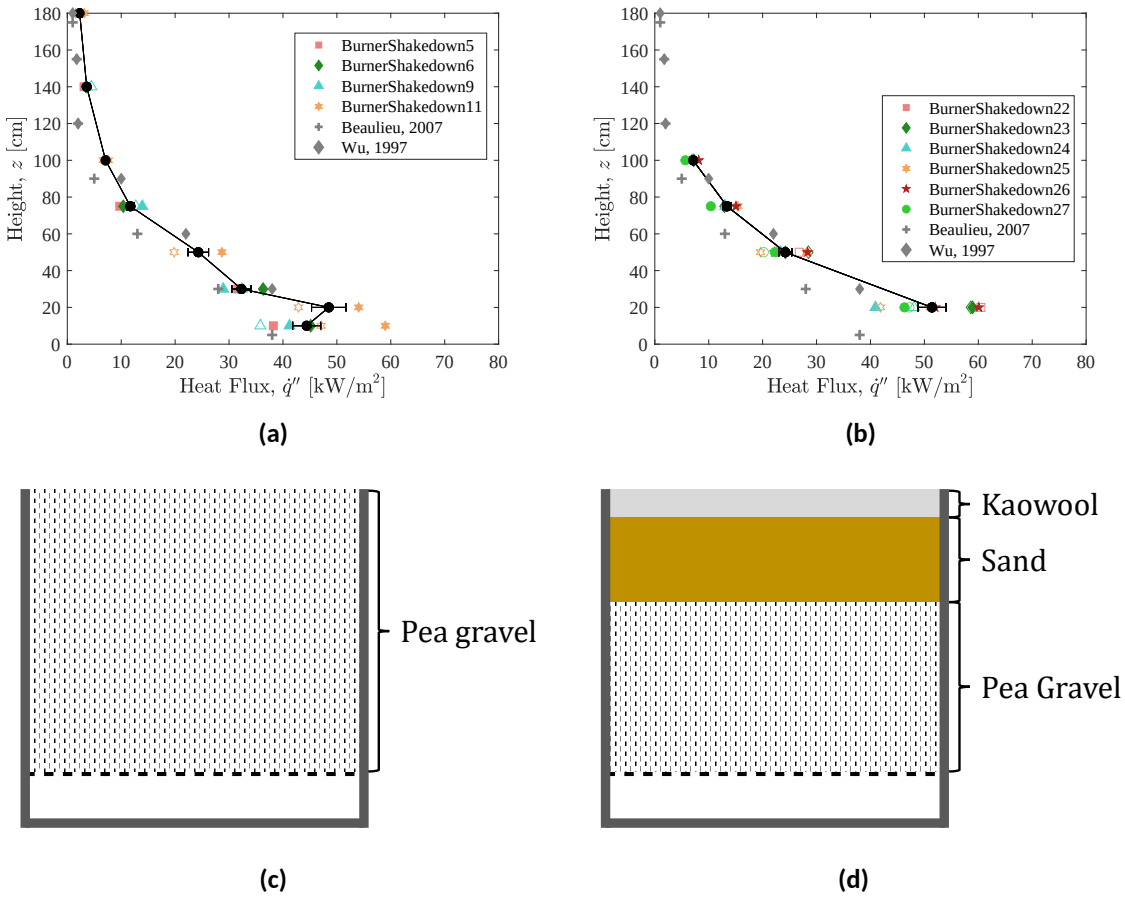

Fig. 12. Height-resolved measurements of centerline burner flame heat flux (a and b) and schematics of burner fill in two configurations (c and d). Error bars indicate expanded uncertainty of the heat flux measurements (U_c; 95% confidence interval, coverage factor = 2), as described in Appendix B.2.

Table 3. Burner flame heat flux along the centerline ($y = 0$) of panel walls, 20 s, 40 s, 60 s, and 80 s after burner ignition; Final Burner Configuration, Tests 7-66

		Total Heat flux, $\dot{q}''_{\text{burner}}$ **[kW m^{-2}]**			
Time [s]	HRR [kW]	z = 20 cm	z = 50 cm	z = 75 cm	z = 100 cm
20	22±8.5	20.5±1.9	8.4±0.8	5.0±0.6	2.9±0.3
40	50±6.9	41.9±2.3	17.2±1.2	9.8±0.8	5.7±0.4
60	59±6.7	45.7±2.3	19.0±1.1	10.2±0.7	6.0±0.4
80	63±7.0	51.4±2.4	24.2±1.1	13.4±0.7	7.1±0.4

Error bars indicate an expanded uncertainty ($u_{\text{exp}}(\dot{q}''_{\text{burner}})$)

Table 4. Spatially-resolved measurements of burner flame heat flux during steady flaming; Final Burner Configuration, Tests 7-66

	Total Heat flux, q''_{burner} [kW m^{-2}]				
Height, z [cm]	**HF y$=-25$ cm**	**HF y$=-15$ cm**	**HF y$=$0**	**HF y$=$15 cm**	**HF y$=$25 cm**
20	35.2$\pm$2.8	50.9$\pm$4.6	51.4$\pm$2.6	57.3$\pm$3.1	39.9$\pm$3.7
50	20.8$\pm$2.3	19$\pm$1.0	24.2$\pm$1.2	22.5$\pm$1.5	19.6$\pm$1.2
75	6.7$\pm$0.8	8.9$\pm$0.8	13.4$\pm$0.8	12.5$\pm$0.7	9.1$\pm$0.5
100	3.8$\pm$0.3	4.6$\pm$0.3	7.1$\pm$0.4	5.8$\pm$0.3	6.2$\pm$0.4

Error bars indicate an expanded uncertainty ($u_{\text{exp}}(\dot{q}''_{\text{burner}})$)

2.5. Test Procedure

The parallel panel apparatus was used to conduct two types of experiments: (1) Burner Shakedown tests that were used to characterize the heat feedback profile from the rectangular propane burner used as ignition source to an inert wall (i.e., the Marinite support panel) and (2) Ignitability and fire growth experiments that were used to characterize time-resolved flame heat feedback, heat release rate, and gaseous species production during upward flame spread over the parallel panel walls. The test procedure of ignitability and fire growth experiments can be described as follows:

- Initial Setup:
  - For select tests (PMMA R1, R2; PBT R1; and all XLPE tests), cover surface[11] of parallel panel Marinite walls with aluminum foil.
  - For samples known to melt, flow, and/or drip: cover the sides of the propane burner, parallel panel support frame, and the gypsum board within 1 m of the parallel panel support frame with a layer of aluminum foil.
  - Measure initial sample mass.
  - Prepare and mount test specimen to either wall of the parallel panel frame. Sample should be secured to frame along edges and every 20 cm to 30 cm across its surface.
  - If used, install and secure water-cooled heat flux gauges (and water lines) at various heights across the surface of the sample. Confirm sufficient water flow and data acquisition prior to further setup.
  - Call NIST Fire Department and deactivate (place in bypass) automatic fire suppression systems.
  - Turn on exhaust fans and open makeup air dampers.
  - Verify that area carbon monoxide (CO) detectors and alarms are functioning.
  - Turn on measurement and data acquisition (DAQ) systems and verify that they are functioning.
  - Turn on lighting and verify camera settings.
  - Prepare the ignition source (spark, pilot tube).
  - Confirm adequate water supply to gauges. Cover and protect back/exposed surfaces of measurement devices using thermal insulation and/or a radiation shield.
  - Verify that all fire suppression water lines are functioning properly.
  - Prepare NFRL data acquisition system to record data (heat release, species yields, and flame heat flux) and video.

[11] Test-specific details regarding this sample-back-surface boundary condition are provided in Appendix C.

  - Photograph initial test setup.

- Safety Briefing:
  - Define roles and responsibilities of test personnel.
  - Identify unique hazards of material of interest (e.g., dripping, firebrand formation, hazardous gaseous volatile production) and define unique test steps (e.g., removal of shields protecting selected heat flux gauges).
  - Confirm sufficient (and stable) exhaust flow [kg/s].
  - Confirm automatic fire suppression systems in bypass, fire department notified.
  - Confirm area carbon monoxide (CO) detectors and alarms are functioning.
  - Restrict access to test area, signs posted indicating “Test in Progress”.

- Data Logging, Ignition, and Testing:
  - Acquire background data (e.g., heat release rate baseline).
  - Begin video recording.
  - Ignite fire: Supply gas to propane burner, apply pilot to top of burner until sustained ignition observed, remove pilot flame.
  - If sustained uniform ignition of samples is achieved across the base of both parallel panel walls, turn off gas flow to burner. If needed (e.g., for samples that support significant melt flow and/or dripping) cover top of burner with metal shield.
  - If present, remove shields from heat flux gauges after continuous flaming is observed at those locations.

- End of Test:
  - Allow sample to burn to completion OR suppress fire as needed at a time determined by the Test Director in consultation with the Safety Officer (e.g., due to formation of a large pool fire).
  - Verify all test samples fully extinguished and any remaining sample and frame cool to 50°C.
  - Acquire post-test background heat release rate baseline.
  - Re-activate automatic fire suppression systems.
  - Collect, weigh, and dispose of any remaining unburned material, residue and/or char.
  - Safely remove water-cooled heat flux gauges from panel walls.

- Secure, store, and/or discard post-test debris.
- Remove debris from top of propane burner; replace sand / kaowool blanket at top of burner as needed.
- Clean, paint, and recalibrate, heat flux gauges as needed.

3. Results and Discussion

This section presents a summary of experimental results — qualitative descriptions of material burning behavior and an analysis of quantitative measurement data (e.g., measured heat release rate and wall flame heat flux) — recorded for each of the materials considered in this work. Measurement results are presented separately for each material, in alphabetical order, with the exception of PMMA, poly(methyl methacrylate), which is presented first as an exemplar case to demonstrate the procedure used to process all measurement data for further analysis (especially wall flame heat flux measurements). The selected results presented in this section are designed to facilitate interpretation of the aggregate of measurement data obtained from repeated experiments on the same material (e.g., in this section, plots are provided to show average wall flame heat flux profiles across the height of samples at a selection of representative fire sizes); thus, not all measurement data recorded from every experiment is presented here. A complete presentation of measurements recorded in each individual experiment (e.g., all heat flux data, and related heat flux gauge temperatures, measured at all times and fire sizes throughout each experiment) is provided, with limited further analysis, in Appendix C.

3.1. Burning Behavior, Heat Release Rate, and Wall Flame Heat Flux

3.1.1. PMMA - poly(methyl methacrylate)

Heat Release Rate and Observed Burning Behavior

The PMMA[12] studied in this work is a cast, black sample that was selected because of its tendency to maintain its density while burning, insignificant melt flow, simple decomposition kinetics, and low transparency to infrared radiation. Although multiple experimental [93–96] and computational modeling [97–99] studies of the flammability response of PMMA exist in the literature, the measurement data presented in Vol. 1 and Vol. 2 of this report represents one of the first attempts to perform a series of pyrolysis experiments across a range of scales (from mg-scale thermal analysis tests up to 2.5 m wall flame spread tests), to determine all relevant thermophysical properties of this material, and to use these results to simulate material flammability behavior in response to a variety of fire-like environments. Note: several of these outcomes will be discussed in later volumes of this report.

[12] Samples of this PMMA were also made available to participants of the Measurement and Computation of Fire Phenomena (MaCFP) Working Group, an international collaboration, the general objective of which is to establish a structured effort in the fire research community to make significant and systematic progress in fire modeling, based on a fundamental understanding of fire phenomena. An extensive series of experiments was performed as part of the MaCFP effort [89]: as of July 2020, eighteen institutions from eleven different countries have submitted measurement data obtained from more than 200 separate tests conducted in 9 unique experimental apparatus. A summary of these results is provided elsewhere [89–91]. A recent study presents experimental measurement data, observations, and numerical simulations of the flammability behavior of this same PMMA from mg-scale up to 1.5 m flame spread over PMMA panels in a corner-wall configuration [92].

In total, six parallel panel experiments were conducted on PMMA. For Tests R1 to R5, the preliminary burner configuration was used; Test R6 used the final burner configuration. In the first test, PMMA R1 (the very first experiment conducted in this series), the propane burner was turned off after just 90 s, which led to sustained flaming ignition of only the left ($x = -15$ cm) panel; in this test, ignition of the right panel was not observed until flames had reached the top of the left panel. In Tests R2 to R5, the propane burner was left on for 120 s (i.e., until $t = $ 2:00). In each of these four tests, burner flames could show preferential attachment to one wall (either the left or the right, in some tests alternating sides after approximately 30 s to 45 s). Relatively uniform ignition was observed across the base of both panel walls in Tests R2 and R3.

In test PMMA R4, the burner was briefly turned off at $t = $ 120 s, but it was apparent that sustained flaming ignition of the right panel wall was not achieved; propane flow to the burner was therefore turned back on at $t = $ 150 s, and remained on until $t = $ 210 s. After the burner was turned off in these four tests, although sustained flaming was observed on both walls (at least to a degree), limited flame coverage and/or delayed flame spread was observed on one wall for the first 60 s to 120 s after ignition (i.e., between 120 s$\leq t \leq$ 240 s). In test R5, a crossflow from back to front (i.e., from $+y$ to $-y$) resulted in preferential flame attachement to the front edge ($y = -30$ cm) of panel walls while flames spread upwards. Later in each test, as fires grew larger, uniform flaming was observed across either wall (further details for each test are presented in Appendix C).

Prior to conducting test PMMA R6 (for all materials considered, the seventh test in this series) the propane burner was adjusted (see Sec. 2.4) to improve its uniformity and reproducibility. In Test PMMA R6, although the burner was supplied propane for the same 2 minutes as for Tests R2-R5, visual observations, HRR data, and heat flux measurements suggested that uniform ignition across both panel walls occurred earlier (approximately 100 s after burner ignition). Earlier ignition (of both panels) observed in Test PMMA R6 matches previous observations (see Sec. 2.4) that the final burner configuration (as compared to the preliminary configuration) provided not only more repeatable, uniform flaming conditions but also higher heat fluxes at the base of the panels.

Figure 13 plots measured HRR of all six PMMA tests as a function of time after burner ignition. Measurements from Tests R2, R3, and R6 are highlighted here as relatively uniform ignition of the base of (and subsequent upward flame spread over) both panel walls was observed in these tests and these time-resolved HRR curves may be considered as validation datasets for simulations of fire growth (supported by this specific PMMA, burning in this configuration, when ignited by the propane burner in either of its two configurations). Although delays in ignition due to burner non-uniformity led to shifts (i.e., time delays) in initial fire growth, excluding PMMA R1 (in which only one wall was burning for the majority of the experiment) fire growth rate and peak fire size are quite comparable between each of these experiments. This suggests that measurements (e.g., wall flame heat flux) recorded in separate tests can be analyzed together when compared at the same HRR (rather than simply at the same time).

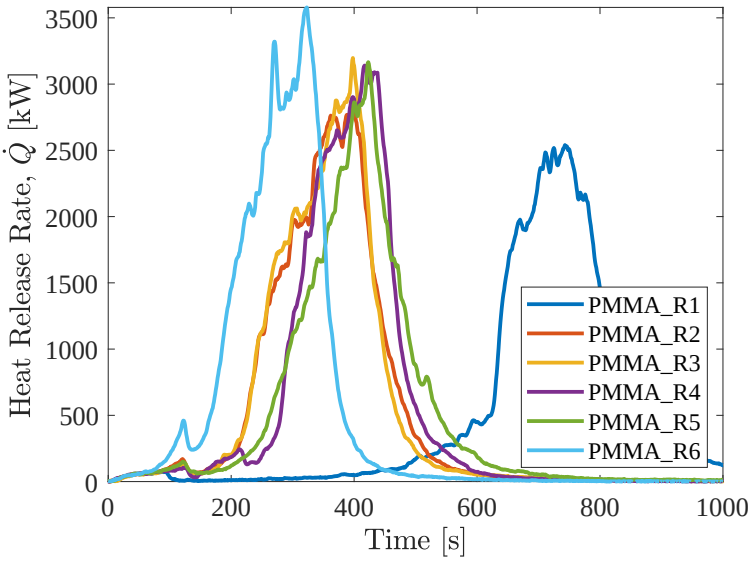

Fig. 13. Measured heat release rate during parallel panel experiments on PMMA. Here, time $t = 0$ is defined by burner ignition.

Images of typical fire development[13] in PMMA tests are presented in Fig. 14. As shown here, after sustained ignition was achieved, flames spread readily upwards across both panel walls. In each test, while total HRR was less than 1.5 MW, the flames on either panel wall remained separate (attached to their respective walls); however, as total fire size increased, these two flames merged to fill the volume between the panel walls. A peak HRR of approximately 3.1 MW (mean of all six repetitions) was observed approximately 240 s to 270 s after ignition/burner shut off. To quantify this fire growth behavior, an average fire growth rate can be defined as $\overline{\frac{d\dot{Q}}{dt}} = \frac{(\dot{Q}_{0.85*\text{peak}} - \dot{Q}_{\text{min}})}{(t_{0.85*\text{peak}} - t_{\text{min}})}$, where $\dot{Q}_{\text{min}}$ is the minimum HRR measured shortly after burner shutoff, $\dot{Q}_{0.85*\text{peak}}$ is equal to 85 % of the peak HRR measured during the test, and t_{min} and $t_{0.85*\text{peak}}$ are the times [s] at which these heat release rates were measured. Tabulated values of $\overline{\frac{d\dot{Q}}{dt}}$ are provided for each material[14] and test repetition in Table 8. For PMMA Tests R2 and R3, $\overline{\frac{d\dot{Q}}{dt}}$ equaled 12.1 kW s^{-1} and 12.2 kW s^{-1}, respectively; for PMMA Test R6, $\overline{\frac{d\dot{Q}}{dt}} = 22.1$ kW s^{-1}.

[13] Representative images of fire development, including flame behavior at ignition, are provided for all test repetitions in Appendix C.

[14] Note: For some materials, the burner was not turned off in a test. In these experiments, average fire growth rate was therefore calculated as: $\overline{\frac{d\dot{Q}}{dt}} = \frac{(\dot{Q}_{0.85*\text{peak}} - 90\text{ kW})}{(t_{\text{peak}} - t_{90\text{ kW}})}$, where $t_{90\text{ kW}}$ is well after propane burner ignition at which HRR measured 90 kW. 90 kW was used rather than the nominal propane burner HRR of 63 kW to allow for the the fire growth rate to be dominated by flame spread across the panels, and to not capture the noise in the HRR measurement. All other terms in this expression are used identically as previously defined.

(a) Just prior to sample ignition

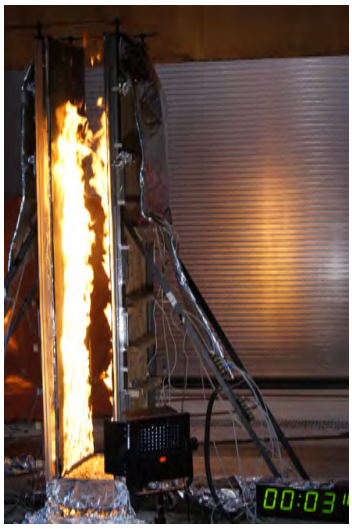

(b) Flame spread 60 s after ignition

(c) Peak HRR, $\dot{Q} = 3.6$ MW

Fig. 14. Fire behavior of PMMA slabs during parallel panel experiments.

Melt flow and dripping was not observed during PMMA tests; however, as samples heated, softened, and/or burned out across their height, small sections of remaining PMMA (which were no longer securely attached to the panel walls) could be observed to fall. Although these sections would typically burn to completion at the base of the panels, a sudden spike or decrease in HRR was measured when this detachment occurred. Four representative images of material burning behavior (pre-test, ignition, peak HRR, end of test) are provided for each experiment (including all six tests on PMMA and all tests on each of the other combustible solids) in Appendix C.

Flame Heat Flux

Flame heat flux measurements were obtained in all six PMMA test repetitions using an array of up to 12 water-cooled heat flux gauges. In each test, gauges were placed at up to 8 out of 9 possible heights, z, across each panel wall. At 4 heights (i.e., $z =$ 0.20 m, 0.50 m, 1.0 m, and 1.8 m) flame heat flux was also recorded at up to 4 locations across the width (y-dimension) of the panel. Careful review and post-processing of this data was required to ensure the quality and reliability of these measurements and to allow for their combined analysis as one aggregate dataset. This process required multiple steps (some manual, others assisted by a series of custom analysis scripts written in MATLAB) conducted in a systematic order. A brief summary of this post-processing procedure is described below:

- First, time-resolved heat flux measurements recorded by each individual gauge (in each test) were manually reviewed alongside test pictures, video (multiple camera angles), and notes taken by hand during each experiment. This allowed for the identification of 'good' data (e.g., when flame coverage was uniform across the sample wall) and 'bad' data (e.g., when sample deformation affected gauge readings or when uneven flaming was observed).

- Next, heat flux measurements were processed such that they could be analyzed as a function of fire size, HRR, (rather then time, t) to minimize the impact of burner variability on final results. This required smoothing of each dataset, determination of the resolution of measurements in HRR-space (i.e., given instantaneous measured fire growth rates for each material and a data reporting frequency of Δt=1 s, what is (on average) the finest interval, $\Delta \dot{Q}$ [kW], at which measurements were reported), and interpolation of measurements to regularly ordered reporting intervals [kW] such that statistics could be calculated for repeated heat flux measurements obtained at the same HRR in different experiments.

- Finally, using this processed data, average profiles (e.g., evolution of flame heat flux at a given location with increases in HRR or the flame heat feedback profile across the surface of the panels at a given HRR) could be calculated and presented. For all materials tested in this work, the same analysis steps and statistics were calculated (given the availability of measurement data).

This post-processing procedure is detailed in this section using PMMA flame heat flux measurements as exemplar data. For heat flux measurements obtained from tests on all other materials, the same processing steps are used but only the final results are presented.

Figure 15 plots total wall flame heat flux, $\dot{q}''_{\text{total}}$, as measured by water-cooled Schmidt-Boelter heat flux gauges positioned at the centerline of panels ($y = 0$) at a height of $z =$ 1.8 m during repeated parallel panel experiments on PMMA. This data was recorded on both the left and right walls (i.e., $x =$ -0.15 m and $x =$ 0.15 m) during tests PMMA R1, R3, and R5. In Fig. 15a, raw, unsmoothed measurements of $\dot{q}''_{\text{total}}$ (i.e., the original measurements, as recorded during the experiment) are plotted as dotted lines as a function of time after

burner ignition. Highlighted on this figure, as solid lines, are recorded values of $\dot{q}''_{\text{total}}$ that were identified by manual review as 'good'. As seen here, the cutoff for 'good' heat flux data occurred well before the end of the experiment.

In general (i.e., for all materials considered in this work), corruption or distortion of $\dot{q}''_{\text{total}}$ data could occur for a variety of reasons, including: sample dripping or melt flow over the front of the gauge, deformation that caused the front surface of the sample to move relative to the heat flux gauge (e.g., sample swelling or growth of an intumescent char layer), sample burnout or fall off, or heavy deposition of soot at the gauge's front surface. For the tests shown in Fig. 15a, $\dot{q}''_{\text{total}}$ measurements are typically identified as 'bad' prior to the end of testing due to sample deformation and/or detachment from the wall; in many instances for PMMA, material detaches from the wall and forms a puddle at the base of the wall on top of the burner, marking the beginning of unacceptable data. Test notes and video also indicated non-uniform flaming across both walls in test PMMA R5, prior to $t = 270$ s (due to a crossflow from back to front of the assembly; i.e., from $+y$ to $-y$). Consequently this subset of data (in Fig. 15a, see light red and dark green curves, prior to $t = 270$ s) is marked as 'bad' and excluded from further analysis. Later in test PMMA R5, when fires grew (i.e., when HRR $>$ 500 kW) and uniform flaming was observed across either wall, measurements of $\dot{q}''_{\text{total}}$ taken on the left wall (which supported continuous flaming throughout the duration of the experiment) converges with those obtained in other test replicates, thus this data is included for further analysis.

For all experiments conducted in this work (including all materials and all heat flux gauge locations) time-resolved measurements of $\dot{q}''_{\text{total}}$ (both 'good' and 'bad', as solid and dotted lines, respectively) are plotted in Appendix B.4. Digital copies of $only$ 'good' heat flux data are also provided (as .csv files) online, as links on the project page of the NIST Fire Calorimetry database: www.https://www.nist.gov/el/fcd/vertical-upward-flamespread-on-parallel-panels.

After 'good' and 'bad' $\dot{q}''_{\text{total}}$ measurements are carefully identified, they are processed such that they can be compared across different experiments at the same fire size (i.e., at the same HRR, $\dot{Q}$); this allows for the calculation of mean values (and related statistics) of repeated $\dot{q}''_{\text{total}}$ measurements recorded at the same HRR in different experiments. First, at each time step (Δt = 1 s) that 'good' data is recorded, a simple running average (+/-3 s interval) of measurement data is calculated to determine the average ('smoothed') HRR and $\dot{q}''_{\text{total}}$ at that time. Both original and 'smoothed' measurements are plotted in Fig 15b (as thin and thick lines, respectively); as seen here, this smoothing removes a substantial amount of noise in $\dot{q}''_{\text{total}}$ measurements while still providing an accurate representation of measured values.

Next, a linear interpolation is performed using these smoothed measurements such that $\dot{q}''_{\text{total}}$ can be reported at regular intervals of HRR ($\Delta\dot{Q}$ [kW]); this allows for direct comparison of $\dot{q}''_{\text{total}}$ data even when obtained at slightly different HRR (in separate experiments). This processing step is required because, although measurement data is recorded at 1 Hz for all experiments, depending on the fire growth rate, $\frac{d\dot{Q}}{dt}$, measured during each test, $\dot{q}''_{\text{total}}$ may be effectively recorded at different intervals [kW] in HRR-space. These intervals are calculated for all experiments across all tests and a minimum $\Delta\dot{Q}$ (i.e., finest

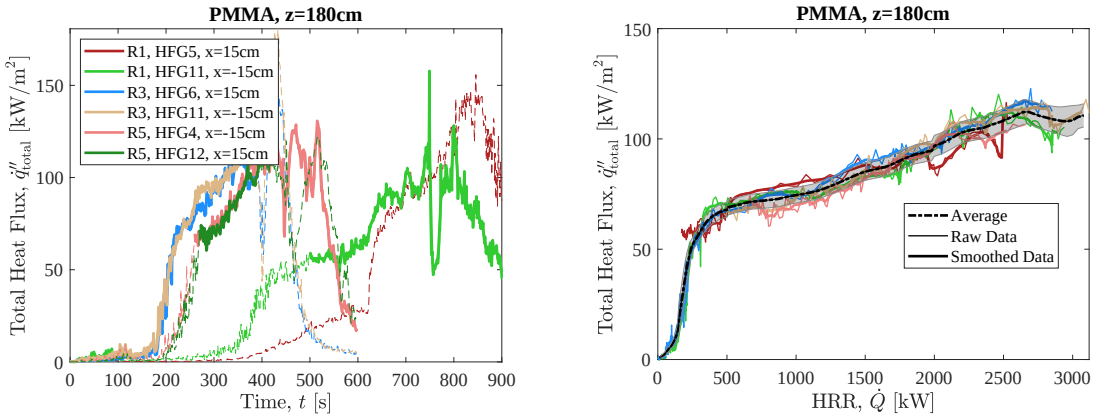

Fig. 15. Total wall flame heat flux measured at $z = 1.8$ m (at the centerline, $y = 0$, of panels) during repeated parallel panel experiments on PMMA, plotted as a function of (a) time after burner ignition and (b) heat release rate, $\dot{Q}$ [kW]. In plot (a) solid and dashed lines represent 'good' and 'bad' data, respectively (see main text). In plot (b) thick and thin lines represent filtered and unfiltered data, respectively [smoothed and unsmoothed data, respectively]. The shaded area around each curve represents the expanded uncertainty of the heat flux measurements (U_c; 95% confidence interval, coverage factor = 2), as described in Appendix B.2.

resolution) is defined for each material such that 90 % of all measurements are resolved within that interval. This interpolation interval, $\Delta\dot{Q}$, could vary for different materials or during different stages of the experiment (e.g., initial versus peak fire growth rate). For PMMA, when $\dot{Q} < 500$ kW, $\Delta\dot{Q} = 10$ kW; and when $\dot{Q} > 500$ kW, $\Delta\dot{Q} = 30$ kW or 40 kW. For most other materials considered in this work[15] (which supported slower fire growth) this reporting interval is defined as $\Delta\dot{Q} = 5$ kW.

Once this interpolation is performed, average values of total heat flux, $\overline{\dot{q}''_{\text{total}}}$, are calculated at each HRR interval, $\dot{Q}_i$, as the mean of interpolated values recorded at a specific height, z, across $\pm 3\Delta\dot{Q}$:

$$\left(\overline{\dot{q}''_{\text{total}}}\right)_i = \frac{1}{\left(\left(\sum_{\text{j}=1}^{N_j} N_i\right)\right)} \sum_{\text{j}=1}^{N_j} \sum_{\text{i}-3}^{i+3} \left(\dot{q}''_{\text{total}}\right)_{\text{i,j}} \tag{1}$$

Here, the subscript j identifies sepeate measurements obtained by unique heat flux gauges at the same height, z, in either (a) the same test on opposite panel walls or (b) repeated tests, on either panel wall. The standard deviation, σ_i, is then calculated at each

[15]For ABS and HIPS, which both supported rapid fire growth, $\Delta\dot{Q} = 10$ kW while $\dot{Q} < 300$ kW and $\Delta\dot{Q}$ varied between 50 kW $\leq \Delta\dot{Q} \leq$ 80 kW while$\dot{Q} > 300$ kW.

HRR, $\dot{Q}_i$, as:

$$\sigma_i = \sqrt{\left(\frac{1}{((\sum_{\mathrm{j}=1}^{N_j} N_i) - 1)} \sum_{\mathrm{j}=1}^{N_j} \sum_{\mathrm{i}-3}^{i+3} \left(\left(\dot{q}''_{\mathrm{total}} \right)_{\mathrm{i,j}} - \left(\overline{\dot{q}''_{\mathrm{total}}} \right)_i \right)^2 \right)} \quad (2)$$

In these two equations, N_j represents the total number of recordings (either from repeated tests, or the same test on opposite panel walls) that provided 'good' measurements of $\dot{q}''_{\mathrm{total}}$ at the location and the heat release rate, $\dot{Q}_i$, of interest; N_i represents the number of $\dot{q}''_{\mathrm{total}}$ measurements available for a given recording in the +/- $3\Delta\dot{Q}$ interval around $\dot{Q}_i$. These same processing steps — i.e., data quality check, smoothing, interpolation, and calculation of statistics — are performed for all heat flux measurements obtained at all location in all tests (and for all materials).

Figure 16 plots total wall flame heat flux, $\dot{q}''_{\mathrm{total}}$, measured at the centerline of panels ($y = 0$) at a height of $z = 1.8$ m during repeated parallel panel experiments on PMMA. Here, colored lines represent 'filtered' $\dot{q}''_{\mathrm{total}}$ data from individual tests and solid crosses indicate linearly interpolated values of $\dot{q}''_{\mathrm{total}}$, plotted at 10 kW $\leq \Delta\dot{Q} \leq$ 40 kW intervals. As seen here, interpolated values of $\dot{q}''_{\mathrm{total}}$ nearly perfectly overlap the 'filtered' $\dot{q}''_{\mathrm{total}}$ curves from which they were determined. The average total heat flux, $\overline{\dot{q}''_{\mathrm{total}}}$, measured in these tests is plotted as a solid black line with shaded gray error bars indicating expanded uncertainty (95 % confidence interval, coverage factor = 2, see Appendix B.4) of measured values obtained within the +/- $3\Delta\dot{Q}$ interval around $\dot{Q}_i$. As seen here, great reproducibility in $\dot{q}''_{\mathrm{total}}$ data is observed between repeated measurements obtained in repeated experiments (and on both the left and right walls) when $\dot{q}''_{\mathrm{total}}$ data is considered as a function of HRR (i.e., fire size).

The analysis procedure outlined above for $\dot{q}''_{\mathrm{total}}$ data obtained at $z = 180$ cm was repeated for measurements recorded at multiple heights between 0.1 m $\leq z \leq 2.2$ m; average wall flame heat fluxes at each height (all obtained along the centerline of panels, $y = 0$) are plotted as a function of HRR in Fig. 17. As shown here, at the beginning of tests (i.e., as flames spread upwards towards each gauge location; see Fig. 17a), $\dot{q}''_{\mathrm{total}}$ rapidly increases at each height. After flames extend beyond each gauge location, the rate of increase of measured heat flux decreases. At higher z, it takes progressively longer in each experiment (thus larger HRR are required) for this inflection point to be observed; this delay corresponds to the additional time needed for the flame front to reach higher heights across the panel walls. At heights $z <$ 1.0 m, $\dot{q}''_{\mathrm{total}}$ measured between 40 kW m^{-2} and 50 kW m^{-2} when flames first extend above the heat flux gauge (i.e., at this inflection point). At $z \geq$ 1.0 m, $\dot{q}''_{\mathrm{total}}$ measured between 50 kW m^{-2} and 75 kW m^{-2} at this inflection point. After continuous flaming is observed across each gauge location (which occurs at approximately $\dot{Q} = 500$ kW), $\dot{q}''_{\mathrm{total}}$ measurements continue gradually increasing by approximately 40 % to 55 %, at all measurement locations (see Fig. 17b). This increase in $\dot{q}''_{\mathrm{total}}$ likely arises due to some combination of: the thickening of flames along each wall (see Fig. 14b vs.

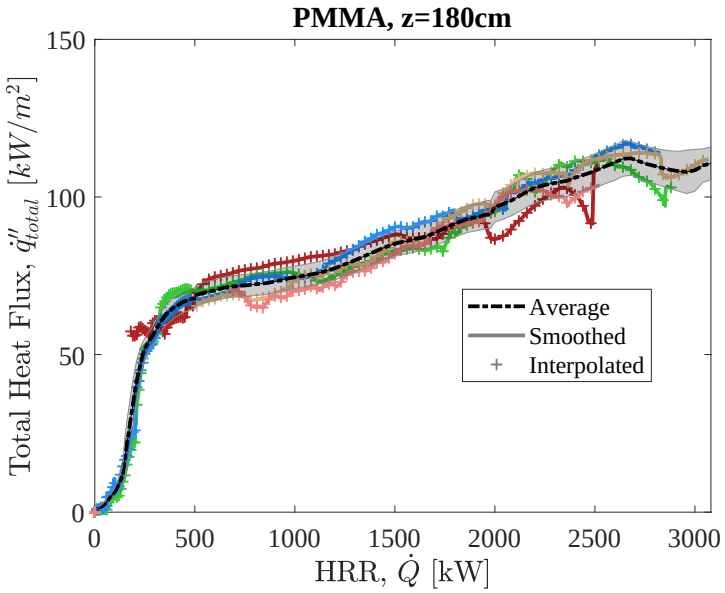

Fig. 16. Total wall flame heat flux measured at $z = 1.8$ m (at the centerline, $y = 0$, of panels) during repeated parallel panel experiments on PMMA. Here, solid lines represent smoothed $\dot{q}^{\text{“}}$total measurements and crosses indicate interpolated values. The gray shaded area around the black average curve represents expanded uncertainty of the heat flux measurements (U_c; 95% confidence interval, coverage factor = 2), as described in Appendix B.2.

Fig. 14c), potentially greater temperatures during prolonged flaming between the panel walls, and further heating (in-depth) of opposing panel walls, which would lead to greater reradiation between panels.

The centerline $\dot{q}''_{\text{total}}$ data shown in Fig. 17 can be converted into spatially resolved profiles ($\dot{q}''_{\text{total}}$ vs. z at a given HRR) by taking the average heat flux measurements recorded all heights, z, at a specific HRR and plotting these values versus their respective heights[16]. Several height-resolved $\dot{q}''_{\text{total}}$ profiles obtained by this procedure (measured at HRR between 300 kW and 2800 kW) are displayed in Fig. 18.

In Fig. 18a, $\dot{q}''_{\text{total}}$ profiles illustrate the change in flame structure during the early stages of fire growth (i.e., $\dot{Q} \leq 500$ kW). Shortly after ignition, continuous flaming is only observed near the base of the panel walls and, correspondingly, $\dot{q}''_{\text{total}}$ measurements are negligible for $z > 0.75$ m. For larger and larger fires, elevated heat flux measurements are recorded at increasing heights across the panel walls until, by $\dot{Q} = 500$ kW (when continuous flames are observed across the full length of panel walls), all measurement locations show approximately $\dot{q}''_{\text{total}} = 50$ kW m^{-2}, or greater. For qualitative comparison, representative images of flame structure taken at each HRR for which $\dot{q}''_{\text{total}}$ profiles are plotted in Fig. 18a are shown in Fig. 19.

[16] Determination of centerlien heat flux profiles can be visualized as taking vertical 'slices' of $\dot{q}''_{\text{total}}$ data plotted in Fig. 17.

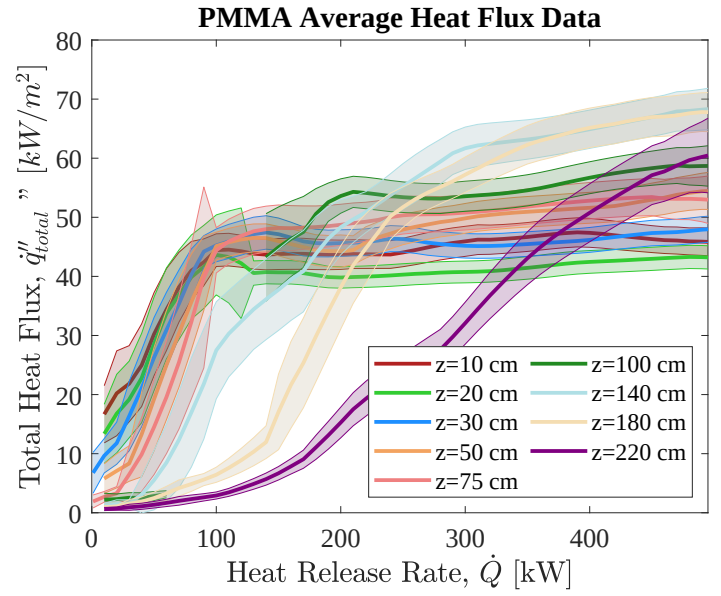

(a)

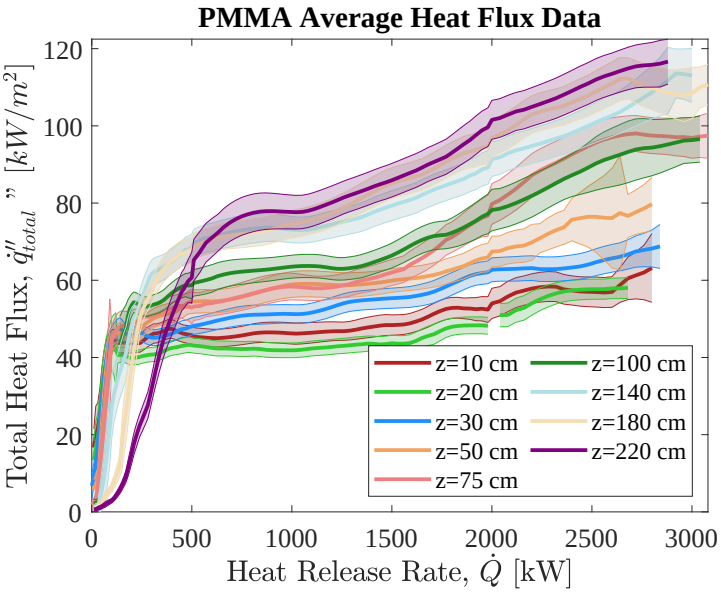

(b)

Fig. 17. Total wall flame heat flux measured at the centerline, $y = 0$, and across the height, z, of panels during repeated experiments on PMMA. In (a), $\dot{q}''_{\text{total}}$ measurements are highlighted during the early stages of fire growth (rapid changes due to upward flame spread); in (b), $\dot{q}''_{\text{total}}$ are shown through the duration of these tests. For each curve, errorbars represent the expanded uncertainty (U_c; 95 % confidence interval, coverage factor = 2).

Fig. 18b, plots several representative wall flame heat flux profiles measured during later stages of these tests, when flames covered the full surface of panel walls. As seen here, $\dot{q}''_{\text{total}}$ monotonically increases with height, z, for all fires when continuous flaming is observed across the panel walls. Specifically, at a measured HRR of 1500 kW, $\dot{q}''_{\text{total}}$ increases from approximately 55 kW m^{-2} at $z = 30$ cm to 86 kW m^{-2} at $z = 220$ cm. Additionally, as HRR increases from 780 kW to 2800 kW, $\dot{q}''_{\text{total}}$ continuously increases (on average by 50 %) at each measurement location across the full height of the panel walls.

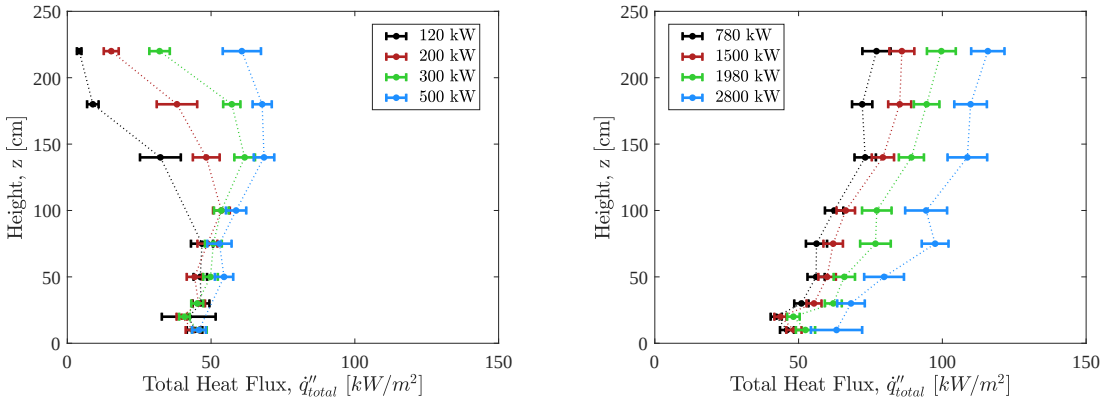

Fig. 18. Height-resolved measurements of total wall flame heat flux measured at the centerline, $y = 0$, of panels during repeated experiments on PMMA. In plot (a), $\dot{q}''_{\text{total}}$ profiles are highlighted during the early stages of fire growth (i.e., $\dot{Q} < 500$ kW); in plot (b), $\dot{q}''_{\text{total}}$ profiles are plotted at the later stages of these tests, when flames covered the full surface of panel walls. Error bars indicate expanded uncertainty of the heat flux measurements (U_c; 95% confidence interval, coverage factor = 2), as described in Appendix B.2.

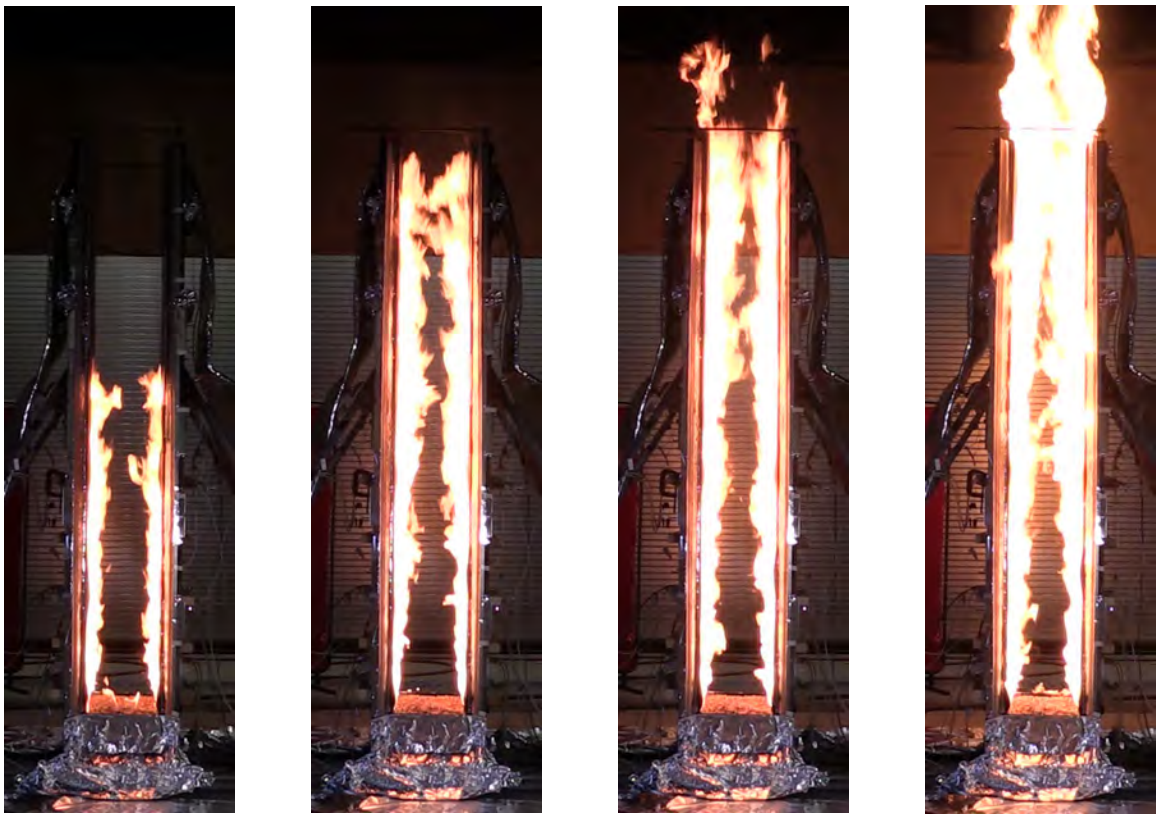

(a) $\dot{Q} = 100$ kW **(b)** $\dot{Q} = 200$ kW **(c)** $\dot{Q} = 300$ kW **(d)** $\dot{Q} = 500$ kW

Fig. 19. Representative images of flame structure during the early stages of fire growth due to upward flame spread over PMMA panels; corresponsding $\dot{q}''_{\text{total}}$ profiles are plotted in Fig. 18a.

3.1.2. ABS, poly(acrylonitrile butadiene styrene)

Heat Release Rate and Observed Burning Behavior

Three parallel panel experiments were conducted on ABS; images of typical fire development in these tests are shown in Fig. 20. In each test, samples ignited readily and the propane burner was turned off after 75 s. Immediately after ignition, the burner was covered with a steel shield (to protect it from molten remnants of ABS panels that would fall down towards the end of tests). Although both walls ignited simultaneously after burner exposure in each test, in Test R1, the front edge of both panel walls (i.e., -30 cm $\leq y \leq -22$ cm) did not support continuous flaming at burner shutoff (i.e., ignition); however, within approximately 55 s after ignition, uniform flaming was observed across the full width of panels walls in Test R1. In all three tests, approximately 60 s after sample ignition, when total HRR was between 1.5 MW and 2.0 MW, the flames on either panel wall merged to fill the volume between the panel walls

As seen in Fig. 20, ABS samples produced a significant amount of soot while burning. Some of this soot attached to the front surface of panels, quickly blackening them; however, most of it was observed to travel upwards with other combustion products, away from the panels and through the exhaust system. In previous tests of laminar flame spread over ABS (15 cm tall, 5 cm wide samples) [73], it was observed that this soot readily adhered to the surface of the polymer, forming a continuous dark layer across the full length of the sample that continued to deposit during burning to create a low density layer (of fairly uniform thickness) that measured up to 3 mm to 3.5 mm thick. In the absence of an external heat flux (in that study, as applied by an external radiant panel) this soot layer "inhibited progression of the pyrolysis front, ultimately causing sample extinction when the initial pyrolysis zone reached burnout". In the full-scale experiments conducted in this work, despite this soot deposition, ABS samples readily supported flame spread across their surface. It is possible that this occurred due to differences in system scale, strength and size of the initial burner used for ignition, and/or radiative heating from the opposite panel and the wall flame it supported.

In Tests R1 and R2, the burning behavior of ABS was highly repeatable: flames spread rapidly across the full height of each panel wall, reaching a peak HRR between 3.5 MW and 3.8 MW approximately 125 s after sample ignition (i.e., at $t = 180$ s to 200 s; see Fig. 21). In ABS Test R3, a strong cross flow (from back to front of samples; i.e., from $+y$ to $-y$) resulted in preferential flame attachement to the front edge ($y = -30$ cm) of panel walls while flames spread upwards; in this test, although flames reached the top of the assembly relatively quickly, uniform flaming was not observed across either wall until later in the test as a result of lateral flame spread. As seen Fig. 21, this resulted in slower rate of rise in HRR and a delayed time to peak HRR, though peak HRR was largely unaffected. This shift in measured HRR behavior is similar to that observed in test PMMA R5, which was also impacted by a strong cross flow (see Fig. 13). It is believed that this cross flow is externally driven (e.g., by the room's configuration and ventilation). Of all the solid materials tested in this work (i.e., neglecting porous polymer foams), ABS samples supported the highest

(a) Ignition

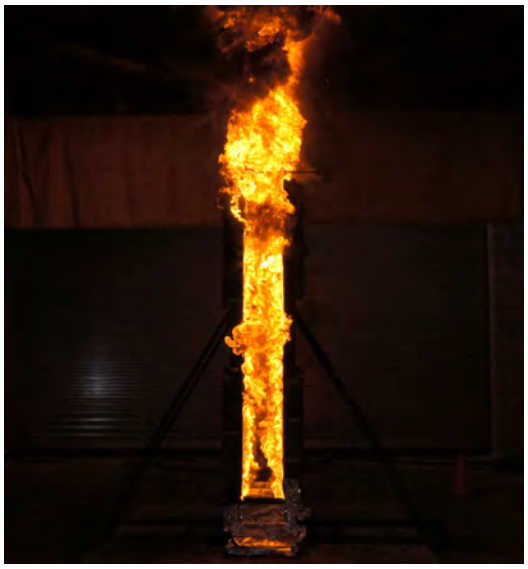

(b) Flame spread 60 s after sample ignition; $\dot{Q} = 2.5$ MW

(c) Peak HRR, $\dot{Q} = 3.8$ MW

(d) Heavy soot formation ($t = 360$ s)

Fig. 20. Fire behavior of ABS slabs during parallel panel experiments.

fire growth rates measured. Specifically, between tests R1 and R2, ABS $\overline{\frac{d\dot{Q}}{dt}}$ averaged 52.3 kW s^{-1}; this is approximately 3.6x greater than the average fire growth rate supported by PMMA panels.

Within 30 s after peak HRR was observed, small sections of the ABS panels were observed to detach from the wall (due to softening/burnout at attachment points) and continue to burn at the base of the panels. Samples were allowed to burn out until complete extinction; however, after approximately $t = 350$ s, complete burnout was observed along the walls and flaming was only observed on sections of the sample that had detached and fallen down from the assembly walls.

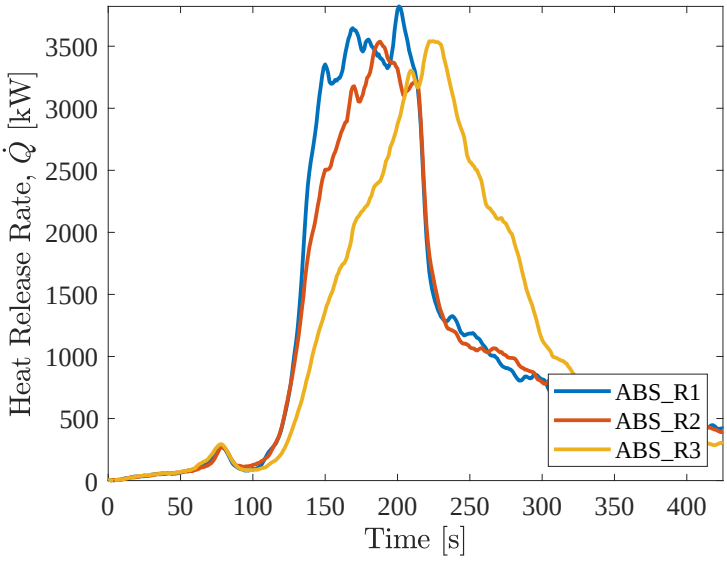

Fig. 21. Measured heat release rate during parallel panel experiments on ABS.

Flame Heat Flux

Figure 22 plots the average value of total wall flame heat flux, $\dot{q}''_{\text{total}}$, measured at the centerline of panels ($y = 0$) at heights 0.3 m $\leq z \leq$ 1.8 m during repeated parallel panel experiments on ABS. As shown here, at each height, $\dot{q}''_{\text{total}}$ rapidly increases at the beginning of tests as fires grow (i.e., as HRR increases and flames spread upwards towards, and over, each gauge location). After flames extend beyond each gauge location, the rate of increase of measured heat flux substantially decreases. Similarly as for tests on PMMA, a progressively higher HRR is required for this inflection point to be observed at higher heights, z; this delay corresponds to the additional time needed for the flame to spread across the panel walls (see Figs. 23a and 24). However, once continuous flaming was observed across the height of samples, the heat flux profile measured for ABS wall flames showed notable differences compared to that measured for PMMA flames.

When continuous flaming is observed across the height of samples, $\dot{q}''_{\text{total}}$ is substantially higher near the top of the assembly for ABS flames than for PMMA flames (see Fig. 23b). Specifically, as seen in Fig. 23, at a measured HRR of 2000 kW, $\dot{q}''_{\text{total}}$ is approximately 114 kW m^{-2} at $z = 220$ cm. Additionally, after flames extend beyond each gauge location (as HRR increases from 800 kW to 3000 kW), $\dot{q}''_{\text{total}}$ continuously increases (on average by 25 %) at each measurement location across the full height of the panel walls (see Fig. 22). Figure 23b, highlights how this increase in $\dot{q}''_{\text{total}}$ occurs fairly uniformly across the height of samples. It is possible that this relative difference between flame heat feedback profiles (and their development) arises because ABS supports dark, sooty, optically thick flames that quickly filled the volume between the two panel walls shortly after sample ig-

nition (see Fig. 20b). Not until $\dot{Q} = 3000$ kW are the flame heat flux profiles supported by ABS and PMMA similar (within their measured uncertainties).

In tests ABS R2 and R3, Repeated measurements of radiation heat flux were obtained at $z =$ 1.0 m, 1.8 m in order to calculate the fraction of total wall heat flux attributed to radiation (i.e., $\dot{q}_{\text{rad}}(\%) = \frac{\dot{q}''_{\text{rad}}}{\dot{q}''_{\text{total}}}$). These results are presented in detail (along with similar radiation measurements obtained for five other materials) in Sec. 3.3.

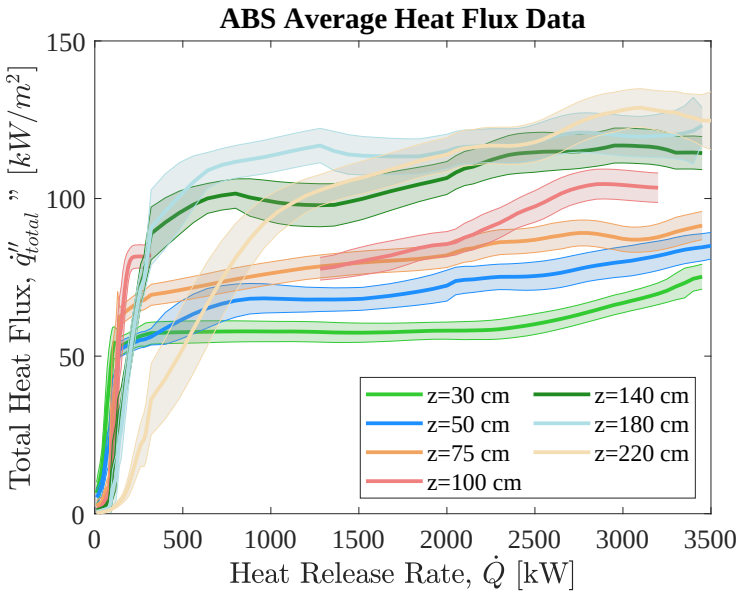

Fig. 22. Total wall flame heat flux measured at the centerline, $y = 0$, and across the height, z, of panels during repeated experiments on ABS. The shaded area around each curve represents expanded uncertainty of the heat flux measurements (U_c; 95% confidence interval, coverage factor = 2), as described in Appendix B.2.

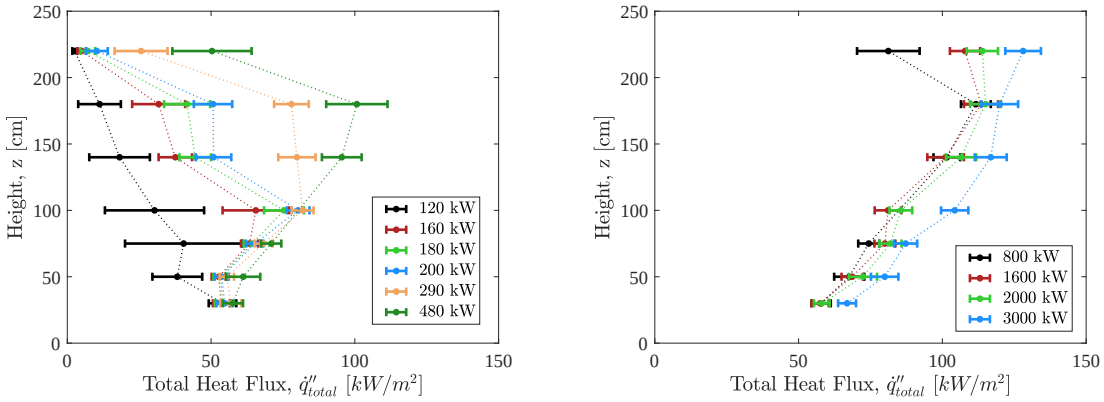

Fig. 23. Height-resolved measurements of total wall flame heat flux measured at the centerline, $y = 0$, of panels during repeated experiments on ABS. In plot (a), $\dot{q}''_{\text{total}}$ profiles are highlighted during the early stages of fire growth (i.e., $\dot{Q} < 500$ kW); in plot (b), $\dot{q}''_{\text{total}}$ profiles are plotted at the later stages of these tests, when flames covered the full surface of panel walls. Error bars indicate expanded uncertainty of the heat flux measurements (U_c; 95% confidence interval, coverage factor = 2), as described in Appendix B.2.

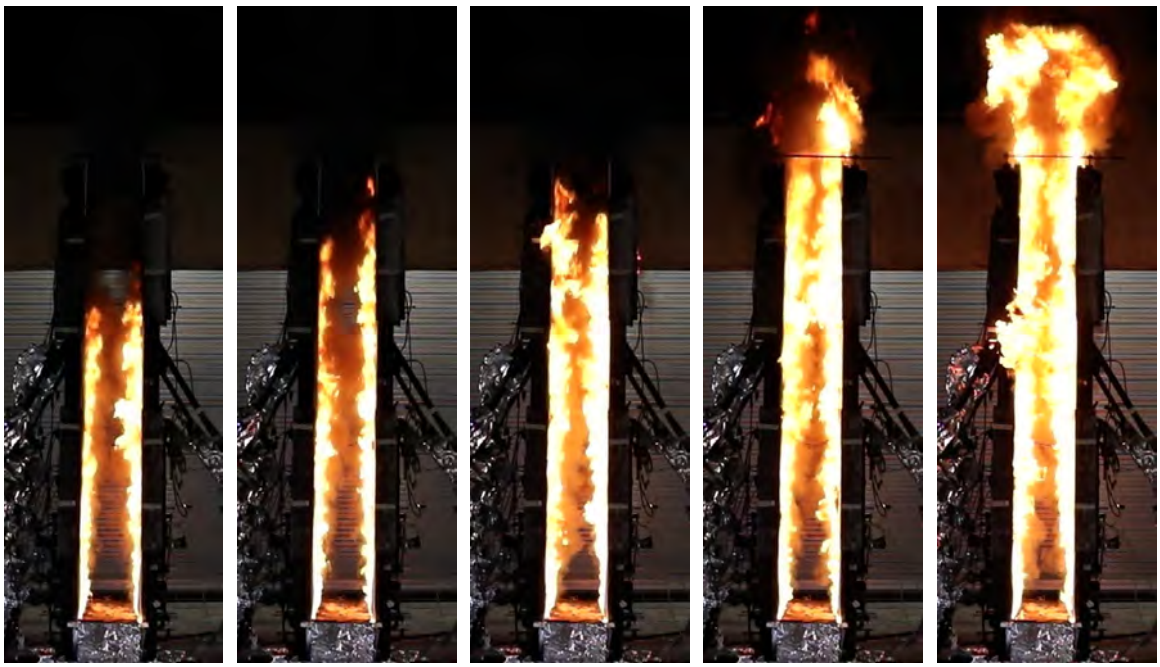

(a) $\dot{Q} = 120$ kW **(b)** $\dot{Q} = 160$ kW **(c)** $\dot{Q} = 200$ kW **(d)** $\dot{Q} = 300$ kW **(e)** $\dot{Q} = 480$ kW

Fig. 24. Representative images of flame structure during the early stages of fire growth due to upward flame spread over ABS panels. Corresponding height-resolved flame heat feedback profiles are plotted in Fig. 23a. Error bars indicate expanded uncertainty of the heat flux measurements (U_c; 95% confidence interval, coverage factor = 2), as described in Appendix B.2.

3.1.3. GPO-1, fiberglass-reinforced polyester laminate

Three parallel panel experiments were conducted on GPO-1; images of typical fire development in these tests are shown in Fig. 25. In Tests R1 and R2, the front 10 cm of one panel (i.e., 20 cm $\leq y \leq$ 30 cm on either the left or right panel) did not initially ignite due to burner non-uniformity; however, sustained flaming was observed on both walls and the burner was turned off between $t = 210$ s and $t = 225$ s. In Test R3, sustained flaming was observed across the full width of both walls and the burner was turned off at $t = 210$ s. Figure 26 plots time-resolved HRR measurements from each of these experiments; as seen here, initial fire growth is quite similar between Tests R1 and R2, but faster in Test R3. Just prior to burner shutoff in each test, wall flames were observed up to $z = 1.5$ m and total HRR measured between 200 kW and 250 kW; however, for 45 s to 60 s immediately after burner shutoff, flames decreased in size and measured HRR reduced by approximately a factor of two. In all three tests, flames gradually spread upwards across the full height of the panel. Although peak measured HRR is highly repeatable, averaging approximately 475 kW and varying by less than 10 % across all three tests, time to peak HRR was much shorter for Test R3 ($t = 410$ s) versus Tests R1 and R2 (approximately $t = 570$ s).

Of all materials tested in this study for which self-sustained flaming and upward flame spread were observed, flame spread was second slowest[17] on GPO-1. Specifically, for Tests R1, R2, and R3, $\overline{\frac{d\dot{Q}}{dt}}$ measured 1.6 kW s^{-1}, 1.4 kW s^{-1}, and 3.7 kW s^{-1}, respectively. This is approximately 0.1x to 0.25x the average fire growth rate supported by PMMA panels. Similarly as tests on PMMA, these results demonstrate that relatively small changes in ignition conditions may propagate into larger deviations in fire growth rate. Throughout the duration of each test, even at peak HRR, the flames on either GPO-1 panel wall remained separate (i.e., attached to their respective walls, without merging). Within approximately 120 s of peak HRR[18], burnout (i.e., local extinction) was first observed near the bottom ($z = 0$) and towards the center (-15 cm $\leq y \leq$ 15 cm) of each wall panel. This burnout front steadily advanced upwards and outwards, leaving behind a residual structure (layers of glass fabric reinforcement) until complete extinction of the samples (towards the end of tests, small flamelets were only observed along the side and upper edges of the assembly). Despite this burnout, samples maintained their original shape, remaining flat against the panel walls throughout experiments. Figure 25 presents a series of representative images from each test showing flame spread and subsequent burnout during these tests.

Figure 27 plots the average value of total wall flame heat flux, $\dot{q}''_{\text{total}}$, measured at the centerline of panels ($y = 0$) at heights 0.1 m $\leq z \leq$ 2.2 m during repeated parallel panel experiments on GPO-1. At each height, $\dot{q}''_{\text{total}}$ steadily increases at the beginning of tests as fires grow and flames spread upwards, towards each gauge location. At some measurement locations, a small spike/discontinuity in $\dot{q}''_{\text{total}}$ is observed at lower heights, z, when

[17] POM-GF samples supported the slowest average fire growth rates measured in this test series.

[18] First observations of the time to burnout at the base of GPO-1 samples varied from test to test, but generally occurred shortly before or after peak HRR was measured.

(a) Shortly after ignition, $\dot{Q} = 120$ kW

(b) Flame spread, $\dot{Q} = 165$ kW

(c) Peak HRR, $\dot{Q} = 498$ kW

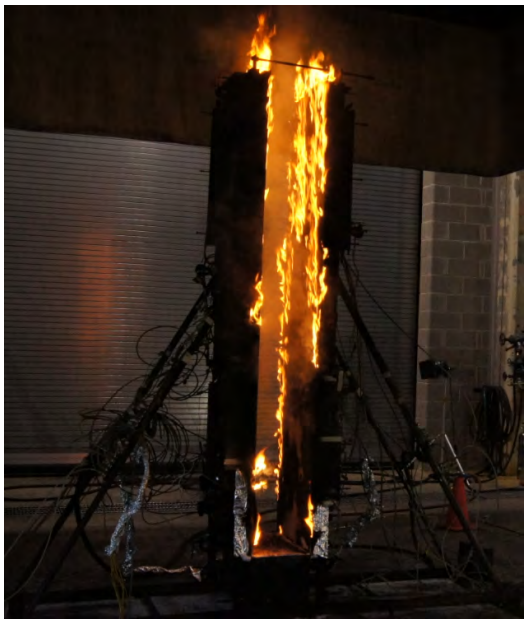

(d) Burnout at base of sample, $\dot{Q} = 160$ kW

Fig. 25. Fire behavior of GPO-1 slabs during parallel panel experiments.

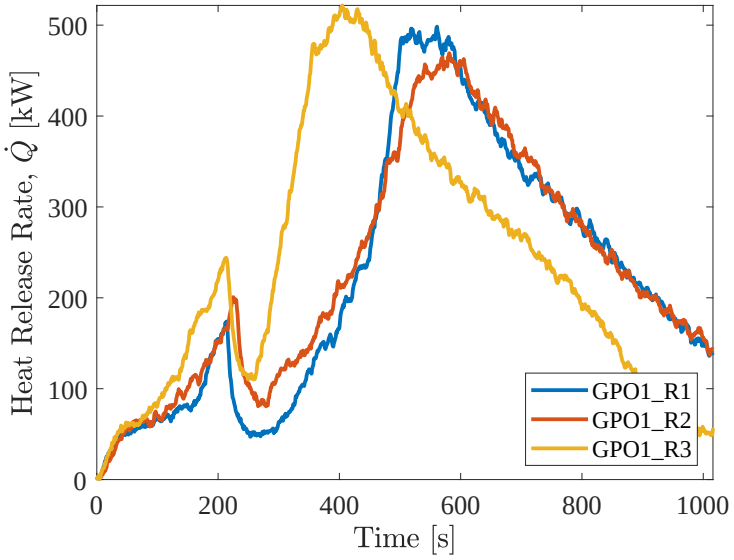

Fig. 26. Measured heat release rate during parallel panel experiments on GPO-1.

$60\,\mathrm{kW} < \dot{\mathrm{Q}} < 100\,\mathrm{kW}$: this represents the transition between the flames supported by the propane burner and the wall panels themselves. Unlike tests on PMMA, after continuous flaming is observed across the surface of each gauge in tests on GPO-1, measured flame heat flux remains relatively constant (at $z < 50$ cm , $\dot{q}''_{\mathrm{total}}$ remains constant, even as measured HRR increases from 150 kW to 400 kW; at $z \geq$75 cm, $\dot{q}''_{\mathrm{total}}$ increases by approximately 5 % after this inflection point). Note: throughout the duration of each test on GPO-1, the flames spreading on either panel wall remained separate (i.e., they did not merge in the volume between the panels).

Figure 28 plots height-resolved wall flame heat flux profiles measured in GPO-1 tests at HRRs of 120 kW, 180 kW, 300 kW, and 450 kW; Fig. .29 shows representative images of flame structure when each of these HRRs was measured in Test GPO-1 R3. As seen here, after flames covered the full surface of panel walls and when $\dot{Q} = 400$ kW, $\dot{q}''_{\mathrm{total}}$ increases as a function of height, z, from approximately 40 kW m^{-2} at $z = 20$ cm to approximately 80 kW m^{-2} at $z = 220$ cm. Compared to PMMA flames, when fire size is the same (e.g., at $\dot{Q} = 400$ kW or 500 kW) and when both support continuous flames across the full length of panel walls, $\dot{q}''_{\mathrm{total}}$ is higher in GPO-1 tests. It is possible that this occurs due to increased reradiation from front surface of the opposite panel walls: not only can the front-most layer of glass fabric reinforcement observed at the front surface of samples reach higher temperatures than the surrounding polyester resin (as it remains thermally stable while the sample is continuously exposed to a wall flame) but, because flames spread more slowly in GPO-1 tests, each panel wall has been heated for considerably longer in tests on GPO-1 (vs. in PMMA tests) by the time a HRR or 500 kW is measured.

Repeated measurements of radiation heat flux were also obtained at $z = 0.5$ m, 1.0 m, 1.8 m (in tests GPO-1 R1, R2, and R3) in order to calculate the fraction of total wall heat flux attributed to radiation (i.e., $q_{\text{rad}}(\%) = \frac{\dot{q}''_{\text{rad}}}{\dot{q}''_{\text{total}}}$). These results are presented in detail (along with similar radiation measurements obtained for five other materials) in Sec. 3.3.

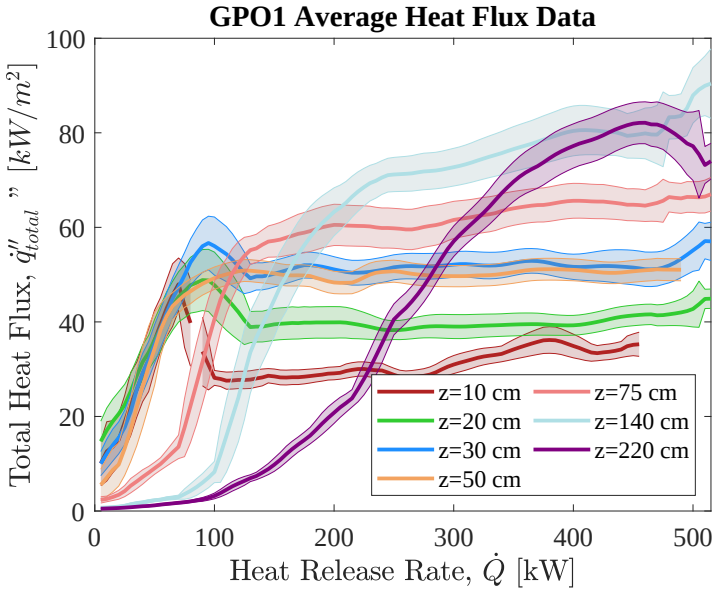

Fig. 27. Total wall flame heat flux measured at the centerline, $y = 0$, and across the height, z, of panels during repeated experiments on GPO-1.The shaded area around each curve represents the expanded uncertainty of the heat flux measurements (U_c; 95% confidence interval, coverage factor = 2), as described in Appendix B.2.

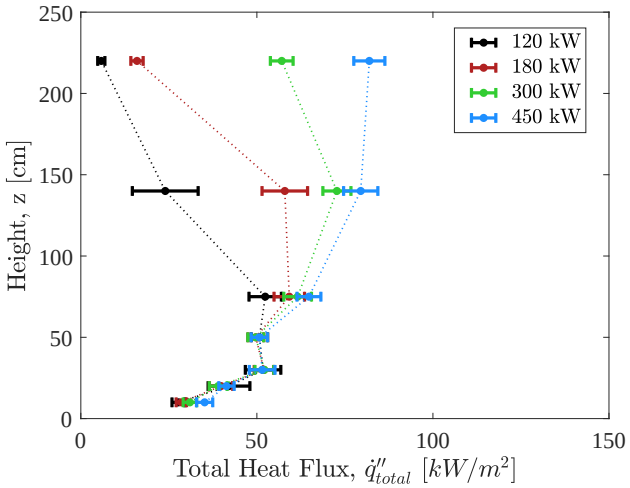

Fig. 28. Height-resolved measurements of total wall flame heat flux measured at the centerline, $y = 0$, of panels during repeated experiments on GPO-1. Error bars indicate expanded uncertainty of the heat flux measurements (U_c; 95% confidence interval, coverage factor = 2), as described in Appendix B.2.

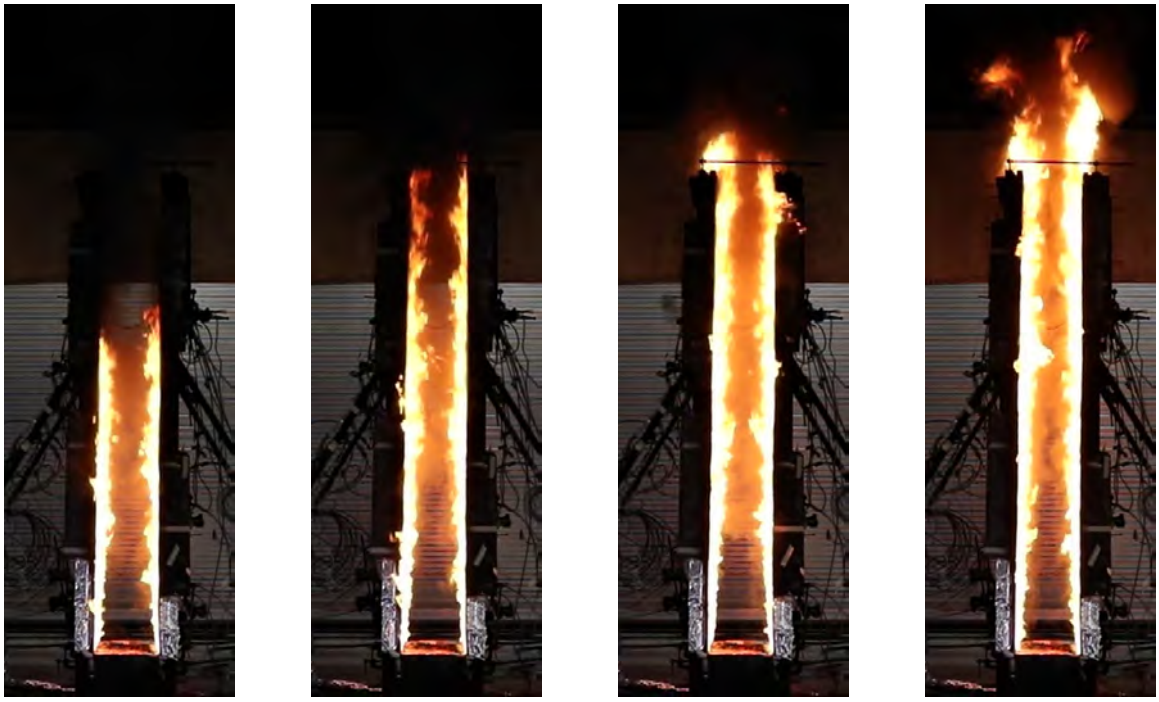

(a) $\dot{Q} = 120$ kW **(b)** $\dot{Q} = 180$ kW **(c)** $\dot{Q} = 300$ kW **(d)** $\dot{Q} = 450$ kW

Fig. 29. Representative images of flame structure during the early stages of fire growth due to upward flame spread over GPO-1 panels. Corresponding height-resolved flame heat feedback profiles are plotted in Fig. 28.

3.1.4. GPO-3, fiberglass-reinforced polyester laminate (Redboard: improved arc- and flame-resistance)

Three[19] parallel panel experiments were conducted on Redboard (GPO-3); images of typical fire behavior in these tests are shown in Fig. 30. In each test, self-sustained flaming could not be achieved: despite application of the propane burner for up to 20 minutes, flame spread was not observed beyond the original preheated region. Figure 30a, shows peak flame height during these tests (wall flames extend only up to the mid-height of the panels, approximately equal to the height of the burner flames) and Fig. 30b, shows unburned sections of the sample (red) at the top of the panel walls following a 20 minute burner exposure. As seen in Fig. 31, peak HRR measured never exceeded 135 kW in any of the three repetitions (note: this value includes the 63 kW of energy released by the propane burner at the base of samples) even though samples were continuously exposed to the propane burner. In each test, samples self-extinguished shortly after the burner was turned off; this result is consistent with the high arc-, carbon-track-, and fire-resistance rating of this material. Flame heat flux measurements were not recorded during experiments on Redboard.

(a) Peak HRR, $\dot{Q} = 135$ kW

(b) After 20 min. exposure to 63 kW burner

Fig. 30. Fire behavior of GPO-3 (Redboard) slabs during parallel panel experiments.

[19] For the third repetition, Test_R3, Redboard panels were only 1.22 m tall. Measured peak HRR and total heat release in this test was similar to that observed when using full sizes, 2.44 m tall, panels, as flames were never observed to spread above $z = 1.22$ m.

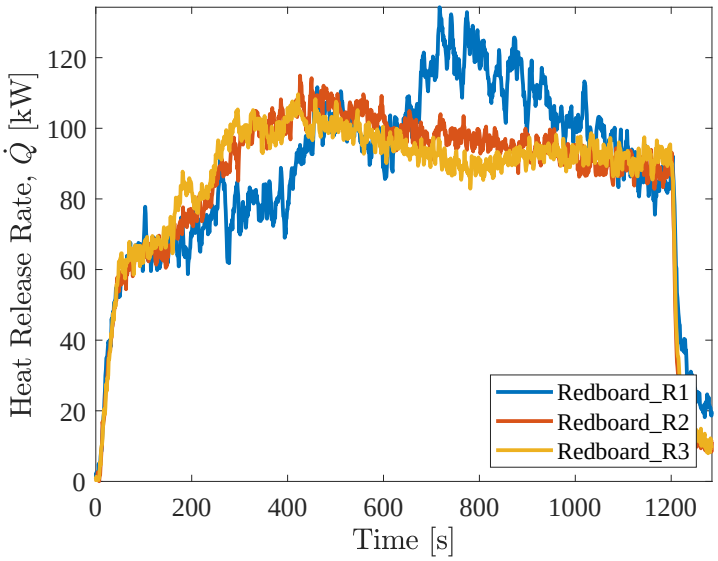

Fig. 31. Measured heat release rate during parallel panel experiments on GPO-3 (Redboard).

3.1.5. HDPE, high density polyethylene

HDPE is known to melt at relatively low temperatures (130°C to 135°C) [100, 101] and it has been shown that this can have a strong impact on the burning behavior of and flame spread over HDPE-jacketed copper wires [102]. In this parallel panel test series, significant melting of HDPE panels was observed after peak burning (which created a potentially hazardous pool fire that was particularly difficult to extinguish and clean up), thus only one test was conducted on this material. Figure 32 provides a representative series of images illustrating burning behavior during this test on HDPE.

Although HDPE burned vigorously in the parallel panel configuration, sustained flaming ignition of the panel walls (and subsequent burner extinction) was not observed until $t = 230$ s. After ignition, flames rapidly spread upwards to the top of the assembly, reaching a peak HRR of 2.8 MW just 100 s after sample ignition (i.e., at $t = 330$ s); this equates to an average spread rate of $\overline{\frac{d\dot{Q}}{dt}} = 26.7$ kW s^{-1}, which is approximately 1.84x the average fire growth rate supported by PMMA panels. Figure 33 plots total HRR measured during this test on HDPE. Flame heat flux measurements were not recorded during experiments on HDPE due to expected melting behavior.

Only minor dripping / melt flow was observed at the front surface of samples prior to peak burning; however, shortly after this peak HRR was observed, a significant melt flow event occurred in which approximately half of the total specimen mass softened, detached from the panel walls, and fell to the burner and surrounding platform below. Measured HRR decreased substantially following this melt flow event, though the polymer melt continued burning as a pool fire until manual suppression (by water-line). Note: as seen in Fig. 32d, the flaming polymer melt produced during this test on HDPE was particularly difficult to extinguish. Application of water by a hose line would splash and spread this polymer melt (which could still continue burning), similarly as a liquid pool fire might behave.

(a) Burner application

(b) Sample ignition $t = 230$ s

(c) Peak HRR, $\dot{Q} = 2.8$ MW

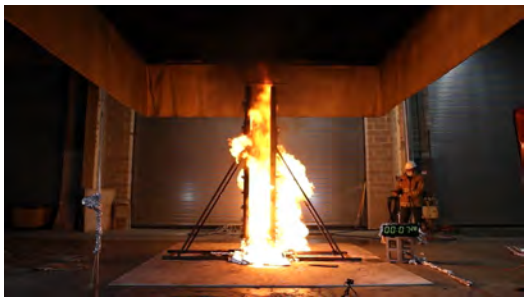

(d) Suppression of pool fire, $t = 448$ s

Fig. 32. Fire behavior of HDPE slabs burning in parallel panel configuration.

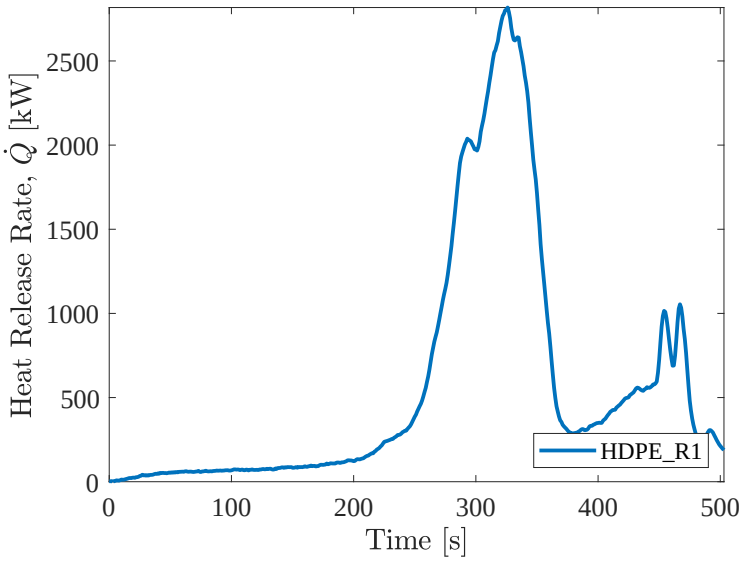

Fig. 33. Measured heat release rate of HDPE slabs burning in parallel panel configuration.

3.1.6. HIPS, high impact polystyrene

Four parallel panel experiments were conducted on HIPS. Additionally, one experiment was conducted using a single HIPS panel (opposite panel, including Marinite insulation, removed). Images of typical fire behavior in HIPS parallel panel tests are shown in Fig. 34; as seen here, HIPS samples produced a significant amount of soot while burning. Much like ABS, previous tests at the bench scale have demonstrated that soot formed by burning slabs of HIPS can adhere to the front surface of the polymer, continuously thickening and forming a thermally stable layer that can ultimately cause auto-extinction of samples (so long as samples remain in place without significant dripping or melt flow). In these full-scale experiments, however, although soot readily formed and adhered to the front surface of panels, blackening them (as well as any exposed surfaces of the parallel panel assembly), much of the soot was carried upwards and away with other combustion products and significant dripping event occurred within minutes after ignition. Although the exhaust system was increased to its maximum flow rate during these tests, during periods of peak burning and soot production, the density of soot in the exhaust flow system exceeded the maximum limit of the measurement system (i.e., across the path length of the laser, the soot was optically thick; see further discussion in Section. 3.4 and test-specific results in Appendix C).

For each repeated parallel panel test on HIPS, ignition was achieved by approximately $t = 75$ s, at which point the propane burner was turned off and the burner was covered with a steel shield. As seen in Fig. 35, time-resolved HRR mesaured in tests R1, R2, and R4 was highly repeatable. For test R3, although the maximum rate of rise of HRR and peak HRR were similar to that measured in the other three tests, rapid fire growth occured approximately 20 s sooner. In Test R3, flames ignited uniformly across the base of each panel wall. In Tests R1, R2, and R4, the front 10 cm (approximately $y \leq$ -20 cm) of the right panel ($x = 15$ cm) did not ignite initially; lateral flame spread was observed in these tests and wall flames covered the full surface of both panel walls within 80 s to 90 s after ignition. In all four tests, shortly after the burner was turned off, a minor decrease in fire size was observed; by $t = 115$ s in Test R3 and by approximately $t = 130$ s in Tests R1, R2, and R4, flame tips were first observed to reach the top of the panel walls, at which point a rapid increase in measured HRR was recorded. For all parallel panel tests conducted on HIPS, $\overline{\frac{d\dot{Q}}{dt}}$ averaged 38.2 kW s^{-1}; this is approximately 2.6x greater than the average fire growth rate supported by PMMA panels. Neglecting porous polymer foams, HIPS samples supported the second highest fire growth rates measured in this test series (close to that measured for ABS: $\overline{\frac{d\dot{Q}}{dt}} \simeq$ 52.3 kW s^{-1})

After a period of approximately 30 s, during which time fires burned at or near a peak HRR between 3.0 MW and 3.2 MW while maintaining their shape, HIPS panels were observed to detach from the wall and fall to the base of the panel assembly where they continued burning. After approximately $t = 480$ s, complete sample separation from the walls was observed and flaming was only observed on parts of the sample that had detached and fallen down to the base of the assembly. Periodically, water was applied to contain the

(a) Ignition

(b) Peak HRR, $\dot{Q} = 3.0\,\mathrm{MW}$

(c) Dripping and Heavy Soot Formation

(d) Continued burning and heavy soot formation of pool fire

Fig. 34. Fire behavior of HIPS slabs burning in parallel panel configuration.

melt pool and protect the back of the parallel panel assembly from direct flame exposure; however, this drip pool was allowed to burn until auto-extinction.

Figure 36 plots the average value of total wall flame heat flux, $\dot{q}''_{\mathrm{total}}$, measured at the centerline of panels ($y = 0$) at heights 0.2 m $\leq z \leq$ 1.8 m during repeated parallel panel experiments on HIPS. As seen here, at each height, $\dot{q}''_{\mathrm{total}}$ rapidly increases at the beginning of tests as HRR increases and flames spread upwards towards, and over, each gauge location. After flames extend beyond each gauge location (which takes progressively longer at higher heights, z) the rate of increase of measured heat flux substantially decreases.

Similarly as for ABS, after continuous flaming is observed across the full height of HIPS panels, $\dot{q}''_{\mathrm{total}}$ measurements demonstrate a strong dependence on height, z (i.e., $\dot{q}''_{\mathrm{total}}$ is substantially higher near the top of the assembly). Specifically, as seen in Fig. 37, at a measured HRR of 1000 kW, $\dot{q}''_{\mathrm{total}}$ increases from approximately 60 kW m^{-2} at $z = 30$ cm

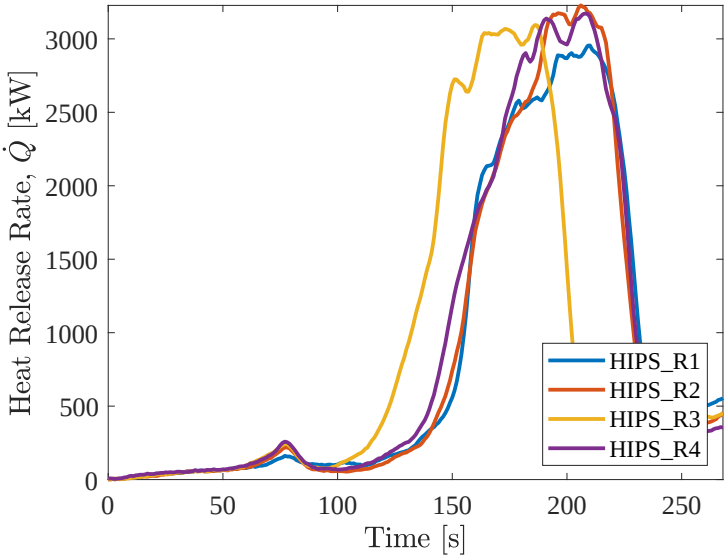

Fig. 35. Measured heat release rate of HIPS slabs burning in parallel panel configuration.

to approximately 120 kW m^{-2} at $z = 220$ cm. Additionally, as seen in Fig. 36, after continuous flaming is observed across each gauge location (consider measurements between 400 kW$\leq \dot{Q} \leq$ 3000 kW), $\dot{q}''_{\text{total}}$ measurements increase by (on average) just 20 % across the full length of samples (comparatively, in tests on PMMA, $\dot{q}''_{\text{total}}$ continues increasing by approximately 40 % to 55 % after this inflection point)[20]. It is possible that this occurs because dark, sooty, optically thick flames quickly filled the volume between the two panel walls (see Fig. 34).

[20] Note: by the time this inflection point is observed, $\dot{q}''_{\text{total}}$ is substantially higher for both ABS and HIPS flames (than for PMMA flames), with $\dot{q}''_{\text{total}} \geq$ 75 kW m^{-2} for all heights $z \geq 0.75$ m.

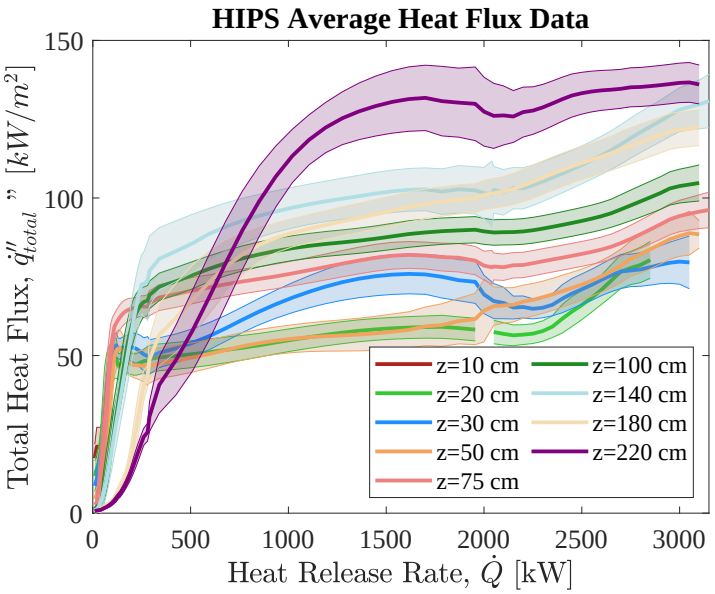

Fig. 36. Total wall flame heat flux measured at the centerline, $y = 0$, and across the height, z, of panels during repeated experiments on HIPS. The shaded area around each curve represents the expanded uncertainty of the heat flux measurements (U_c; 95% confidence interval, coverage factor = 2), as described in Appendix B.2.

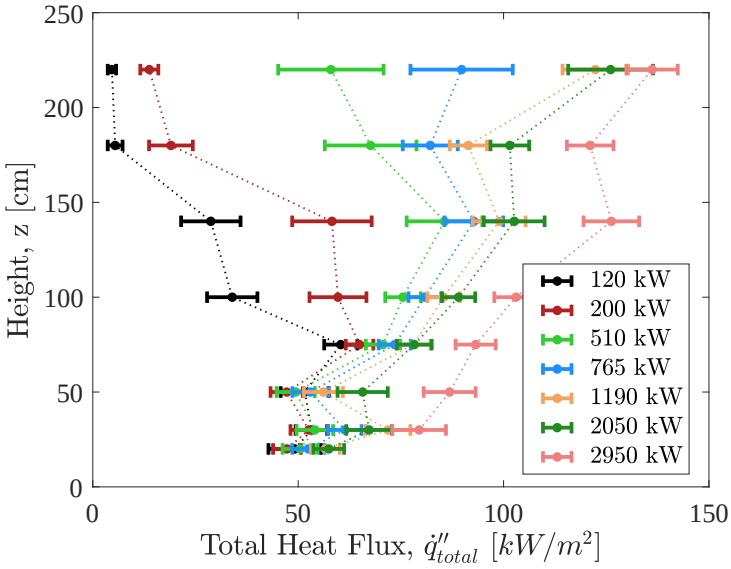

Fig. 37. Height-resolved measurements of total wall flame heat flux measured at the centerline, $y = 0$, of panels during repeated experiments on HIPS. Error bars indicate expanded uncertainty of the heat flux measurements (U_c; 95% confidence interval, coverage factor = 2), as described in Appendix B.2.

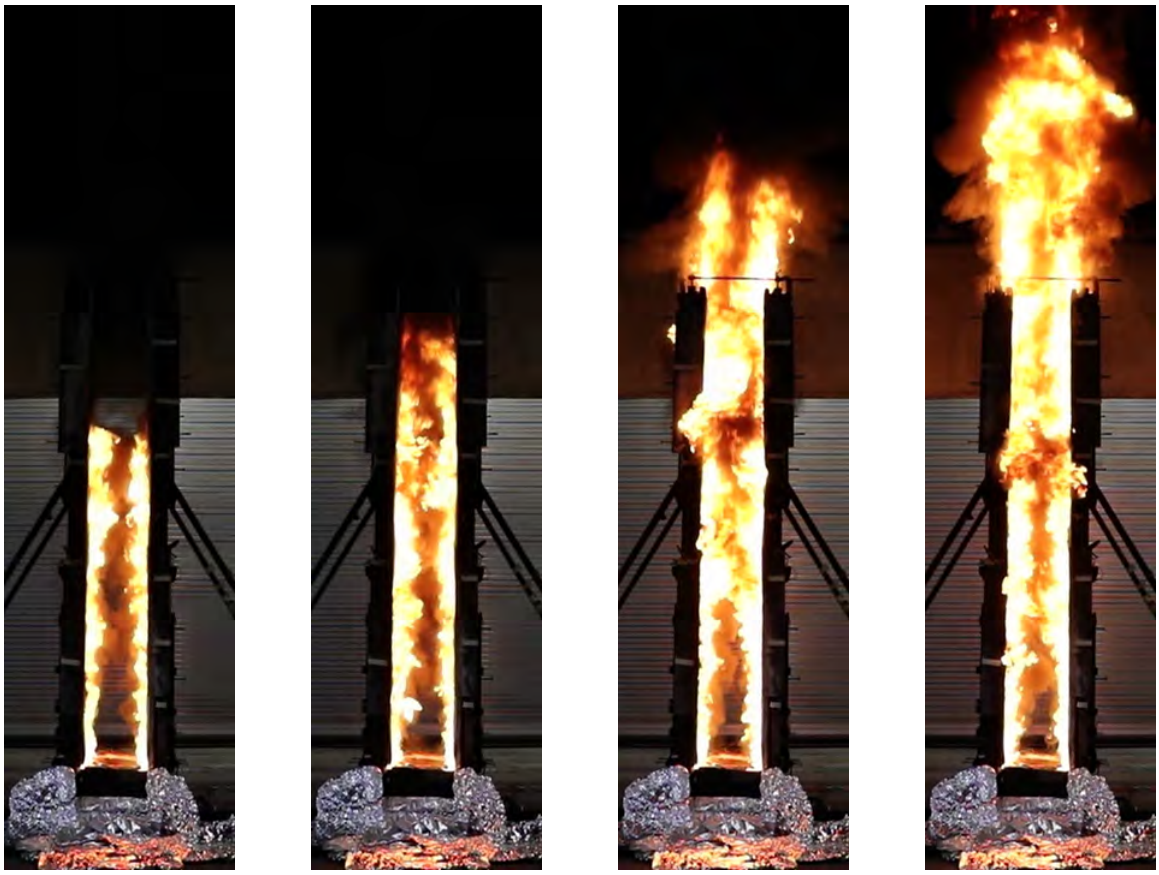

(a) $\dot{Q} = 120$ kW **(b)** $\dot{Q} = 200$ kW **(c)** $\dot{Q} = 510$ kW **(d)** $\dot{Q} = 765$ kW

Fig. 38. Representative images of flame structure during the early stages of fire growth due to upward flame spread over HIPS panels. Corresponding height-resolved flame heat feedback profiles are plotted in Fig. 37.

Figure 39 plots measurement data (HRR and flame heat flux) demonstrating the impact of sample configuration (parallel panel versus single panel) on measured fire growth rate and flame heat flux. As seen in Fig. 39a, fire growth rate was considerably slower in the single panel test: with just one panel burning, it required approximately 3x longer (200 s versus 70 s) after the burner was turned off for a rapid increase in HRR to be observed. Although fire growth rate was considerably slower for the single panel test, peak HRR was only approximately half that measured in the parallel panel test. Thus, nominally, peak HRR scaled with sample surface area.

Figure 39b plots measured flame to wall heat flux along the centerline of panel walls, $\dot{q}''_{\text{total}}$, versus width-normalized HRR, $\dot{Q}/w$ (here, w represents total sample width: in the single panel configuration, $w = 0.6$ m; in the parallel panel configuration, $w = 1.2$ m). As seen here, in the single panel configuration, larger values of $\dot{Q}/w$ are required before rapid increases in $\dot{q}''_{\text{total}}$ are measured; however, peak, quasi-steady state $\dot{q}''_{\text{total}}$ is generally comparable or slightly higher (10% to 20% higher)[21]. This demonstrates that, at the same relative fire size (i.e., $\dot{Q}/w$) flame height (i.e., region of the sample exposed to elevated flame heat fluxes) is lower in the single panel configuration. Because flame to wall heat fluxes under the continuous flame sheet were not measured to be lower in the single panel configuration, this suggests that burning configuration (i.e., single versus parallel panel) primarily affects fire growth rate by altering flame structure.

Repeated measurements of radiation heat flux were also obtained in parallel panel tests at $z = 0.5$ m, 1.0 m, 1.8 m (in tests HIPS R1, R2, and R4) in order to calculate the fraction of total wall heat flux attributed to radiation (i.e., $q_{\text{rad}}(\%) = \frac{\dot{q}''_{\text{rad}}}{\dot{q}''_{\text{total}}}$). To validate this measurement technique versus other results available in the literature [59, 60], measurements of radiation heat flux were also obtained at $z = 1.0$ m and 1.8 m when HIPS burned in the single panel configuration. These results are presented in detail (along with similar radiation measurements obtained for five other materials) in Sec. 3.3.

[21] For $\dot{Q}/w$ between 200 kW/m and 1600 kW/m, flame heat flux measurements at $z = 50$ cm are considerably higher in the single panel configuration (versus parallel panel configuration); this behavior is inconsistent with heat flux measurements at $z = 30$ cm and $z = 75$ cm. It is possible that sample deformation (e.g., dripping, warping, or panel separation) affected this measurement; however, only one single panel test was conducted and this result cannot be confirmed.

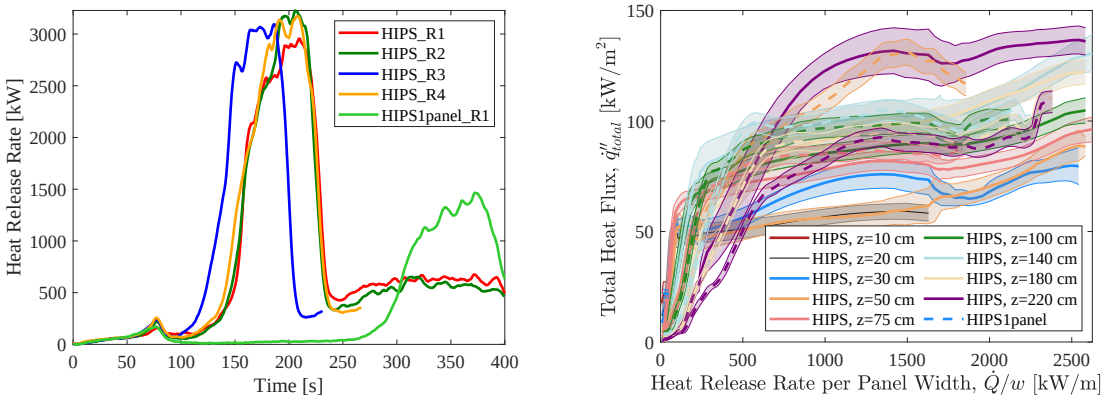

(a) **(b)**

Fig. 39. Comparison of fire growth rate and flame heat flux measurements for HIPS burning in the parallel panel or single panel configurations. Fig. (a) demonstrates the delay in fire growth rate and reduced peak HRR observed in the single panel test. Fig. (b) shows reduced flame heat fluxes at all heights in the single panel configuration when plotted as a function of width-normalized HRR, $\dot{Q}/w$. The shaded area around each curve represents the expanded uncertainty of the heat flux measurements (U_c; 95% confidence interval, coverage factor = 2), as described in Appendix B.2.

3.1.7. OSB, oriented strand board

Three parallel panel experiments were conducted on OSB; images of typical fire development in these tests are shown in Fig. 40. Although the moisture content of OSB panels was not measured prior to testing, the panels were stored (for a minimum of 7 days) in a room that maintained an average humidity of 25 %. In the first test, OSB R1, it appeared that strong ignition of samples had been achieved (flame tips were observed above $z = 2.0$ m; HRR $>$ 300 kW) and so the propane burner was turned off at $t = 135$ s. However, after burner shutoff, wall flames were not self-sustaining, thus the burner was turned back on at $t = 165$ s. Throughout the duration of the second and third tests (OSB R2 and R3) the burner was continuously supplied with propane. Figure 41 plots time-resolved HRR measurements from each of these experiments; in all three tests, flames spread upwards across the full height of the panels, reaching an initial peak fire size of approximately 600 kW between 180 s and 210 s after burner ignition.

Note: in Test OSB R3, due to poor initial performance of the propane burner (flaming only observed along the front edge of the burner, -30 cm $\leq y \leq$ 25 cm), ignition was cancelled after the first attempt (burner quickly turned off after 15 s) and the test restarted. During the second attempt at ignition, burner flaming was more uniform; however, because the burner and gas lines were pre-loaded with propane, initial burner HRR (and resulting flame heat flux) increased faster than normal (as discussed in Sec. 2.4). As a result, in this test, sample ignition occured earlier (at $t = 11$ s in Test R3, versus $t = 39$ s and 45 s in Tests R1 and R2, respectively) and initial HRR was slightly higher during the first 60 s of the experiment (see Fig. 41).

After this first peak in measured HRR, flames decreased in size[22], remaining fully separate on either panel wall (though still fully covering the surface of both walls) and measured HRR decreased for a period of approximately 200 s. As samples continued to burn, cracking was observed across their front surface and measured HRR increased once again until burnout, separation, and collapse of charred sections of OSB was observed across the surface of the panel walls; at this time, the propane burner was turned off and flames began to gradually self-extinguish[23] (see Fig. 40c). Following extinction of the burner, smoldering of sample remnants continued and smaller flames continued burning in two distinct regions: towards the top of the panels, where OSB was not yet fully charred through and remained attached to the assembly and above a pile embers that had formed at the base of the panels/at the top of the burner.

The two peaks in HRR measured in these experiments likely evolve due to surface charring dynamics and the continued heating of these samples (with finite thickness). Similar results have been observed in previous bench scale tests in which OSB samples were exposed to a range of incident heat fluxes (25 kW m^{-2} to 50 kW m^{-2}) in cone calorimeter experiments [103]. In each case, measured burning rate increases shortly after sample

[22] Note: the rapid decrease and increase in HRR measured during Test R1 between $150\ s \leq t \leq 200\ s$ corresponds to temporary burner shutoff and reignition.

[23] A second peak in measured HRR is observed in each dataset at the time of burner shut off; however, it is possible that larger fires could have been observed had the burner been left on for longer.

ignition before decreasing as a char layer forms and thickens at the surface of samples. This char layer acts as a thermal barrier (insulator), thus decreasing the net heat (from the flame above) available for pyrolysis of the virgin wood below. As samples continue burning, the thermal wave penetrating the sample reaches the backing insulation and the sample is heated through in-depth: at this point, burning rate accelerates and a second peak in HRR is observed. It is possible that the relatively quick development of this second peak in HRR in parallel panel tests on OSB was also influenced by rate at which cracking of the char layer was observed across the surface of panels in these tests (first seen within minutes of ignition).

Although flames quickly spread across the front surface of samples, average fire growth rate (which is calculated here based on the rate of rise in HRR to its first peak) was relatively low, as compared to other materials tested in this work. Between Tests R2 and R3, $\overline{\frac{d\dot{Q}}{dt}}$ averaged 2.2 kW s^{-1}, which is approximately 0.15x the average fire growth rate supported by PMMA panels) due to the low peak HRR observed in these experiments. Note: when the burner was not turned off in a test, average fire growth rate was calculated as: $\overline{\frac{d\dot{Q}}{dt}} = \frac{(\dot{Q}_{0.85*\text{peak}} - 90\text{ kW})}{(t_{\text{peak}} - t_{90\text{ kW}})}$, where $t_{90\text{ kW}}$ is well after burner ignition at which HRR measured 90 kW and all other terms in this expression are used identically as previously defined.

Figure 42 plots the average value of total wall flame heat flux, $\dot{q}''_{\text{total}}$, measured at the centerline of panels ($y = 0$) at heights 0.1 m $\leq z \leq 2.2$ m during repeated parallel panel experiments on OSB. At each height, $\dot{q}''_{\text{total}}$ increases to approximately 75 kW m^{-2} as flames spread upwards, towards, and over the surface of each gauge location. After continuous flaming is observed over each gauge in OSB tests, $\dot{q}''_{\text{total}}$ measurements remain relatively constant across the full height of samples, increasing by no more than 10 % while HRR remains below 500 kW.

A discontinuity is observed in the heat fluxes measured $z = 10, 75, 140,$ and 220 cm when $\dot{Q} > 600$ kW. This discontinuity arises because the flame heat flux data plotted in Fig. 42 only includes measurements recorded while HRR is increasing. As noted above, HRR temporarily decreases (before rising again) during tests on OSB, resulting in two HRR peaks throughout the course of the experiment. In Test OSB R2, HRRs greater than 600 kW were only measured during this second peak in HRR, approximately 300 s after a first HRR peak was measured. As a result, all heat flux data plotted in Fig. 42 when $\dot{Q} > 600$ kW is obtained from Test OSB R2 during this second increase in HRR (i.e., after $t = 400$ s). During the middle stages of all OSB tests, while HRR temporarily decreases before rising again, time-resolved measurements of $\dot{q}''_{\text{total}}$ continue to monotonically increase at all heights $z <$ 140 cm; towards the top of the panel walls, $\dot{q}''_{\text{total}}$ first decreases before increasing along with the second rise in HRR. It is possible that much of this measured increase in $\dot{q}''_{\text{total}}$ arises due to increasing reradiation from the opposite panel wall: as seen in Fig. 40d, after flames spread to the top of the assembly, glowing combustion (i.e., smoldering) is observed across the full surface of OSB panels.

Repeated measurements of radiation heat flux were also obtained at $z = 0.5$ m, 1.0 m, 1.8 m (in tests OSB R1, R2, and R3) in order to calculate the fraction of total wall heat flux

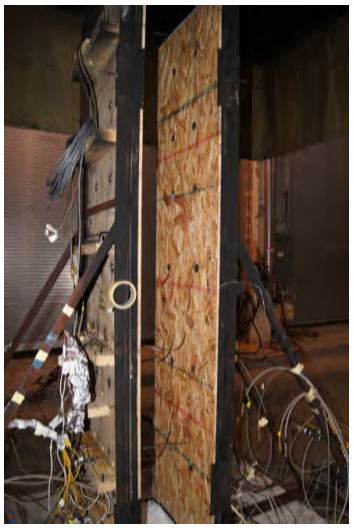

(a) Prior to ignition

(b) Early flame spread, $\dot{Q} = 300$ kW

(c) Near first peak in HRR, $\dot{Q} = 500$ kW

(d) Decay: Local burnout, smoldering (glowing combustion) of charred panels, and continued flaming of remaining sample remnants

Fig. 40. Fire behavior of OSB panels during parallel panel experiments.

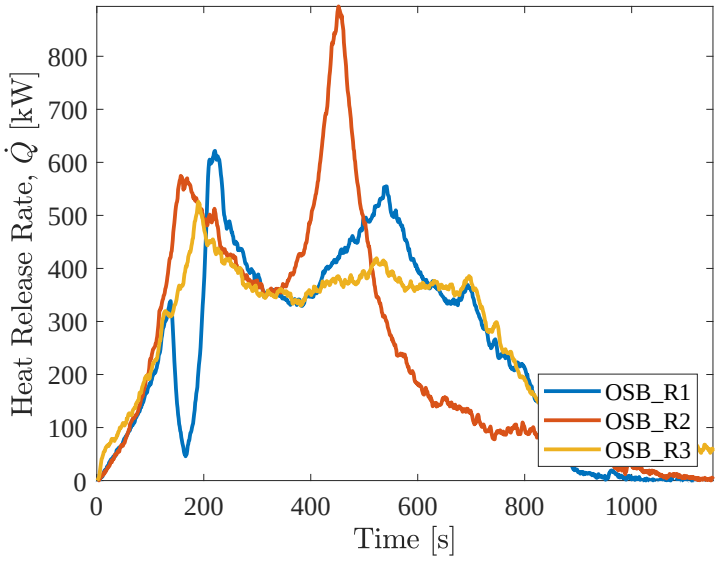

Fig. 41. Measured heat release rate during parallel panel experiments on OSB.

attributed to radiation (i.e., $q_{\text{rad}}(\%) = \frac{\dot{q}''_{\text{rad}}}{\dot{q}''_{\text{total}}}$). These results are presented in detail (along with similar radiation measurements obtained for five other materials) in Sec. 3.3.

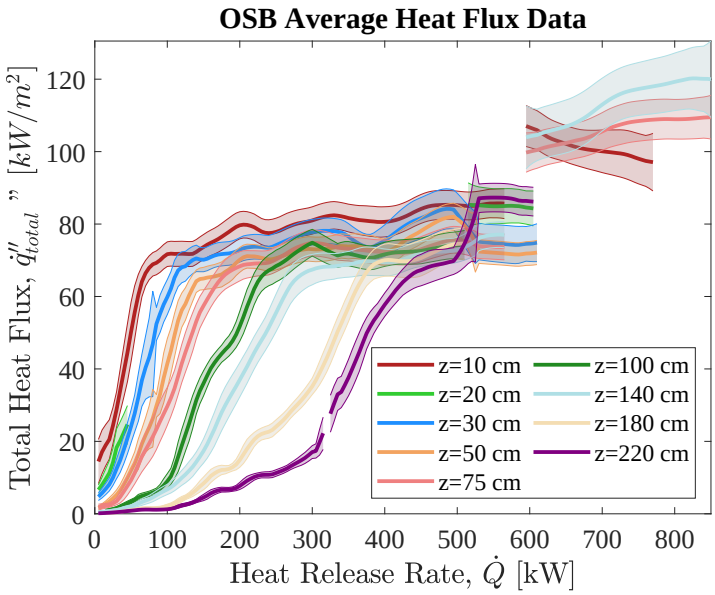

Fig. 42. Total wall flame heat flux measured at the centerline, $y = 0$, and across the height, z, of panels during repeated experiments on OSB. The shaded area around each curve represents the expanded uncertainty of the heat flux measurements (U_c; 95% confidence interval, coverage factor = 2), as described in Appendix B.2.

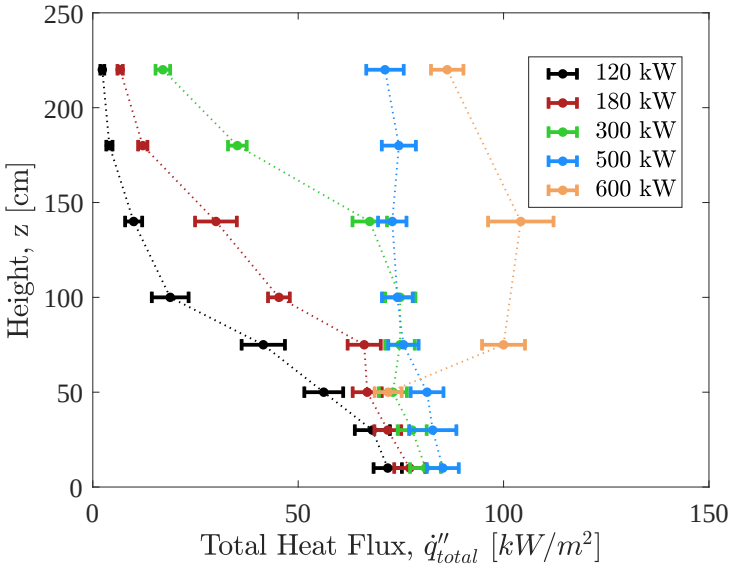

Fig. 43. Height-resolved measurements of total wall flame heat flux measured at the centerline, $y = 0$, of panels during repeated experiments on OSB. From left to right, $\dot{q}''_{\text{total}}$ profiles are plotted as HRR increases during upward flames spread and until the later stages of these tests, after peak HRR was measured, while HRR decreases when flames still covered the full surface of panel walls (i.e., before local burnout is observed at the base of samples). Error bars indicate expanded uncertainty of the heat flux measurements (U_c; 95% confidence interval, coverage factor = 2), as described in Appendix B.2.

(a) $\dot{Q} = 120$ kW **(b)** $\dot{Q} = 180$ kW **(c)** $\dot{Q} = 300$ kW **(d)** $\dot{Q} = 500$ kW **(e)** $\dot{Q} = 600$ kW

Fig. 44. Representative images of flame structure during the early stages of fire growth due to upward flame spread over OSB panels. Corresponding height-resolved flame heat feedback profiles are plotted in Fig. 43.

3.1.8. PBT, poly(butylene terepthalate)

One parallel panel test was conducted on PBT in this series; flame heat flux measurements were not recorded during this experiment. Local ignition of either wall was first observed by $t = 170$ s (see Fig. 45a and the propane burner was turned off at $t = 210$ s, at which point sustained flaming was observed across the surface of either panel wall and flame tips just reached the top of the assembly. After burner shutoff, as seen in Fig. 46, measured HRR increased rapidly, reaching 2.7 MW approximately 50 s later (i.e. by $t = 260$ s). This equates to an average fire growth rate of $\overline{\frac{d\dot{Q}}{dt}} = 56.0$ kW s^{-1}, which is comparable to the value calculated for ABS panels (52.3 kW s^{-1}). PBT is known to melt at approximately 225°C (roughly 180°C before its primary decomposition reaction) and its melt flow behavior during burning is known to affect its performance in standard fire tests [104, 105]. In this full-scale test, small drips were first observed to fall from the sample shortly after sustained flaming was observed. From $t = 260$ s until $t = 310$ s (i.e., the time at which peak HRR was observed), measured HRR remained relatively constant, increasing or decreasing slightly as relatively small (≤ 10 cm) sections of PBT detached from the assembly walls, fell to the base of the assembly, and continued burning.

Unlike most of the other materials tested in this work, which were large enough to cover the full surface of each parallel panel wall, PBT was obtained in the form of 1.22 m long, 0.30 m wide slabs that were attached side by side, four each on either panel wall. Because samples were not continuous across the width and height of the parallel panel walls (where they were attached to the assembly by a series of flat, metal clamps) they could detach more easily while burning. By $t = 310$ s, the edges of most PBT sections had separated from the assembly walls, at which point a significant melt flow / dripping event occurred and the majority of the remaining PBT fell down, where it continued burning as a pool fire. Molten PBT that dripped or spread to the back sides of the parallel panel assembly was extinguished (suppression by application of water) and the remaining drip pool closest to the burner was allowed to burn until self-extinction.

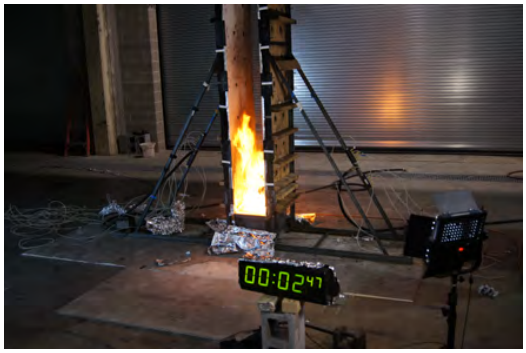

(a) Ignition of base of panel walls, just prior to burner shutoff

(b) Peak HRR, $\dot{Q} = 2.8$ MW

Fig. 45. Fire behavior of PBT slabs burning in parallel panel configuration.

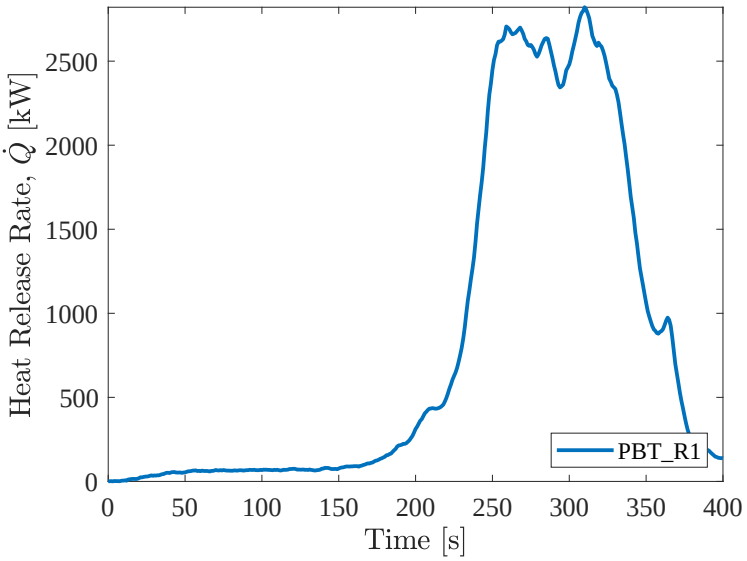

Fig. 46. Measured heat release rate of HIPS slabs burning in parallel panel configuration.

3.1.9. PMMA-PVC alloy (Kydex)

Two parallel panel tests were conducted on a PMMA-PVC alloy (Kydex); flame heat flux measurements were not recorded during these experiments. Burning behavior in these tests was repeatable and shared characteristics of separate experiments on pure PMMA and pure PVC slabs (see discussions in Sections 3.1.1 and 3.1.12, respectively). In PMMA-PVC Tests R1 and R2, the propane burner was continuously supplied with propane until $t = 600$ s, though measured HRR was approximately 15 % of its peak value $t = 300$ s. Representative images of typical fire development in these tests are shown in Fig. 47. Sample ignition likely occurred at $t = 90$ s, as evidenced by increased flame heights, heavy soot formation, and measured HRR exceeding $\dot{Q} = 120$ kW (i.e., twice the value of the propane burner; see Fig. 48).

Much like tests on PMMA panels, flames spread upwards across the surface of PMMA-PVC panels, with flame tips reaching the top of the panel assembly by approximately $t = 180$ s to $t = 195$ s. However, both peak HRR ($\dot{Q} \simeq 1.1$ MW) and average fire growth rate ($\overline{\frac{d\dot{Q}}{dt}} = 5.1$ kW s^{-1}) were approximately 3x lower in PMMA-PVC tests than in PMMA tests. As seen in Fig. 47, throughout the duration of tests on PMMA-PVC, significant quantities of soot were produced. Soot production was similarly observed during the burning of PVC samples with measured soot yields, Y_{soot}, of PMMA-PVC samples comparable to those of PVC samples (see discussion in Sec. 3.4) and both approximately 10x to 20x greater than Y_{soot} measured for PMMA. Note: although the soot yields measured during the burning of PMMA-PVC and PVC panels in this configuration were similar, peak fire sizes and total energy released in PMMA-PVC tests was significantly greater (factor of 2?x), resulting in substantially greater total soot production.

Figure 47b plots measured HRR from each of these experiments; as seen here, fire growth rate was highly repeatable during the early stages of each test. After $t = 180$ s, as samples continued to heat in-depth across their height, measured HRR increased, reaching a peak value of $\dot{Q} \simeq 1.1$ MW. Several secondary burning behaviors may have affected observed fire growth behavior. First, PMMA-PVC samples charred at their front surface. In some locations, this char layer may have formed an effective fire barrier; in others, charred sample remnants were observed to detach from the panel walls and fall to the top of the burner. Written observations made during experiments (prior to peak burning) also indicated that, along sample edges, small sections of PMMA-PVC slabs could separate from the assembly walls (in some cases folding forwards, but not fully detaching). When this behavior was observed, visual observations suggested that fire size could vary considerably: increasing or decreasing depending on whether the detached sample continued burning in place (at both its front and back surface) or fell to the base of the assembly. Following burner extinction at $t = 600$ s, sample remnants that had fallen to the top of the burner were allowed to continue burning (flaming combustion) until self-extinction (which occurred between $t = 2100$ s and $t = 2700$ s). These fires remained relatively small, $\dot{Q} < 30$ kW, and appeared to sustain themselves, in part due to their configuration: i.e., the charred sample remnants arranged in this porous matrix could retain heat

(a) Ignition of panel walls, approximately 90 s after burner exposure

(b) Peak HRR, $\dot{Q} = 1.1$ MW

(c) Continued burning of (and heavy soot formation) charred sample remnants at the base of panels, towards the end of a test

Fig. 47. Fire behavior of PMMA-PVC slabs during parallel panel experiments.

while oxgygen penetrated the pile in-depth (as evidenced by visual observations of glowing and flaming), thus sustaining combustion in a manner not observed when charred panels remain separated, flat against the parallel panel assembly. Compared to PMMA panels, which burned to completion, approximately half of the initial mass of PMMA-PVC samples remained at the end of each of these experiments (mostly as partially degraded and/or charred residue).

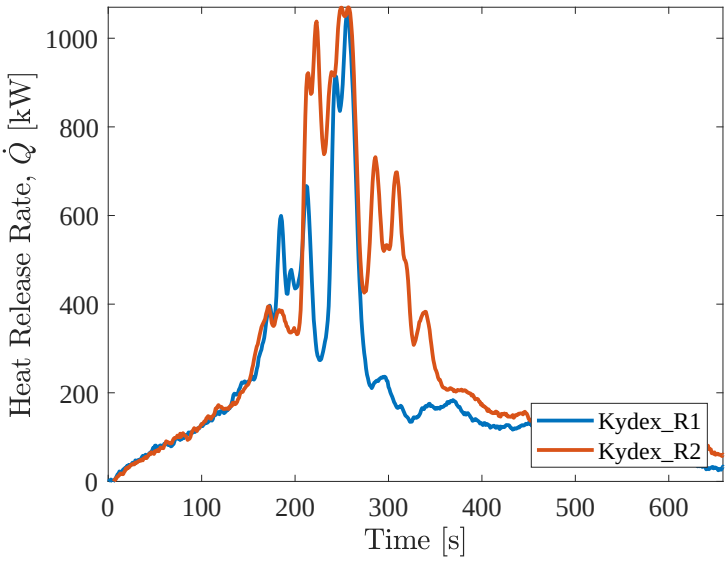

Fig. 48. Measured heat release rate of PMMA-PVC slabs burning in parallel panel configuration.

3.1.10. Polyiso, polyisocyanurate foam

Eight total tests were conducted on (nominally) the same polyisocyanurate foam of three different initial thicknesses: 13 mm , 25 mm , and 51 mm (nominally, 0.5 in., 1.0 in., and 2.0 in. thick). In the figures, tables, and text below, these three materials are referred to as Polyiso05, Polyiso, and Polyiso2, respectively. Flame heat flux measurements were not recorded during experiments on Polyiso foam.

Polyiso panels tested in this work consisted of a polyiso core bonded to Kraft-paper-reinforced aluminum facers on each side; both sides have a reflective surface. Prior to testing, the aluminum foil facer (and paper reinforcement) was completely removed from one side of the panels. This side was exposed to the burner flame, while the back side of the panel (with original foil facer still intact) was attached to the Marinite walls of the parallel panel assembly. As seen in Fig. 49a, panels were held in place by lengths of 12 gauge steel wire that were stretched horizontally across the front surface of panels (from $y = -15$ cm to $y = 15$ cm), pushed through the panels themselves, and connected at the back side of the assembly; six such connections were made at various heights, 0.4 m $\leq z \leq$ 2.2 m. For samples of all thicknesses, a horizontal strip of this same wire was also wrapped around the entire front surface of samples and affixed to the back of the panel at up to four heights between $z = 0.25$ m and $z = 2.2$ m. For Tests R2 and R3 on Polyiso05, which burned to completion (see Fig. 52a), additional lengths of wire were wrapped around the front of the sample to help hold it in place.

For each thickness of polyiso tested in this work, sample ignition and self-sustained flaming was readily observed within seconds of ignition of the burner. Of all the materials tested in this work (including each of the other porous foams), flame spread was most rapid over polyiso panels (i.e., shortest time to peak HRR), with peak HRRs observed between $t = 16$ s and $t = 23$ s in each of the eight experiments. Although time to peak HRR did not demonstrate any obvious dependence on sample thickness, peak HRR $decreased$ slightly with increasing sample thickness. This resulted in average fire growth rates of ($\overline{\frac{d\dot{Q}}{dt}} = 137.2$ kW s^{-1}, 129.1 kW s^{-1}, and 112.1 kW s^{-1} for Polyiso05, Polyiso, and Polyiso2, respectively). On average, in the parallel panel configuration tested here, $\overline{\frac{d\dot{Q}}{dt}}$ was approximately 8.7x higher for Polyiso foam as compared to solid PMMA slabs.

Because of this rapid flame spread, a discrete sample ignition time could not be reliably defined in real time (i.e., as experiments were conducted) and so, to improve test to test repeatability, the propane burner was left on throughout the duration of experiments. In general, polyiso samples retained their shape throughout the duration of experiments (see Fig. 52 with burnout observed only near the base of 1 in.- and 2 in.-thick polyiso samples (after prolonged burner exposure and extinction of the upper regions of the panels). The Polyiso05 samples maintained their shape throughout the duration of experiments, but would fragment and separate from the panel walls towards the end of tests as they burned to completion (see Fig. 52a).

As seen in Fig. 50, despite the rapid ignition and fire growth supported by polyiso samples (and the breakup of 13 mm thick samples towards the end of tests), burning behav-

ior of polyiso slabs was highly repeatable[24]. While measured total heat release, THR, increased with sample thickness (average THR =18 MJ, 31 MJ, and 38 MJ, for Polyiso05, Polyiso, and Polyiso2, respectively). Peak HRR *decreased* with sample thickness (the average peak HRR of Polyiso05, Polyiso, and Polyiso2 measured 1.03 MW, 0.96 MW, and 0.79 MW, respectively). Residue yield — i.e., final mass remaining at the end of the test divided by initial sample mass μ_{res}) — increased with sample thickness (average μ_{res} =0.17, 0.27, and 0.57 for Polyiso05, Polyiso, and Polyiso2, respectively. The heat of combustion measured for polyiso foam samples burning in the parallel panel configuration showed no statistically significant dependence on sample thickness, averaging 21.2 kJ g^{-1} across all 8 tests.

Unique time-resolved HRR profiles are observed for each of the three thicknesses tested here. Both 0.5 in. and 1.0 in. thick samples show two peaks in HRR (for Polyiso05, these peaks are approximately 10 s apart and support approximately the same HRR; for 1.0 in.-thick samples, these peaks are separated by approximately 60 s apart, and second peak HRR measured 0.3x to 0.5x that of of the first) whereas only one peak and a monotonic decay in HRR is observed for 2.0 in thick samples. Collectively, these results (along with visual observation of sample residue (Fig. 52) suggest that, although flammable, thicker polyiso panels retained some of their capabilities as thermal insulators while burning thus limiting the involvment of the backside of panels. While the thinnest polyiso samples quickly heated through in-depth, burning nearly to completion, it took longer for a thermal wave to reach the back surface of 1.0 in thick panels and the 2.0 in. thick samples were thick enough (at least in this burning configuration, with this burner exposure) to never heat through in-depth to sufficient temperatures such that complete thermal decomposition of the sample was observed.

[24]Note: the slight delay in the rapid rise in HRR measured in Tests Polyiso05_R3 and Polyiso_R1 appears to be related to sample ignition behavior. In both of these tests, burner flames first ignited along the back edge of the assembly (i.e., at $y = 30$ cm); seconds later, flames were observed across the width of the base of samples.

(a) Mounting of Polyiso panels prior to ignition

(b) Initial flame height seconds after ignition of 2.0 in. thick polyiso samples

Fig. 49. Polyiso samples prior to and shortly after ignition in parallel panel tests.

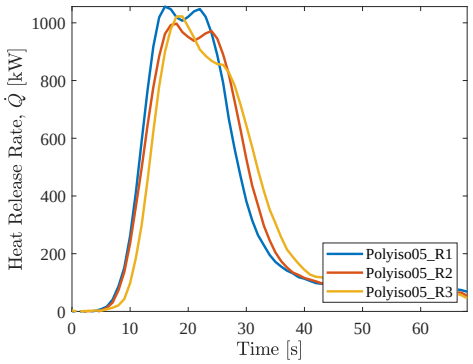

(a) Nominal thickness = 0.5 in.

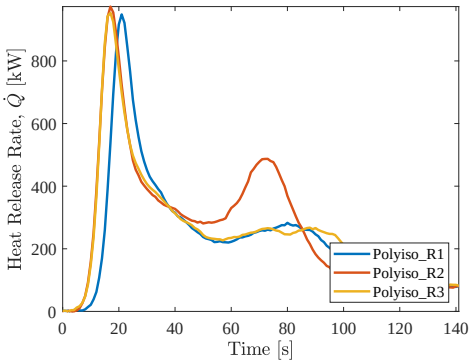

(b) Nominal thickness = 1.0 in.

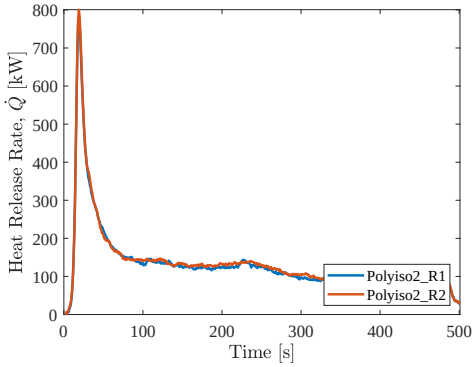

(c) Nominal thickness = 2.0 in.

Fig. 50. Measured heat release rate of polyisocyanurate foam samples burning in parallel panel configuration.

(a) Nominal thickness = 0.5 in., $\dot{Q} = 1.02$ MW

(b) Nominal thickness = 1.0 in., $\dot{Q} = 0.97$ MW

(c) Nominal thickness = 2.0 in., $\dot{Q} = 0.80$ MW

Fig. 51. Peak fire size in parallel panel tests on polyiso samples of three thickness. Measured peak HRR *decreased* with sample thickness (the average peak HRR of 13 mm, 25 mm, and 51 mm thick samples measured 1.03 MW, 0.96 MW, and 0.79 MW, respectively).

(a) Nominal thickness = 0.5 in., complete burnout and fragmentation of residue

(b) Nominal thickness = 1.0 in., near complete burnout, residue mostly in tact

(c) Nominal thickness = 2.0 in., unburnt sample visible at backside of panels away from burner

Fig. 52. Variations in remaining sample residue in parallel panel tests on polyisocyanurate foam samples of three different thickness.

3.1.11. POM-GF, glass-fiber reinforced poly(oxymethylene)

Previous measurements show that POM melts at relatively low temperatures (between 165°C and 180°C [100, 106]). In preliminary tests (bench scale flame spread experiments on 30 cm tall samples) it was observed that pure POM slabs can melt and flow readily while burning in a vertical configuration (this melt flow can have a strong impact on its fire growth behavior) but POM samples reinforced with chopped glass fibers would better retain their shape while burning [25]. In full scale parallel panel tests conducted in this work, continuous (but relatively slow) melt flow was observed at the front surface of each panel throughout the duration of experiments. Shortly after peak HRR was observed, a significant melt flow event occurred, at which point the lower half of each sample slab had softened and/or melted substantially such that it fully detached from the panel walls, and fell to the burner and surrounding platform below. Although polymer melt continued burning as a pool fire at the base of the assembly, measured HRR dropped precipitously following this melt flow event. As tests continued, POM-GF remained attached to the panel walls at $z > 1.2$ m and continued burning in place for an additional 60 s to 150 s before total collapse. The melt pool at the base of the panel walls was allowed to gradually burn out until approximately 50 minutes to 60 minutes after burner ignition.

Local sample softening, ignition, and flame attachment (to the panel walls) was first observed near the base of the assembly at approximately $t = 30$ s; however, the propane burner was not turned off until approximately $t = 180$ s, when sustained, uniform flaming across the width of panel walls (with advancement of the wall flame front beyond the original height of the burner flames). In Tests R1 and R2, a crossflow from front to back (i.e., from $-y$ to $+y$) resulted in preferential flame attachment to the back edge ($y =$+30 cm) of panel walls. In Test R3, the same initial burning behavior was observed, however the crossflow of air moved from back to front of the assembly (i.e., from $+y$ to $-y$).

Although approximately 10 cm of the front edge (i.e., -30 cm $\leq y \leq -20$ cm) of both panel walls in Test R1 and just the right panel wall in Test R2; or the back edge, 20 cm $\leq y \leq 30$ cm, in Test R3) did not initially ignite due to this crossflow (and the resulting non-uniformity of the burner flame), in all tests, sustained flaming was similarly observed on both panel walls after the burner was turned off at $t = 180$ (Fig. 53a). As seen in Figs. 53b and 53c, lateral flame spread allowed for near-uniform coverage of either panel wall approximately 200 s to 240 s after sample ignition. This figure also demonstrates the unique nature of flames supported by burning POM-GF samples: even at peak burning ($\dot{Q} \simeq 500$ kW when flame tips extended beyond $z =$2.5 m) soot production was not observed

[25] Preliminary flame spread tests were conducted on 30 cm tall, 5 cm wide slabs of pure POM and POM reinforced by 20 wt.% chopped glass-fibers (i.e., the POM-GF tested in this work at full scale). In these tests, both samples were ignited at their base and flames were allowed to spread freely upwards. Melting and dripping (flaming) of pure POM was observed shortly after ignition; however, POM-GF samples showed limited melt flow at their surface and generally maintained their shape (though thermal bowing was observed).

and flames remained nearly transparent[26]. Note: POM-GF slabs used for Test R3 were slightly thicker than those used in Tests R1 and R2 (approximately 9.5 mm thick versus 7.0 mm thick) resulting in (1) a slightly lower initial fire growth rate and (2) a longer period of steady burning where the POM-GF slabs remained fixed to the panel walls before ultimately softening, melting, and detaching.

Figure 54 plots time-resolved measurements of HRR from repeated tests on POM-GF panels; as seen here, fire growth was highly repeatable. In all tests, initial fire growth during burner application (0 s $< t <$ 180 s) was nearly identical. After burner shutoff, flames gradually spread upwards across the full height of the panels, reaching a peak fire size of approximately 500 kW by $t = 577$ s in Test R1 and $t = 663$ s in Test R2. Of all materials tested in this work for which self-sustained flaming and upward flame spread were observed, fire growth was slowest on POM-GF. Specifically, $\overline{\frac{d\dot{Q}}{dt}}$ averaged 0.98 kW s^{-1}, which is approximately 0.07x the average fire growth rate supported by PMMA panels.

Figure 55 plots the average value of total wall flame heat flux, $\dot{q}''_{\text{total}}$, measured at the centerline of panels ($y = 0$) at heights 0.2 m $\leq z \leq 2.2$ m during repeated parallel panel experiments on POM-GF. A similar trend is observed here as for each of the materials tested in this work: at each height, $\dot{q}''_{\text{total}}$ steadily increases at the beginning of tests as fires grow and flames spread upwards, towards each gauge location. However, as panels continued burning, polymer melt flow at the front surface of each sample could cover the surface of heat flux gauges, thus invalidating their measurements. As a result, there is a limited availability of flame heat flux data at higher HRR, especially at lower measurement locations. At heights $z \geq$ 180 cm, $\dot{q}''_{\text{total}}$ measurements were still obtained after continuous flaming is observed across the surface of the panel walls (for HRR up to 450 kW). As seen in Fig. 55, measured flame heat flux remains relatively constant at each height after steady flaming is observed.

Fig. 56 plots height-resolved wall flame heat flux profiles measured in GPO-1 tests at heat release rates between 120 kW and 500 kW. As seen here, at all heights, z, after continuous flaming was observed at each measurement location, $\dot{q}''_{\text{total}}$ reaches approximately 50 kW m^{-2}. When flames were observed across the full length of panel walls, $\dot{q}''_{\text{total}}$ is notably lower for POM-GF than for all other materials tested in this work (when compared at the same HRR). It is possible that this is a result of the limited soot production by, and radiation heat ransfer from, these (mostly) transparent, and relatively thin[27] flames. Repeated measurements of radiation heat flux were obtained at $z =$ 1.0 m, 1.8 m, and 2.0 m (in tests POM-GF R1, R2, and R3) in order to calculate the fraction of total wall heat flux attributed to radiation (i.e., $q_{\text{rad}}(\%) = \frac{\dot{q}''_{\text{rad}}}{\dot{q}''_{\text{total}}}$): of all materials tests in this work, $q_{\text{rad}}(\%)$ was lowest for POM-GF. These results are presented in detail (along with similar radiation measurements obtained for five other materials) in Sec. 3.3.

[26] Unfortunately, the yellow and orange highlights captured in photographs somewhat hide the predominantly transparent, blue flames that were observed during testing.

[27] Throughout the duration of each test on POM-GF, even at peak HRR, the flames spreading on either panel wall remained separate (i.e., they did not merge in the volume between the panels) and mostly transparent.

(a) Initial flame height shortly after the sample is ignited and the burner is covered in Test R3 ($t = 194$ s).

(b) Flame sheet covering left panel wall in Test R3, showing transparent blue flame ($t = 280$ s)

(c) Flame sheet covering base of left panel wall in Test R3; still primarily transparent, and reaching the top of assembly ($t = 438$ s)

(d) Flame sheet covering left panel wall up to z =1.5 m in Test R3, flame tips above top of assembly ($t = 576$ s)

(e) Flame sheet covering full surface of left panel wall in Test R3 near peak burning, $\dot{Q} > 450$ kW ($t = 650$ s)

(f) Continued burning of melted POM-GF at the front base of panels, towards the end of Test R3 ($t = 1474$ s)

Fig. 53. Representative fire behavior of POM-GF slabs during parallel panel experiments. These images are from the rear of the setup. ”Left panel wall” refers to the left panel when viewing from the front of the setup.

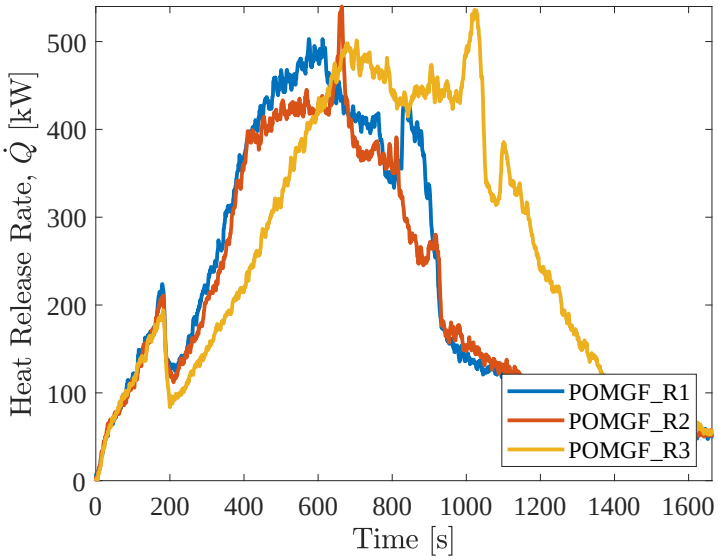

Fig. 54. Measured heat release rate of POM-GF slabs burning in parallel panel configuration.

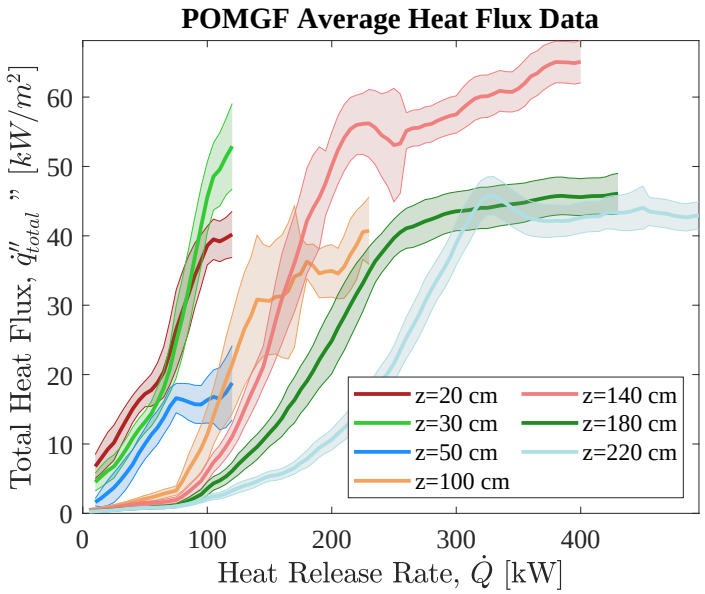

Fig. 55. Total wall flame heat flux measured at the centerline, $y = 0$, and across the height, z, of panels during repeated experiments on POM-GF. The shaded area around each curve represents the expanded uncertainty of the heat flux measurements (U_c; 95% confidence interval, coverage factor = 2), as described in Appendix B.2.

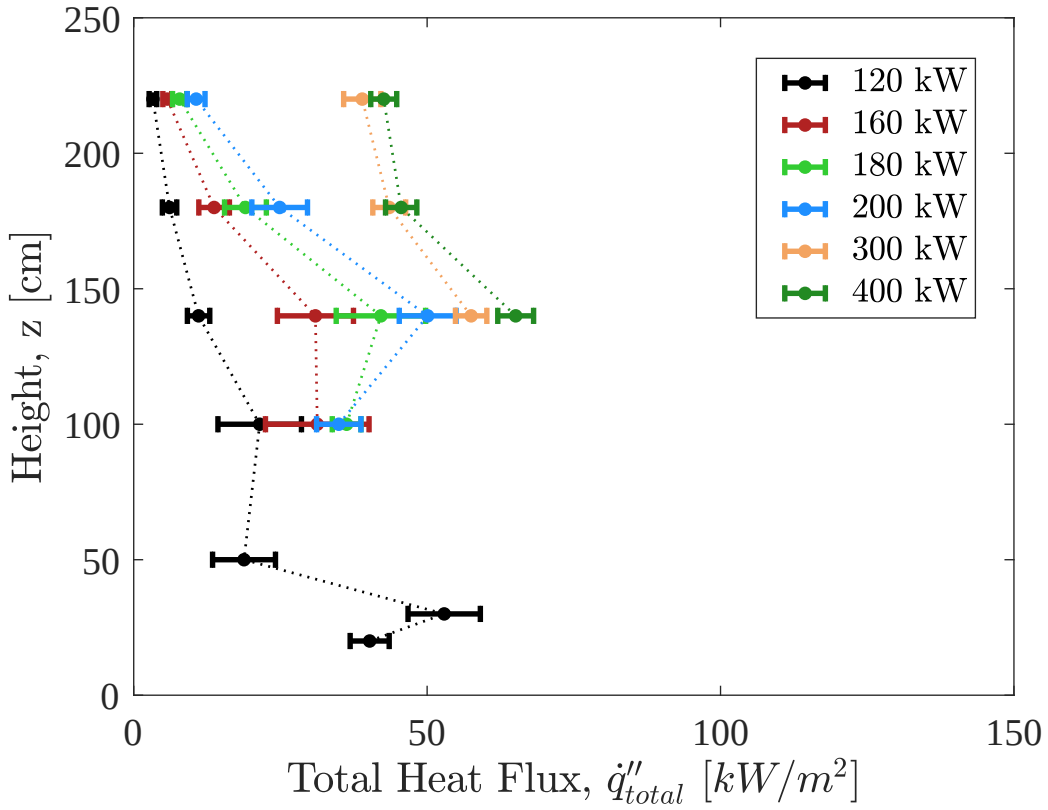

Fig. 56. Height-resolved measurements of total wall flame heat flux measured at the centerline, $y = 0$, of panels during repeated experiments on POM-GF. As seen here, $\dot{q}''_{\text{total}}$ reaches a peak value of approximately 50 kW m^{-2} at all measurement locations when steady flaming is observed. As fire size (i.e., $\dot{Q}$) increases, heat flux data is not available at lower heights due to polymer melt flow over the surface of the lower heat flux gauges. Error bars indicate expanded uncertainty of the heat flux measurements (U_c; 95% confidence interval, coverage factor = 2), as described in Appendix B.2.

3.1.12. PVC, poly(vinyl chloride)

Two parallel panel tests were conducted on PVC. In Test R1, to determine if self-sustained flaming of samples could be achieved, the propane burner was turned off twice when flames were observed at or above $z = 1$ m on both panel walls. After each burner shutoff, flames quickly began to extinguish and so the burner was reignited and allow to burn until $t = 1500$ s. In Test R2, the burner was continuously supplied propane until $t = 1200$ s. As seen in Fig. 58, throughout the majority of tests, total HRR measured approximately $\dot{Q} = 130$ kW (note: this value includes the contribution from the propane burner, approximately 63 kW). Although fires remained relatively small throughout the duration of each test (HRR$<$250 kW; flames typically remaining below $z = 1.5$ m) as seen in Fig. 57, heavy smoke formation occurred throughout the duration of tests. Significant charring was also observed across the height of samples, most notably towards the base of the assembly, where PVC panels were continuously exposed to flames from the propane burner. In both tests, flame spread was not observed across the height of samples, although temporary increases in fire size allowed flame tips to reach up to approximately $z = 2$ m. Measured increases in HRR always coincided with visual observation of taller flames (i.e., involvement and burning of a larger region of the panel walls); in some cases, these increases in HRR were observed after partial separation (local) of the edges of PVC slabs from the parallel panel assembly or detachment of the char layer at their front surface.

A limited amount of heat flux data is available from each test repetition on PVC; these measurements are plotted in Fig. 59 from ignition until the first decrease in HRR (i.e., in Test R1, until the burner was first shut off at $t = 180$ s, and, in Test R2, until approximately $t = 260$ s, when the char layer was observed to thicken at the sample's surface). At each height, $\dot{q}''_{\text{total}}$ steadily increases as fires grow, with higher heat fluxes always observed at lower heights, z. This confirms the repeatability of measurements obtained at different locations in either test repetition. Note: heat flux measurements plotted in Fig. 59 include heat transfer from the flames supported by the propane burner, which account for at least 50 % of total heat released in the dataset presented here.

(a) Peak HRR, $\dot{Q} = 236$ kW

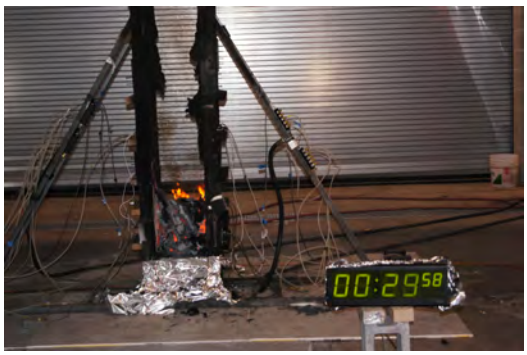

(b) Charring at base of PVC panels at end of test

Fig. 57. Fire behavior of PVC slabs during parallel panel experiments.

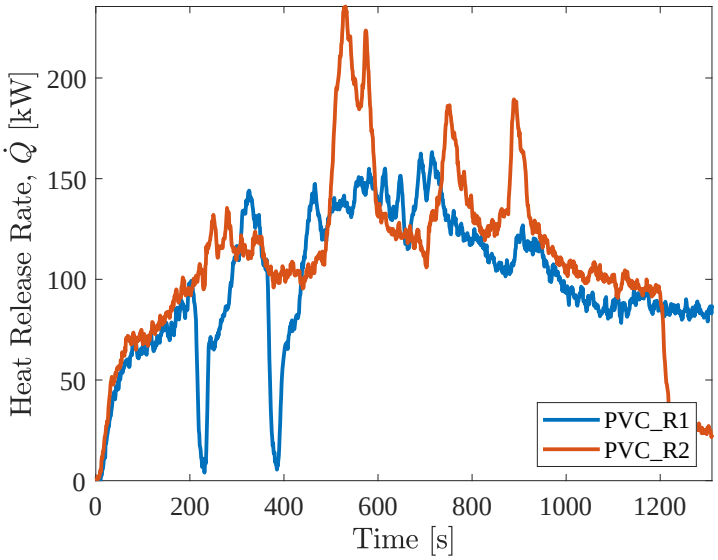

Fig. 58. Measured heat release rate of PVC slabs burning in parallel panel configuration.

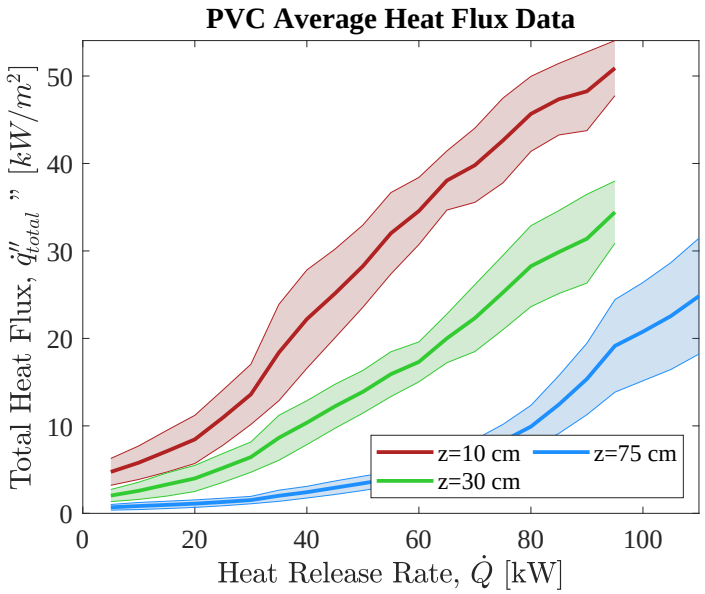

Fig. 59. Total wall flame heat flux measured at the centerline, $y = 0$, and across the height, z, of panels during repeated experiments on PVC. The shaded area around each curve represents the expanded uncertainty of the heat flux measurements (U_c; 95% confidence interval, coverage factor = 2), as described in Appendix B.2.

3.1.13. SIS Wire, switchboard wire

Two parallel panel tests were conducted on SIS wire. As seen in Fig. 60a, in each test, between 90 and 96 strands of SIS wire were attached to a 60 cm wide strip of wood that was attached to (or folded over) the top of either wall of the parallel panel assembly. SIS wire strands were evenly distributed (in a single layer) across the width of samples and held in place using lengths of 12 gauge steel wire that wrapped around either panel wall at four locations: $z \simeq$0.1 m, 0.5 m, 1.0 m, and 1.5 m. In Test R1, SIS wire was layered directly against the Marinite board insulation of the parallel panel assembly. In Test R2, a 6.2 mm thick layer of Redboard (GPO-3) was first attached to the Marinite and then the SIS Wire was placed in front to determine if the combined fuel load could support flaming combustion.

In each test, despite prolonged burner exposure (15 minutes in Test 1; 25 minutes in Test 2) flame spread over samples was not observed and total flame extinction was observed once the propane burner was turned off. Production of thick, white/gray smoke throughout the duration of propane burner application indicated the generation of high molecular weight gaseous pyrolyzates that did not burn. As seen in Fig. 61 total HRR peaked shortly after burner ignition, though it never exceeded $\dot{Q} = 150$ kW in either experiment, and then settled to a quasi-steady value of 95 kW or 70 kW (with or without the presence of Redboard behind SIS Wire) throughout the remainder of the test. Note: measured HRR includes the contribution from the propane burner, $\dot{Q} = 60$ kW. These results are consistent with previous measurements on Redboard (see Sec. 3.1.4 and demonstrate that the SIS Wire tested here (in this configuration and with this particular, though reasonably severe, ignition source) does not represent a significant fuel load and will not support self-sustained flaming.

Flame heat flux measurements were recorded at four heights ($z =$ 20, 50, 100, and 140 cm) during SIS Wire Test R2. These measurements are plotted as a function of time in Fig. 62. As seen here, measured flame heat flux — absolute value and flame extension length (i.e., height, z, at which elevated heat fluxes are measured) — is only slightly greater than that measured in response to application of the propane burner against an inert wall.

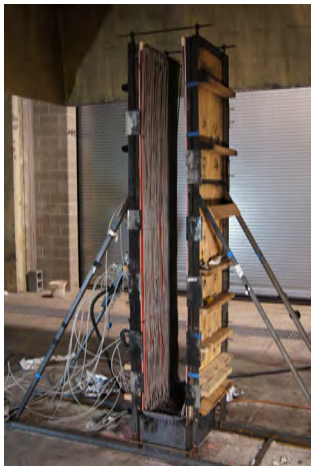

(a) Distribution of SIS Wire across the left panel wall in Test R2

(b) Peak HRR, $\dot{Q} = 142$ kW

(c) Burnout at base of panels after 25 minute burner exposure

Fig. 60. Fire behavior of SIS Wire during parallel panel experiments.

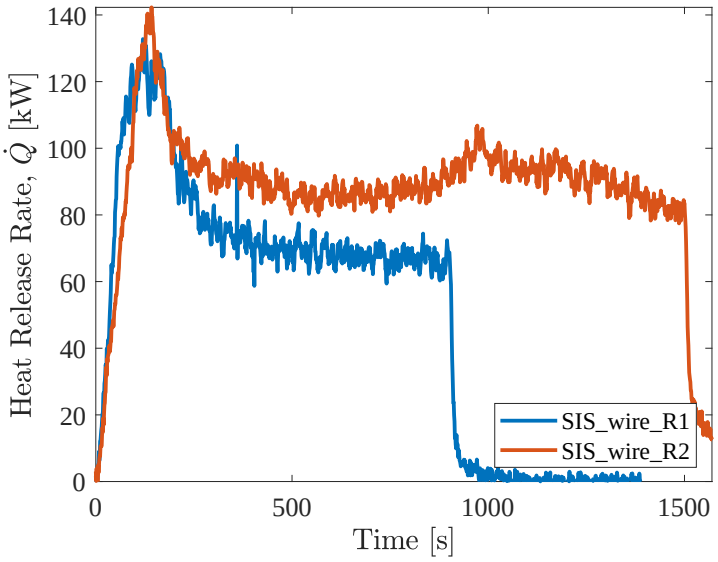

Fig. 61. Measured heat release rate of SIS Wire burning in parallel panel configuration.

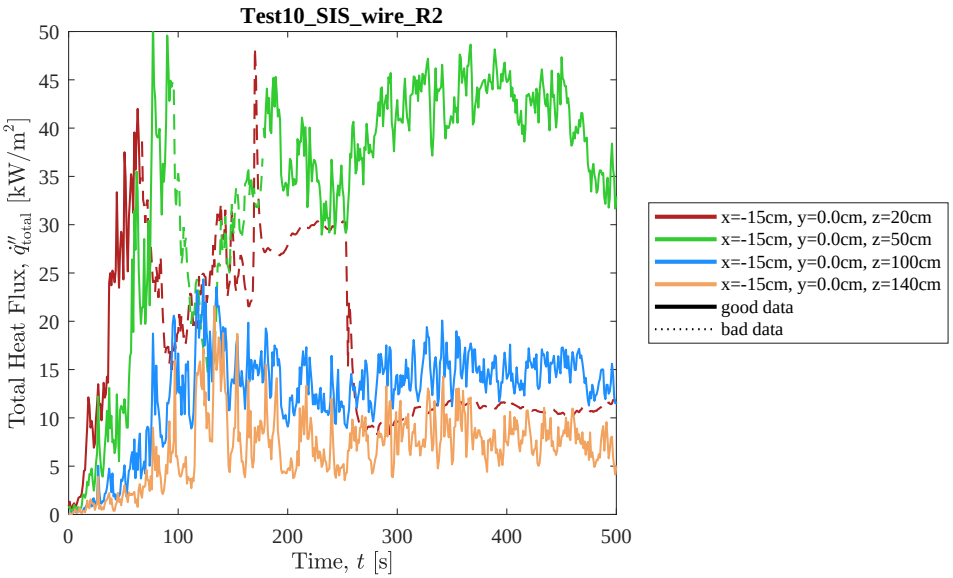

Fig. 62. Total wall flame heat flux measured at the centerline, $y = 0$, and across the height, z, of GPO-3 panels covered with 96 vertically-oriented strands of SIS Wire.

3.1.14. Western Red Cedar

Four parallel panel experiments were conducted on Western Red Cedar. Although the moisture content of Western Red Cedar panels was not measured prior to testing, the panels were stored (for a minimum of 7 days in a room) that maintained an average humidity of 25 %. In Test R1, multiple attempts were made to turn off the burner when flame tips were observed above $z = 2.0$ m; however, sustained flaming of samples was not maintained after the burner was turned off. Thus, for the remainder of test R1 ($t > 220$ s), and throughout the duration of Tests R2, R3, and R4, the burner was continuously supplied with propane. Likely, the inability of this material to sustain flaming in this test configuration without an external heat source arises, at least in part, due to the char layer that forms at the sample's front surface during burning. This char layer is thermally stable and can act as an insulator, thus decreasing the net heat transfer (from the flame above) available for pyrolysis of the virgin wood below. Images of typical fire behavior in these tests are shown in Fig. 63. As seen here, the front surface of Western Red Cedar samples quickly blackened and charred after burner exposure; however, as seen in Fig. 63d, in tests R2, R3, and R4, although surface charring was observed (especially near the propane burner), samples remained fully intact[28] throughout the duration of experiments (approximately 400 s to 600 s). However, in Test R1, when panel walls were exposed to the burner for more than 1200 s, sustained smoldering combustion (i.e., glowing) *was* observed across the lower half of samples (i.e., near the flames of the propane burner) after the burner was turned off.

Figure 64 plots time-resolved HRR measurements from each of these experiments. In all tests, when the burner was continuously kept on (i.e., Tests R2, R3, and R4), burning behavior (i.e., fire growth rate, time to peak HRR, and decay behavior) was highly repeatable: flames spread readily across the full height of the panels, but fire growth was short lived and fires remained relatively small (in these three tests, an average peak HRR of approximately 370 kW was measured between 90 s and 120 s after burner ignition). After this peak HRR was measured, fires quickly decreased in size to approximately 150 kW (including the contribution from the 63 kW propane burner). In these three tests, the burner was turned off before a second increase in HRR was observed because fires were no longer growing and continued heating appeared to risk damage to the heat flux gauges embedded in each sample[29].

[28] The relatively slow charring behavior of Western Red Cedar (i.e., prior to $t = 600$ s, limited cracking of the char layer was observed and thus detachment, falloff, and/or burnout of charred sample remnants did not occur; additionally, after the burner was turned off, self-sustained smoldering combustion at the sample's surface was not achieved) differs from that of OSB samples, which readilly showed signs of cracking and glowing combustion across their surface much earlier in experiments (see Sec. 3.1.7).

[29] Unlike most of the other materials tested in this work, which were wide enough to cover the full surface of each parallel panel wall, Western Red Cedar was obtained in the form of 2.5 m long, 0.28 m wide planks (approximately 0.021 m thick) that were attached side by side (two each, centered on either panel wall). A crack could form and widen during prolonged burning along the centerline of these two planks, exposing heat flux gauges positioned across the height of the sample at $y = 0$ cm).

(a) Ignition

(b) Peak HRR, $\dot{Q} = 322$ kW

(c) Charring at the front surface of samples (top) and continued flaming (bottom, near burner) at time, $t = 160$ s after ignition

(d) Extinction shortly after burner shutoff: charring at the front surface of samples and smoldering combustion near the burner

Fig. 63. Fire behavior of Western Red Cedar panels during parallel panel experiments.

For test R1, in which Red Cedar samples were exposed to the propane burner for twice as long, a gradual (but small; i.e., $< 10\,\%$) increase in HRR was measured between $t = 600$ s and $t = 1200$ s. During this time, the panels continued heating in-depth, and cracks in the char layer developed across the lower half of the panel walls. In this test, continued smoldering (glowing combustion) and local flaming was observed after the burner was turned off until samples were finally extinguished by application of water (hose stream).[30]

Although flames quickly spread across the front surface of the samples, the peak HRR was relatively low compared to other materials tested. The average rate of increase in the HRR for Test R2, R3, and R4, starting from the time the fire reached 63 kW and ending at its peak, is 1.8 kW/s, approximately 10 % of the growth rate of PMMA and half that of OSB.

Figure 65 plots the average value of total wall flame heat flux, $\dot{q}''_{\text{total}}$, measured at the centerline of panels ($y = 0$) at heights 0.1 m $\leq z \leq 2.2$ m during repeated parallel panel

[30] The behavior of Western Red Cedar panels after extended exposure to the propane burner — i.e., cracking of the char layer, increased HRR later in experiments, and sustained glowing combustion near the base of panel walls after burner shutoff — is similar to that observed at earlier times in tests on OSB samples (see Sec. 3.1.7).

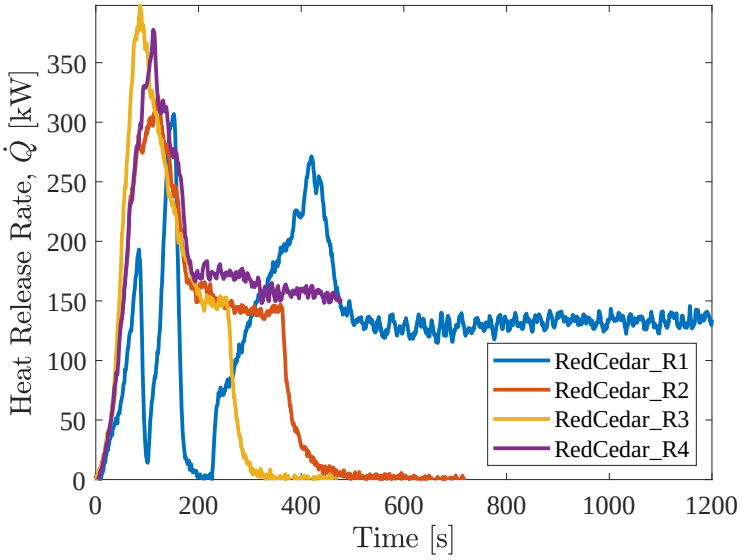

Fig. 64. Measured heat release rate during parallel panel experiments on Western Red Cedar.

experiments on Western Red Cedar. After continuous flaming was observed across each gauge location, $\dot{q}''_{\text{total}}$ maintains a fairly steady value between approximately 70 kWm^{-2} (at $z > 75$ cm) and 80 kWm^{-2} (at lower heights, where the panel walls are continuously exposed to the propane burner flames). Similarly as in tests on OSB (the other wood-based material tested in this work), after continuous flaming is observed over each gauge and *while* HRR continues to increase at the start of the test, $\dot{q}''_{\text{total}}$ can increase by 10 % to 15 % (potentially due to increasing reradiation from the opposite panel wall). For Western Red Cedar samples, this increase is only measured near the base of the sample (i.e., near the flames of the propane burner, where sample charring is most pronounced); however, for OSB, $\dot{q}''_{\text{total}}$ increases at all heights. Similarly, distinct differences in smoldering behavior were observed at each sample's surface. In tests on OSB, after flames spread to the top of the assembly, char cracking and glowing combustion (i.e., smoldering) is observed across the full surface of panels (see Fig. 40d); however, in tests on Western Red Cedar, panels remain mostly black (no evidence of smoldering) above $z > 1.2$ m, with glowing combustion only observed across parts of the sample that were continuously exposed to the propane burner flames (see Figs. 63c and 63d). For both materials, the flames spreading on either panel wall remained separate (i.e., they did not merge in the volume between the panels) throughout the duration of tests while $\dot{Q} < 650$ kW.

Measurements of radiation heat flux were obtained at $z = 0.5$ m and 1.0 m (in Test R3) in order to calculate the fraction of total wall heat flux attributed to radiation (i.e., $q_{\text{rad}}(\%) = \frac{\dot{q}''_{\text{rad}}}{\dot{q}''_{\text{total}}}$). These results are presented in detail (along with similar radiation measurements obtained for five other materials) in Sec. 3.3.

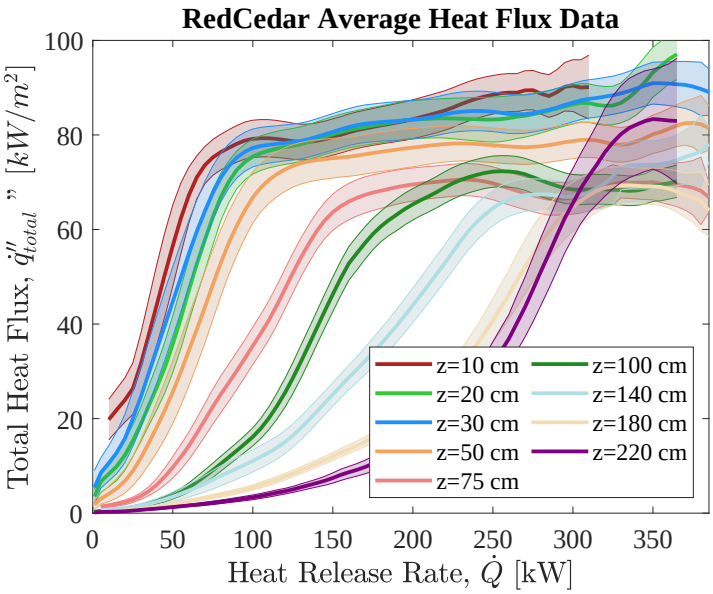

Fig. 65. Total wall flame heat flux measured at the centerline, $y = 0$, and across the height, z, of panels during repeated experiments on Western Red Cedar. The shaded area around each curve represents the expanded uncertainty of the heat flux measurements (U_c; 95% confidence interval, coverage factor = 2), as described in Appendix B.2.

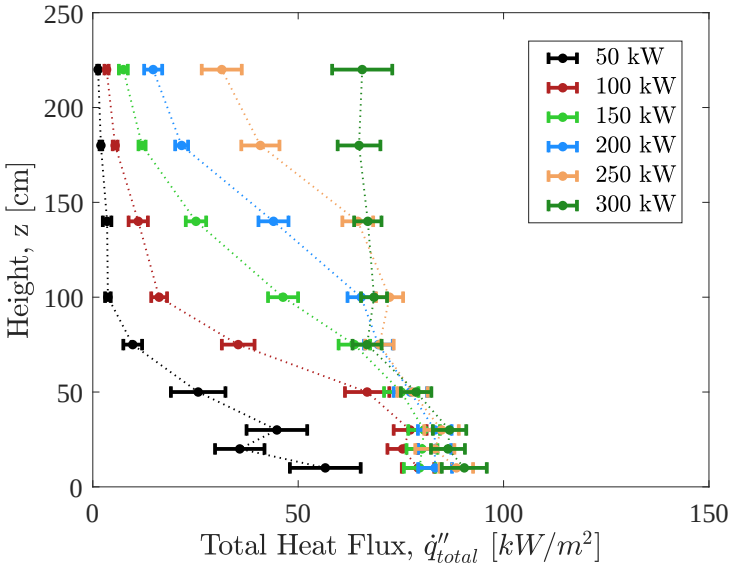

Fig. 66. Height-resolved measurements of total wall flame heat flux measured at the centerline, $y = 0$, of panels during repeated experiments on Western Red Cedar. Error bars indicate expanded uncertainty of the heat flux measurements (U_c; 95% confidence interval, coverage factor = 2), as described in Appendix B.2.

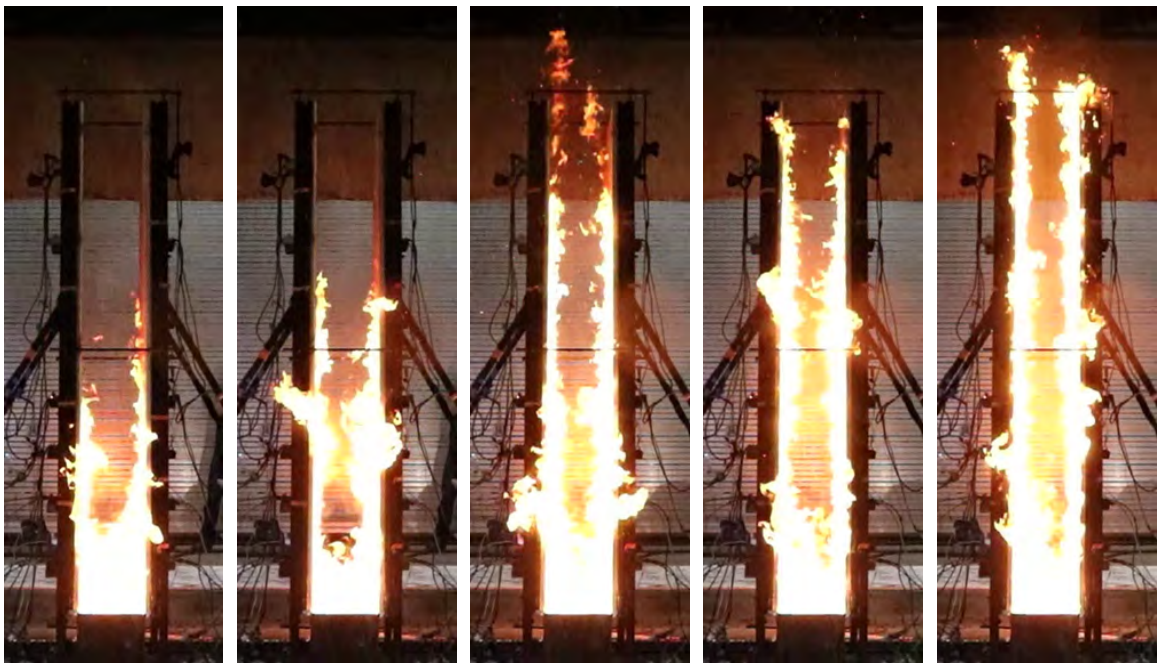

(a) $\dot{Q} = 100$ kW **(b)** $\dot{Q} = 150$ kW **(c)** $\dot{Q} = 200$ kW **(d)** $\dot{Q} = 250$ kW **(e)** $\dot{Q} = 300$ kW

Fig. 67. Representative images of flame structure during the early stages of fire growth due to upward flame spread over Western Red Cedar panels. Corresponding height-resolved flame heat feedback profiles are plotted in Fig. 66.

3.1.15. XLPE, cross-linked polyethylene foam

Eight total tests were conducted on (nominally) the same XLPE foam of the same initial thicknesses with three different densities: 2 lb/ft^3, 4 lb/ft^3, and 6 lb/ft^3 (i.e., 2.57×10^{-2} kg m^{-3}, 5.14×10^{-2} kg m^{-3} and 7.71×10^{-2} kg m^{-3}). In the figures, tables, and text below, these three materials are referred to as XLPE2, XLPE4, and XLPE6, respectively. XLPE panels were held in place by lengths of 12 gauge steel wire that were stretched horizontally across the front surface of panels (from $y = -15$ cm to $y = 15$ cm), pushed through the panels themselves, and connected at the back side of the assembly; six such connections were made at various heights, 0.4 m$\leq z \leq$2.2 m. Samples were also held in place by a series of long, flat steel clamps that attached along the edges of the parallel panel assembly. Flame heat flux measurements were not recorded during experiments during XLPE foam tests.

For each thickness of XLPE tested in this work, sample ignition was achieved by approximately $t = 30$ s (as evidenced by self-sustained wall flames spreading beyond $z = 1.0$ m on each panel wall) at which point, the propane burner was turned off and then covered with a steel shield (to protect it from flaming portions of XLPE panels that would drip/fall down towards the end of tests). Following ignition, flames spread rapidly over XLPE panels, which were allowed to burn out until complete extinction leaving little solid residue behind. Figure 68 plots a series of representative images depicting fire growth during Test R2 on XLPE4. Note: just 11 s separates Figs. 68a and 68d in which measured HRR increases from 250 kW to 2000 kW.

Figure 69 plots time-resolved HRR measurements from all parallel panel tests conducted on XLPE foam. As seen here, fire development (i.e., time to ignition, fire growth rate, and peak fire size) was highly repeatable, except in test XLPE2 R1, which showed delayed fire growth (though similar peak fire growth rate and peak fire size as compared to other test repetitions on this material). As seen in Fig. 70, which shows representative burner flame structure during these two tests, the delayed fire growth in test XLPE2 R1 may arise due to non-uniformity (from wall to wall) of the burner flame (see related discussion in Sec. 2.4). Additionally, Test XLPE2 R2 was the only test on XLPE foam in which the burner was not covered by a steel shield after sample ignition (see Table 5); the application of this burner shield was observed to immediately decrease the thickness of wall flames near the base of samples and to reduce overall fire size.

Time-resolved measurements of HRR are smooth and continuous for all tests on XLPE2 because these samples remained attached to the panel walls (until complete burnout) throughout the duration of burning. However, shortly after peak HRR was observed in tests on XLPE4 and XLPE6, but prior to complete burnout, small sections of the panels were observed to detach from the wall and to continue burning at the base of the assembly. As seen in Fig. 69c, sudden increases or decreases in HRR could be measured when this detachment occurred; this behavior was more pronounced for the higher density XLPE6 samples. For XLPE4, the initial rise in HRR measured at ignition ($t = 35$ s) in Test R1 was notably larger than that measured in Tests R2 and R3, potentially due to the additional time needed before the burner could be safely shielded (see Table 5).

Table 5. Timing of burner shutoff (propane flow) and shield application in XLPE foam tests

Test	Burner off	Shield On
XLPE2 R1	$t = 41$ s	$t = 67$ s
XLPE2 R2	$t = 41$ s	No Shield
XLPE4 R1	$t = 40$ s	$t = 41$ s
XLPE4 R2	$t = 35$ s	$t = 36$ s
XLPE4 R3	$t = 36$ s	$t = 38$ s
XLPE6 R1	$t = 41$ s	$t = 51$ s
XLPE6 R2	$t = 41$ s	$t = 50$ s
XLPE6 R3	$t = 40$ s	$t = 48$ s

For each test on XLPE foam, peak HRRs between 2.8 MW to 4.2 MW were measured approximately 30 s to 40 s after the burner was turned off. No systematic sensitivity to sample density was observed in peak HRR or time to peak HRR measured in each of these XLPE tests. It is possible that trends (with respect to sample density) in peak HRR and the time at which it was observed are occluded due to detachment of sections of XLPE4 and XLPE6 samples from the panel walls (see Fig2. 69b and 69c). Both average fire growth rate[31], $\overline{\frac{d\dot{Q}}{dt}}$, and total heat release[32] increased monotonically with sample density. The calculated average fire growth rates (126 kW s$^{-1} \leq \overline{\frac{d\dot{Q}}{dt}} \leq 184$ kW s^{-1}) for XLPE foam samples were the highest measured of all materials tested in this work. On average, in the parallel panel configuration tested here, $\overline{\frac{d\dot{Q}}{dt}}$ was approximately 11.0x higher for XLPE foam as compared to solid PMMA slabs. The heat of combustion measured during parallel panel tests on XLPE foam showed no statistically significant dependence on sample density, averaging 38.2 kJ g^{-1} across all 8 tests.

[31]Measured $\overline{\frac{d\dot{Q}}{dt}}$ (average value between repeated tests) increased with sample density from 127 kW s^{-1}, to 168 kW s^{-1}, and to 184 kW s^{-1} for XLPE2, XLPE4, and XLPE6, respectively.

[32]Measured total heat release (THR, average value between repeated tests) increased with sample density from 103 MJ, to 178 MW, and to 286 MW for XLPE2, XLPE4, and XLPE6, respectively.

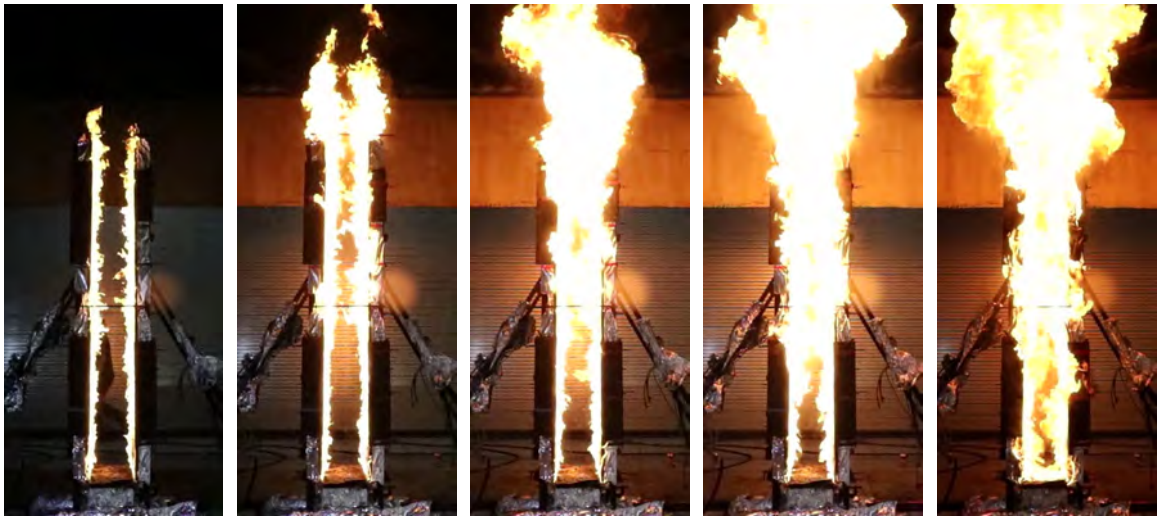

(a) $\dot{Q} = 250$ kW, $t = 50$ s | **(b)** $\dot{Q} = 500$ kW, $t = 53$ s | **(c)** $\dot{Q} = 1000$ kW, $t = 56$ s | **(d)** $\dot{Q} = 2000$ kW, $t = 61$ s | **(e)** $\dot{Q} = 2875$ kW, $t = 75$ s

Fig. 68. Representative images of flame structure during rapid fire growth over XLPE4 panels.

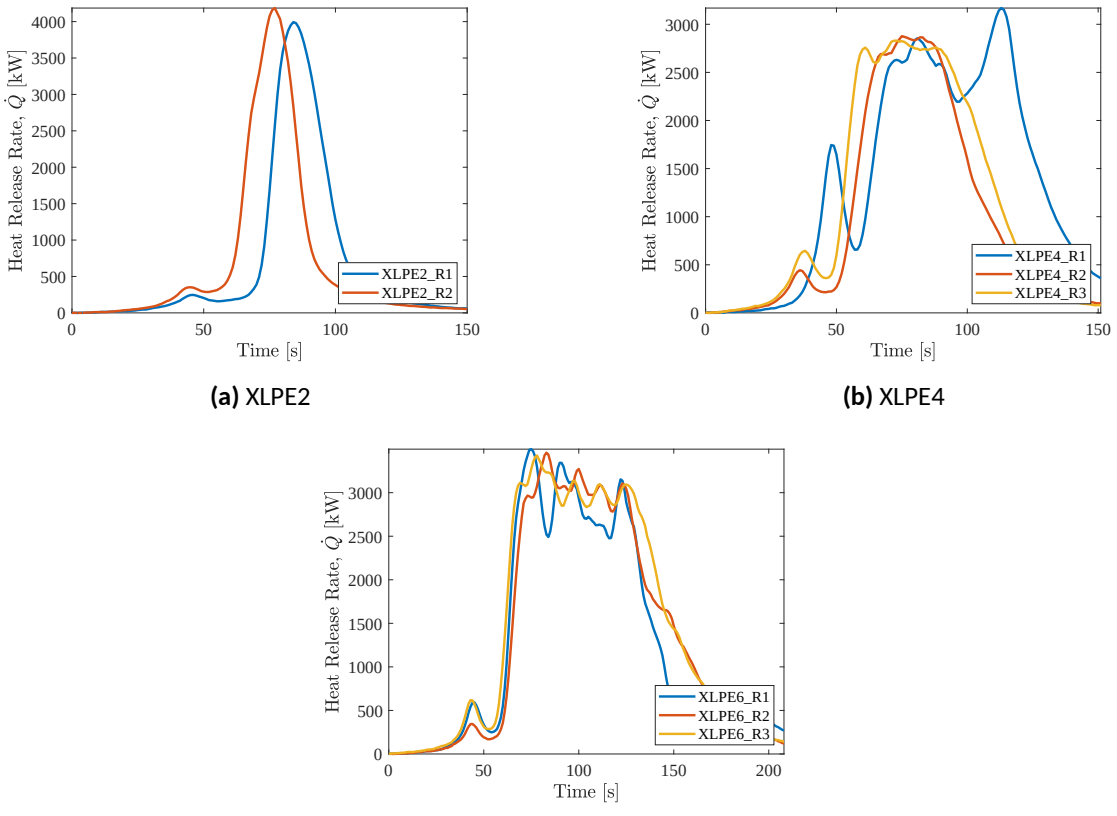

(a) XLPE2

(b) XLPE4

(c) XLPE6

Fig. 69. Measured heat release rate of polyiso slabs burning in parallel panel configuration.

(a) Test XLPE2_R1 showing preferential flame attachment to the right wall ($x = 15$ cm)

(b) Test XLPE2_R2 showing uniform flame attachment to both panel walls

Fig. 70. Burner flame structure at $t = 16$ s (i.e., as samples begin to ignite) in XLPE2 tests. Non-uniform burner flame structure in Test XLPE2 R1 (left) may have contributed to the delayed rise in measured HRR (see Fig. 69).

3.1.16. XPS, extruded polystyrene foam

Twelve total tests were conducted on XPS panels that were produced by two different manufacturers (see Table 1) in two different colors (green or pink). It is not expected that the color of these samples would significantly affect material flammibility response; rather, these two samples were considered to explore the variability in burning behavior of different samples of nominally the same material (obtained from two different sources). Both green and pink panels were tested in two different initial thicknesses: 25 and 51 mm (nominally 1.0, and 2.0 in. thick). In the figures, tables, and text below, tests on these two materials are therefore referred to by sample color and thickness (e.g., XPSgreen1 or XPSpink2). XPS panels were held in place by lengths of 12 gauge steel wire that were stretched horizontally across the front surface of panels (from $y = -15$ cm to $y = 15$ cm), pushed through the panels themselves, and connected at the back side of the assembly; six such connections were made at various heights, 0.4 m$\leq z \leq$2.2 m. For samples of all thicknesses, a horizontal strip of this same wire was also wrapped around the entire front surface of samples and affixed to the back of the panel at up to four heights between $z = 0.25$ m and $z = 2.2$ m. Flame heat flux measurements were not recorded during experiments during tests on XPS foam.

For each thickness of XPS foam tested in this work, sample ignition was achieved by approximately $t = 25$ s (as evidenced by notable soot production and the presence of wall flames extending up to approximately $z = 0.75$ m). Following ignition, the propane burner was kept on and flames spread rapidly over both XPS panels. Images of typical fire behavior in these tests are shown in Fig. 71; as seen here, XPS samples produced a significant amount of soot while burning. Peak burning was observed for each test between $t = 60$ s and $t = 80$ s, at which point flaming sections of panels were observed to detach from the wall and fall to the base of the panel assembly where they continued burning. After approximately $t = 120$ s to $t = 150$ s, complete burnout was observed along the walls and flaming was only observed on parts of the sample that had detached and fallen down from the panel walls. This drip pool was allowed to burn until complete extinction, leaving little solid residue behind; flame extinction occurred shortly after the propane burner was turned off (typically at $t = 600$ s).

Figure 72 plots time-resolved HRR measurements from all parallel panel tests conducted on XPS foam. As seen here, all tests (except for Test XPSgreen1 R3) demonstrated rapid fire growth and qualitatively similar time-resolved HRR profiles; however, measured time to ignition (and the onset of rapid fire growth) was not as repeatable in XLPE foam tests as that observed in tests on other materials. Specifically, although the maximum rate of rise of HRR was fairly similar between repeated tests, time to peak HRR and, especially for thinner samples, peak HRR showed notable variations. A careful analysis of test notes, pictures, and video indicated that these variations could primarily be attributed variations in ignition conditions and sample burnout/meltflow (especially for thinner samples).

To account for variations in sample ignition behavior, Figs. 72c and 72d plot time-resolved HRR measured in XPS foam tests with a time shift such that fire growth in repeated experiments is compared beginning at the same fire size, $\dot{Q} = 130$ kW, after sample ignition.

(a) $\dot{Q} = 75$ kW

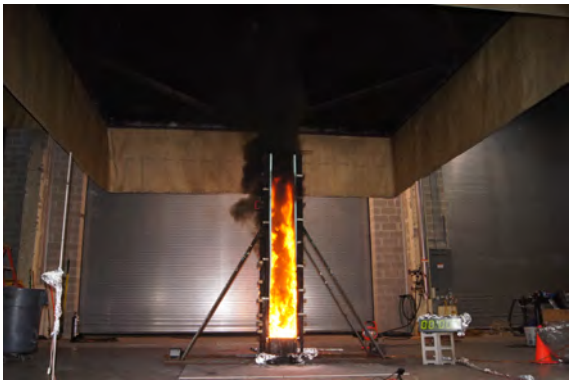

(b) $\dot{Q} = 250$ kW

(c) $\dot{Q} = 1500$ kW

Fig. 71. Representative images of flame structure during the early stages of fire growth due to upward flame spread over XPS foam panels.

That is, in these two plots, a new time scale is defined as $t - t_{130\ \mathrm{kW}}$, where $t_{130\ \mathrm{kW}}$ is uniquely determined in each test as the first time at which measured heat release rate exceeded $\dot{Q} = 130$ kW. This fire size was selected as it is approximately twice the HRR of the propane burner at steady state[33] and, at this HRR, flame tips still extend to just the midpoint (1.4 m$\leq z \leq 1.5$ m) of the panel walls.

For 2 in. thick samples of XPS foam, application of this time-shift greatly improves reproducibility in the HRR profiles measured in repeated experiments (see Fig. 72d). Specifically, without this time shift, measured time to peak HRR varies within a $\pm$19 s for green foam tests and a $\pm$6 s window for pink foam tests; however, with this time shift, time to peak HRR ($t - t_{130\ \mathrm{kW}}$) varies with $\pm$2 s for both foams. This result suggests that measured variations in fire growth rate during these tests on XPS foams are less likely due to variations in material composition and/or thermophysical properties and more strongly affected by initial test conditions[34]. This further highlights the extreme sensitivity of flame spread and fire growth rate over these foams to even minor changes in ignition conditions. Note: with this time shift, peak HRR is repeatedly measured several seconds later in tests on XPSgreen versus XPSpink.

For 1 in. thick samples of XPS foam, application of this time-shift improves the reproducibility of apparent fire growth rate and time to peak HRR measured in XPSpink1 tests; however, significant deviations are still observed in XPSgreen1 tests, especially Test XPSgreen1_R3 (see Fig. 72c). It is believed that this is a result of deformation (i.e., shrinking/collapse) of XPS foams when heated. During all tests on XPS foam, it was observed that the sample would collapse (i.e., shrink away, in the x-direction) where exposed to the burner. For thicker samples, ignition could still occur because enough material remained to burn in place while the front surface of the panels heated and collapsed; however, for thinner samples, this shrinkage effectively allowed the foam to recede away from the burner without igniting. In some cases, this would just lead to delayed fire growth or reduced peak HRR as burnout (or melting/collapse) was observed towards the base of the panels prior to full involvement and burning of the top of the sample. However, in Test R3 on XPSgreen1, the sample fully collapsed (shrank, melted, detached from the sample wall, and/or burned away) below $z < 1.2$ m and did not support flame attachment or burning farther downstream (i.e., at higher heights, z). At the start of XPSgreen1 Test R3, it was observed that foam panels were notably thinner (18.3 mm to 18.6 mm) than their nominal, average thickness (25 mm).

Comparing the two XPS foam types (i.e., XPSgreen vs. XPSpink) and thicknesses tested here, the following observations can be made. First, peak HRR does not show a statistically significant dependence on foam type when both panels burn to completion in this config-

[33] Note: HRR measurements shown in Fig. 72a are not corrected for the HRR of the propane burner, which was left on throughout the duration of experiments.

[34] The rapid fire growth observed in Test XPSgreen2 R1 (nearly 20 s shift in peak HRR, as compared to Tests R2 and R3) may have resulted from early ignition of the back edge (i.e., $y = 30$ cm) of the left panel wall. In this test, when ignition was finally observed across the base of the panel walls (i.e., when $t = 0$ was defined during the experiment), flames were already observed up to z =25 cm along this back edge of the left wall (flame attachment at this location was first observed at $t = -3$ s).

uration. However, on average, peak HRR increases with sample thickness from 1.11 MW for 1 in. thick samples to 1.67 MW for 2 in. thick samples (neglecting tests R2 and R3 on XPSgreen1, due to sample collapse and resulting limited fire growth). At both thicknesses, time to peak HRR was slightly shorter in tests on XPSpink versus those conducted on XPS-green. Neglecting the results from tests R2 and R3 on XPSgreen1, average fire growth rate was fairly similar [35] for both types and thicknesses of XPS foam, averaging 44.1 kW s^{-1}. The calculated average fire growth rate for XPS foam was slightly higher than that supported by solid HIPS samples ($\overline{\frac{d\dot{Q}}{dt}}$ averaged 38.2 kW s^{-1}); this is approximately 3.0x greater than the average fire growth rate supported by PMMA panels.

[35] Calculated $\overline{\frac{d\dot{Q}}{dt}}$ is slightly lower for XPSgreen samples, but this difference is not statistically significant.

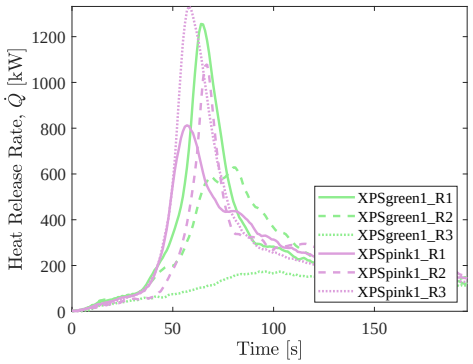

(a) 1 in. (25 mm) thick samples

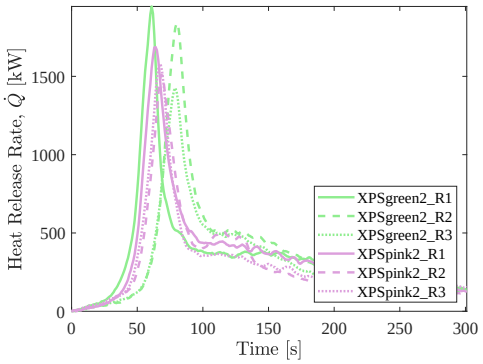

(b) 2 in. (51 mm) thick samples

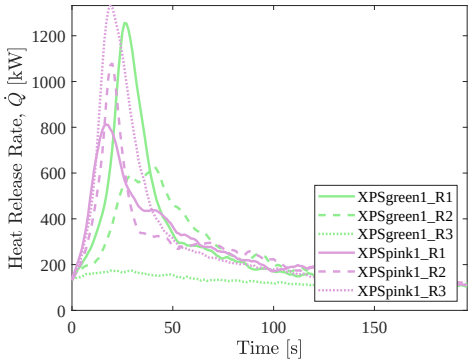

(c) 1 in. (25 mm) thick samples, time shifted

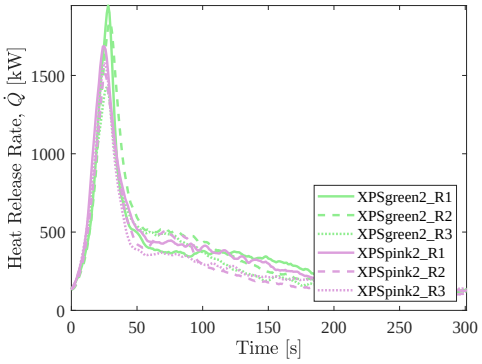

(d) 2 in. (51 mm) thick samples, time shifted

Fig. 72. Measured heat release rate of XPS foam slabs burning in parallel panel configuration. Note: in plots (a) and (b), HRR is plotted as measured, as a function of time after burner ignition; in plots (c) and (d), HRR is time-shifted, such that time $t = 0$ corresponds to the first time in the experiments when measured HRR equaled or exceeded 130 kW.

3.2. Scaling of Flame Heat Flux Data During Fully-Involved Burning

In the previous section, similarity was observed in measured flame heat feedback profiles across the full length of the panel walls when continuous flaming was observed (that is, for each material, it appeared that measured flame heat flux could be expressed as a simple function of HRR and height above the burner: $q^{''} = f(z, \dot{Q})$). As seen in Fig. 73, we identified a means to collapse/scale this data accordingly and so we have provided several representative plots of flame heat flux (measured at all locations, times, and HRRs when steady flaming was observed) versus a normalized length scale ($f(z, \dot{Q}) = (c_1 + c_2 * \dot{Q} * z + (c_3 + c_4 * \dot{Q})$).

Table 6. Tabulated values of constants used to scale flame heat flux data (c_1, c_2, c_3, and c_4) as $f(\dot{Q}, z)$ = q''_{total} (see Fig. 73).

Material	c_1	c_2	c_3	c_4
ABS	6.4E-5	0.4353	0.0117	34.2538
HIPS	1.6E-5	0.3434	0.0133	32.0329
PMMA	5.1E-5	0.1199	0.0085	39.5806

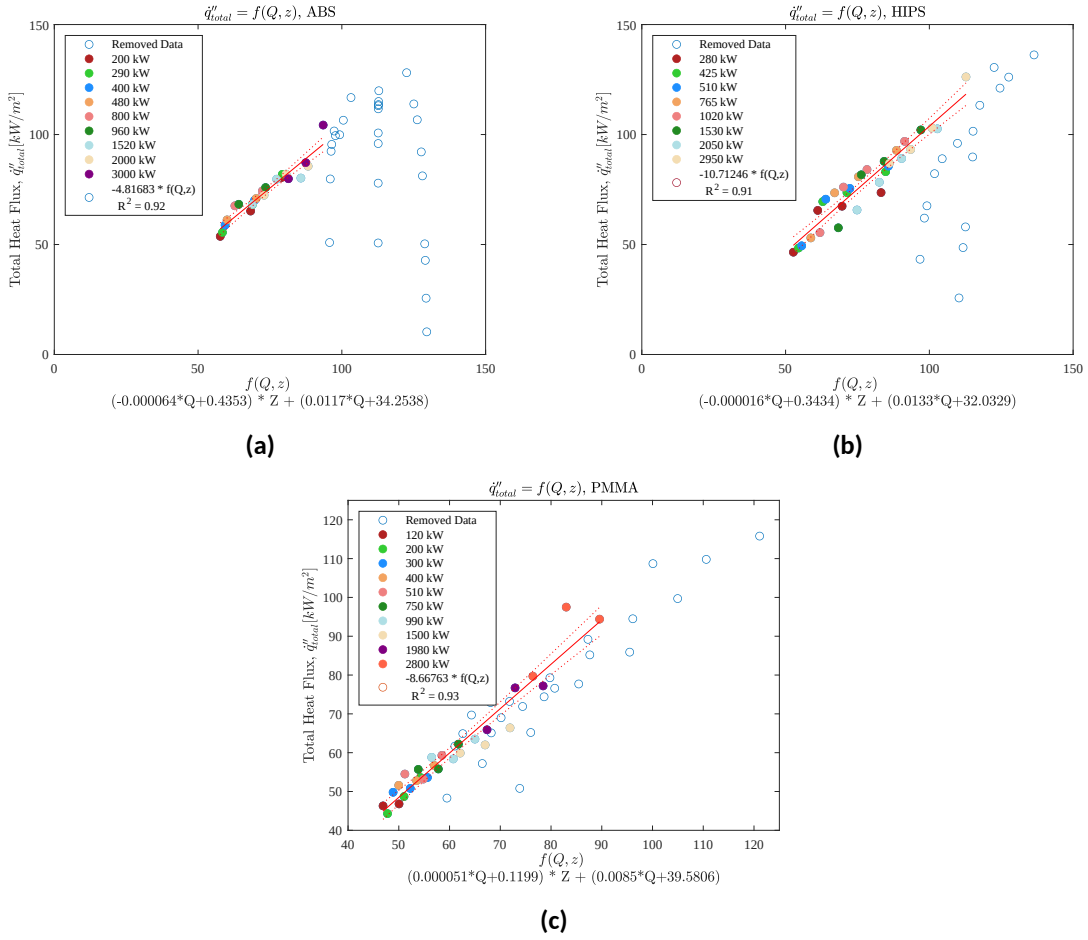

Fig. 73. Heat flux data taken while the materials have full flame coverage; collapsed into a single fit as a function of both heat release rate and height on the panel. Open circles represent flame heat flux measurements at $z > z_f$ (i.e., downstream of the continuous flaming region). Constants (c_1, c_2, c_3, *and* c_4) are shown in Table 6 for each material.

3.3. Radiative Fraction of Total Wall Flame Heat Flux, $q_{\text{rad}}(\%)$

The fraction of total wall flame heat flux attributed to radiation ($q_{\text{rad}}(\%) = \dot{q}''_{\text{rad}}/\dot{q}''_{\text{total}}$) was determined by measuring $\dot{q}''_{\text{rad}}$ and $\dot{q}''_{\text{total}}$ with a pair of water-cooled Schmidt-Boelter heat flux gauges, one fitted with a ZnSe window for the radiative component only, 7.5 cm from the centerline. These measurements were made at up to four heights, $z = 0.50$ m, 1.0 m, 1.8 m, and 2.2 m. To protect both gauge's front surfaces from deposits, they were shielded during the initial stages of experiments by small, custom fitted pieces of insulation (see Fig. 5). Once steady flaming conditions were observed across the surface of both gauges, the shields were removed by pulling a wire connected to the spring-loaded tension rods holding them in place (see Fig. 74), and a "clean gauge" measurement of heat flux was recorded. In separate tests, shields were removed at different times based on the time needed for continuous flaming to be observed across the panel wall at the gauge location of interest; at the same height, shields were always removed simultaneously to expose both the total heat flux gauge and the radiometer to flames at the same time. Calibration, setup, and use of these two heat flux gauges is discussed in detail in Sec. 2.3.3 of this report.

Fig. 74. Senior Technician Laurean DeLauter safely removes shields from heat flux gauges to enable measurements of flame-to-surface radiation heat flux during Test ABS R3.

Figure 75 plots time-resolved measurements of $\dot{q}''_{\text{rad}}$ and $\dot{q}''_{\text{total}}$ recorded by two pairs of shielded heat flux gauges positioned at $z =$ 1.0 m and $z =$ 1.8 m during Test OSB R2. A rapid increase in measured heat flux was observed when the gauge shields were removed

at $t = 180$ s. Similar rapid increases in heat flux were observed whenever the shields were removed successfully[36].

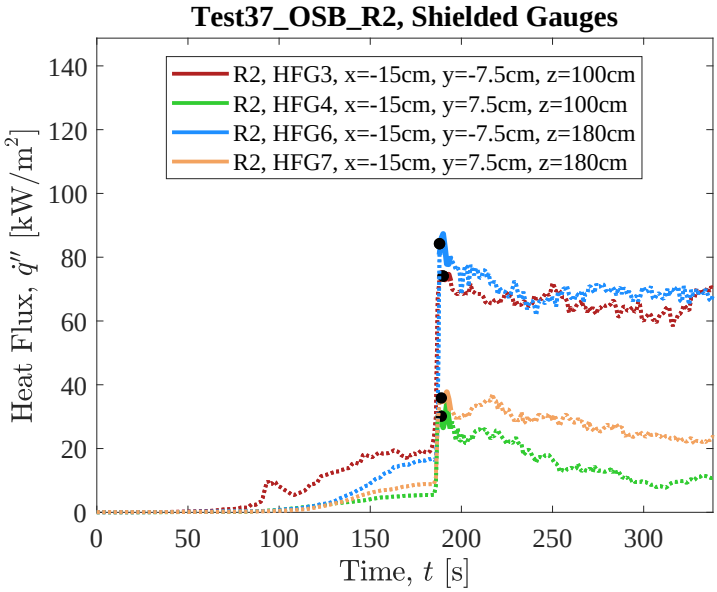

Fig. 75. Measured total and radiation heat flux at $z = 1.0$ m and $z = 1.8$ m during Test OSB R2.

In a few experiments, $\dot{q}''_{\text{total}}$ increased after shield removal when flames continued to grow (e.g., growing thicker or taller if and when fire size, HRR, continued to increase) or when panel walls continued heating later in tests (e.g., due to smoldering combustion of wood-based samples or prolonged exposure and continued heating of thermally stable samples such as the glass fiber reinforcement of GPO-1). Although continuous flaming was observed across the surface of each heat flux gauge when shields were removed, in most cases measured flame heat flux, especially $\dot{q}''_{\text{rad}}$, decreased after shield removal. This could occur due to a variety of physical changes at the gauge's front surface including: soot deposition, melting or dripping of heated sections of sample that were originally above the heat flux gauge, physical deformation of the sample panel such that its front surface was no longer flush with the front surface of the gauge. In all tests, a decrease in measured $\dot{q}''_{\text{rad}}$ was consistently observed by the radiometers after shield removal for these reasons (most notably, soot deposition) and due to the gradual degradation (i.e., reduction in transmissivity) of their ZnSe windows. Consequently, given the potential for measured flame heat flux to vary after shield removal, $\dot{q}''_{\text{rad}}$ and $\dot{q}''_{\text{total}}$ are therefore reported as discrete values: specifically as the maximum average heat flux (6 s running average) recorded within 10 s

[36] In a few experiments, shields could not be simultaneously removed from both the radiometer and total heat flux gauge (e.g., if the shields shifted or became embedded into the wall due to sample melting or other deformation). In these tests, a rapid increase in measured heat flux was therefore not observed and $q_{\text{rad}}(\%)$ was not calculated from this data.

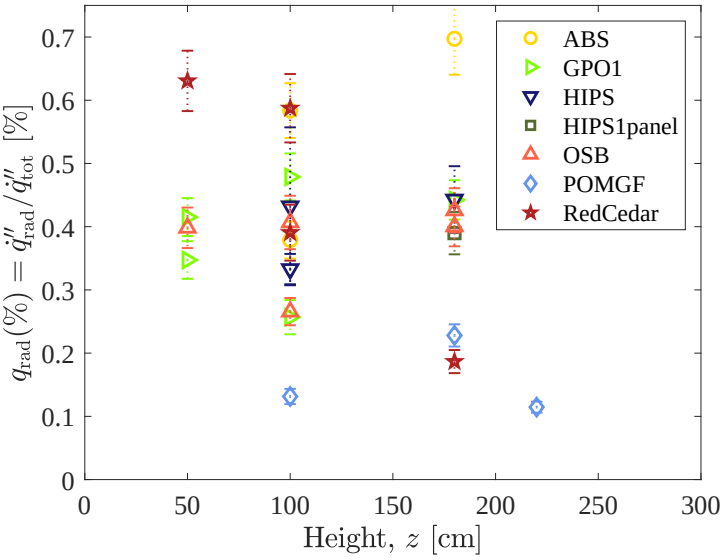

Fig. 76. Radiative fraction of total wall flame heat flux, $q_{\mathrm{rad}}(\%)$, measured at multiple heights, z, when continuous flaming was supported by six materials (ABS, GPO-1, HIPS, OSB, and POM). Error bars indicate expanded uncertainty of the heat flux measurements (U_c; 95% confidence interval, coverage factor = 2), as described in Appendix B.2.

of shield removal. This subset of measurement data used for the calculation of $\dot{q}''_{\mathrm{rad}}$ and $\dot{q}''_{\mathrm{total}}$ is highlighted as the bolded sections of heat flux measurements plotted in Fig. 75.

Table 7 lists $\dot{q}''_{\mathrm{rad}}$ and $\dot{q}''_{\mathrm{total}}$ measurements obtained shortly after shield removal in all replicate tests on ABS, GPO-1, HIPS, POM-GF, OSB, and Western Red Cedar. Included in this table are the gauge locations and measured HRR at the time of shield removal. Uncertainties reported in this table represent expanded uncertainties (95 % confidence interval), which are calculated with explicit consideration for gauge calibration uncertainty 2.28 % and fluctuations measured values during the 6 s averaging window after shield removal (mean random error due to fluctuations during testing, approximately 2.4 %). A detailed description of this uncertainty calculation is provided in Appendix B.2.

Also provided in Table 7 are calculated values of radiative fraction, $q_{\mathrm{rad}}(\%)$. To visualize potential trends in this measurement data, $q_{\mathrm{rad}}(\%)$ is plotted as function of height in Fig. 76 and as a function of HRR in Fig. 77. As seen here, $q_{\mathrm{rad}}(\%)$ shows a strong dependence on material composition but limited systematic variation as a function of measurement height or fire size.

For the least sooty of these fuels, (POM-GF, which produced a blue, nearly transparent flame; see Fig. 53) $q_{\mathrm{rad}}(\%)$ averaged just 16 %. Conversely, for ABS and HIPS (which supported large, sooty fires; see Secs. 3.1.2 and 3.1.6) $q_{\mathrm{rad}}(\%)$ averaged closer to 40 %. Note: this average does not include the two highest radiative fractions measured in ABS Test R2 ($q_{\mathrm{rad}}(\%) = 58.4$ % and 69.7 %), which were both obtained shortly after peak HRR was

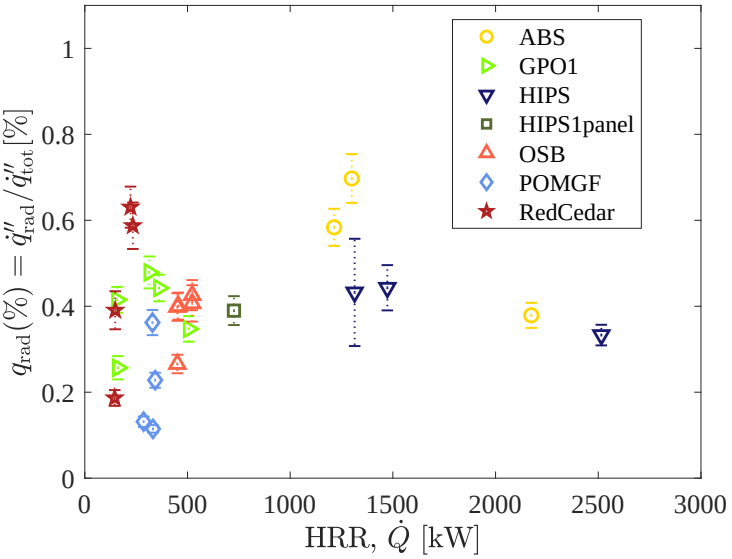

Fig. 77. Radiative fraction of total wall flame heat flux, $q_{\rm rad}(\%)$, measured at multiple HRR, $\dot{Q}$, when continuous flaming was supported by six materials (ABS, GPO-1, HIPS, OSB, POM-GF, and Western Red Cedar). Error bars indicate expanded uncertainty of the heat flux measurements (U_c; 95% confidence interval, coverage factor = 2), as described in Appendix B.2.

observed when ABS samples had completely detached from the apparatus walls (due to softening/burnout at attachment points) but continued to burn at the base of the assembly[37]. The qualitative observation of increasing radiative fraction with increasing sample sooting propensity is consistent with measured values of soot yield, $Y_{\rm soot}$, presented in Sec. 3.4; similar observations of flame radiance from plastic pool fires (including PMMA, POM, and HIPS) and gaseous wall fires of different smoke yields have been made elsewhere [107, 108].

The radiative fractions measured here, even for the highly sooty flames (presumably optically thick) produced by ABS and HIPS, are notably lower than those calculated in previous works (both for solid fuels [59, 60] and gaseous wall burners [109, 110]). These previous studies reported that heat transfer in large, turbulent wall flames is dominated by radiation

[37] In Test ABS R2, heat flux gauge shields did not remove cleanly when pulled (likely because they had become stuck to the panel walls as the material softened) and the gauges were only uncovered when the sample (and these shields) completely detached from the panel walls. At this time, a sudden increase in $\dot{q}''_{\rm rad}$ and $\dot{q}''_{\rm total}$ was measured at both $z = 100$ cm and $z = 180$ cm, HRR still exceeded 1.2 MW, and the volume between the panel walls was fully engulfed in flames. This allowed for an estimate of $q_{\rm rad}(\%)$; however, it is emphasized that the sample burning configuration at this time (flames filled the volume between the panel walls, but this fuel was formed by the pyrolysis of ABS that was burning in a pool fire configuration at the base of the assembly and the panel walls themselves were uncovered marinite insulation panels) is not the same as for all other measurements plotted in Fig. 76 (sample slabs lining each panel wall). Time resolved measurements of $\dot{q}''_{\rm rad}$ and $\dot{q}''_{\rm total}$ from Test ABS R2 are presented in Appendix C.

(75 % to 80 % of total heat transfer at heights above 75 cm to 100 cm). In these previous measurements on solid fuels, PMMA slabs up to 3.56 m tall were burned in the vertical configuration (single panel, 41 cm to 91 cm wide, with water cooled sidewalls). Total flame to wall flame heat flux was calculated by measuring local sample burning rate and material heat of vaporization and radiation heat transfer from flame to wall was estimated by means of a gray flame analysis and using measurements (from a narrow angle radiometer) of flame radiation away from the wall. Measurements of gaseous wall flames supported in a similar configuration — porous, water-cooled gas burners up to 65 cm tall, with water-cooled sidewall(s) — also calculated $\dot{q}''_{\rm rad}$ using a radiometer positioned at a distance away from the wall and either a large (65 cm by 38 cm water-cooled heat transfer plate) above the burners or highly spatially-resolved measurements of temperature across the flame sheet. It is highlighted that total heat fluxes, $\dot{q}''_{\rm total}$, measured in this work (parallel panel configuration) can be a factor of 2x to 3x greater than those reported in previous studies; this may be one factor influencing the relative difference in calculated $q_{\rm rad}(\%)$.

To assess how sample configuration affected measurements of $q_{\rm rad}(\%)$, an additional experiment was conducted on HIPS in which one of the parallel panel walls was removed. This allowed the opposite panel to burn freely without the influence of a nearby obstruction on air entrainment, flame structure, or reradiation. In Table 7, this test is listed as HIPS1Panel R1. Measurements of $\dot{q}''_{\rm rad}$, $\dot{q}''_{\rm total}$, and $q_{\rm rad}(\%)$ are relatively similar (even at a different HRR) when HIPS burned in the single wall or parallel panel configuration, as seen in Figs. 76 and 77 and in Table 7. It should be noted that the shields were removed from the gauges well after flame spread occurred across the gauge locations and flames are presumably optically thick. Therefore, it is inferred that heat flux measurements in these tests are primarily from the optically-thick and sooty flames, and not as much from re-radiation of the opposite panel.

Both high and low values of $q_{\rm rad}(\%)$ are measured in separate tests on Western Red Cedar. This variation arises primarily due to the state of the flame and glowing char oxidation in the opposite panel at the time of gauge shield removal. In Western Red Cedar Test R2, at the time of shield removal (HRR=150 kW), flame tips only intermittently covered the heat flux gauges at $z = 100$ cm and they were not present at all at $z = 180$ cm. Additionally, although the full length of the sample showed at least some signs of blackening at the time of shield removal, cracks in the char and evidence of active smoldering were only observed near the propane burner flames (i.e., below $z < 100$ cm). Consequently, in this test, reduced heat fluxes were measured by shielded gauges at both $z = 100$ cm and 180 cm. At $z = 180$ cm, the measured value of $q_{\rm rad}(\%) = 19$ % confirms that heating occurs primarily by convection (heating from the thermal plume rising above the flames). In Western Red Cedar Test R3, substantially higher values of $q_{\rm rad}(\%)$ (approximately 60 %) are measured at both $z = 50$ cm and $z = 100$ cm. At the time of shield removal in Test R3, fire size was approximately 50 % greater than that in Test R2 (i.e., HRR = 240 kW), flame tips extended up to the top of the panel walls, but only intermittent flaming was observed across each gauge location. Most importantly, both panel walls were brightly glowing due to smoldering combustion, providing significantly higher radiation from the opposite panel

wall than heat fluxes measured from the flames of any other material tests at the time of shield removal.

For OSB, $q_{\text{rad}}(\%)$ was measured at three heights (z =50 cm, 100 cm, and 180 cm) with repeat measurements taken at 100 cm and 180 cm. In each test, at the time of shield removal, HRR measured between 450 kW and 520 kW and flames covered the full length of the panel walls (flames measured approximately 8 cm to 10 cm thick on either wall). For 4 out of 5 of these measurements, $q_{\text{rad}}(\%)$ measured approximately 40 %$\pm$3 %; each of these measurements was obtained before peak HRR was measured. In OSB Test R1, shields were removed just after peak HRR and $q_{\text{rad}}(\%)$ measured 27 %; it is possible that this difference in measured radiative fraction arises due to the local variations in smoldering/glowing behavior at the surface of the developing char layer (see description in Section 3.1.7).

For GPO-1, $q_{\text{rad}}(\%)$ was measured at three heights (z = 50 cm, 100 cm, and 180 cm) with repeat measurements taken at 50 cm and 100 cm. For each of 5 of these measurements, $q_{\text{rad}}(\%)$ measured between 26 % and 48 %. No significant correlation was observed between $q_{\text{rad}}(\%)$ variations and either (a) measurement location, (b) HRR, or (c) time at which the shields were removed. It is noted, however, that individually q''_{rad} and q''_{total} do increase with gauge height, except for the measurements from a single experiment. In test R1, the shields are pulled much earlier (i.e., at a lower HRR) than in the other experiments. Since the glass fibers in this material are highly thermally stable and likely could maintain elevated temperatures above the pyrolysis temperature of the materials tested in this work, sample surface temperature (and resulting surface reradiation to the opposite wall) may have increased in all tests except for R1, where the sample has not been heated for nearly as long as the samples in the other tests.

Table 7. Tabulated values of radiative and total flame heat flux .

Test	z [m]	HRR [kW]	$\dot{q}''_{\text{rad}}$ [kW/m^2]	$\dot{q}''_{\text{total}}$ [kW/m^2]	$q_{\text{rad}}(\%)$ [%]
ABS					
ABS R2	1.0	1200	110.7 ± 2.4	189.6 ± 2.8	58 ± 4.3
ABS R3	1.0	2220	25.3 ± 2.9	66.7 ± 2.5	38 ± 2.9
ABS R2	1.8	1300	157.2 ± 2.6	225.5 ± 3.2	70 ± 5.7
GPO-1					
GPO R1	0.5	160	20.2 ± 2.5	48.7 ± 2.6	42 ± 3.0
GPO R3	0.5	510	15 ± 3.4	43.3 ± 2.6	35 ± 3.0
GPO R1	1.0	160	16.2 ± 4.6	63 ± 2.5	26 ± 2.7
GPO R2	1.0	310	29.1 ± 2.7	60.8 ± 2.8	48 ± 3.7
GPO R3	1.8	360	31.3 ± 2.4	70.7 ± 2.6	44 ± 3.1
HIPS					
HIPS R2	1.0	1300	32.1 ± 10.9	74.3 ± 9.5	43 ± 12.5
HIPS R4	1.0	2520	31 ± 2.5	93.2 ± 2.6	33 ± 2.4
HIPS R2	1.8	1470	50.1 ± 5.3	113.2 ± 2.6	44 ± 5.3
HIPS1panel R1	1.8	730	39.7 ± 2.9	101.9 ± 3.2	39 ± 3.4
OSB					
OSB R1	0.5	450	27.5 ± 2.9	69.1 ± 2.8	40 ± 3.2
OSB R1	1.0	450	19.5 ± 3.1	73.4 ± 2.7	27 ± 2.2
OSB R2	1.0	520	30.1 ± 4.5	74.1 ± 2.5	41 ± 4.2
OSB R2	1.8	520	35.9 ± 2.8	84.2 ± 3.0	43 ± 3.5
OSB R3	1.8	460	30.9 ± 3.0	77.1 ± 2.6	40 ± 3.2
POM					
POM R2	2.2	330	5.8 ± 2.6	50.8 ± 2.8	12 ± 0.9
POM R3	1.0	290	9.3 ± 2.4	70.5 ± 3.9	13 ± 1.2
POM R3	1.8	340	11.6 ± 2.7	51 ± 2.8	23 ± 1.8
Western Red Cedar					
Red Cedar, R3	0.5	220	42.4 ± 2.8	67.2 ± 2.6	63 ± 4.8
Red Cedar, R2	1.0	150	21 ± 3.2	53.7 ± 4.7	39 ± 4.4
Red Cedar, R3	1.0	230	40.2 ± 3.6	68.5 ± 2.9	59 ± 5.4
Red Cedar, R2	1.8	150	2.7 ± 2.7	14.5 ± 4.1	19 ± 1.8

3.4. Heat Release and Product Yields

Table 8 provides a summary of the heat release rate measurements. "Ignition Time" is defined here as the first time in the experiment at which the measured heat release rate exceeds the burner HRR by both 20 % and 5 kW [38].

"Heat Released" [MJ] is corrected for the presence of the propane burner by removing its contribution (i.e., subtracting the product of [average burner heat release rate] and [burner application duration]). "Peak HRR" is not corrected for contribution of the propane burner and therefore the burner may contribute to reported Peak HRR in some tests. "Growth Rate" is calculated as the average rate of increase of the HRR from just after the burner is shut off until the HRR reaches 85 % of its peak value. In cases where the burner is not shut off, the growth rate is calculated starting from the time at which the HRR is 90 kW.

"Heat of combustion" is the total energy released (kJ) per unit mass (g) of gaseous volatiles produced over the entire experiment. The mass of gaseous volatiles produced was calculated as measured total mass lost (initial minus final mass) when measurements of both the initial and final mass of the sample was available. In some cases, one or both of these values was not recorded (e.g., due to significant melt flow, difficulty completely removing sample remnants from base of the parallel panel assembly and/or the cement board at the base of this apparatus, or the inability to measure final sample mass after the test was complete due to continued production of hazardous volatiles). When sample remnants could not be cleanly or completed removed from the ground and/or the test apparatus at the end of an experiment, uncertainty in final sample mass was correspondingly increased (estimated as a Type B uncertainty).

Measured ignition time varied by a factor of up to 30, with low density materials (i.e., polymer foams) igniting and growing to peak HRR substantially faster than other materials. In general, fire growth rates were highest for these foams, but also positively correlated with peak fire size and heat of combustion; thus, for the large fires supported by highly energetic materials such as ABS, HDPE, and HIPS, the growth rate was comparable to that of some foams (e.g., each of XPS foams tests). For XLPE tests conducted on nominally the same material with three different densities (i.e., 2.57×10^{-2} kg m^{-3}, 5.14×10^{-2} kg m^{-3} and 7.71×10^{-2} kg m^{-3}), peak HRR and time to peak HRR did not demonstrate a dependence on sample density (potentially due to sample detachment prior to complete burnout, see Sec. 3.1.15); however, both the fire growth rate and total heat released monotonically increased with sample density. XLPE heat of combustion showed no statistically significant dependence on sample density, averaging 38 kJ/g across all 8 tests.

In general, the total amount of heat released increased with the heat of combustion and amount of material available (e.g., fires supported by solid HDPE samples yielded larger Total HR than low-density XLPE foams); however, clear outliers in this trend arise

[38] The second criteria (5 kW) ensured that ignition would not be mistakenly identified very early on in an experiment, as the burner's HRR was still increasing. For most tests, this ignition time (as identified by HRR measurements) coincides with the time at which sustained, uniform flaming was first observed across the base of both panel walls.

if and when sample deformation strongly impacted material burning behavior. For example, although PMMA has a lower heat of combustion than ABS or HIPS, it maintained its shape (and attachment to the panel walls) for significantly longer during these experiments, thus they had comparable amounts of energy released. Sample deformation also strongly affected fire growth rate and peak HRR in tests on polymer foams. As discussed in Section 3.1.16, XPS foam samples would rapidly shrink when exposed to the burner and, for thinner samples, this caused the foam to completely recede without igniting. In some cases, this would just lead to delayed fire growth or reduced peak HRR as burnout (or melting/collapse) was observed towards the base of the panels prior to full involvement and burning of the top of the sample; in others, the sample fully collapsed (shrank, melted, detached from the sample wall, and/or burned away) without supporting sustained flaming farther downstream.

Depending on the physical and thermal stability of the virgin material, increases in sample thickness affected burning behavior in different ways. For example, in tests on XPS foams between 25 mm and 51 mm thick (XPS foams were observed to burn to completion leaving little solid residue behind, see Sec. 3.1.16), peak HRR and growth rate both *increase* with sample thickness. However, in tests on polyiso foams between 13 mm and 51 mm thick, peak HRR and growth rate both *decrease* with increasing sample thickness (polyiso foam produced a relatively stable porous char that mostly retained its shape throughout the duration of burning; see Sec. 3.1.10).

Table 8. Tabulated values of fire size, growth rate, and energy release

Polymer	Ignition Time[A] [s]	Ignition HRR [kW]	Peak HRR [kW]	Time to Peak [min]	Growth Rate [kW/s]	Heat Released [MJ]	Heat of Combustion [kJ/g]
"Pure" Synthetic Polymers							
HDPE R1	126	74.4	2817 ± 167	5.4	26.7	284 ± 18	NM
HIPS R1	36	55.5	2955 ± 152	3.5	37.4	509 ± 29	28.3 ± 1.7
HIPS R2	33	51.7	3228 ± 166	3.4	33.0	504 ± 29	28.0 ± 1.6
HIPS R3	50	65.5	3094 ± 159	3.1	47.6	535 ± 31	28.1 ± 1.7
HIPS R4	43	64.3	3173 ± 163	3.5	34.7	513 ± 32	28.7 ± 1.9
HIPS1panel R1	43	61.9	1465 ± 76	6.2	5.9	274 ± 17	28.8 ± 1.9
PBT R1	139	74.5	2821 ± 169	5.2	56.0	375 ± 25	NM
PMMA R1	91	74.5	2540 ± 111	12.4	4.0	506 ± 24	24.4 ± 1.2
PMMA R2	83	75.5	2882 ± 125	6.6	12.1	506 ± 24	24.4 ± 1.2
PMMA R3	86	75.3	3197 ± 139	6.6	12.2	506 ± 23	24.4 ± 1.2
PMMA R4	82	74.5	3140 ± 137	7.0	15.8	504 ± 24	24.3 ± 1.2
PMMA R5	78	74.3	3166 ± 138	7.1	10.6	504 ± 24	24.3 ± 1.2
PMMA R6	58	71.2	3579 ± 156	5.4	22.1	503 ± 23	24.3 ± 1.2
PVC R1	141	75	163.2 ± 8.8	11.9	1.1	61.9 ± 9	NM
PVC R2	118	75	236 ± 12	8.9	0.1	84 ± 9.7	NM
Copolymers							
ABS R1	33	51.2	3821 ± 228	3.4	63.7	547 ± 35	29.3 ± 1.9
ABS R2	35	54.4	3538 ± 211	3.1	40.9	566 ± 36	29.7 ± 1.9
ABS R3	34	53.3	3541 ± 181	3.8	28.3	550 ± 31	28.6 ± 1.7
PMMA-PVC alloy R1	45	64.4	1060 ± 67	4.3	4.8	111 ± 11	9.6 ± 1.0
PMMA-PVC alloy R2	47	64.3	1070 ± 68	4.3	5.5	182 ± 17	10.42 ± 1.0
Porous Polymer Foams							
XLPE 2# R1	27	45	3992 ± 237	1.4	142.7	101.4 ± 6.7	37.3 ± 2.6
XLPE 2# R2	21	38.9	4186 ± 248	1.3	110.8	104.9 ± 7	37.1 ± 2.6
XLPE 4# R1	25	45.4	3169 ± 162	1.9[C]	56.9	211 ± 11	37.9 ± 2.8
XLPE 4# R2	23	73.8	2876 ± 146	1.3	134.4	149.1 ± 8.3	36.9 ± 3.3
XLPE 4# R3	18	61.6	2830 ± 144	1.2	200.7	174.4 ± 9.5	37.5 ± 3.1
XLPE 6# R1	25	42.3	3500 ± 207	1.3	196.3	278 ± 17	39.4 ± 4
XLPE 6# R2	25	43	3459 ± 205	1.4	147.2	280 ± 17	39.9 ± 2.5
XLPE 6# R3	26	75.1	3427 ± 203	1.3	208.1	304	39.7
PolyIso (0.5 in.) R1	7	26.8	1056 ± 64	0.3	153.4	18.6 ± 1.4	20.6 ± 2.5
PolyIso (0.5 in.) R2	7	26.2	997 ± 61	0.3	124.6	18.2 ± 1.4	21.1 ± 2.7
PolyIso (0.5 in.) R3	9	50	1022 ± 62	0.3	133.6	17.9 ± 1.4	18.7 ± 2.2
PolyIso (1 in.) R1	11	27.3	949 ± 58	0.4	120.0	28.6 ± 3.6	21.7 ± 2.9
PolyIso (1 in.) R2	8	31.5	974 ± 59	0.3	125.3	32 ± 3	21.9 ± 2.2
PolyIso (1 in.) R3	8	24.3	954 ± 58	0.3	141.9	31 ± 3	21.4 ± 2.2
PolyIso (2 in.) R1	9	21	784 ± 48	0.4	112.3	37.6 ± 4.8	22.1 ± 2.9
PolyIso (2 in.) R2	9	26.3	801 ± 49	0.4	111.8	38.8	21.8 ± 2.8
XPS (Green 1 in.) R1	31	74.1	1255 ± 76	1.1	38.6	54.9 ± 6.5	26.1 ± 3.2
XPS (Green 1 in.) R2	31	73.6	628 ± 39	1.4	15.1	49.1 ± 6.2	23.3 ± 3
XPS (Green 1 in.) R3	32	51	174 ± 10	1.6	2.9	22.9 ± 3.8	25.4 ± 9
XPS (Green 2 in.) R1	26	73.6	1946 ± 117	1	55.4	105 ± 10	24.5 ± 2.4
XPS (Green 2 in.) R2	9	19.1	1839 ± 95	1.3	48.0	110 ± 10	26.2 ± 3
XPS (Green 2 in.) R3	27	45.8	1426 ± 74	1.3	37.0	97.8 ± 9.1	27.5 ± 3.4

Table 8 – *Continued on next page*

Polymer	Ignition Time[A] [s]	Ignition HRR [kW]	Peak HRR [kW]	Time to Peak [min]	Growth Rate [kW/s]	Heat Released [MJ]	Heat of Combustion [kJ/g]
XPS (Pink 1 in.) R1	33	76.5	812 ± 50	1	37.8	50.4 ± 6.2	26.1 ± 3.3
XPS (Pink 1 in.) R2	25	42.4	1080 ± 65	1.1	45.6	47.1 ± 6	24.3 ± 3.2
XPS (Pink 1 in.) R3	22	39.5	1332 ± 80	1	54.1	55.3 ± 6.3	28.7 ± 3.4
XPS (Pink 2 in.) R1	22	38.4	1687 ± 101	1.1	52.1	100.6 ± 9.2	27.9 ± 2.6
XPS (Pink 2 in.) R2	22	39	1510 ± 78	1.2	39.7	84.5 ± 8.4	27.4 ± 3.7
XPS (Pink 2 in.) R3	28	72.2	1580 ± 81	1.1	43.7	93.2 ± 8.2	30.3 ± 3
Composite Materials							
GPO-1 R1	130	75	498 ± 31	9.4	1.6	235 ± 17	21.7 ± 1.7
GPO-1 R2	113	75	469 ± 29	9.7	1.4	246 ± 17	22.5 ± 1.7
GPO-1 R3	86	75	522 ± 32	6.8	3.7	232 ± 16	21.2 ± 1.6
GPO-3 R1	240	74.9	134.3 ± 9.2	12.0	0.1	43 ± 8.7	NM
GPO-3 R2	184	74.7	115 ± 8	7.1	0.2	37.8 ± 8.3	NM
GPO-3 R3	165	76.2	110 ± 7.7	7.0	0.5	36.2 ± 8	NM
POM-GF R1	19	34.4	503 ± 28	9.6	1.3	387 ± 26	15.5 ± 2
POM-GF R2	18	36.2	540 ± 29	11.1	0.8	367 ± 24	14.76 ± 0.97
POM-GF R3	22	38.8	536 ± 29	17.1	0.9	452 ± 29	14.52 ± 0.94
Other Materials							
SIS Wire R1	39	59.6	132.8 ± 9.5	1.4	1.0	16 ± 5.3	NM
SIS Wire + GPO-3 R1	63	71.6	142 ± 10	1.2	1.3	47 ± 10	NM
OSB R1	39	58.9	622 ± 38	3.7	3.1[D]	243 ± 18	14.9 ± 3.3
OSB R2	45	63.4	894 ± 54	3.5	1.8[D]	243 ± 17	14.9 ± 1.9
OSB R3	11[E]	47.4	526 ± 28	3.2	2.6	262 ± 18	16.2 ± 1.1
Western Red Cedar R1	50	66.5	307 ± 17	2.6	3.7	139 ± 14	NM
Western Red Cedar R2	27	44.5	322 ± 18	2.1	4.6	44.4 ± 4.1	11.9 ± 1.4
Western Red Cedar R3	27	44.7	398 ± 22	1.5	7.4	38.8 ± 3.2	12.5 ± 1.5
Western Red Cedar R4	29	47.7	378 ± 21	1.9	4.7	65.1 ± 5.7	12.6 ± 1.3

NM = Not Measured

[A] Ignition time is defined when measured HRR was both 5 kW and 20 % above the burner HRR

[B] Peak HRR includes contribution from burner used for sample ignition (nominally 63 kW)

[C] This peak is measured after partial sample detachment, see Fig 69

[D] Calculated based on initial rise in HRR

[E] See discussion in Sec. 3.1.7

Table 9 provides average gas species and soot yields for each of the materials tested in this work. The smoke particulate generated by the fire is measured via the light extinction of a HeNe laser beam across the center of the exhaust duct (assuming a specific extinction coefficient[75] of flame generated smoke: 8.71 $m^2/g \pm 0.47$ m^2/g). The design and implementation of this optical technique is described elsewhere [74]. Gas species and soot yields are calculated by dividing the time integral (from sample ignition to burnout) of species mass flow rate in the exhaust hood by the measured total mass loss of the fuels. These yields therefore represent the mass of species generated per unit mass of fuel consumed. Residue Yield, μ_{res}, is calculated by dividing the final mass by the initial mass of the item; this value should not necessarily be interpreted as a char yield because final mass could include glass-fiber reinforcement and/or portions of the original sample that detached from the parallel panel apparatus during the course of the experiment without burning to completion (e.g., due to melt flow, dripping, or simply separating from the wall because of burnout of the material near mounting supports).

Gaseous species yields are corrected for CO and CO_2 generation by the propane burner by assuming that propane flames burn similarly in the presence of each combustible solid vs. in open air, and subtracting the expected amount of CO and CO_2 generated during the burner application duration. For fuels with gas-phase active flame retardants (e.g., SIS Wire or chlorinated materials such as PVC and PMMA-PVC), propane combustion may not be complete, thus this correction (i.e., subtraction) may *under*estimate CO generation by the propane burner flames and thus *over*estimate the calculated CO yield of the combustible solid of interest.

For tests on GPO-3, HDPE, PBT, and SIS Wire, sample masses were not measured at the end of experiments. Total mass loss during tests on these four materials (which is needed for the calculation of combustion product yields) was therefore unknown and instead estimated by dividing measured Total Heat Release by a representative heat of combustion [111]. A representative upper-bound heat of combustion (which provides a conservative estimate of product yields) was calculated for each of these fuels on the basis of microscale combustion calorimetry experiments [73, 112]. These experiments will be presented in detail in Volume 2 of this report. Heats of complete combustion (energy release per gram fuel *burned*) measured in the MCC for each of these fuels are summarized:

- $\Delta H_{\text{c,complete}}^{\text{HDPE}} = 46.1$ kJ/g
- $\Delta H_{\text{c,complete}}^{\text{GPO}-3} = 16.9$ kJ/g
- $\Delta H_{\text{c,complete}}^{\text{PBT}} = 23.7$ kJ/g
- $\Delta H_{\text{c,complete}}^{\text{SISWire}} = 28.3$ kJ/g

Uncertainty in these heats of complete combustion (when used as surrogates to characterize large scale burning behavior in the parallel panel assembly) is estimated as 15% (type B uncertainty). This uncertainty is explicitly considered in calculations of soot and gaseous species yields for each of these four fuels.

Table 9. Tabulated values of soot, residue, and gaseous species yields

Polymer	Test #	y_{CO} [g/g]	y_{CO_2} [g/g]	y_{soot} [g/g]	μ_{res} [%]
'Pure' Synthetic Polymers					
HDPE[B]	R1	0.015 ± 0.003	2.81 ± 0.6	0.019 ± 0.005	65.8 ± 0.9
HIPS	R1	0.068 ± 0.002	2.139 ± 0.084	0.2 ± 0.027	8.6 ± 1.4
HIPS	R2	0.062 ± 0.002	2.085 ± 0.068	0.198 ± 0.027	8.9 ± 0.7
HIPS	R3	0.066 ± 0.003	2.082 ± 0.081	0.21 ± 0.027	3.5 ± 1.4
HIPS	R4	0.063 ± 0.003	2.108 ± 0.083	0.2 ± 0.028	9.2 ± 1.4
HIPS1panel	R1	0.07 ± 0.003	2.23 ± 0.1	0.157 ± 0.021	3.5 ± 2.9
PBT[C]	R1	0.057 ± 0.012	3.01 ± 0.64	0.079	NM
PMMA	R1	0.005 ± 0.001	2.196 ± 0.085	0.005 ± 0.001	0.0 ± 1.4
PMMA	R2	0.005 ± 0.001	2.208 ± 0.085	0.005 ± 0.000	0.0 ± 1.4
PMMA	R3	0.005 ± 0.000	2.198 ± 0.085	0.005 ± 0.000	0.0 ± 1.4
PMMA	R4	0.004 ± 0.001	2.219 ± 0.085	BDL	0.0 ± 1.4
PMMA	R5	0.004 ± 0.001	2.194 ± 0.084	BDL	0.0 ± 1.4
PMMA	R6	0.004 ± 0.001	2.247 ± 0.086	0.005 ± 0.000	0.0 ± 1.4
PVC	R1	0.193 ± 0.03	1.45 ± 0.22	0.209 ± 0.041	NM
PVC	R2	0.161 ± 0.02	1.31 ± 0.17	0.183 ± 0.033	NM
Copolymers					
ABS	R1	0.054 ± 0.002	2.178 ± 0.079	0.166 ± 0.023	1.9 ± 0.4
ABS	R2	0.057 ± 0.002	2.183 ± 0.082	0.167 ± 0.022	2.0 ± 1.1
ABS	R3	0.055 ± 0.002	2.141 ± 0.083	0.166 ± 0.022	1.0 ± 1.5
PMMA-PVC alloy	R1	0.103 ± 0.005	0.62 ± 0.027	0.1 ± 0.018	53.1 ± 1.1
PMMA-PVC alloy	R2	0.108 ± 0.004	0.719 ± 0.028	0.107 ± 0.017	29.2 ± 1.1
Porous Polymer Foams					
XLPE 2#	R1	0.021 ± 0.000	2.8 ± 0.12	0.017 ± 0.004	0.0 ± 2.1
XLPE 2#	R2	0.020 ± 0.000	2.67 ± 0.11	0.018 ± 0.004	0.0 ± 2.0
XLPE 4#	R1	0.022 ± 0.001	2.7 ± 0.17	0.026 ± 0.004	0.0 ± 5.1
XLPE 4#	R2	0.020 ± 0.002	2.61 ± 0.21	0.025 ± 0.004	0.0 ± 7.0
XLPE 4#	R3	0.020 ± 0.001	2.66 ± 0.19	0.024 ± 0.004	0.0 ± 6.1
XLPE 6#	R1	0.021 ± 0.002	2.87 ± 0.25	0.032 ± 0.005	0.0 ± 8.0
XLPE 6#	R2	0.020 ± 0.000	2.914 ± 0.096	0.028 ± 0.004	0.0 ± 0.8
XLPE 6#	R3	0.020 ± 0.000	2.78 ± 0.1	0.030 ± 0.004	0.0 ± 0.7
PolyIso (0.5 in.)	R1	0.072 ± 0.007	1.98 ± 0.2	0.061 ± 0.01	16.7 ± 7.9
PolyIso (0.5 in.)	R2	0.07 ± 0.007	1.94 ± 0.2	0.063 ± 0.011	21.1 ± 7.8
PolyIso (0.5 in.)	R3	0.053 ± 0.005	1.64 ± 0.16	0.057 ± 0.009	11.9 ± 7.8
PolyIso (1 in.)	R1	0.073 ± 0.004	2.06 ± 0.12	0.055 ± 0.01	35.9 ± 2.7
PolyIso (1 in.)	R2	0.066 ± 0.004	1.97 ± 0.1	0.023 ± 0.01	14.1 ± 2.8
PolyIso (1 in.)	R3	0.076 ± 0.004	1.95 ± 0.1	0.059 ± 0.008	30.6 ± 2.8
PolyIso (2 in.)	R1	0.098 ± 0.005	1.961 ± 0.096	0.050 ± 0.008	58.1 ± 1.4
PolyIso (2 in.)	R2	0.092 ± 0.004	1.938 ± 0.093	0.049 ± 0.007	56.3 ± 1.4
XPS (Green 1 in.)	R1	0.089 ± 0.004	2.142 ± 0.096	0.145 ± 0.019	0.0 ± 2.7
XPS (Green 1 in.)	R2	0.080 ± 0.004	1.835 ± 0.082	0.141 ± 0.02	0.0 ± 2.7
XPS (Green 1 in.)	R2	0.075 ± 0.024	1.85 ± 0.59	0.134 ± 0.046	48.9 ± 16.1 [A]
XPS (Green 2 in.)	R1	0.084 ± 0.003	1.852 ± 0.071	0.171 ± 0.022	0.0 ± 1.3
XPS (Green 2 in.)	R2	0.081 ± 0.006	1.96 ± 0.15	0.155 ± 0.025	0.4 ± 6.7
XPS (Green 2 in.)	R3	0.082 ± 0.007	2.11 ± 0.18	0.149 ± 0.024	12.3 ± 7.0
XPS (Pink 1 in.)	R1	0.088 ± 0.004	2.09 ± 0.097	0.142 ± 0.022	0.0 ± 2.9

Table 9 – *Continued on next page*

Polymer	Test #	y_{CO} [g/g]	y_{CO_2} [g/g]	y_{soot} [g/g]	μ_{res} [%]
XPS (Pink 1 in.)	R2	0.082 ± 0.004	1.971 ± 0.091	0.154 ± 0.021	0.0 ± 2.9
XPS (Pink 1 in.)	R3	0.075 ± 0.004	2.16 ± 0.1	0.138 ± 0.02	0.0 ± 2.9
XPS (Pink 2 in.)	R1	0.08 ± 0.003	2.139 ± 0.084	0.167 ± 0.022	0.0 ± 1.6
XPS (Pink 2 in.)	R2	0.072 ± 0.007	2.03 ± 0.2	0.139 ± 0.03	16.3 ± 7.7
XPS (Pink 2 in.)	R3	0.082 ± 0.005	2.35 ± 0.14	0.151 ± 0.021	16.1 ± 3.9
Composite Materials					
GPO-1	R1	0.050 ± 0.002	2.069 ± 0.092	0.033 ± 0.005	69.1 ± 0.8
GPO-1	R2	0.050 ± 0.002	2.005 ± 0.089	0.032 ± 0.007	68.8 ± 0.8
GPO-1	R3	0.049 ± 0.002	1.979 ± 0.088	0.035 ± 0.005	68.8 ± 0.8
GPO-3[C]	R1	0.127 ± 0.036	2.78 ± 0.8	BDL	NM
GPO-3[C]	R2	0.162 ± 0.055	3.6 ± 1.1	0.007 ± 0.003	NM
GPO-3[C]	R3	0.149 ± 0.045	3.11 ± 0.93	0.018 ± 0.007	NM
POM-GF	R1	0.008 ± 0.001	1.43 ± 0.17	BDL	25.4 ± 8.4
POM-GF	R2	0.006 ± 0.000	1.318 ± 0.048	BDL	25.8 ± 0.3
POM-GF	R3	0.007 ± 0.000	1.303 ± 0.048	BDL	20.4 ± 0.7
Other Materials					
SIS Wire[C]	R1	0.038 ± 0.15	1.7 ± 0.66	0.44 ± 0.18	NM
SIS Wire + GPO-3[C]	R1	0.42 ± 0.12	2.73 ± 0.82	0.272 ± 0.090	NM
OSB	R1	0.016 ± 0.003	1.55 ± 0.33	BDL	31.0 ± 7.3
OSB	R2	0.027 ± 0.003	1.48 ± 0.17	0.003 ± 0.002	31.0 ± 7.3
OSB	R3	0.030 ± 0.001	1.604 ± 0.064	0.002 ± 0.001	31.0 ± 1.2
Western Red Cedar	R1	0.11 ± 0.025	1.87 ± 0.43	BDL	NM
Western Red Cedar	R2	0.024 ± 0.002	1.147 ± 0.096	BDL	83.5 ± 1.3
Western Red Cedar	R3	0.018 ± 0.002	1.22 ± 0.12	0.003 ± 0.001	85.4 ± 1.3
Western Red Cedar	R4	0.039 ± 0.003	1.169 ± 0.077	0.004 ± 0.001	74.5 ± 1.3

Continued from previous page

BDL = Below Detection Limit

NM = Not Measured

[A] Material did not sustain flame spread during testing, therefore was not entirely consumed, see Sec.3.1.16

[B] Residue yield, μ_{res}, estimated by dividing measured Total Heat Release by a representative heat of combustion[111]

[C] An initial mass was not taken for this material. Therefore, residue yield, μ_{res}, cannot be estimated.

4. Conclusions and Future Work

4.1. Summary of Results

This report presents measurements of heat release rate, product yields, and heat flux obtained from a series of 90 full-scale fire experiments, including 66 conducted on 18 unique combustible solids. The primary focus of this research is to quantify how material composition affects ignition, fire growth, and peak fire size in large fires. A variety of materials was thus selected in order to provide a wide range of material compositions and burning behaviors such as swelling, charring, dripping, and soot formation. Materials tested include: natural and synthetic polymers, copolymers, fiberglass-reinforced composite materials, porous polymer foams, and electrical cables. Additionally, for several of these materials (i.e., PolyIso, XLPE, and XPS foam) samples of nominally the same material were tested with different densities or thicknesses or from two different suppliers. Two formulations of glass-fiber-reinforced polyester resins with different arc-resistance ratings (i.e., GPO-1 and GPO-3) were also tested.

Fig. 78 highlights flame structure of each of the materials at an HRR of approximately 400 kW. Notable differences in flame structure (e.g., flame thickness, length, and continuity), soot production, and brightness/flame color can be observed for each of these materials even when compared at the same relative fire size (HRR). Fig. 79 illustrates flame structure of each of the materials at their respective peak HRRs (100 kW to 4200 kW). This series of images highlights how material composition can strongly impact peak fire size.

Measurement data presented in this study also reinforces that (even for same material) ignitability, fire growth rate, and peak fire size may be strongly affected by both (1) ignition conditions and (2) sample deformation (e.g., due to swelling, melt flow, dripping, and/or intumescence). Small changes in initial conditions may propagate into comparatively large differences in fire growth (positive feedback) and thus it is critical to carefully characterize ignition source size (HRR and exposure length scale), strength (i.e., incident heat flux), and duration in order to ensure test respectability and reproducibility (as well as fire model accuracy). Although sample deformation is well known to strongly impact material flammability response, it remains challenging to ensure these behaviors do not affect the results of standard test methods, that they are accurately and completely characterized in research experiments, and that they (and their effects on wall/flame interactions) are described with suitable accuracy (and reasonable computation cost) in numerical simulations.

This study also offers a comprehensive set of validation data for computational fluid dynamics (CFD) simulations of large scale fire growth due to flame spread over the surface of combustible solids. Selected measurement data is presented and analyzed in this report; representative images and detailed descriptions of individual experiments are provided in Appendix C. A complete set of all measurement data and videos recorded during these experiments is available online on the NIST Fire Calorimetry Database [1]: https://www.nist.gov/el/fcd/vertical-upward-flamespread-on-parallel-panels. A summary of key mea-

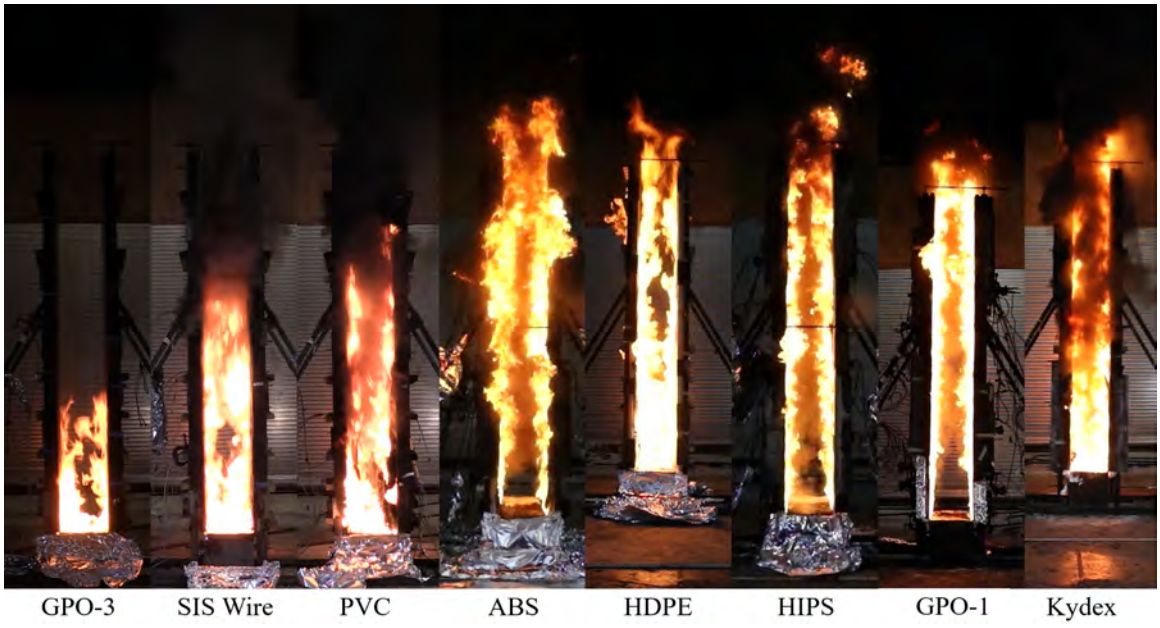

(a)

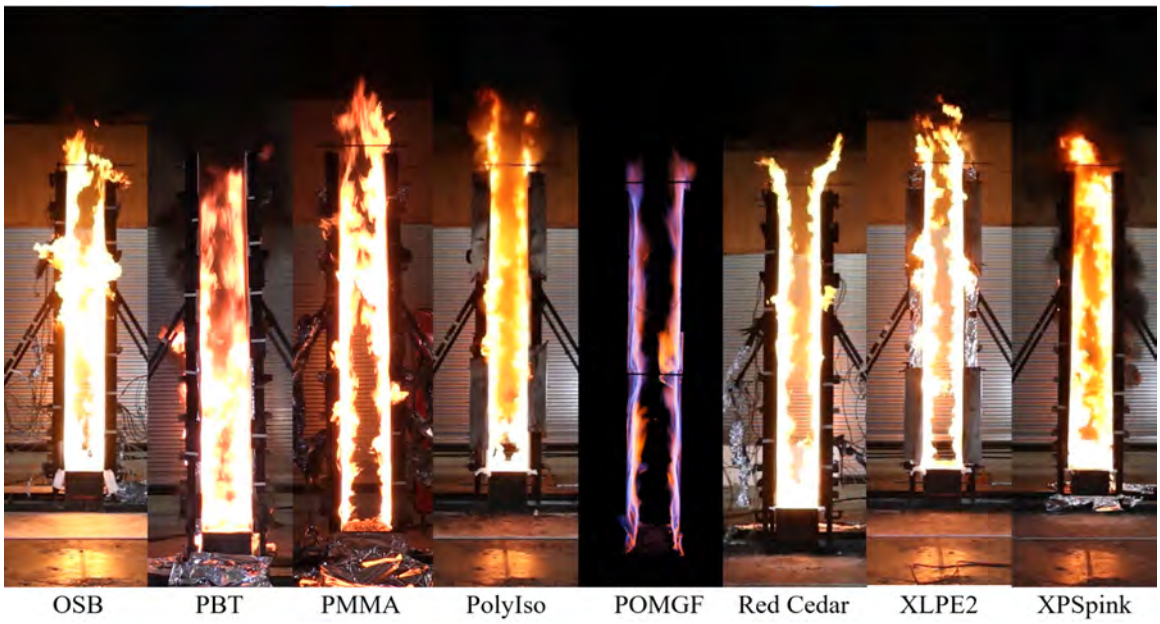

(b)

Fig. 78. Representative flame structure of each of the materials tested in this work when HRR = 400 kW. Note: in the top row of images, flame structure for GPO-3, SIS Wire, and PVC flame structure is shown when heat release rate measured approximately 100 kW, 150 kW, and 250 kW, respectively. These are the peak heat release rates measured during tests on these three materials; these three HRRs are not corrected to account for the contribution of the propane burner used for sample ignition (nominally, 63 kW).

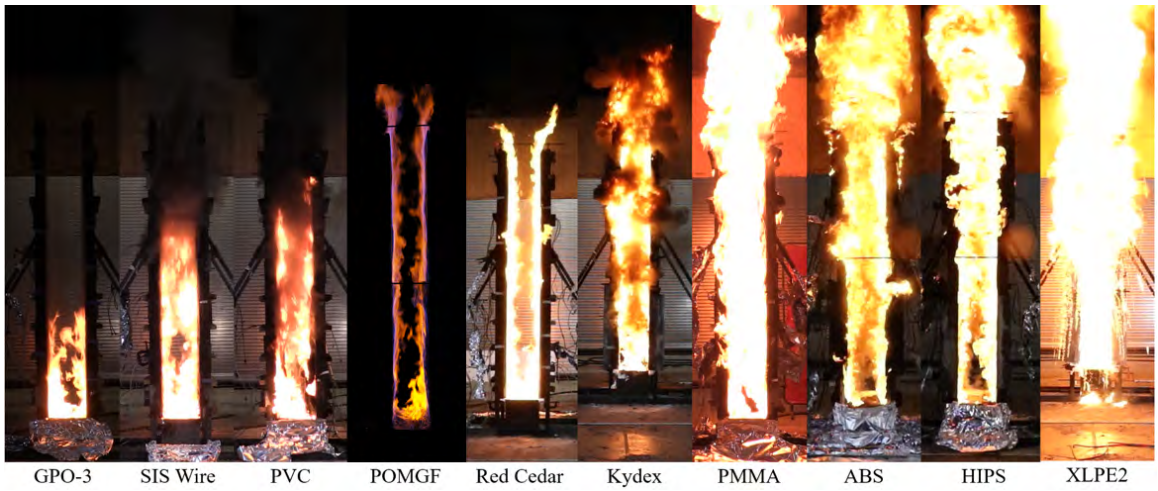

Fig. 79. Representative flame structure of selected materials tested in this work at their respective peak heat release rates (peak HRR).

surement data (fire size and growth rate, heat transfer, and species production) obtained during these experiments is provided in the sections below.

4.2. Fire Size (Heat Release Rate, HRR)

Figure 80 plots a representative heat release rate (HRR) curve of each of the materials tested in this work. Significant differences in ignition time, growth rate, and peak HRR are observed as a result of differences in material composition. These values are reported in Table 8. Between the 18 different materials, ignition time varied by a factor of approximately 30, both Peak HRR and time to Peak HRR varied by two orders of magnitude, and the heat of combustion (energy release per gram of gaseous volatiles produced) varied by up to a factor of four. As highlighted in Sec. 3, it was observed that fire growth rate and peak HRR could be strongly affected by sample deformation; often, peak HRR was measured concurrently with a significant melt flow event or sample detachment from the panel walls. It is emphasized that this parallel panel test configuration provides a fairly severe flame spread scenario (e.g., due flame confinement and the potential for reradiation between panel walls). As noted in Sec. 3.1.6, fire growth due to upward flame spread over (and continued burning of) HIPS panels was considerably faster in the parallel panel configuration versus a single panel burning independently (similar ignition conditions).

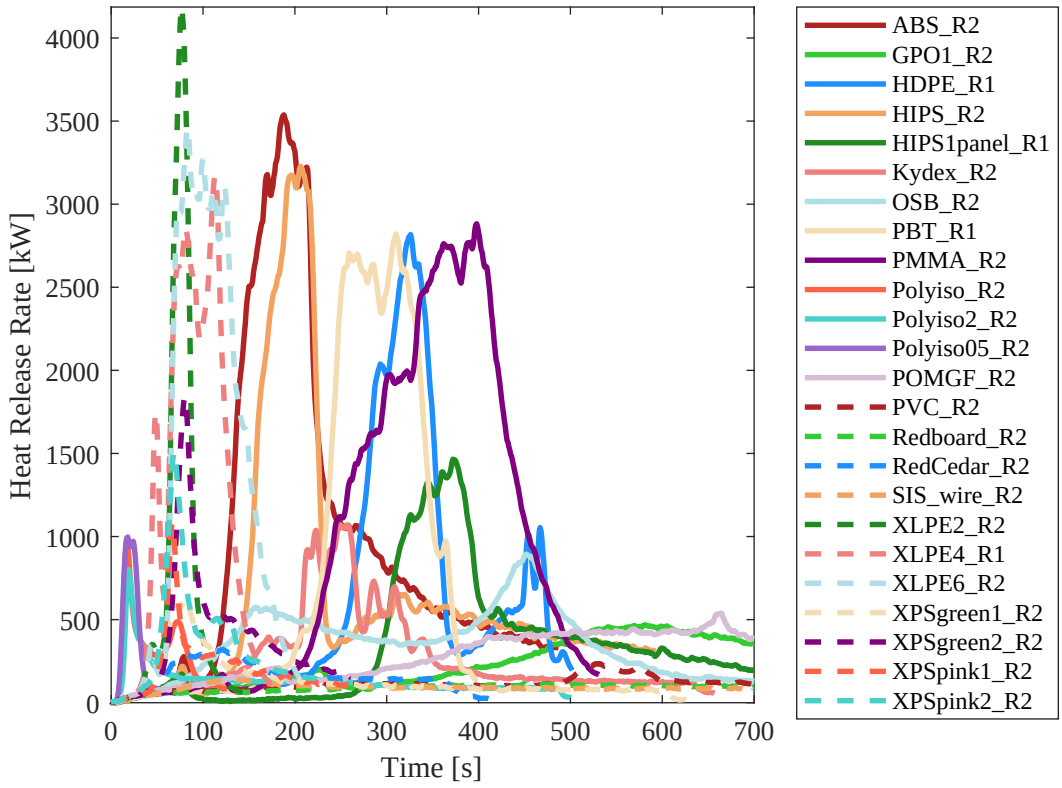

Fig. 80. Time-resolved measurements of total HRR obtained during the burning of each of the materials tested in this work (one representative HRR profile is provided for each material, even when replicate data was available).

4.3. Heat Transfer

Flame-to-surface heat transfer was measured across the full length of panel walls in experiments involving ABS, GPO-1, HIPS, OSB, PMMA, POM-GF, PVC, SIS Wire, Western Red Cedar. Width-resolved measurements of flame heat flux were also recorded in this experimental series at three heights ($z = 50$ cm, 100 cm, and 180 cm); this dataset will be analyzed further in future volumes of this work to quantify potential variations of flame heat flux and flame structure across the width of the panel walls as these fires developed.

Careful processing and analysis of heat flux measurements (see Section 3.1.1) allowed for height-resolved flame heat feedback profiles to be defined as a function of HRR. Figure 81 provides heat feedback profiles measured during tests on PMMA alongside representative images of flame structure at heat release rates between 120 kW $\leq$ HRR $\leq$ 2800 kW. Figure 82 plots several exemplary flame heat feedback profiles measured for seven materials at three heat release rates (approximately 300 kW, 1 MW, and 3 MW). These heat feedback profiles can be used as a validation set for CFD simulations of this configuration. Note: in Fig. 82a, the elevated heat fluxes measured at low heights ($z < 0.75$ m) during tests on OSB and Western Red Cedar likely arise due to the presence of flames supported by the propane burner, which was left on to ensure the continued burning of these two materials (but turned off during tests on each of the other materials shown in this figure), and local smoldering (i.e., glowing combustion) of the wood panels.

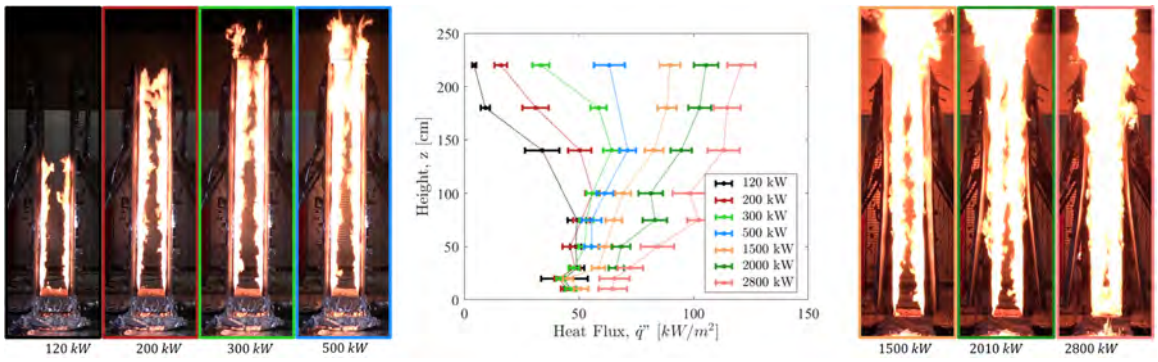

Fig. 81. Height-resolved measurements of total flame to wall heat flux (as measured by an array of water-cooled, Schmidt-Boelter heat flux gauges) during upward flame spread over black, cast PMMA, and representative images of flame structure for measured heat release rates between 120 kW $\leq \dot{Q} \leq$ 2800 kW. Error bars indicate expanded uncertainty of the heat flux measurements (U_c; 95% confidence interval, coverage factor = 2), as described in Appendix B.2.

For one material, HIPS, centerline heat flux measurements were recorded as panels burned both in the parallel panel and the single panel configuration. Results presented in Sec. 3.1.6 suggest that this change in burning configuration primarily affects fire growth rate by altering flame height (rather than due to significant changes in peak flame heat flux under the continuous region of the wall flame). Future experiments are planned to better understand this relationship by quantifying the impact of sample configuration and panel

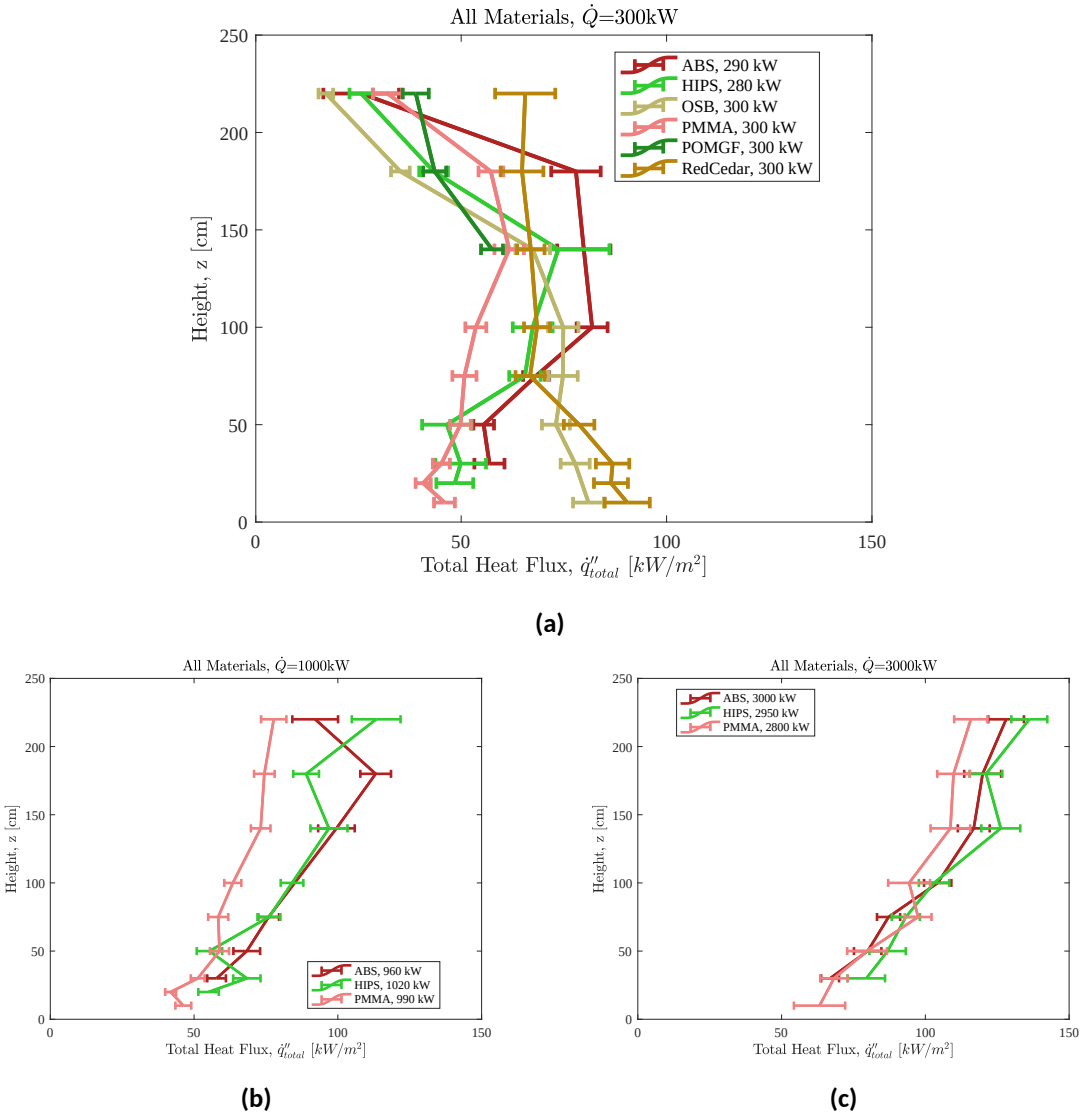

Fig. 82. Height-resolved measurements of total wall flame heat flux measured at the centerline, $y = 0$, of panels during repeated experiments on (ABS, HIPS, and PMMA). In (a), $\dot{q}''_{\text{total}}$ profiles are highlighted during the early stages of fire growth (i.e., $\dot{Q} = 300$ kW); in (b) and (c), $\dot{q}''_{\text{total}}$ profiles are plotted at the later stages of these tests, when flames covered the full surface of panel walls. Error bars indicate expanded uncertainty of the heat flux measurements (U_c; 95% confidence interval, coverage factor = 2), as described in Appendix B.2.

spacing on flame structure, flame heat feedback, and fire growth rate. These results will enhance our understanding of (and ability to predict) of common fire scenarios of higher complexity (e.g., electrical enclosure fires or facade fires).

For 6 materials (ABS, GPO-1, HIPS, OSB, POM-GF, and Western Red Cedar), the fraction of total wall flame heat flux attributed to radiation was determined at four heights ($z = 0.50$ m, 1.0 m, 1.8 m, and 2.2 m) in multiple tests by simultaneously measuring $\dot{q}''_{\text{rad}}$ and $\dot{q}''_{\text{total}}$ with a pair of water-cooled Schmidt-Boelter heat flux gauges (one radiometer and one total heat flux gauge placed side by side). As discussed in Sec. 3.3, in this configuration, the radiative fraction of the heat flux demonstrated a strong dependence on material composition but limited systematic variations as a function of height or fire size (so long as a continuous flame sheet was supported over the measurement location). In general, the radiative fraction was higher for sootier fires (e.g., ABS and HIPS) versus less sooty fires (e.g., POM-GF). However, elevated radiative fractions were also observed for wood-based materials when smoldering (i.e., glowing combustion) at the surface.

4.4. Species Yields

Carbon monoxide (CO), carbon dioxide (CO_2), and soot yields were measured in experiments conducted in this test series. Soot yields varied substantially from undetectable (POM-GF) to approximately 0.21 for styrene-containing polymers (i.e., ABS, HIPS, and XPS foam).

4.5. Future Work

Additional volumes of this report will include measurement data from a series of mg- and g-scale experiments conducted on all 18 materials studied in this work. These bench-scale experiments — including thermogravimetric analysis (TGA), differential scanning calorimetry (DSC), microscale combustion calorimetry (MCC), and pyrolysis of coupon sized slabs in a well-controlled, 1-dimensional heating environment — and the systematic method by which their measurement data will be analyzed [113–116] are specifically designed to allow for determination (i.e., calibration) of the material properties controlling heating, decomposition, and production of gaseous volatiles by each of these materials. Collectively, the measurement data obtained from each of these experiments (from bench- to full-scale) will thus provide a comprehensive database of experimental measurements needed to calibrate pyrolysis models for combustible solids, use these models for quantitative prediction of fire growth using CFD tools, and validate the simulation results.

Future work can consider the impact of key secondary factors that affect fire growth rate, flame structure, and/or flame heat feedback mechanisms: e.g., type and strength of ignition source, aging of fuels, ventilation conditions, physical phenomena (e.g., melt flow and dripping), and configuration factors such as panel spacing or fuel packing density, wall size, orientation, and geometry. Some such experiments are ongoing and will be presented in related publications, currently in preparation (e.g., Ref. [117]). These configuration factors may be of great interest as previous cable fire research has demonstrated that, "the parameter that has the most effect on the test results [i.e., the fire response of cables in real-scale tests] is the method of mounting the tested cables" [43]. Additionally, further analysis can explore relationships between quantities measured in tests conducted at different scales as part of this experimental test series (e.g., correlating flame length, flame heat flux distribution, and $q_{\mathrm{rad}}(\%)$ with fuel composition, sooting tendency, or Y_{soot} or correlating measured fire growth rate to key material properties derived from small-scale measurement data such as decomposition reaction temperature [118] or the the fire growth capacity (FGC) [119]).

References

[1] M.F. Bundy and R.A. Bryant. Nist fire calorimetry database (fcd). https://doi.org/10.18434/mds2-2314(Accessed 2023-03-13), 2020.

[2] Organization for Economic Cooperation and Development (OECD) Nuclear Energy Agency (NEA) Committee on the Safety of Nuclear Installations (CSNI). Fire project report: Collection and analysis of fire events (2010-2013) – extensions in the database and applications. Technical Report NEA/CSNI/R (2015)14, NEA CSNI, 2015.

[3] EPRI. Fire events database and generic ignition frequency model for u.s. nuclear power plants. Technical Report 1003111, Electric Power Research Institute, Palo Alto, California, 2001.

[4] R. Wachowiak and A. Lindeman. The updated fire events database: Description of content and fire event classification guidance. Technical Report 1025284, Electric Power Research Institute, Palo Alto, California, July 2013.

[5] I.T. Leventon, K.B. McGrattan, R.D. Davis, K. Hamburger, and N. Melly. Characteristics of nuclear power plant fires involving electrical enclosures. NIST Technical Note 2215, National Institute of Standards and Technology, 2021.

[6] S.P. Nowlen, M. Kazarians, and F. Wyant. Risk methods insights gained from fire incidents. NUREG NUREG/CR-6738, Nuclear Regulatory Commission, Washington, D.C., 2001.

[7] V. Babrauskas. *Ignition Handbook*. Fire Science Publishers, Issaquah, Washington USA, 1st edition, 2003. Co-published by the Society of Fire Protection Engineers.

[8] V. Babrauskas. Electrical fires. In *SFPE Handbook of Fire Protection Engineering*, chapter 22, pages 662–705. Springer, New York, NY, 5th edition, 2016.

[9] V. Babrauskas. *Ignition Handbook*. Fire Science Publishers, Issaquah, Washington USA, 1st edition, 2003. Co-published by the Society of Fire Protection Engineers.

[10] Marcelo M Hirschler. Survey of fire testing of electrical cables. *Fire and materials*, 16(3):107–118, 1992.

[11] V. Babrauskas, R.D. Peacock, E. Braun, R.W. Bukowski, and W.W. Jones. *Fire Performance of Wire and Cable: Reaction-to-Fire Tests–A Critical Review of the Existing Methods and of New Concepts*. US Department of Commerce, Technology Administration, National Institute of Standards and Technology, 1991.

[12] J. Martinka. Traditional approach to assessment of fire hazards of electrical cables. In *Fire Hazards of Electrical Cables*, pages 55–66. Springer, 2022.

[13] K.B. McGrattan and S. Bareham. Cable heat release, ignition, and spread in tray installations during fire (christifire) phase 2: Vertical shafts and corridors. NUREG NUREG/CR-7010, Nuclear Regulatory Commission, Washington, D.C., 2013.

[14] Electric Power Research Institute (EPRI) and Office of Nuclear Regulatory Research (RES) U.S. Nuclear Regulatory Commission. Fire pra methodology for nuclear power facilities volume 2: Detailed methodology. NUREG EPRI TR-1011989 and NUREG/CR-6850, Nuclear Regulatory Commission, Rockville, MD, 2005.

[15] United States. Office of the Federal Register. *Code of Federal Regulations (10 CFR 50.48)*, volume Fire Protection. US General Services Administration, National Archives and Records Service, 2005.

[16] United States Nuclear Regulatory Commission. Implementation of fire protection requirements (generic letter no. 86-10), 1986.

[17] American Society for Testing and Materials International. *ASTM E84-21a: Standard Test Method for Surface Burning Characteristics of Building Materials*, 2021.

[18] National Fire Protection Association. Performance-based standard for fire protection for light water reactor electric generating plants. Technical Report NFPA 805, 2020.

[19] Electric Power Research Institute (EPRI) and Office of Nuclear Regulatory Research (RES) U.S. Nuclear Regulatory Commission. Methodology for modeling fire growth and suppression response for electrical cabinet fires in nuclear power plants. Technical Report 3002016051/NUREG-2230, Nuclear Regulatory Commission, Washington, D.C., 2020.

[20] K.B. McGrattan and S. Bareham. Heat release rates of electrical enclosure fires (helen-fire). NUREG NUREG/CR-7197, Nuclear Regulatory Commission, Washington, D.C., 2016.

[21] N. Melly. Nuclear power plant fire ignition frequency and non-suppression probability estimation using the updated fire events database: United states fire event experience through 2009(nureg-2169, epri 3002002936). NUREG NUREG/CR-2169, Nuclear Regulatory Commission, Washington, D.C., 2015.

[22] NRC/EPRI. Peak heat release rates and effect of obstructed plume. NUREG NUREG/CR-2178 volume 1, Nuclear Regulatory Commission, Washington, D.C., 2016.

[23] K.B. McGrattan and I.T. Leventon. Oxygen-limited fires inside under-ventilated enclosures (olive-fire). NIST Technical Note 2232, National Institute of Standards and Technology, Gaithersburg, Maryland, 2022.

[24] O.A. Ezekoye, M.J. Hurley, J.L. Torero, and K.B. McGrattan. Applications of heat transfer fundamentals to fire modeling. *Journal of Thermal Science and Engineering Applications*, 5(2), 2013.

[25] A. Alvarez, B.J. Meacham, N.A. Dembsey, and J.R. Thomas. Twenty years of performance-based fire protection design: challenges faced and a look ahead. *Journal of Fire Protection Engineering*, 23(4):249–276, 2013.

[26] NRC/EPRI. Verification and validation of selected fire models for nuclear power plant applications. NUREG NUREG-1824 // EPRI 1011999, volumes 1-7, Nuclear Regulatory Commission, Washington, D.C., 2007.

[27] FA Williams. Mechanisms of fire spread. In *Symposium (International) on Combustion*, volume 16, pages 1281–1294. Elsevier, 1977.

[28] A.C. Fernandez-Pello and T. Hirano. Controlling mechanisms of flame spread. *Combustion Science and Technology*, 32(1-4):1–31, 1983.

[29] K. Annamalai and M. Sibulkin. Flame spread over combustible surfaces for laminar flow systems part i: Excess fuel and heat flux. *Combustion Science and Technology*, 19(5-6):167–183, 1979.

[30] M. Annamalai, K. Sibulkin. Flame spread over combustible surfaces for laminar flow systems part ii: Flame heights and fire spread rates. *Combustion Science and Technology*, 19(5-6):185–193, 1979.

[31] L Audouin, L Rigollet, H Prétrel, W Le Saux, and M Röwekamp. Oecd prisme project: Fires in confined and ventilated nuclear-type multi-compartments-overview and main experimental results. *Fire Safety Journal*, 62:80–101, 2013.

[32] J.M Chavez. An experimental investigation of internally ignited fires in nuclear power plant control cabinets: Part 1: Cabinet effects tests. NUREG NUREG/CR-4527-1, Nuclear Regulatory Commission, Washington, D.C., 1987.

[33] O. Riese. Fire behaviour of cables with insulation materials frequently used in nuclear power plants. In *19th International Conference on Structural Mechanics In Reactor Technology (SMiRT 19)*, 2007.

[34] C.M. Lannon, S.I. Stoliarov, J.M. Lord, and I.T. Leventon. A methodology for predicting and comparing the full-scale fire performance of similar materials based on small-scale testing. *Fire and Materials*, 42(7):710–724, 2018.

[35] I.T. Leventon. *Prediction of Upward Flame Spread over Polymers*. PhD thesis, University of Maryland, 2016.

[36] Y. Pizzo, J.L. Consalvi, and B. Porterie. A transient pyrolysis model based on the b-number for gravity-assisted flame spread over thick pmma slabs. *Combustion and Flame*, 156(9):1856–1859, 2009.

[37] Y. Zhou, J. Gong, L. Jiang, and C. Chen. Orientation effect on upward flame propagation over rigid polyurethane foam. *International Journal of Thermal Sciences*, 132:86–95, 2018.

[38] M.J. Gollner, , C.H. Miller, , W. Tang, , and A.V. Singh. The effect of flow and geometry on concurrent flame spread. *Fire Safety Journal*, 91:68–78, 2017.

[39] X. Huang and Y. Nakamura. A review of fundamental combustion phenomena in wire fires. *Fire Technology*, 56(1):315–360, 2020.

[40] J.E. Mendez, D. Lange, J.P. Hidalgo, and M.S. McLaggan. Effect of cavity parameters on the fire dynamics of ventilated façades. *Fire safety journal*, 133:103671, 2022.

[41] K. Livkiss, S. Svensson, B. Husted, and P. van Hees. Flame heights and heat transfer in facade system ventilation cavities. *Fire Technology*, 54:689–713, 2018.

[42] J. Park, J. Brucker, R. Seballos, B. Kwon, and Y-T Liao. Concurrent flame spread over discrete thin fuels. *Combustion and Flame*, 191:116–125, 2018.

[43] SJ Grayson, Patrick Van Hees, Andrea M Green, H Breulet, and U Vercellotti. Assessing the fire performance of electric cables (fipec). *Fire and materials*, 25(2):49–60, 2001.

[44] H.K. Hasegawa, N.J. Alvares, A.E. Lipska-Quinn, D.G. Beason, S.J. Priante, and K.L. Foote. Fire-protection research for doe facilities: Fy 82 year-end report. 9 1983.

[45] H.K. Hasegawa, N.J. Alvares, A.E. Lipska-Quinn, D.G. Beason, S.J. Priante, K.L. Foote, and K Staggs. Fire protection research for doe facilities: Fy 83 year-end report. 1984.

[46] M. Siemon, O. Riese, B. Forell, D. Krönung, and W. Klein-Heßling. Experimental and numerical analysis of the influence of cable tray arrangements on the resulting mass loss rate and fire spreading. *Fire and Materials*, 43(5):497–513, 2019.

[47] D.L. Urban, P. Ferkul, S. Olson, G.A. Ruff, J. Easton, S. James, Y.T. Liao, C. Li, C. Fernandez-Pello, L. Torero, J, G. Legros, C. Eigenbrod, N. Smirnov, S. Rouvreau, and G. Toth, B. Jomaas. Flame spread: effects of microgravity and scale. *Combustion and Flame*, 199:168–182, 2019.

[48] P.A. Beaulieu and N.A. Dembsey. Effect of oxygen on flame heat flux in horizontal and vertical orientations. *Fire Safety Journal*, 43(6):410–428, 2008.

[49] D. Alibert, M. Coutin, M. Mense, Y. Pizzo, and B. Porterie. Effect of oxygen concentration on the combustion of horizontally-oriented slabs of pmma. *Fire Safety Journal*, 91:182–190, 2017.

[50] Y. Konno, N. Hashimoto, and O. Fujita. Downward flame spreading over electric wire under various oxygen concentrations. *Proceedings of the Combustion Institute*, 37(3):3817–3824, 2019.

[51] J. Mangs and O. Keski-Rahkonen. Full scale fire experiments on electronic cabinets. VTT Publications VTT186, VTT Technical Research Centre of Finland, Espoo, Finland, 1994.

[52] J. Mangs and O. Keski-Rahkonen. Full scale fire experiments on electronic cabinets ii. VTT Publications VTT269, VTT Technical Research Centre of Finland, Espoo, Finland, 1996.

[53] J. Mangs and O. Keski-Rahkonen. On the fire dynamics of vehicles and electrical equipment. VTT Publications VTT269, VTT Technical Research Centre of Finland, Espoo, Finland, 2004.

[54] W. Plumecocq, M. Coutin, S. Melis, and L. Rigollet. Characterization of closed-doors electrical cabinet fires in compartments. *Fire safety journal*, 46(5):243–253, 2011.

[55] S.P. Nowlen. Quantitative data on the fire behavior of combustible materials found in nuclear power plants: A literature review. NUREG NUREG/CR-4679, Nuclear Regulatory Commission, Washington, D.C., 1987.

[56] K. McGrattan, S. Hostikka, R. McDermott, J. Floyd, C. Weinschenk, and K. Overholt. Fire dynamics simulator user's guide. *NIST special publication*, 1019(6):1–339, 2013.

[57] A.V. Singh and M.J. Gollner. A methodology for estimation of local heat fluxes in steady laminar boundary layer diffusion flames. *Combustion and Flame*, 162(5):2214–2230, 2015.

[58] T. Ahmad and G.M. Faeth. An investigation of the laminar overfire region along upright surfaces. *Journal of Heat Transfer*, 1978.

[59] L. Orloff, J. De Ris, and G.H. Markstein. Upward turbulent fire spread and burning of fuel surface. In *Symposium (International) on Combustion*, volume 15, pages 183–192. Elsevier, 1975.

[60] L. Orloff, A.T. Modak, and R.L. Alpert. Burning of large-scale vertical surfaces. In *Symposium (International) on Combustion*, volume 16, pages 1345–1354. Elsevier, 1977.

[61] B.Y. Lattimer. Heat transfer from fires to surface. In *SFPE Handbook of Fire Protection Engineering*, chapter 28, pages 745–798. Springer, New York, NY, 5th edition, 2016.

[62] G.J. Fiola, D.M. Chaudhari, and S.I. Stoliarov. Comparison of pyrolysis properties of extruded and cast poly (methyl methacrylate). *Fire Safety Journal*, 120:103083, 2021.

[63] T. Nyazika, M. Jimenez, F. Samyn, and S. Bourbigot. Pyrolysis modeling, sensitivity analysis, and optimization techniques for combustible materials: A review. *Journal of fire sciences*, 37(4-6):377–433, 2019.

[64] A. Witkowski, A.A. Stec, and T.R. Hull. Thermal Decomposition of Polymeric Materials. In *SFPE Handbook of Fire Protection Engineering*, chapter 32, pages 167–254. Springer, New York, NY, 5th edition, 2016.

[65] S.I. Stoliarov and J. Li. Parameterization and validation of pyrolysis models for polymeric materials. *Fire Technology*, 52:79–91, 2016.

[66] A. Tewarson, M. Khan, P.K. Wu, and R.G Bill Jr. Flammability evaluation of clean room polymeric materials for the semiconductor industry. *Fire and Materials*, 25(1):31–42, 2001.

[67] FM Approvals LLC. American National Standard for Cleanroom Materials Flammability Test Protocol. Standard ANSI/FM 4910-2021, Norwood, MA, USA, 2021.

[68] R.A. Bryant and M.F. Bundy. The NIST 20 MW Calorimetry measurement system for large-fire research. NIST Technical Note 2077, National Institute of Standards and Technology, Gaithersburg, Maryland, 2019.

[69] H.E. Collins, S. Levine, W. Minner, V.A. Moore, V.W. Panciera, K.V. Seyfrit, and Hanauer S.H. Recommendations related to browns ferry fire. NUREG NUREG-0050, Nuclear Regulatory Commission, Washington, D.C., 1976.

[70] E.L. Jordan. Fire in compressible material at dresden unit 3. NRC Information Notice NRC-IN-86-35, Nuclear Regulatory Commission Office of Inspection and Enforcement, Washington, D.C., 1986.

[71] B.K. Grimes. Personnel hazards and other problems from smoldering fire-retardant material in the drywell of a boiling-water reactor. NRC Information Notice NRC-IN-94-26, Nuclear Regulatory Commission Office of Nuclear Reactor Regulation, Washington, D.C., 1986.

[72] M.J. Case. Combustibility of epoxy floor coatings at commercial nuclear power plants. NRC Information Notice NRC-IN-07-26, Nuclear Regulatory Commission Office of Nuclear Reactor Regulation, Washington, D.C., 1986.

[73] I.T. Leventon, K.T. Korver, and S.I. Stoliarov. A generalized model of flame to surface heat feedback for laminar wall flames. *Combustion and Flame*, 179:338–353, 2017.

[74] G.W. Mulholland, E.L. Johnsson, M.G. Fernandez, and D.A. Shear. Design and testing of a new smoke concentration meter. *Fire and Materials*, 24(5):231–243, 2000.

[75] George W Mulholland and Carroll Croarkin. Specific extinction coefficient of flame generated smoke. *Fire and Materials*, 24(5):227–230, 2000.

[76] G.A. Marxman. Combustion in the turbulent boundary layer on a vaporizing surface. In *Symposium (International) on Combustion*, volume 10, pages 1337–1349. Elsevier, 1965.

[77] B. Boust, J. Sotton, S.A. Labuda, and M. Bellenoue. A thermal formulation for single-wall quenching of transient laminar flames. *Combustion and flame*, 149(3):286–294, 2007.

[78] I.T. Leventon and S.I. Stoliarov. Evolution of flame to surface heat flux during upward flame spread on poly (methyl methacrylate). *Proceedings of the Combustion Institute*, 34(2):2523–2530, 2013.

[79] J.G. Quintiere, M. Harkleroad, and Y. Hasemi. Wall flames and implications for upward flame spread. *Combustion Science and Technology*, 48(3-4):191–222, 1986.

[80] W.M. Pitts, J. R. Lawson, and J.R. Shields. Report of test fr 4014,". *NIST/BFRL Calibration System for Heat-Flux Gages*, 2001.

[81] W.M. Pitts, A.V. Murthy, J.L. De Ris, J-R Filtz, K. Nygård, D. Smith, and I. Wetterlund. Round robin study of total heat flux gauge calibration at fire laboratories. *Fire Safety Journal*, 41(6):459–475, 2006.

[82] V. Babrauskas. Development of the cone calorimeter a bench-scale heat release rate apparatus based on oxygen consumption. *Fire and Materials*, 8(2):81–95, 1984.

[83] Medtherm, Hunstville, AL. *APPROXIMATE TRANSMITTANCE OF 1MM THICK ZINC SELENIDE WINDOW*, 2015.

[84] B.K. Tsai, C.E. Gibson, A.V. Murthy, E.A. Early, D.P. Dewitt, and R.D. Saunders. Heat-flux sensor calibration. NIST Special Publication 250-65, National Institute of Standards and Technology, Gaithersburg, Maryland, 2004.

[85] I.T. Leventon. Calibration of Water-Cooled Schmidt Boelter Heat Flux Gauges in Response to Multiple Radiation Heat Sources. NIST Technical Note *In Preparation*, National Institute of Standards and Technology.

[86] Bernard Béland. Heating of damaged conductors. *Fire Technology*, 18(3):229–236, 1982.

[87] P.A. Beaulieu. Parallel Panel Experiments of FRP Composites. Technical Report 0003024286, FM Global, Norwood, Massachusetts, December 2007.

[88] P. Wu. Parallel Wall Fire Tests with PMMA and FRPPMMA. Technical Memorandum 0003024286, FM Global, December 1997.

[89] I.T. Leventon, B. Batiot, M.C. Bruns, S. Hostikka, Y. Nakamura, P. Reszka, and S.I. Stoliarov. The macfp condensed phase working group: A structured, global effort towards pyrolysis model development. *Journal of ASTM International*, 1642:10–29, 2022.

[90] B. Batiot, M. Bruns, S. Hostikka, I. Leventon, Y. Nakamura, P. Reszka, T. Rogaume, and S. Stoliarov. Preliminary summary of experimental measurements: Predecisional draft report submitted to the 2021 MaCFP condensed phase work-

shop. https://github.com/MaCFP/matl-db/releases/download/v1.0.0/MaCFP_2021_Report_Part_I_Experimental.pdf, archived: https://perma.cc/T6LR-95A2.

[91] B. Batiot, M. Bruns, S. Hostikka, I. Leventon, Y. Nakamura, P. Reszka, T. Rogaume, and S. Stoliarov. Measurement and Computation of Fire Phenomena (MaCFP) Condensed Phase Material Database. https://github.com/MaCFP/matl-db, Commit: 77c5f3f6a6316c9bced06908f2c6b0c93c88a03d, DOI: https://doi.org/10.18434/mds2-2586.

[92] D.M. Chaudhari, G.J. Fiola, and S.I. Stoliarov. Experimental analysis and modeling of buoyancy-driven flame spread on cast poly (methyl methacrylate) in corner configuration. *Polymer Degradation and Stability*, page 109433, 2020.

[93] T. Kashiwagi and T.J. Ohlemiller. A study of Oxygen Effects on Nonflaming Transient Gasification of PMMA and PE Dduring Thermal Irradiation. In *Symposium (International) on Combustion*, volume 19, pages 815–823. Elsevier, 1982.

[94] T. Hirata, T. Kashiwagi, and J. E. Brown. Thermal and oxidative degradation of poly (methyl methacrylate): Weight loss. *Macromolecules*, 18(7):1410–1418, 1985.

[95] A. Tewarson and S. D. Ogden. Fire behavior of polymethylmethacrylate. *Combustion and flame*, 89(3-4):237–259, 1992.

[96] B. T. Rhodes and J. G. Quintiere. Burning rate and flame heat flux for pmma in a cone calorimeter. *Fire Safety Journal*, 26(3):221–240, 1996.

[97] J.-L. Consalvi, Y. Pizzo, and B. Porterie. Numerical analysis of the heating process in upward flame spread over thick pmma slabs. *Fire Safety Journal*, 43(5):351–362, 2008.

[98] I. T. Leventon, J. Li, and S. I. Stoliarov. A flame spread simulation based on a comprehensive solid pyrolysis model coupled with a detailed empirical flame structure representation. *Combustion and Flame*, 162(10):3884–3895, 2015.

[99] K. Fukumoto, C. Wang, and J. Wen. Large eddy simulation of upward flame spread on pmma walls with a fully coupled fluid-solid approach. *Combustion and Flame*, 190:365–387, 2018.

[100] S.I. Stoliarov and R.N. Walters. Determination of the heats of gasification of polymers using differential scanning calorimetry. *Polymer Degradation and Stability*, 93(2):422–427, 2008.

[101] A. Tewarson. Flammability of polymers. *Plastics and the Environment*, pages 403–489, 2003.

[102] Y. Kobayashi, Y. Konno, X. Huang, S. Nakaya, M. Tsue, N. Hashimoto, O. Fujita, and C. Fernandez-Pello. Effect of insulation melting and dripping on opposed flame spread over laboratory simulated electrical wires. *Fire Safety Journal*, 95:1–10, 2018.

[103] J. Gong, H. Zhou, H. Zhu, C.G. McCoy, and S.I. Stoliarov. Development of a pyrolysis model for oriented strand board: Part ii—thermal transport parameterization and bench-scale validation. *Journal of Fire Sciences*, page 07349041211036651, 2021.

[104] S.V. Levchik, D.A. Bright, G.R. Alessio, and S. Dashevsky. Synergistic action between aryl phosphates and phenolic resin in pbt. *Polymer degradation and stability*, 77(2):267–272, 2002.

[105] M. Matzen, B. Kandola, C. Huth, and B. Schartel. Influence of flame retardants on the melt dripping behaviour of thermoplastic polymers. *Materials*, 8(9):5621–5646, 2015.

[106] J. Li and S.I. Stoliarov. Measurement of kinetics and thermodynamics of the thermal degradation for non-charring polymers. *Combustion and Flame*, 160:1287–1297, 2013.

[107] GH Markstein. Radiative properties of plastics fires. In *Symposium (International) on Combustion*, volume 17, pages 1053–1062. Elsevier, 1979.

[108] G.H. Markstein and J. De Ris. Wall-fire radiant emission—part 2: Radiation and heat transfer from porous-metal wall burner flames. In *Symposium (International) on Combustion*, volume 24, pages 1747–1752. Elsevier, 1992.

[109] J. De Ris and L. Orloff. The role of buoyancy direction and radiation in turbulent diffusion flames on surfaces. In *Symposium (International) on Combustion*, volume 15, pages 175–182. Elsevier, 1975.

[110] D. Zeng, G. Xiong, G. Agarwal, and Y. Wang. Experimental study of flame heat transfer in a vertical turbulent wall fire. *Proceedings of the Combustion Institute*, 38(3):4477–4484, 2021.

[111] M.F. Bundy. User's Guide for Fire Calorimetry Database (FCD). https://www.nist.gov/system/files/documents/2020/11/19/FCD_User_Guide_v4a.pdf.

[112] American Society for Testing and Materials International. *ASTM D7309-21b: Standard Test Method for Determining Flammability Characteristics of Plastics and Other Solid Materials Using Microscale Combustion Calorimetry*, 2021.

[113] M.C. Bruns and I.T. Leventon. Automated fitting of thermogravimetric analysis data. *Fire and Materials*, 45(3):406–414, 2021.

[114] M.C. Bruns and I.T. Leventon. Design of a material flammability property database. Philadelphia, PA, August 2016. American Chemical Society National Meeting.

[115] M.C. Bruns and I.T. Leventon. Automated characterization of pyrolysis kinetics and heats of combustion of flammable materials. Atlantic City, NJ, October 2019. Triennial International Fire & Cabin Safety Research Conference.

[116] M.C. Bruns and I.T. Leventon. Automated characterization of heat capacities and heats of gasification of combustion of flammable materials. Atlantic City, NJ, October 2022. Triennial International Fire & Cabin Safety Research Conference.

[117] I.T. Leventon, K. De Lannoye, and A.A. Chernovsky. Characterization of fire growth over commercial polymers in the nist intermediate scale flame spread apparatus. NIST Technical Note (In Preparation), National Institute of Standards and Technology, 2024.

[118] Y. Ding, I.T. Leventon, and S.I. Stoliarov. An analysis of the sensitivity of the rate of buoyancy-driven flame spread on a solid material to uncertainties in the pyrolysis and combustion properties. is accurate prediction possible? *Polymer Degradation and Stability*, 214:110405, 2023.

[119] R.E. Lyon, N. Safronava, S. Crowley, and R.N. Walters. A molecular-level fire growth parameter. *Polymer Degradation and Stability*, 186:109478, 2021.

[120] B.N. Taylor, C.E. Kuyatt, et al. Guidelines for evaluating and expressing the uncertainty of nist measurement results. NIST Technical Note 1297, National Institute of Standards and Technology, Gaithersburg, Maryland, 1994.

Appendices

A. Material Manufacturer and Distributor Information

Table 10. Materials Tested - Manufacturer and Distributor Information

Material	Manufacturer	Trade Name	Distributor
'Pure' Synthetic Polymers			
High Density Polyethylene (HDPE)	Rochling Engineering Plastics	Polystone G Natural HDPE	Modern Plastics
High Impact Polystyrene (HIPS)	Spartech	HIPS	Curbell Plastics
Polybutylene Terepthalate (PBT)	Ensinger	HYDEX 4101 PBT	Curbell Plastics
Poly(methyl methacrylate) (PMMA)	Evonik	Acrylite 9H01 GT	Acrylite Shop (https://www.acrylite.co/cast-black-9h01-gt.html)
Poly(vinyl chloride) (PVC)	Röchling Industrial	Type I PVC Sheet	Piedmont Plastics
Copolymers			
Poly(Acrylonitrile Butadiene Styrene) (ABS)	King Plastics	King KPC ABS	Piedmont Plastics
PMMA-PVC alloy (Kydex)	Sekisui	Kydex 100	Laird Plastics
Porous Polymer Foams			
Cross Linked Polyethylene (XLPE 2#)	Three-Sixty Solutions	SOLU-CELL-P2000	New England Foam
Cross Linked Polyethylene (XLPE 4#)	Three-Sixty Solutions	SOLU-CELL-P4000	New England Foam
Cross Linked Polyethylene XLPE 6#	Three-Sixty Solutions	SOLU-CELL-P6000	New England Foam
Poly(Isocyanurate) (PolyIso)	RMAX	Thermasheath	The Home Depot
Extruded Polystyrene (XPS)	Kingspan Insulation	GreenGuard XPS Insulation Board	Lowe's
Extruded Polystyrene (XPS)	Owens Corning	FOAMULAR 150 & FOAMULAR 250 Foam	The Home Depot
Composite Materials			
GPO-1	Haysite Reinforced Plastics	Glastic, GPO-1	Professional Plastics
GPO-3	Haysite Reinforced Plastics	Redboard	Professional Plastics
Poly(oxymethylene) (POM-GF)	Ensinger	Delrin 570	EMCO Plastics (1/4 in. samples) and Laird plastics (3/8 in. samples)
Other Materials			
SIS Wire	Rockbestos	12 AWG RSCC FIREWALL® TYPE XHHW-2 ORSIS 600V (UL) VY-1 NU-CLEAR Gray 2017	Rockbestos
Oriented Strand Board (OSB)	Georgia Pacific	OSB Sheating (7/16 CAT, PS2-10-compliant)	Lowe's
Western Red Cedar	The Hardwood Store of North Carolina	Western Red Cedar	The Hardwood Store of NC

B. Uncertainty of Measurements

Measurements presented in this report include heat release rate, heat flux, sensor positions, and species yields (e.g., soot, CO, CO_2). Derived quantities calculated on the basis of these measurements (e.g., heat of combustion, or radiation fraction of total flame heat flux to the panels walls) are also calculated on the basis of these measurements. For each measurand, Type A and/or Type B uncertainties, combined standard uncertainties, and total expanded uncertainties were evaluated as presented below. Here, the following definitions apply:

- Bias: uncertainties from the calibration of the sensor
- Precision: uncertainty in the ability of the measurement instrument to resolve information from the sensor
- Random Error: result of a measurement minus the mean that would result from an infinite number of measurements of the same measurand carried out under repeatability conditions (i.e., uncertainty due to random, unpredictable variations in the measurement process).
- Type A Uncertainties: those which are evaluated by statistical methods
- Type B Uncertainties: those which are evaluated by other means

Type A uncertainties were determined using the method defined by Taylor and Kuyatt [120]. Type B uncertainties were estimated by other means such as the information available in manufacturer's specifications, from past experience, or engineering judgment.

In many cases (e.g., calculation of heat release rate or radiation fraction), a measurement quantity, y, is not measured directly, but is instead calculated as a function of N other measured quantities:

$$y = f(x_i, x_2, ..., x_N) \tag{B.1}$$

Included in the quantities x_i are both measured quantities and quantities that take into account other sources of variability (e.g., different observers, or instruments). When each of these parameters are uncorrelated, the combined standard uncertainty of a measurement result, $u_c(y)$, is calculated as:

$$u_c(y) = \sqrt{\left(\sum_{i=1}^{N} \left(\frac{\partial f}{\partial x_i}\right)^2 u^2(x_i)\right)} \tag{B.2}$$

where $u(x_i)$ is the standard uncertainty of each input parameter and the partial derivatives, $\frac{\partial f}{\partial x_i}$, are referred to as sensitivity coefficients. Thus, the combined standard uncertainty of a measurement result, u_c. is obtained by combining the individual standard uncertainties using the law of propagation of uncertainty (i.e., the "root-sum-of-squares").

A series of repeated measurements allows for the calculation of statistics of their uncertainties during steady burning or flaming conditions; in this case, the standard deviation, σ_y, or the standard deviation of the mean, $\sigma_{mean,y} = \sigma_y/\sqrt{N}$, of the output estimate is considered an uncertainty component. The expanded uncertainty, U_c, is defined as:

$$U_c(y) = k\sqrt{u_c(y)^2 + \sigma_{mean,y}^2} \tag{B.3}$$

where the coverage factor, k, is taken as equal to 2, so that the expanded uncertainty, U_c, corresponds to a confidence level of approximately a 95%.

In the exemplary calculations provided below, average values of random errors for a given measurement quantity are provided (often estimated as $\sigma_{mean,y}$ of repeated measurements of the same value) in order to offer a representative calculation of the expanded uncertainty of a given measurement quantity. It is emphasized that the random errors reported in this appendix are exemplary and measurements (and their respective random errors) of the same type/quantity recorded in different locations, in different experiments, and/or at different times during an experiment may vary from these values.

B.1. Heat Release Rate

Heat Release Rate

All tests conducted in this study were performed underneath the 3 MW calorimeter in the National Fire Research Laboratory (NFRL). The measurement uncertainty (total expanded uncertainty) for this calorimeter (calculated as per Bryant and Bundy [68]) is defined as as 6.5% to 7.0% for heat release rates between 0.5 MW $\leq \mathrm{HRR} \leq$ 3.0 MW (average value, 6.8%) for generic combustible fuels. Measurement repeatability improves for larger fires and larger exhaust flows, and therefore its contribution to uncertainty decreases for these conditions. Peak heat release rate is often a desired parameter from a fire test. Preliminary experiments [68] suggest that the 3 MW calorimeter can accurately resolve a fire event with a peak lasting more than 15 s. For smaller fires (e.g., the burner flame used for ignition) heat release rate is considerably lower than the standard operating range of the 3 MW calorimeter; thus the expanded uncertainty of such lower HRR measurements is defined as 10 % (type B uncertainty).

Heat of Combustion

Heat of combustion, ΔH_c, measured during these parallel panel tests is calculated as as the integral of heat release rate measured throughout the duration of experiments (corrected for energy release by the propane burner while it is turned on) divided by total mass lost

during the experiment:

$$\Delta H_c = \frac{\left(\int_{t_{ign}}^{t_{ext}} \dot{Q}\, dt - \int_{t_{ign}}^{t_{burner\ off}} \dot{Q}_{burner}\, dt\right)}{m_{initial} - m_{final}} = \frac{THR}{\Delta m} \tag{B.4}$$

Here, t_{ign} represents the start of the test, i.e., the time when the burner is first ignited; $t_{burner\ off}$ represents the time when the burner is turned off; and t_{ext} represents the time at which extinction of sample flames was observed. The symbol $\dot{Q}$ represents total measured heat release rate and $\dot{Q}_{burner}$ represents energy from the propane burner flames; the difference between these two integral values can be defined as total heat released by the combustible solid, THR. Here, $\dot{Q}_{burner}$ is estimated as equal to the steady state heat release rate measured in burner shakedown tests (i.e., $\dot{Q}_{burner}$ = 63 kW; see Section 2.4).

The primary sources of uncertainty in ΔH_c are thus measurement uncertainty in (1) total heat released, $U_{THR} = 6.8\%$ and (2) measured mass loss, $0.1\% \leq U_{\Delta m} \leq 4.0\%$[39]. Expanded uncertainty in measured heat of combustion can thus be calculated as:

$$U_{\Delta H_c} = 2\sqrt{u_{THR}^2 + u_{\Delta m}^2} \tag{B.5}$$

Defining a representative value of $U_{\Delta m} = 1.5\ \%$, expanded uncertainty in ΔH_c can be calculated as: $U_{\Delta H_c} = 2\sqrt{\frac{6.8\%}{2}^2 + \frac{1.5\%}{2}^2} = 7.0\ \%$.

B.2. Heat Flux Measurements

Heat flux measurements reported in this work were determined by scaling the voltage generated by the thermopile of a Schmidt-Boelter heat flux gauge by a calibration constant that quantifies gauge sensitivity in units of kW m^{-2} mV^{-1}. Further details regarding heat flux gauge calibration are presented in Section 2.3.3 of this report.

The considered sources of error in heat flux measurements are thus: (a) random error due to fluctuations in heat flux readings during testing, (b) bias due to uncertainty in the calibration constant, and (c) the precision of the DAQ system used to resolve measurements from these gauges. Random error due to fluctuations during experiments is estimated by calculating the standard deviation of the mean of repeated measurements obtained within a +/- 3 s window (in all tests, heat flux measurements were obtained at 1 Hz). This random error varies as a function of gauge location, material type, and test number, thus a single combined uncertainty, u_c, cannot be defined for all heat measurements, rather it is defined uniquely (on a test-specific-basis, as needed) throughout this report. To provide further guidance on interpretation of this data, u_c for heat flux measurements is calculated below assuming random error in heat flux gauge readings can be approximated by its average value across tests (approximately 4.4 %). As seen in the example calculations below, for both the comprehensive and expedited calibration techniques,

[39] Note: large test to test variability in reported $U_{\Delta m}$ arises due to differences in material melt/dripping behavior, total amount of sample residue remaining at the end of an experiment, and the relative ease (or difficulty) in cleanly removing this residue at the completion of each test.

total uncertainty in heat flux measurements was dominated by this random error (fluctuations during testing).

B.2.1. Total Heat Flux to Panel Walls

Tests 1 - 15, 20, 37, 45; all Burner Shakedowns
For the first series of experiments, heat flux gauges were calibrated by direct comparison to an internal reference gauge (which was calibrated by the Radiometric Physics Division of NIST) when both were exposed to the same, steady incident heat flux supplied by a high-temperature tungsten lamp [80]. This calibration procedure is described in Section 2.3.3 of this report. The combined uncertainty of this calibration technique is calculated as the root sum of squares of the individual uncertainty components: blackbody calibration (1.5%), tungsten lamp calibration repeatbility (0.5%), and measured average drift in gauge sensitivity (1.3%).

- Precision (DAQ system: 0.01 %
- Calibration Bias (accuracy in tungsten lamp calibration apparatus): $\sqrt{1.5^2 + 0.5^2 + 1.3^2}$=2.08%
- Random error (mean random error due to fluctuations during testing): 4.4 %
- Combined Standard Uncertainty: $u_c(y) = 4.9\%$
- Total Expanded Uncertainty, $U_c(y) = 9.8\%$

Tests 16-19, 21-36, 38-44, and 46-66;
For the experiments conducted later in this test series, heat flux gauges were recalibrated by an expedited calibration procedure, as described in Section 2.3.3. Following this approach, at the *start of* a new round of testing, heat flux gauges were recalibrated as per the tungsten lamp procedure described above; however, *during* this test series, after gauges were cleaned and repainted, an average sensitivity coefficient was prescribed as the calculated mean value of all recent calibration results[40].

For each gauge, prior to testing, this average calibration was spot checked (but not adjusted) by placing the heat flux gauge of interest side by side with a secondary reference gauge, such that they were both positioned 2.54 cm below the center of the radiant heater of a cone calorimeter [82]. The cone heater was set to approximately 800°C to provide an incident radiant heat flux of approximately 50 kW m^{-2} and the response of the freshly painted gauge was recorded. On average (236 total spot checks), measured gauge response matched the reference value within 1%. Thus, this 1% average deviation is included as an additional source of uncertainty (bias) when calculating combined uncertainty, u_c. The combined uncertainty of this calibration technique was calculated as the root sum of

[40] A review of the historical record from all calibrations conducted on all gauges used in this project indicates that, after cleaning and repainting, individual calibrations (conducted as per the tungsten lamp method [80]) matched their average value within, on average, 0.85%.

squares of the individual uncertainty components: blackbody calibration (1.5%), tungsten lamp calibration repeatability (0.5%), cone calorimeter calibration repeatability (0.75%), and measured average drift in gauge sensitivity (1.3%).

- Precision (DAQ system): 0.01 %
- Calibration Bias (accuracy of tungsten lamp calibration, transfer calibration to cone heat flux gauge): $\sqrt{1.5^2 + 0.5^2 + 0.75^2 + 1.3^2}$=2.21%
- Calibration Bias (average variation of calibration spot checks): 1.0 %
- Random error (mean random error due to fluctuations during testing): 4.4 %
- Combined Standard Uncertainty: $u_c(y) = 5.0\%$
- Total Expanded Uncertainty, $U_c(y) = 10.0\%$

B.2.2. Radiation Heat Flux to Panel Walls

Measurements of radiation heat flux to the panel walls, $\dot{q}''_{\text{rad}}$, were obtained using water-cooled Schmidt-Boelter heat flux gauges that had been fitted at their front surface with a 1 mm thick ZnSe window of viewing angle 150°. This configuration will be referred to as a radiometer. Prior to each test, after cleaning and repainting of gauges, ZnSe windows were cleaned (soaked in an acetone solution and gently wiped with an acetone-soaked cotton cloth), reattached to a total heat flux gauge, and then calibrated beneath the heater of a cone calorimeter as per the expedited calibration procedure described above. Because this calibration requires comparison to a secondary standard (i.e., the cone calorimeter reference gauge), the uncertainty of this gauge's calibration constant (2.08%) is included as an additional source uncertainty when calculating u_c for the radiometer.

- Precision (DAQ system): 0.01 %
- Calibration Bias (accuracy of tungsten lamp calibration, transfer calibration to cone heat flux gauge): $\sqrt{1.5^2 + 0.75^2 + 0.75^2 + 1.3^2}$=2.28%
- Random error (mean random error due to fluctuations during testing): 2.4 %
- Combined Standard Uncertainty: $u_c(y) = 4.2\%$
- Total Expanded Uncertainty, $U_c(y) = 8.4\%$

B.2.3. Radiative Fraction of Total Heat Flux to Panel Walls

In this work, the fraction of total flame heat flux attributed to radiation was calculated as $q_{rad}(\%) = \frac{\dot{q}''_{\text{rad}}}{\dot{q}''_{\text{total}}}$, where, $\dot{q}''_{\text{rad}}$, represents radiation heat transfer to the wall and $\dot{q}''_{\text{total}}$, represents total heat transfer to the wall. In this work, multiple tests were conducted in which $\dot{q}''_{\text{rad}}$ and $\dot{q}''_{\text{total}}$ were measured by a pair of water-cooled heat flux gauges each located at the same height, z, and 7.5 cm from the centerline, $y = 0$, of one wall. To protect the gauge's surface from deposits (which could reduce gauge sensitivity, especially that of the radiometer), both of these gauges were shielded during the initial stages of experiments by small, custom fitted pieces of insulation. Once steady flaming conditions were observed across the surface of both gauges, the shields were removed and a 'clean gauge' measurement of incident heat flux was recorded.

For each measurement, (a) random error due to fluctuations in heat flux readings shortly after shield removal, (b) bias due to uncertainty in the calibration constant, and (c) the precision of the DAQ system used to resolve measurements from these gauges. Given the potential for measured flame heat flux to vary after shield removal, $\dot{q}''_{\text{rad}}$ and $\dot{q}''_{\text{total}}$ are calculated and reported as discrete values: specifically as the maximum average heat flux (during a 3 s running average) recorded within 10 s of shield removal. Random error in $\dot{q}''_{\text{rad}}$ and $\dot{q}''_{\text{total}}$ are thus estimated as the standard deviation of the mean of "good"[41] heat flux measurements obtained during this time period; precision and bias components of uncertainty are defined as noted above.

The combined standard uncertainty of $q_{rad}(\%)$ is therefore calculated as the root sum of squares of u_c of both $\dot{q}''_{\text{rad}}$ and $\dot{q}''_{\text{total}}$:

$$u_c\left(q_{rad}(\%)\right) = \sqrt{\left(u_c(\dot{q}''_{\text{rad}})\right)^2 + \left(u_c(\dot{q}''_{\text{total}}\right)^2} \tag{B.6}$$

The expanded uncertainty of $q_{rad}(\%)$ is defined as:

$$U_c\left(q_{rad}(\%)\right) = k * u_c\left(q_{rad}(\%)\right) \tag{B.7}$$

where the coverage factor, k, is taken as equal to 2, to define a confidence level of approximately a 95%.

B.2.4. Radiative Heat Flux Away From Panel Walls

The heat flux gauge positioned beneath the corner of the 3 MW calorimeter's exhaust hood to measure radiation heat transfer away from the panel walls was calibrated by direct comparison to an internal reference gauge (secondary standard which was originally calibrated by the Radiometric Physics Division of NIST) when both were exposed to the same, steady incident heat flux supplied by a high-temperature tungsten lamp. The combined uncertainty, u_c, for this heat flux gauge is thus calculated as follows:

[41] Heat flux measurements recorded by each individual gauge (in each test) were identified as "good" (e.g., when flame coverage was uniform across the sample wall) or "bad" (e.g., when sample deformation affected gauge readings or when uneven flaming was observed) as discussed in Sec. 3.1.1.

- Precision (DAQ system): 0.01 %
- Calibration Bias (accuracy of tungsten lamp calibration): $\sqrt{1.5^2 + 0.75^2 + 1.3^2}$=2.16%
- Random error (mean random error due to fluctuations in heat flux readings during testing): 4.1 %
- Combined Standard Uncertainty: $u_c(y) = 5.4\%$
- Total Expanded Uncertainty, $U_c(y) = 10.8\%$

B.3. Species Yields, Y_{CO}, $Y_{\mathrm{CO_2}}$, and Y_{soot}

The generation rates of combustion products (carbon monoxide, CO; carbon dioxide, CO_2; soot) are calculated over the time period from ignition (t_{ign}) to fire out (t_{out}). These two events are marked electronically in the data file and are required in order to generate the standard report reported in the Fire Calorimetry Database [1]. Species yields are calculated by dividing the total amount of a species generated between t_{ign} and t_{out} by the mass of fuel consumed by the fire, Δm_{fuel}. This mass, Δm_{fuel}, can estimated by the two different methods listed below. If both fuel consumption measurements are available, the value used to calculate species yields is the one with lower uncertainty.

- Mass loss by load cell measurements: Δm_{fuel} is calculated as the difference in specimen mass measured (by a load cell) before and after the test. Here, uncertainty includes the reported accuracy of the load cell (Type A uncertainty) and estimates (Type B uncertainty) of how well the sample residue could be collected and measured at the end of a test (e.g., sample residue could be lost if stuck to the panel assembly *or* remnants of aluminum foil, drywall, or marinite could have become embedded in the sample residue/melt pool). On average, this uncertainty averaged 4.4 %.
- Mass loss by calorimetry: Δm_{fuel} is calculated by dividing the measured total heat release (THR) by a measured fuel heat of combustion (here, heats of combustion measured in the MCC are used; see discussion in Sec 3.4). Uncertainty in measured heat release is discussed above; uncertainty in these heats of complete combustion (when used as surrogates to characterize large scale burning behavior in the parallel panel assembly) is estimated as 15% (type B uncertainty).

Gaseous Species Yields: Y_{CO} and $Y_{\mathrm{CO_2}}$

The total amounts of product species generated are given by:
Total CO_2 = $\frac{M_{\mathrm{CO_2}}}{M_{\mathrm{air}}} \sum_{t=t_{ign}}^{t_{out}} [X_{\mathrm{CO_2}} - X^0_{\mathrm{CO_2}}] \dot{m}_e \Delta t$
Total CO = $\frac{M_{\mathrm{CO}}}{M_{\mathrm{air}}} \sum_{t=t_{ign}}^{t_{out}} [X_{\mathrm{CO}} - X^0_{\mathrm{CO}}] \dot{m}_e \Delta t$

where:
$\dot{m}_e$ = mass flow rate in exhaust duct, [kg/s]
M_i = molecular weight of gas i, [kg/kmole]
X_i = volume fraction of exhaust gas i, [L/L]
X_i^0 = volume fraction of ambient gas i, [L/L]

and the species yields are thus given by:
CO_2 Yield = $Y_{CO_2} = \frac{\text{Total } CO_2}{\Delta m_{\text{fuel}}}$
CO Yield = $Y_{CO} = \frac{\text{Total CO}}{\Delta m_{\text{fuel}}}$

The combined uncertainty of each product species is calculated as the root sum of squares of the individual uncertainty components: (1) total amount of species generated and (2) mass of fuel consumed by the fire, Δm_{fuel}. A full uncertainty budget for measured values of carbon monoxide and carbon dioxide is provided in Ref. [68]; for simplicity, expanded uncertainties are reported here:

- $\frac{U_c(\text{CO})}{X_{\text{CO}}}$ = 0.0052
- $\frac{U_c(\text{CO}_2)}{X_{\text{CO}_2}}$ = 0.0012.

Gaseous species yields are corrected for CO and CO_2 generation by the propane burner by assuming that propane flames burn similarly in the presence of each combustible solid vs. in open air, and subtracting the expected amount of CO and CO_2 generated during the burner application duration. For fuels with gas-phase active flame retardants (e.g., SIS Wire or chlorinated materials such as PVC and PMMA-PVC), propane combustion may not be complete, thus this correction (i.e., subtraction) may $under$estimate CO generation by the propane burner flames and thus $over$estimate the calculated CO yield of the combustible solid of interest.

Soot Yield: Y_{soot}

The smoke particulate generated by the fire is measured via the light extinction of a HeNe laser beam across the center of the exhaust duct (assuming a specific extinction coefficient [75] of flame generated smoke: 8.71 $m^2/g \pm 0.47$ m^2/g). The design and implementation of this optical technique (and reported experimental uncertainties) are described elsewhere [74].

In several parallel panel tests, the density of smoke in the exhaust duct was sufficiently high that measured intensity (Si photodiode detector) was zero: $I(t) = 0$. At these times in the tests, soot generation rate is thus greater than that which can be accurately measured. Soot yields are therefore calculated by integrating measured soot generation rate between calculated t_{ign} and t_{out} $only$ when $I(t) > 0$ and dividing this value be a reduced mass loss (sample mass burned only during this time period, when $I(t) > 0$). This reduced mass loss

was calculated by scaling total sample mass loss, Δm_{fuel}, by the ratio of [measured heat release during this time period] divided by [total heat released during the experiment].

B.4. Sensor Location

Precision, bias, and random error of all sensor location measurements are estimated as Type B Uncertainties.

Heat Flux Gauges Mounted in Panel Walls

- Precision (ability to read tape measure with eye): 1 mm
- Bias (accuracy of tape measure increments): 1 mm
- Random error (estimate based on alignment of bottom panel of sample slab): 5 mm
- Combined Standard Uncertainty: $u_c(y) = 5.2$ mm
- Total Expanded Uncertainty, $U_c(y) = 10.4$ mm

Heat Flux Gauge Positioned Away From Panel Walls

In all tests, the parallel panel apparatus was positioned at the center of the NFRL's 3 MW exhaust hood; this exhaust hood measures 6.1 m by 6.1 m square. To measure radiation heat transfer at a distance away from the panels, a Schmidt-Boelter heat flux gauge was positioned directly beneath one corner of this exhaust hood. Uncertainty in the location of this heat flux gauge is calculated as follows:

- Precision (ability to align heat flux gauge with corner of exhaust hood): 15 cm
- Bias (accuracy of tape measure increments): 1 cm
- Random error (e.g., movement of gauge between test repetitions): 2.5 cm
- Combined Standard Uncertainty: $u_c(y) = 15.2$ cm
- Total Expanded Uncertainty, $U_c(y) = 30.5$ cm

C. Test-Specific Experimental Results: Measurement Data and Sample Behavior

C.1. ABS - Poly(acrylonitrile butadiene styrene)

Test 47 ABS R1

Test Description
1/4 in. thick, 24 in. wide, 96 in. tall panels of ABS backed by aluminum foil (bottom 1 foot on the right side ONLY) mounted to 1 in. thick Marinite board. Panels were ignited using a rectangular propane burner (60 kW nominal heat release rate) filled with layers of Pea Gravel, Sand, and Kaowool Insulation (i.e., the 'Final Burner configuration'; see Fig. 12). Burner flames uniformly attached to both panel walls after approximately 15 s and the burner was shut off ($t = 76$ s) and shielded ($t = 88$ s) after sustained, uniform flaming of panels. Flame to wall heat flux measurements were not recorded in this test.

(a) Pre-test

(b) Ignition

(c) Peak HRR

(d) End of Test

Fig. 83. Photographs of Test 47 ABS R1.

Heat Release Rate, Heat Flux at a Distance, and Species Yields

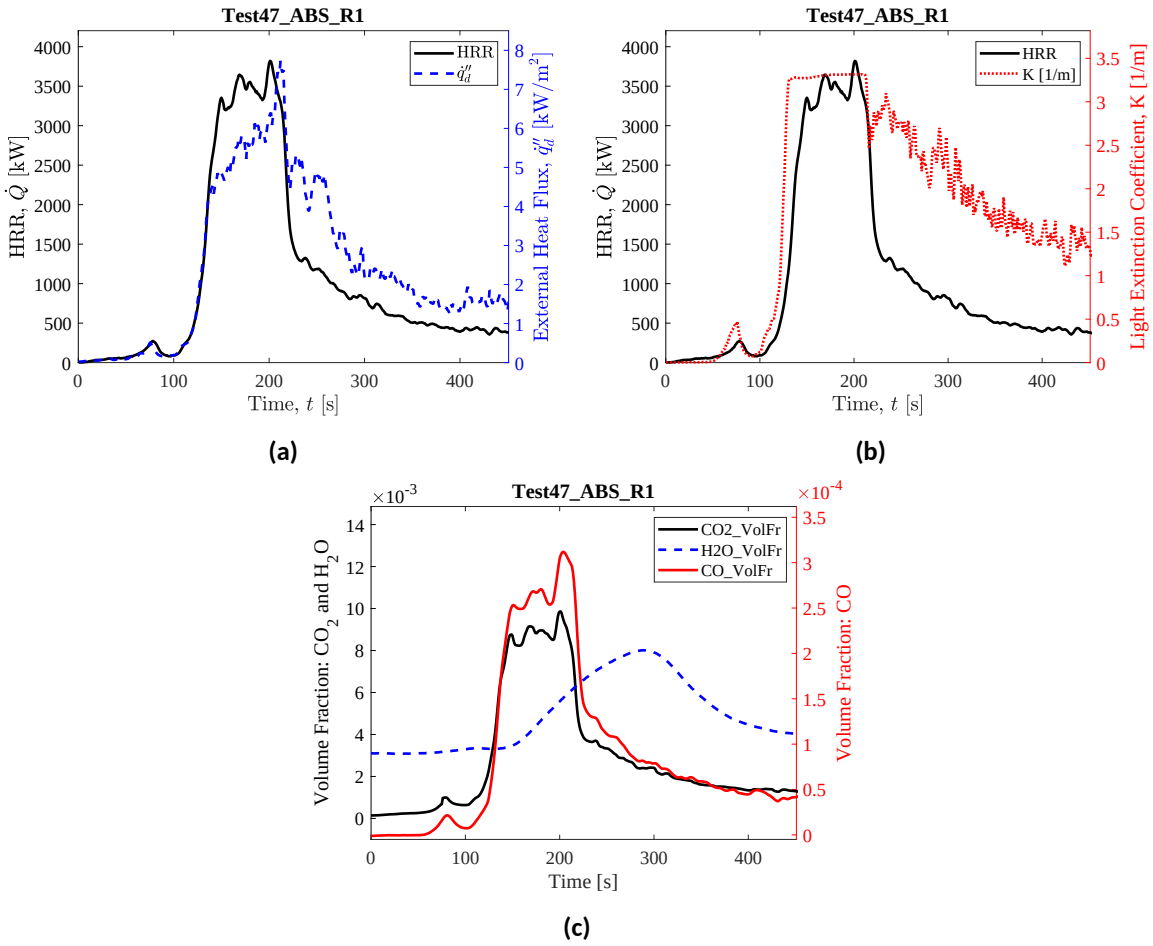

Fig. 84. Test 47 ABS R1: (a) Heat release rate and heat flux at a distance, $\dot{q}''_{\mathrm{d}}$ (here, $\dot{q}''_{\mathrm{d}}$ is measured at x =-220 cm, y =-310 cm, z =90 cm); (b) Heat release rate and light extinction coefficient, K (smoke particulate in exhaust duct [111]); (c) Time-resolved volume fractions of CO_2, H_2O, and CO.

Test 51 ABS R2

Test Description
1/4 in. thick, 24 in. wide, 96 in. tall panels of ABS mounted to 1 in. thick Marinite board. Panels were ignited using a rectangular propane burner (60 kW nominal heat release rate) filled with layers of Pea Gravel, Sand, and Kaowool Insulation (i.e., the 'Final Burner configuration'; see Fig. 12). Burner flames were fairly uniform shortly after the burner was turned on the burner was shut off ($t = 77$ s) and shielded ($t = 85$ s) after sustained flaming of panels. Heat flux gauges were mounted flush with the fuel's surface between $z = 20$ cm and $z = 180$ cm. Shielded radiometers and total heat flux gauges were positioned side by side at $z =$100 cm and $z = 180$ cm. The heat flux shields were removed at $t =$132 s.

(a) Pre-test

(b) Ignition

(c) Peak HRR

(d) End of Test

Fig. 85. Photographs of Test 51 ABS R2.

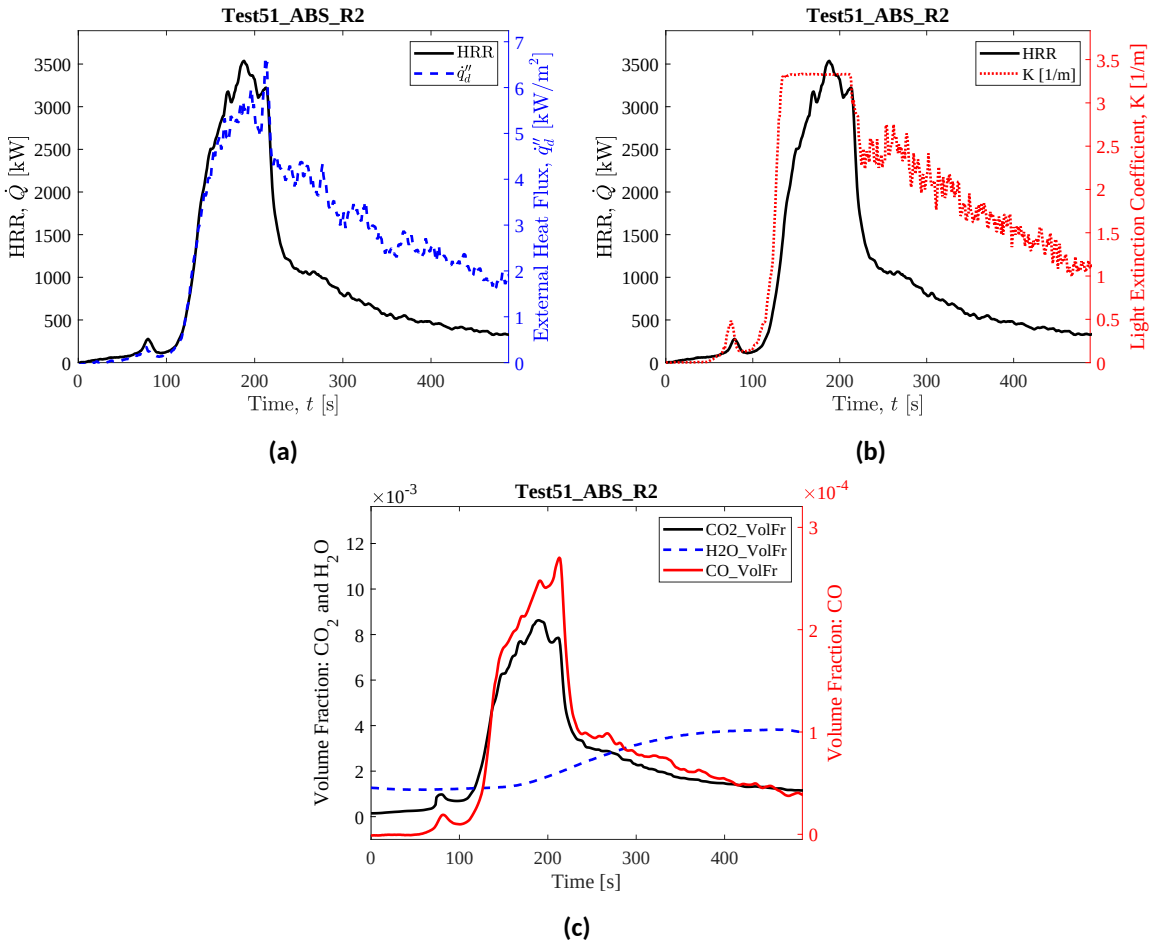

Fig. 86. Test 51 ABS R2: (a) Heat release rate and heat flux at a distance, $\dot{q}''_{\mathrm{d}}$ (here, $\dot{q}''_{\mathrm{d}}$ is measured at x =-220 cm, y =-310 cm, z =90 cm); (b) Heat release rate and light extinction coefficient, K (smoke particulate in exhaust duct [111]); (c) Time-resolved volume fractions of CO_2, H_2O, and CO.

Flame Heat Flux

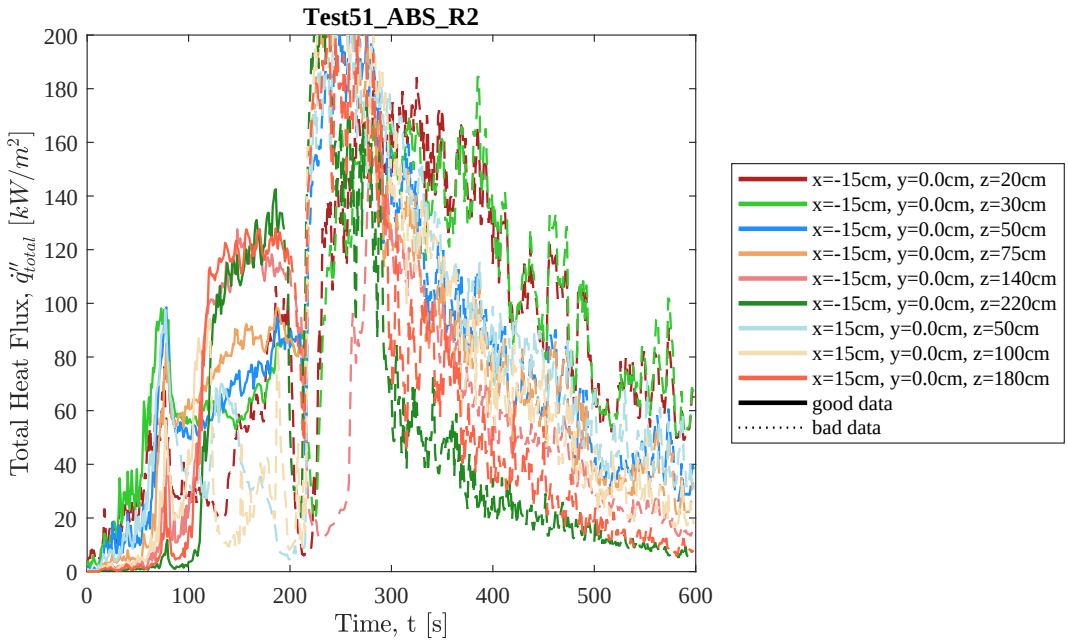

Fig. 87. Total flame to surface flame heat flux to water-cooled Schmidt-Boelter heat flux gauges as measured in Test 51 ABS R2. Here, raw, unsmoothed original measurments are plotted from each gauges as a function of time. Solid lines highlight values of $\dot{q}''_{\text{total}}$ that were identified by manual review as ”good” (see Sec. 3.1.1) and dotted lines represent ”bad” measurement data that should not be considered for further analysis.

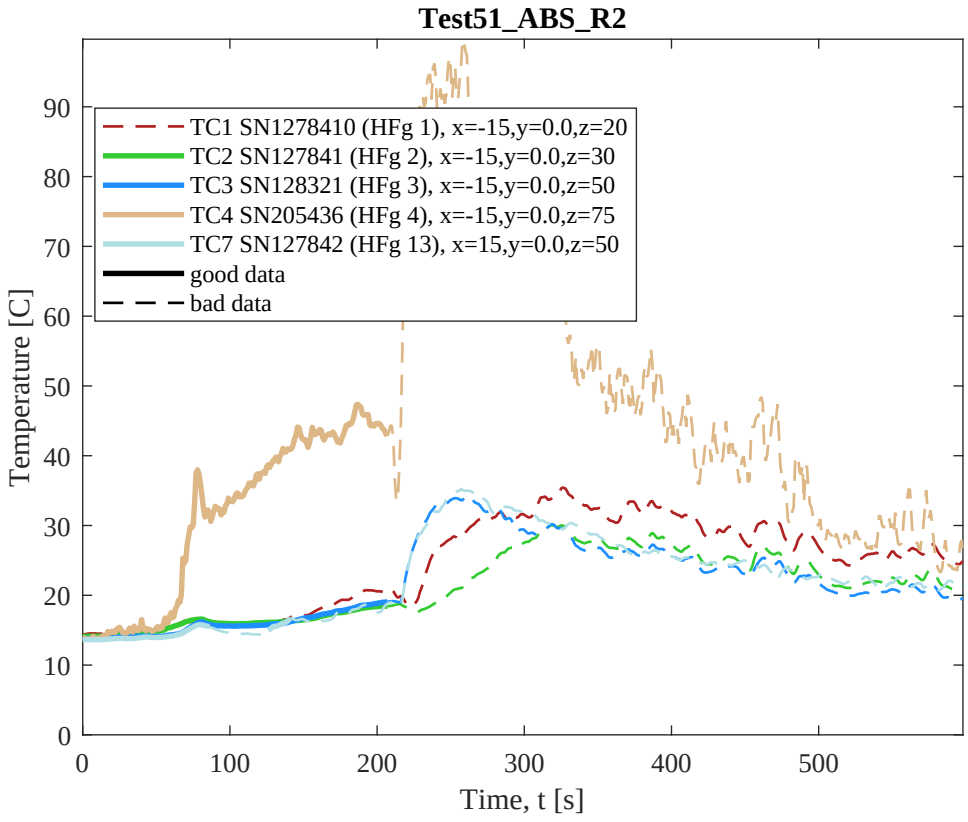

Fig. 88. Temperature of water-cooled Schmidt-Boelter heat flux gauges during Test 51 ABS R2.

Shielded Gauges

Measurements of total and radiation heat flux recorded by shielded heat flux gauges (Sec. efssec: qrad). Gauge shields were removed at 235, 229, 227, and 231 seconds (gauges 5, 6, 8 and 9, respectively).

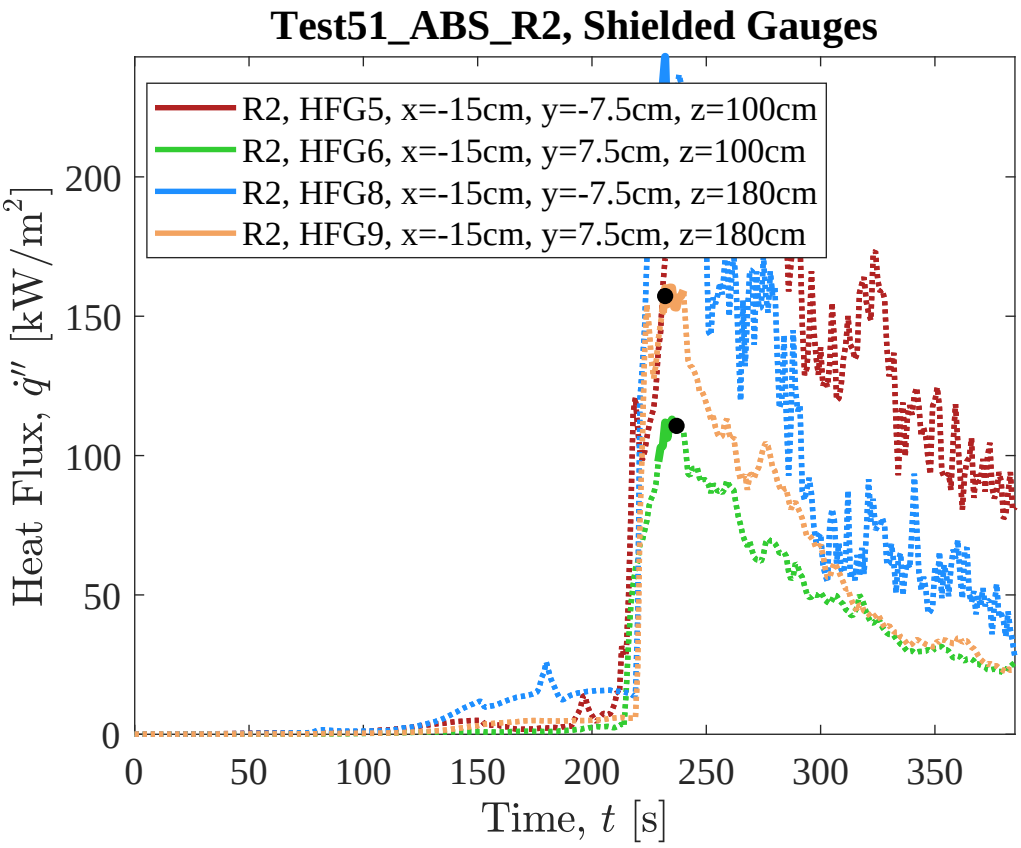

Fig. 89. Shielded gauge data for Test51 ABS R2.

Test 53 ABS R3

Test Description

1/4 in. thick, 24 in. wide, 96 in. tall panels of ABS mounted to 1 in. thick Marinite board. Panels were ignited using a rectangular propane burner (60 kW nominal heat release rate) filled with layers of Pea Gravel, Sand, and Kaowool Insulation (i.e., the 'Final Burner configuration'; see Fig. 12). The burner was shut off ($t = 77$ s) and shielded ($t = 88$ s) after sustained flaming of panels. Unforunately, a significant cross flow was observed during these tests (from back to front of the assembly), thus the flames do not cover centerline gauges or the back side of the panels as the flames spread upwards across the panels. Although flames reached the top of the assembly relatively quickly, uniform flaming was not observed across either wall until later in the test, as a result of lateral flame spread. Heat flux gauges were mounted flush with the fuel's surface between $z = 30$ cm and $z = 180$ cm. Shielded radiometers and total heat flux gauges were positioned side by side at $z =$100 cm and $z = 180$ cm. The heat flux shields were removed at $t =$174 s (after flames were observed to fully cover both gauge locations).

(a) Pre-test

(b) Ignition

(c) Peak HRR

(d) End of Test

Fig. 90. Photographs of Test 53 ABS R3.

Heat Release Rate, Heat Flux at a Distance, and Species Yields

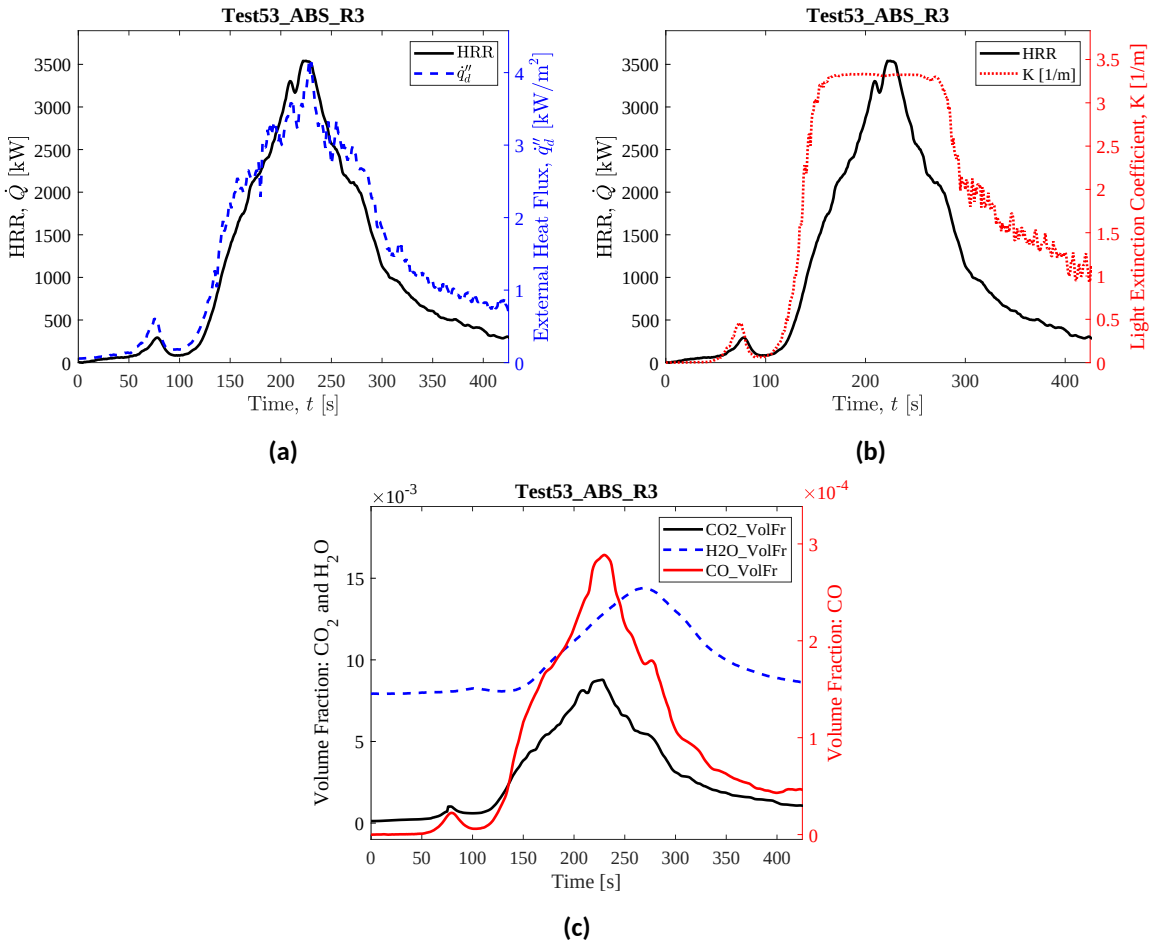

Fig. 91. Test 53 ABS R3: (a) Heat release rate and heat flux at a distance, $\dot{q}''_{\mathrm{d}}$ (here, $\dot{q}''_{\mathrm{d}}$ is measured at x =300 cm, y =-305 cm, z =90 cm); (b) Heat release rate and light extinction coefficient, K (smoke particulate in exhaust duct [111]); (c) Time-resolved volume fractions of CO_2, H_2O, and CO.

Flame Heat Flux

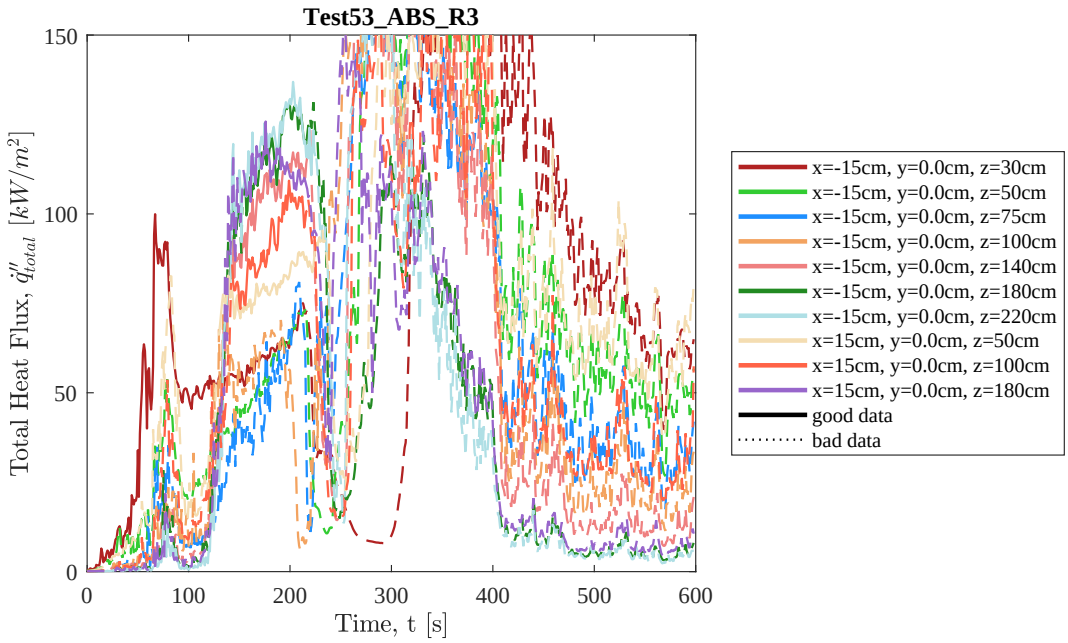

Fig. 92. Total flame to surface flame heat flux to water-cooled Schmidt-Boelter heat flux gauges as measured in Test 53 ABS R3. Here, raw, unsmoothed original measurments are plotted from each gauges as a function of time. Solid lines highlight values of $\dot{q}''_{\text{total}}$ that were identified by manual review as ”good” (see Sec. 3.1.1) and dotted lines represent ”bad” measurement data that should not be considered for further analysis.

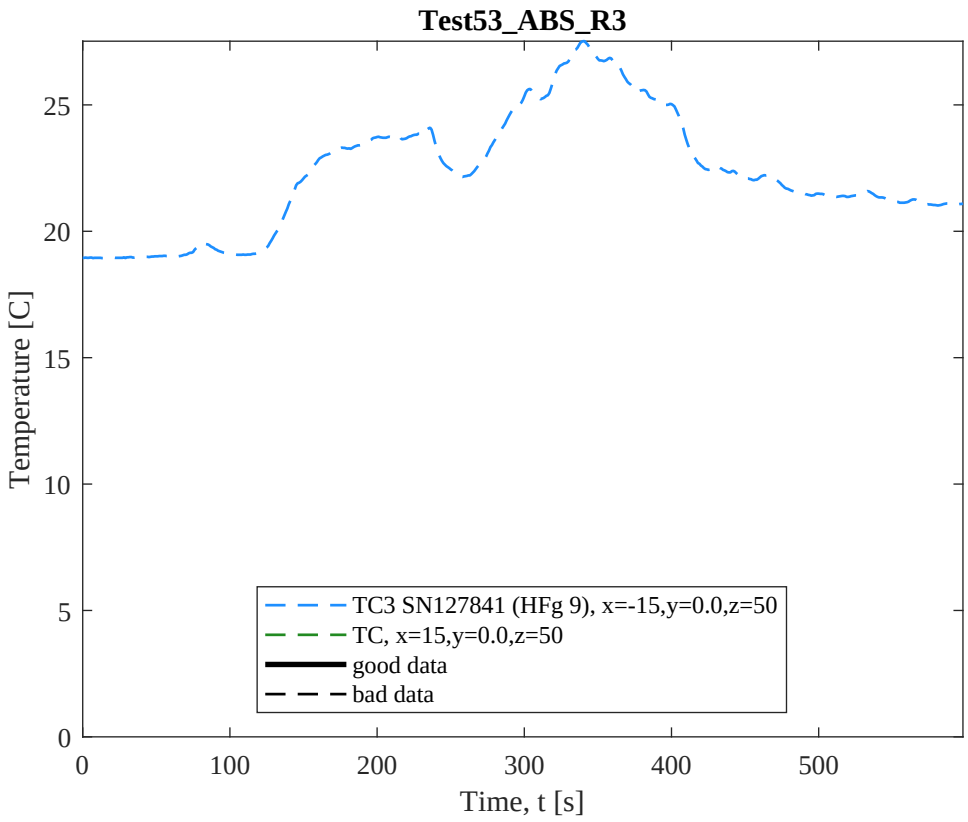

Fig. 93. Temperature of water-cooled Schmidt-Boelter heat flux gauges during Test 53 ABS R3.

Shielded Gauges

Measurements of total and radiation heat flux recorded by shielded heat flux gauges (Sec. efssec: qrad). Gauge shields were removed at 175, 176, and 176 seconds (gauges 5, 6, and 8, respectively).

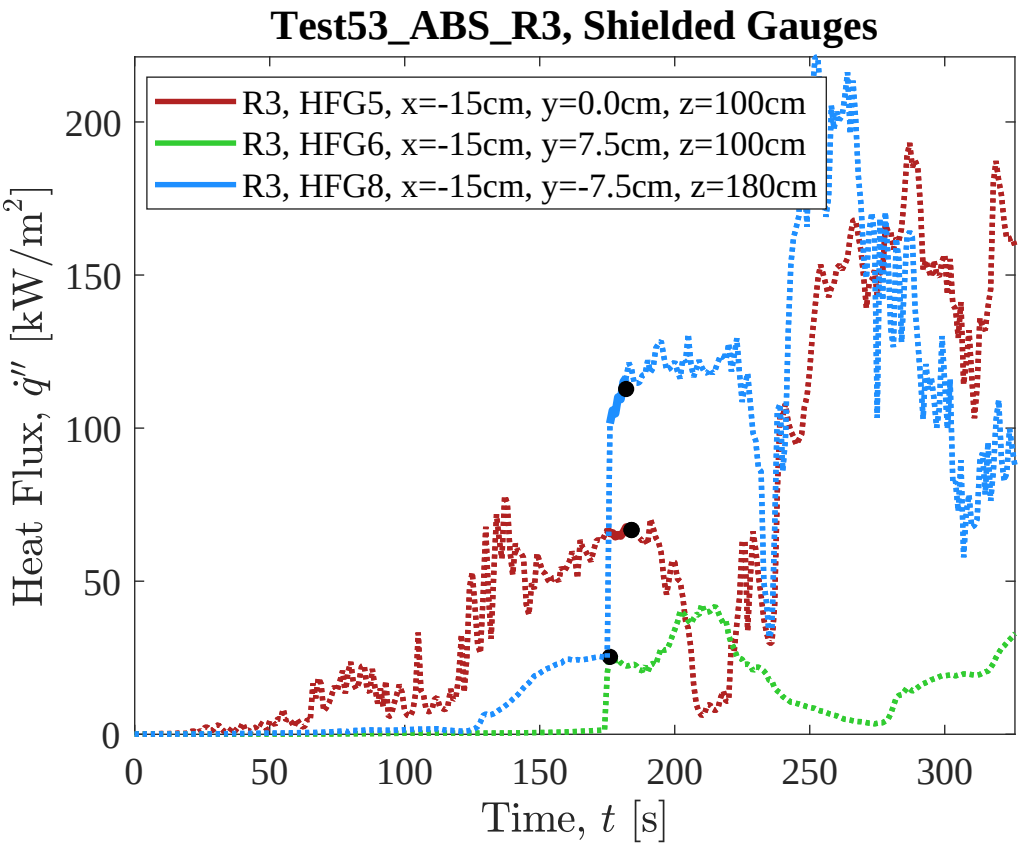

Fig. 94. Shielded gauge data for Test53 ABS R3.

C.2. GPO-1 - Fiberglass-Reinforced Polyester laminate (limited arc- and flame-resistance)

Test 17 GPO1 R1

Test Description

1/4 in. thick, 24 in. wide, 96 in. tall panels of GPO-1 mounted to 1 in. thick Marinite board. Panels were ignited using a rectangular propane burner (60 kW nominal heat release rate) filled with layers of Pea Gravel, Sand, and Kaowool Insulation (i.e., the 'Final Burner configuration'; see Fig. 12). In this test, although propane burner flames tended to attach more to the right wall than to the left, the front 10 cm (i.e., 20 cm $\leq y \leq 30$ cm) of the right panel did not initially ignite due to burner non-uniformity; however, sustained flaming was observed on both walls (slightly higher flames along the right wall) by the time that the burner was shut off ($t = 215$ s). Heat flux gauges were mounted flush with the fuel's surface, primarily between $z = 20$ cm and $z = 50$ cm, with one gauge at $z = 220$ cm. Heat flux measurements recorded on the right wall at $z = 50$ cm and $y = 25$ cm are lower than expected throughout the first 3?00 s of the test due to limite flame coverage resulting from burner non-uniformity. Shielded radiometers and total heat flux gauges were positioned side by side at z =50 cm and $z = 100$ cm. The heat flux shields were removed at t =392 s.

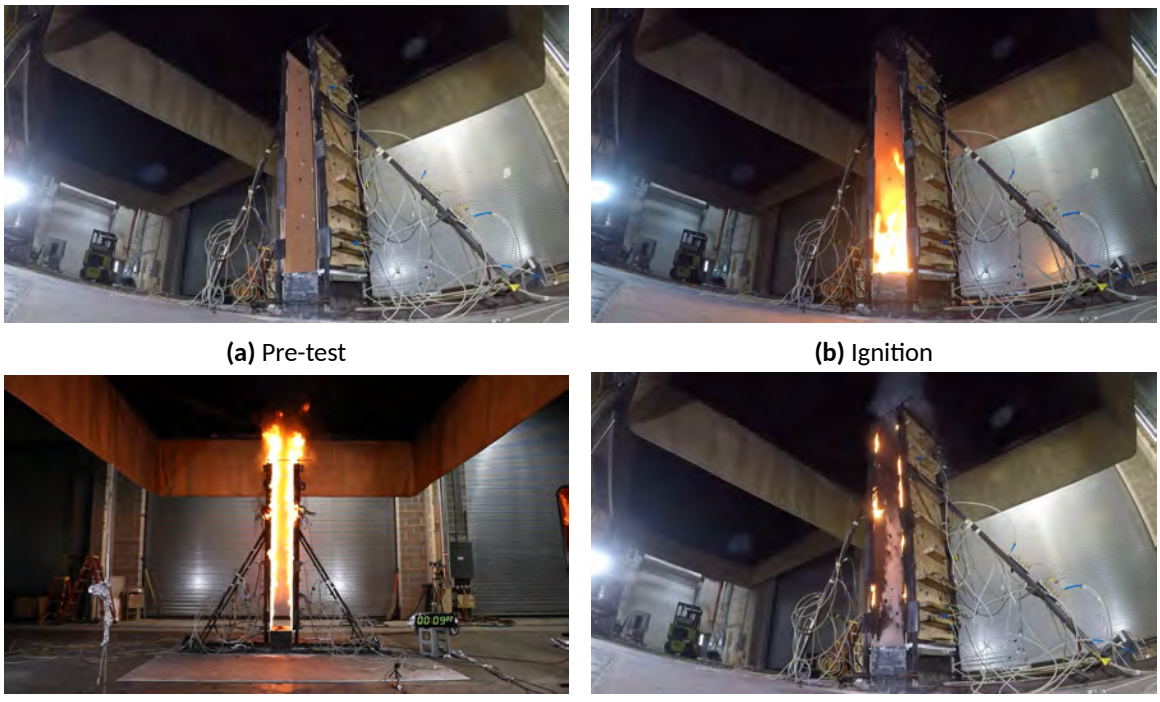

(a) Pre-test

(b) Ignition

(c) Peak HRR

(d) End of Test

Fig. 95. Photographs of Test 17 GPO1 R1.

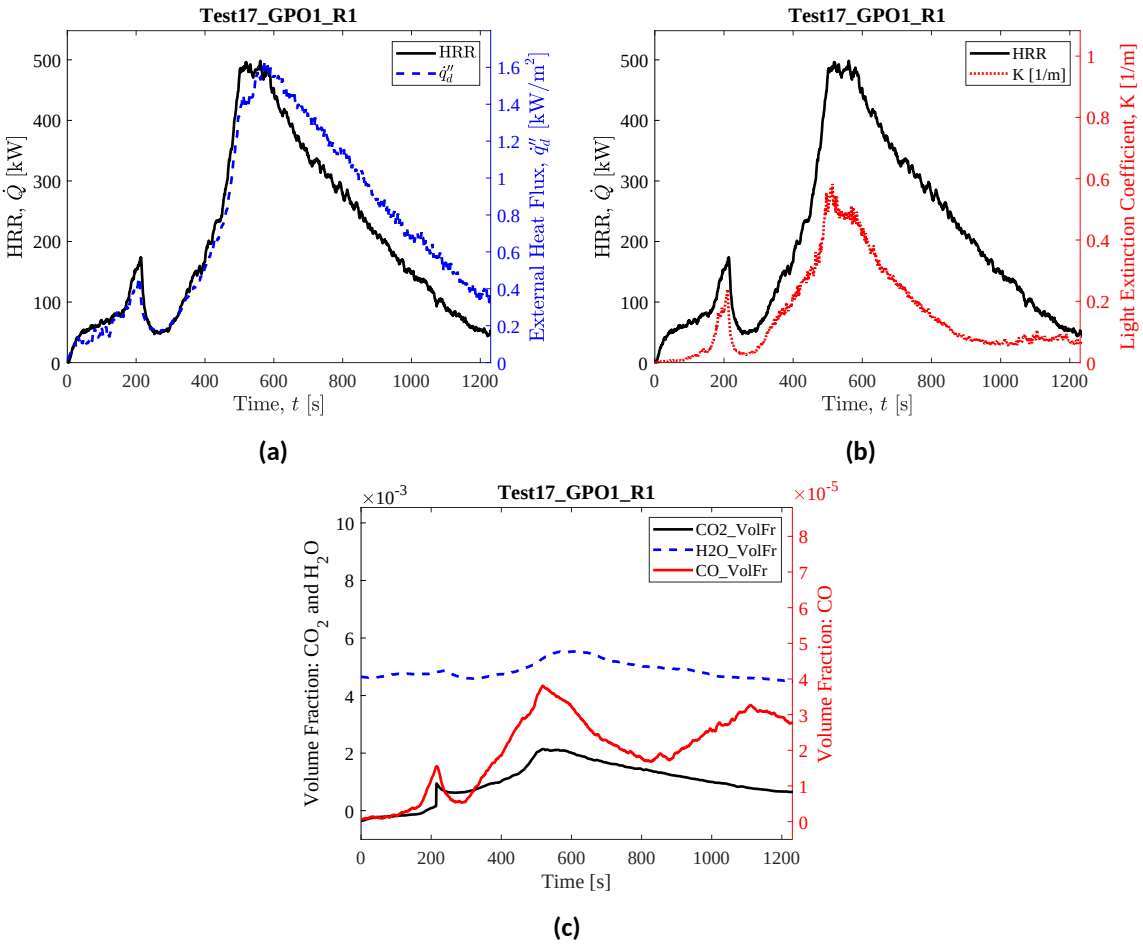

Fig. 96. Test 17 GPO1 R1: (a) Heat release rate and heat flux at a distance, $\dot{q}''_{\mathrm{d}}$ (here, $\dot{q}''_{\mathrm{d}}$ is measured at x =-100 cm, y =-300 cm, z =90 cm); (b) Heat release rate and light extinction coefficient, K (smoke particulate in exhaust duct [111]); (c) Time-resolved volume fractions of CO_2, H_2O, and CO.

Flame Heat Flux

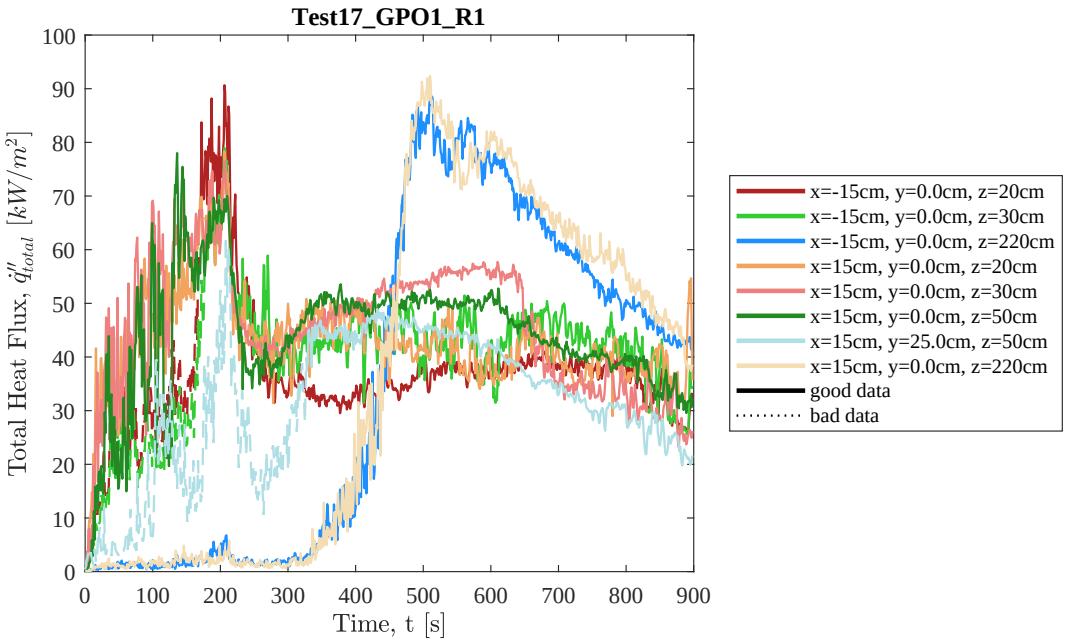

Fig. 97. Total flame to surface flame heat flux to water-cooled Schmidt-Boelter heat flux gauges as measured in Test 17 GPO1 R1. Here, raw, unsmoothed original measurments are plotted from each gauges as a function of time. Solid lines highlight values of $\dot{q}''_{\text{total}}$ that were identified by manual review as ”good” (see Sec. 3.1.1) and dotted lines represent ”bad” measurement data that should not be considered for further analysis.

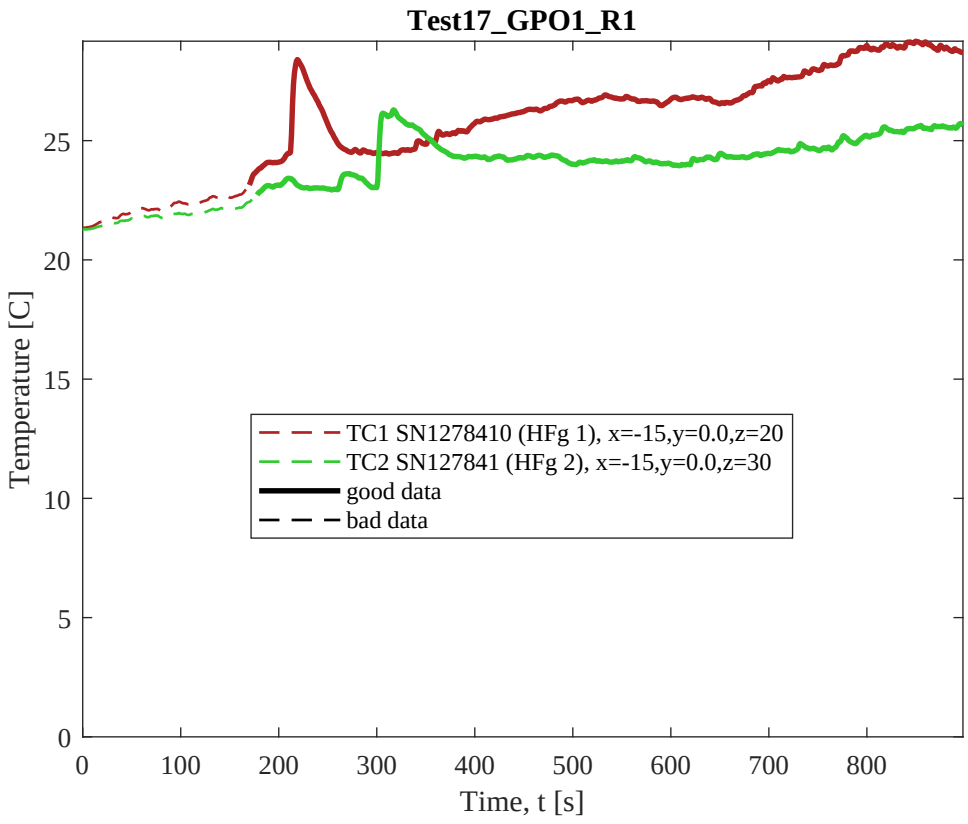

Fig. 98. Temperature of water-cooled Schmidt-Boelter heat flux gauges during Test 17 GPO1 R1.

Shielded Gauges

Measurements of total and radiation heat flux recorded by shielded heat flux gauges (Sec. efssec: qrad). Gauge shields were removed at 394, 394, 397, and 395 seconds (gauges 3, 4, 5 and 6, respectively).

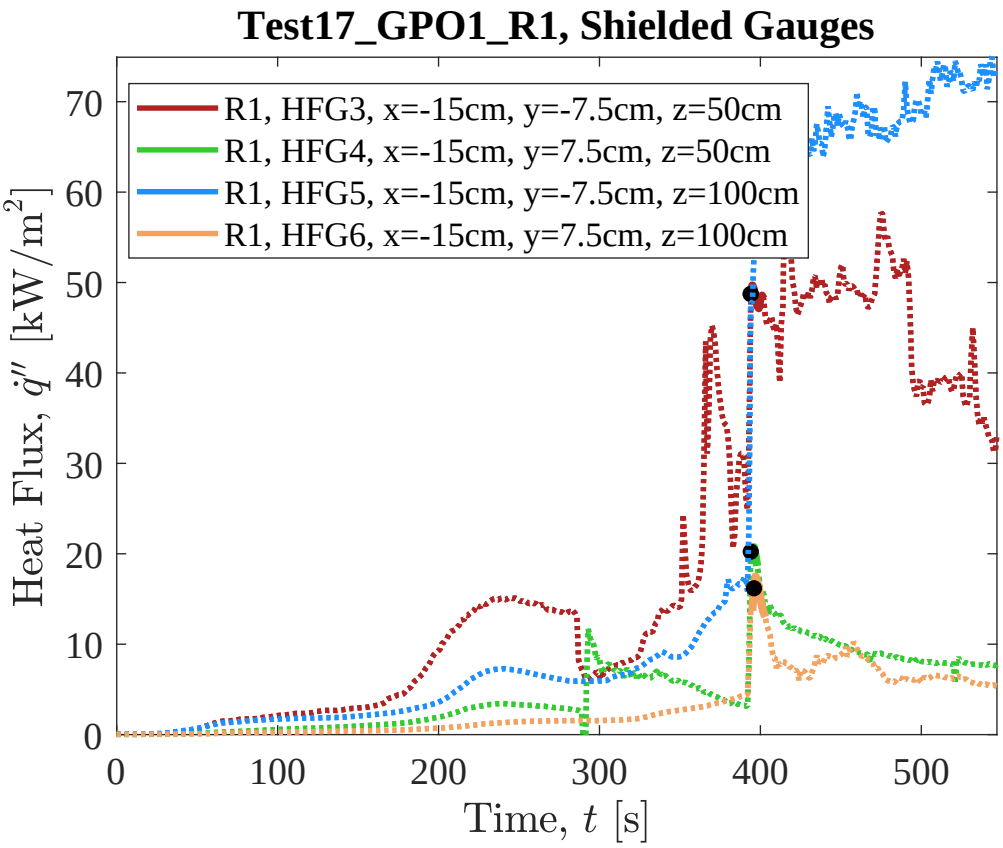

Fig. 99. Shielded gauge data for Test17 GPO1 R1.

Test 40 GPO1 R2

Test Description

1/4 in. thick, 24 in. wide, 96 in. tall panels of GPO-1 backed by aluminum foil (bottom 2 feet only) mounted to 1 in. thick Marinite Board. Panels were ignited using a rectangular propane burner (60 kW nominal heat release rate) filled with layers of Pea Gravel, Sand, and Kaowool Insulation (i.e., the 'Final Burner configuration'; see Fig. 12. In this test, the front 15 cm (i.e., -30 cm $\leq y \leq -15$ cm) of the left panel did not initially ignite due to burner non-uniformity (limited burner flame attachment at the front side of the left panel wall); however, sustained flaming was observed on both walls by the time that the burner was shut off ($t = 228$ s). Heat flux gauges were mounted flush with the fuel's surface between $z = 10$ cm and $z = 140$ cm. Shielded radiometers and total heat flux gauges were positioned side by side at z =100 cm and $z = 180$ cm. The lower heat flux shields were removed at t =470 s and the upper heat flux shields were removed at t =546 s; however, reliable measurements of both total and radiation flame heat flux were obtained only at $z = 100$ cm.

(a) Pre-test

(b) Ignition

(c) Peak HRR

(d) End of Test

Fig. 100. Photographs of Test 40 GPO1 R2.

Heat Release Rate, Heat Flux at a Distance, and Species Yields

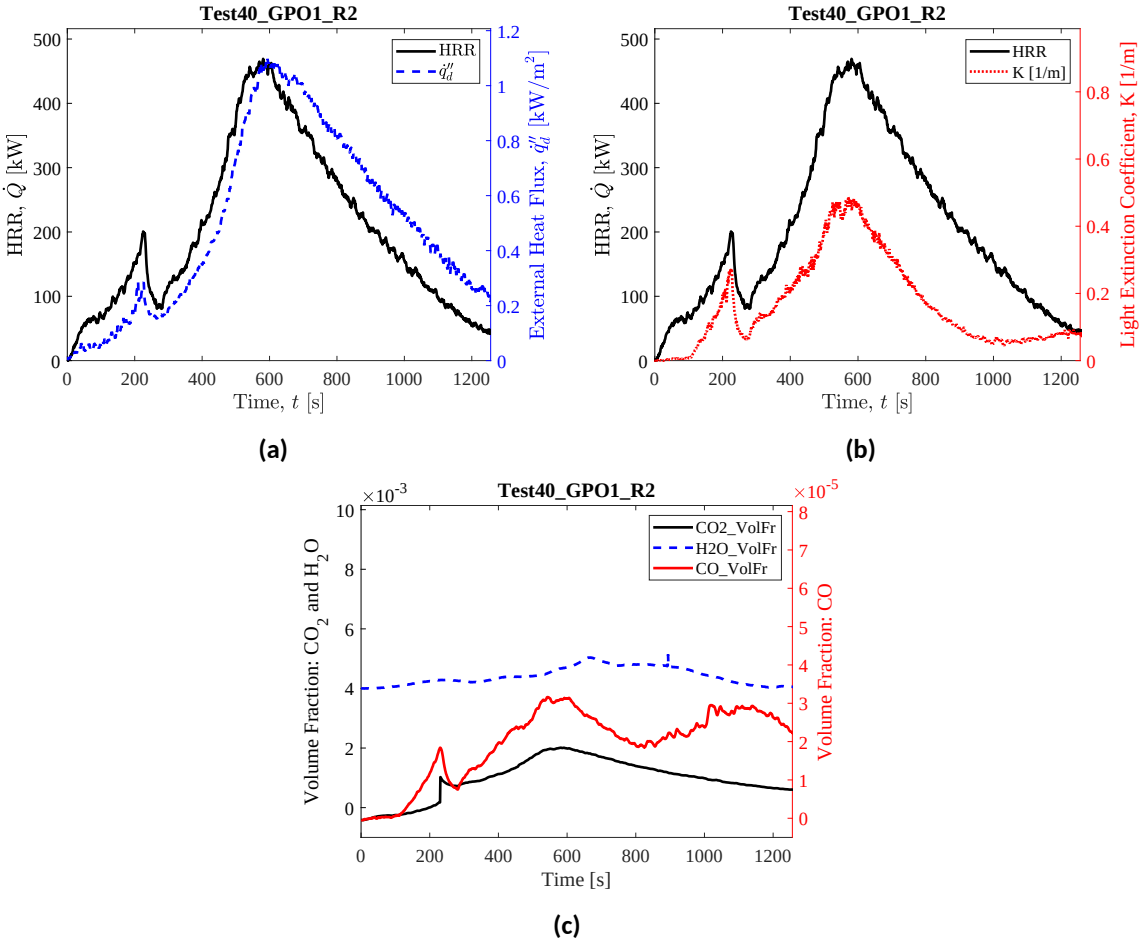

Fig. 101. Test 40 GPO1 R2: (a) Heat release rate and heat flux at a distance, $\dot{q}''_{\mathrm{d}}$ (here, $\dot{q}''_{\mathrm{d}}$ is measured at x =-232 cm, y =-300 cm, z =90 cm); (b) Heat release rate and light extinction coefficient, K (smoke particulate in exhaust duct [111]); (c) Time-resolved volume fractions of CO_2, H_2O, and CO.

Flame Heat Flux

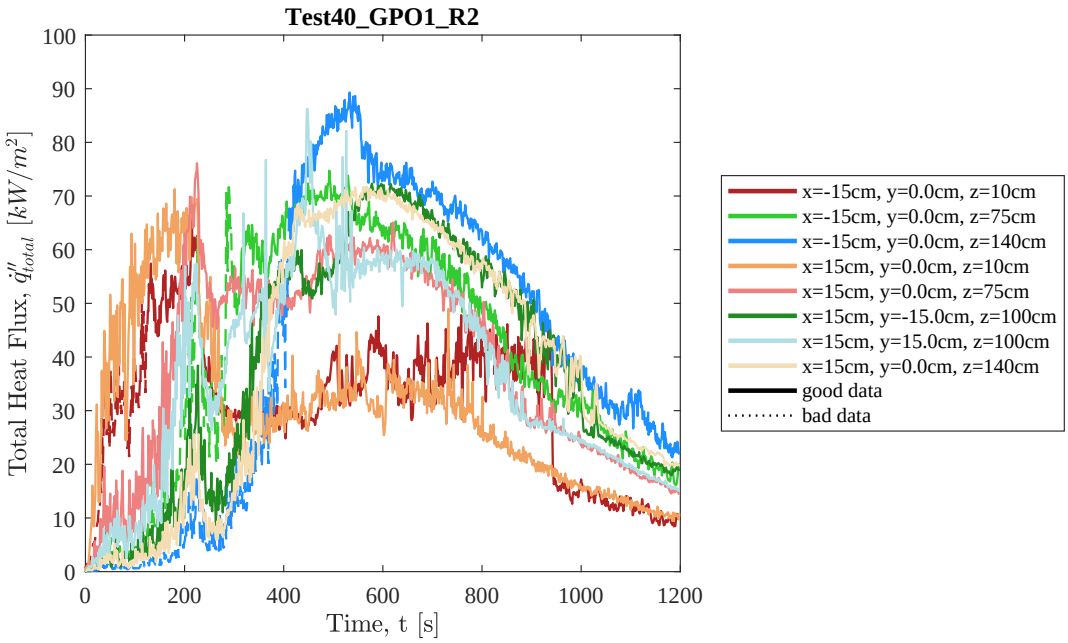

Fig. 102. Total flame to surface flame heat flux to water-cooled Schmidt-Boelter heat flux gauges as measured in Test 40 GPO1 R2. Here, raw, unsmoothed original measurments are plotted from each gauges as a function of time. Solid lines highlight values of $\dot{q}''_{\text{total}}$ that were identified by manual review as ”good” (see Sec. 3.1.1) and dotted lines represent ”bad” measurement data that should not be considered for further analysis.

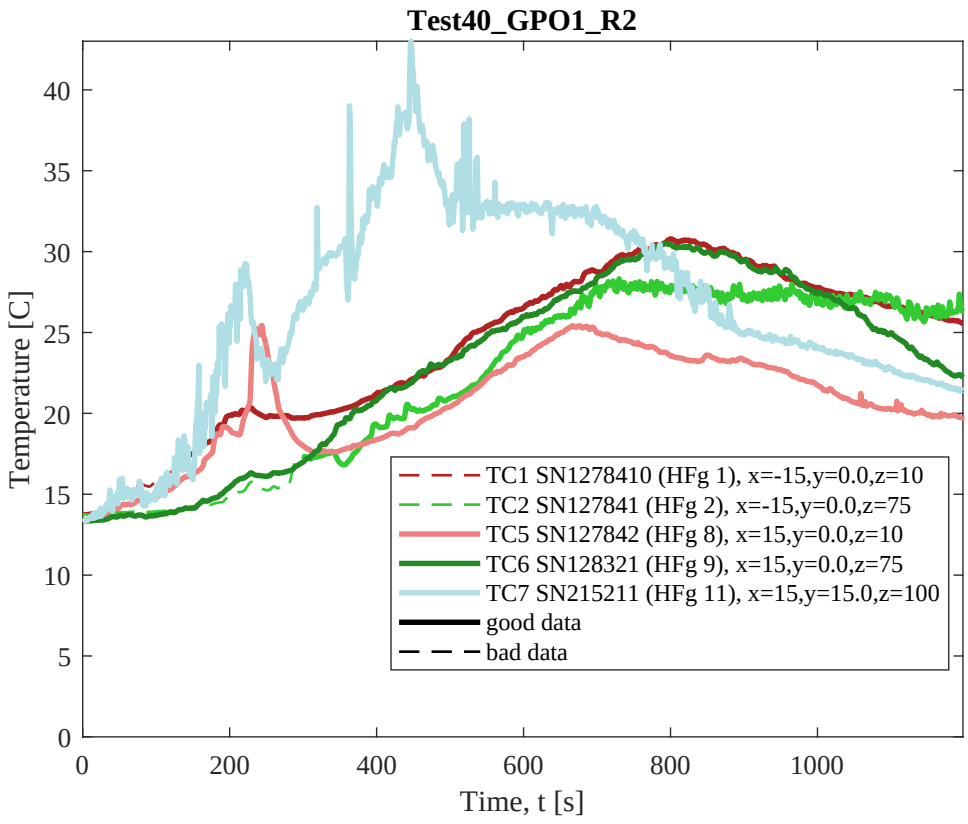

Fig. 103. Temperature of water-cooled Schmidt-Boelter heat flux gauges during Test 40 GPO1 R2.

Shielded Gauges

Measurements of total and radiation heat flux recorded by shielded heat flux gauges (Sec. efssec: qrad). Gauge shields were removed at 470, 470, and 546 seconds (gauges 3, 4, and 6, respectively).

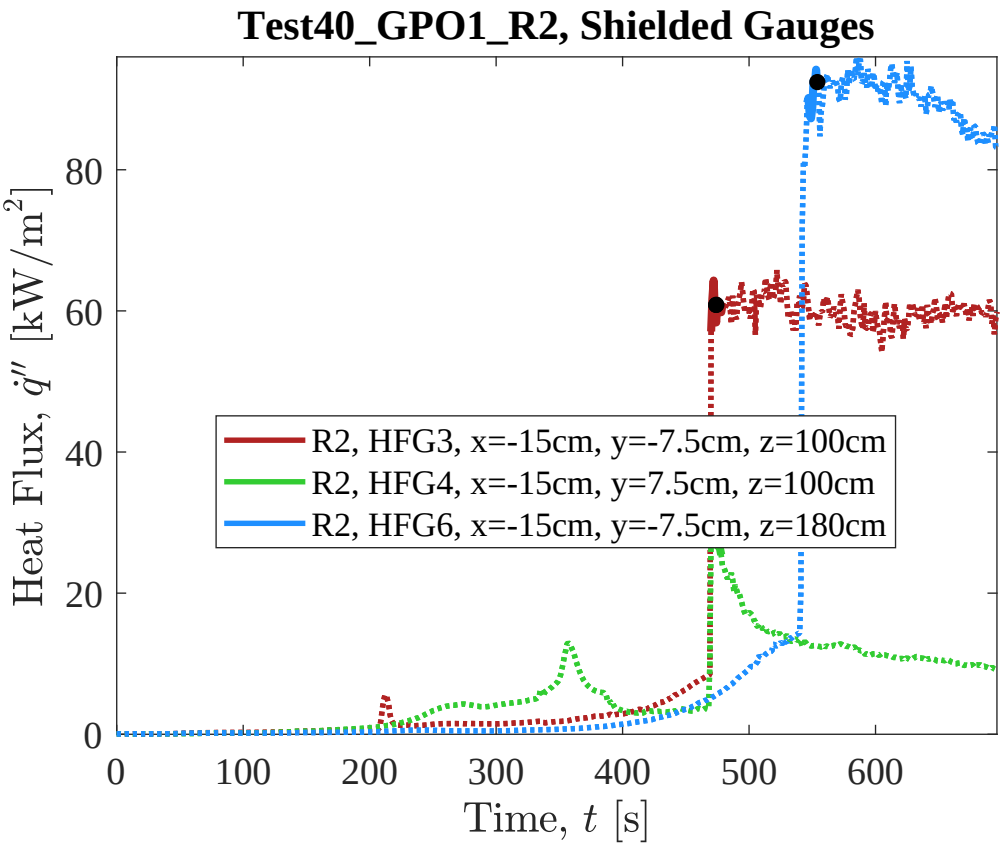

Fig. 104. Shielded gauge data for Test40 GPO1 R2.

Test 49 GPO1 R3

Test Description
1/4 in. thick, 24 in. wide, 96 in. tall panels of GPO-1 mounted to 1 in. thick Marinite board. Panels were ignited using a rectangular propane burner (60 kW nominal heat release rate) filled with layers of Pea Gravel, Sand, and Kaowool Insulation (i.e., the 'Final Burner configuration'; see Fig. 12). The burner was shut off ($t = 210$ s) after sustained, uniform flaming of both panel walls. Heat flux gauges were mounted flush with the fuel's surface between $z = 20$ cm and $z = 180$ cm. Shielded radiometers and total heat flux gauges were positioned side by side at $z =$50 cm and $z = 180$ cm. The lower heat flux shields were removed at $t =$396 s and the upper heat flux shields were removed at $t =$545 s; reliable measurements of both total and radiation flame heat flux were obtained at both heights.

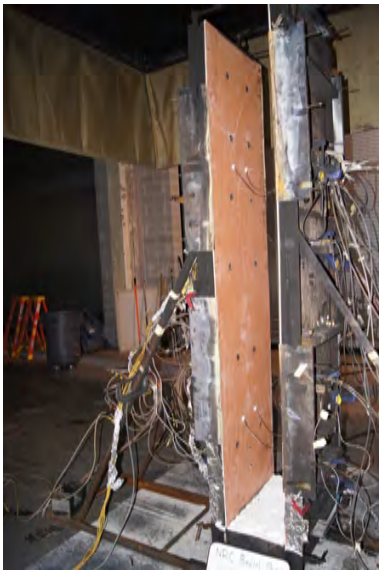

(a) Pre-test

(b) Ignition

(c) Peak HRR

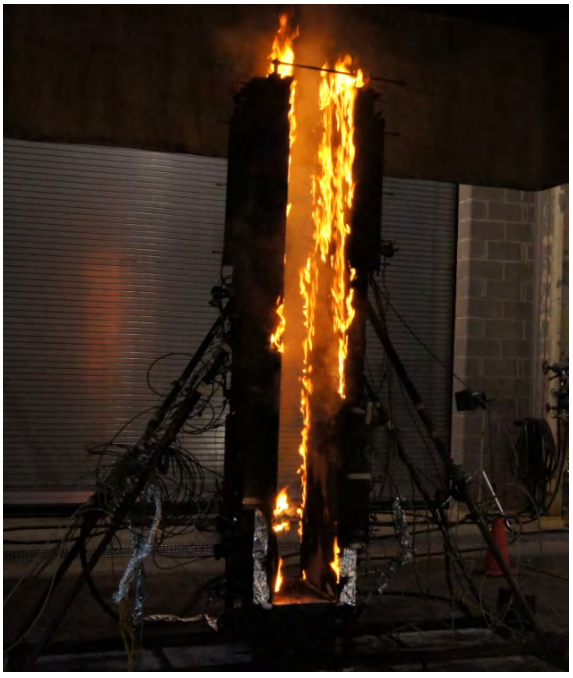

(d) End of Test

Fig. 105. Photographs of Test 49 GPO1 R3.

Heat Release Rate, Heat Flux at a Distance, and Species Yields

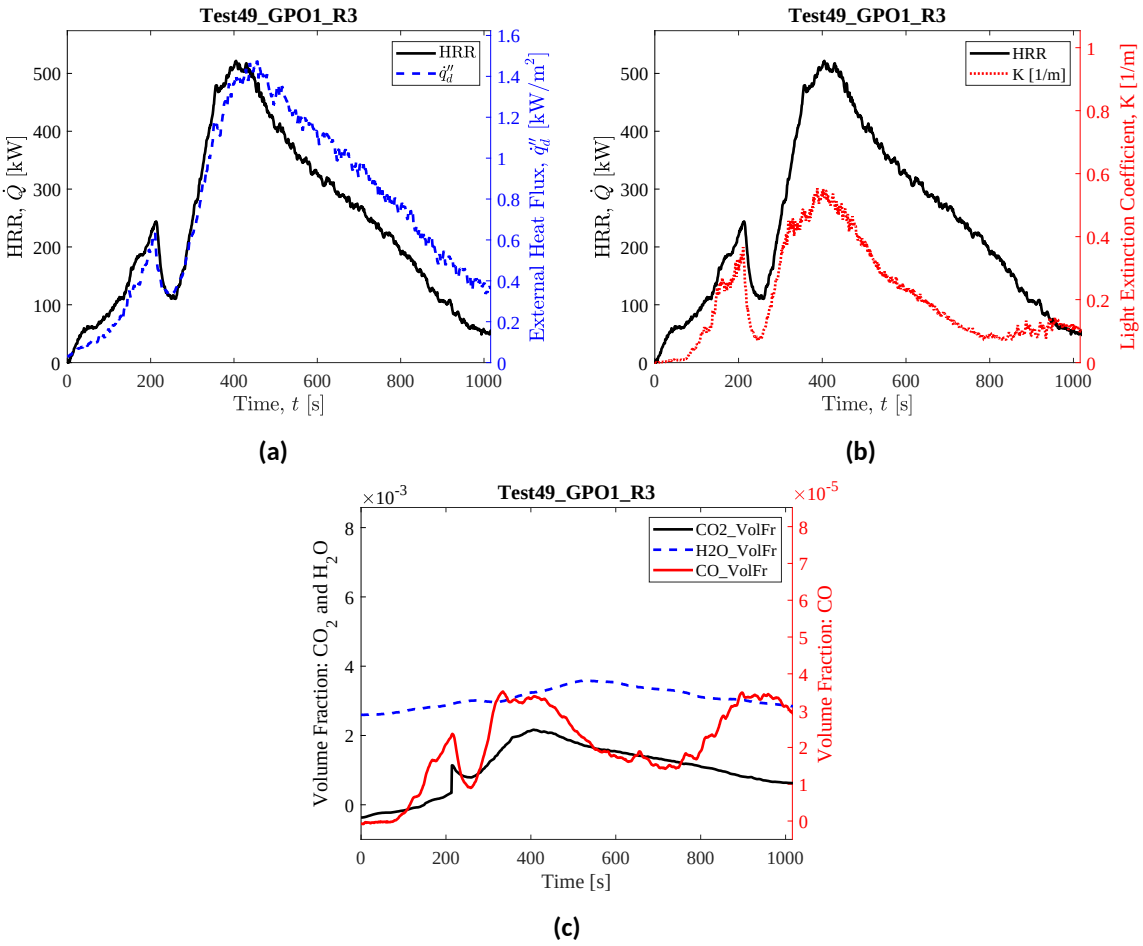

Fig. 106. Test 49 GPO1 R3: (a) Heat release rate and heat flux at a distance, $\dot{q}''_{\mathrm{d}}$ (here, $\dot{q}''_{\mathrm{d}}$ is measured at x =-220 cm, y =-310 cm, z =90 cm); (b) Heat release rate and light extinction coefficient, K (smoke particulate in exhaust duct [111]); (c) Time-resolved volume fractions of CO_2, H_2O, and CO.

Flame Heat Flux

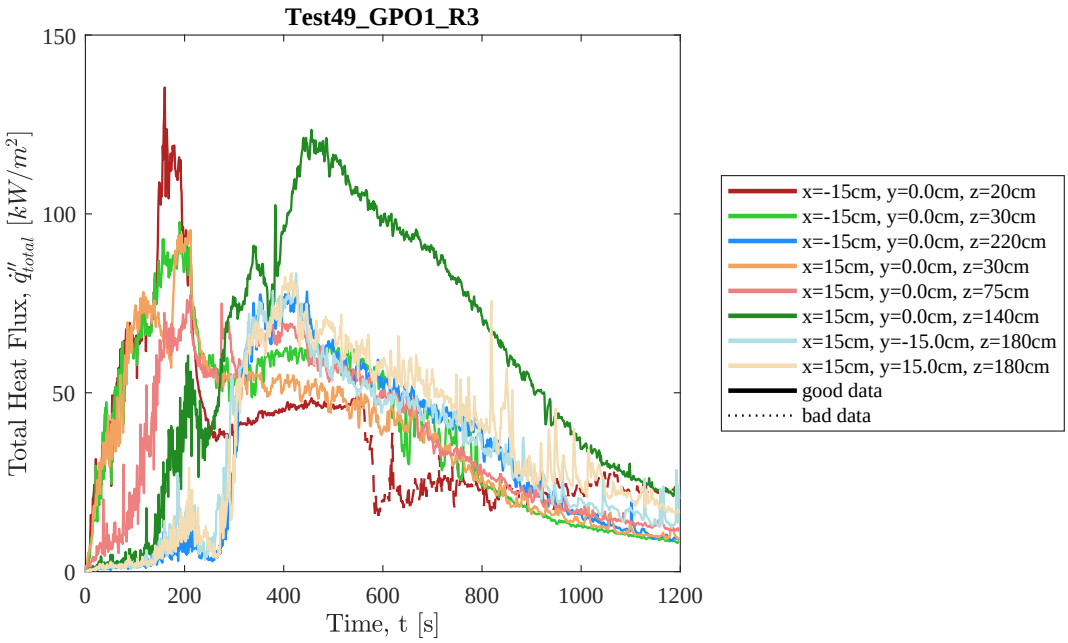

Fig. 107. Total flame to surface flame heat flux to water-cooled Schmidt-Boelter heat flux gauges as measured in Test 49 GPO1 R3. Here, raw, unsmoothed original measurments are plotted from each gauges as a function of time. Solid lines highlight values of $\dot{q}''_{\text{total}}$ that were identified by manual review as ”good” (see Sec. 3.1.1) and dotted lines represent ”bad” measurement data that should not be considered for further analysis.

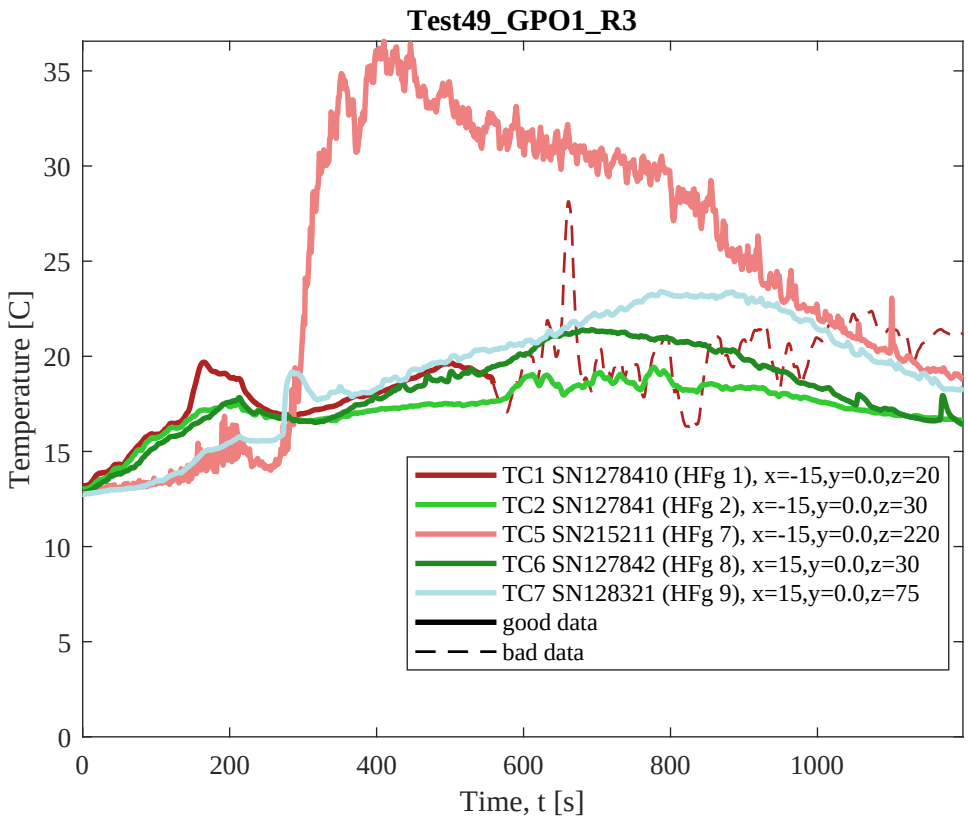

Fig. 108. Temperature of water-cooled Schmidt-Boelter heat flux gauges during Test 49 GPO1 R3.

Shielded Gauges

Measurements of total and radiation heat flux recorded by shielded heat flux gauges (Sec. efssec: qrad). Gauge shields were removed at 398, 396, 553, and 545 seconds (gauges 3, 4, 5 and 6, respectively).

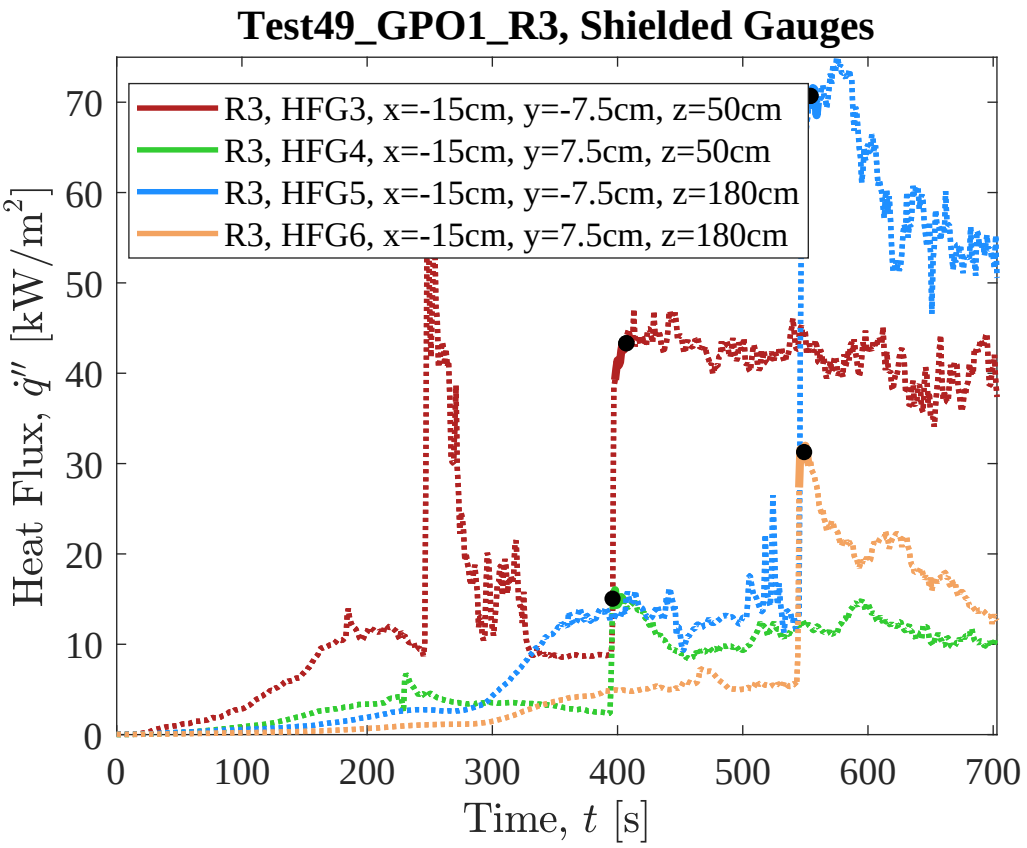

Fig. 109. Shielded gauge data for Test49 GPO1 R3.

C.3. HDPE - High Density Polyethylene

Test 16 HDPE R1

Test Description

1/4 in. thick, 24 in. wide, 96 in. tall panels of HDPE mounted to 1 in. thick Marinite board. Panels were ignited using a rectangular propane burner (60 kW nominal heat release rate) filled with layers of Pea Gravel, Sand, and Kaowool Insulation (i.e., the 'Final Burner configuration'; see Fig. 12). The burner was shut off ($t = 231$ s) after sustained flaming of panels; both walls ignited uniformly across their base. Heat flux gauges were not installed in HDPE panels due to expected melting behavior. Just 100 s after sample ignition (i.e., at $t = 330$ s), significant melt flow was observed across the front surface of the panel followed by complete collapse of the HDPE slabs.

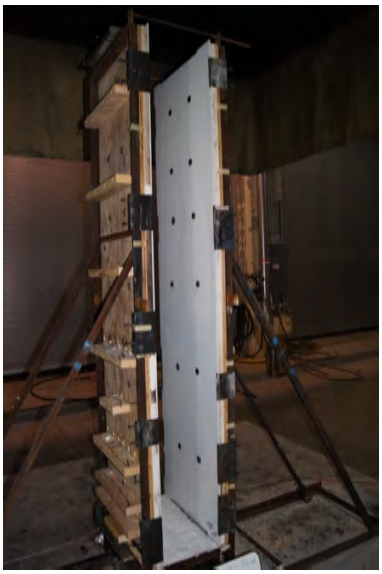

(a) Pre-test

(b) Ignition

(c) Peak HRR

(d) End of Test

Fig. 110. Photographs of Test 16 HDPE R1.

Heat Release Rate, Heat Flux at a Distance, and Species Yields

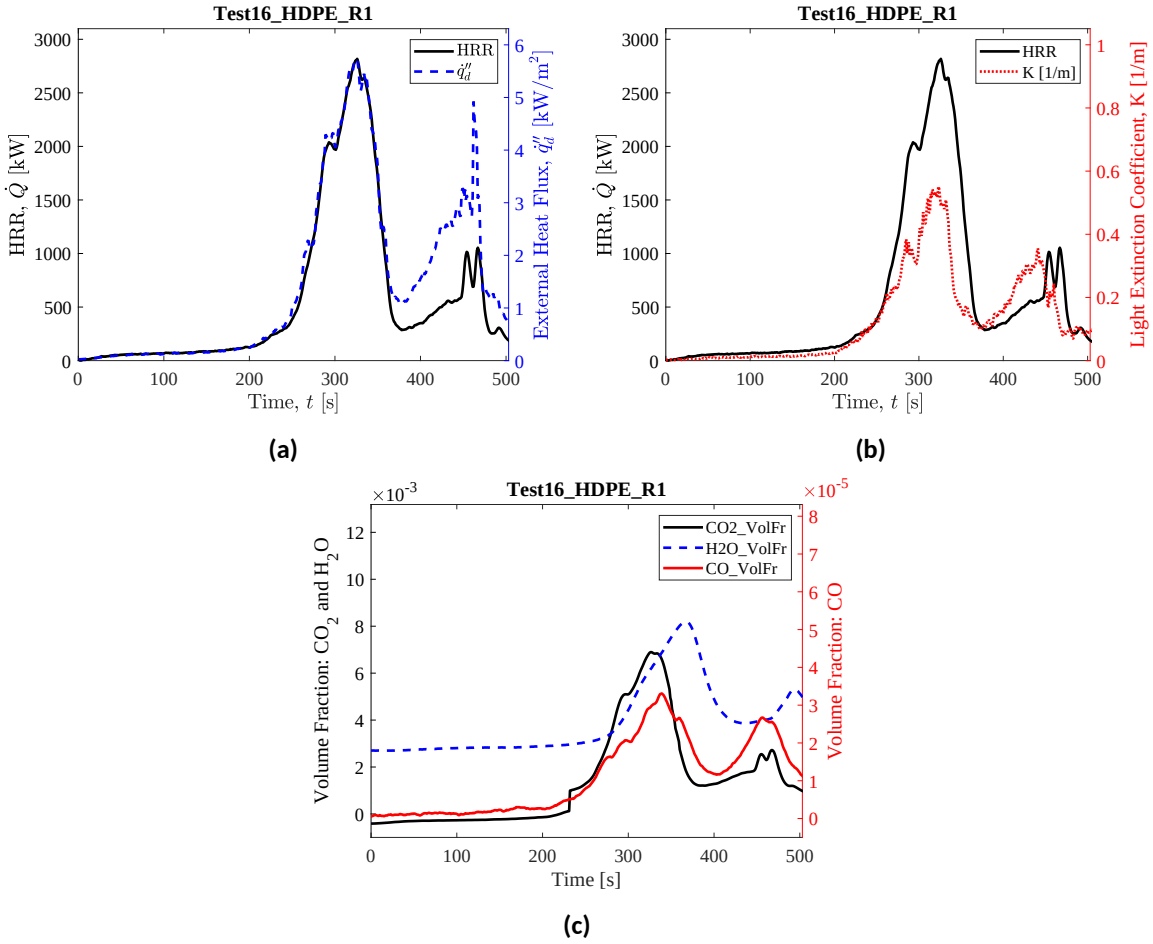

Fig. 111. Test 16 HDPE R1: (a) Heat release rate and heat flux at a distance, $\dot{q}''_{\mathrm{d}}$ (here, $\dot{q}''_{\mathrm{d}}$ is measured at x =-100 cm, y =-300 cm, z =90 cm); (b) Heat release rate and light extinction coefficient, K (smoke particulate in exhaust duct [111]); (c) Time-resolved volume fractions of CO_2, H_2O, and CO.

C.4. HIPS - High Impact Polystyrene

Test 45 HIPS R1

Test Description
1/4 in. thick, 24 in. wide, 96 in. tall panels of HIPS mounted to 1 in. thick Marinite board. Panels were ignited using a rectangular propane burner (60 kW nominal heat release rate) filled with layers of Pea Gravel, Sand, and Kaowool Insulation (i.e., the 'Final Burner configuration'; see Fig. 12). The burner was shut off ($t = 77$ s) and shielded ($t = 108$ s) after sustained flaming of both walls was achieved. In this test, the front 10 cm (i.e., -30 cm $\leq y \leq 20$ cm) of the right panel did not initially ignite due to burner non-uniformity; however, lateral flame spread was observed in this test and wall flames covered the full surface of both panel walls within 90 s after ignition. Heat flux gauges were mounted flush with the fuel's surface between $z = 20$ cm and $z = 50$ cm. Shielded radiometers and total heat flux gauges were positioned side by side at $z =$50 cm and $z = 100$ cm; however, reliable measurements of both total and radiation flame heat flux were note obtained at either location.

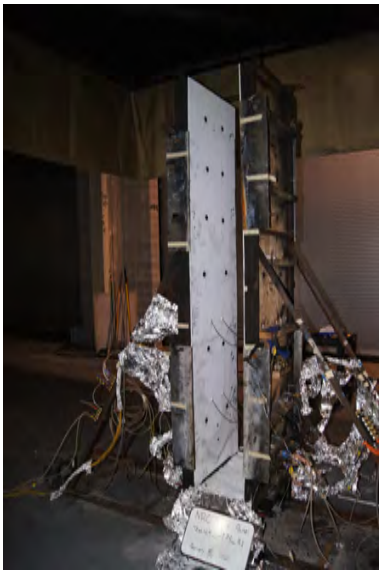

(a) Pre-test

(b) Ignition

(c) Peak HRR

(d) End of Test

Fig. 112. Photographs of Test 45 HIPS R1.

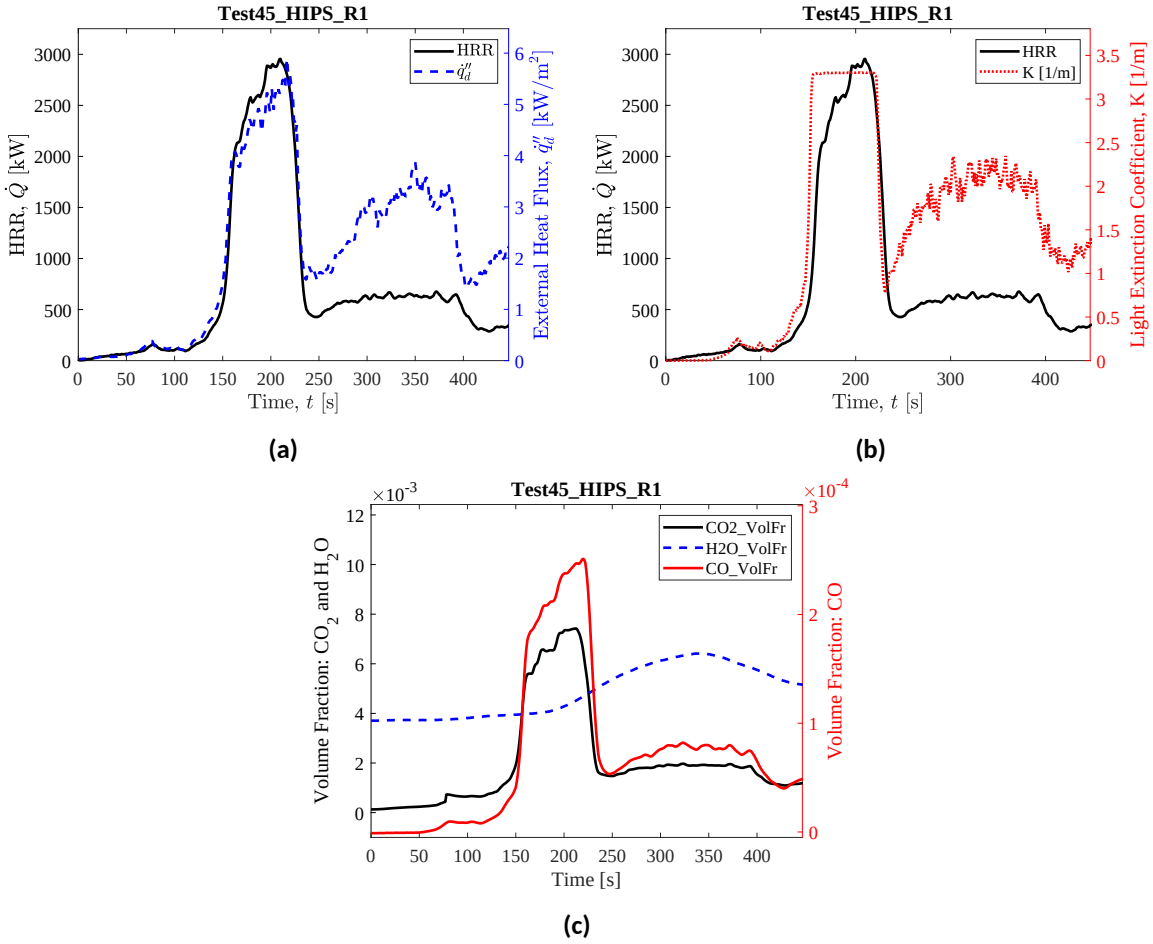

Fig. 113. Test 45 HIPS R1: (a) Heat release rate and heat flux at a distance, $\dot{q}''_{\mathrm{d}}$ (here, $\dot{q}''_{\mathrm{d}}$ is measured at x =-220 cm, y =-310 cm, z =90 cm); (b) Heat release rate and light extinction coefficient, K (smoke particulate in exhaust duct [111]); (c) Time-resolved volume fractions of CO_2, H_2O, and CO.

Flame Heat Flux

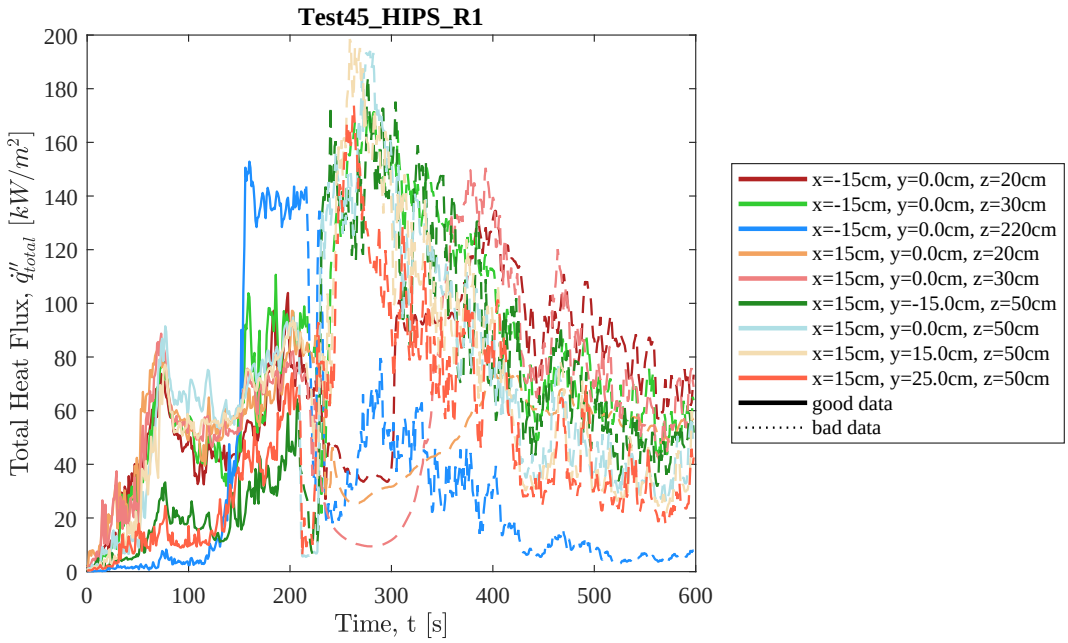

Fig. 114. Total flame to surface flame heat flux to water-cooled Schmidt-Boelter heat flux gauges as measured in Test 45 HIPS R1. Here, raw, unsmoothed original measurments are plotted from each gauges as a function of time. Solid lines highlight values of $\dot{q}''_{\text{total}}$ that were identified by manual review as ”good” (see Sec. 3.1.1) and dotted lines represent ”bad” measurement data that should not be considered for further analysis.

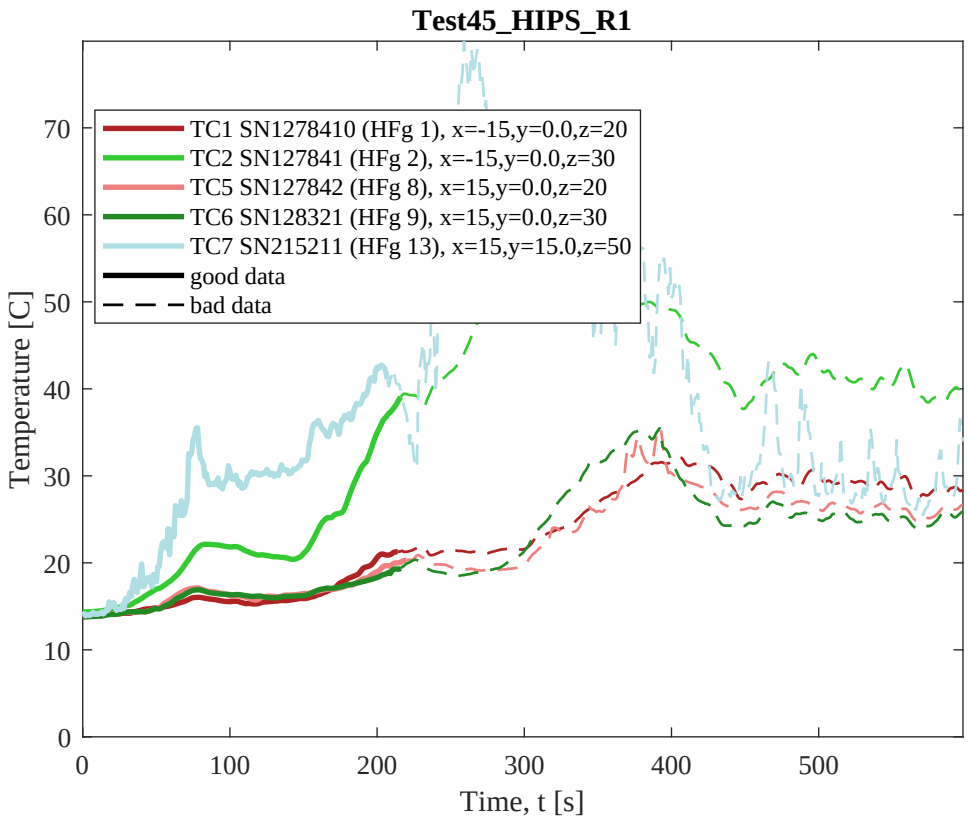

Fig. 115. Temperature of water-cooled Schmidt-Boelter heat flux gauges during Test 45 HIPS R1.

Test 46 HIPS R2

Test Description

1/4 in. thick, 24 in. wide, 96 in. tall panels of HIPS mounted to 1 in. thick Marinite board. Panels were ignited using a rectangular propane burner (60 kW nominal heat release rate) filled with layers of Pea Gravel, Sand, and Kaowool Insulation (i.e., the 'Final Burner configuration'; see Fig. 12). The burner was shut off ($t = 77$ s) and shielded ($t = 77$ s) after sustained flaming of both walls was achieved. In this test, the front 10 cm (i.e., -30 cm $\leq y \leq 20$ cm) of the right panel did not initially ignite due to burner non-uniformity; however, lateral flame spread was observed in this test and wall flames covered the full surface of both panel walls within 90 s after ignition. Heat flux gauges were mounted flush with the fuel's surface between $z = 10$ cm and $z = 140$ cm. Shielded radiometers and total heat flux gauges were positioned side by side at z =100 cm and $z = 180$ cm. The heat flux shields were removed at t =228 s; reliable measurements of both total and radiation flame heat flux were obtained at both heights.

(a) Pre-test

(b) Ignition

(c) Peak HRR

(d) End of Test

Fig. 116. Photographs of Test 46 HIPS R2.

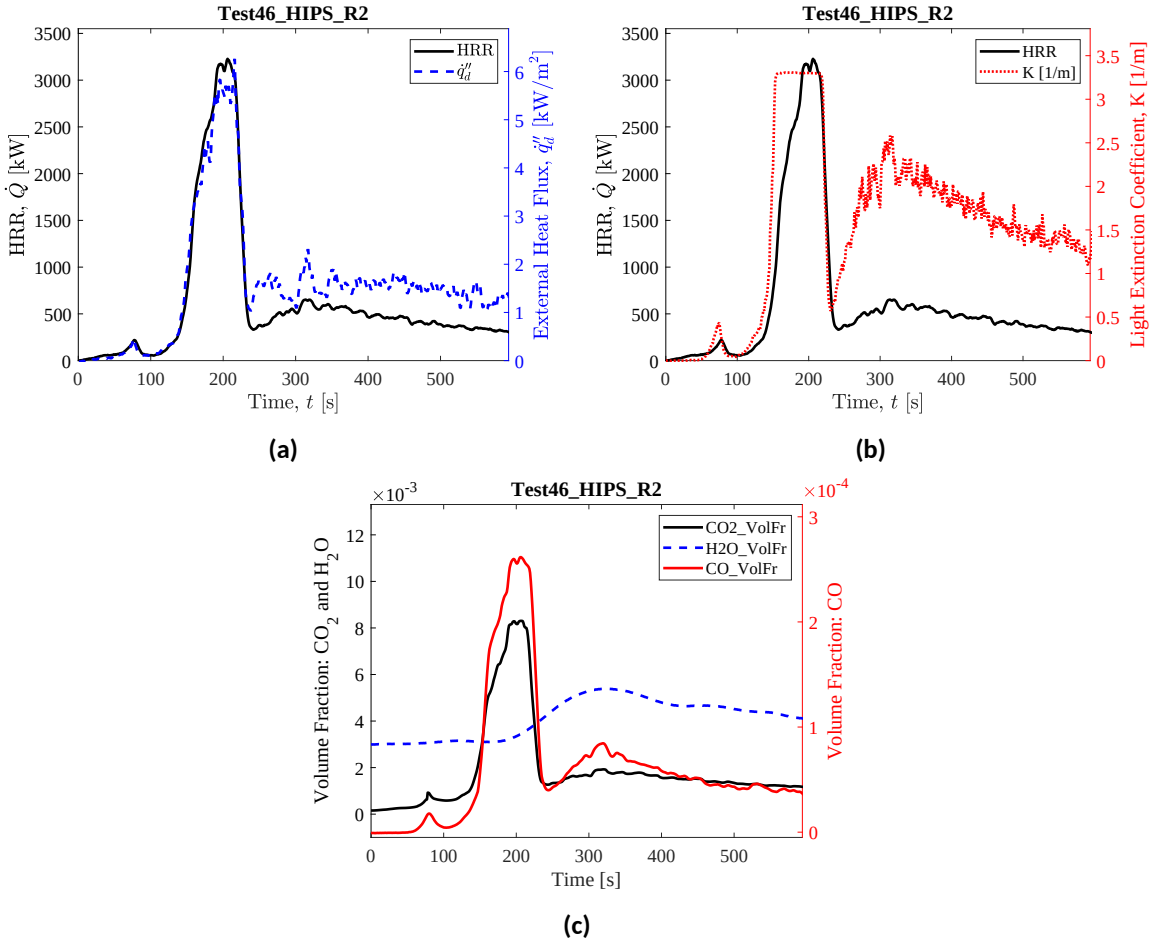

Fig. 117. Test 46 HIPS R2: (a) Heat release rate and heat flux at a distance, $\dot{q}''_{\mathrm{d}}$ (here, $\dot{q}''_{\mathrm{d}}$ is measured at x =-220 cm, y =-310 cm, z =90 cm); (b) Heat release rate and light extinction coefficient, K (smoke particulate in exhaust duct [111]); (c) Time-resolved volume fractions of CO_2, H_2O, and CO.

Flame Heat Flux

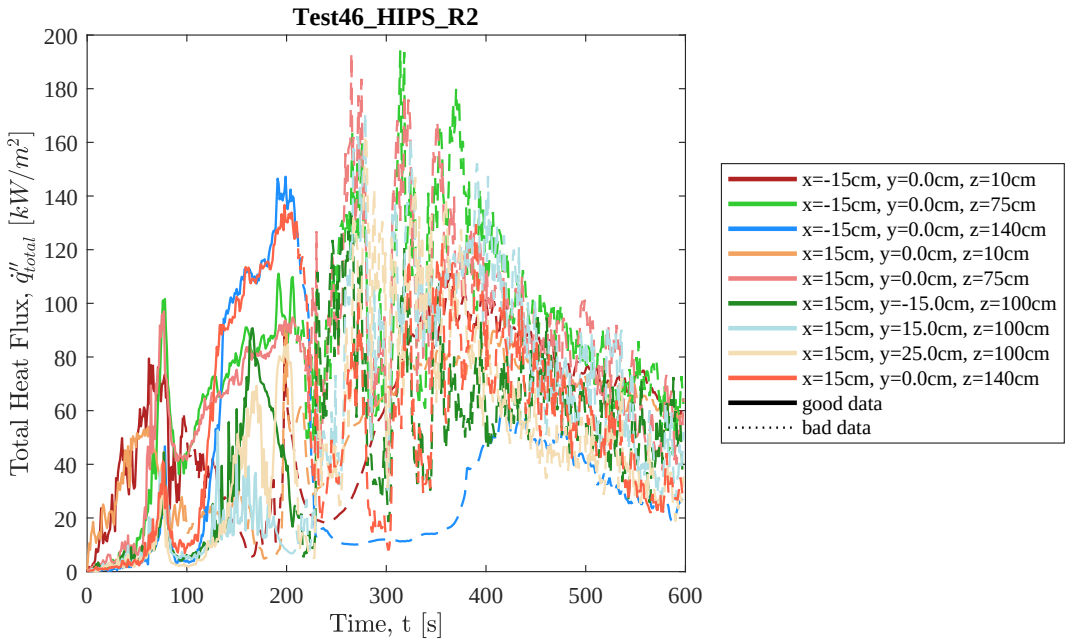

Fig. 118. Total flame to surface flame heat flux to water-cooled Schmidt-Boelter heat flux gauges as measured in Test 46 HIPS R2. Here, raw, unsmoothed original measurments are plotted from each gauges as a function of time. Solid lines highlight values of $\dot{q}''_{\text{total}}$ that were identified by manual review as ”good” (see Sec. 3.1.1) and dotted lines represent ”bad” measurement data that should not be considered for further analysis.

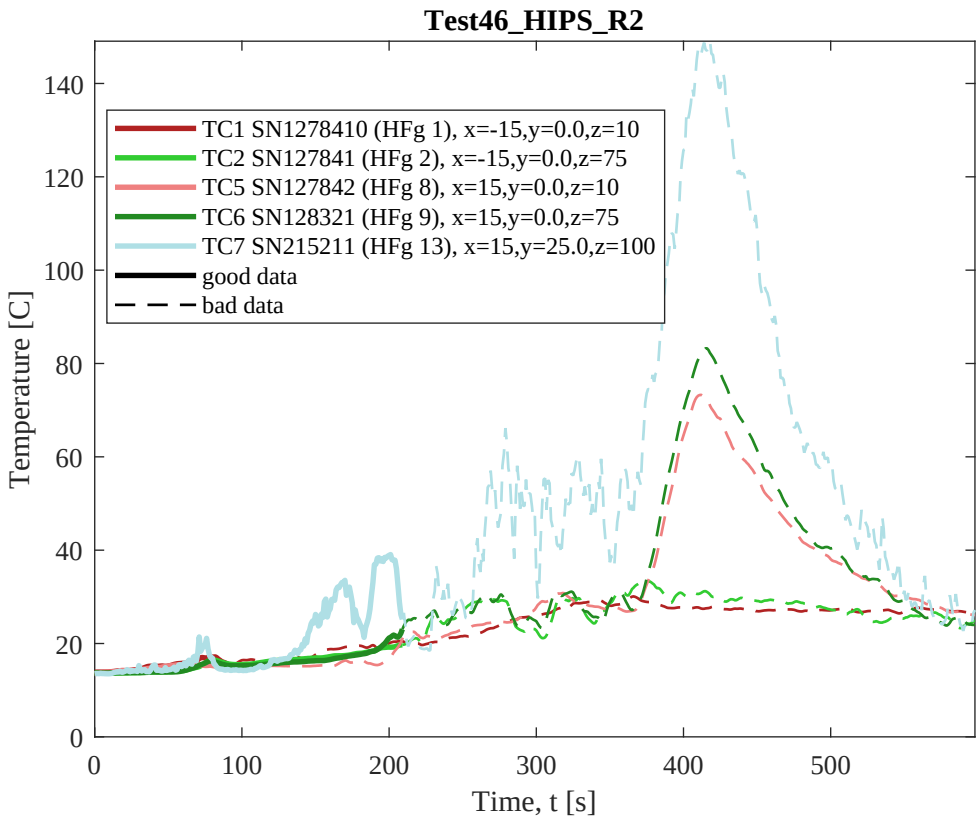

Fig. 119. Temperature of water-cooled Schmidt-Boelter heat flux gauges during Test 46 HIPS R2.

Shielded Gauges

Measurements of total and radiation heat flux recorded by shielded heat flux gauges (Sec. efssec: qrad). Gauge shields were removed at 228, 227, 226, and 226 seconds (gauges 3, 4, 6 and 7, respectively).

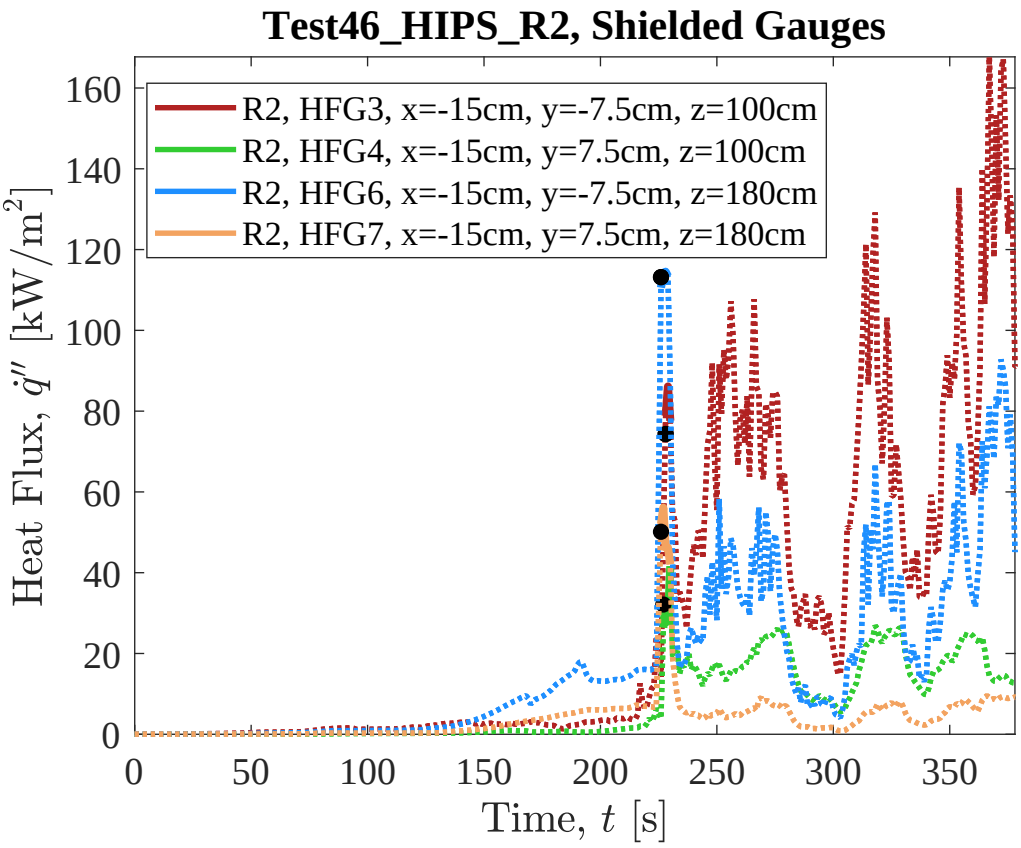

Fig. 120. Shielded gauge data for Test46 HIPS R2.

Test 52 HIPS R3

Test Description
1/4 in. thick, 24 in. wide, 96 in. tall panels of HIPS mounted to 1 in. thick Marinite board. Panels were ignited using a rectangular propane burner (60 kW nominal heat release rate) filled with layers of Pea Gravel, Sand, and Kaowool Insulation (i.e., the 'Final Burner configuration'; see Fig. 12). The burner was shut off ($t = 77$ s) and shielded ($t = 77$ s) after uniform, sustained flaming of both walls was achieved. Flame to wall heat flux measurements were not recorded in this test.

(a) Pre-test

(b) Ignition

(c) Peak HRR

(d) End of Test

Fig. 121. Photographs of Test 52 HIPS R3.

Heat Release Rate, Heat Flux at a Distance, and Species Yields

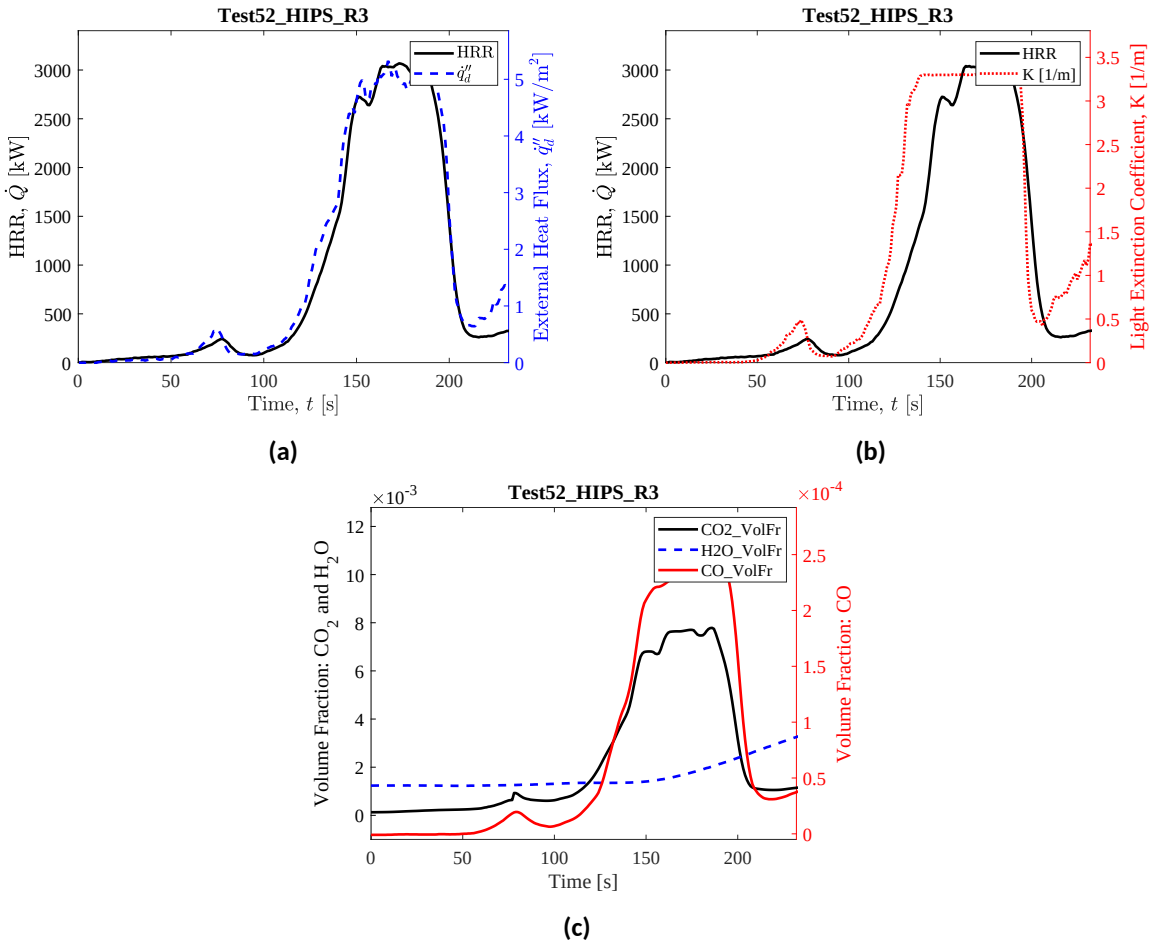

Fig. 122. Test 52 HIPS R3: (a) Heat release rate and heat flux at a distance, $\dot{q}''_{\mathrm{d}}$ (here, $\dot{q}''_{\mathrm{d}}$ is measured at x =-220 cm, y =-310 cm, z =90 cm); (b) Heat release rate and light extinction coefficient, K (smoke particulate in exhaust duct [111]); (c) Time-resolved volume fractions of CO_2, H_2O, and CO.

Test 56 HIPS R4

Test Description
1/4 in. thick, 24 in. wide, 96 in. tall panels of HIPS mounted to 1 in. thick Marinite Board. Panels were ignited using a rectangular propane burner (60 kW nominal heat release rate) filled with layers of Pea Gravel, Sand, and Kaowool Insulation (i.e., the 'Final Burner configuration'; see Fig. 12). The burner was shut off ($t = 77$ s) and shielded ($t = 78$ s) after sustained flaming of both walls was achieved. In this test, the front 10 cm (i.e., (i.e., -30 cm $\leq y \leq 20$ cm) of the right panel did not initially ignite due to burner non-uniformity; however, lateral flame spread was observed in this test and wall flames covered the full surface of both panel walls within 90 s after ignition. Heat flux gauges were mounted flush with the fuel's surface between $z = 30$ cm and $z = 180$ cm. Shielded radiometers and total heat flux gauges were positioned side by side at z =100 cm and $z = 180$ cm. An attempt was made to remove the heat flux shields at t =165 s; however, the shields covering the total heat flux gauges shifted (independently) earlier in the test and the shield covering the upper radiometer could not be removed until approximately $t = 235$ s.

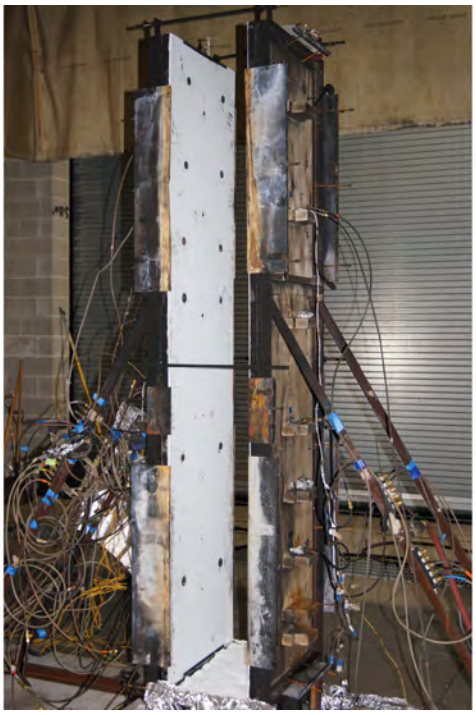

(a) Pre-test

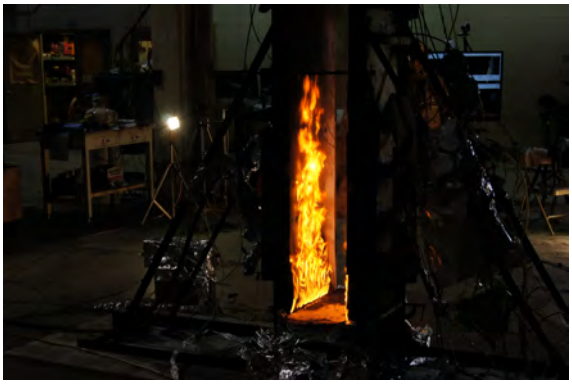

(b) Ignition

(c) Peak HRR

(d) End of Test

Fig. 123. Photographs of Test 56 HIPS R4.

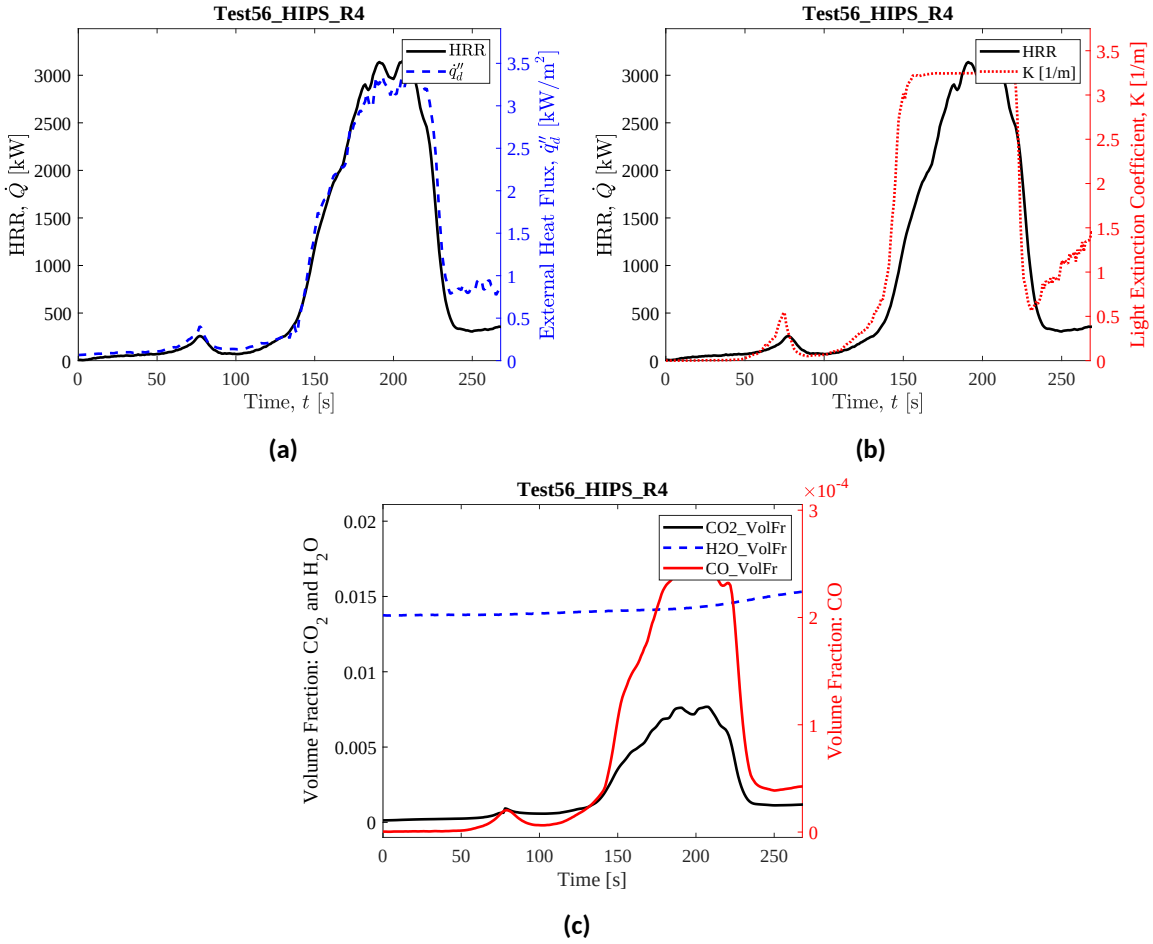

Fig. 124. Test 56 HIPS R4: (a) Heat release rate and heat flux at a distance, $\dot{q}''_{\mathrm{d}}$ (here, $\dot{q}''_{\mathrm{d}}$ is measured at x =300 cm, y =-305 cm, z =90 cm); (b) Heat release rate and light extinction coefficient, K (smoke particulate in exhaust duct [111]); (c) Time-resolved volume fractions of CO_2, H_2O, and CO.

Flame Heat Flux

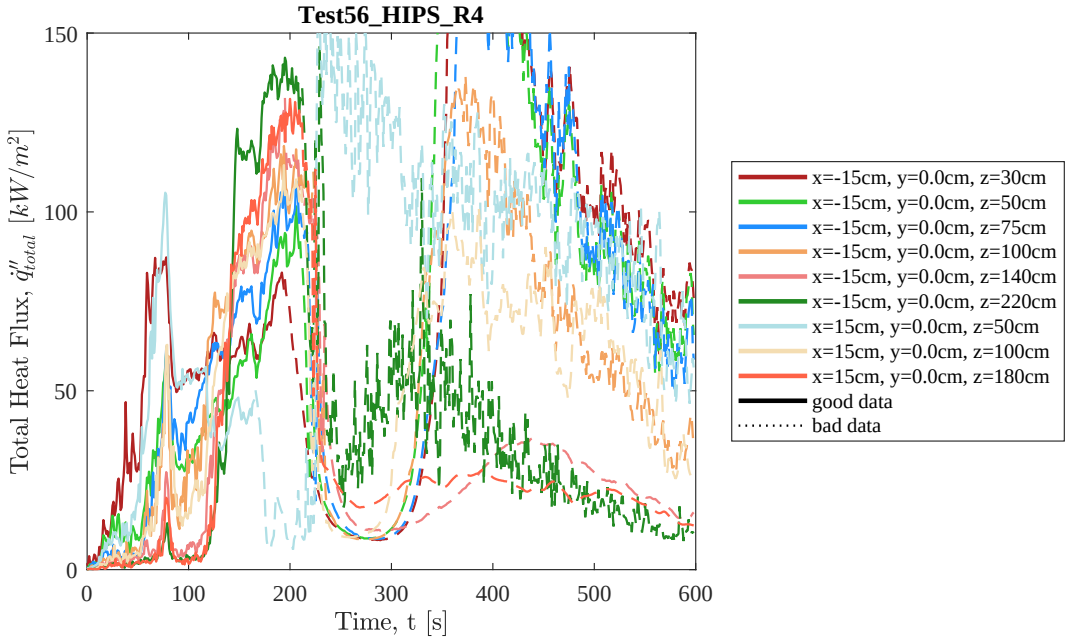

Fig. 125. Total flame to surface flame heat flux to water-cooled Schmidt-Boelter heat flux gauges as measured in Test 56 HIPS R4. Here, raw, unsmoothed original measurments are plotted from each gauges as a function of time. Solid lines highlight values of $\dot{q}''_{\text{total}}$ that were identified by manual review as ”good” (see Sec. 3.1.1) and dotted lines represent ”bad” measurement data that should not be considered for further analysis.

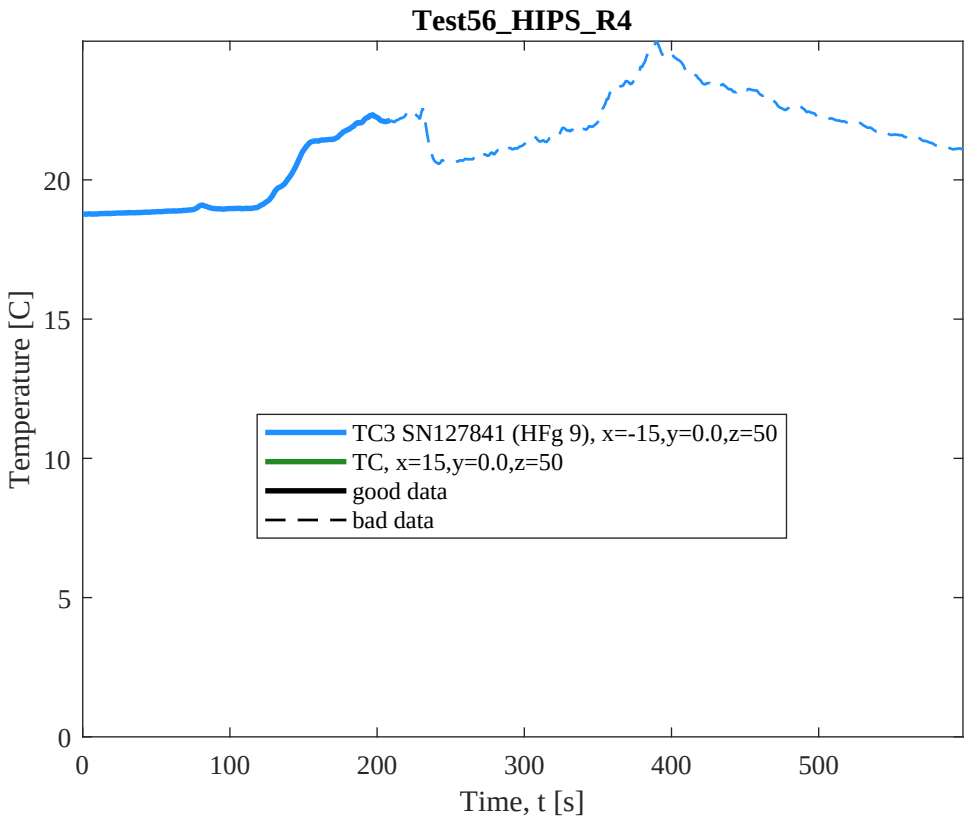

Fig. 126. Temperature of water-cooled Schmidt-Boelter heat flux gauges during Test 56 HIPS R4.

Shielded Gauges

Measurements of total and radiation heat flux recorded by shielded heat flux gauges (Sec. efssec: qrad). Gauge shields were removed at 156, 167, and 230 seconds (gauges 5, 6, and 8, respectively).

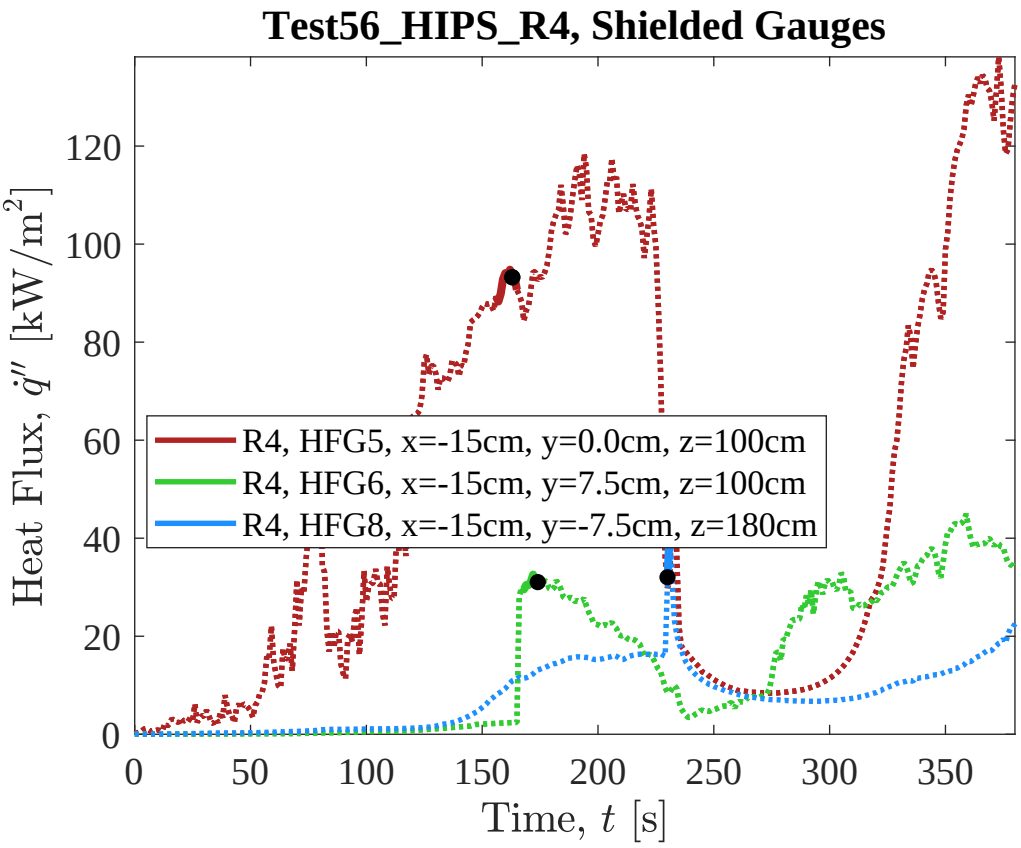

Fig. 127. Shielded gauge data for Test56 HIPS R4.

Test 66 HIPS1panel R1

Test Description

One panel of 1/4 in. thick, 24 in. wide, 96 in. tall HIPS mounted to 1 in. thick Marinite board. Opposite this panel, at the base of the assembly, a 50 cm tall, 60 cm wide panel of marinite was installed to control airflow near the burner at the start of the test. The panel was ignited using a rectangular propane burner (60 kW nominal heat release rate) filled with layers of Pea Gravel, Sand, and Kaowool Insulation (i.e., the 'Final Burner configuration'; see Fig. 12). The burner was shut off ($t = 75$ s) and shielded ($t = 80$ s) after sustained flaming after sustained flaming was achieved across the base of the panel wall. Peak HRR was measured at $t =$ 314 s; shortly thereafter, HRR quickly decreased as the sample detached from the panel wall. Although peak HRR for this 1panel HIPS test was approximately half that of the standard parallel panel tests (approximately 1.5 MW versus 3 MW), average fire growth rate was substantially slower (5.7 kW/s versus 38.2 kW/s, on average). Heat flux gauges were mounted flush with the fuel's surface between $z = 30$ cm and $z = 220$ cm. Shielded radiometers and total heat flux gauges were positioned side by side at $z =$100 cm and $z = 180$ cm. The lower heat flux shields were removed at $t =$287 s and the upper heat flux shields were removed at $t =$304 s; however, reliable measurements of both total and radiation flame heat flux were obtained only at $z = 180$ cm.

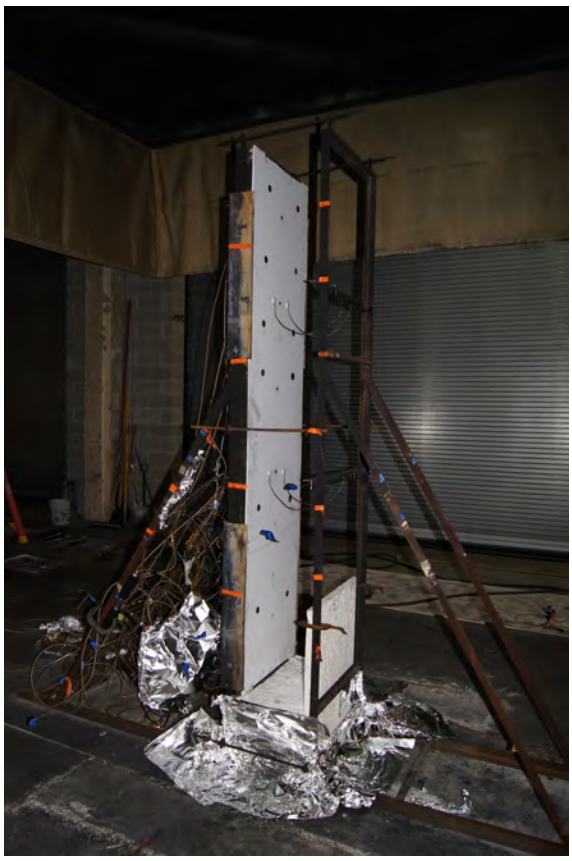

(a) Pre-test

(b) Ignition

(c) Peak HRR

(d) End of Test

Fig. 128. Photographs of Test 66 HIPS1panel R1.

Heat Release Rate, Heat Flux at a Distance, and Species Yields

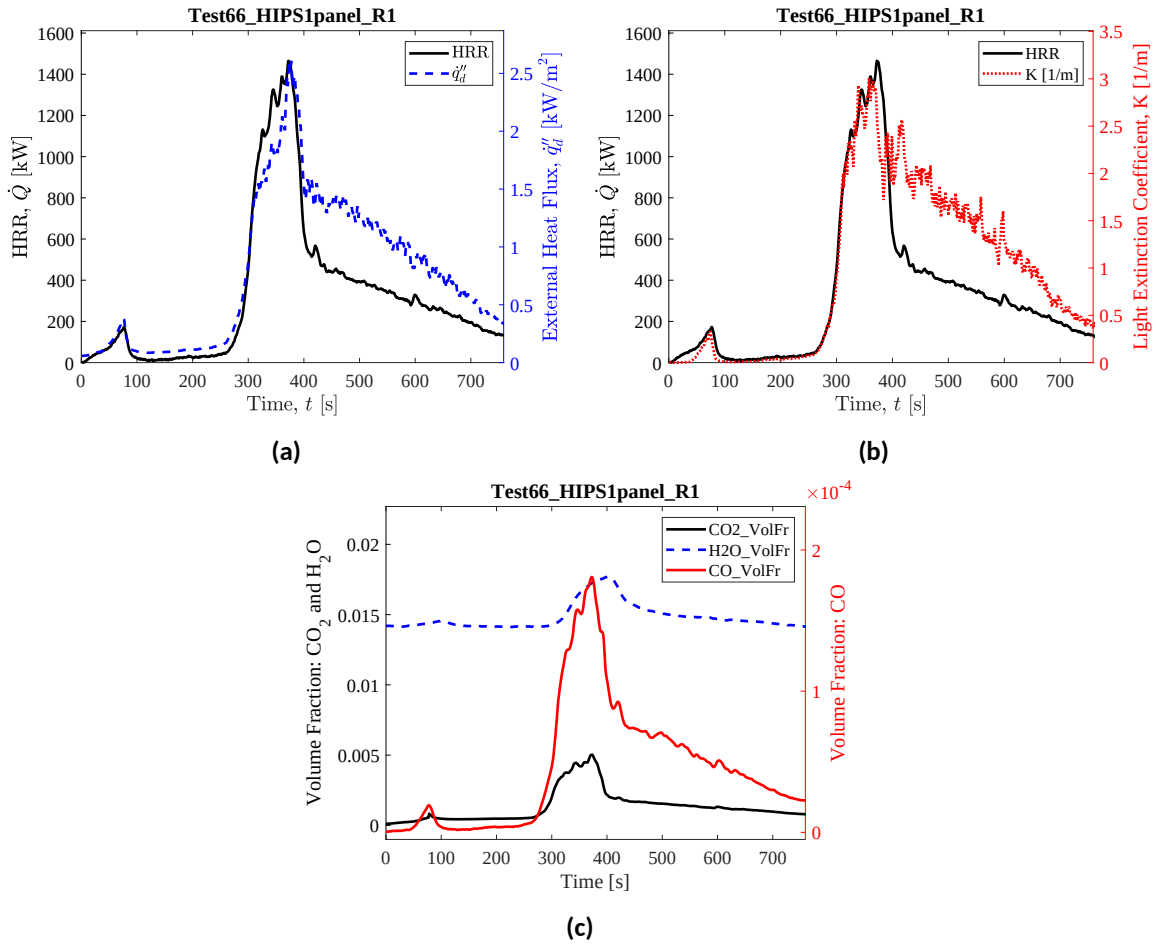

Fig. 129. Test 66 HIPS1panel R1: (a) Heat release rate and heat flux at a distance, $\dot{q}''_{\mathrm{d}}$ (here, $\dot{q}''_{\mathrm{d}}$ is measured at x =300 cm, y =-305 cm, z =90 cm); (b) Heat release rate and light extinction coefficient, K (smoke particulate in exhaust duct [111]); (c) Time-resolved volume fractions of CO_2, H_2O, and CO.

Flame Heat Flux

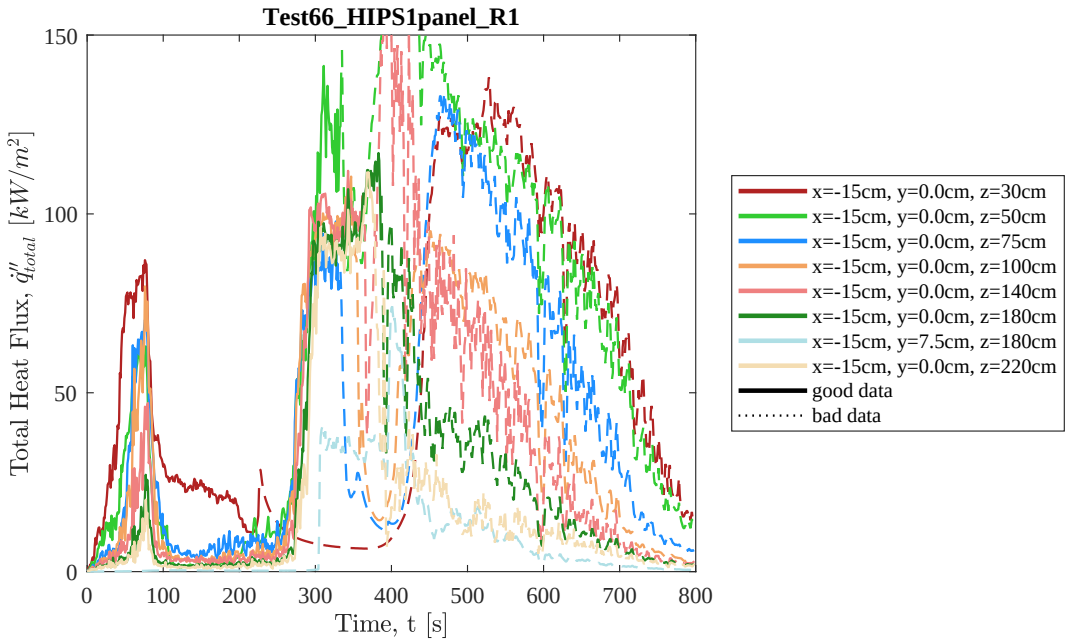

Fig. 130. Total flame to surface flame heat flux to water-cooled Schmidt-Boelter heat flux gauges as measured in Test 66 HIPS1panel R1. Here, raw, unsmoothed original measurments are plotted from each gauges as a function of time. Solid lines highlight values of $\dot{q}''_{\text{total}}$ that were identified by manual review as ”good” (see Sec. 3.1.1) and dotted lines represent ”bad” measurement data that should not be considered for further analysis.

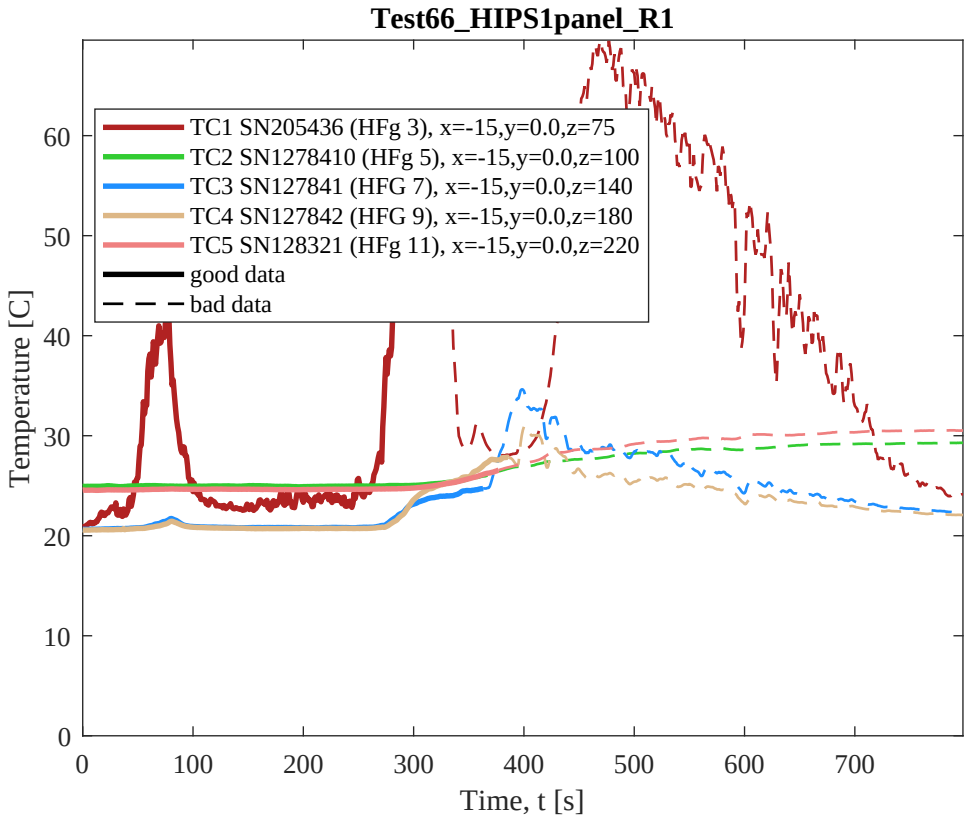

Fig. 131. Temperature of water-cooled Schmidt-Boelter heat flux gauges during Test 66 HIPS1panel R1.

Shielded Gauges

Measurements of total and radiation heat flux recorded by shielded heat flux gauges (Sec. efssec: qrad). Gauge shields were removed at 286, 308, and 307 seconds (gauges 4, 8 and 10, respectively).

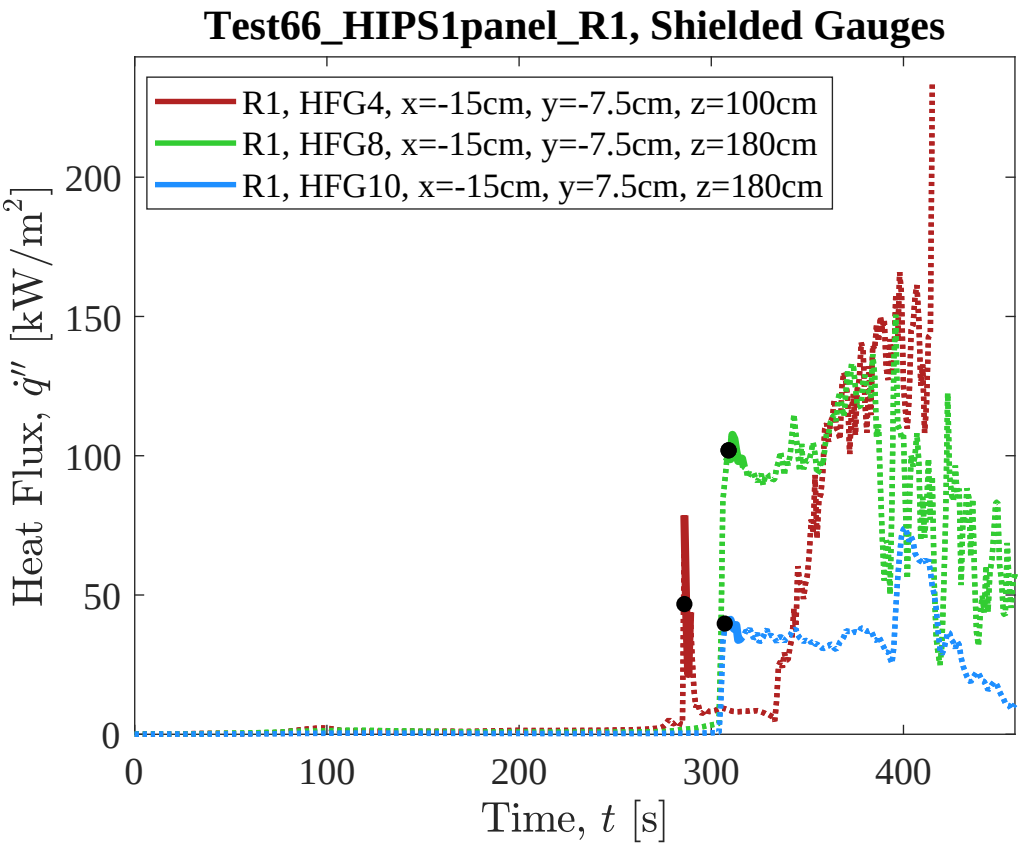

Fig. 132. Shielded gauge data for Test66 HIPS1panel R1.

C.5. OSB - Oriented Strand Board

Test 20 OSB R1

Test Description
7/16 in. thick, 24 in. wide, 96 in. tall panels of OSB mounted to 1 in. thick Marinite board (new Marinite). Panels were ignited using a rectangular propane burner (60 kW nominal heat release rate) filled with layers of Pea Gravel, Sand, and Kaowool Insulation (i.e., the 'Final Burner configuration'; see Fig. 12). The burner was initially shut off ($t = 135$ s) when flame tips were observed above $z = 2.0$ m and total HRR 300 kW; however, after burner shutoff, wall flames were not self-sustaining, and so the burner was turned back on at $t = 165$ s. The burner was kept on until $t = 540$ s at which point flames began to gradually self-extinguish. Heat flux gauges were mounted flush with the fuel's surface between $z = 20$ cm and $z = 50$ cm. Shielded radiometers and total heat flux gauges were positioned side by side at $z =$50 cm and $z = 100$ cm. The heat flux shields were removed at $t =$256 s and reliable measurements of both total and radiation flame heat flux were obtained at both heights.

(a) Pre-test

(b) Ignition

(c) Peak HRR

(d) End of Test

Fig. 133. Photographs of Test 20 OSB R1.

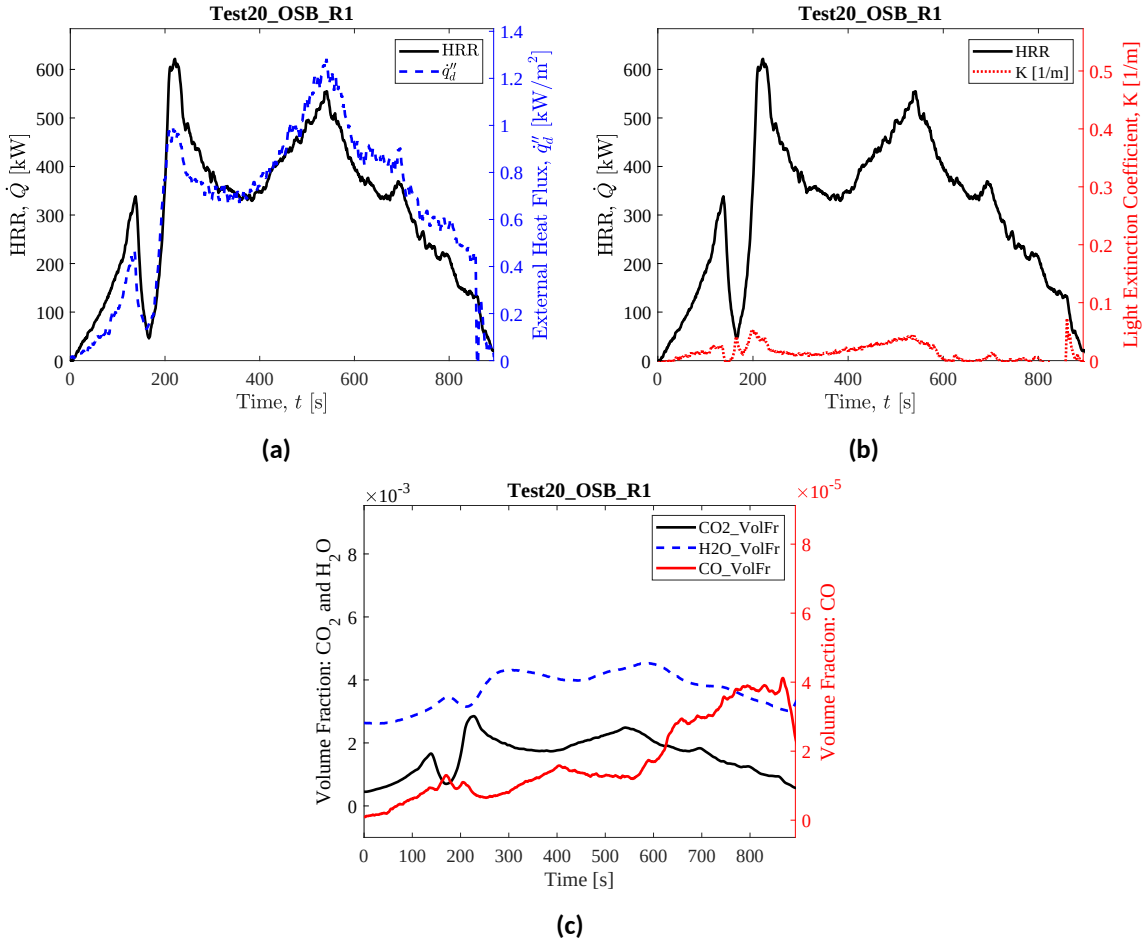

Fig. 134. Test 20 OSB R1: (a) Heat release rate and heat flux at a distance, $\dot{q}''_{\mathrm{d}}$ (here, $\dot{q}''_{\mathrm{d}}$ is measured at x =-150 cm, y =-300 cm, z =90 cm); (b) Heat release rate and light extinction coefficient, K (smoke particulate in exhaust duct [111]); (c) Time-resolved volume fractions of CO_2, H_2O, and CO.

Flame Heat Flux

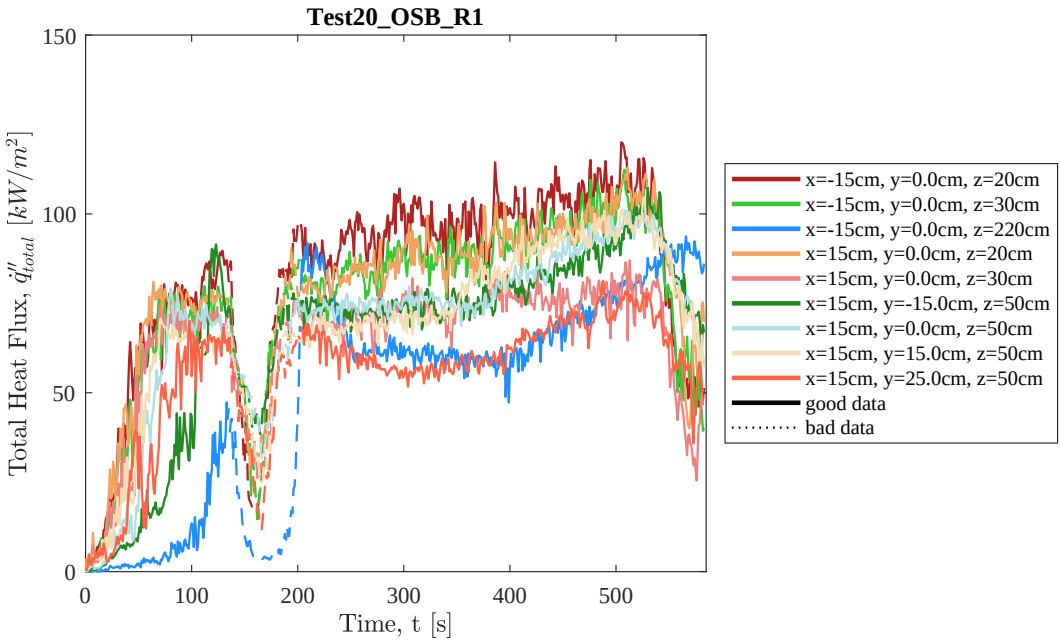

Fig. 135. Total flame to surface flame heat flux to water-cooled Schmidt-Boelter heat flux gauges as measured in Test 20 OSB R1. Here, raw, unsmoothed original measurments are plotted from each gauges as a function of time. Solid lines highlight values of $\dot{q}''_{\text{total}}$ that were identified by manual review as ”good” (see Sec. 3.1.1) and dotted lines represent ”bad” measurement data that should not be considered for further analysis.

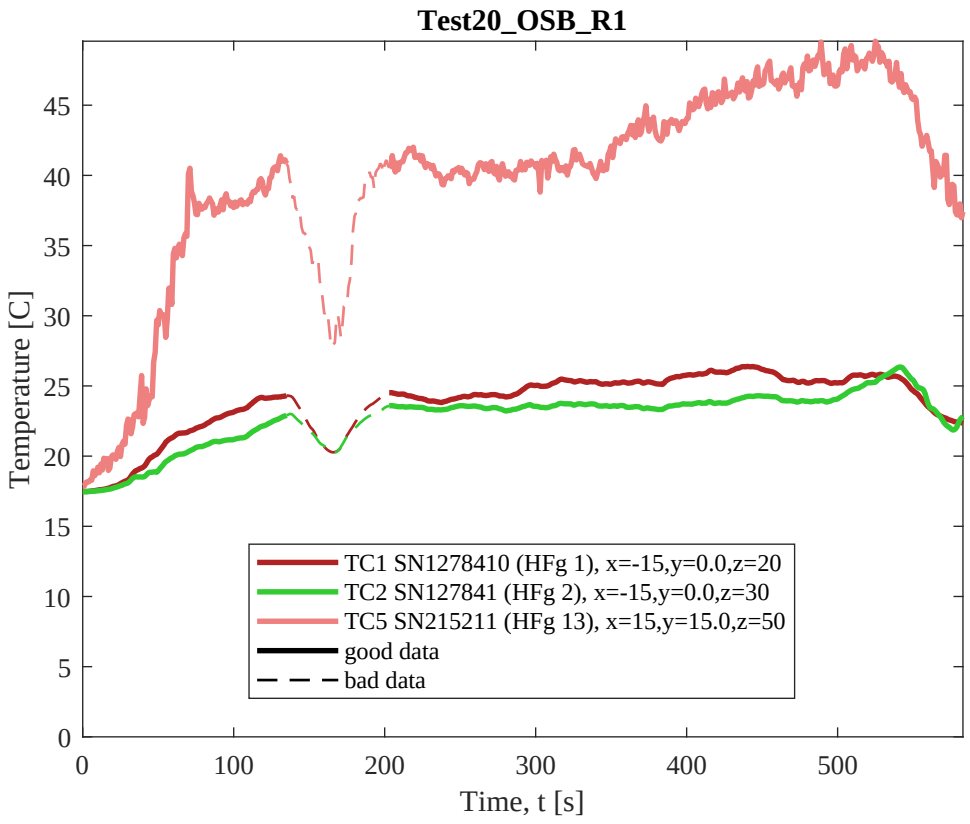

Fig. 136. Temperature of water-cooled Schmidt-Boelter heat flux gauges during Test 20 OSB R1.

Shielded Gauges

Measurements of total and radiation heat flux recorded by shielded heat flux gauges (Sec. efssec: qrad). Gauge shields were removed at 260 seconds.

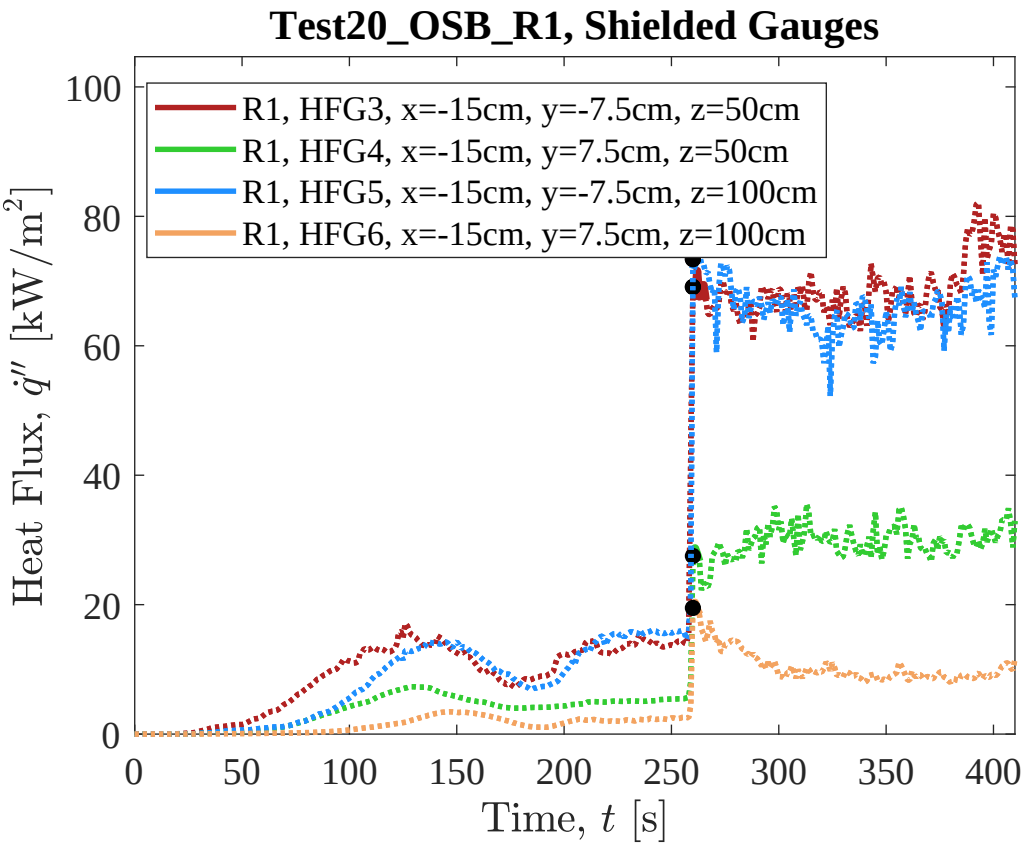

Fig. 137. Shielded gauge data for Test20 OSB R1.

Test 37 OSB R2

Test Description
7/16 in. thick, 24 in. wide, 96 in. tall panels of OSB mounted to 1 in. thick Marinite board (new Marinite). Panels were ignited using a rectangular propane burner (60 kW nominal heat release rate) filled with layers of Pea Gravel, Sand, and Kaowool Insulation (i.e., the 'Final Burner configuration'; see Fig. 12). The was burner kept on until $t = 460$ s at which point flames began to gradually self-extinguish. Heat flux gauges were mounted flush with the fuel's surface between $z = 10$ cm and $z = 140$ cm. Shielded radiometers and total heat flux gauges were positioned side by side at z =100 cm and $z = 180$ cm. The heat flux shields were removed at t =188 s and reliable measurements of both total and radiation flame heat flux were obtained at both heights.

(a) Pre-test

(b) Ignition

(c) Peak HRR

(d) End of Test

Fig. 138. Photographs of Test 37 OSB R2.

Heat Release Rate, Heat Flux at a Distance, and Species Yields

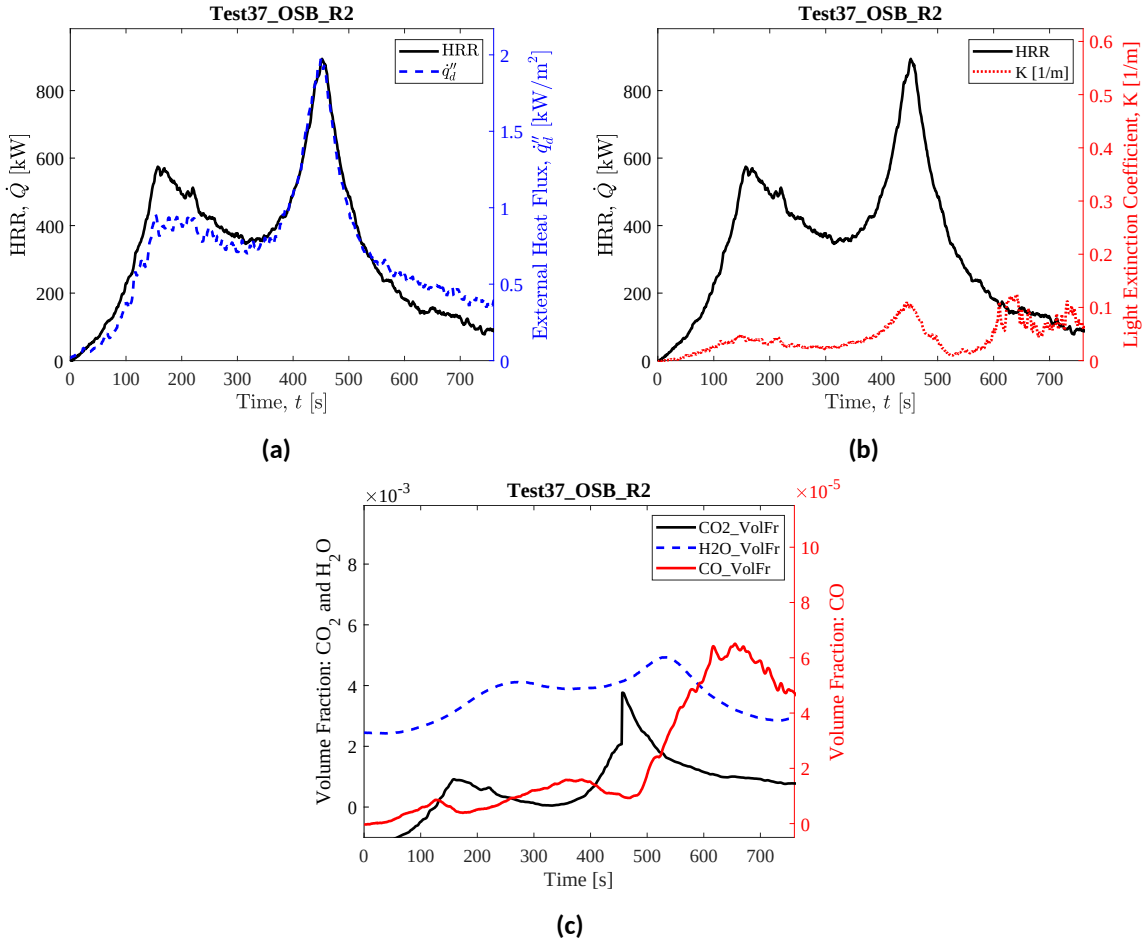

Fig. 139. Test 37 OSB R2: (a) Heat release rate and heat flux at a distance, $\dot{q}''_{\mathrm{d}}$ (here, $\dot{q}''_{\mathrm{d}}$ is measured at x =-232 cm, y =-300 cm, z =90 cm); (b) Heat release rate and light extinction coefficient, K (smoke particulate in exhaust duct [111]); (c) Time-resolved volume fractions of CO_2, H_2O, and CO.

Flame Heat Flux

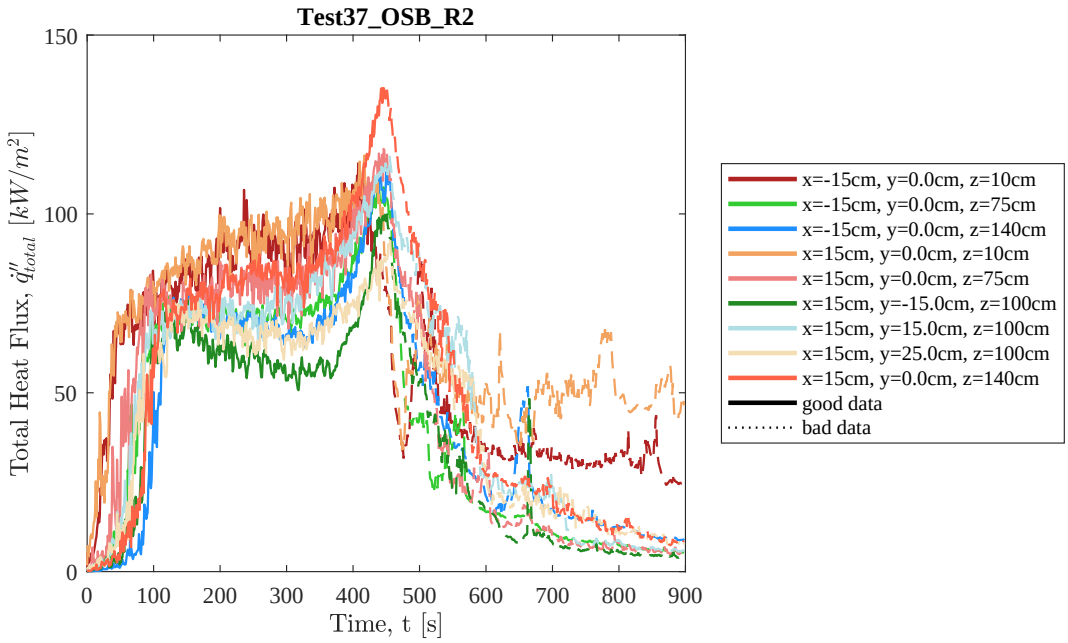

Fig. 140. Total flame to surface flame heat flux to water-cooled Schmidt-Boelter heat flux gauges as measured in Test 37 OSB R2. Here, raw, unsmoothed original measurments are plotted from each gauges as a function of time. Solid lines highlight values of $\dot{q}''_{\text{total}}$ that were identified by manual review as ”good” (see Sec. 3.1.1) and dotted lines represent ”bad” measurement data that should not be considered for further analysis.

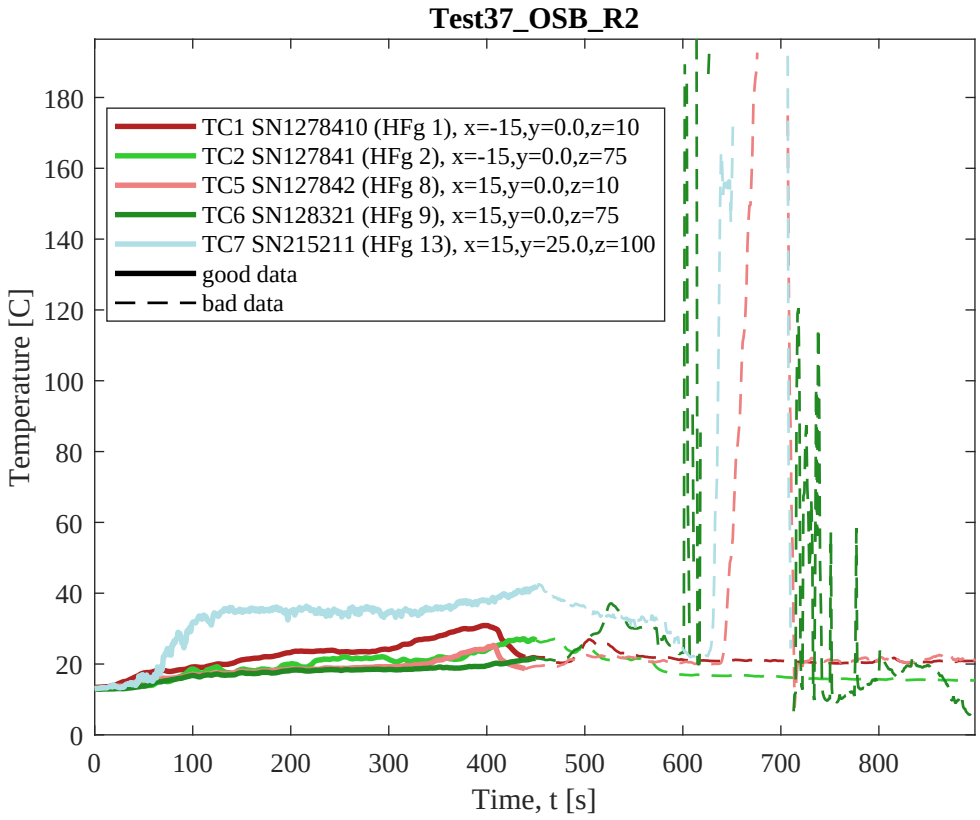

Fig. 141. Temperature of water-cooled Schmidt-Boelter heat flux gauges during Test 37 OSB R2.

Shielded Gauges

Measurements of total and radiation heat flux recorded by shielded heat flux gauges (Sec. efssec: qrad). Gauge shields were removed at 188 seconds.

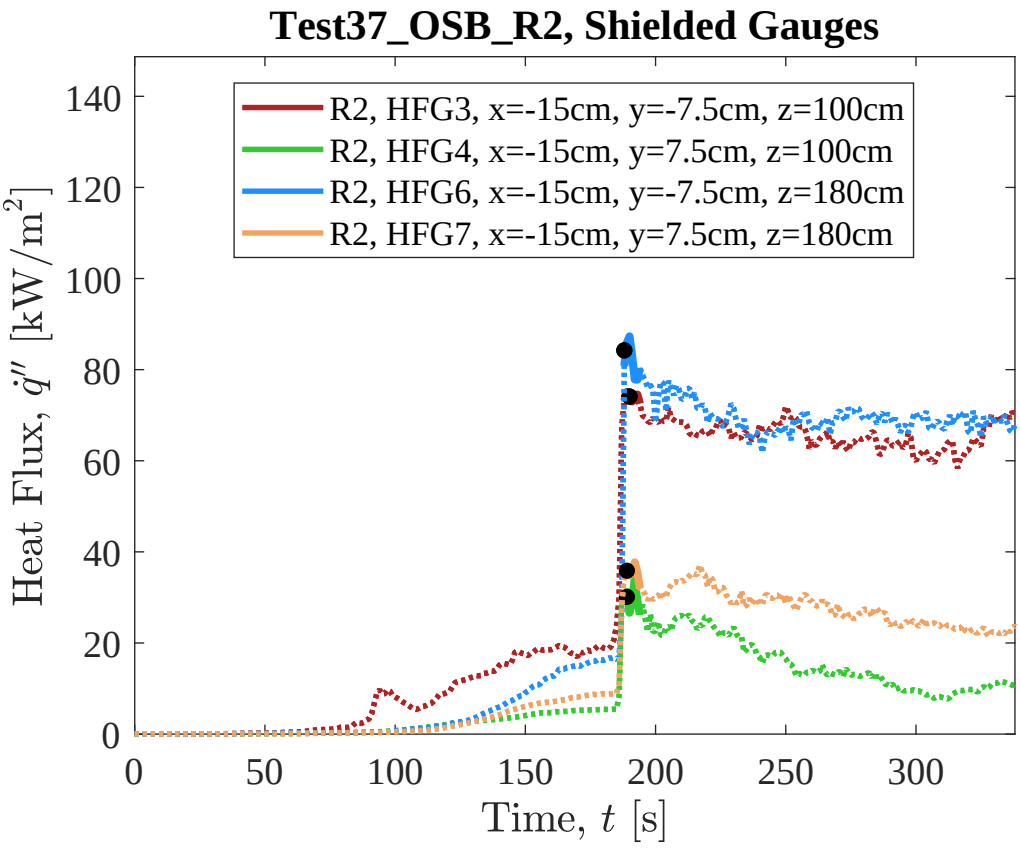

Fig. 142. Shielded gauge data for Test37 OSB R2.

Test 57 OSB R3

Test Description

7/16 in. thick, 24 in. wide, 96 in. tall panels of OSB mounted to 1 in. thick Marinite Board. Panels were ignited using a rectangular propane burner (60 kW nominal heat release rate) filled with layers of Pea Gravel, Sand, and Kaowool Insulation (i.e., the 'Final Burner configuration'; see Fig. 12). The burner was kept on until $t = 720$ s at which point flames began to gradually self-extinguish; . Heat flux gauges were mounted flush with the fuel's surface between $z = 30$ cm and $z = 220$ cm. Shielded radiometers and total heat flux gauges were positioned side by side at $z = 180$ cm. The heat flux shields were removed at $t = 171$ s; reliable measurements of both total and radiation flame heat flux were obtained.

Note: in Test OSB R3, due to poor initial performance of the propane burner (flaming only observed along the front edge of the burner, -30 cm $\leq y \leq$ 25 cm), ignition was cancelled after the first attempt (burner quickly turned off after 15 s) and the test restarted. During the second attempt at ignition, burner flaming was substantially more uniform; however, because the burner and gas lines were pre-loaded with propane, initial burner HRR (and resulting flame heat flux) increased faster than normal (as discussed in Sec. 2.4). As a result, in this test, sample ignition occured earlier (at $t = 11$ s in Test R3, versus $t = 39$ s and 45 s in Tests R1 and R2, respectively) and initial HRR was slightly higher during the first 60 s of the experiment (see Fig. 41).

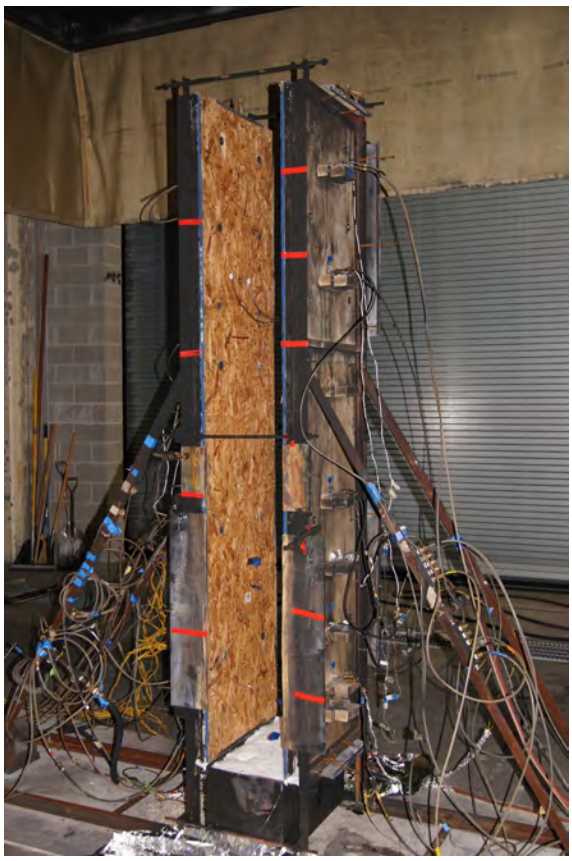

(a) Pre-test

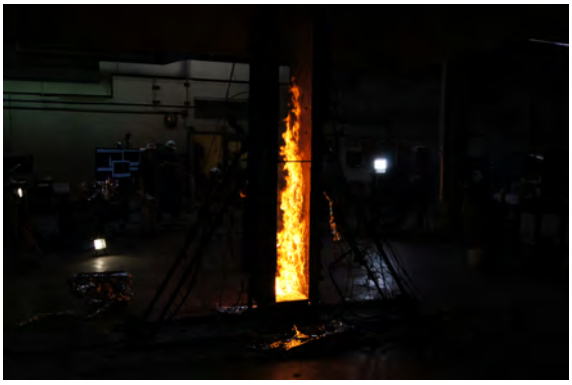

(b) Ignition

(c) Peak HRR

(d) End of Test

Fig. 143. Photographs of Test 57 OSB R3.

Heat Release Rate, Heat Flux at a Distance, and Species Yields

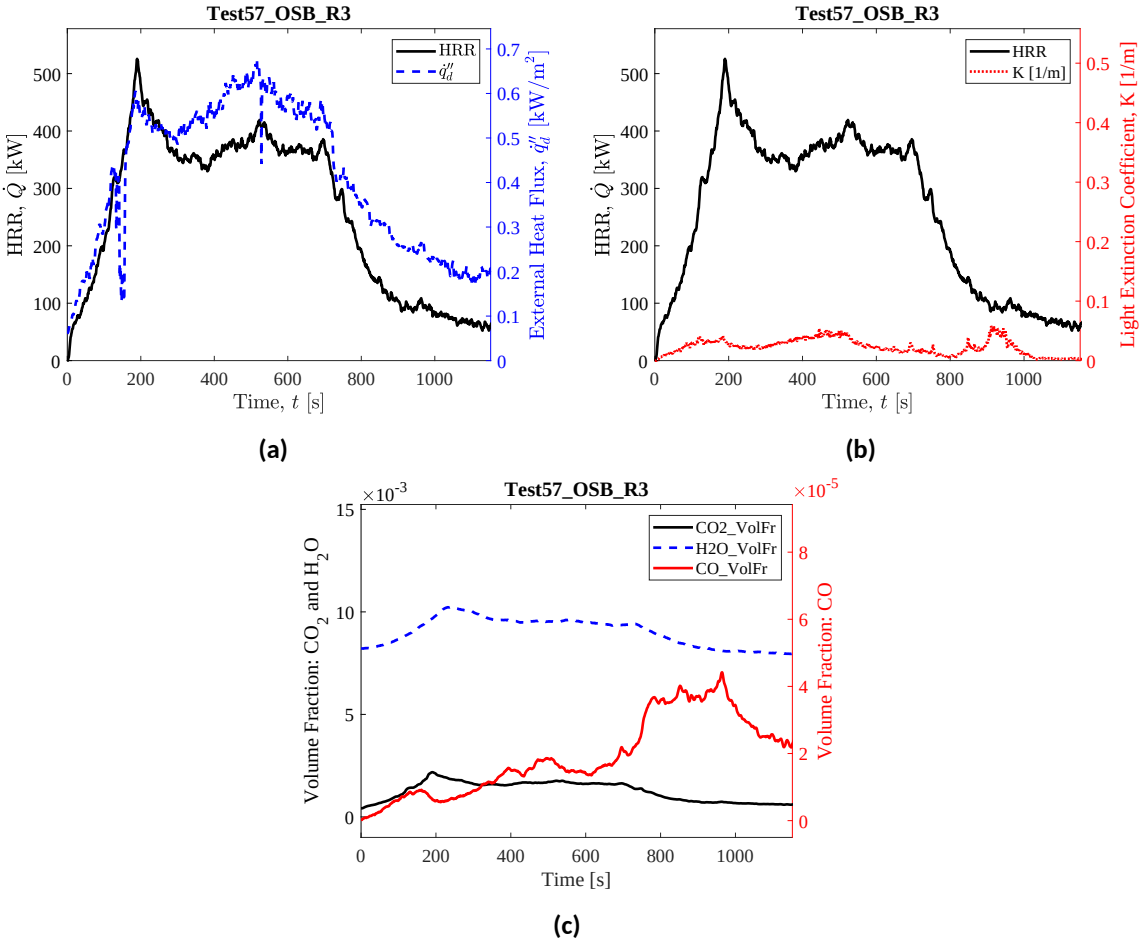

Fig. 144. Test 57 OSB R3: (a) Heat release rate and heat flux at a distance, $\dot{q}''_{\mathrm{d}}$ (here, $\dot{q}''_{\mathrm{d}}$ is measured at x =300 cm, y =-305 cm, z =90 cm); (b) Heat release rate and light extinction coefficient, K (smoke particulate in exhaust duct [111]); (c) Time-resolved volume fractions of CO_2, H_2O, and CO.

Flame Heat Flux

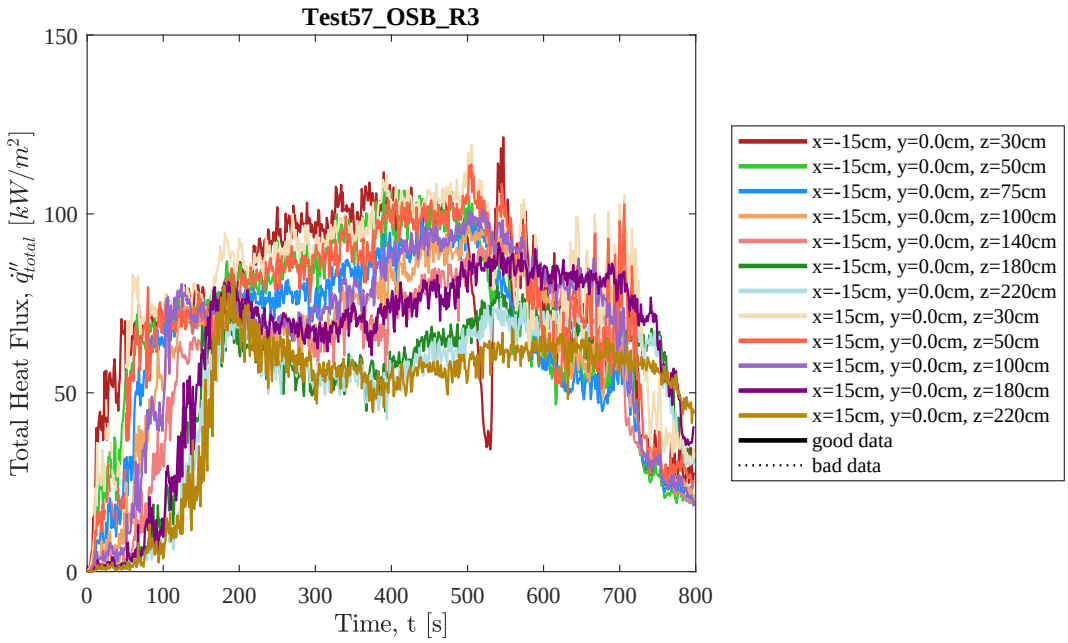

Fig. 145. Total flame to surface flame heat flux to water-cooled Schmidt-Boelter heat flux gauges as measured in Test 57 OSB R3. Here, raw, unsmoothed original measurments are plotted from each gauges as a function of time. Solid lines highlight values of $\dot{q}''_{\text{total}}$ that were identified by manual review as ”good” (see Sec. 3.1.1) and dotted lines represent ”bad” measurement data that should not be considered for further analysis.

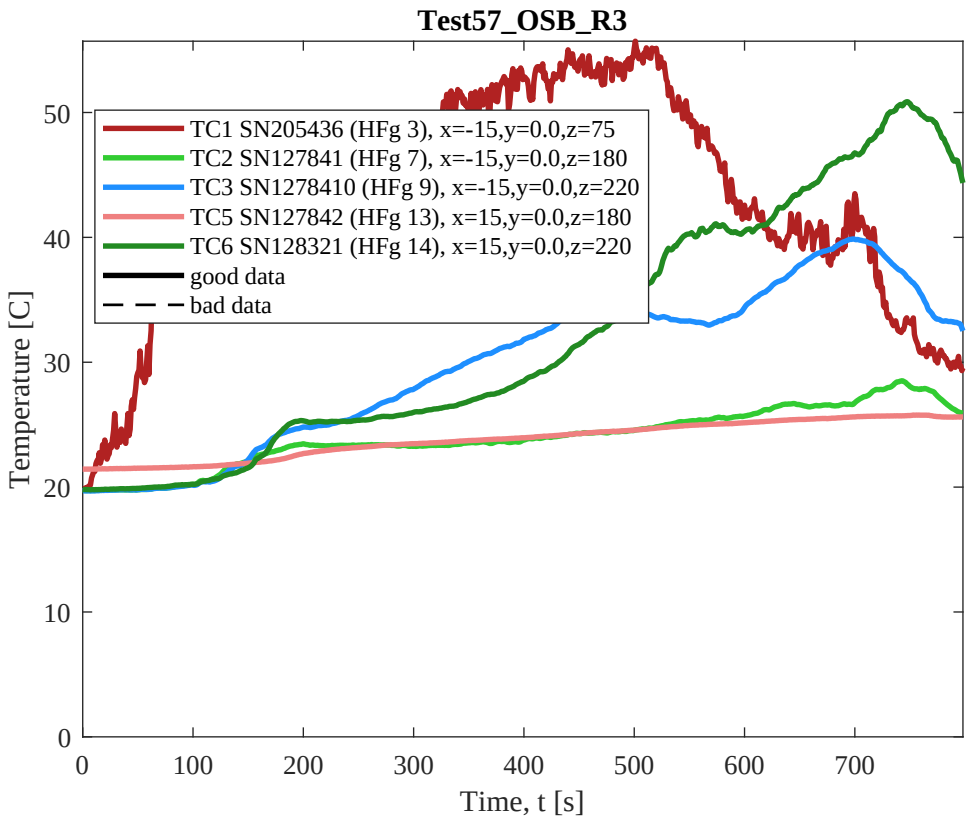

Fig. 146. Temperature of water-cooled Schmidt-Boelter heat flux gauges during Test 57 OSB R3.

Shielded Gauges

Measurements of total and radiation heat flux recorded by shielded heat flux gauges (Sec. efssec: qrad). Gauge shields were removed at 171 seconds and 172 seconds (gauges 6 and 8, respectively).

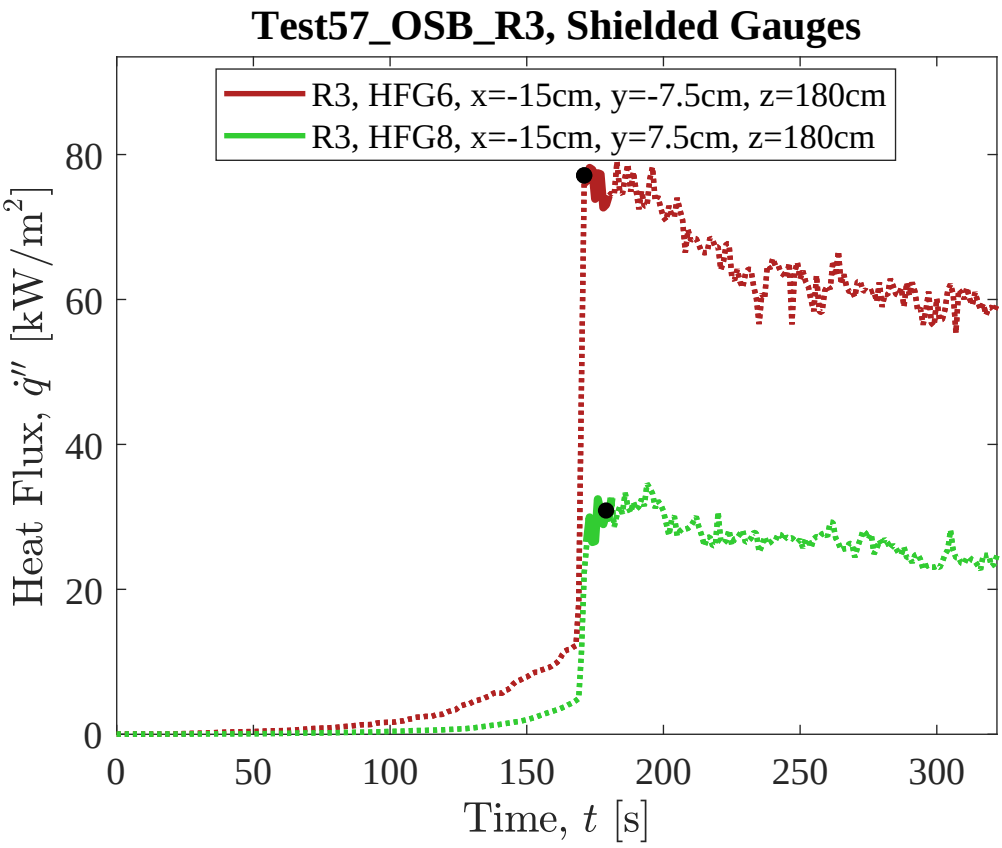

Fig. 147. Shielded gauge data for Test57 OSB R3.

C.6. PBT - Poly(Butylene Terepthalate)

Test 12 PBT R1

Test Description

1/4 in. thick, 24 in. wide, 96 in. tall (in four sections, each 12 in.x48in.) panels of PBT backed by aluminum foil layer mounted to 1 in. thick Marinite board. Panels were ignited using a rectangular propane burner (60 kW nominal heat release rate) filled with layers of Pea Gravel, Sand, and Kaowool Insulation (i.e., the 'Final Burner configuration'; see Fig. 12). The burner was shut off ($t = 211$ s) after sustained flaming of panels; both walls ignited uniformly across their base. By $t = 310$ s, the edges of most PBT sections had separated from the assembly walls, at which point a significant melt flow / dripping event occurred and the majority of the remaining PBT fell down, where it continued burning as a pool fire. Molten PBT that dripped or spread to the back sides of the parallel panel assembly was extinguished (suppression by application of water) and the remaining drip pool closest to the burner was allowed to burn until self-extinction. Flame to wall heat flux measurements were not recorded in this test.

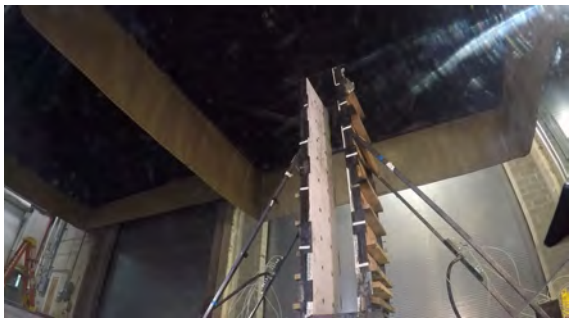

(a) Pre-test

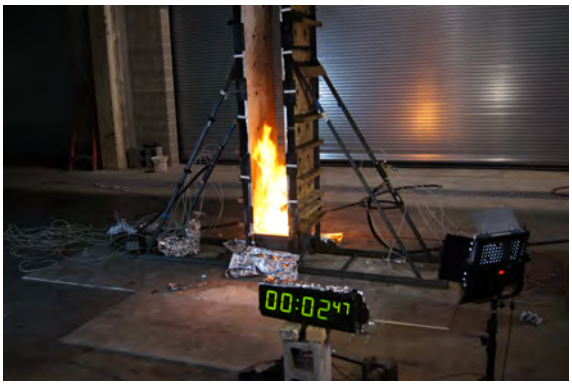

(b) Ignition

(c) Peak HRR

(d) End of Test

Fig. 148. Photographs of Test 12 PBT R1.

Heat Release Rate, Heat Flux at a Distance, and Species Yields

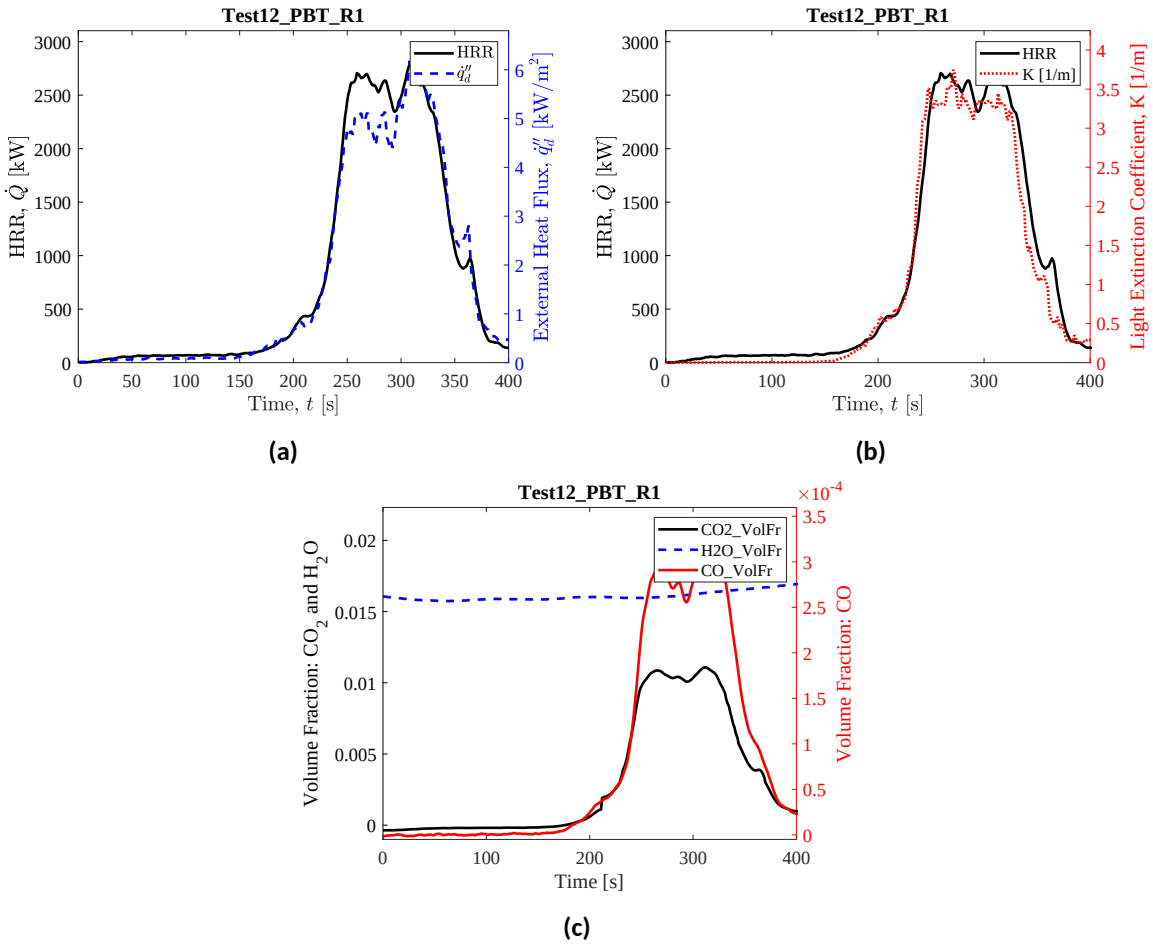

Fig. 149. Test 12 PBT R1: (a) Heat release rate and heat flux at a distance, $\dot{q}''_{\mathrm{d}}$ (here, $\dot{q}''_{\mathrm{d}}$ is measured at x =-100 cm, y =-300 cm, z =90 cm); (b) Heat release rate and light extinction coefficient, K (smoke particulate in exhaust duct [111]); (c) Time-resolved volume fractions of CO_2, H_2O, and CO.

C.7. PMMA - Poly(Methyl Methacrylate)

Test 1 PMMA R1

Test Description

1/4 in. thick, 24 in. wide, 96 in. tall panels of cast Black PMMA backed by aluminum foil layer mounted to 1 in. thick Marinite board. Panels were ignited using a rectangular propane burner (60 kW nominal heat release rate) filled with Pea Gravel (i.e., the 'Preliminary Burner configuration'; see Fig. 12. In this experiment (the first of the series) the burner was turned off too early (at $t = 90$ s) and sustained flaming of only the left panel wall was achieved. The right panel wall did not ignite until $t = 620$ s (ignition first observed at the top of the assembly). Heat flux gauges were mounted flush with the fuel's surface between $z = 10$ cm and $z = 180$ cm.

(a) Pre-test

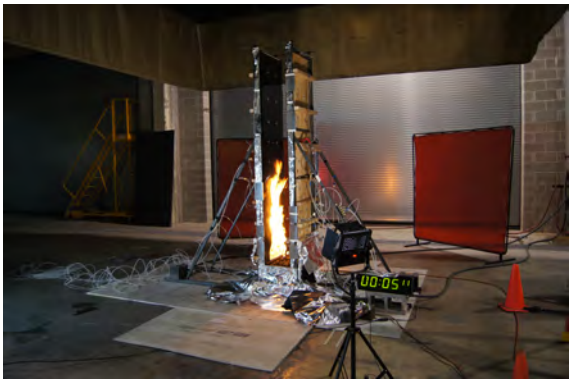

(b) Ignition

(c) Peak HRR

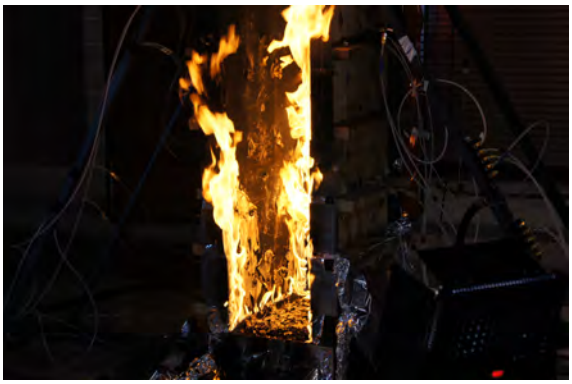

(d) End of Test

Fig. 150. Photographs of Test 1 PMMA R1.

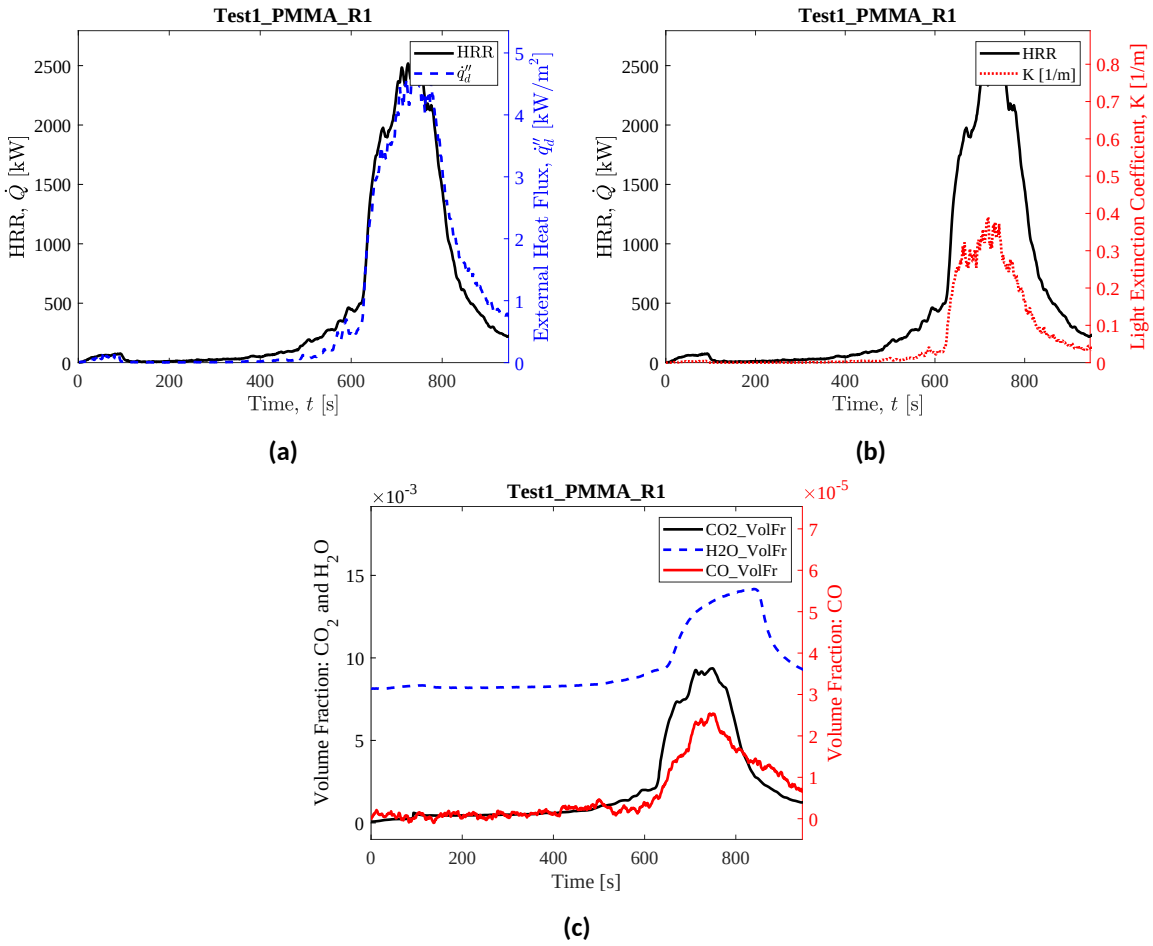

Fig. 151. Test 1 PMMA R1: (a) Heat release rate and heat flux at a distance, $\dot{q}''_{\mathrm{d}}$ (here, $\dot{q}''_{\mathrm{d}}$ is measured at x =-95 cm, y =-300 cm, z =90 cm); (b) Heat release rate and light extinction coefficient, K (smoke particulate in exhaust duct [111]); (c) Time-resolved volume fractions of CO_2, H_2O, and CO.

Flame Heat Flux

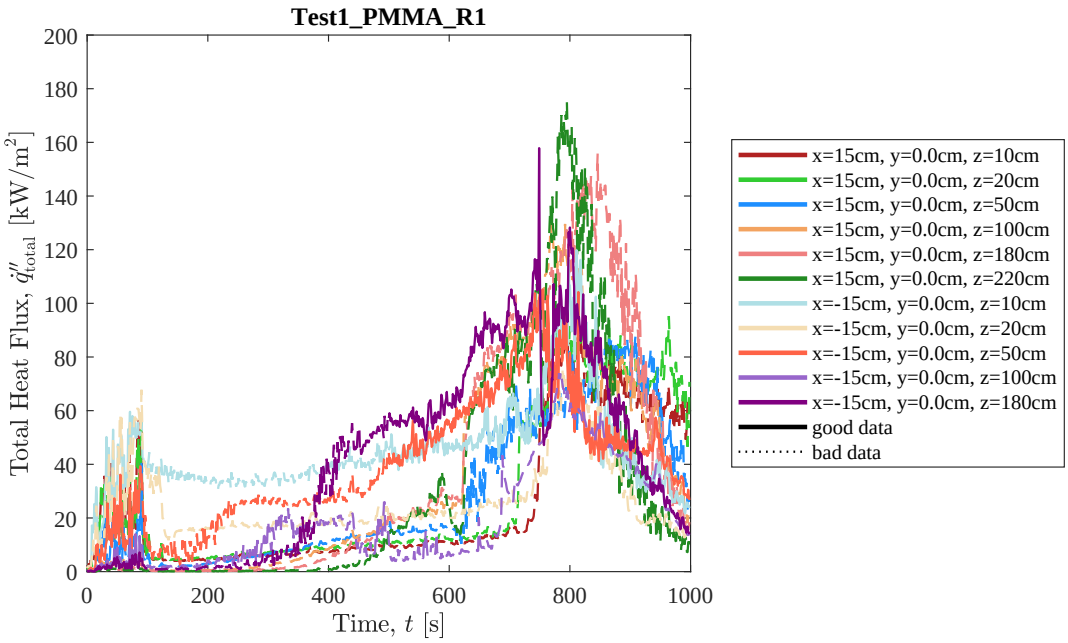

Fig. 152. Total flame to surface flame heat flux to water-cooled Schmidt-Boelter heat flux gauges as measured in Test 1 PMMA R1. Here, raw, unsmoothed original measurments are plotted from each gauges as a function of time. Solid lines highlight values of $\dot{q}''_{\text{total}}$ that were identified by manual review as ”good” (see Sec. 3.1.1) and dotted lines represent ”bad” measurement data that should not be considered for further analysis.

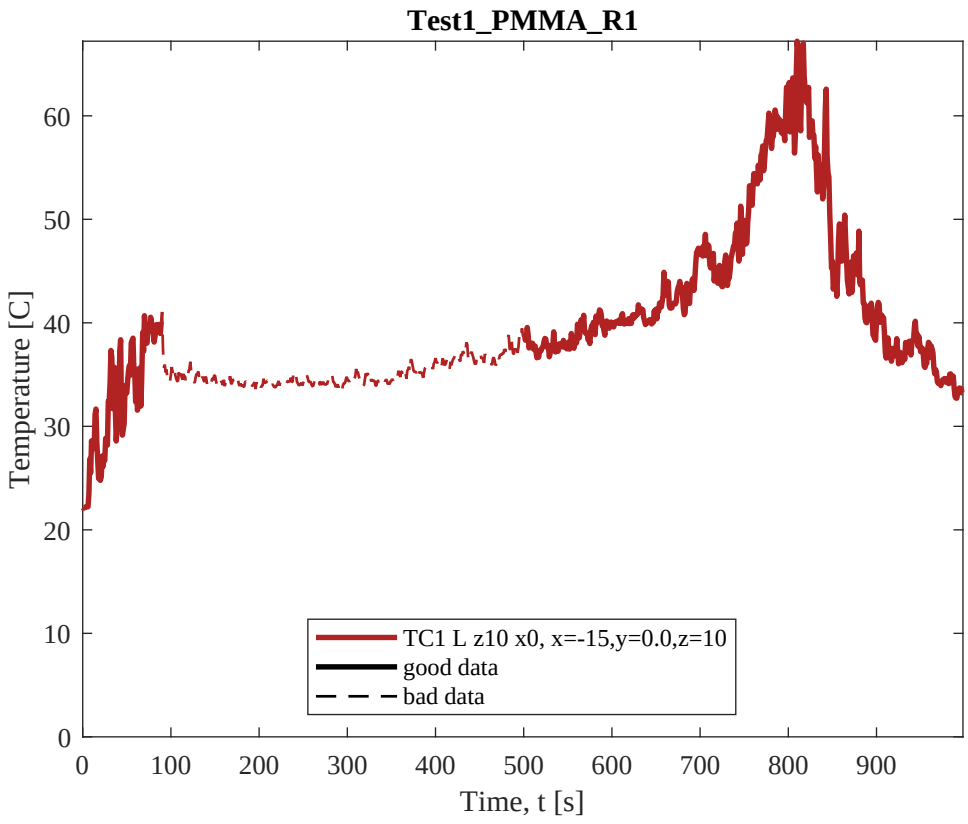

Fig. 153. Temperature of water-cooled Schmidt-Boelter heat flux gauges during Test 1 PMMA R1.

Test 2 PMMA R2

Test Description

1/4 in. thick, 24 in. wide, 96 in. tall panels of cast Black PMMA backed by aluminum foil layer mounted to 1 in. thick Marinite board. Panels were ignited using a rectangular propane burner (60 kW nominal heat release rate) filled with Pea Gravel (i.e., the 'Preliminary Burner configuration'; see Fig. 12. Although flames appeared to grow thicker and longer along the left panel wall until $t = 60$ s, the burner was shut off ($t = 120$ s) after sustained, uniform flaming of both panel walls. Heat flux gauges were mounted flush with the fuel's surface between $z = 10$ cm and $z = 140$ cm. The edges of this PMMA panel were not sufficiently clamped to the parallel panel apparatus - this allowed for deformation of the PMMA slab and eventual corruption of heat flux measurements recorded at the mid-height of the panel walls.

(a) Pre-test

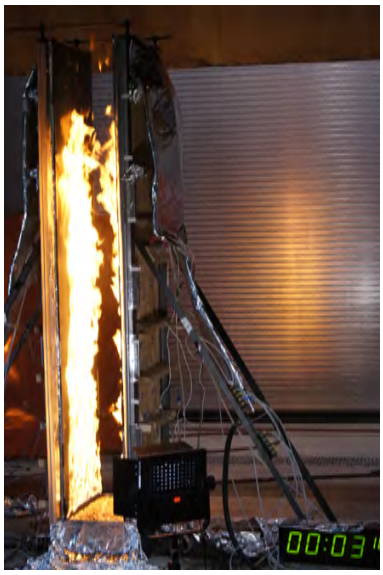

(b) Ignition

(c) Peak HRR

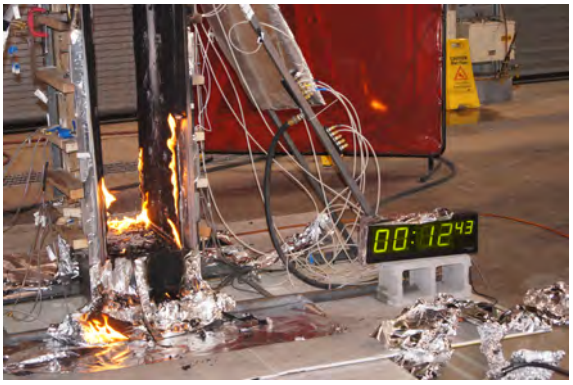

(d) End of Test

Fig. 154. Photographs of Test 2 PMMA R2.

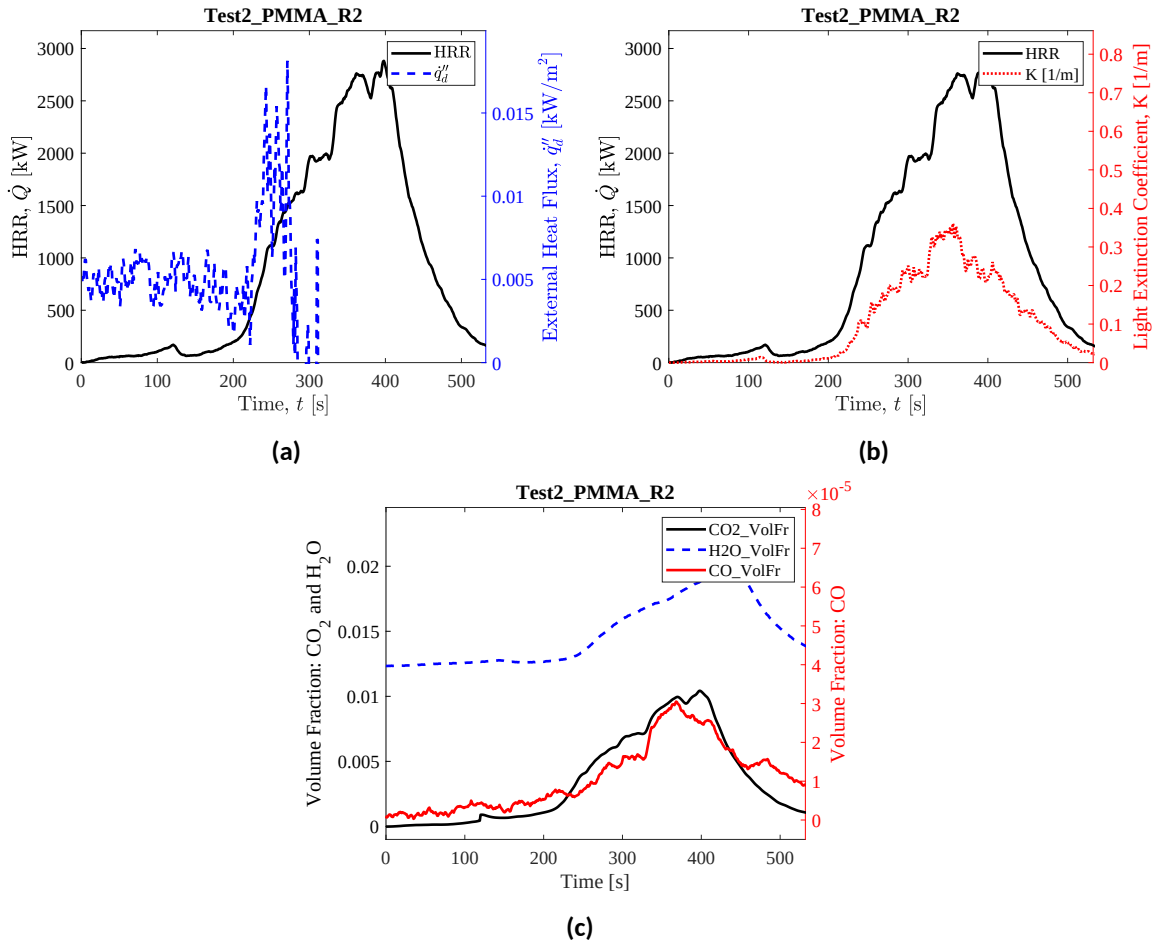

Fig. 155. Test 2 PMMA R2: (a) Heat release rate and heat flux at a distance, $\dot{q}''_{\mathrm{d}}$ (here, $\dot{q}''_{\mathrm{d}}$ is measured at x =-300 cm, y =-300 cm, z =90 cm); (b) Heat release rate and light extinction coefficient, K (smoke particulate in exhaust duct [111]); (c) Time-resolved volume fractions of CO_2, H_2O, and CO.

Flame Heat Flux

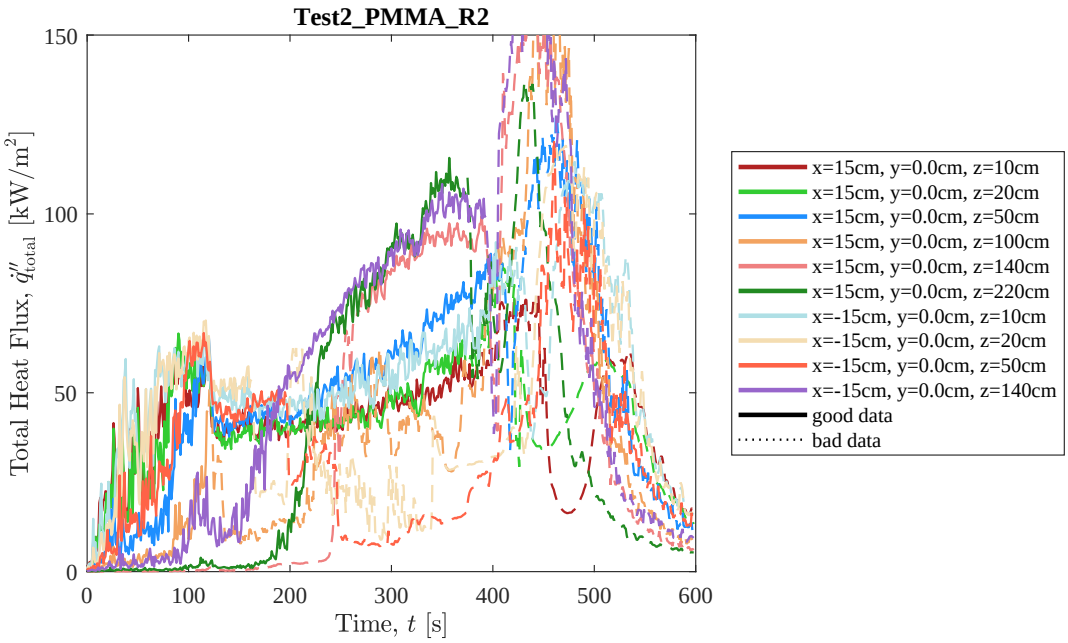

Fig. 156. Total flame to surface flame heat flux to water-cooled Schmidt-Boelter heat flux gauges as measured in Test 2 PMMA R2. Here, raw, unsmoothed original measurments are plotted from each gauges as a function of time. Solid lines highlight values of $\dot{q}''_{\text{total}}$ that were identified by manual review as ”good” (see Sec. 3.1.1) and dotted lines represent ”bad” measurement data that should not be considered for further analysis.

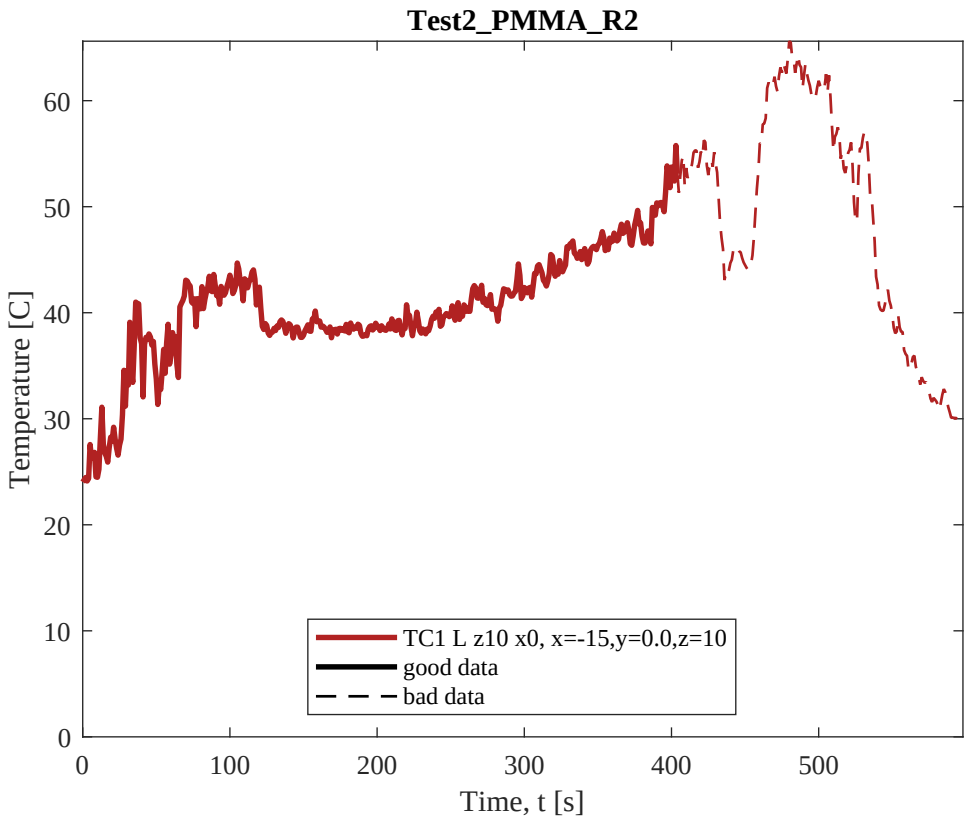

Fig. 157. Temperature of water-cooled Schmidt-Boelter heat flux gauges during Test 2 PMMA R2.

Test 3 PMMA R3

Test Description

1/4 in. thick, 24 in. wide, 96 in. tall panels of cast Black PMMA mounted to 1 in. thick Marinite board. Panels were ignited using a rectangular propane burner (60 kW nominal heat release rate) filled with Pea Gravel (i.e., the 'Preliminary Burner configuration'; see Fig. 12. For the first minute that the burner was turned on, flames would alternate (approximate duration, 30 s) between primarily covering just the left and then just the right wall. Nevertheless, the burner was shut off at $t = 120$ s and sustained, uniform flaming of both panel walls was observed. Heat flux gauges were mounted flush with the fuel's surface between $z = 20$ cm and $z = 220$ cm.

(a) Pre-test

(b) Ignition

(c) Peak HRR

(d) End of Test

Fig. 158. Photographs of Test 3 PMMA R3.

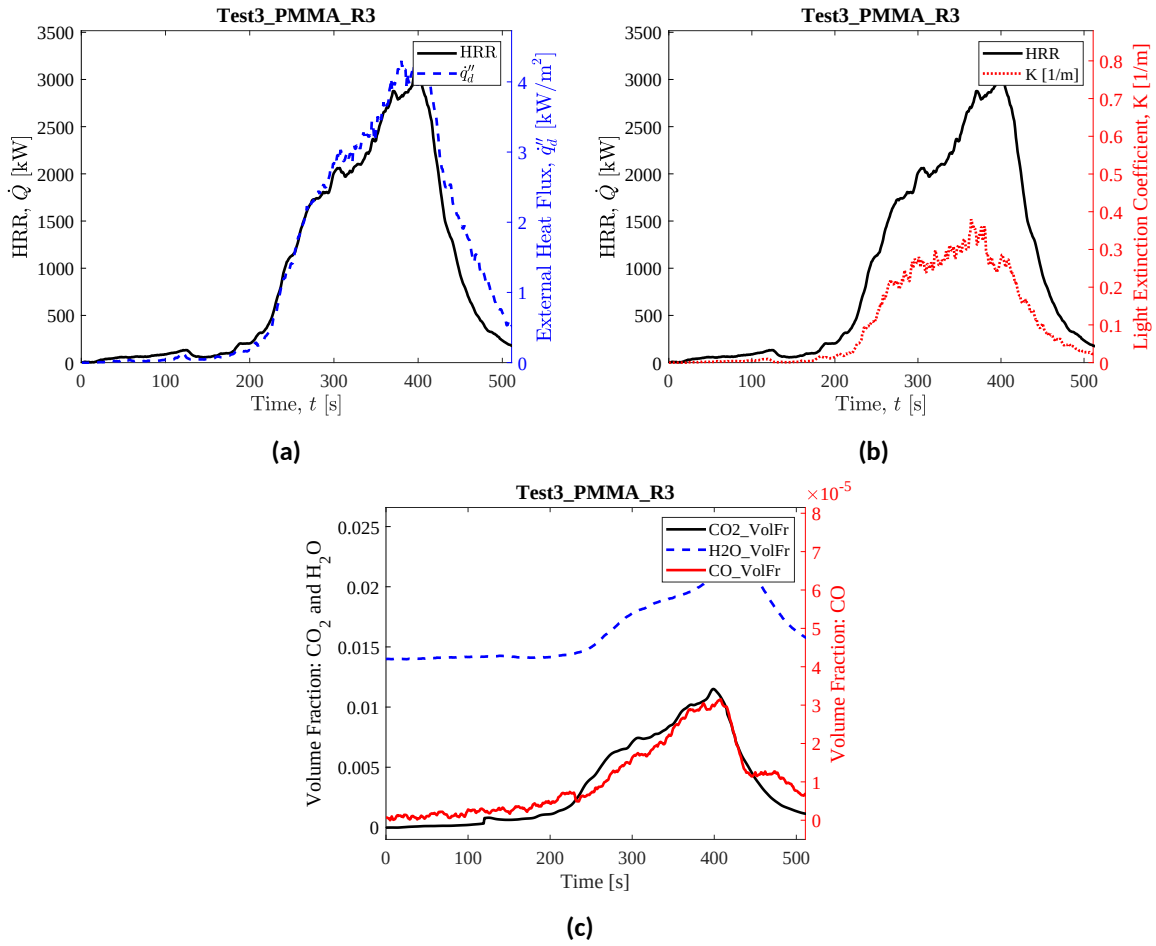

Fig. 159. Test 3 PMMA R3: (a) Heat release rate and heat flux at a distance, $\dot{q}''_{\mathrm{d}}$ (here, $\dot{q}''_{\mathrm{d}}$ is measured at x =-300 cm, y =-300 cm, z =90 cm); (b) Heat release rate and light extinction coefficient, K (smoke particulate in exhaust duct [111]); (c) Time-resolved volume fractions of CO_2, H_2O, and CO.

Flame Heat Flux

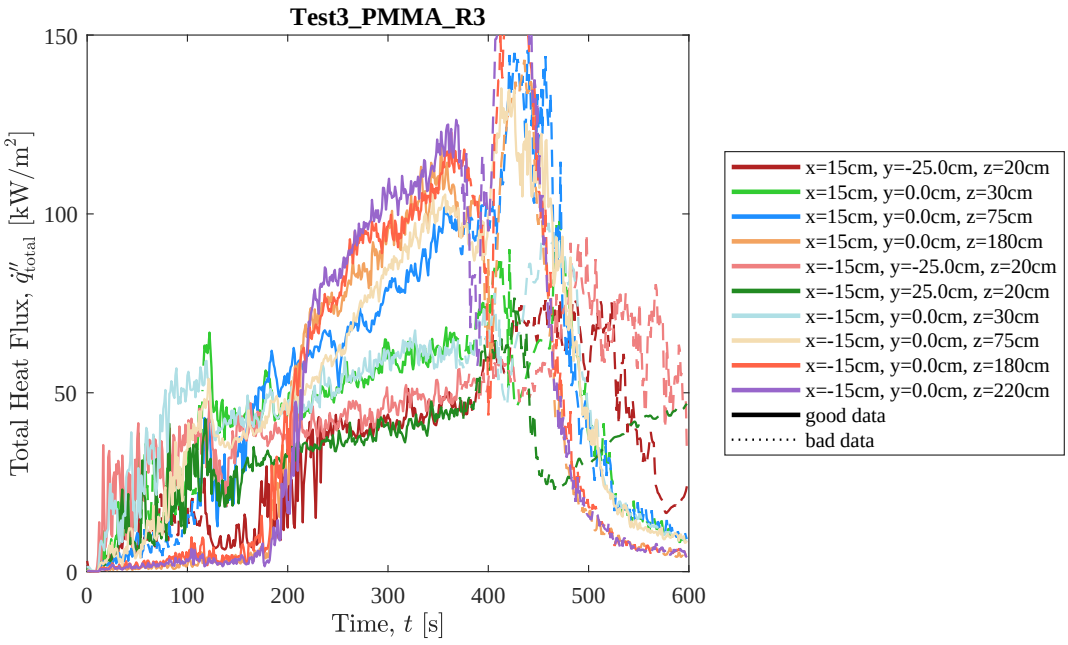

Fig. 160. Total flame to surface flame heat flux to water-cooled Schmidt-Boelter heat flux gauges as measured in Test 3 PMMA R3. Here, raw, unsmoothed original measurments are plotted from each gauges as a function of time. Solid lines highlight values of $\dot{q}''_{\text{total}}$ that were identified by manual review as ”good” (see Sec. 3.1.1) and dotted lines represent ”bad” measurement data that should not be considered for further analysis.

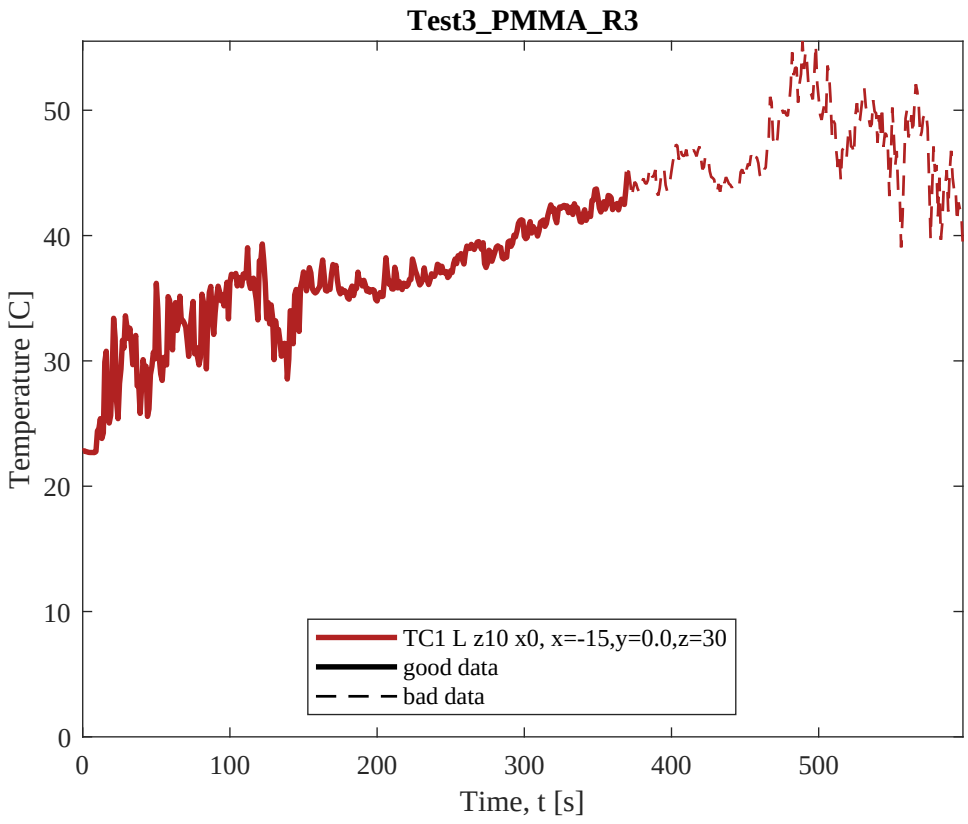

Fig. 161. Temperature of water-cooled Schmidt-Boelter heat flux gauges during Test 3 PMMA R3.

Test 4 PMMA R4

Test Description

1/4 in. thick, 24 in. wide, 96 in. tall panels of cast Black PMMA mounted to 1 in. thick Marinite board. Panels were ignited using a rectangular propane burner (60 kW nominal heat release rate) filled with Pea Gravel (i.e., the 'Preliminary Burner configuration'; see Fig. 12. The burner was briefly shut off ($t = 120$ s) but it was apparent that sustained flaming ignition of the right panel wall was not achieved (burner flames appeared t attached primarly towards the back ($-y$) of the left panel wall; only weak ignition was observed at the base of the right wall); propane flow to the burner was therefore turned back on at $t = 150$ s, and kept on until $t = 210$ s. Heat flux gauges were mounted flush with the fuel's surface between $z = 100$ cm and $z = 220$ cm.

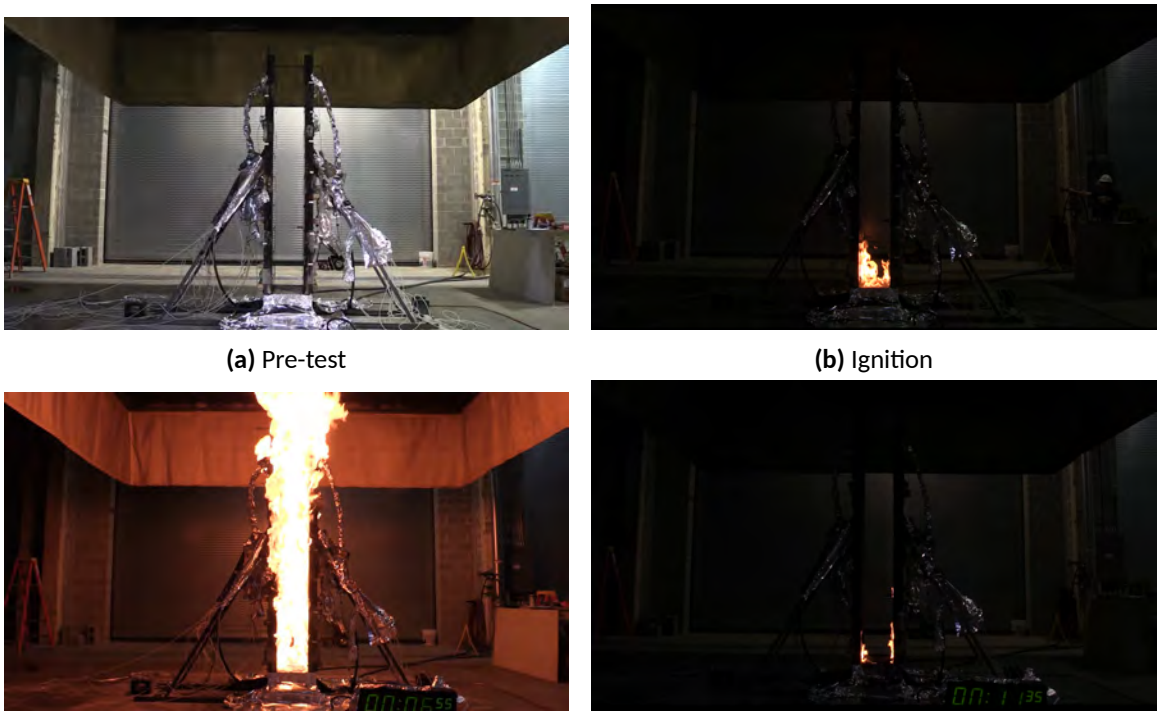

(a) Pre-test

(b) Ignition

(c) Peak HRR

(d) End of Test

Fig. 162. Photographs of Test 4 PMMA R4.

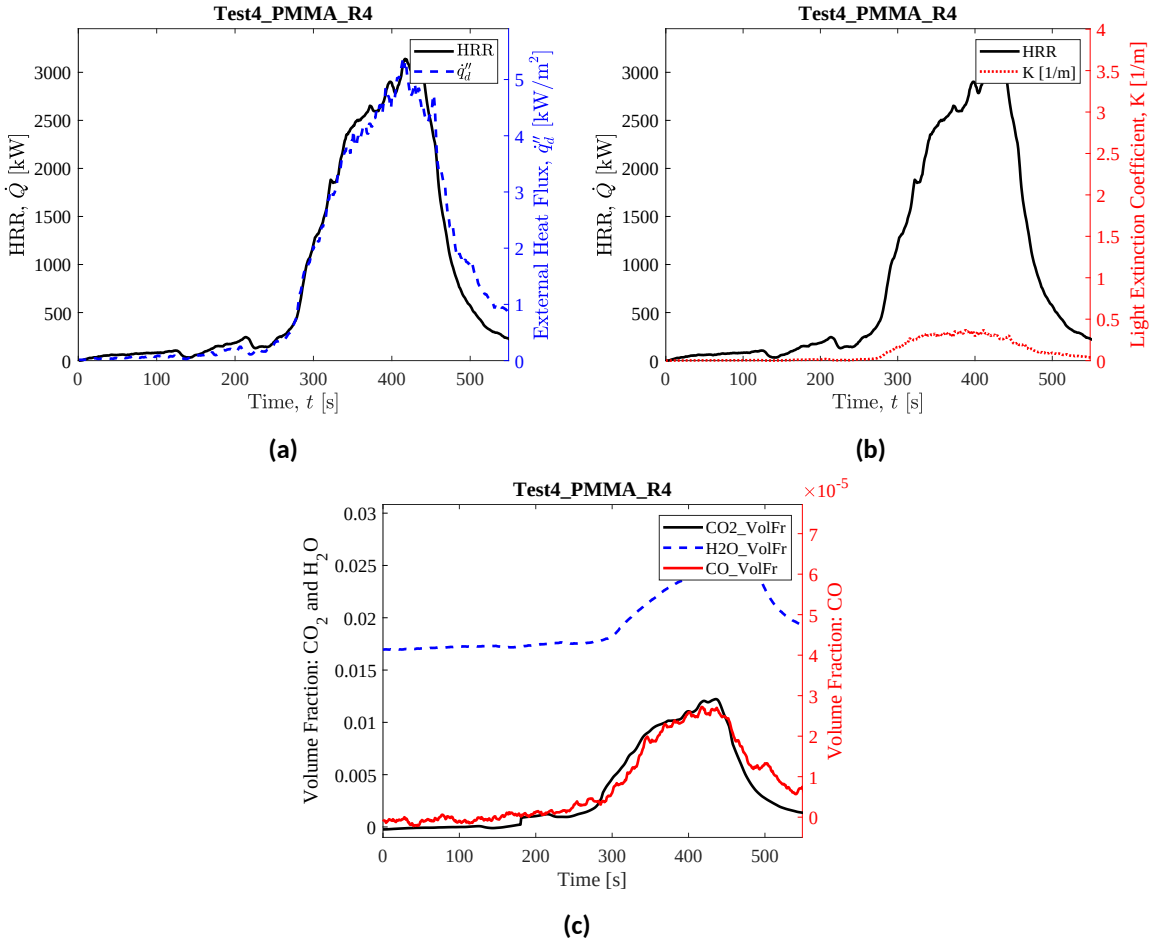

Fig. 163. Test 4 PMMA R4: (a) Heat release rate and heat flux at a distance, $\dot{q}''_{\mathrm{d}}$ (here, $\dot{q}''_{\mathrm{d}}$ is measured at x =-300 cm, y =-300 cm, z =90 cm); (b) Heat release rate and light extinction coefficient, K (smoke particulate in exhaust duct [111]); (c) Time-resolved volume fractions of CO_2, H_2O, and CO.

Flame Heat Flux

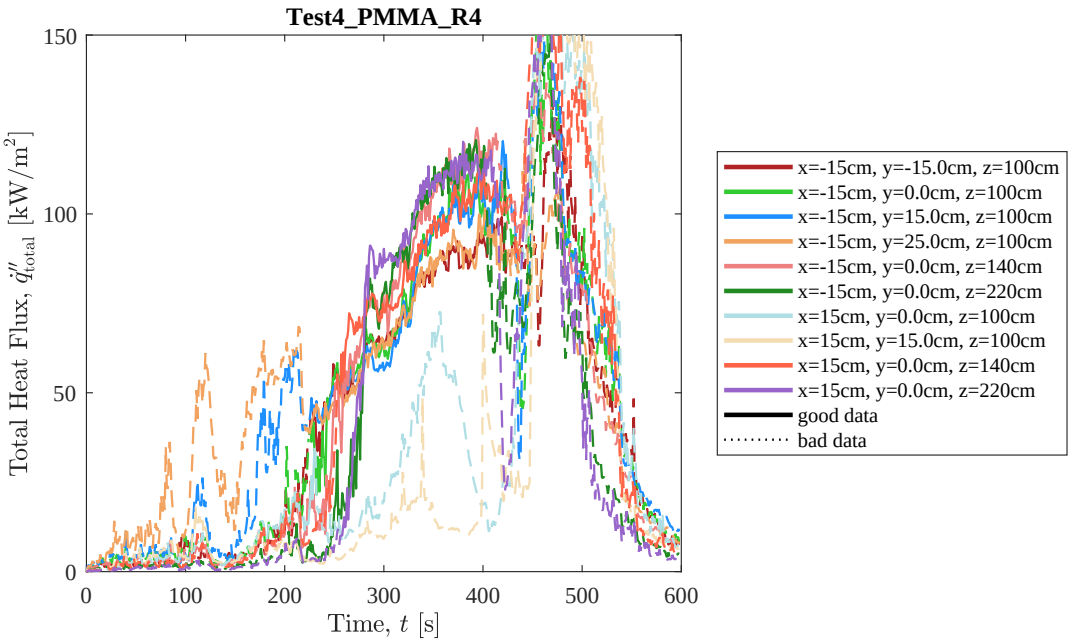

Fig. 164. Total flame to surface flame heat flux to water-cooled Schmidt-Boelter heat flux gauges as measured in Test 4 PMMA R4. Here, raw, unsmoothed original measurments are plotted from each gauges as a function of time. Solid lines highlight values of $\dot{q}''_{\text{total}}$ that were identified by manual review as ”good” (see Sec. 3.1.1) and dotted lines represent ”bad” measurement data that should not be considered for further analysis.

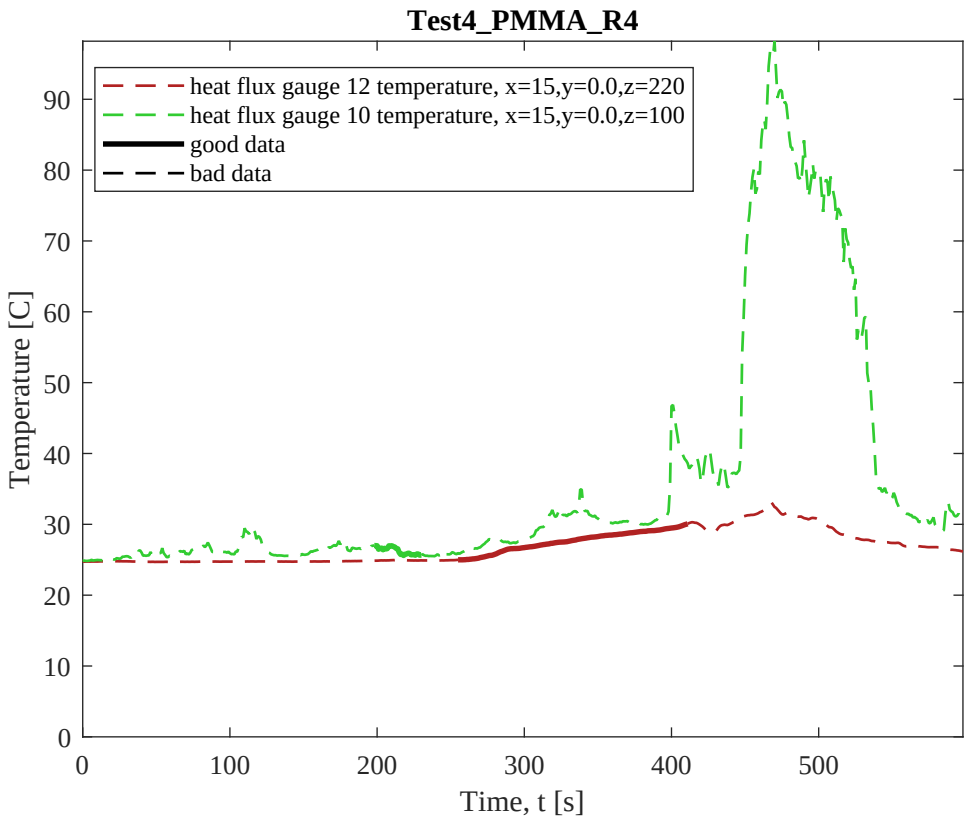

Fig. 165. Temperature of water-cooled Schmidt-Boelter heat flux gauges during Test 4 PMMA R4.

Test 5 PMMA R5

Test Description

1/4 in. thick, 24 in. wide, 96 in. tall panels of cast Black PMMA mounted to 1 in. thick Marinite board. Panels were ignited using a rectangular propane burner (60 kW nominal heat release rate) filled with Pea Gravel (i.e., the 'Preliminary Burner configuration'; see Fig. 12. The burner was shut off ($t = 120$ s) after sustained, uniform flaming of both panel walls; however, a crossflow from back to front (i.e., from $+y$ to $-y$) resulted in preferential flame attachement to the front edge ($y = -30$ cm) of panel walls while flames spread upwards. Later in this test ($t = 660$ s), as fires grew larger (stronger fire-induced buoyant flow), uniform flaming was observed across the width of both panel walls. Heat flux gauges were mounted flush with the fuel's surface between $z = 30$ cm and $z = 180$ cm.

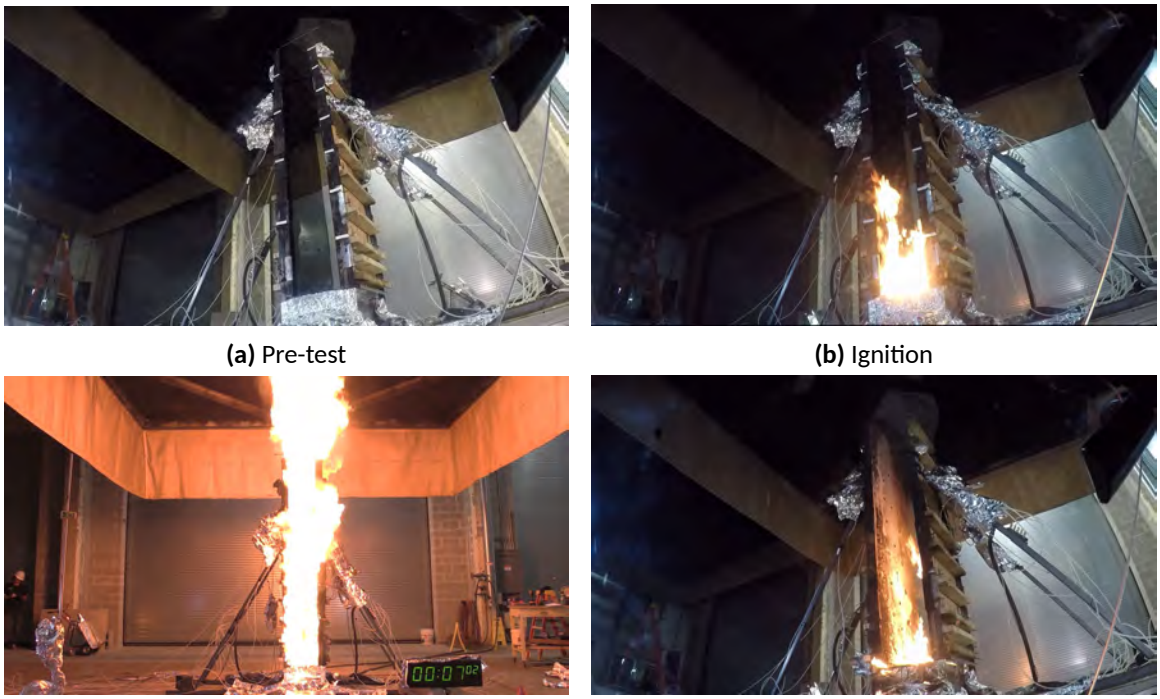

(a) Pre-test

(b) Ignition

(c) Peak HRR

(d) End of Test

Fig. 166. Photographs of Test 5 PMMA R5.

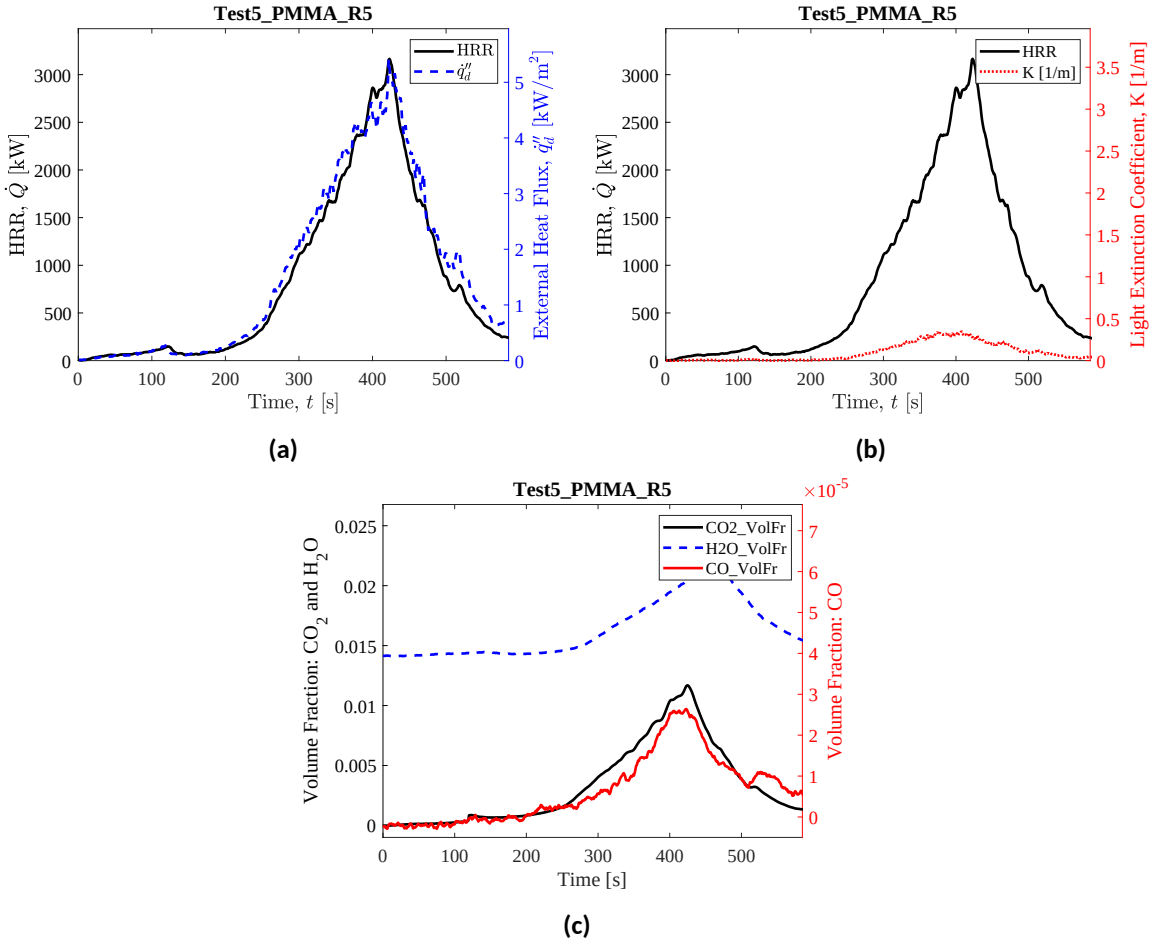

Fig. 167. Test 5 PMMA R5: (a) Heat release rate and heat flux at a distance, $\dot{q}''_{\mathrm{d}}$ (here, $\dot{q}''_{\mathrm{d}}$ is measured at x =-100 cm, y =-300 cm, z =90 cm); (b) Heat release rate and light extinction coefficient, K (smoke particulate in exhaust duct [111]); (c) Time-resolved volume fractions of CO_2, H_2O, and CO.

Flame Heat Flux

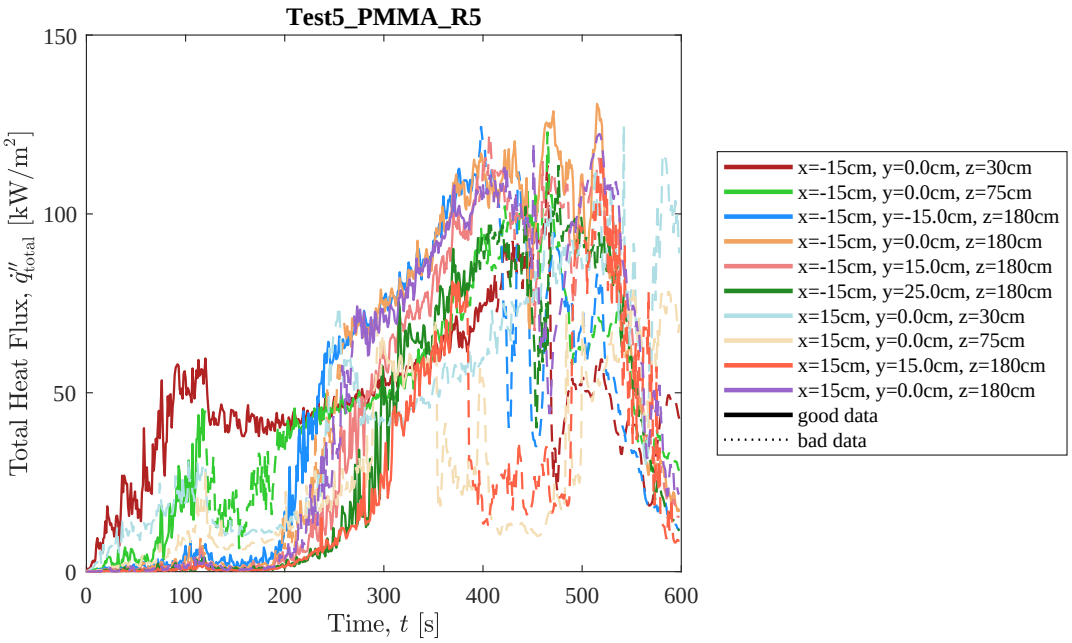

Fig. 168. Total flame to surface flame heat flux to water-cooled Schmidt-Boelter heat flux gauges as measured in Test 5 PMMA R5. Here, raw, unsmoothed original measurments are plotted from each gauges as a function of time. Solid lines highlight values of $\dot{q}''_{\text{total}}$ that were identified by manual review as ”good” (see Sec. 3.1.1) and dotted lines represent ”bad” measurement data that should not be considered for further analysis.

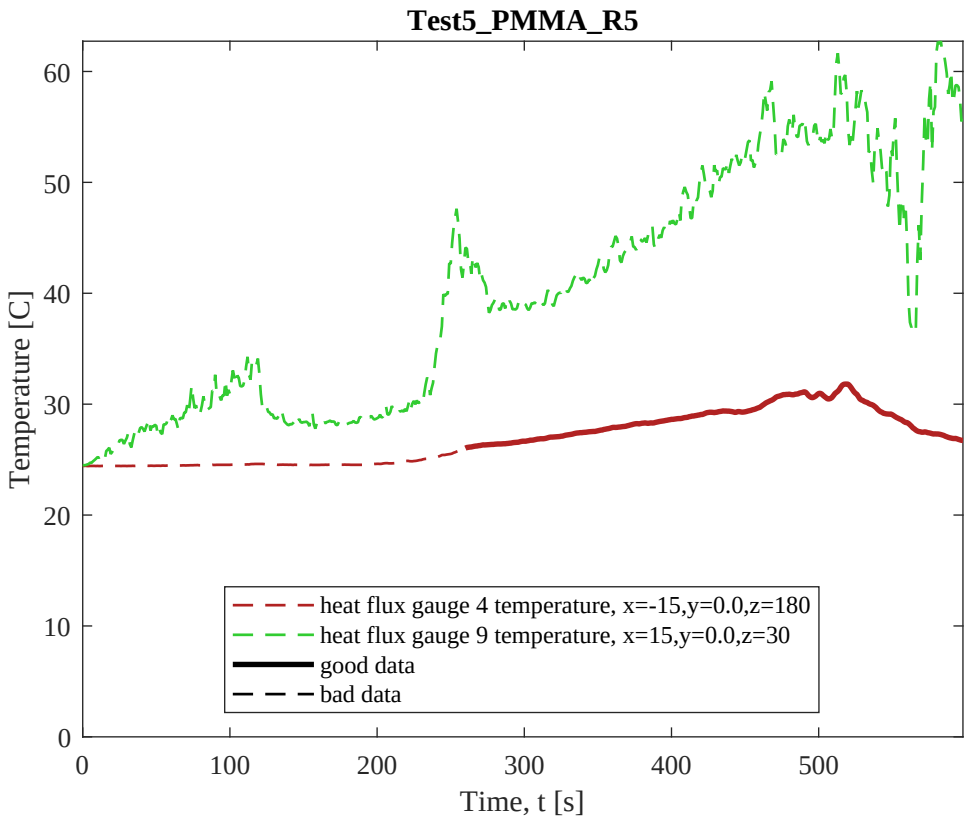

Fig. 169. Temperature of water-cooled Schmidt-Boelter heat flux gauges during Test 5 PMMA R5.

Test 7 PMMA R6

Test Description

1/4 in. thick, 24 in. wide, 96 in. tall panels of cast Black PMMA mounted to 1 in. thick Marinite board. Panels were ignited using a rectangular propane burner (60 kW nominal heat release rate) filled with layers of Pea Gravel, Sand, and Kaowool Insulation (i.e., the 'Final Burner configuration'; see Fig. 12); this new burner configuration provided significantly more uniform flaming conditions throughout the time it was on. The burner was shut off at $t = 120$ s to match the timing of tests R2-R5; however, visual observations, HRR data, and heat flux measurements all suggested that uniform ignition across both panel walls occurred at approximately $t = 100$ s. Heat flux gauges were mounted flush with the fuel's surface between $z = 50$ cm and $z = 100$ cm.

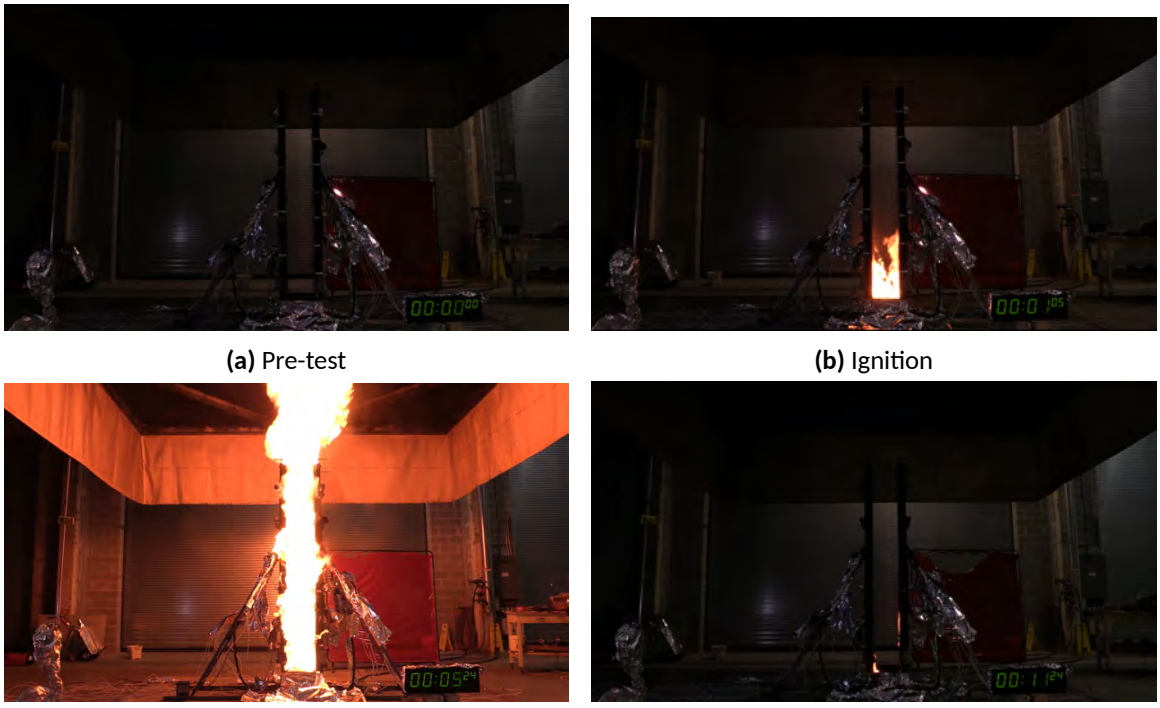

(a) Pre-test

(b) Ignition

(c) Peak HRR

(d) End of Test

Fig. 170. Photographs of Test 7 PMMA R6.

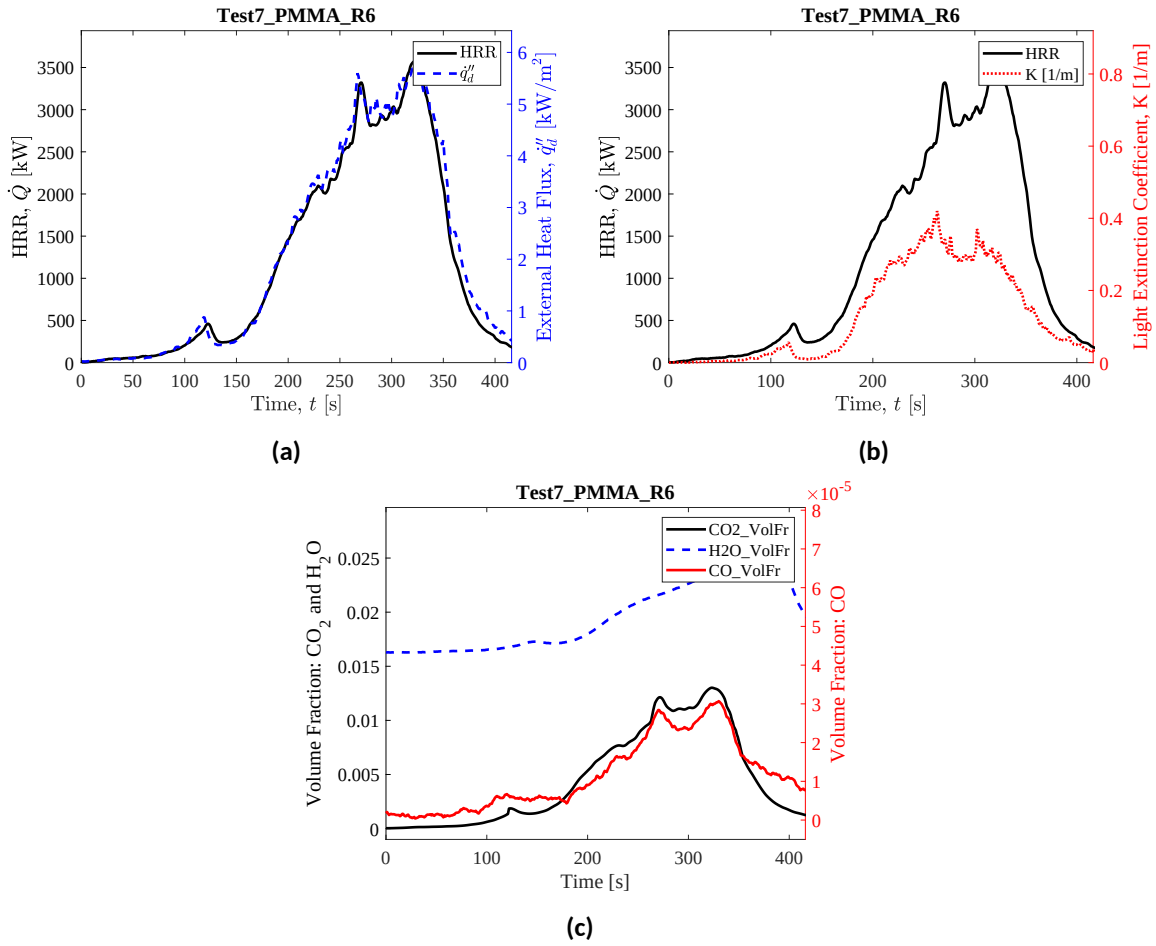

Fig. 171. Test 7 PMMA R6: (a) Heat release rate and heat flux at a distance, $\dot{q}''_{\mathrm{d}}$ (here, $\dot{q}''_{\mathrm{d}}$ is measured at x =-100 cm, y =-300 cm, z =90 cm); (b) Heat release rate and light extinction coefficient, K (smoke particulate in exhaust duct [111]); (c) Time-resolved volume fractions of CO_2, H_2O, and CO.

Flame Heat Flux

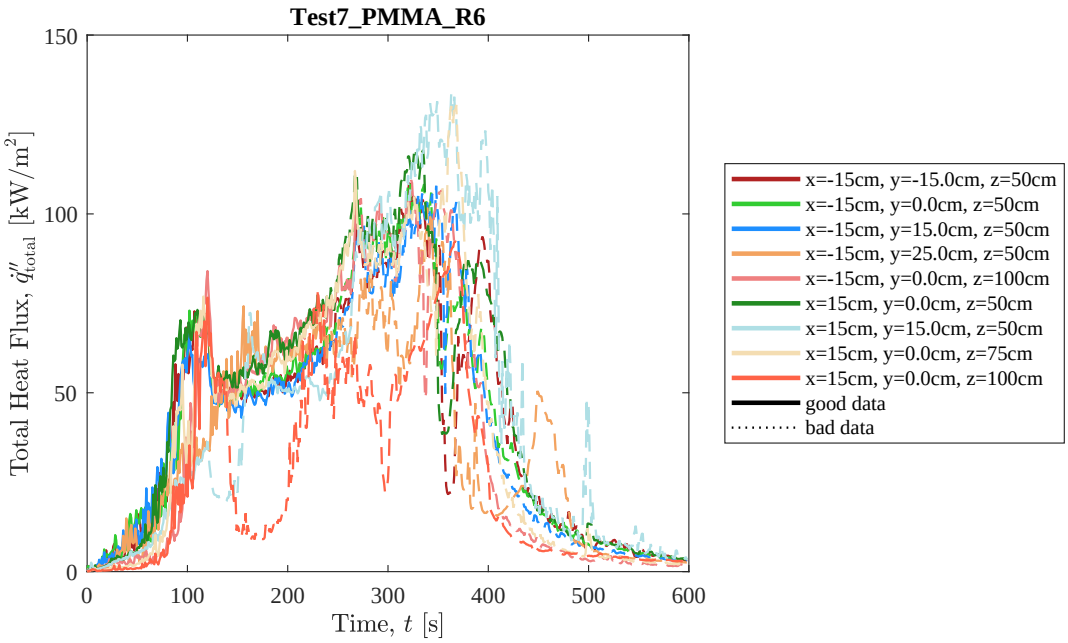

Fig. 172. Total flame to surface flame heat flux to water-cooled Schmidt-Boelter heat flux gauges as measured in Test 7 PMMA R6. Here, raw, unsmoothed original measurments are plotted from each gauges as a function of time. Solid lines highlight values of $\dot{q}''_{\text{total}}$ that were identified by manual review as ”good” (see Sec. 3.1.1) and dotted lines represent ”bad” measurement data that should not be considered for further analysis.

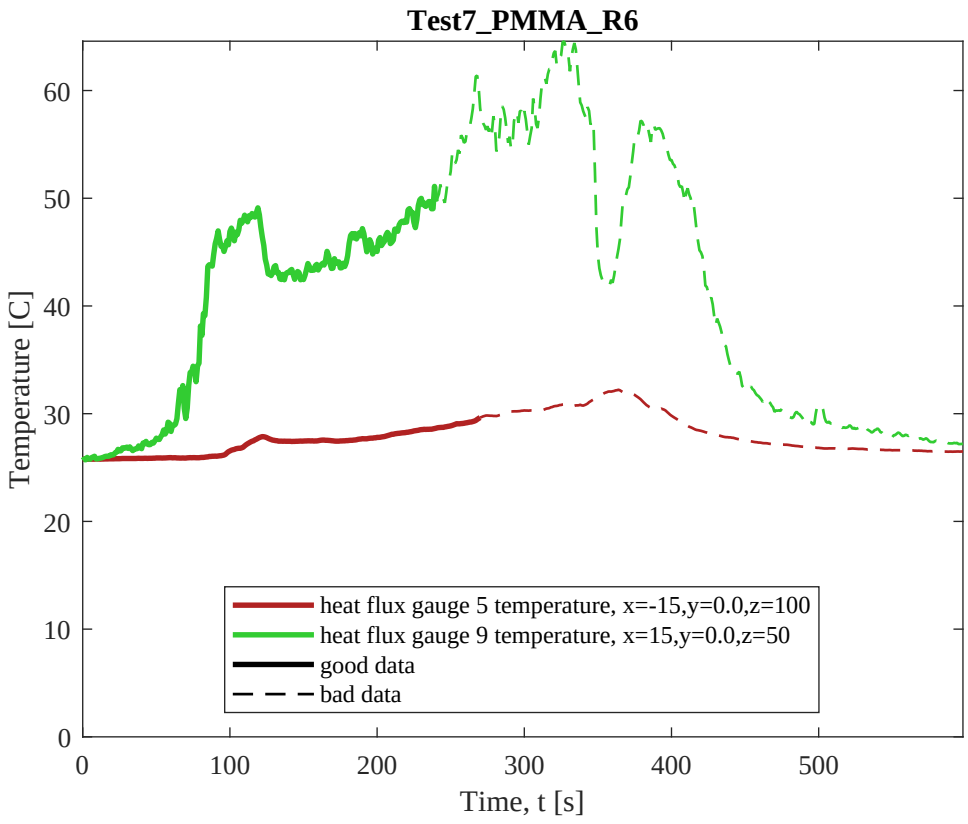

Fig. 173. Temperature of water-cooled Schmidt-Boelter heat flux gauges during Test 7 PMMA R6.

C.8. PMMA-PVC alloy (Kydex)

Test 29 PMMA-PVC R1

Test Description
1/4 in. thick, 24 in. wide, 96 in. tall panels of Kydex mounted to 1 in. thick Marinite board. Panels were ignited using a rectangular propane burner (60 kW nominal heat release rate) filled with layers of Pea Gravel, Sand, and Kaowool Insulation (i.e., the 'Final Burner configuration'; see Fig. 12). The propane burner was continuously supplied with propane until $t = 600$ s. Flaming conditions appeared relatively uniform (from left to right panel wall) though substantial soot production was observed, HRR remained relatively low later in the test while the burner remained on, and the panel walls quickly self-extinguished after the burner was turned off. Following burner extinction, sample remnants that had fallen to the top of the burner continued to burn for approximately 25 minutes. Flame to wall heat flux measurements were not recorded in this test.

(a) Pre-test

(b) Ignition

(c) Peak HRR

(d) End of Test

Fig. 174. Photographs of Test 29 PMMA-PVC R1.

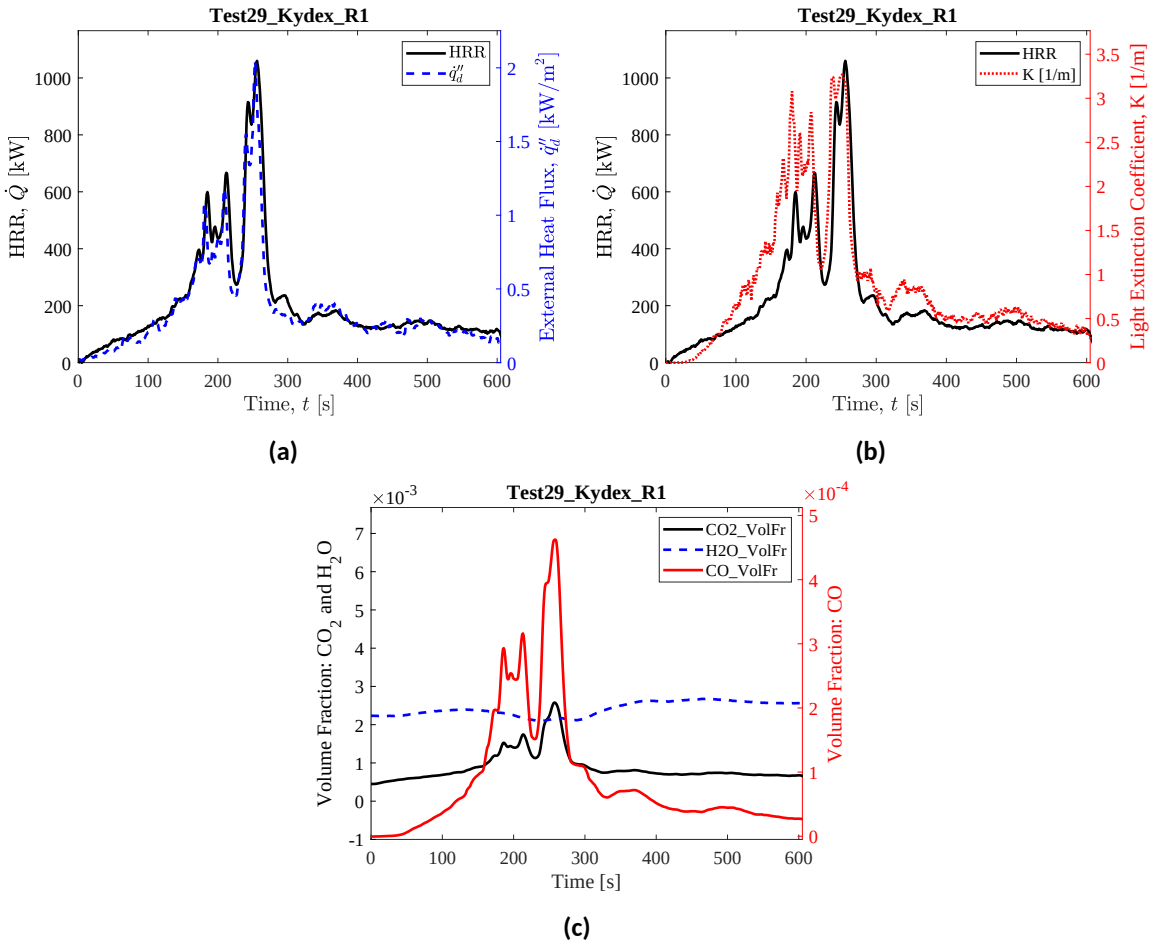

Fig. 175. Test 29 PMMA-PVC R1: (a) Heat release rate and heat flux at a distance, $\dot{q}''_{\mathrm{d}}$ (here, $\dot{q}''_{\mathrm{d}}$ is measured at x =-232 cm, y =-300 cm, z =90 cm); (b) Heat release rate and light extinction coefficient, K (smoke particulate in exhaust duct [111]); (c) Time-resolved volume fractions of CO_2, H_2O, and CO.

Test 30 PMMA-PVC R2

Test Description

1/4 in. thick, 24 in. wide, 96 in. tall panels of Kydex mounted to 1 in. thick Marinite board. Panels were ignited using a rectangular propane burner (60 kW nominal heat release rate) filled with layers of Pea Gravel, Sand, and Kaowool Insulation (i.e., the 'Final Burner configuration'; see Fig. 12). The propane burner was continuously supplied with propane until $t = 600$ s. Flaming conditions appeared relatively uniform (from left to right panel wall) though substantial soot production was observed, HRR remained relatively low later in the test while the burner remained on, and the panel walls quickly self-extinguished after the burner was turned off. Following burner extinction, sample remnants that had fallen to the top of the burner continued to burn for approximately 25 minutes. Flame to wall heat flux measurements were not recorded in this test.

(a) Pre-test

(b) Ignition

(c) Peak HRR

(d) End of Test

Fig. 176. Photographs of Test 30 PMMA-PVC R2.

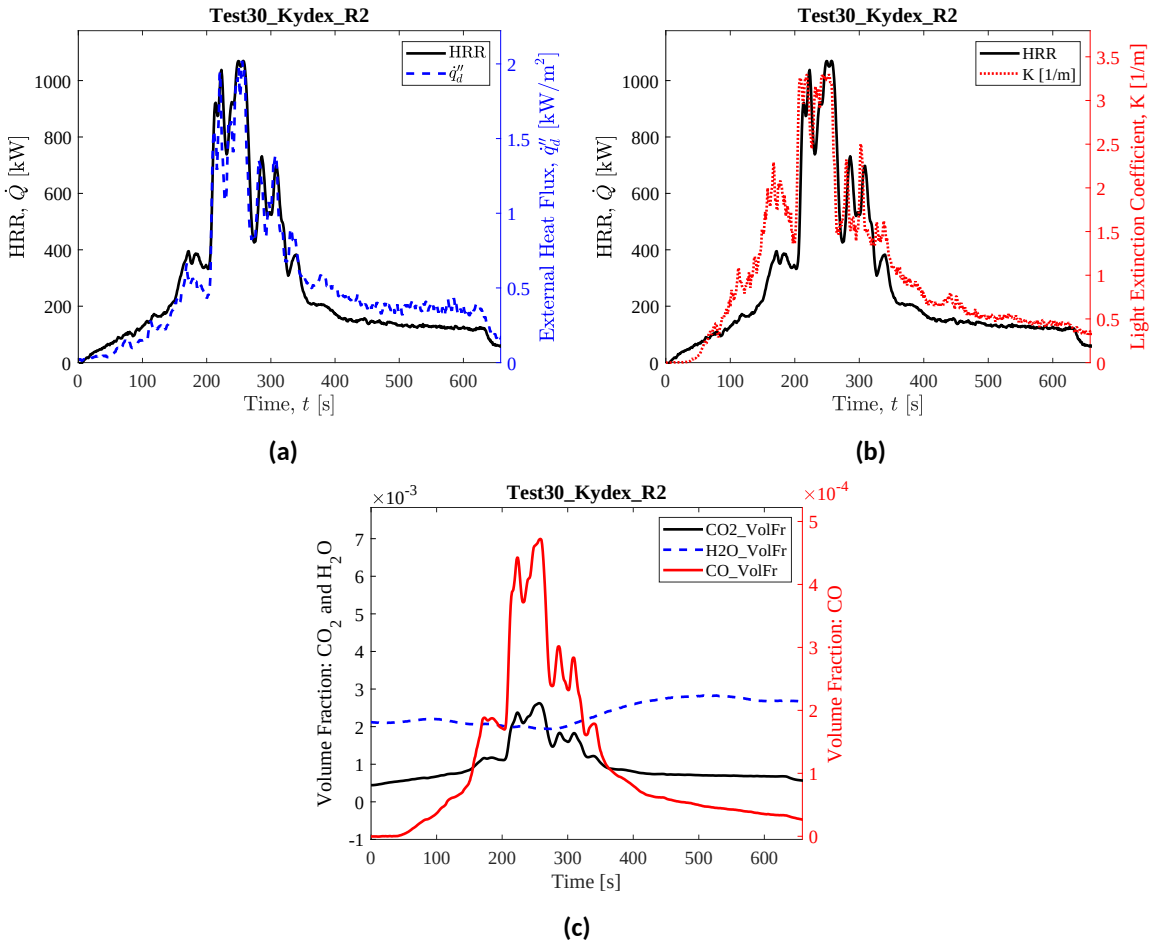

Fig. 177. Test 30 PMMA-PVC R2: (a) Heat release rate and heat flux at a distance, $\dot{q}''_{\mathrm{d}}$ (here, $\dot{q}''_{\mathrm{d}}$ is measured at x =-232 cm, y =-300 cm, z =90 cm); (b) Heat release rate and light extinction coefficient, K (smoke particulate in exhaust duct [111]); (c) Time-resolved volume fractions of CO_2, H_2O, and CO.

C.9. Polyiso - Polyisocyanurate Foam

Test 31 Polyiso05 R1

Test Description
1/2 in. thick, 24 in. wide, 96 in. tall panels of Polyisocyanurate Foam held by wire to 1 in. thick Marinite board. Panels were ignited using a rectangular propane burner (60 kW nominal heat release rate) filled with layers of Pea Gravel, Sand, and Kaowool Insulation (i.e., the 'Final Burner configuration'; see Fig. 12). Wall flames ignited uniformly (across the base of both panel walls) within seconds of burner ignition and the burner was left on throughout the duration of the test (throughout flame spread, peak HRR, and decay). The burner was shut off ($t = 61$ s) and wall flames extinguished within approximately 40 s. Approximately 17 % of the sample mass remained at the end of this test (light, flaky char that had mostly detached from the panel walls). Flame to wall heat flux measurements were not recorded in this test.

(a) Pre-test

(b) Ignition

(c) Peak HRR

(d) End of Test

Fig. 178. Photographs of Test 31 Polyiso05 R1.

Heat Release Rate, Heat Flux at a Distance, and Species Yields

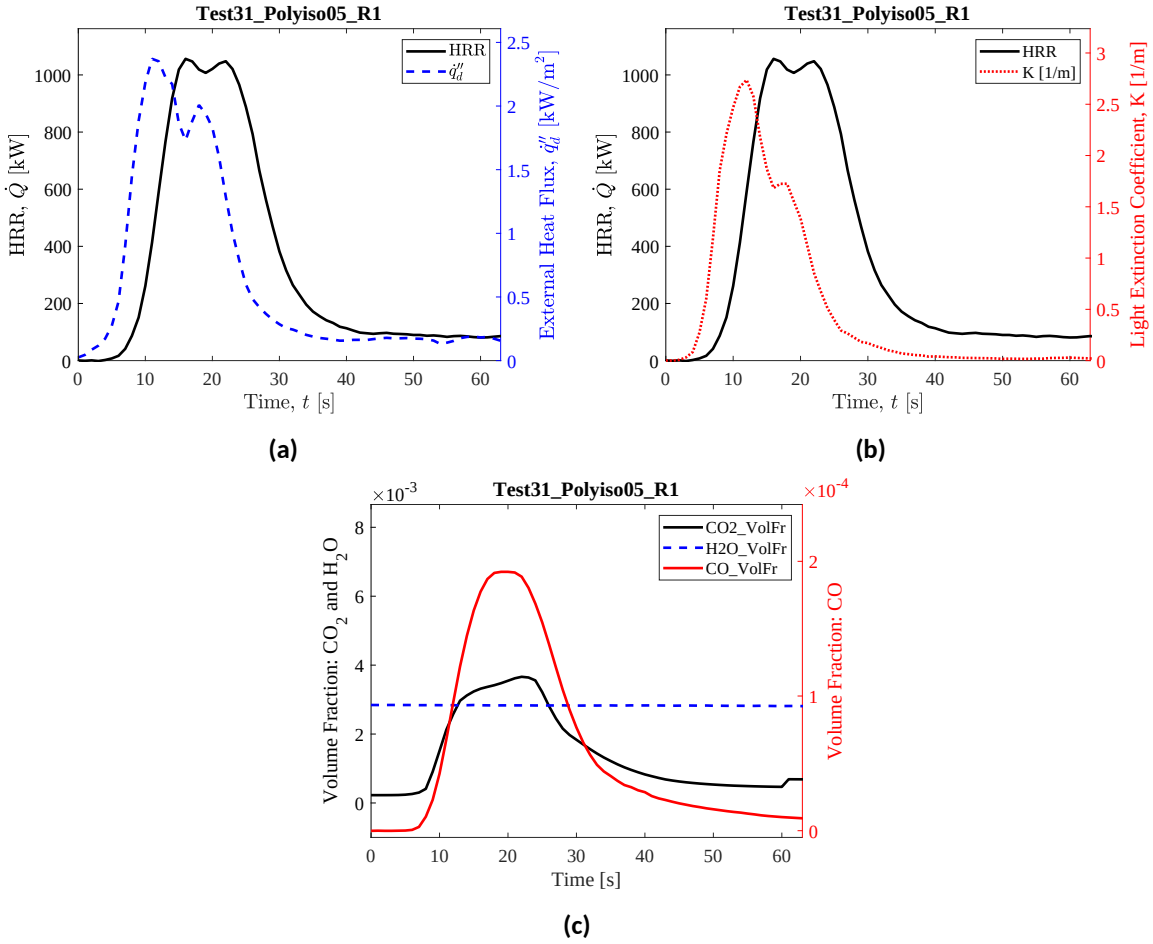

Fig. 179. Test 31 Polyiso05 R1: (a) Heat release rate and heat flux at a distance, $\dot{q}''_{\mathrm{d}}$ (here, $\dot{q}''_{\mathrm{d}}$ is measured at x =-232 cm, y =-300 cm, z =90 cm); (b) Heat release rate and light extinction coefficient, K (smoke particulate in exhaust duct [111]); (c) Time-resolved volume fractions of CO_2, H_2O, and CO.

Test 32 Polyiso05 R2

Test Description

1/2 in. thick, 24 in. wide, 96 in. tall panels of Polyisocyanurate Foam held by wire to 1 in. thick Marinite board. Panels were ignited using a rectangular propane burner (60 kW nominal heat release rate) filled with layers of Pea Gravel, Sand, and Kaowool Insulation (i.e., the 'Final Burner configuration'; see Fig. 12). Wall flames ignited uniformly (across the base of both panel walls) within seconds of burner ignition and the burner was left on throughout the duration of the test (throughout flame spread, peak HRR, and decay). The burner was shut off ($t = 61$ s) and wall flames extinguished within approximately 30 s. Approximately 21 % of the sample mass remained at the end of this test (light, flaky char that had mostly detached from the panel walls). Flame to wall heat flux measurements were not recorded in this test.

(a) Pre-test

(b) Ignition

(c) Peak HRR

(d) End of Test

Fig. 180. Photographs of Test 32 Polyiso05 R2.

Heat Release Rate, Heat Flux at a Distance, and Species Yields

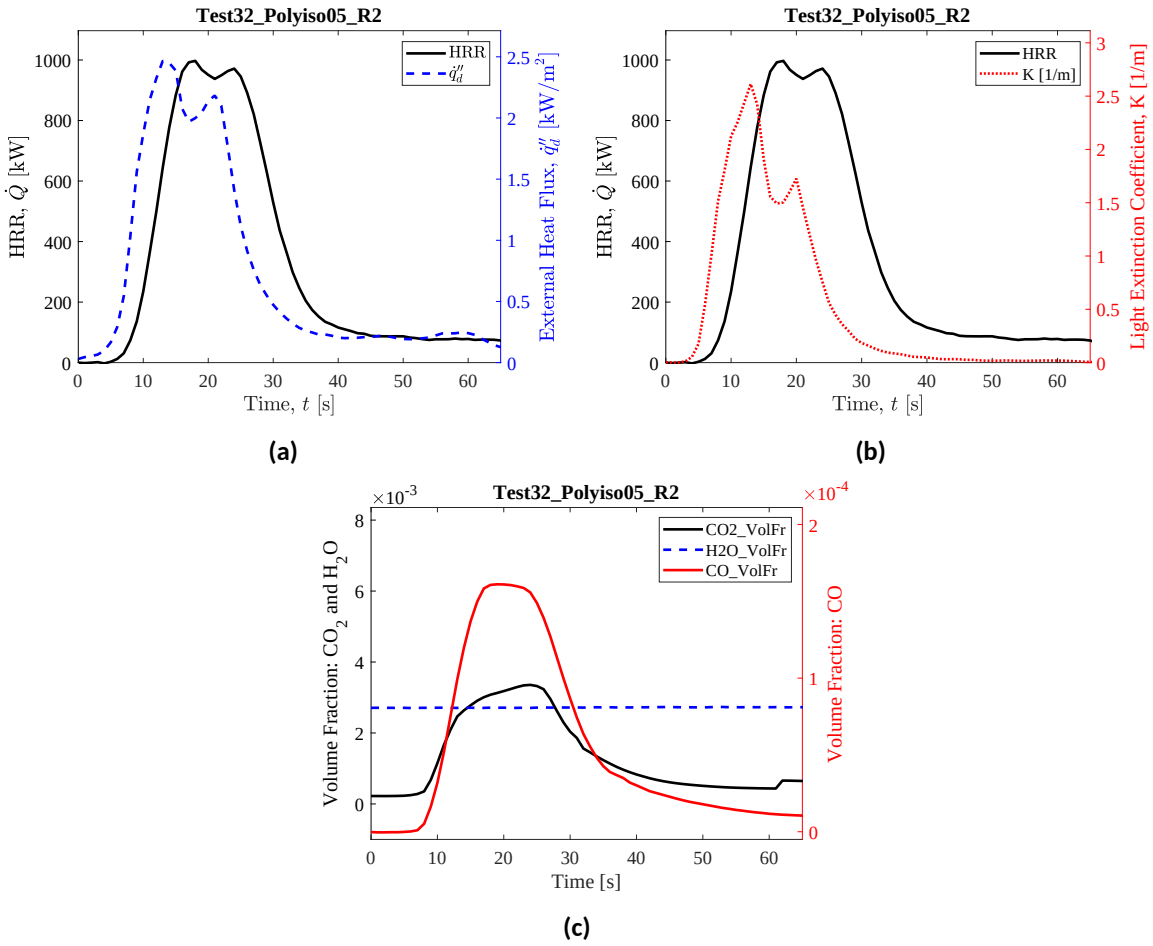

Fig. 181. Test 32 Polyiso05 R2: (a) Heat release rate and heat flux at a distance, $\dot{q}''_{\mathrm{d}}$ (here, $\dot{q}''_{\mathrm{d}}$ is measured at x =-232 cm, y =-300 cm, z =90 cm); (b) Heat release rate and light extinction coefficient, K (smoke particulate in exhaust duct [111]); (c) Time-resolved volume fractions of CO_2, H_2O, and CO.

Test 44 Polyiso05 R3

Test Description

1/2 in. thick, 24 in. wide, 96 in. tall panels of Polyisocyanurate Foam held by wire to 1 in. thick Marinite board. Panels were ignited using a rectangular propane burner (60 kW nominal heat release rate) filled with layers of Pea Gravel, Sand, and Kaowool Insulation (i.e., the 'Final Burner configuration'; see Fig. 12). Wall flames ignited uniformly (across the base of both panel walls) within seconds of burner ignition and the burner was left on throughout the duration of the test (throughout flame spread, peak HRR, and decay). The burner was shut off ($t = 61$ s) and wall flames extinguished within approximately 40 s. Approximately 12 % of the sample mass remained at the end of this test (light, flaky char that had mostly detached from the panel walls). Flame to wall heat flux measurements were not recorded in this test.

(a) Pre-test

(b) Ignition

(c) Peak HRR

(d) End of Test

Fig. 182. Photographs of Test 44 Polyiso05 R3.

Heat Release Rate, Heat Flux at a Distance, and Species Yields

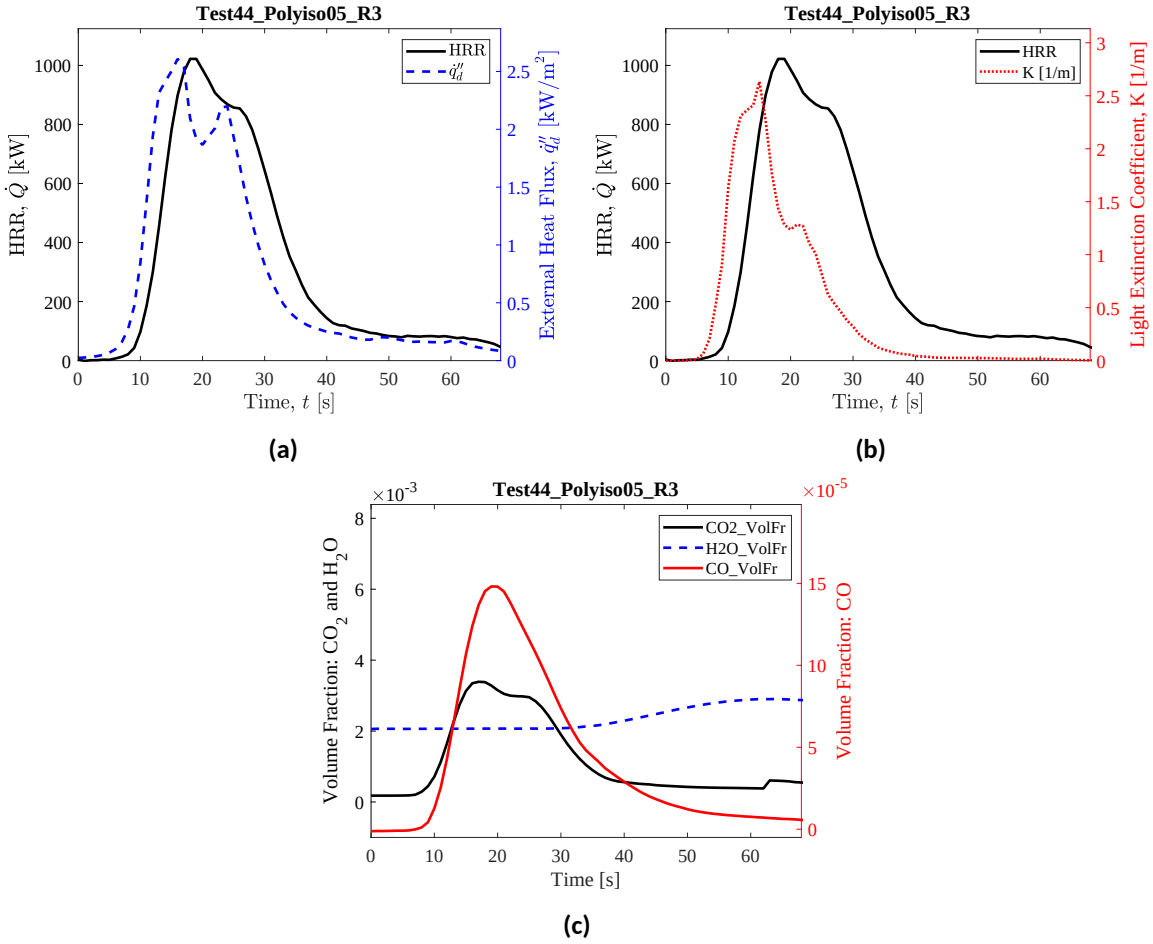

Fig. 183. Test 44 Polyiso05 R3: (a) Heat release rate and heat flux at a distance, $\dot{q}''_{\mathrm{d}}$ (here, $\dot{q}''_{\mathrm{d}}$ is measured at x =-232 cm, y =-300 cm, z =90 cm); (b) Heat release rate and light extinction coefficient, K (smoke particulate in exhaust duct [111]); (c) Time-resolved volume fractions of CO_2, H_2O, and CO.

Test 21 Polyiso1 R3

Test Description

1 in. thick, 24 in. wide, 96 in. tall panels of Polyisocyanurate Foam held by wire to 1 in. thick Marinite board. Panels were ignited using a rectangular propane burner (60 kW nominal heat release rate) filled with layers of Pea Gravel, Sand, and Kaowool Insulation (i.e., the 'Final Burner configuration'; see Fig. 12). Wall flames ignited uniformly (across the base of both panel walls) within seconds of burner ignition and the burner was left on throughout the duration of the test (throughout flame spread, peak HRR, and decay). The burner was shut off ($t = 393$ s) and wall flames extinguished within approximately 40 s. Approximately 36 % of the sample mass remained at the end of this test (a mostly continuous char layer that remained attached to the panel walls, though cracked in some places and detached from the panel assembly closer to the burner). Flame to wall heat flux measurements were not recorded in this test.

(a) Pre-test

(b) Ignition

(c) Peak HRR

(d) End of Test

Fig. 184. Photographs of Test 21 Polyiso1 R3.

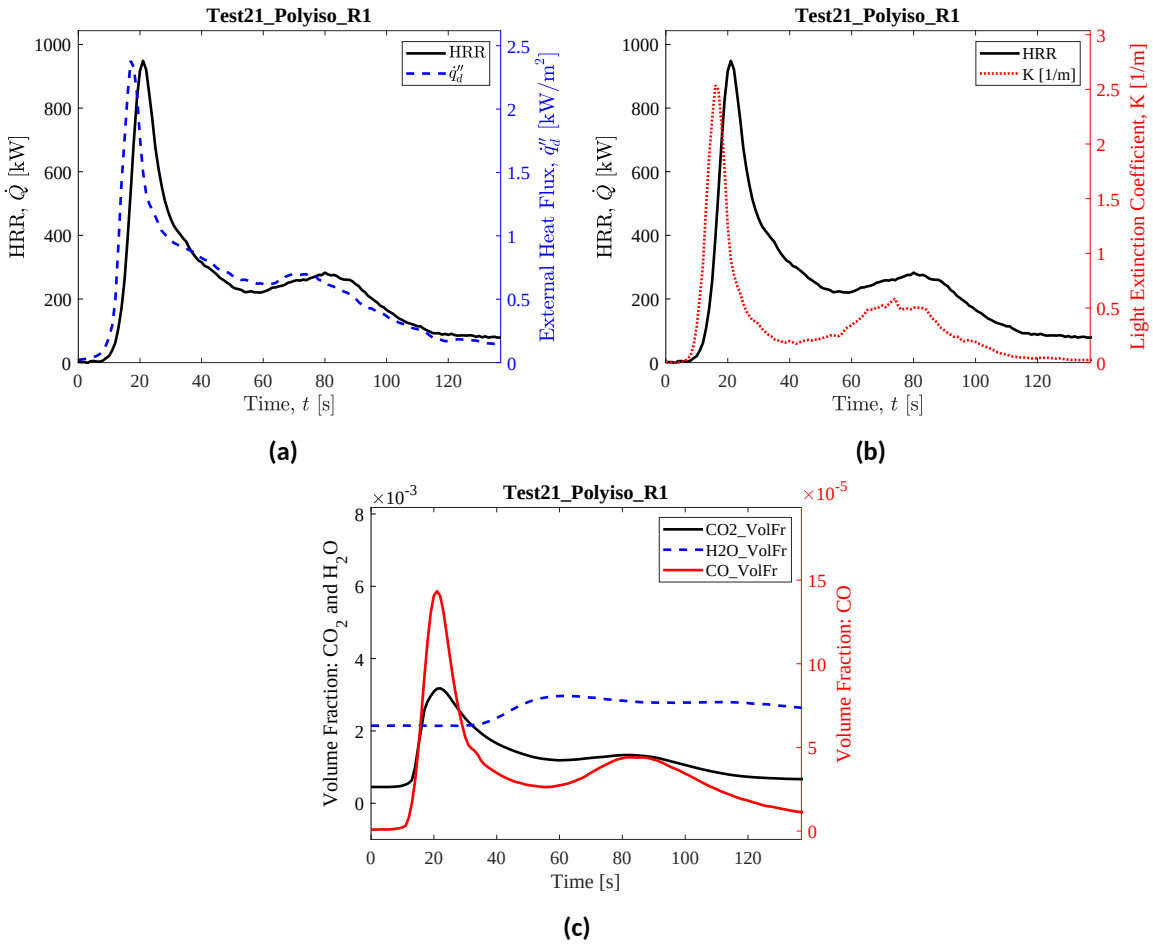

Fig. 185. Test 21 Polyiso1 R3: (a) Heat release rate and heat flux at a distance, $\dot{q}''_{\mathrm{d}}$ (here, $\dot{q}''_{\mathrm{d}}$ is measured at x =-150 cm, y =-300 cm, z =90 cm); (b) Heat release rate and light extinction coefficient, K (smoke particulate in exhaust duct [111]); (c) Time-resolved volume fractions of CO_2, H_2O, and CO.

Test 24 Polyiso1 R2

Test Description

1 in. thick, 24 in. wide, 96 in. tall panels of Polyisocyanurate Foam held by wire to 1 in. thick Marinite board. Panels were ignited using a rectangular propane burner (60 kW nominal heat release rate) filled with layers of Pea Gravel, Sand, and Kaowool Insulation (i.e., the 'Final Burner configuration'; see Fig. 12). Wall flames ignited uniformly (across the base of both panel walls) within seconds of burner ignition and the burner was left on throughout the duration of the test (throughout flame spread, peak HRR, and decay). The burner was shut off ($t = 224$ s) and wall flames extinguished within approximately 80 s. Approximately 14 % of the sample mass remained at the end of this test (a mostly continuous char layer that remained attached to the panel walls, though cracked in some places and detached from the panel assembly closer to the burner). Flame to wall heat flux measurements were not recorded in this test.

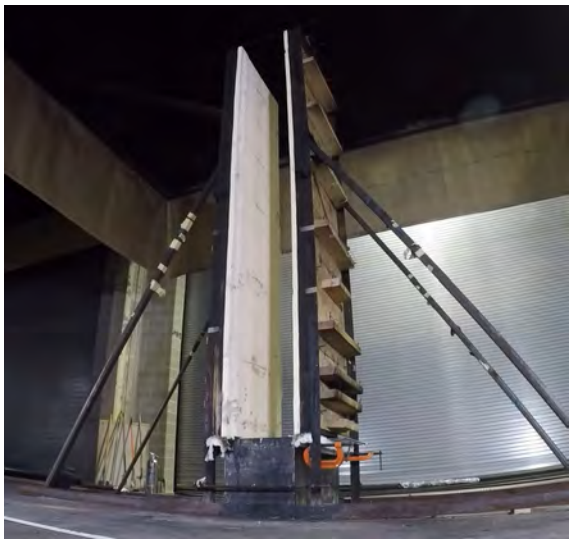

(a) Pre-test

(b) Ignition

(c) Peak HRR

(d) End of Test

Fig. 186. Photographs of Test 24 Polyiso1 R2.

Heat Release Rate, Heat Flux at a Distance, and Species Yields

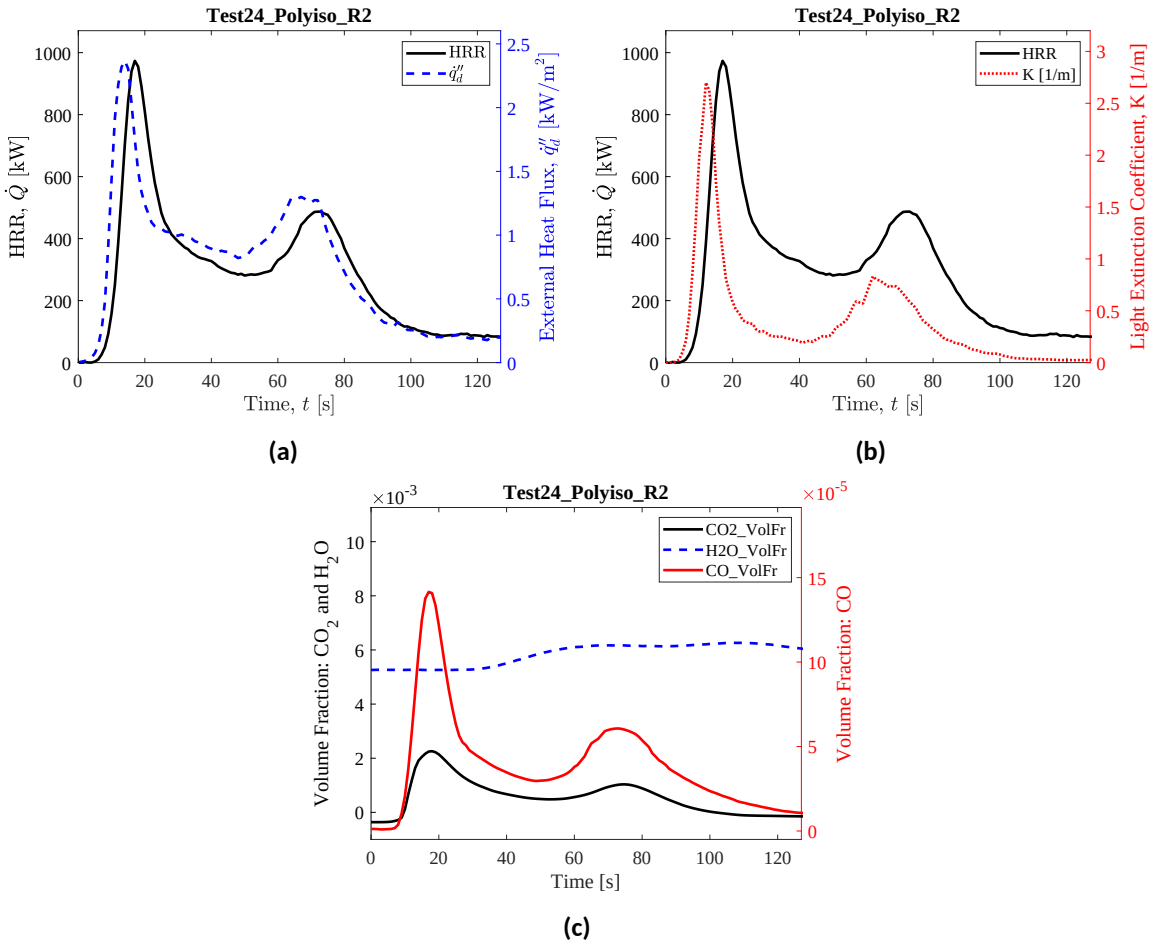

Fig. 187. Test 24 Polyiso1 R2: (a) Heat release rate and heat flux at a distance, $\dot{q}''_{\mathrm{d}}$ (here, $\dot{q}''_{\mathrm{d}}$ is measured at x =-150 cm, y =-300 cm, z =90 cm); (b) Heat release rate and light extinction coefficient, K (smoke particulate in exhaust duct [111]); (c) Time-resolved volume fractions of CO_2, H_2O, and CO.

Test 25 Polyiso1 R3

Test Description

1 in. thick, 24 in. wide, 96 in. tall panels of Polyisocyanurate Foam held by wire to 1 in. thick Marinite board. Panels were ignited using a rectangular propane burner (60 kW nominal heat release rate) filled with layers of Pea Gravel, Sand, and Kaowool Insulation (i.e., the 'Final Burner configuration'; see Fig. 12). Wall flames ignited uniformly (across the base of both panel walls) within seconds of burner ignition and the burner was left on throughout the duration of the test (throughout flame spread, peak HRR, and decay). The burner was shut off ($t = 221$ s) and wall flames extinguished within approximately 80 s. Approximately 31 % of the sample mass remained at the end of this test (a mostly continuous char layer that remained attached to the panel walls, though cracked in some places and detached from the panel assembly closer to the burner). Flame to wall heat flux measurements were not recorded in this test.

(a) Pre-test

(b) Ignition

(c) Peak HRR

(d) End of Test

Fig. 188. Photographs of Test 25 Polyiso1 R3.

Heat Release Rate, Heat Flux at a Distance, and Species Yields

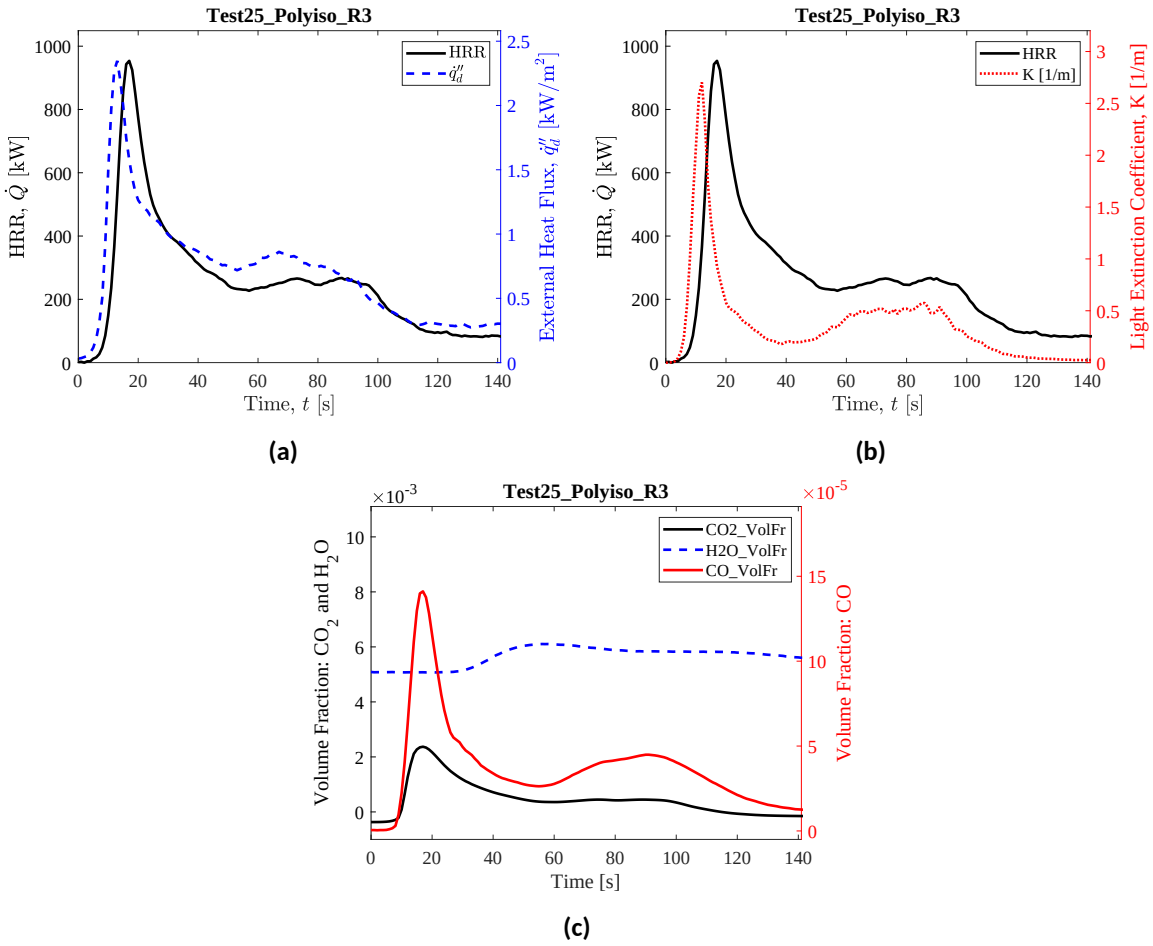

Fig. 189. Test 25 Polyiso1 R3: (a) Heat release rate and heat flux at a distance, $\dot{q}''_{\mathrm{d}}$ (here, $\dot{q}''_{\mathrm{d}}$ is measured at x =-150 cm, y =-300 cm, z =90 cm); (b) Heat release rate and light extinction coefficient, K (smoke particulate in exhaust duct [111]); (c) Time-resolved volume fractions of CO_2, H_2O, and CO.

Test 26 Polyiso2 R1

Test Description

2 in. thick, 24 in. wide, 96 in. tall panels of Polyisocyanurate Foam held by wire to 1 in. thick Marinite board. Panels were ignited using a rectangular propane burner (60 kW nominal heat release rate) filled with layers of Pea Gravel, Sand, and Kaowool Insulation (i.e., the 'Final Burner configuration'; see Fig. 12). Wall flames ignited uniformly (across the base of both panel walls) within seconds of burner ignition and the burner was left on throughout the duration of the test (throughout flame spread, peak HRR, and decay). The burner was shut off ($t = 485$ s) and wall flames extinguished within approximately 80 s. Approximately 58 % of the sample mass remained at the end of this test (above $z = 1.0$ m, a layer of black char covered unburnt polyiso foam that remained attached to the panel walls; closer to the burner, the material had burned through, leaving only lightweight char remnants that had detached from the panel walls). Flame to wall heat flux measurements were not recorded in this test.

(a) Pre-test

(b) Ignition

(c) Peak HRR

(d) End of Test

Fig. 190. Photographs of Test 26 Polyiso2 R1.

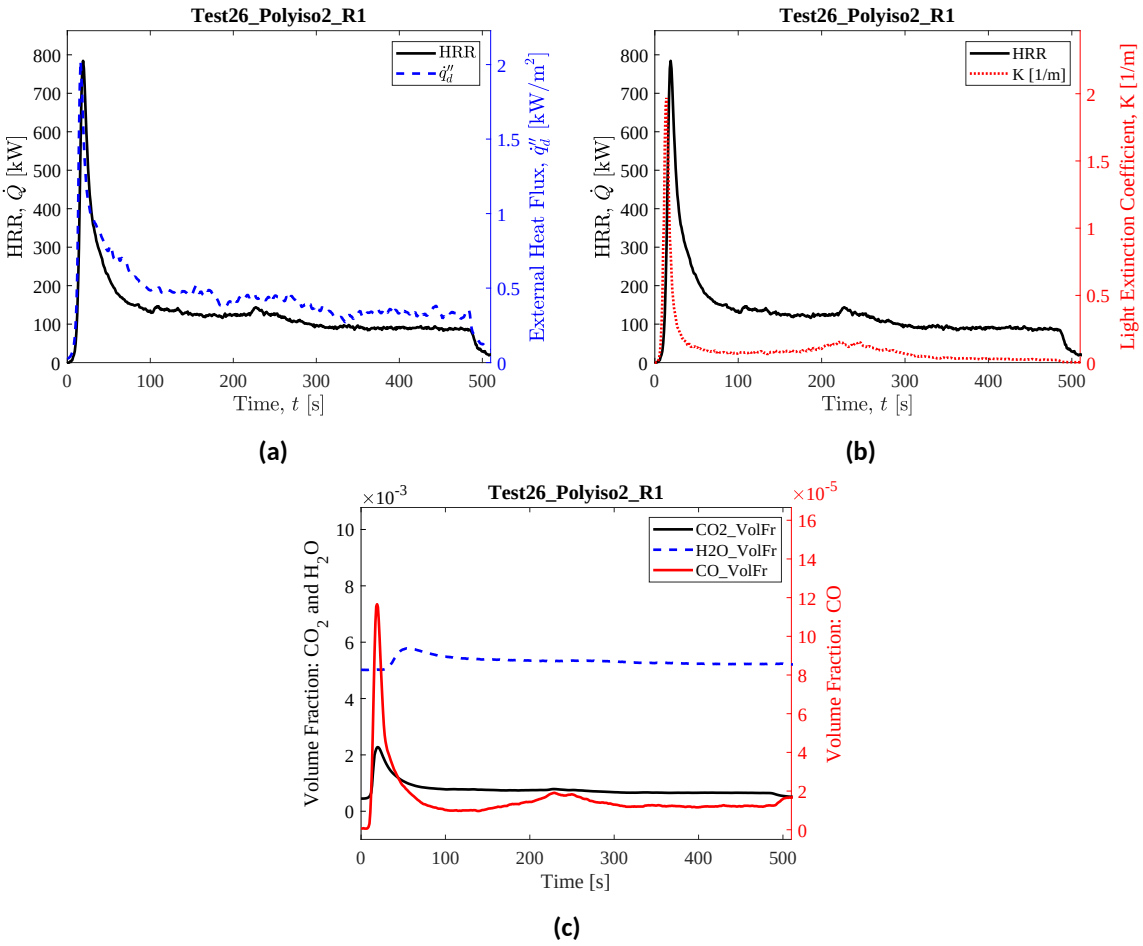

Fig. 191. Test 26 Polyiso2 R1: (a) Heat release rate and heat flux at a distance, $\dot{q}''_{\mathrm{d}}$ (here, $\dot{q}''_{\mathrm{d}}$ is measured at x =-150 cm, y =-300 cm, z =90 cm); (b) Heat release rate and light extinction coefficient, K (smoke particulate in exhaust duct [111]); (c) Time-resolved volume fractions of CO_2, H_2O, and CO.

Test 27 Polyiso2 R2

Test Description

2 in. thick, 24 in. wide, 96 in. tall panels of Polyisocyanurate Foam held by wire to 1 in. thick Marinite board. Panels were ignited using a rectangular propane burner (60 kW nominal heat release rate) filled with layers of Pea Gravel, Sand, and Kaowool Insulation (i.e., the 'Final Burner configuration'; see Fig. 12). Wall flames ignited uniformly (across the base of both panel walls) within seconds of burner ignition and the burner was left on throughout the duration of the test (throughout flame spread, peak HRR, and decay). The burner was shut off ($t = 486$ s) and wall flames extinguished within approximately 60 s. Approximately 56 % of the sample mass remained at the end of this test (above $z = 1.0$ m, a layer of black char covered unburnt polyiso foam that remained attached to the panel walls; closer to the burner, the material had burned through, leaving only lightweight char remnants that had detached from the panel walls). Flame to wall heat flux measurements were not recorded in this test.

(a) Pre-test

(b) Ignition

(c) Peak HRR

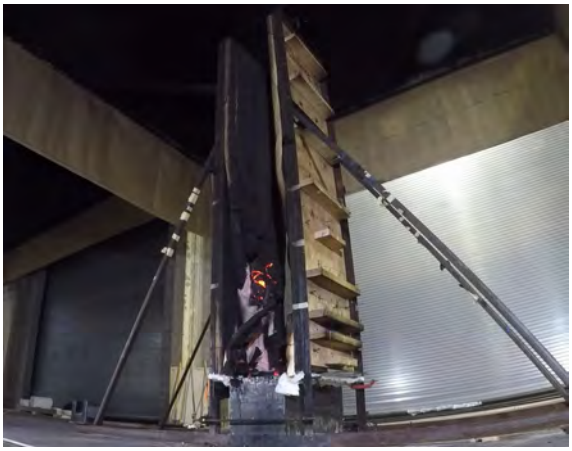

(d) End of Test

Fig. 192. Photographs of Test 27 Polyiso2 R2.

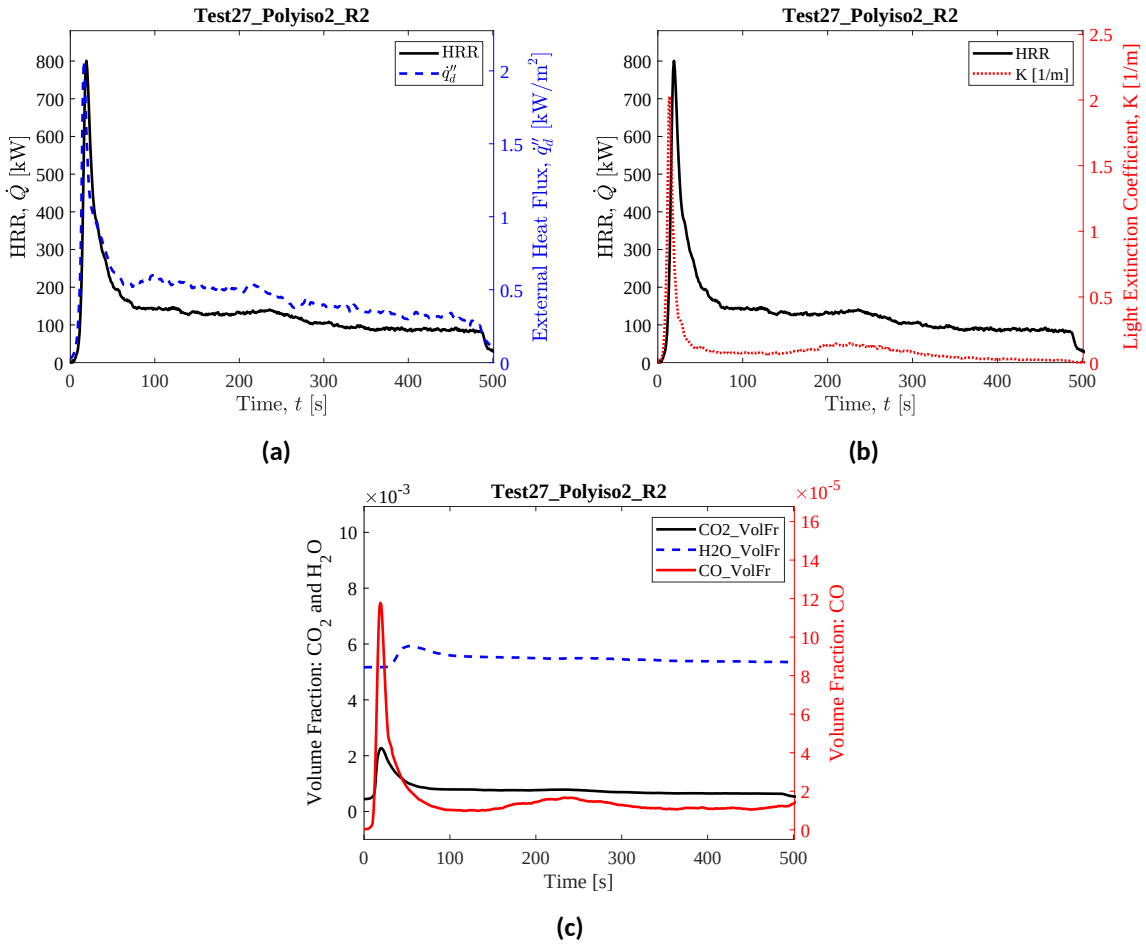

Fig. 193. Test 27 Polyiso2 R2: (a) Heat release rate and heat flux at a distance, $\dot{q}''_{\mathrm{d}}$ (here, $\dot{q}''_{\mathrm{d}}$ is measured at x =-150 cm, y =-300 cm, z =90 cm); (b) Heat release rate and light extinction coefficient, K (smoke particulate in exhaust duct [111]); (c) Time-resolved volume fractions of CO_2, H_2O, and CO.

C.10. POM-GF - Poly(Oxymethylene) reinforced with chopped Glass Fibers

Test 28 POMGF R1

Test Description

1/4 in. thick, 24 in. wide, 96 in. tall (in two sections, each 24 in.x48in.) panels of POM-GF mounted to 1 in. thick Marinite board. Panels were ignited using a rectangular propane burner (60 kW nominal heat release rate) filled with layers of Pea Gravel, Sand, and Kaowool Insulation (i.e., the 'Final Burner configuration'; see Fig. 12). The burner was shut off ($t = 181$ s) after sustained ignition along the base of both of panels. The front 10 cm (i.e., 20 cm $\leq y \leq 30$ cm) of both panel walls were not initially covered by the flame sheet due to burner non-uniformity. Lateral flame spread allowed for flame coverage across the width of panel walls by $t = 480$ s. The sample slabs would warp while heating (undulating profile from bottom to top of the assembly) but remain mostly attached to the panel walls until a sudden melt flow event. Sudden decreases in HRR measured at $t = 720$ s (partial collapse of lower slabs, $z < 1.2$ m) and then $t = 840$ s and $t = 900$ s (collapse of the upper right and then upper left slabs, $z > 1.2$ m) correspond to significant melt flow events. Heat flux gauges were mounted flush with the fuel's surface between $z = 20$ cm and $z = 50$ cm. Later in the test, melt flow limited availability of heat flux measurements at lower heights. Shielded radiometers and total heat flux gauges were positioned side by side at $z =$20 cm and $z = 50$ cm. An attempt was made to remove the heat flux shields at $t =$330 s; however, they had become embedded in polymer melt and could not be removed cleanly. As a result, 'clean gauge' measurements of radiation and total flame heat flux could only obtained, with additional post-processing, at $z = 50$ cm.

(a) Pre-test

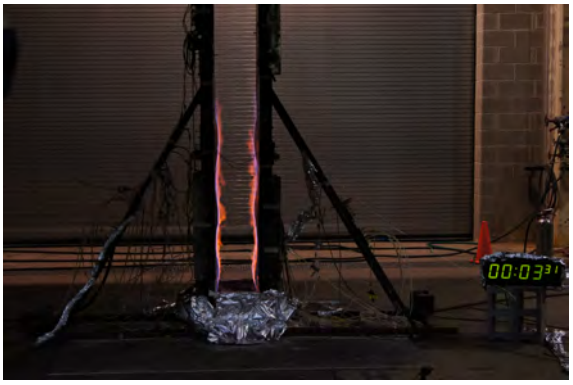

(b) Ignition

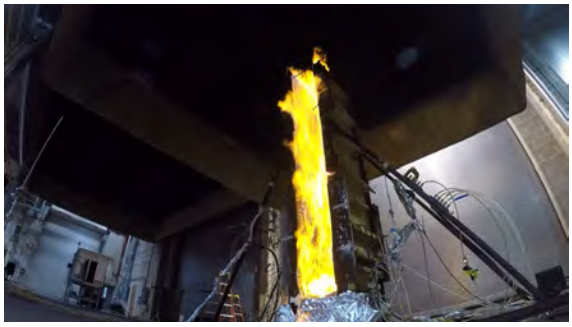

(c) Peak HRR

(d) End of Test

Fig. 194. Photographs of Test 28 POMGF R1.

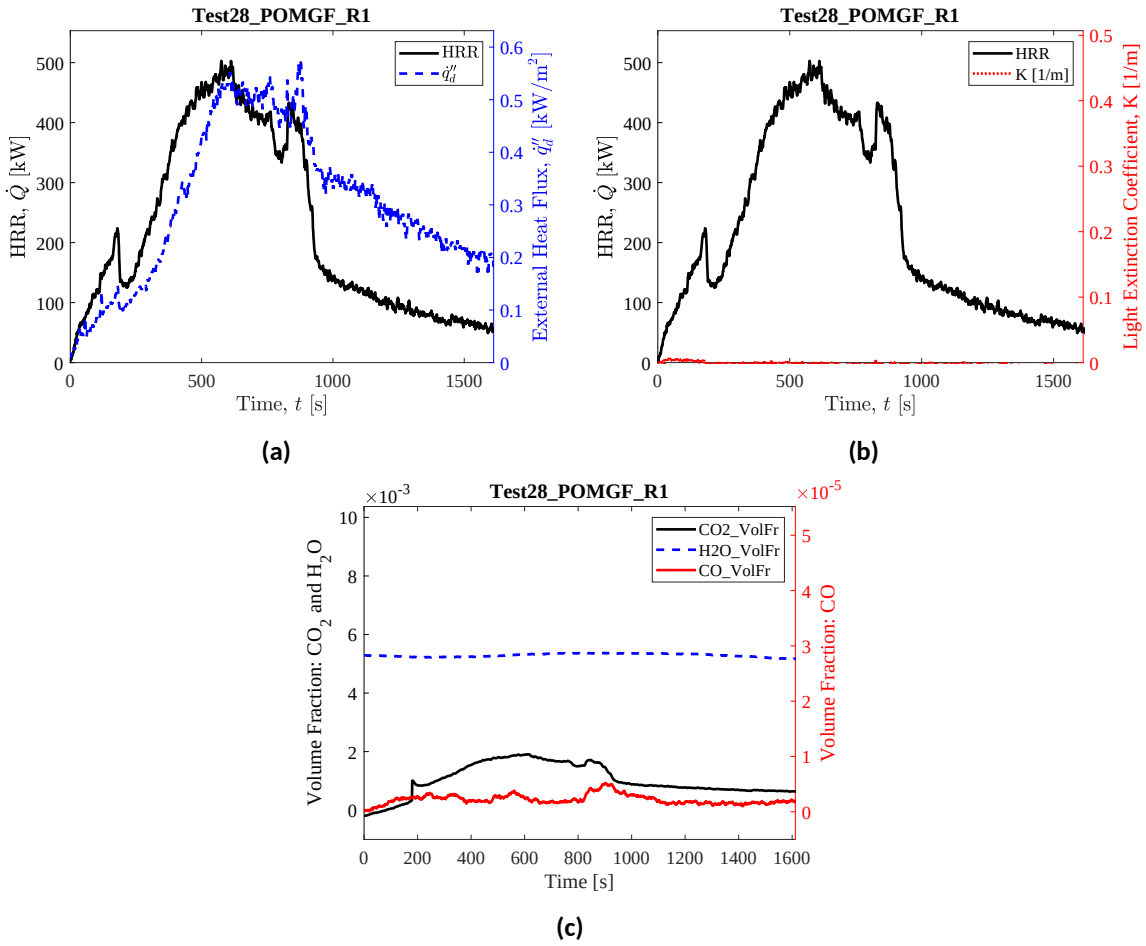

Fig. 195. Test 28 POMGF R1: (a) Heat release rate and heat flux at a distance, $\dot{q}''_{\mathrm{d}}$ (here, $\dot{q}''_{\mathrm{d}}$ is measured at x =-200 cm, y =-300 cm, z =90 cm); (b) Heat release rate and light extinction coefficient, K (smoke particulate in exhaust duct [111]); (c) Time-resolved volume fractions of CO_2, H_2O, and CO.

Flame Heat Flux

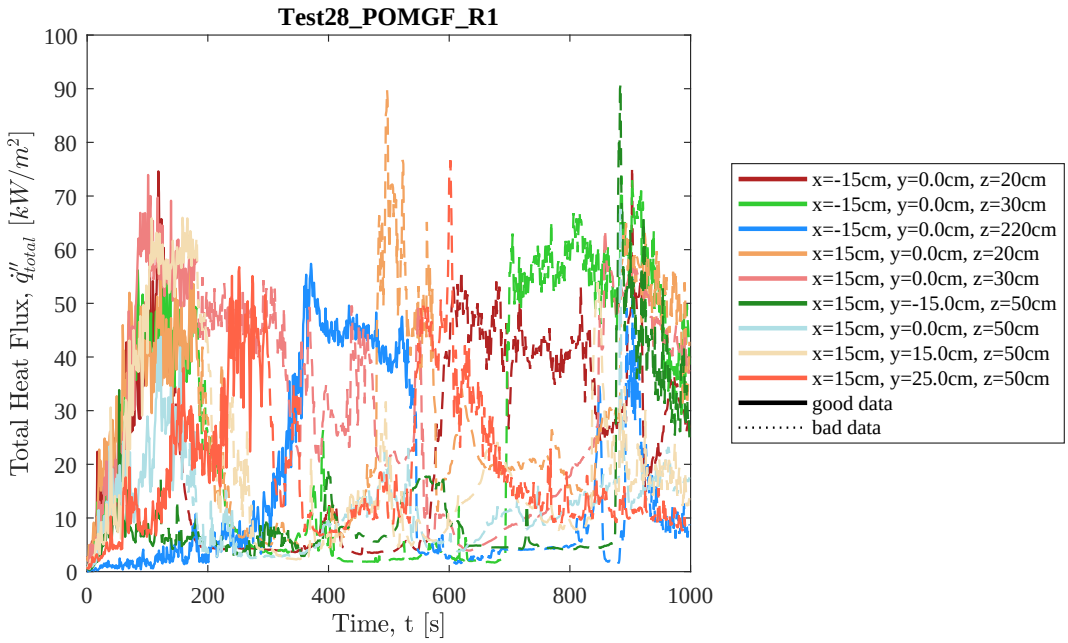

Fig. 196. Total flame to surface flame heat flux to water-cooled Schmidt-Boelter heat flux gauges as measured in Test 28 POMGF R1. Here, raw, unsmoothed original measurments are plotted from each gauges as a function of time. Solid lines highlight values of $\dot{q}''_{\text{total}}$ that were identified by manual review as ”good” (see Sec. 3.1.1) and dotted lines represent ”bad” measurement data that should not be considered for further analysis.

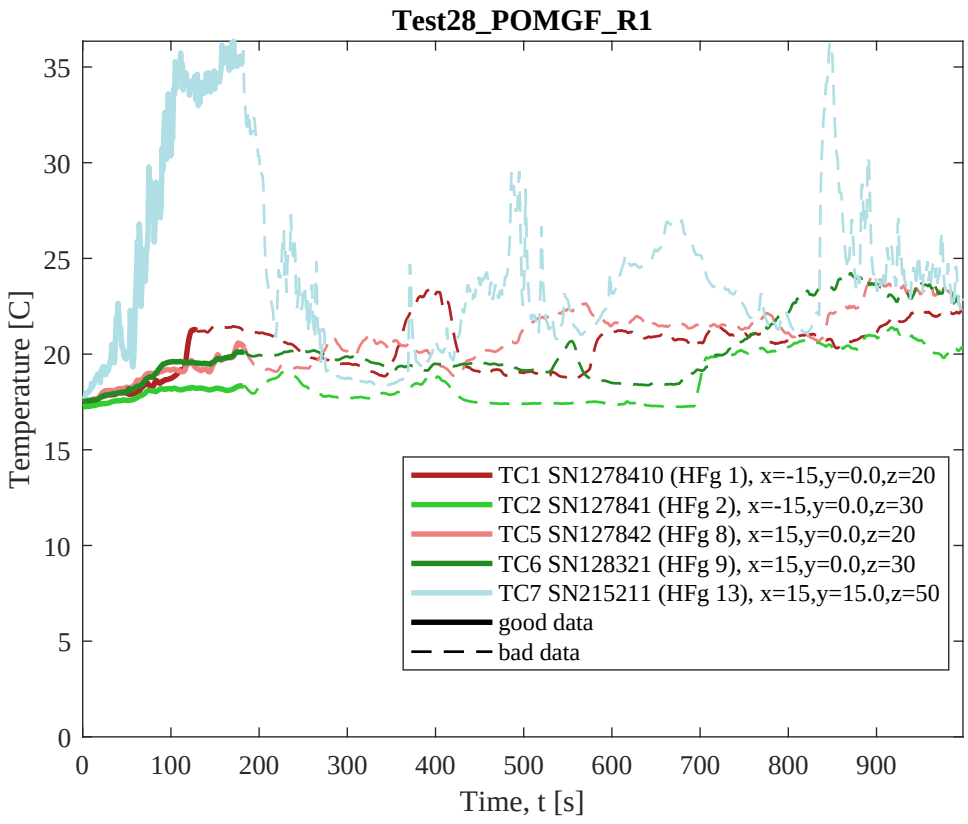

Fig. 197. Temperature of water-cooled Schmidt-Boelter heat flux gauges during Test 28 POMGF R1.

Shielded Gauges

Measurements of total and radiation heat flux recorded by shielded heat flux gauges (Sec. efssec: qrad). Gauge shields were removed at 379, and 368 seconds (gauges 5 and 6, respectively).

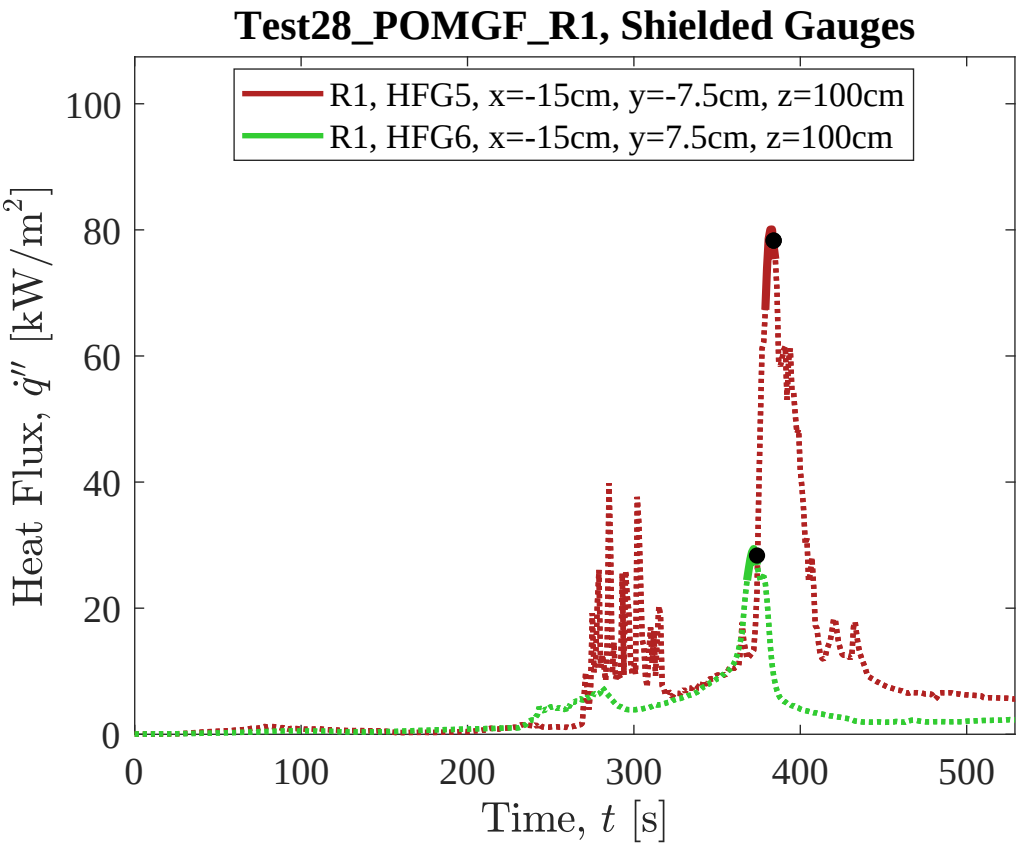

Fig. 198. Shielded gauge data for Test28 POMGF R1.

Test 50 POMGF R2

Test Description

1/4 in. thick, 24 in. wide, 96 in. tall (in two sections, each 24 in.x48in.) panels of POM-GF mounted to 1 in. thick Marinite board. Panels were ignited using a rectangular propane burner (60 kW nominal heat release rate) filled with layers of Pea Gravel, Sand, and Kaowool Insulation (i.e., the 'Final Burner configuration'; see Fig. 12). The burner was shut off ($t = 181$ s) and shielded ($t = 206$ s) after sustained ignition along the base of both of panels. The front 10 cm (i.e., 20 cm $\leq y \leq 30$ cm) of the right panel wall was not initially covered by the flame sheet due to burner non-uniformity; however, flames spread laterally to cover the base of this wall by $t = 260$ s. The sample slabs would warp while heating (undulating profile from bottom to top of the assembly) but remain mostly attached to the panel walls until a sudden melt flow event. A sudden spike and decrease in HRR measured at $t = 645$ s corresponds to partial collapse of lower left POMGF slab, $z < 1.2$ m. Further decreases in HRR measured at $t = 800$ s and $t = 910$ s correspond to collapse of the upper right and then upper left slabs, $z > 1.2$ m. Heat flux gauges were mounted flush with the fuel's surface between $z = 100$ cm and $z = 220$ cm (only these higher locations were selected to limit the impact of polymer melt flow on heat flux measurements). Shielded radiometers and total heat flux gauges were positioned side by side at $z =$180 cm and $z = 220$ cm. The lower heat flux shields were removed at $t =$356 s and the upper heat flux shields were removed at $t =$381 s; however, reliable measurements of both total and radiation flame heat flux were obtained only at $z = 220$ cm.

(a) Pre-test

(b) Ignition

(c) Peak HRR

(d) End of Test

Fig. 199. Photographs of Test 50 POMGF R2.

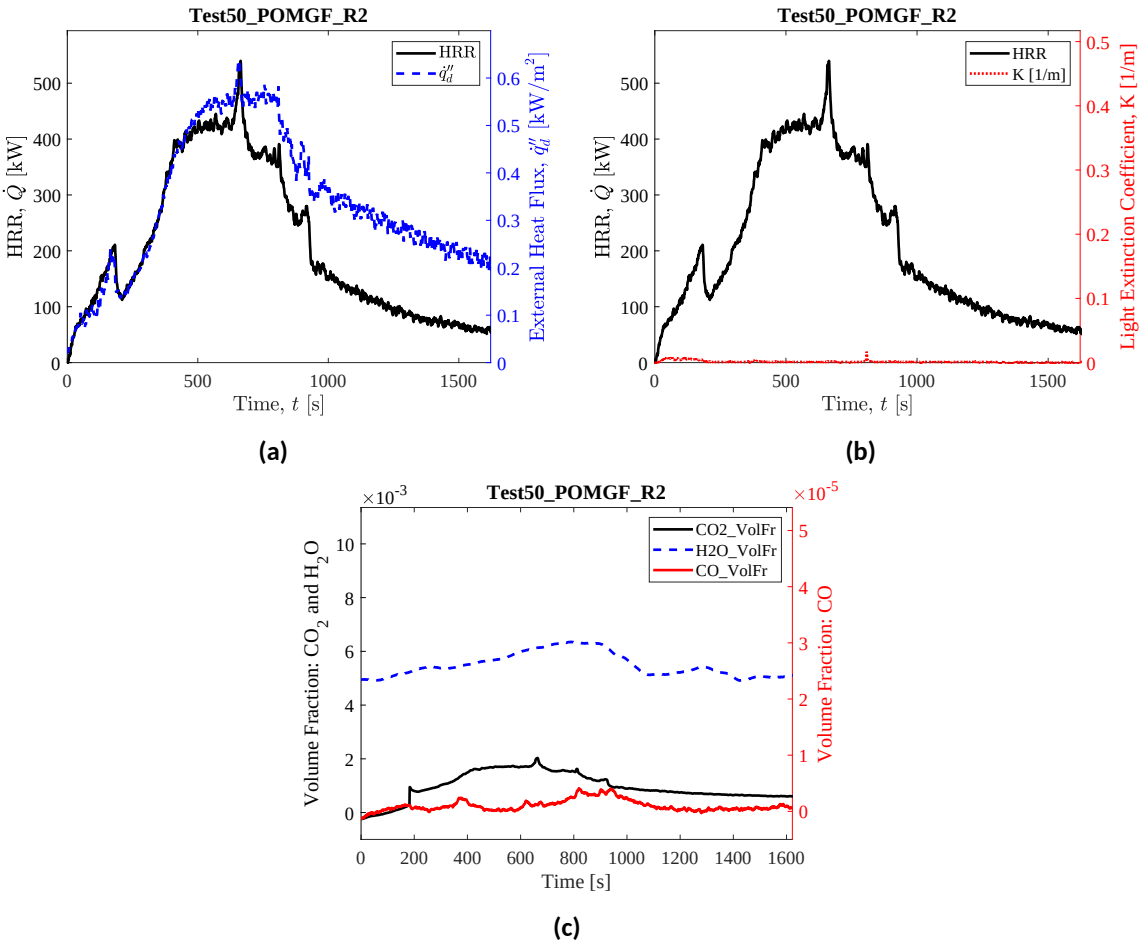

Fig. 200. Test 50 POMGF R2: (a) Heat release rate and heat flux at a distance, $\dot{q}''_{\mathrm{d}}$ (here, $\dot{q}''_{\mathrm{d}}$ is measured at x =-220 cm, y =-310 cm, z =90 cm); (b) Heat release rate and light extinction coefficient, K (smoke particulate in exhaust duct [111]); (c) Time-resolved volume fractions of CO_2, H_2O, and CO.

Flame Heat Flux

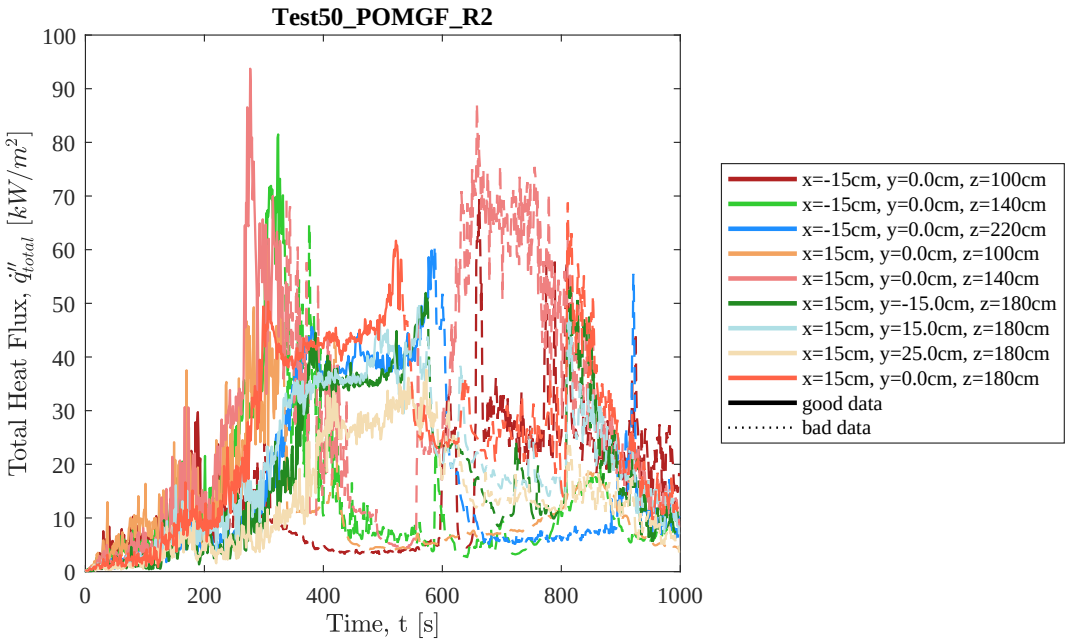

Fig. 201. Total flame to surface flame heat flux to water-cooled Schmidt-Boelter heat flux gauges as measured in Test 50 POMGF R2. Here, raw, unsmoothed original measurments are plotted from each gauges as a function of time. Solid lines highlight values of $\dot{q}''_{\text{total}}$ that were identified by manual review as ”good” (see Sec. 3.1.1) and dotted lines represent ”bad” measurement data that should not be considered for further analysis.

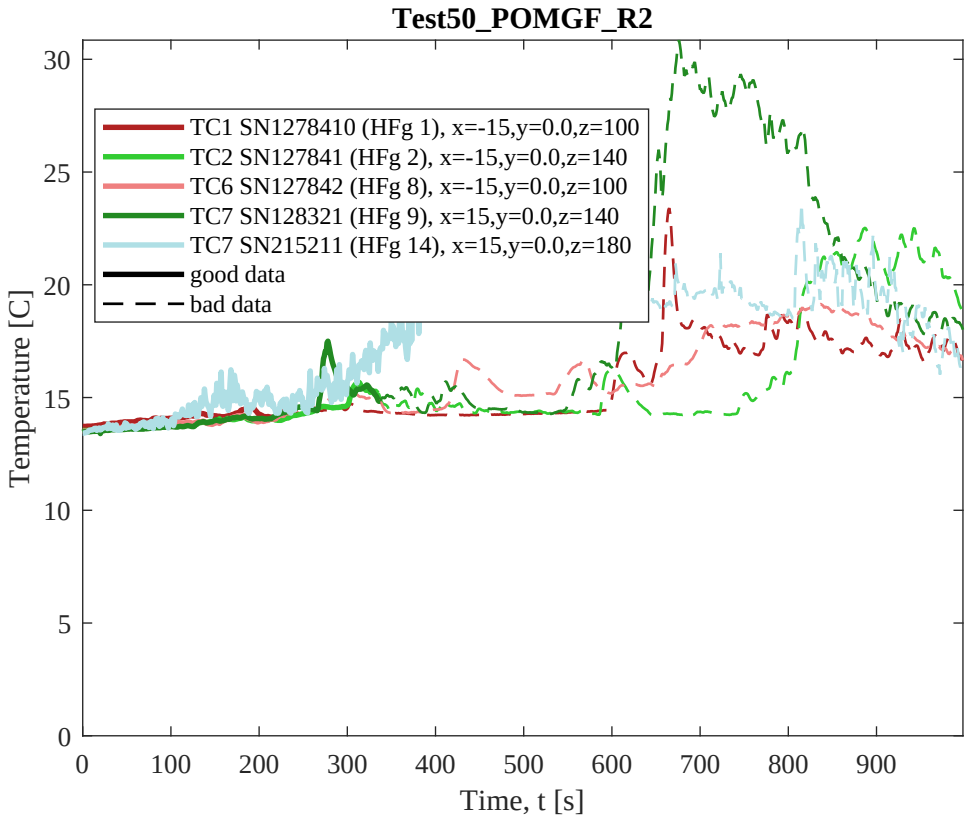

Fig. 202. Temperature of water-cooled Schmidt-Boelter heat flux gauges during Test 50 POMGF R2.

Shielded Gauges

Measurements of total and radiation heat flux recorded by shielded heat flux gauges (Sec. efssec: qrad). Gauge shields were removed at 360, 383, and 382 seconds (gauges 3, 5 and 7, respectively).

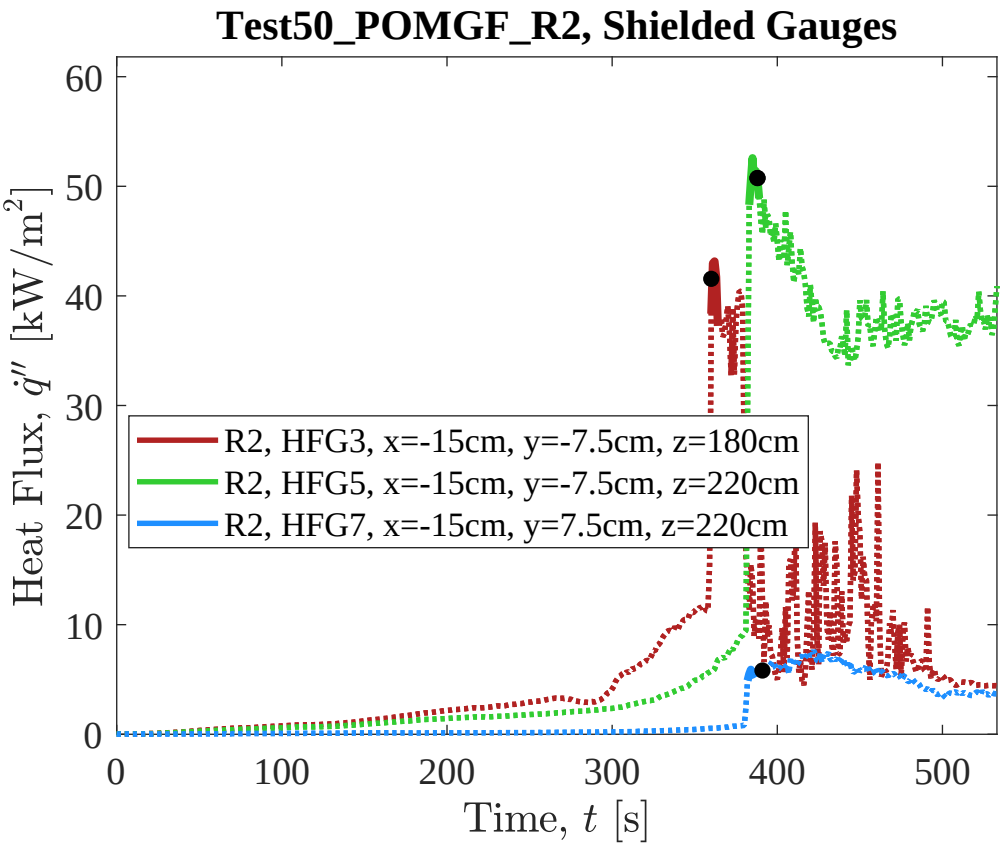

Fig. 203. Shielded gauge data for Test50 POMGF R2.

Test 61 POMGF R3

Test Description

3/8 in. thick, 24 in. wide, 96 in. tall (in two sections, each 24 in.x48in.) panels of POM-GF mounted to 1 in. thick Marinite board. Panels were ignited using a rectangular propane burner (60 kW nominal heat release rate) filled with layers of Pea Gravel, Sand, and Kaowool Insulation (i.e., the 'Final Burner configuration'; see Fig. 12). The burner was shut off ($t = 184$ s) and shielded ($t = 205$ s) after sustained ignition along the base of both of panels. The back 10 cm (i.e., 20 cm $\leq y \leq 30$ cm) of the left panel wall was not initially covered by the flame sheet due to burner non-uniformity; however, flames spread laterally to cover this wall as the sample contiued to burn. The sample slabs mostly maintained their shape while heating, staying attached to the panel walls as polymer melt flowed downwards across their front, heated surface. A sudden spike and decrease in HRR measured at $t = 1000$ s corresponds to the upper right slab. Heat flux gauges were mounted flush with the fuel's surface between $z = 100$ cm and $z = 220$ cm (only these higher locations were selected to limit the impact of polymer melt flow on heat flux measurements). Shielded radiometers and total heat flux gauges were positioned side by side at $z =$100 cm and $z = 180$ cm. The lower heat flux shields were removed at $t =$450 s and the upper heat flux shields were removed at $t =$515 s; reliable measurements of both total and radiation flame heat flux were obtained both heights.

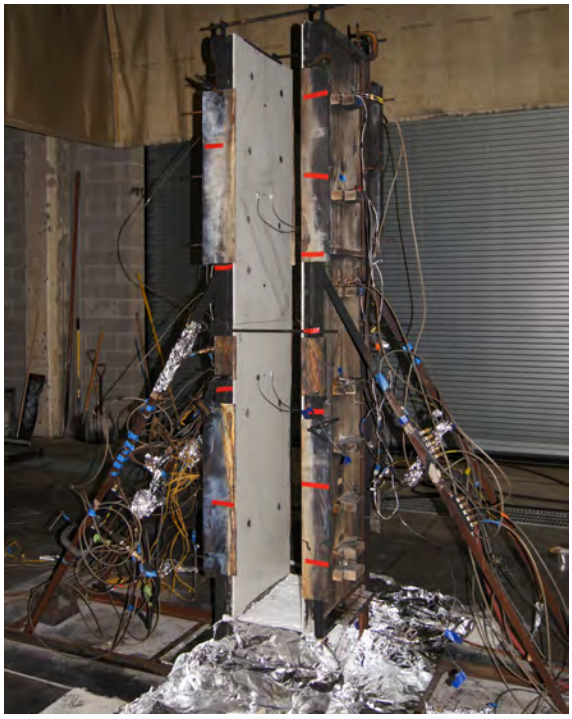

(a) Pre-test

(b) Ignition

(c) Peak HRR

(d) End of Test

Fig. 204. Photographs of Test 61 POMGF R3.

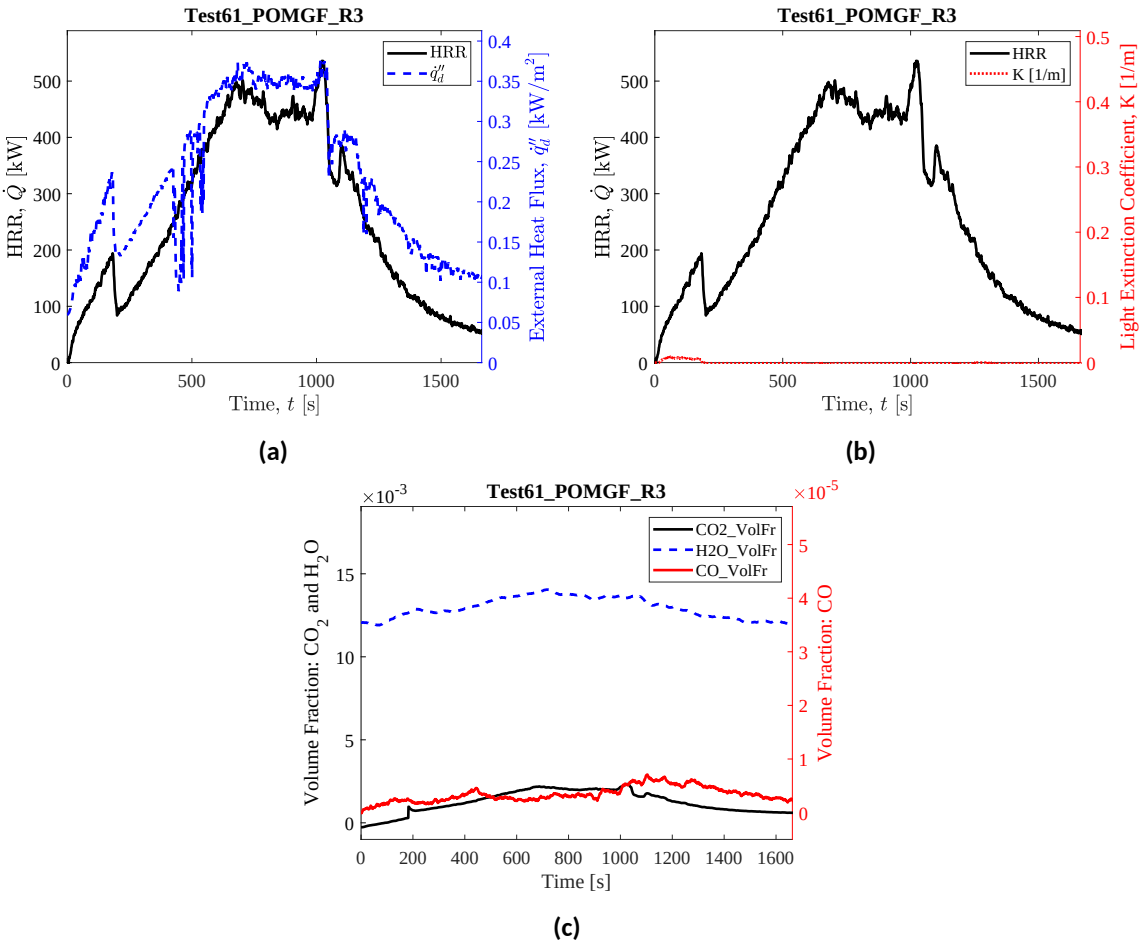

Fig. 205. Test 61 POMGF R3: (a) Heat release rate and heat flux at a distance, $\dot{q}''_{\mathrm{d}}$ (here, $\dot{q}''_{\mathrm{d}}$ is measured at x =300 cm, y =-305 cm, z =90 cm); (b) Heat release rate and light extinction coefficient, K (smoke particulate in exhaust duct [111]); (c) Time-resolved volume fractions of CO_2, H_2O, and CO.

Flame Heat Flux

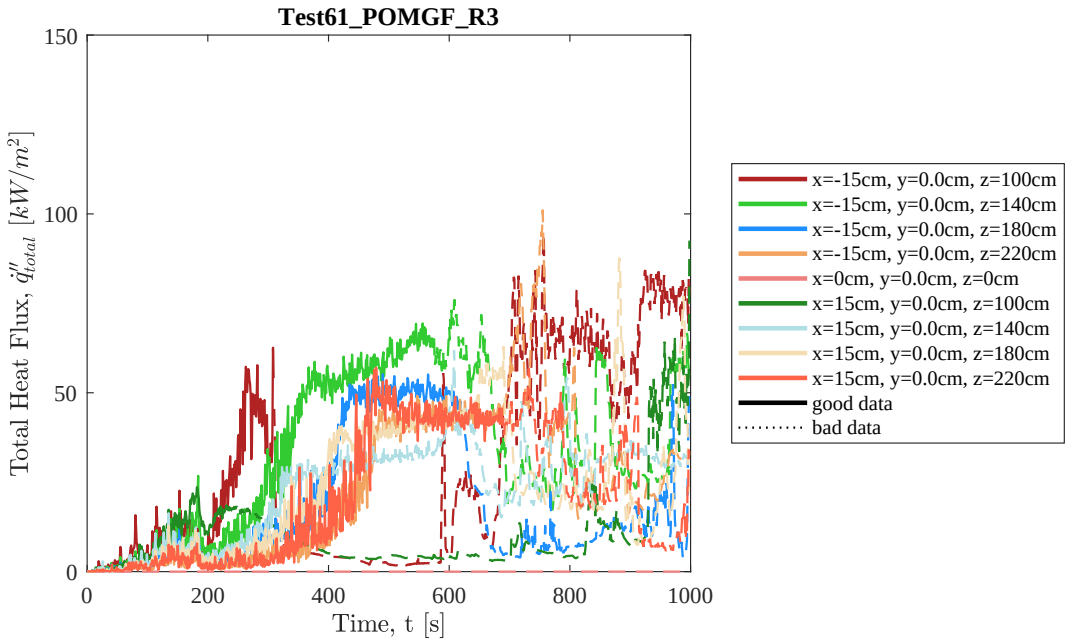

Fig. 206. Total flame to surface flame heat flux to water-cooled Schmidt-Boelter heat flux gauges as measured in Test 61 POMGF R3. Here, raw, unsmoothed original measurments are plotted from each gauges as a function of time. Solid lines highlight values of $\dot{q}''_{\text{total}}$ that were identified by manual review as ”good” (see Sec. 3.1.1) and dotted lines represent ”bad” measurement data that should not be considered for further analysis.

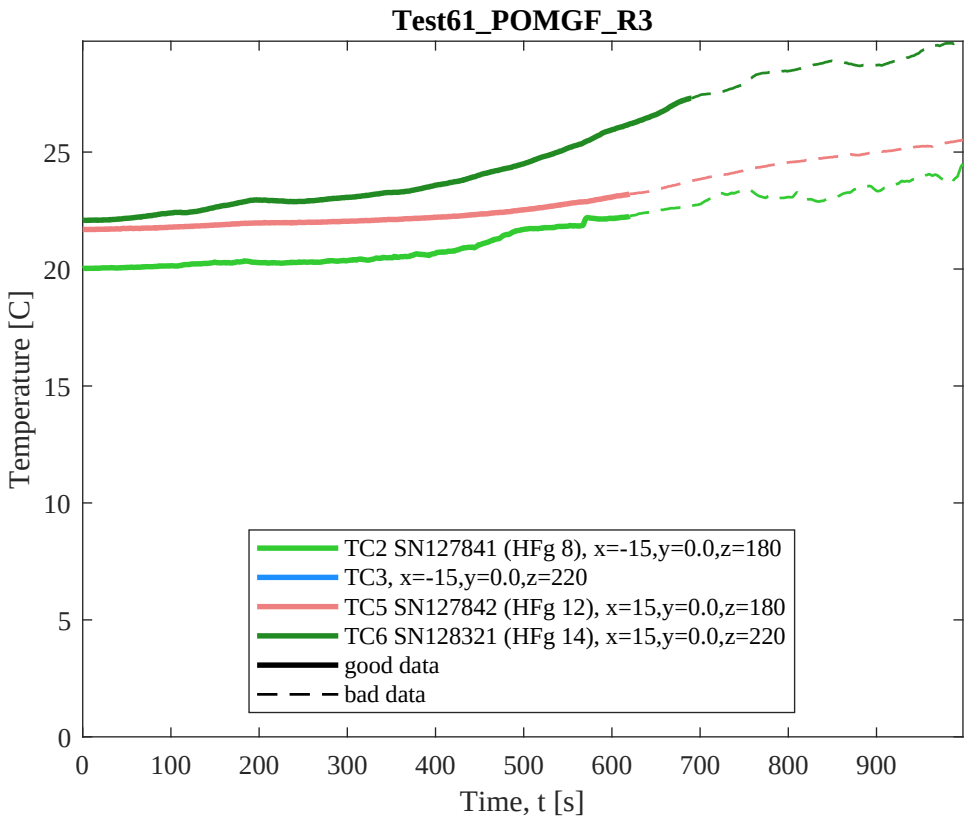

Fig. 207. Temperature of water-cooled Schmidt-Boelter heat flux gauges during Test 61 POMGF R3.

Shielded Gauges

Measurements of total and radiation heat flux recorded by shielded heat flux gauges (Sec. efssec: qrad). Gauge shields were removed at 449, 450, 517, and 517 seconds (gauges 1, 3, 6 and 7, respectively).

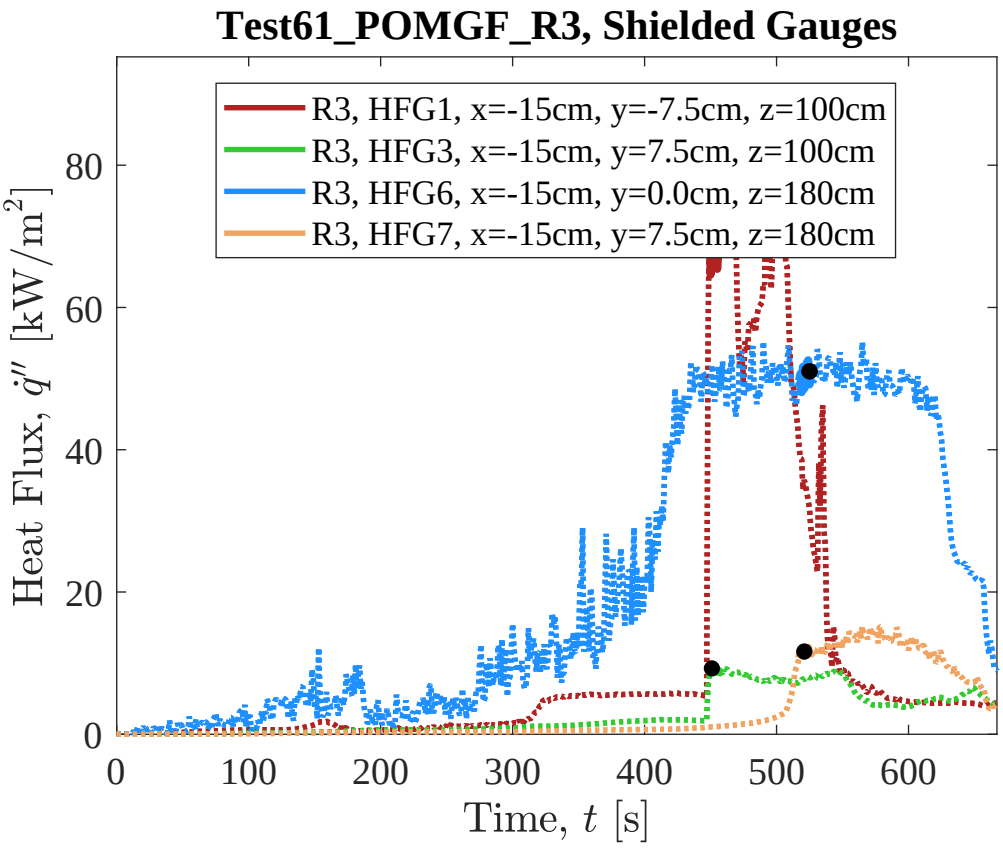

Fig. 208. Shielded gauge data for Test61 POMGF R3.

C.11. PVC - Polyvinyl Chloride

Test 11 PVC R1

Test Description
1/4 in. thick, 24 in. wide, 96 in. tall (in two sections, each 24 in.x48in.) panels of PVC mounted to 1 in. thick Marinite board. Panels were ignited using a rectangular propane burner (60 kW nominal heat release rate) filled with layers of Pea Gravel, Sand, and Kaowool Insulation (i.e., the 'Final Burner configuration'; see Fig. 12). The burner was shut off twice ($t = 210$ s and $t = 360$ s) and re-ignited at $t = 230$ s and $t = 380$ s before being left on throughout remainder of experiment. Rapid decreases in flame height and measured HRR showed that sustained flaming of this material could not be maintained when the burner was turned off. Heat flux gauges were mounted flush with the fuel's surface between $z = 20$ cm and $z = 180$ cm; however, heat flux measurements are not considered reliable after the burner is shut off at $t = 210$ s.

(a) Pre-test

(b) Ignition

(c) Peak HRR

(d) End of Test

Fig. 209. Photographs of Test 11 PVC R1.

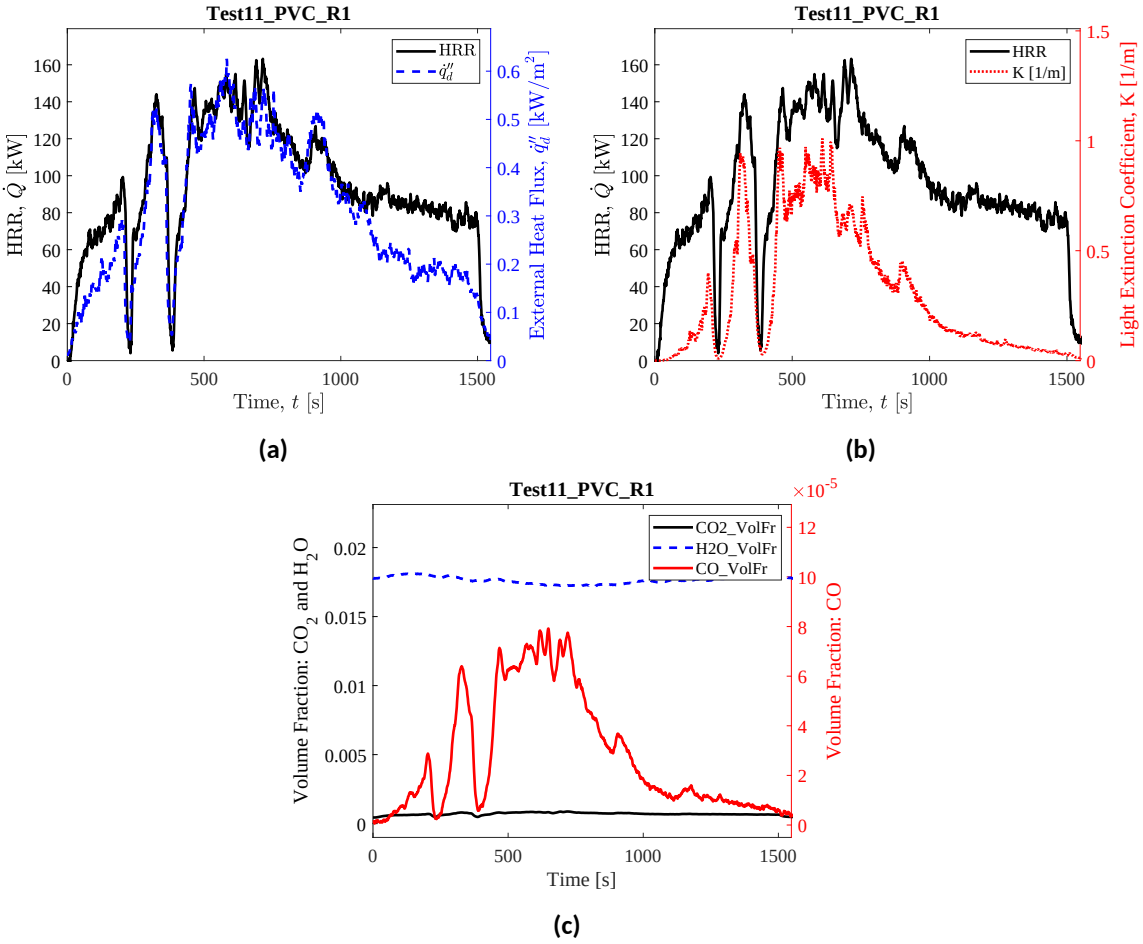

Fig. 210. Test 11 PVC R1: (a) Heat release rate and heat flux at a distance, $\dot{q}''_{\mathrm{d}}$ (here, $\dot{q}''_{\mathrm{d}}$ is measured at x =-100 cm, y =-300 cm, z =90 cm); (b) Heat release rate and light extinction coefficient, K (smoke particulate in exhaust duct [111]); (c) Time-resolved volume fractions of CO_2, H_2O, and CO.

Flame Heat Flux

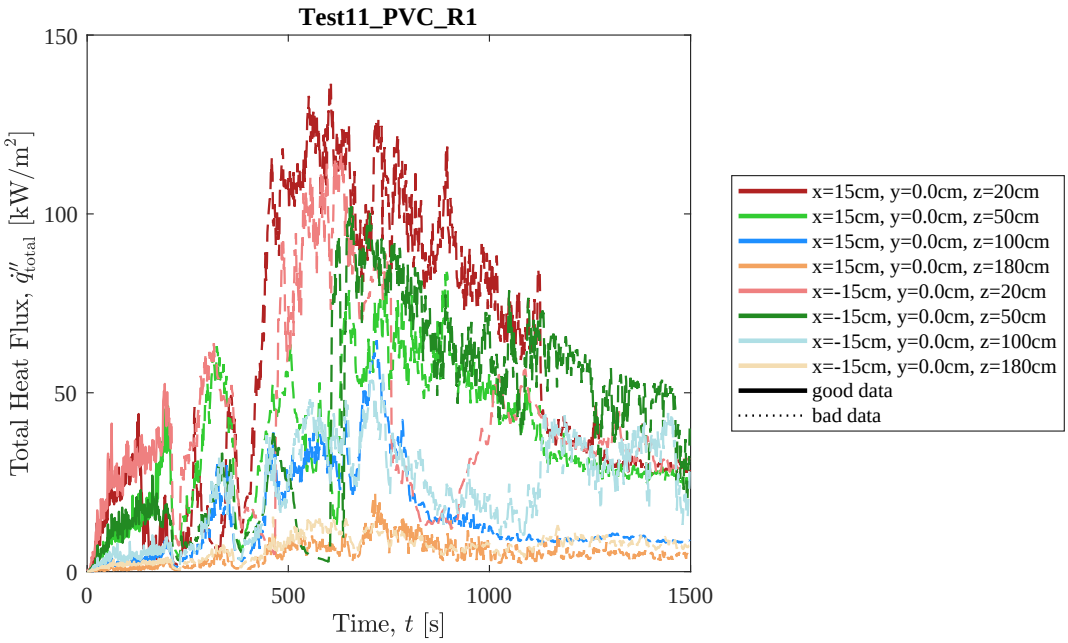

Fig. 211. Total flame to surface flame heat flux to water-cooled Schmidt-Boelter heat flux gauges as measured in Test 11 PVC R1. Here, raw, unsmoothed original measurments are plotted from each gauges as a function of time. Solid lines highlight values of $\dot{q}''_{\text{total}}$ that were identified by manual review as ”good” (see Sec. 3.1.1) and dotted lines represent ”bad” measurement data that should not be considered for further analysis.

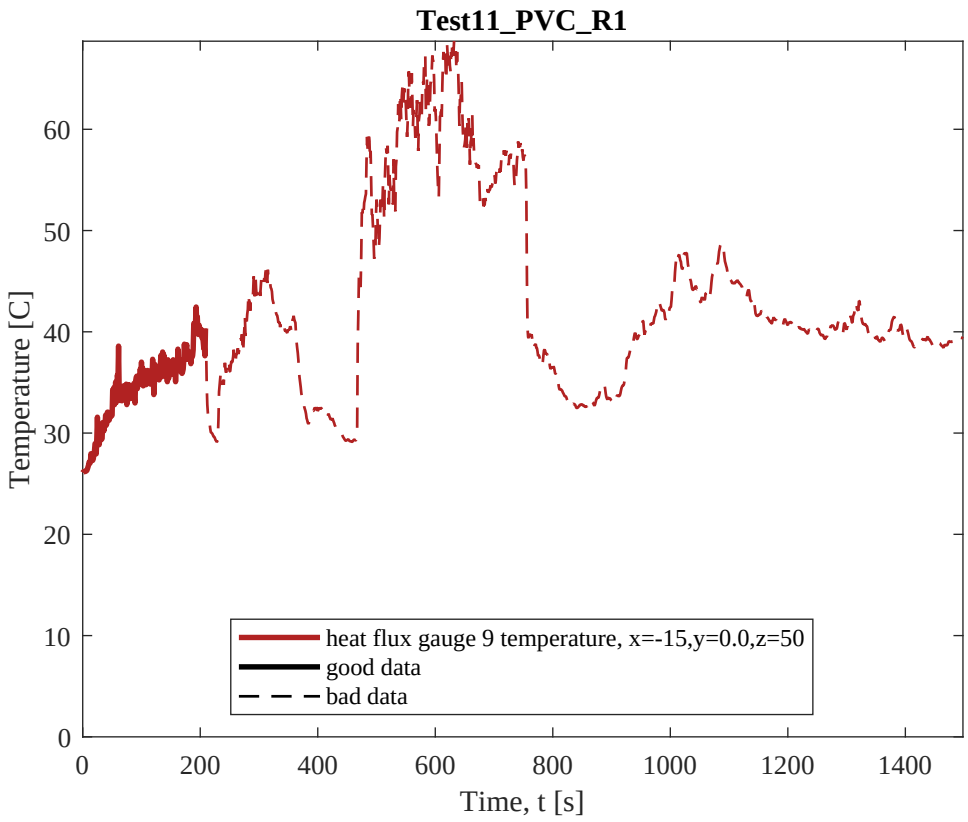

Fig. 212. Temperature of water-cooled Schmidt-Boelter heat flux gauges during Test 11 PVC R1.

Test 13 PVC R2

Test Description

1/4 in. thick, 24 in. wide, 96 in. tall (in two sections, each 24 in.x48in.) panels of PVC mounted to 1 in. thick Marinite board. Panels were ignited using a rectangular propane burner (60 kW nominal heat release rate) filled with layers of Pea Gravel, Sand, and Kaowool Insulation (i.e., the 'Final Burner configuration'; see Fig. 12). The burner was kept on until 1200 s. Throughout this time, measured HRR remained relatively low (approximately 100 kW to 150 kW); however, brief increases in fire size were observe when portions of the PVC panels would detach from the panel walls and (a) continue at their back surface or (b) fall, and coninue burning at the base of the assembly. Heat flux gauges were mounted flush with the fuel's surface between $z = 20$ cm and $z = 75$ cm; however, after $t = 480$ s, heat flux measurements are not considered reliable due to sample detachment from the panel walls.

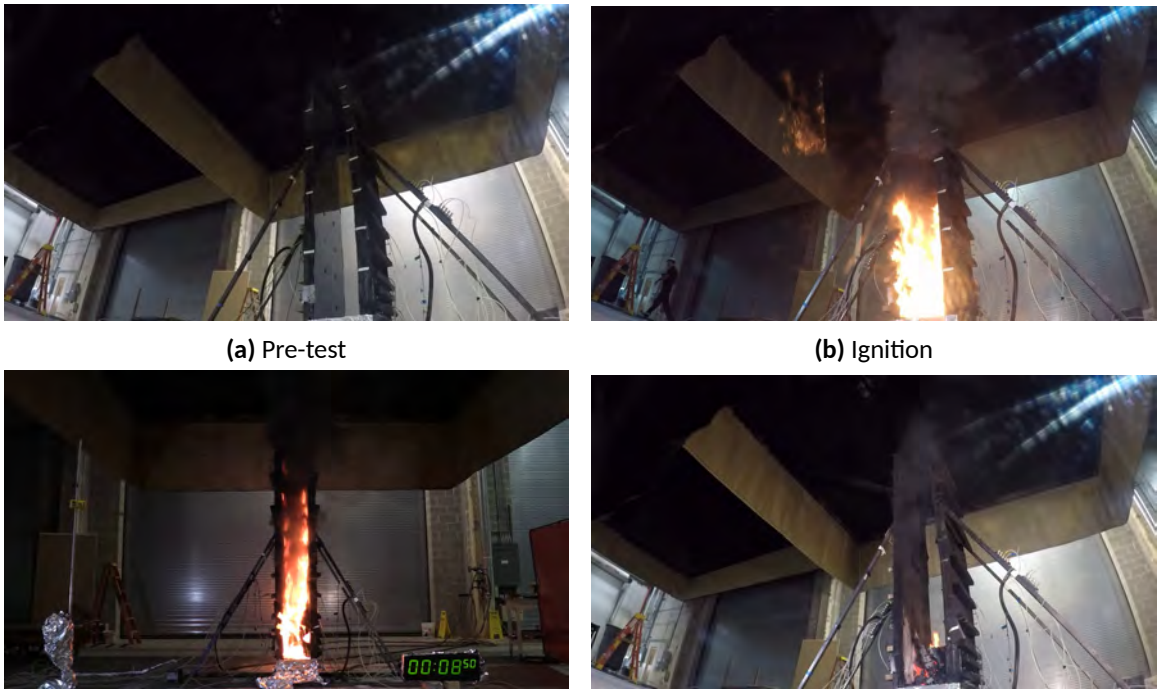

(a) Pre-test

(b) Ignition

(c) Peak HRR

(d) End of Test

Fig. 213. Photographs of Test 13 PVC R2.

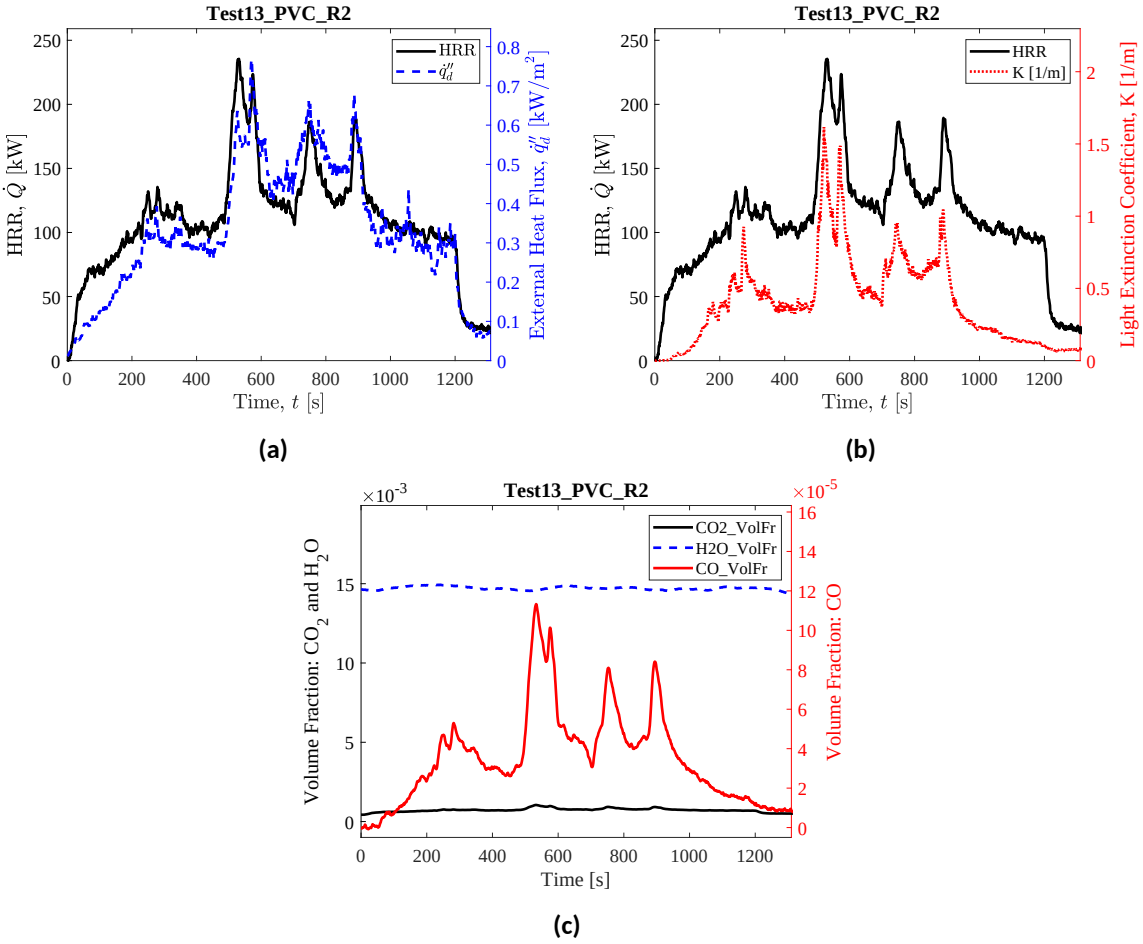

Fig. 214. Test 13 PVC R2: (a) Heat release rate and heat flux at a distance, $\dot{q}''_{\mathrm{d}}$ (here, $\dot{q}''_{\mathrm{d}}$ is measured at x =-100 cm, y =-300 cm, z =90 cm); (b) Heat release rate and light extinction coefficient, K (smoke particulate in exhaust duct [111]); (c) Time-resolved volume fractions of CO_2, H_2O, and CO.

Flame Heat Flux

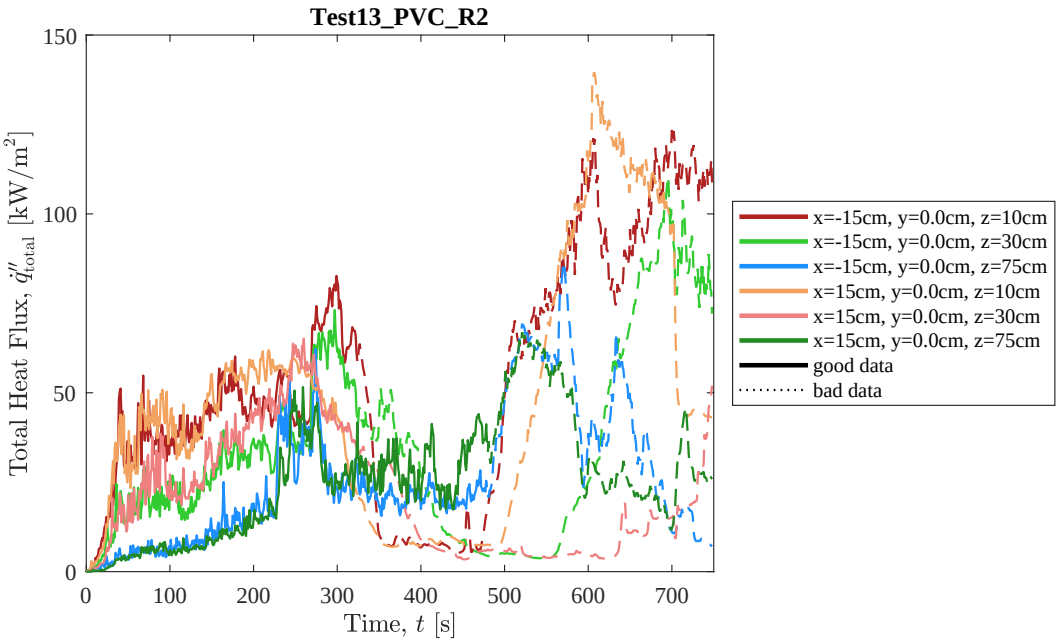

Fig. 215. Total flame to surface flame heat flux to water-cooled Schmidt-Boelter heat flux gauges as measured in Test 13 PVC R2. Here, raw, unsmoothed original measurments are plotted from each gauges as a function of time. Solid lines highlight values of $\dot{q}''_{\text{total}}$ that were identified by manual review as ”good” (see Sec. 3.1.1) and dotted lines represent ”bad” measurement data that should not be considered for further analysis.

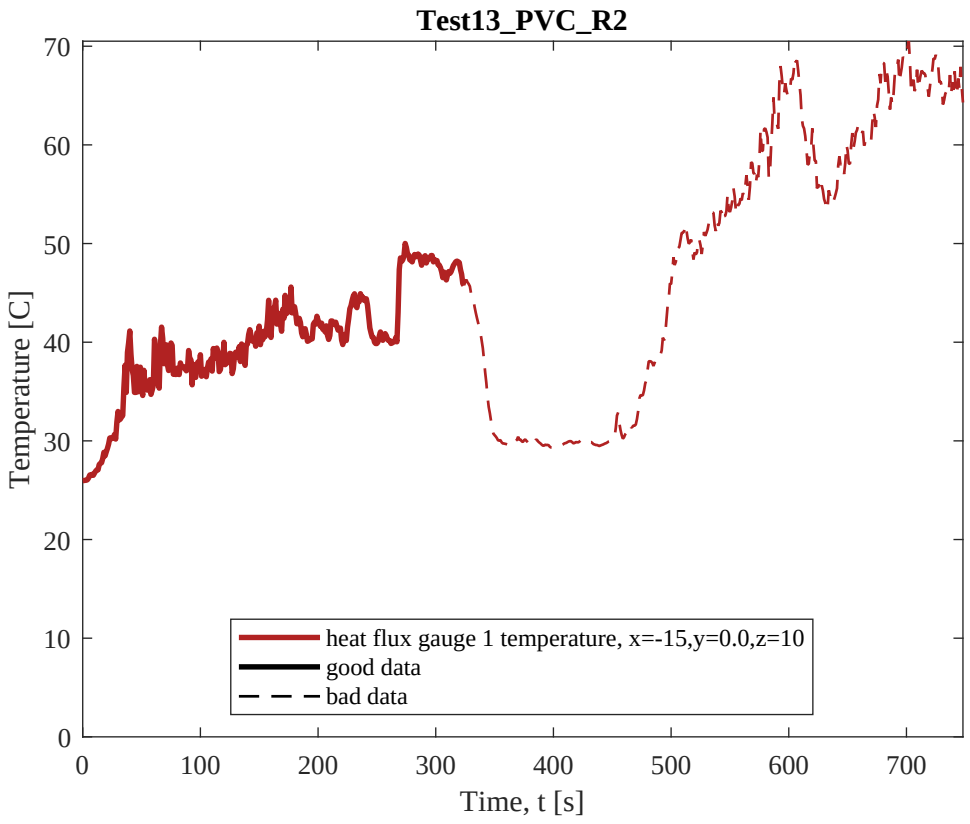

Fig. 216. Temperature of water-cooled Schmidt-Boelter heat flux gauges during Test 13 PVC R2.

C.12. GPO-3 (Redboard) - Fiberglass-Reinforced Polyester laminate (limited arc- and flame-resistance)

Test 6 Redboard R1

Test Description

1/4 in. thick, 24 in. wide, 96 in. tall (in two sections, each 24 in.x48in.) panels of GPO-3 mounted to 1in. thick Marinite board. Panels were ignited using a rectangular propane burner (60 kW nominal heat release rate) filled with Pea Gravel (i.e., the 'Preliminary Burner configuration'; see Fig. 12. Just prior to ignition, the sand in this burner was removed and replaced. The burner was kept on until 1200 s; however, measured HRR remained relatively low, gradually increasing to a peak value of 134 kW at 720 s before steadilly decaying as the sample burned out, leaving behind layers of fiberglass reinforcement. The sample self-extinguished shortly after the burner was turned off. Flame to wall heat flux measurements were not recorded in this test.

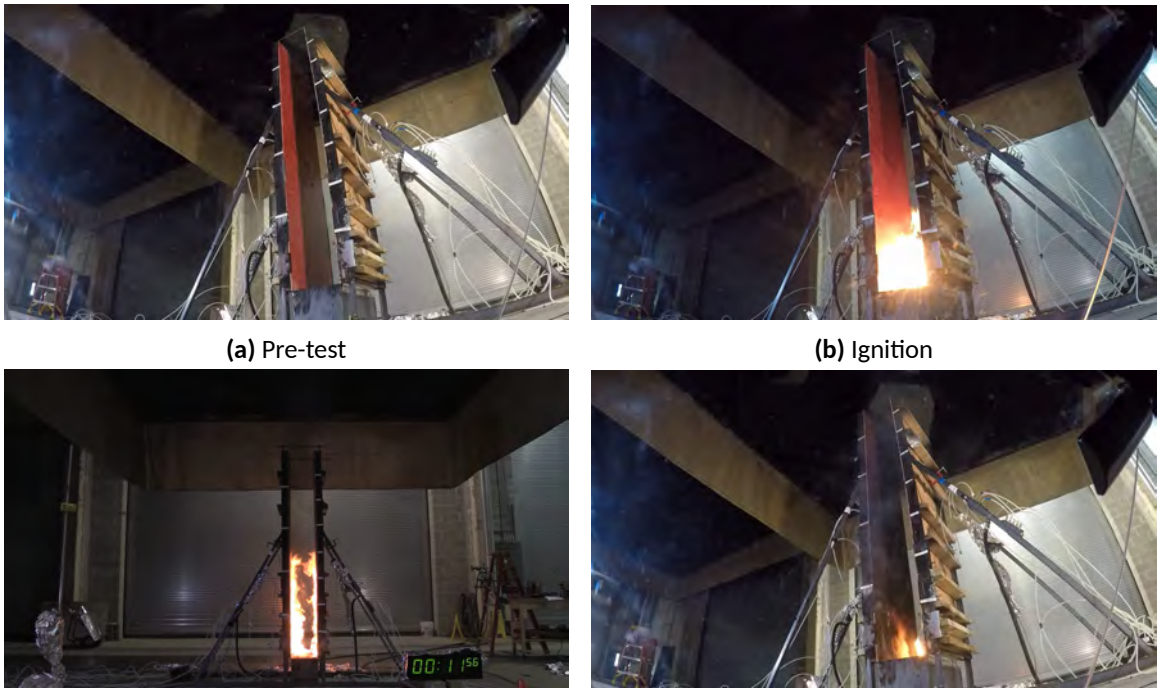

(a) Pre-test

(b) Ignition

(c) Peak HRR

(d) End of Test

Fig. 217. Photographs of Test 6 Redboard R1.

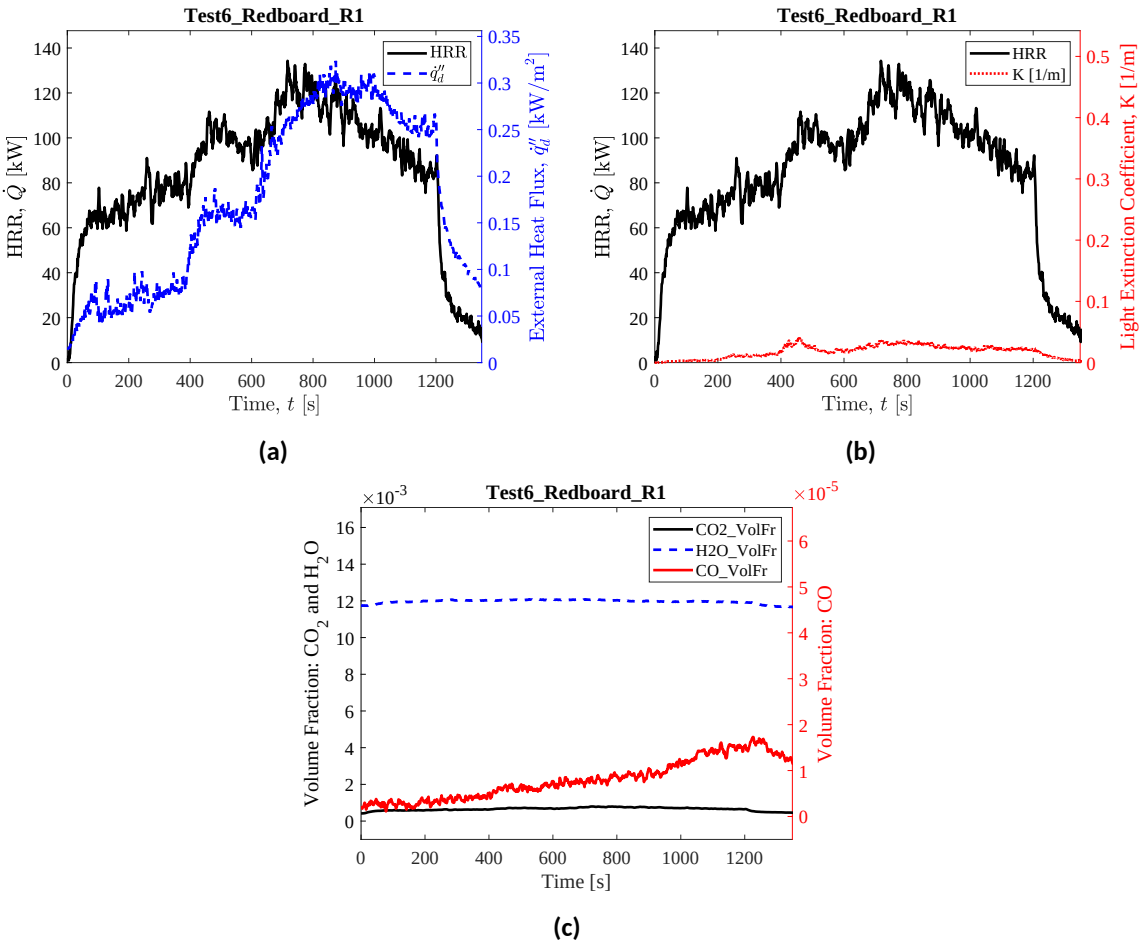

Fig. 218. Test 6 Redboard R1: (a) Heat release rate and heat flux at a distance, $\dot{q}''_{\mathrm{d}}$ (here, $\dot{q}''_{\mathrm{d}}$ is measured at x =-100 cm, y =-300 cm, z =90 cm); (b) Heat release rate and light extinction coefficient, K (smoke particulate in exhaust duct [111]); (c) Time-resolved volume fractions of CO_2, H_2O, and CO.

Test 8 Redboard R2

Test Description

1/4 in. thick, 24 in. wide, 96 in. tall (in two sections, each 24 in.x48in.) panels of GPO-3 mounted to 1in. thick Marinite board. Panels were ignited using a rectangular propane burner (60 kW nominal heat release rate) filled with layers of Pea Gravel, Sand, and Kaowool Insulation (i.e., the 'Final Burner configuration'; see Fig. 12). The burner was kept on until 1200 s; however, measured HRR remained relatively low, gradually increasing to a peak value of 115 kW at 426 s before steadilly decaying as the sample burned out, leaving behind layers of fiberglass reinforcement. The sample self-extinguished shortly after the burner was turned off. Flame to wall heat flux measurements were not recorded in this test.

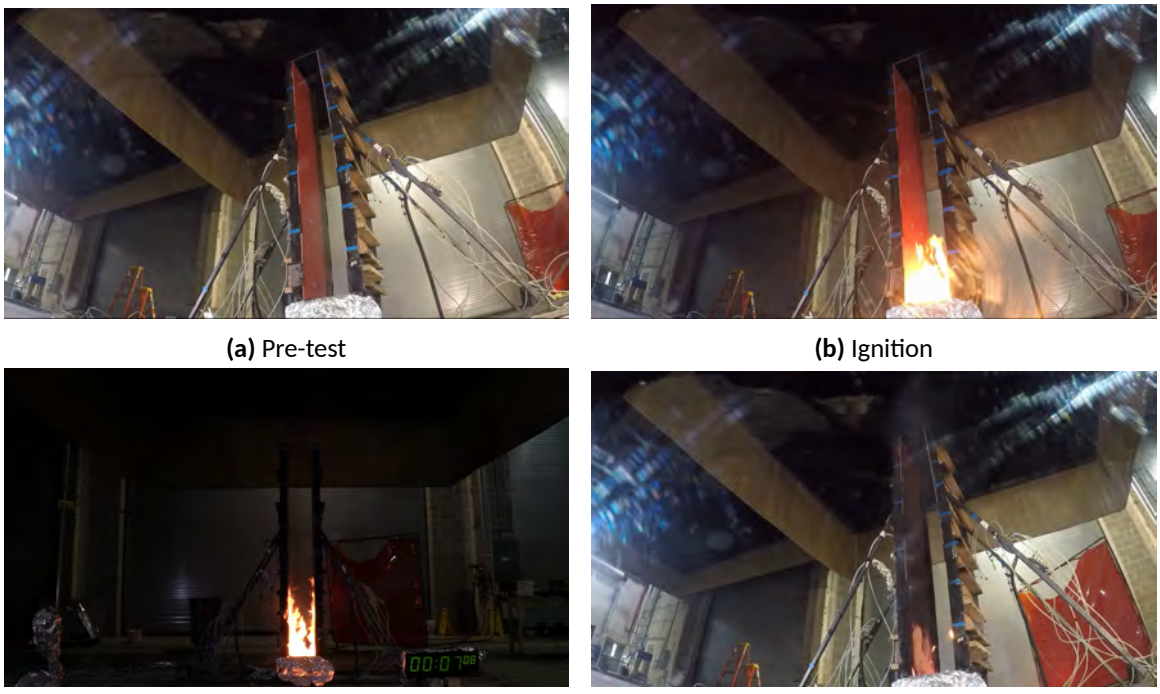

(a) Pre-test

(b) Ignition

(c) Peak HRR

(d) End of Test

Fig. 219. Photographs of Test 8 Redboard R2.

Heat Release Rate, Heat Flux at a Distance, and Species Yields

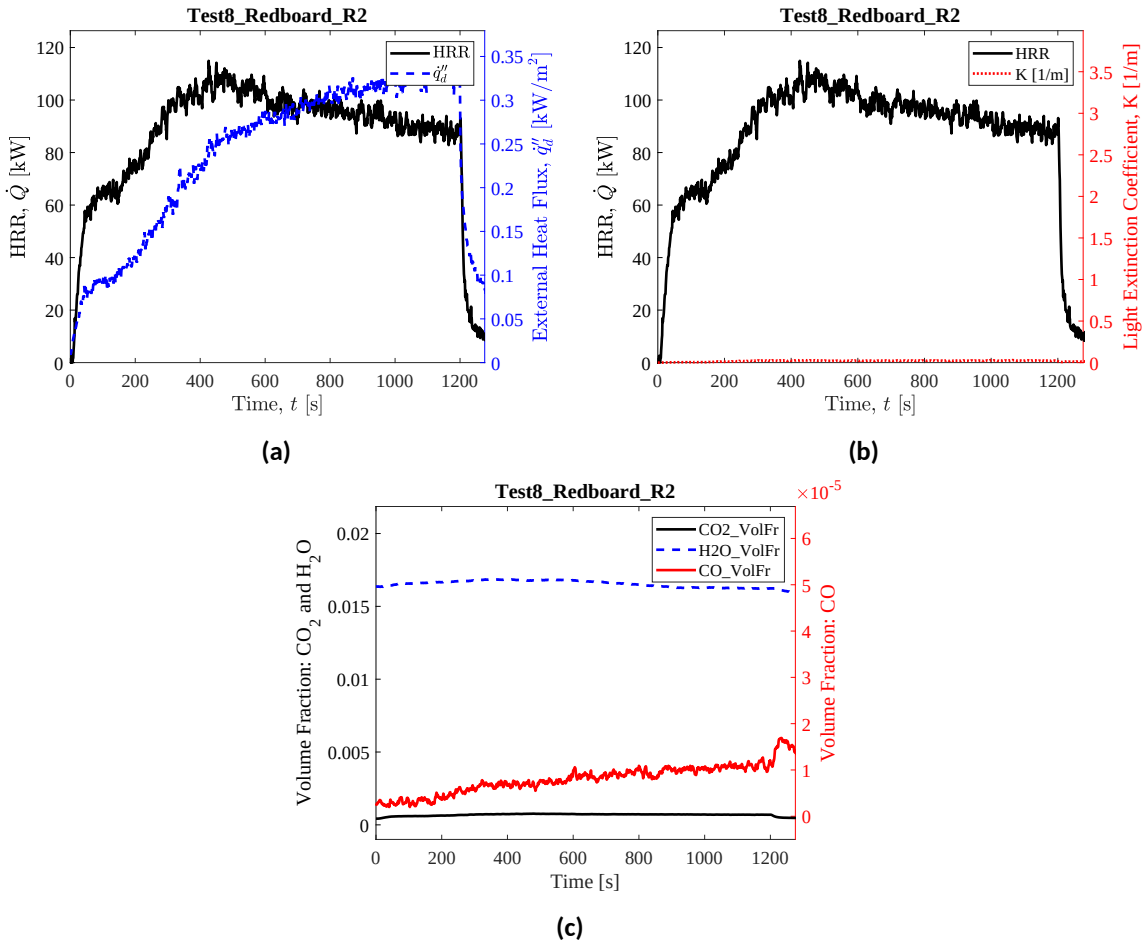

Fig. 220. Test 8 Redboard R2: (a) Heat release rate and heat flux at a distance, $\dot{q}''_{\mathrm{d}}$ (here, $\dot{q}''_{\mathrm{d}}$ is measured at x =-100 cm, y =-300 cm, z =90 cm); (b) Heat release rate and light extinction coefficient, K (smoke particulate in exhaust duct [111]); (c) Time-resolved volume fractions of CO_2, H_2O, and CO.

Test 14 Redboard R3

Test Description

1/4 in. thick, 24 in. wide, 48in.tall panels of GPO-3 mounted to 1 in. thick Marinite board. Panels were ignited using a rectangular propane burner (60 kW nominal heat release rate) filled with layers of Pea Gravel, Sand, and Kaowool Insulation (i.e., the 'Final Burner configuration'; see Fig. 12).burner on throughout experiment. The burner was kept on until 1200 s; however, measured HRR remained relatively low, gradually increasing to a peak value of 110 kW at 426 s before steadilly decaying as the sample burned out, leaving behind layers of fiberglass reinforcement. The sample self-extinguished shortly after the burner was turned off. Flame to wall heat flux measurements were not recorded in this test.

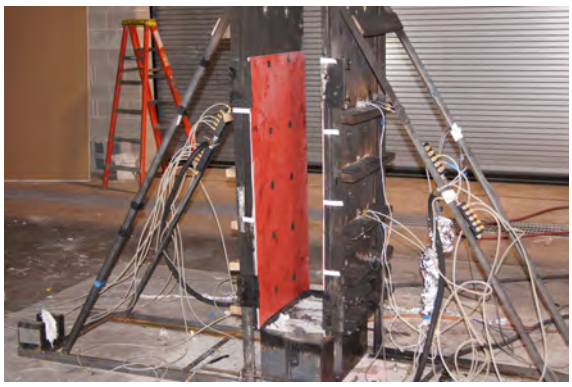

(a) Pre-test

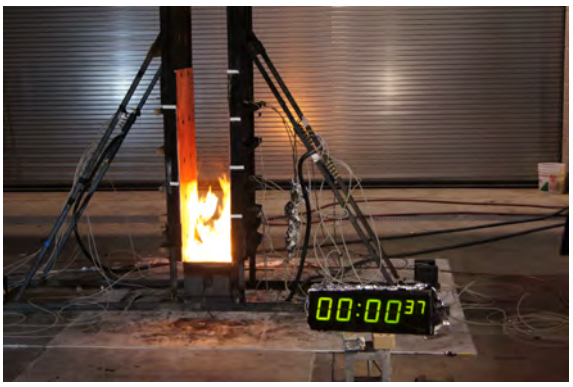

(b) Ignition

(c) Peak HRR

(d) End of Test

Fig. 221. Photographs of Test 14 Redboard R3.

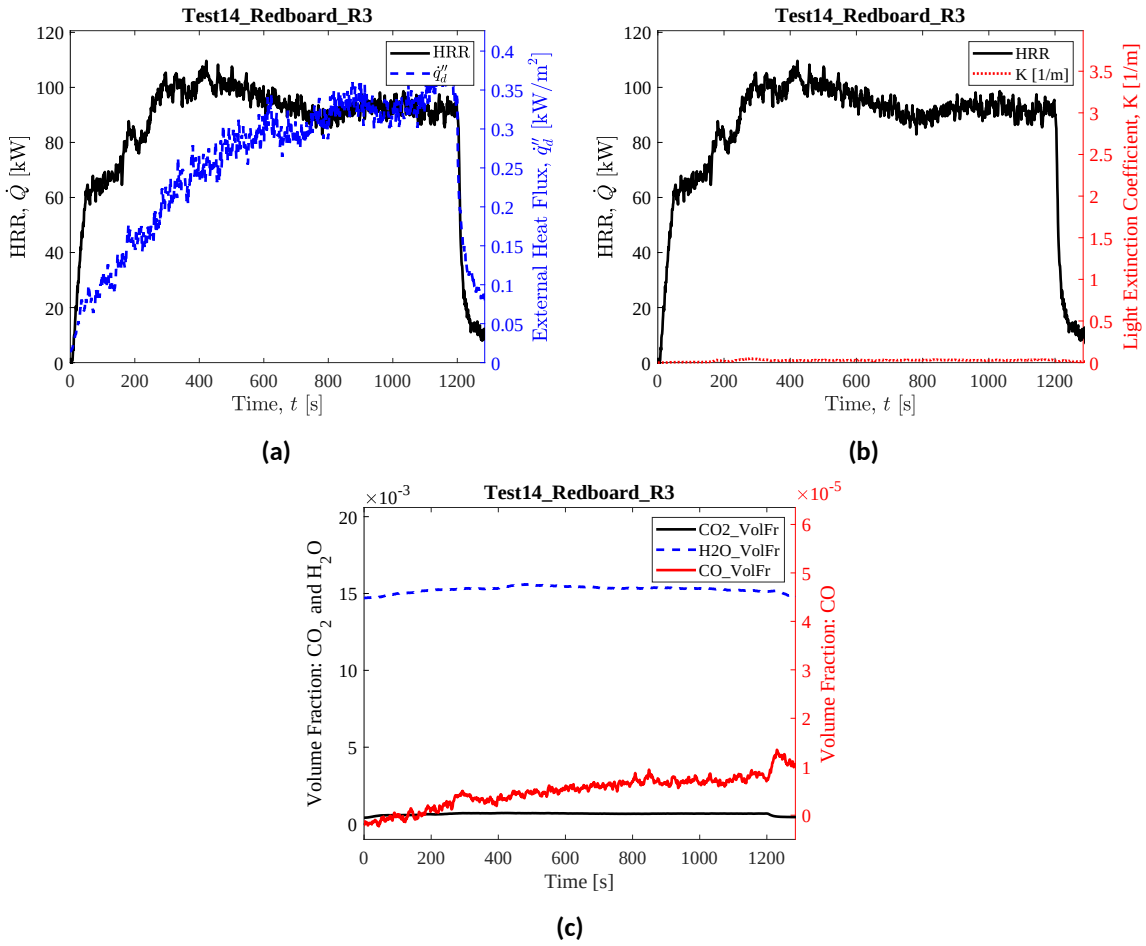

Fig. 222. Test 14 Redboard R3: (a) Heat release rate and heat flux at a distance, $\dot{q}''_{\mathrm{d}}$ (here, $\dot{q}''_{\mathrm{d}}$ is measured at x =-100 cm, y =-300 cm, z =90 cm); (b) Heat release rate and light extinction coefficient, K (smoke particulate in exhaust duct [111]); (c) Time-resolved volume fractions of CO_2, H_2O, and CO.

C.13. Western Red Cedar

Test 15 RedCedar R1

Test Description
7/8 in. thick, 22.5in. wide, 96 in. tall (in two sections, each 11.25in.x96in.) planks of Western Red Cedar mounted to 1in. thick Marinite board (new Marinite). Panels were ignited using a rectangular propane burner (60 kW nominal heat release rate) filled with layers of Pea Gravel, Sand, and Kaowool Insulation (i.e., the 'Final Burner configuration'; see Fig. 12). The burner was shut off twice ($t = 80$ s and $t = 150$ s) and re-ignited at $t = 100$ s and $t = 220$ s before being left on throughout remainder of experiment. Rapid decreases in flame height and measured HRR showed that sustained flaming of this material could not be maintained when the burner was turned off. Heat flux gauges were mounted flush with the fuel's surface between $z = 20$ cm and $z = 220$ cm; however, heat flux measurements are only considered reliable until the burner is first shut off at $t = 80$ s. Shielded radiometers and total heat flux gauges were positioned side by side at $z =$50 cm and $z = 100$ cm. The heat flux shields were removed at $t =$452 s and reliable measurements of both total and radiation flame heat flux were obtained at both heights.

(a) Pre-test

(b) Ignition

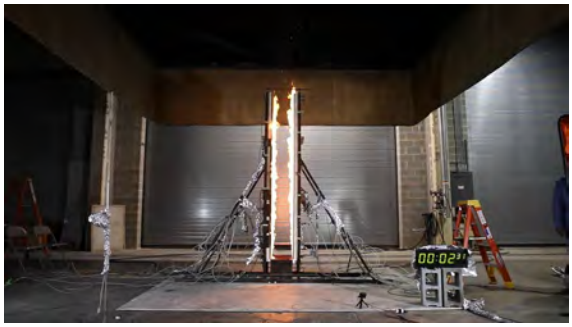

(c) Peak HRR

(d) End of Test

Fig. 223. Photographs of Test 15 RedCedar R1.

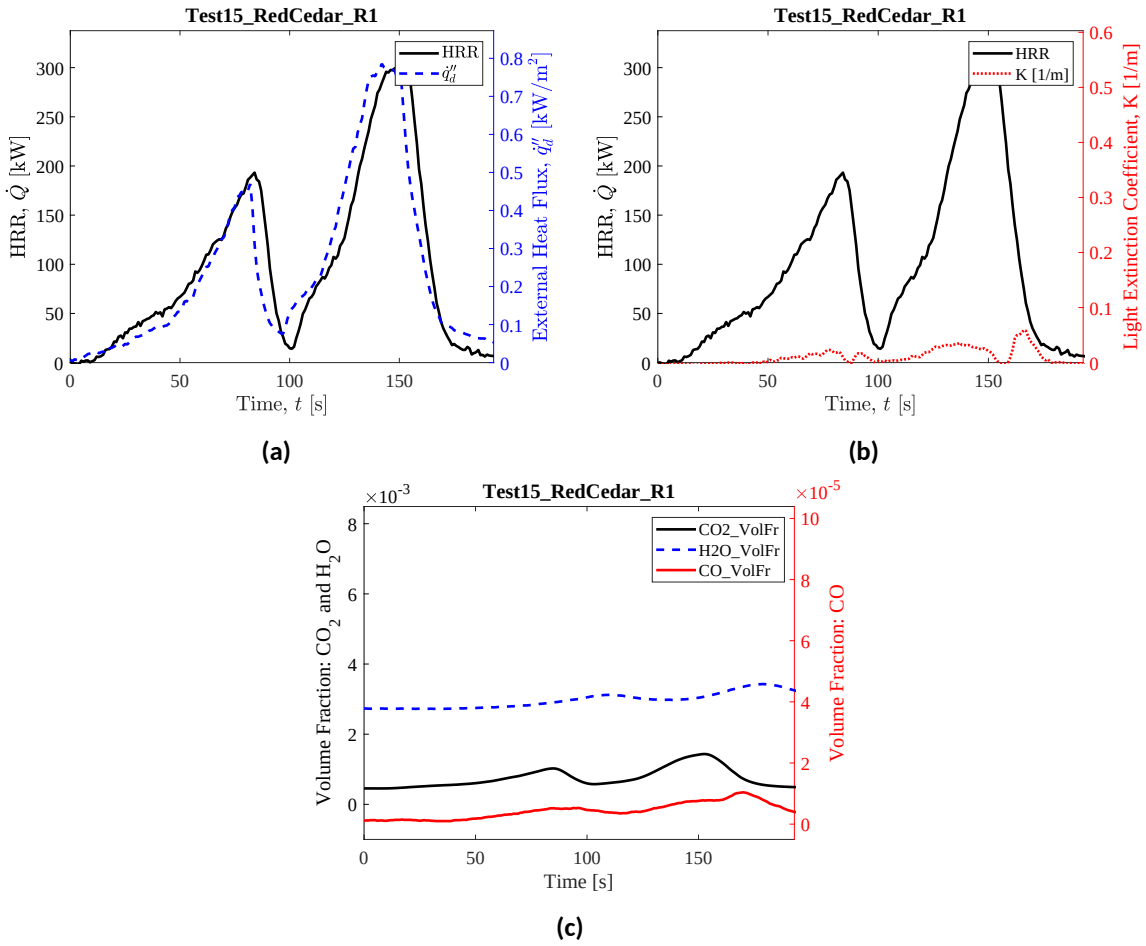

Fig. 224. Test 15 RedCedar R1: (a) Heat release rate and heat flux at a distance, $\dot{q}''_{\mathrm{d}}$ (here, $\dot{q}''_{\mathrm{d}}$ is measured at x =-100 cm, y =-300 cm, z =90 cm); (b) Heat release rate and light extinction coefficient, K (smoke particulate in exhaust duct [111]); (c) Time-resolved volume fractions of CO_2, H_2O, and CO.

Flame Heat Flux

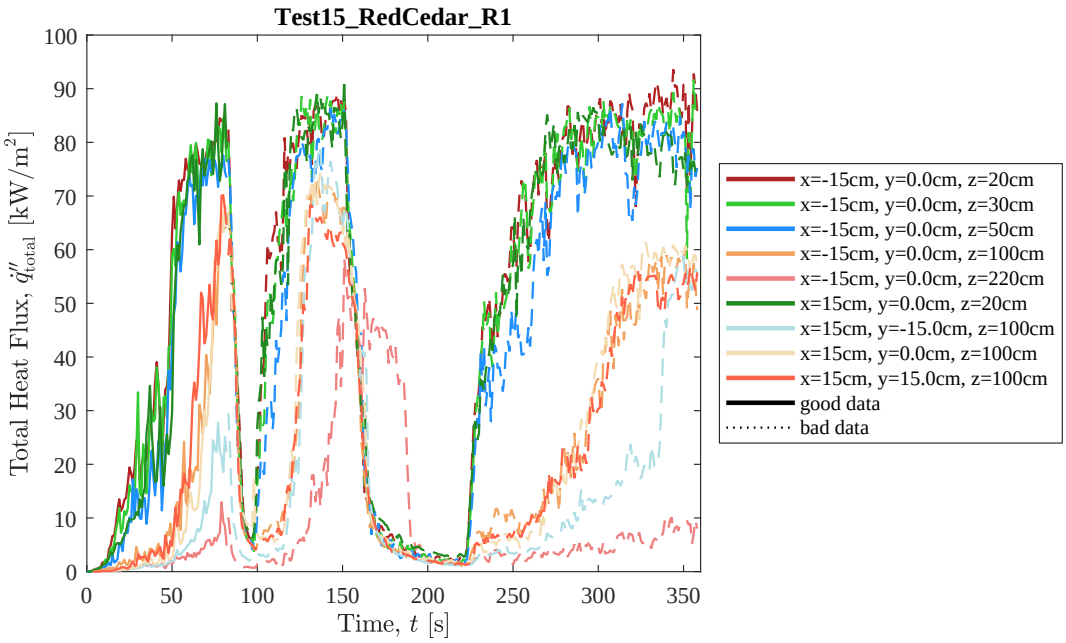

Fig. 225. Total flame to surface flame heat flux to water-cooled Schmidt-Boelter heat flux gauges as measured in Test 15 RedCedar R1. Here, raw, unsmoothed original measurments are plotted from each gauges as a function of time. Solid lines highlight values of $\dot{q}''_{\text{total}}$ that were identified by manual review as ”good” (see Sec. 3.1.1) and dotted lines represent ”bad” measurement data that should not be considered for further analysis.

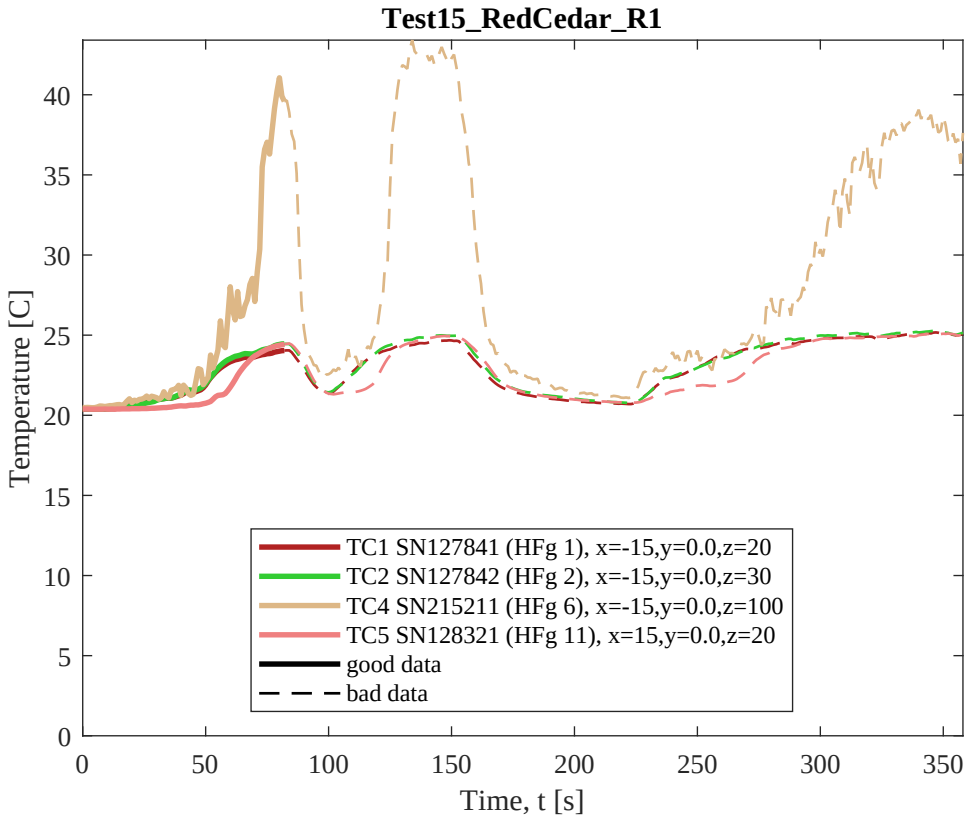

Fig. 226. Temperature of water-cooled Schmidt-Boelter heat flux gauges during Test 15 RedCedar R1.

Shielded Gauges

Measurements of total and radiation heat flux recorded by shielded heat flux gauges (Sec. efssec: qrad). Gauge shields were removed at 454 seconds.

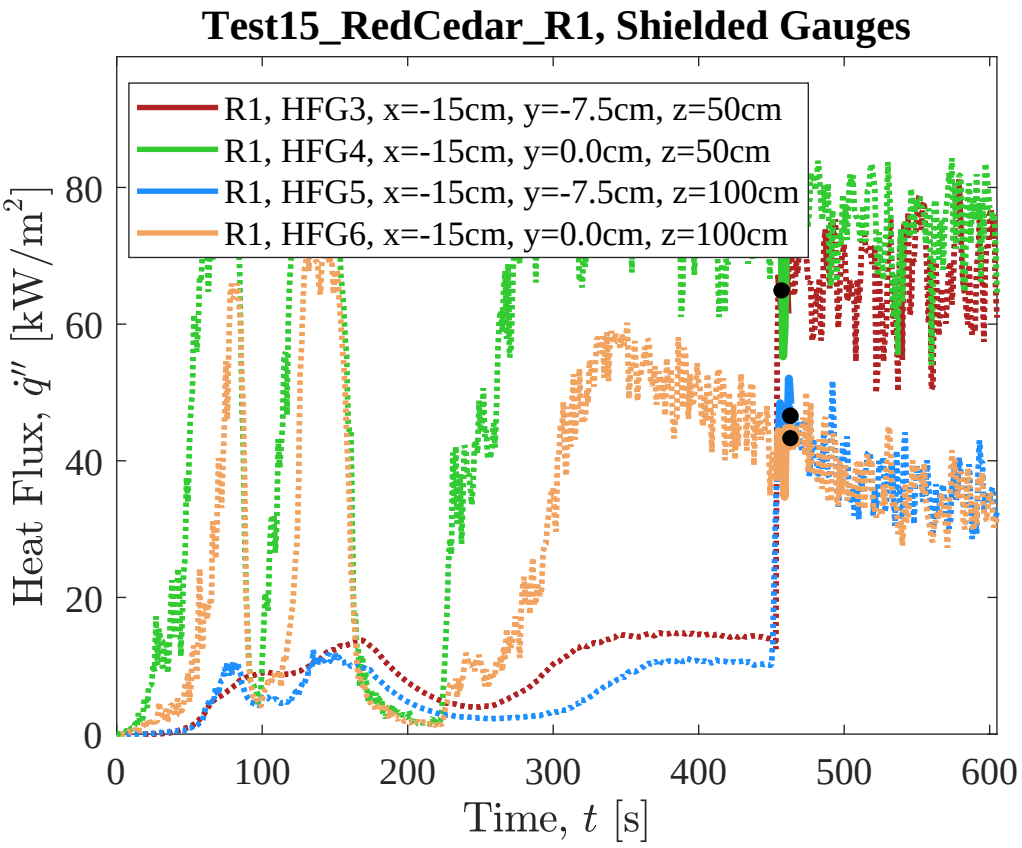

Fig. 227. Shielded gauge data for Test15 RedCedar R1.

Test 22 RedCedar R2

Test Description
7/8 in. thick, 22.5in. wide, 96 in. tall (in two sections, each 11.25in.x96in.) planks of Western Red Cedar mounted to 1in. thick Marinite board (new Marinite). Panels were ignited using a rectangular propane burner (60 kW nominal heat release rate) filled with layers of Pea Gravel, Sand, and Kaowool Insulation (i.e., the 'Final Burner configuration'; see Fig. 12). The burner was kept on throughout the experiment until $t = 360$ s. Heat flux gauges were mounted flush with the fuel's surface between $z = 10$ cm and $z = 140$ cm; heat flux measurements are considered reliable for further analysis until peak HRR was measured. Shielded radiometers and total heat flux gauges were positioned side by side at $z =$100 cm and $z = 180$ cm. The heat flux shields were removed at $t =$452 s and reliable measurements of both total and radiation flame heat flux were obtained at both heights; however, at the time of shield removal, flame tips only intermittently covered the heat flux gauges at $z =$100 cm and they were not present at all at $z =$100 cm thus, in this test, reduced heat fluxes were measured by both of these shielded gauges at both heights.

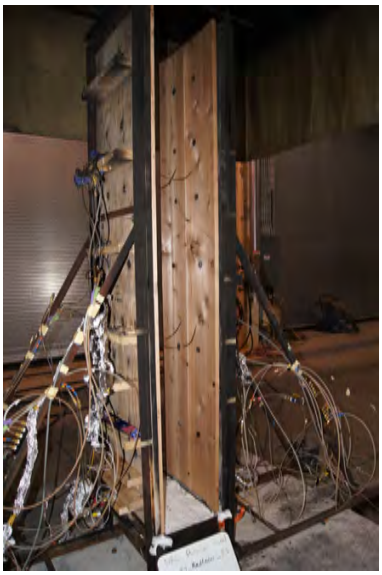

(a) Pre-test

(b) Ignition

(c) Peak HRR

(d) End of Test

Fig. 228. Photographs of Test 22 RedCedar R2.

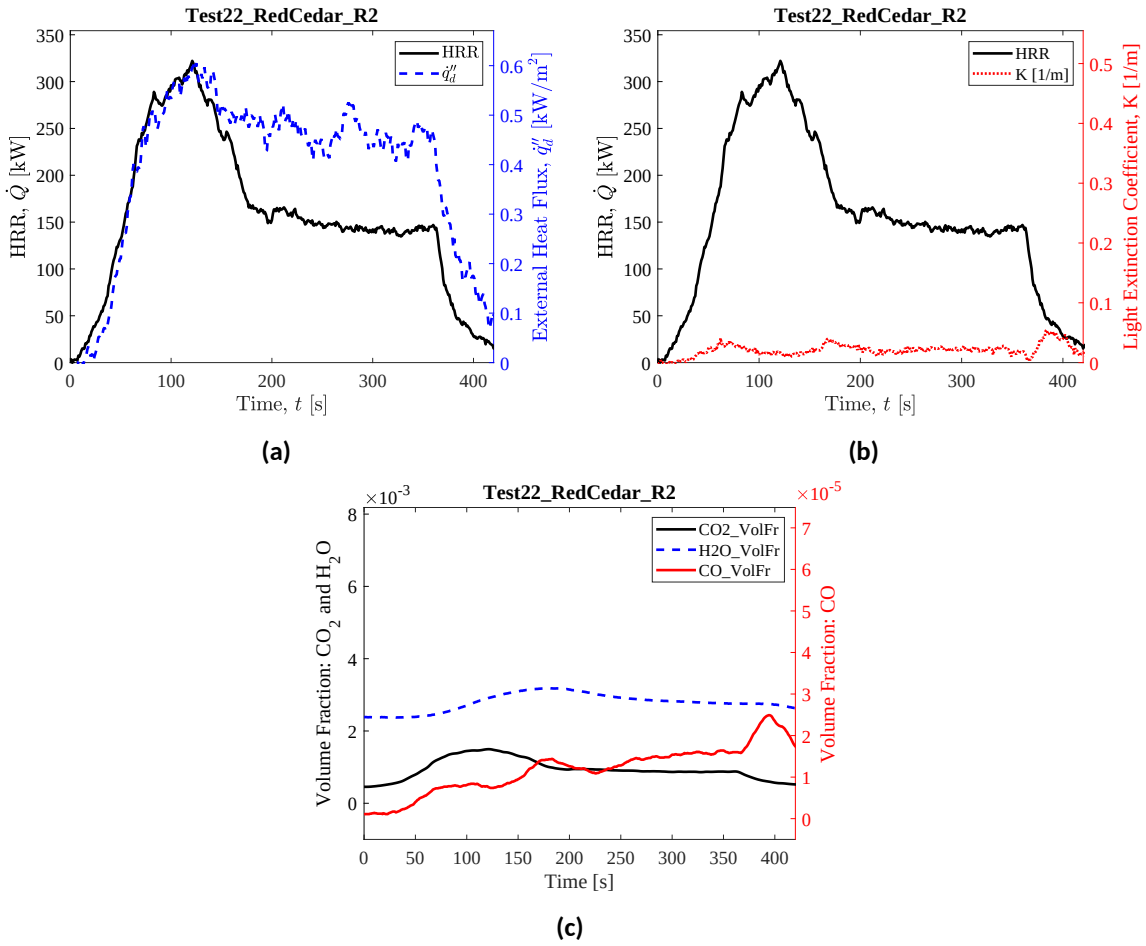

Fig. 229. Test 22 RedCedar R2: (a) Heat release rate and heat flux at a distance, $\dot{q}''_{\mathrm{d}}$ (here, $\dot{q}''_{\mathrm{d}}$ is measured at x =-150 cm, y =-300 cm, z =90 cm); (b) Heat release rate and light extinction coefficient, K (smoke particulate in exhaust duct [111]); (c) Time-resolved volume fractions of CO_2, H_2O, and CO.

Flame Heat Flux

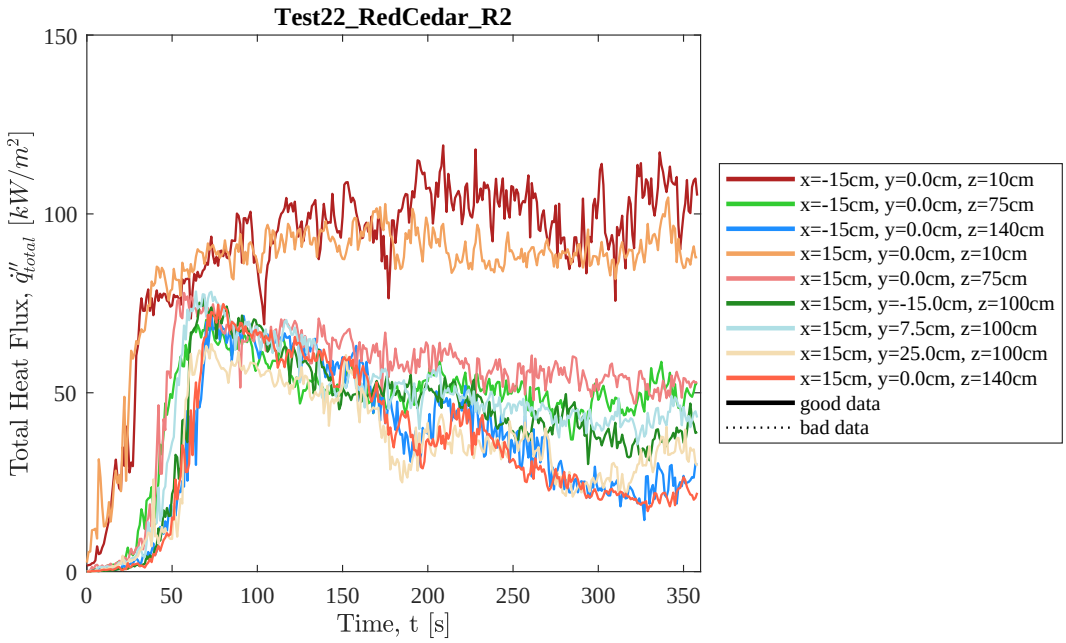

Fig. 230. Total flame to surface flame heat flux to water-cooled Schmidt-Boelter heat flux gauges as measured in Test 22 RedCedar R2. Here, raw, unsmoothed original measurments are plotted from each gauges as a function of time. Solid lines highlight values of $\dot{q}''_{\text{total}}$ that were identified by manual review as ”good” (see Sec. 3.1.1) and dotted lines represent ”bad” measurement data that should not be considered for further analysis.

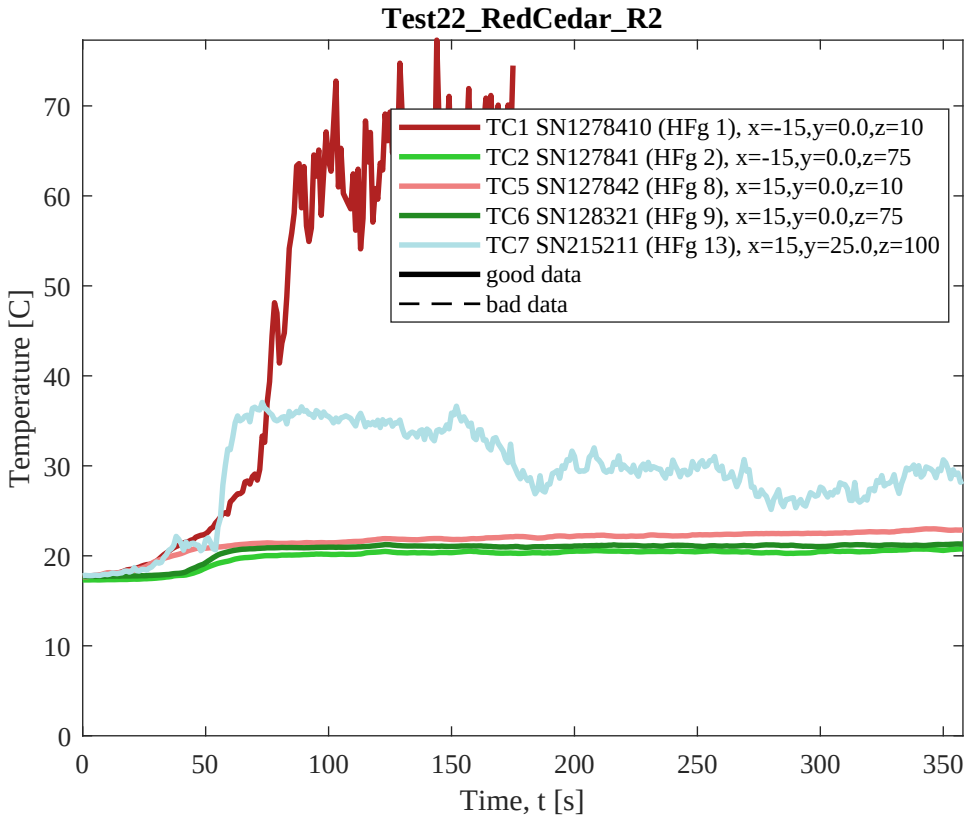

Fig. 231. Temperature of water-cooled Schmidt-Boelter heat flux gauges during Test 22 RedCedar R2.

Shielded Gauges

Measurements of total and radiation heat flux recorded by shielded heat flux gauges (Sec. efssec: qrad). Gauge shields were removed at 244, 245, 242, and 243 seconds (gauges 3, 4, 6 and 7, respectively).

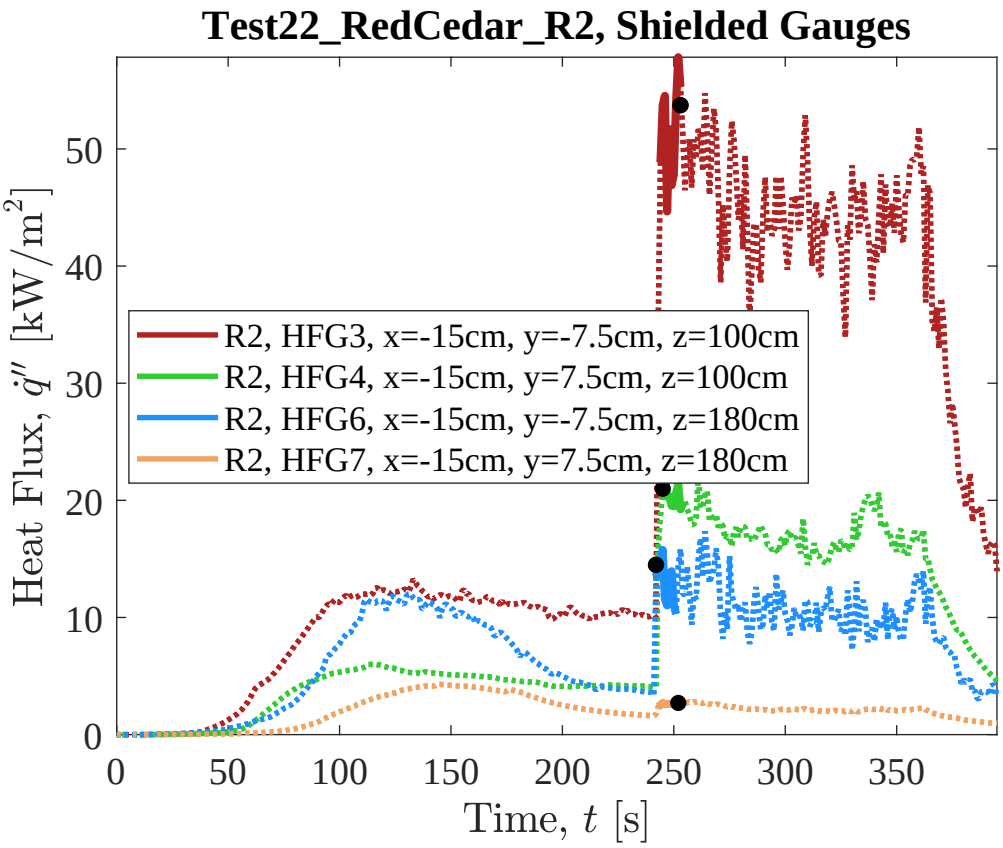

Fig. 232. Shielded gauge data for Test22 RedCedar R2.

Test 43 RedCedar R3

Test Description

7/8 in. thick, 22.5in. wide, 96 in. tall (in two sections, each 11.25in.x96in.) planks of Western Red Cedar mounted to 1in. thick Marinite board (new Marinite). Panels were ignited using a rectangular propane burner (60 kW nominal heat release rate) filled with layers of Pea Gravel, Sand, and Kaowool Insulation (i.e., the 'Final Burner configuration'; see Fig. 12). The burner was kept on throughout the experiment until $t = 360$ s. Heat flux gauges were mounted flush with the fuel's surface between $z = 30$ cm and $z = 180$ cm; heat flux measurements are considered reliable for further analysis until peak HRR was measured. Shielded radiometers and total heat flux gauges were positioned side by side at $z =$50 cm and $z = 100$ cm. The heat flux shields were removed at $t =$148 s and reliable measurements of both total and radiation flame heat flux were obtained at both heights. At the time of shield removal in this test, fire size was approximately 50 % greater than that in Test R2 (i.e., HRR = 240 kW) and flame tips extended up to the top of the panel walls, though only intermittent flaming was observed across each gauge location. Importantly, both panel walls were glowing (smoldering combustion) - this provided significantly higher radiation from the opposite panel wall. As a result, in this test, substantially higher values of $q_{\mathrm{rad}}(\%)$ are measured at both heights.

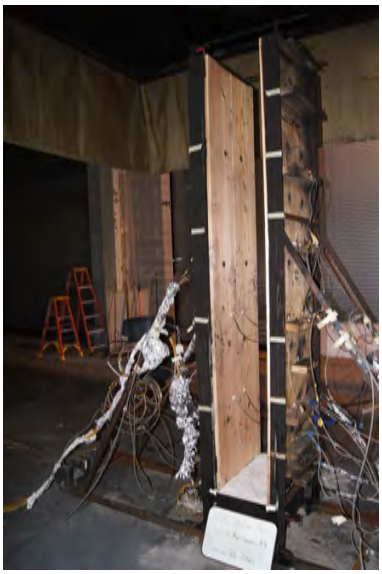

(a) Pre-test

(b) Ignition

(c) Peak HRR

(d) End of Test

Fig. 233. Photographs of Test 43 RedCedar R3.

Heat Release Rate, Heat Flux at a Distance, and Species Yields

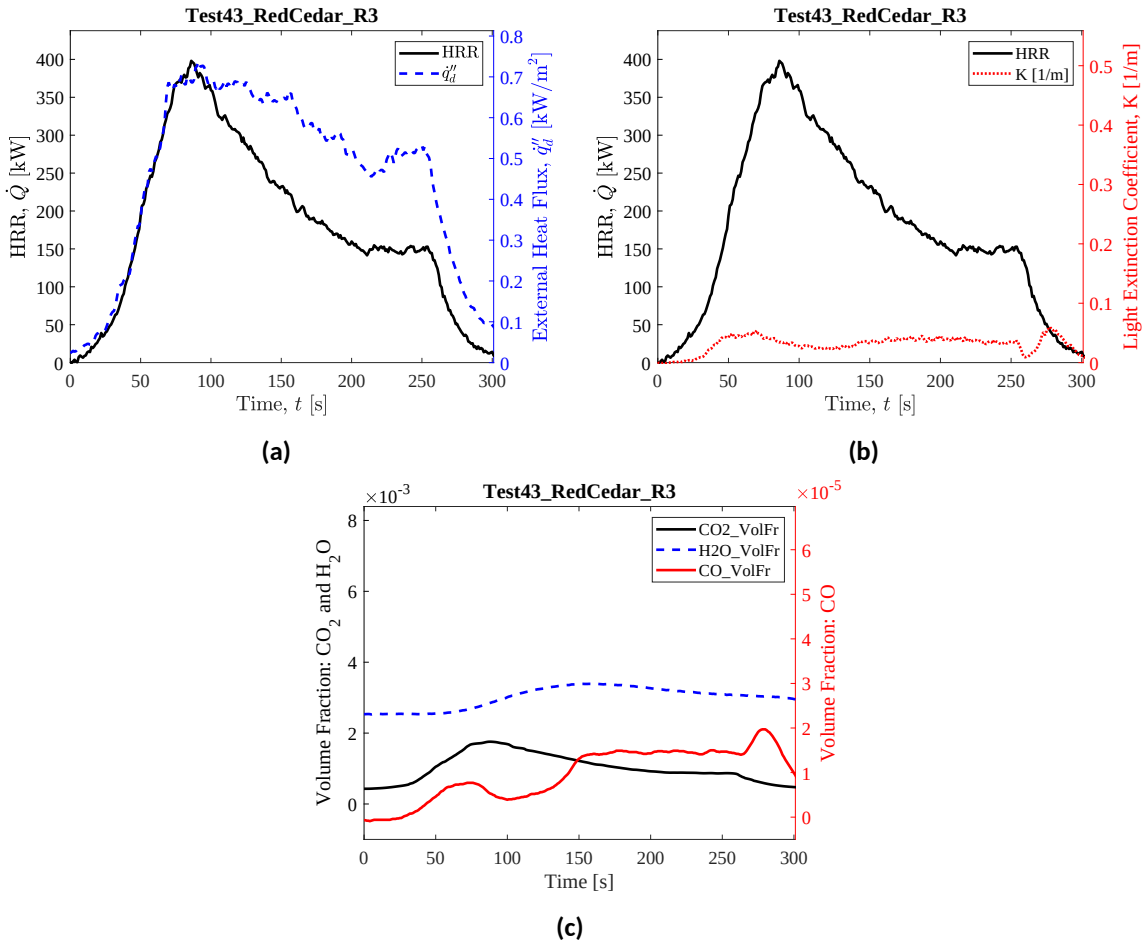

Fig. 234. Test 43 RedCedar R3: (a) Heat release rate and heat flux at a distance, $\dot{q}''_{\mathrm{d}}$ (here, $\dot{q}''_{\mathrm{d}}$ is measured at x =-232 cm, y =-300 cm, z =90 cm); (b) Heat release rate and light extinction coefficient, K (smoke particulate in exhaust duct [111]); (c) Time-resolved volume fractions of CO_2, H_2O, and CO.

Flame Heat Flux

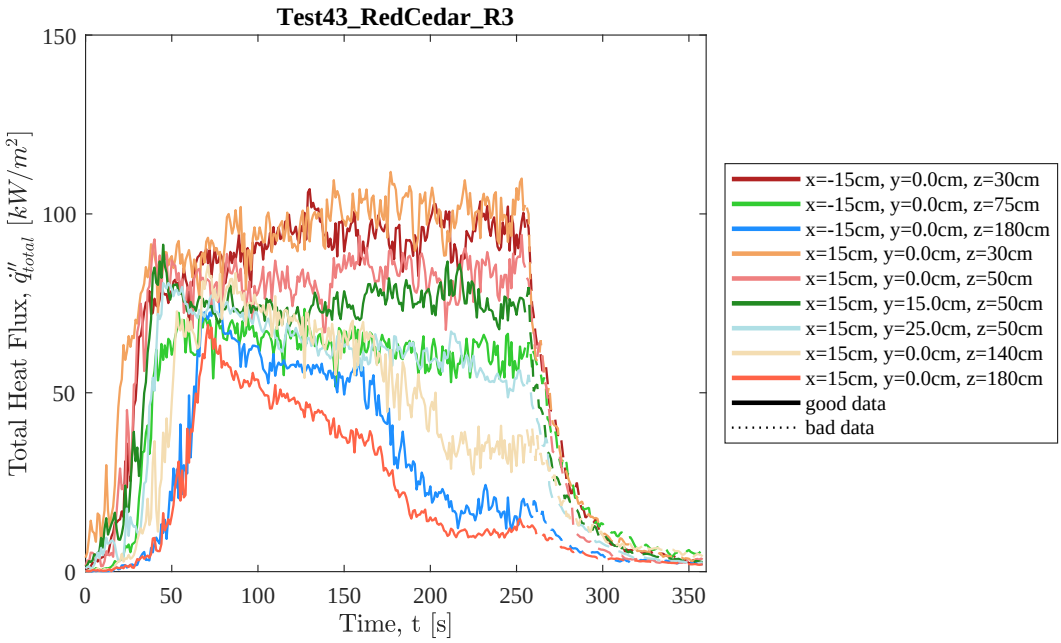

Fig. 235. Total flame to surface flame heat flux to water-cooled Schmidt-Boelter heat flux gauges as measured in Test 43 RedCedar R3. Here, raw, unsmoothed original measurments are plotted from each gauges as a function of time. Solid lines highlight values of $\dot{q}''_{\text{total}}$ that were identified by manual review as ”good” (see Sec. 3.1.1) and dotted lines represent ”bad” measurement data that should not be considered for further analysis.

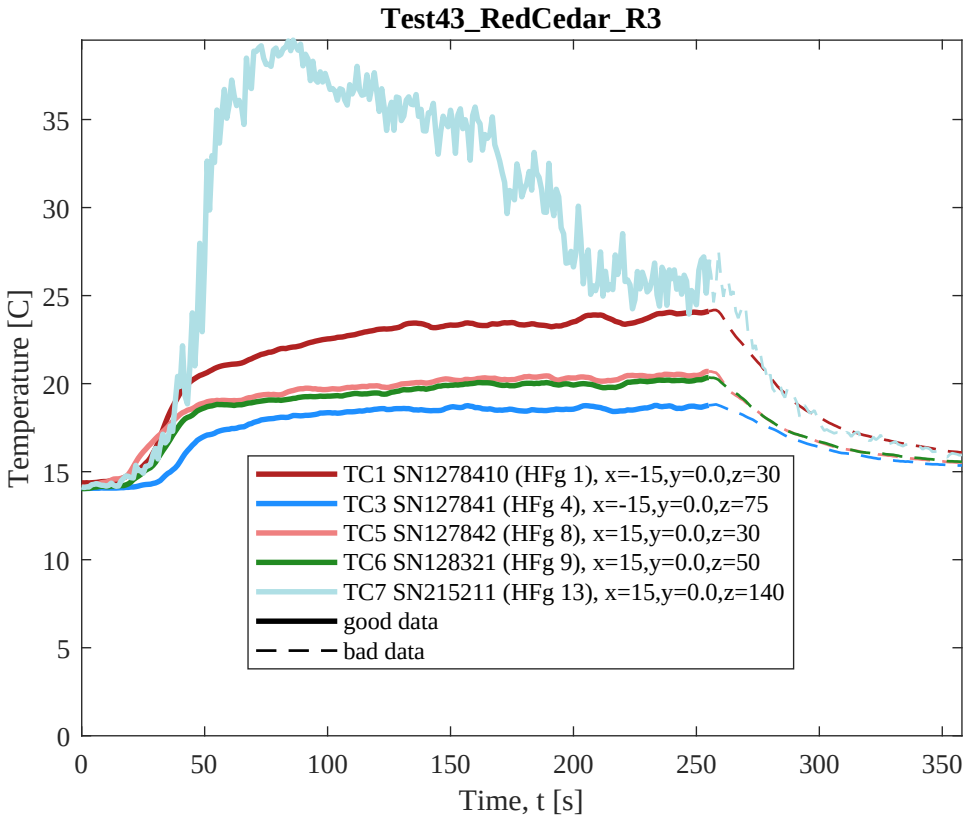

Fig. 236. Temperature of water-cooled Schmidt-Boelter heat flux gauges during Test 43 RedCedar R3.

Shielded Gauges

Measurements of total and radiation heat flux recorded by shielded heat flux gauges (Sec. efssec: qrad). Gauge shields were removed at 148, 148, 146, and 147 seconds (gauges 2, 3, 5 and 6, respectively).

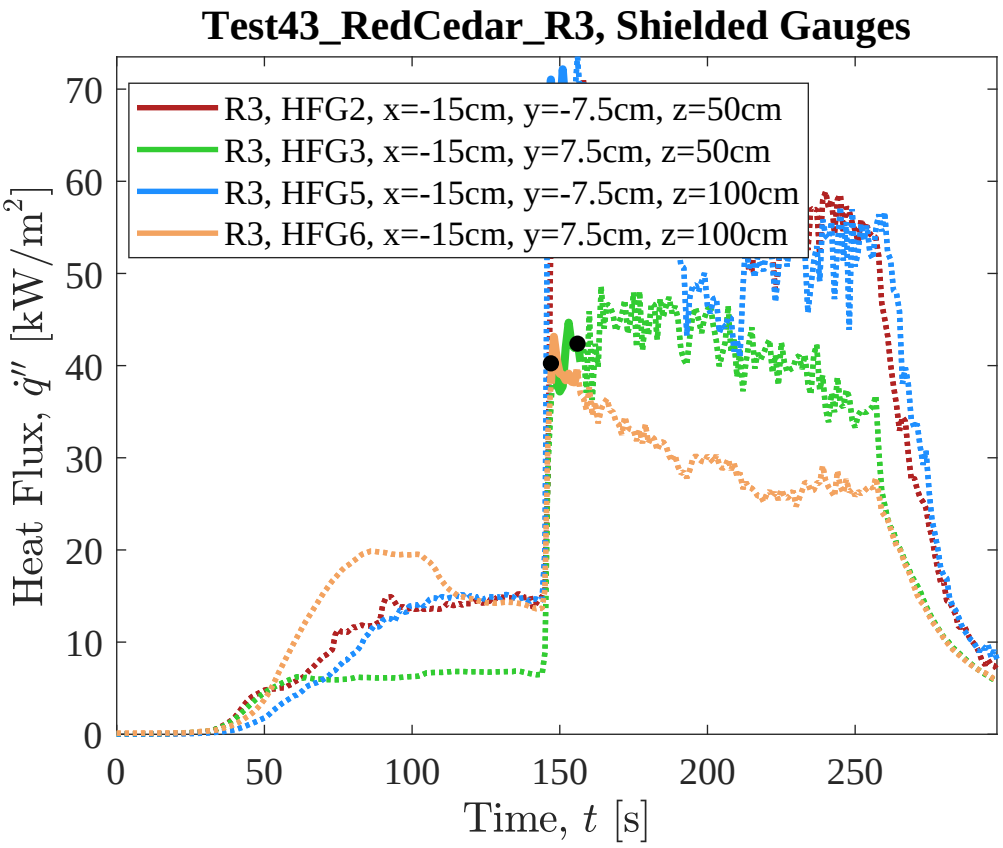

Fig. 237. Shielded gauge data for Test43 RedCedar R3.

Test 65 RedCedar R4

Test Description
7/8 in. thick, 22.5in. wide, 96 in. tall (in two sections, each 11.25in.x96in.) planks of Western Red Cedar mounted to 1in. thick Marinite board (new Marinite). Panels were ignited using a rectangular propane burner (60 kW nominal heat release rate) filled with layers of Pea Gravel, Sand, and Kaowool Insulation (i.e., the 'Final Burner configuration'; see Fig. 12). The burner was kept on throughout the experiment until $t = 480$ s. Heat flux gauges were mounted flush with the fuel's surface between $z = 20$ cm and $z = 20$ cm; heat flux measurements are considered reliable for further analysis until peak HRR was measured.

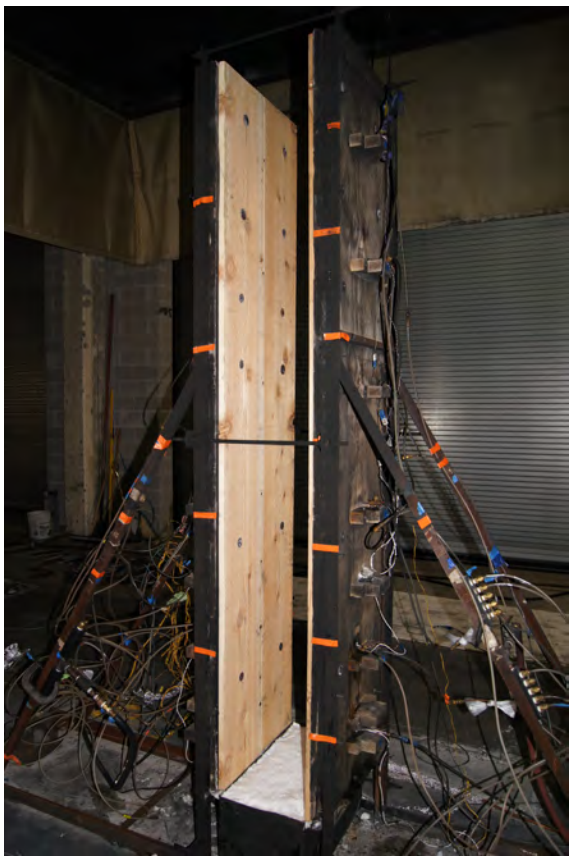

(a) Pre-test

(b) Ignition

(c) Peak HRR

(d) End of Test

Fig. 238. Photographs of Test 65 RedCedar R4.

Heat Release Rate, Heat Flux at a Distance, and Species Yields

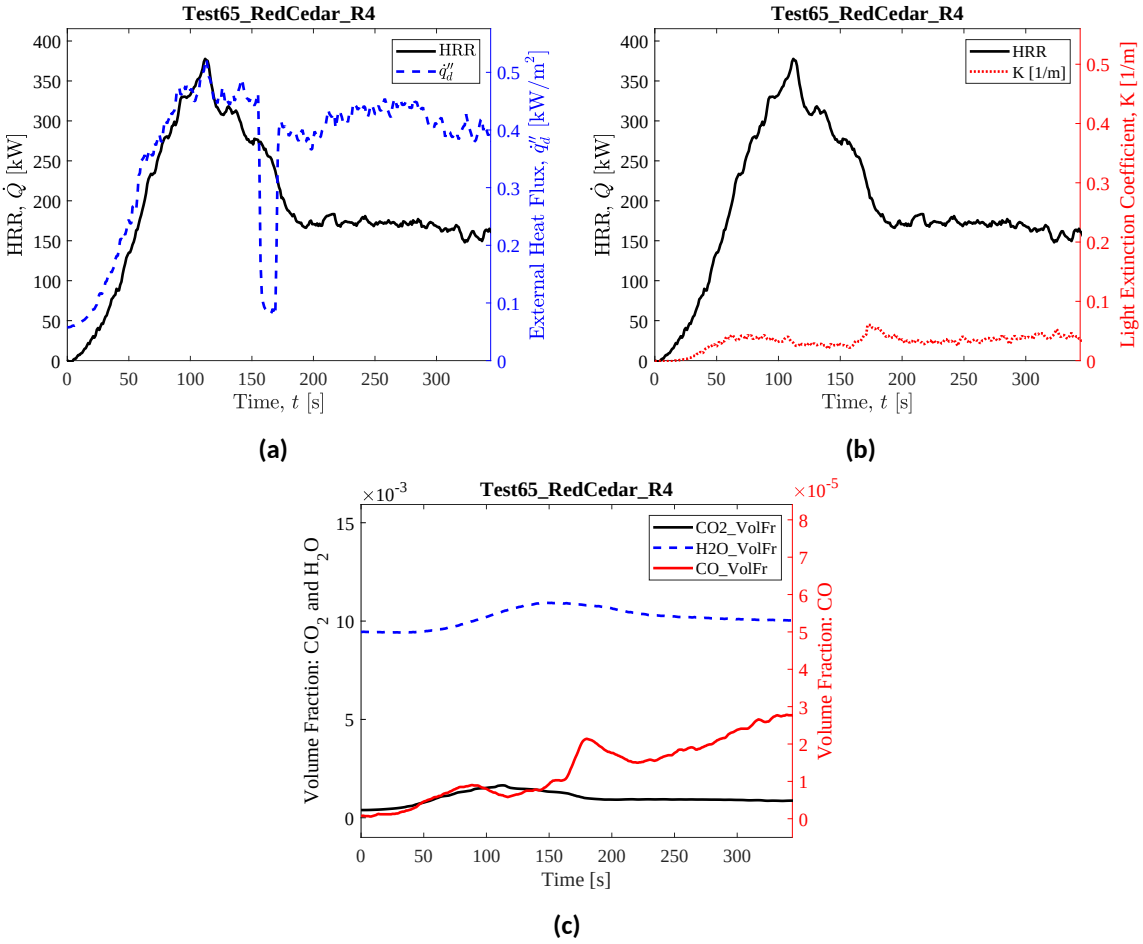

Fig. 239. Test 65 RedCedar R4: (a) Heat release rate and heat flux at a distance, $\dot{q}''_{\mathrm{d}}$ (here, $\dot{q}''_{\mathrm{d}}$ is measured at x =300 cm, y =-305 cm, z =90 cm); (b) Heat release rate and light extinction coefficient, K (smoke particulate in exhaust duct [111]); (c) Time-resolved volume fractions of CO_2, H_2O, and CO.

Flame Heat Flux

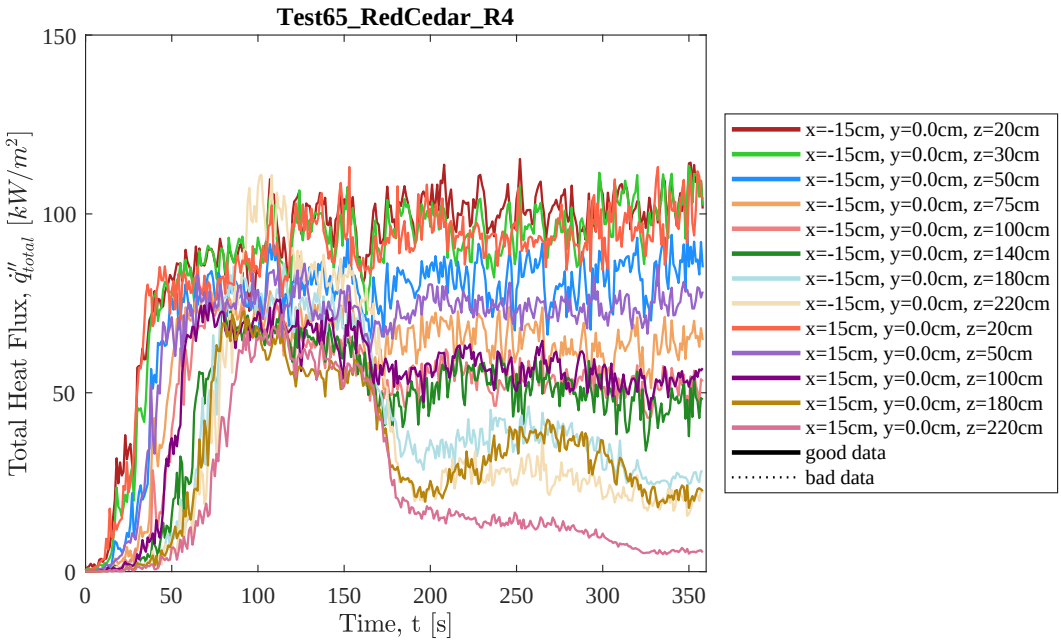

Fig. 240. Total flame to surface flame heat flux to water-cooled Schmidt-Boelter heat flux gauges as measured in Test 65 RedCedar R4. Here, raw, unsmoothed original measurments are plotted from each gauges as a function of time. Solid lines highlight values of $\dot{q}''_{\text{total}}$ that were identified by manual review as ”good” (see Sec. 3.1.1) and dotted lines represent ”bad” measurement data that should not be considered for further analysis.

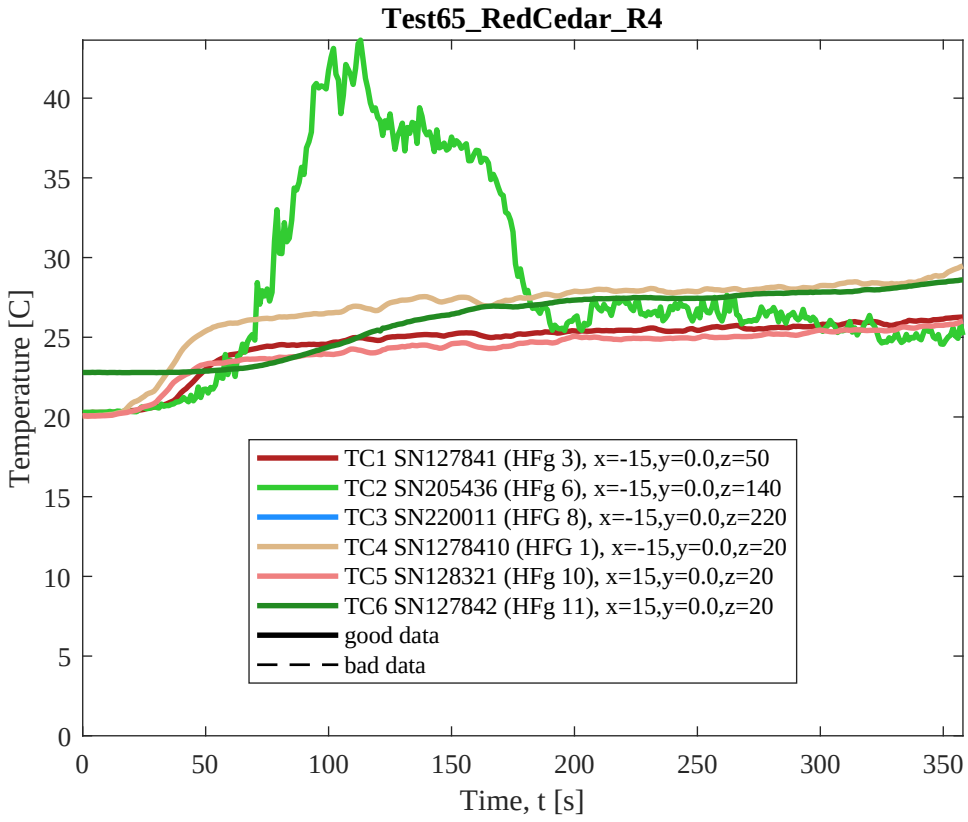

Fig. 241. Temperature of water-cooled Schmidt-Boelter heat flux gauges during Test 65 RedCedar R4.

C.14. SIS Wire - Switchboard Wire

Test 9 SIS Wire R1

Test Description

90 vertically oriented strands of SIS wire, loosely contained w/ steel wire and held to 1in. thick Marinite board with steel wire. Panels were ignited using a rectangular propane burner (60 kW nominal heat release rate) filled with layers of Pea Gravel, Sand, and Kaowool Insulation (i.e., the 'Final Burner configuration'; see Fig. 12). The burner was kept on throughout the experiment until $t = 1500$ s, at which time flames quickly self-extinguished. Flame to wall heat flux measurements were not recorded in this test.

(a) Pre-test

(b) Ignition

(c) Peak HRR

(d) End of Test

Fig. 242. Photographs of Test 9 SIS Wire R1.

Heat Release Rate, Heat Flux at a Distance, and Species Yields

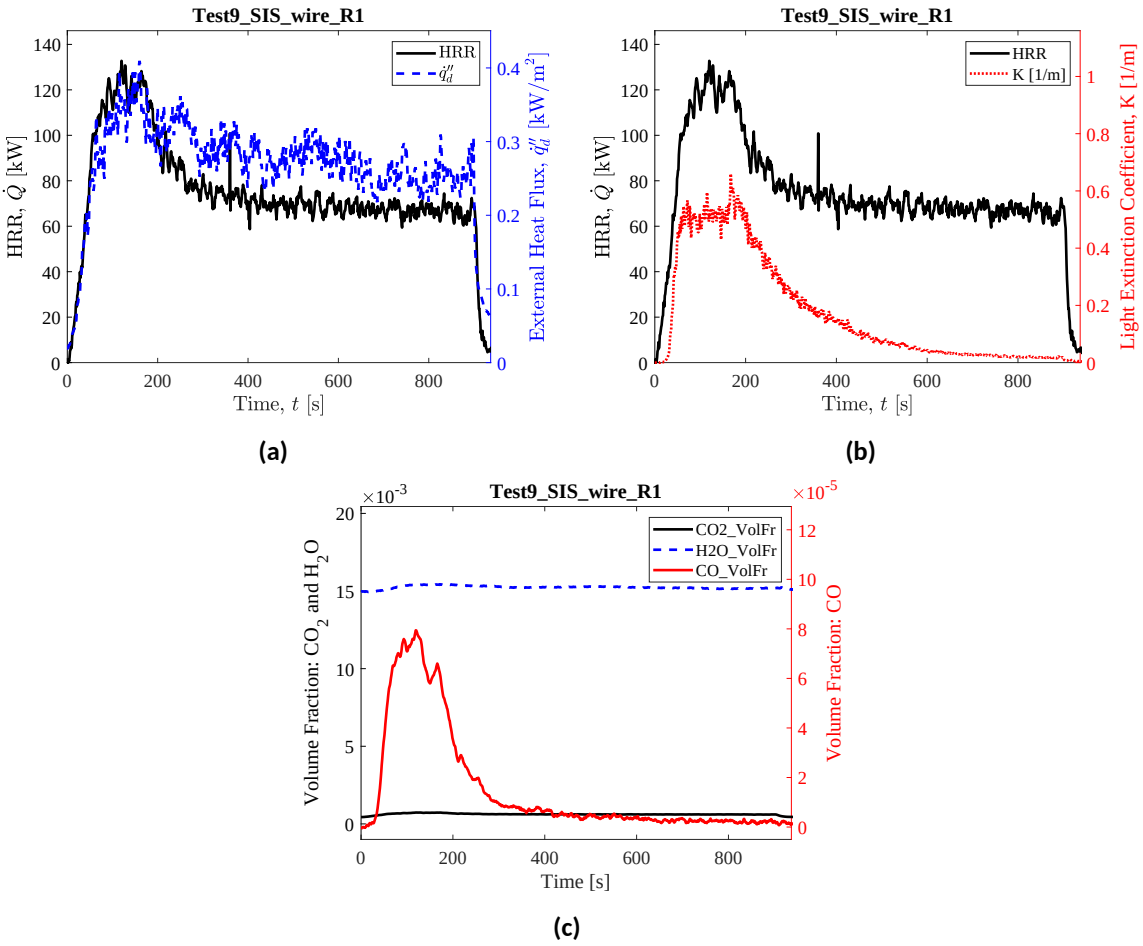

Fig. 243. Test 9 SIS Wire R1: (a) Heat release rate and heat flux at a distance, $\dot{q}''_{\mathrm{d}}$ (here, $\dot{q}''_{\mathrm{d}}$ is measured at x =-100 cm, y =-300 cm, z =90 cm); (b) Heat release rate and light extinction coefficient, K (smoke particulate in exhaust duct [111]); (c) Time-resolved volume fractions of CO_2, H_2O, and CO.

Test 10 SIS Wire R2

Test Description

96 vertically oriented strands of SIS wire, loosely contained w/ steel wire and attached to 1/4 in. thick, 24 in. wide, 96 in. tall (in two sections, each 24 in.x48in.) panels of GPO-3 mounted to 1in. thick Marinite board. Panels were ignited using a rectangular propane burner (60 kW nominal heat release rate) filled with layers of Pea Gravel, Sand, and Kaowool Insulation (i.e., the 'Final Burner configuration'; see Fig. 12). The burner was kept on throughout the experiment until $t = 900$ s, at which time flames quickly self-extinguished. Heat flux gauges were mounted flush with the fuel's surface (left panel only) between $z = 20$ cm and $z = 140$ cm.

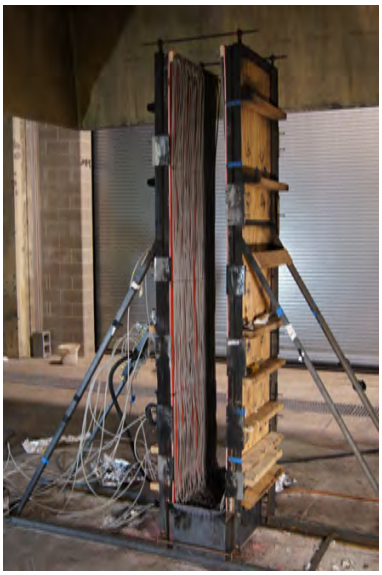

(a) Pre-test

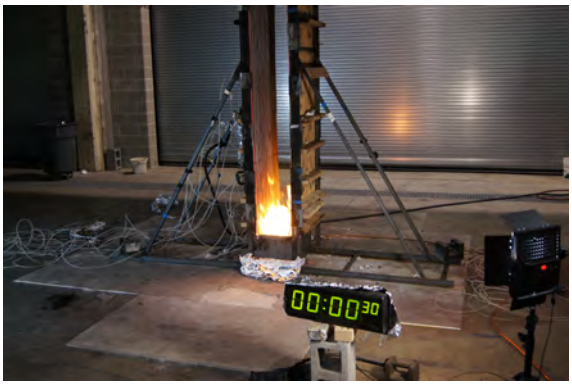

(b) Ignition

(c) Peak HRR

(d) End of Test

Fig. 244. Photographs of Test 10 SIS Wire R2.

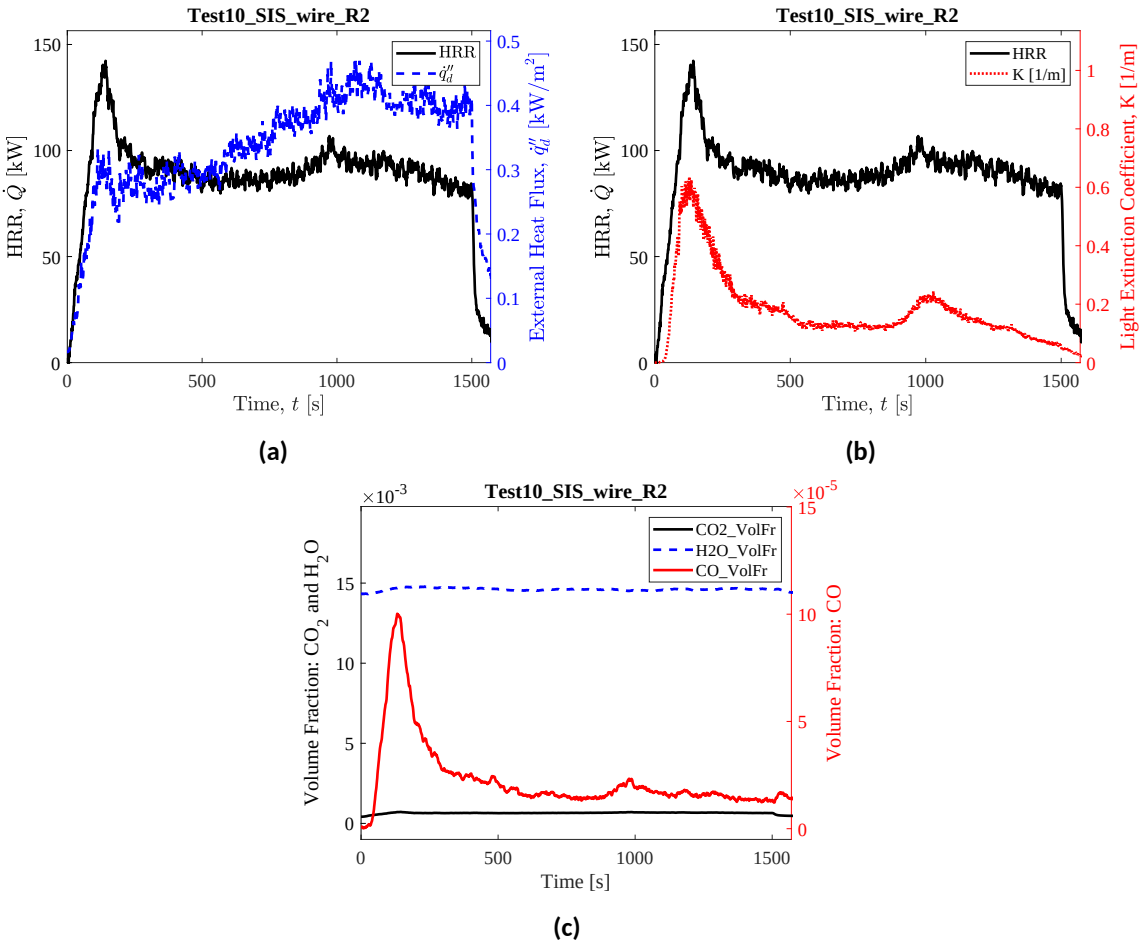

Fig. 245. Test 10 SIS Wire R2: (a) Heat release rate and heat flux at a distance, $\dot{q}''_{\mathrm{d}}$ (here, $\dot{q}''_{\mathrm{d}}$ is measured at x =-100 cm, y =-300 cm, z =90 cm); (b) Heat release rate and light extinction coefficient, K (smoke particulate in exhaust duct [111]); (c) Time-resolved volume fractions of CO_2, H_2O, and CO.

Flame Heat Flux

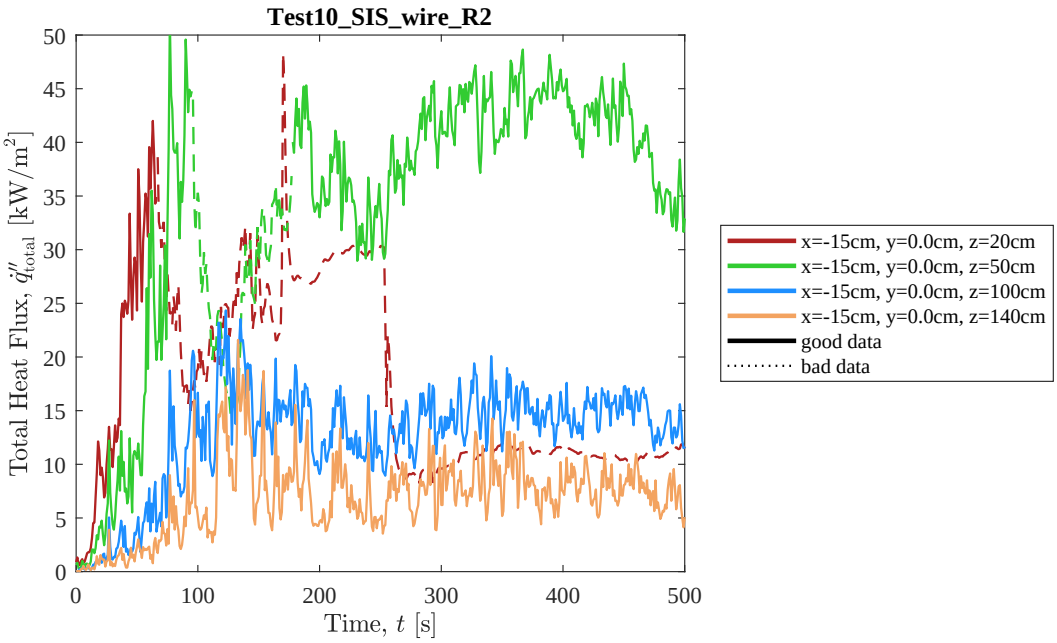

Fig. 246. Total flame to surface flame heat flux to water-cooled Schmidt-Boelter heat flux gauges as measured in Test 10 SIS Wire R2. Here, raw, unsmoothed original measurments are plotted from each gauges as a function of time. Solid lines highlight values of $\dot{q}''_{\text{total}}$ that were identified by manual review as ”good” (see Sec. 3.1.1) and dotted lines represent ”bad” measurement data that should not be considered for further analysis.

C.15. XLPE Foam - Cross-linked Polyethylene Foam

Test 18 XLPE2 R1

Test Description

1 in. thick, 24 in. wide, 96 in. tall panels of XLPE foam (2lb/ft3 density) backed by an alumninum foil layer and held by wire to 1 in. thick Marinite board. Panels were ignited using a rectangular propane burner (60 kW nominal heat release rate) filled with layers of Pea Gravel, Sand, and Kaowool Insulation (i.e., the 'Final Burner configuration'; see Fig. 12). The burner was shut off ($t = 40$ s) and shielded ($t = 50$ s) after sustained flaming of both walls was achieved. Flame to wall heat flux measurements were not recorded in this test.

(a) Pre-test

(b) Ignition

(c) Peak HRR

(d) End of Test

Fig. 247. Photographs of Test 18 XLPE2 R1.

Heat Release Rate, Heat Flux at a Distance, and Species Yields

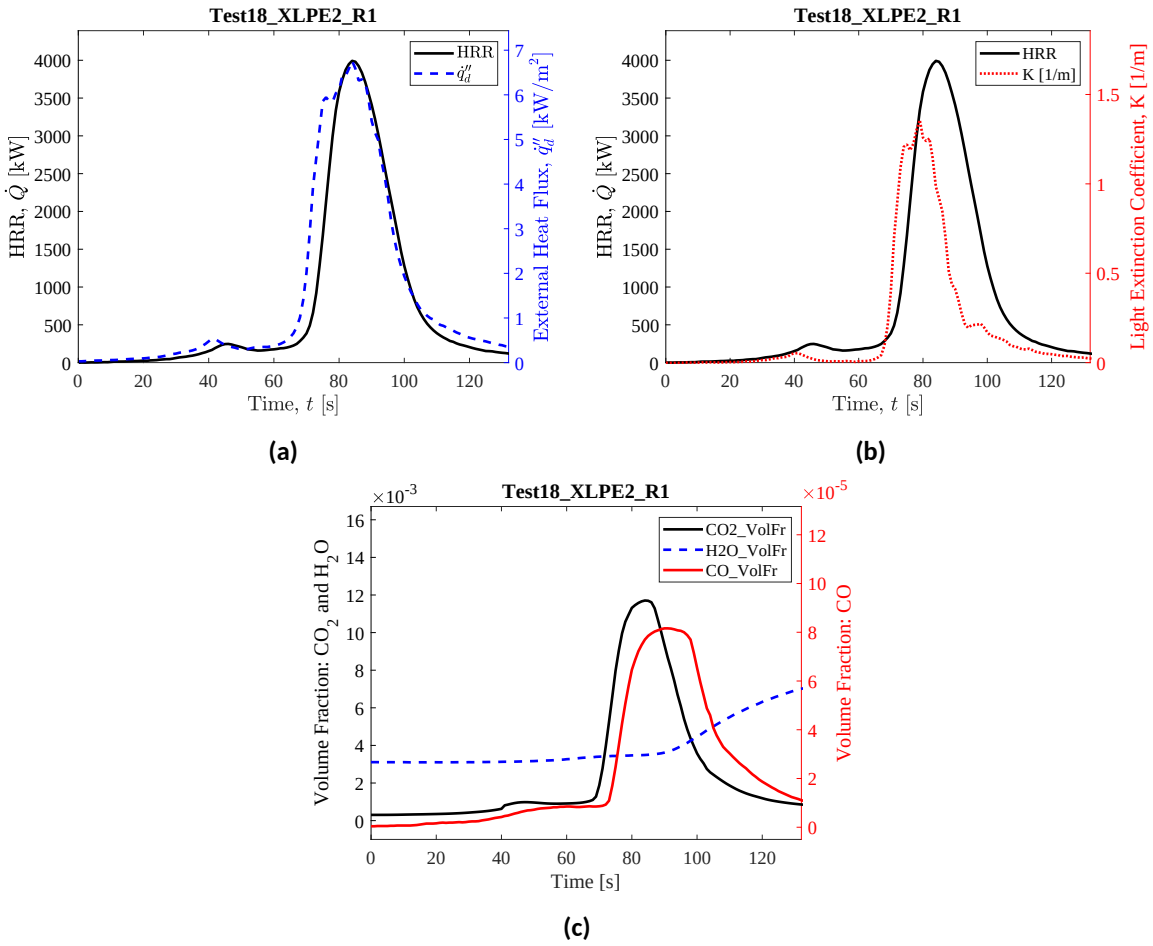

Fig. 248. Test 18 XLPE2 R1: (a) Heat release rate and heat flux at a distance, $\dot{q}''_{\mathrm{d}}$ (here, $\dot{q}''_{\mathrm{d}}$ is measured at x =-100 cm, y =-300 cm, z =90 cm); (b) Heat release rate and light extinction coefficient, K (smoke particulate in exhaust duct [111]); (c) Time-resolved volume fractions of CO_2, H_2O, and CO.

Test 23 XLPE2 R2

Test Description

1 in. thick, 24 in. wide, 96 in. tall panels of XLPE foam (2lb/ft3 density) backed by an alumninum foil layer and held by wire to 1 in. thick Marinite board. Panels were ignited using a rectangular propane burner (60 kW nominal heat release rate) filled with layers of Pea Gravel, Sand, and Kaowool Insulation (i.e., the 'Final Burner configuration'; see Fig. 12). The burner was shut off ($t = 40$ s) but not shielded after sustained flaming of both walls was achieved. This is the only test on XLPE foam where the burner was not shielded; fire growth rate was substantially faster in this test versus XLPE2 Test R1. Flame to wall heat flux measurements were not recorded in this test.

(a) Pre-test

(b) Ignition

(c) Peak HRR

(d) End of Test

Fig. 249. Photographs of Test 23 XLPE2 R2.

Heat Release Rate, Heat Flux at a Distance, and Species Yields

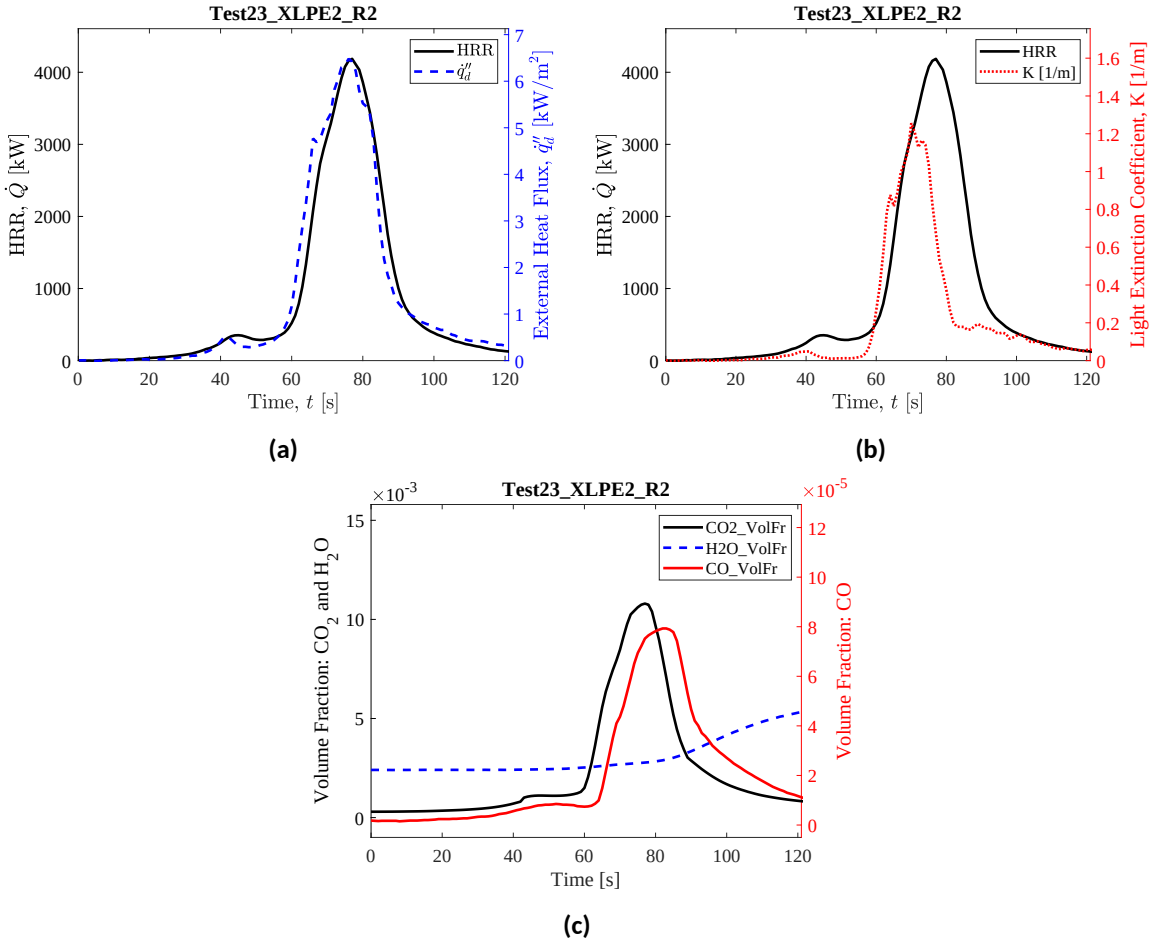

Fig. 250. Test 23 XLPE2 R2: (a) Heat release rate and heat flux at a distance, $\dot{q}''_{\mathrm{d}}$ (here, $\dot{q}''_{\mathrm{d}}$ is measured at x =-150 cm, y =-300 cm, z =90 cm); (b) Heat release rate and light extinction coefficient, K (smoke particulate in exhaust duct [111]); (c) Time-resolved volume fractions of CO_2, H_2O, and CO.

Test 58 XLPE4 R1

Test Description

1 in. thick, 24 in. wide, 96 in. tall panels of XLPE foam (4lb/ft3 density) backed by an alumninum foil layer and held by wire to 1 in. thick Marinite Board. Panels were ignited using a rectangular propane burner (60 kW nominal heat release rate) filled with layers of Pea Gravel, Sand, and Kaowool Insulation (i.e., the 'Final Burner configuration'; see Fig. 12). The burner was shut off ($t = 39$ s) and shielded ($t = 42$ s) after sustained flaming of both walls was achieved. Flame to wall heat flux measurements were not recorded in this test.

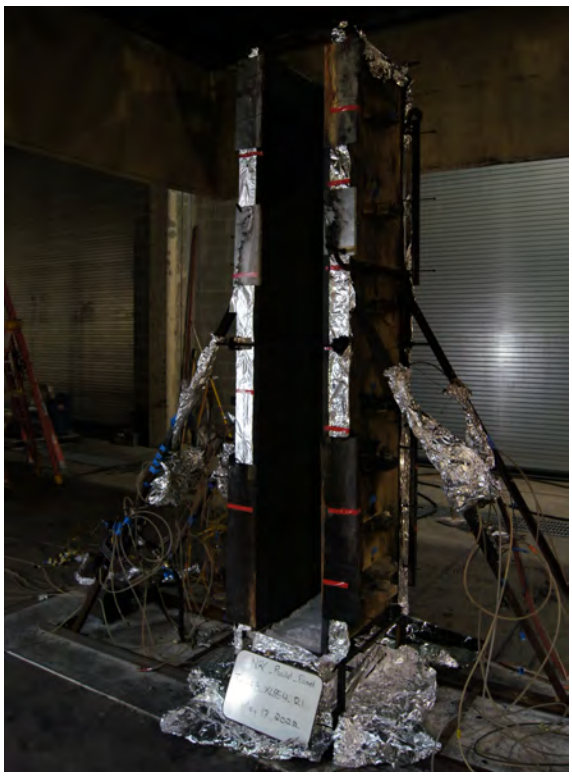

(a) Pre-test

(b) Ignition

(c) Peak HRR

(d) End of Test

Fig. 251. Photographs of Test 58 XLPE4 R1.

Heat Release Rate, Heat Flux at a Distance, and Species Yields

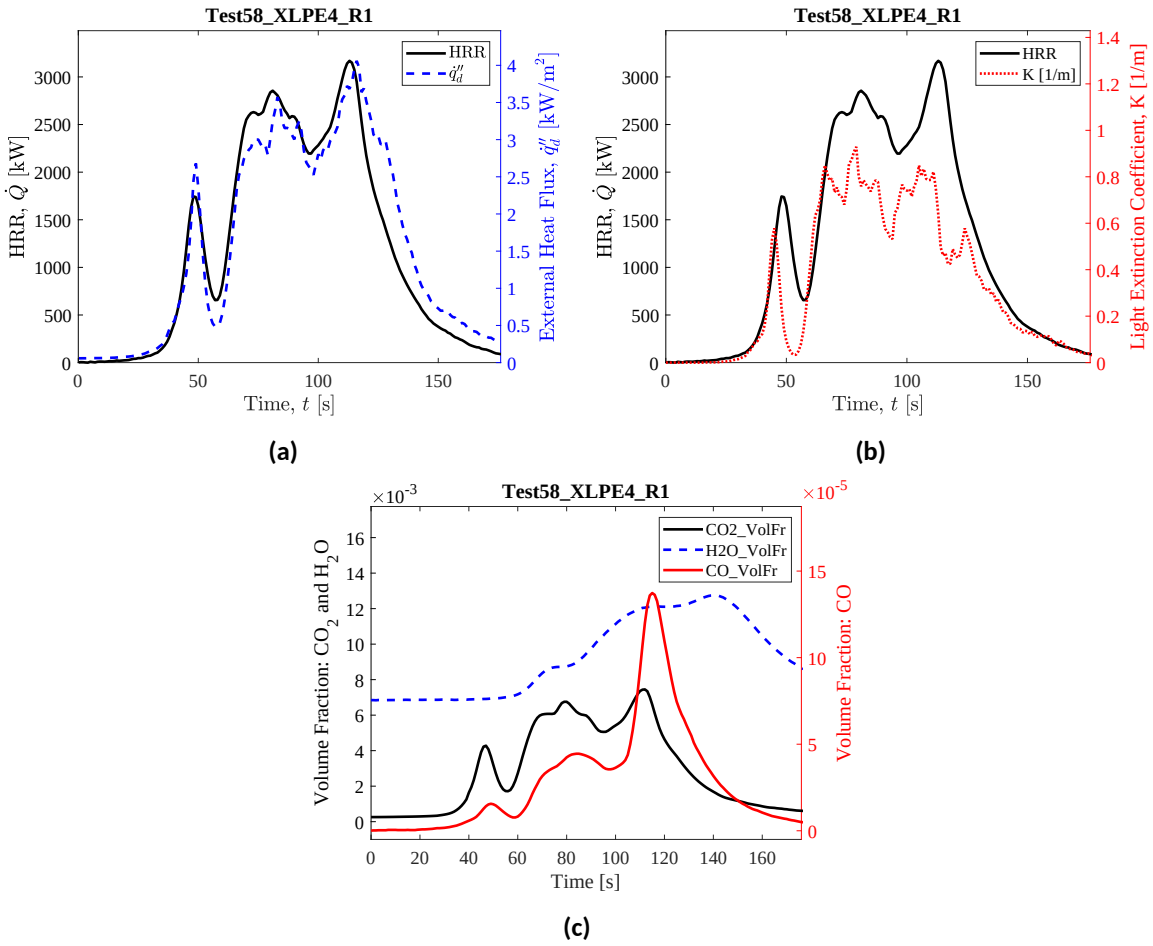

Fig. 252. Test 58 XLPE4 R1: (a) Heat release rate and heat flux at a distance, $\dot{q}''_{\mathrm{d}}$ (here, $\dot{q}''_{\mathrm{d}}$ is measured at x =300 cm, y =-305 cm, z =90 cm); (b) Heat release rate and light extinction coefficient, K (smoke particulate in exhaust duct [111]); (c) Time-resolved volume fractions of CO_2, H_2O, and CO.

Test 59 XLPE4 R2

Test Description
1 in. thick, 24 in. wide, 96 in. tall panels of XLPE foam (4lb/ft3 density) backed by an alumninum foil layer and held by wire to 1 in. thick Marinite Board. Panels were ignited using a rectangular propane burner (60 kW nominal heat release rate) filled with layers of Pea Gravel, Sand, and Kaowool Insulation (i.e., the 'Final Burner configuration'; see Fig. 12). The burner was shut off ($t = 35$ s) and shielded ($t = 37$ s) after sustained flaming of both walls was achieved. Flame to wall heat flux measurements were not recorded in this test.

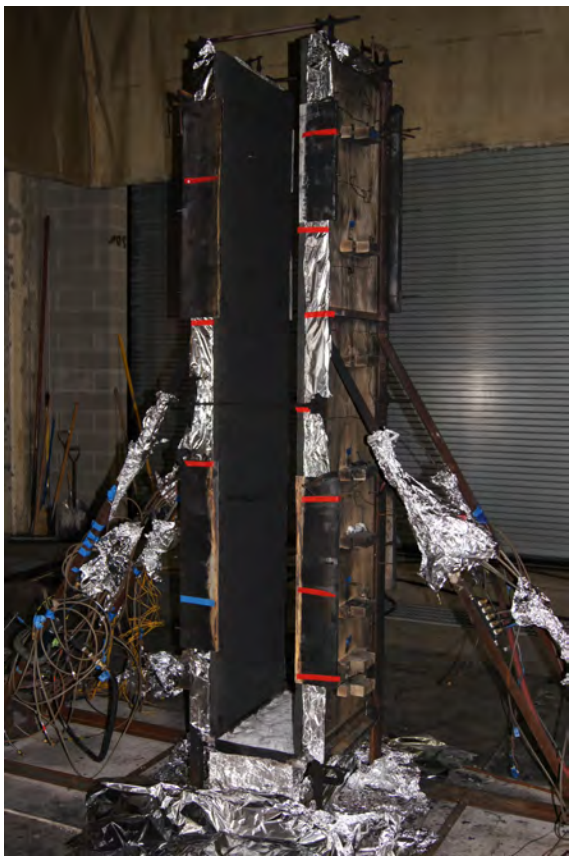

(a) Pre-test

(b) Ignition

(c) Peak HRR

(d) End of Test

Fig. 253. Photographs of Test 59 XLPE4 R2.

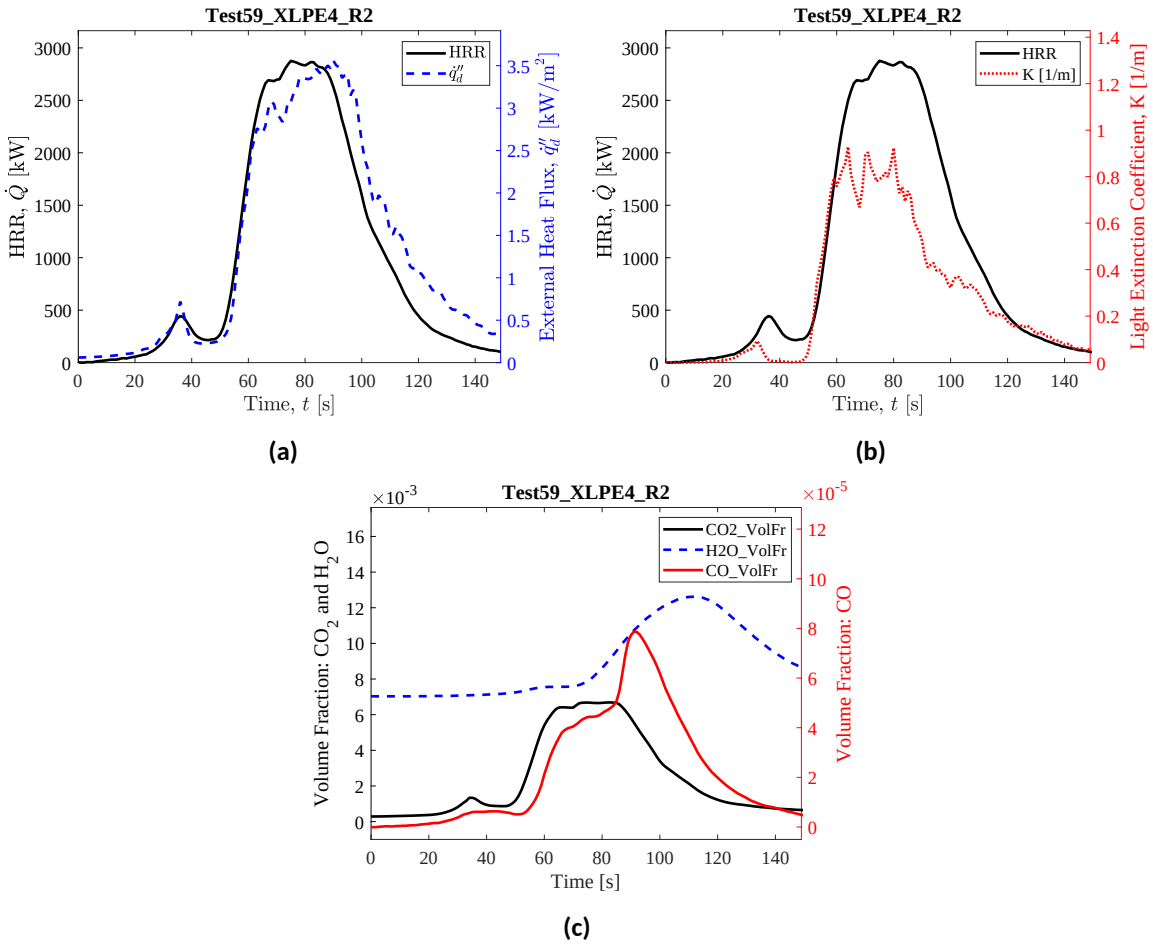

Fig. 254. Test 59 XLPE4 R2: (a) Heat release rate and heat flux at a distance, $\dot{q}''_{\mathrm{d}}$ (here, $\dot{q}''_{\mathrm{d}}$ is measured at x =300 cm, y =-305 cm, z =90 cm); (b) Heat release rate and light extinction coefficient, K (smoke particulate in exhaust duct [111]); (c) Time-resolved volume fractions of CO_2, H_2O, and CO.

Test 60 XLPE4 R3

Test Description
1 in. thick, 24 in. wide, 96 in. tall panels of XLPE foam (4lb/ft3 density) backed by an alumninum foil layer and held by wire to 1 in. thick Marinite Board. Panels were ignited using a rectangular propane burner (60 kW nominal heat release rate) filled with layers of Pea Gravel, Sand, and Kaowool Insulation (i.e., the 'Final Burner configuration'; see Fig. 12). The burner was shut off ($t = 40$ s) and shielded ($t = 40$ s) after sustained flaming of both walls was achieved. Flame to wall heat flux measurements were not recorded in this test.

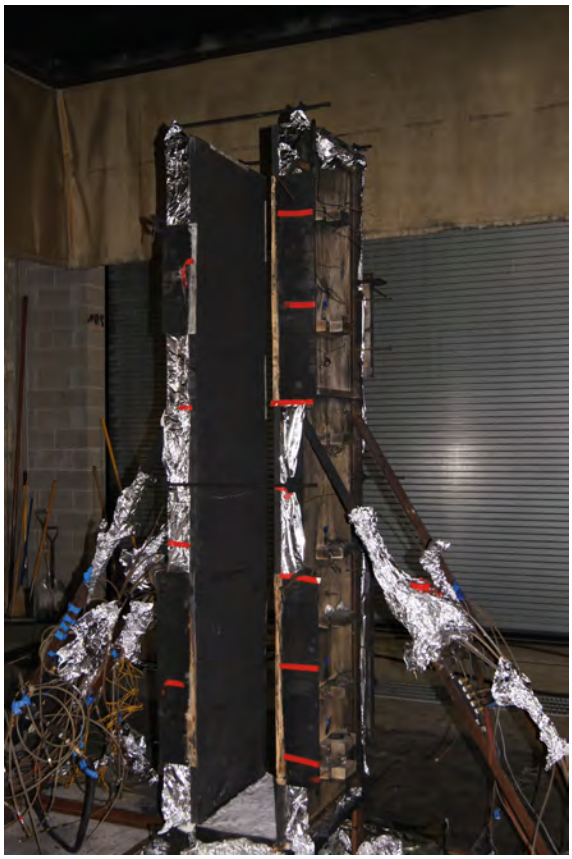

(a) Pre-test

(b) Ignition

(c) Peak HRR

(d) End of Test

Fig. 255. Photographs of Test 60 XLPE4 R3.

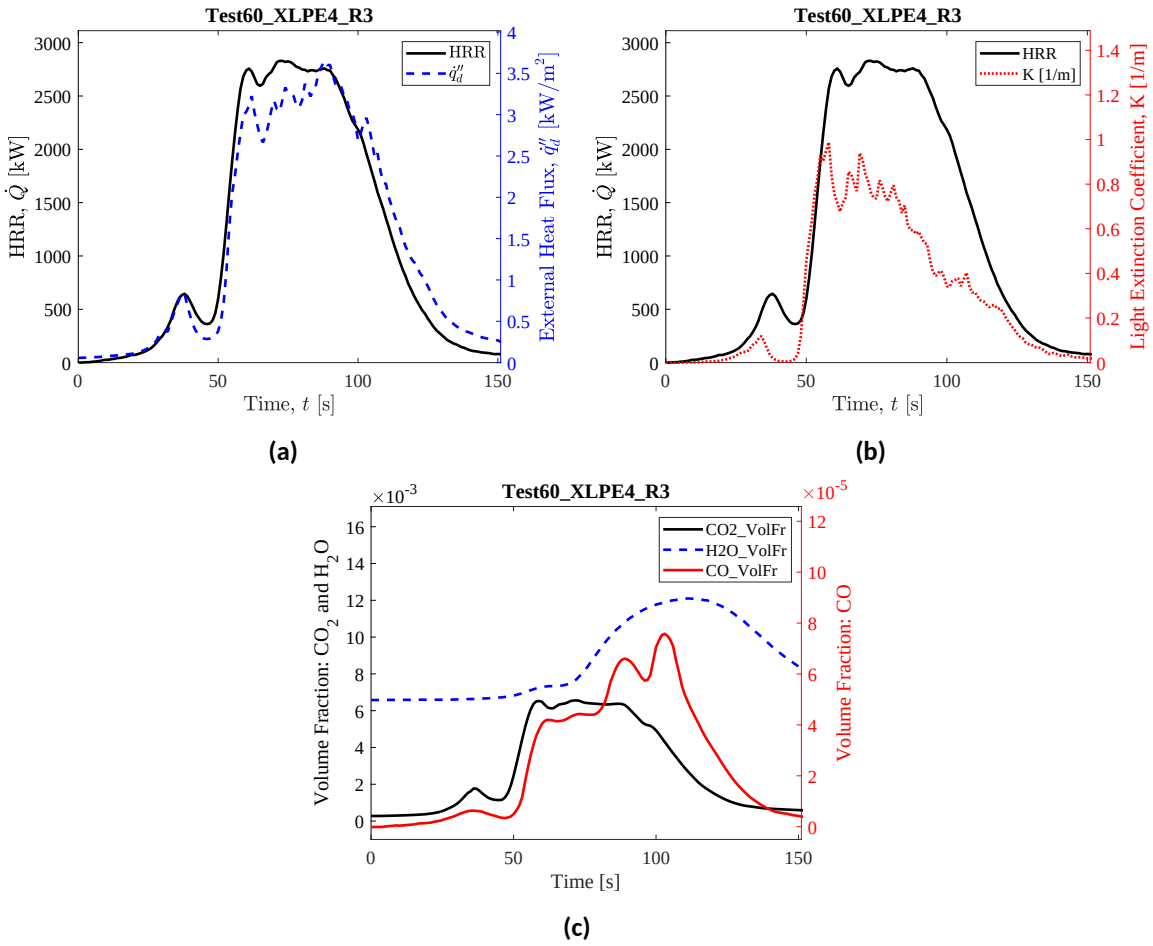

Fig. 256. Test 60 XLPE4 R3: (a) Heat release rate and heat flux at a distance, $\dot{q}''_{\mathrm{d}}$ (here, $\dot{q}''_{\mathrm{d}}$ is measured at x =300 cm, y =-305 cm, z =90 cm); (b) Heat release rate and light extinction coefficient, K (smoke particulate in exhaust duct [111]); (c) Time-resolved volume fractions of CO_2, H_2O, and CO.

Test 19 XLPE6 R1

Test Description

1 in. thick, 24 in. wide, 96 in. tall panels (in two sections, each 24 in.x48in.) of XLPE Foam (6lb/ft3 density) backed by an alumninum foil layer and held by wire to 1 in. thick Marinite board. Panels were ignited using a rectangular propane burner (60 kW nominal heat release rate) filled with layers of Pea Gravel, Sand, and Kaowool Insulation (i.e., the 'Final Burner configuration'; see Fig. 12). The burner was shut off ($t = 41$ s) and shielded ($t = 51$ s) after sustained flaming of both walls was achieved. Flame to wall heat flux measurements were not recorded in this test.

(a) Pre-test

(b) Ignition

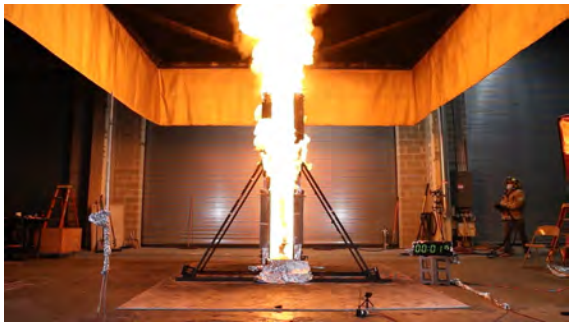

(c) Peak HRR

(d) End of Test

Fig. 257. Photographs of Test 19 XLPE6 R1.

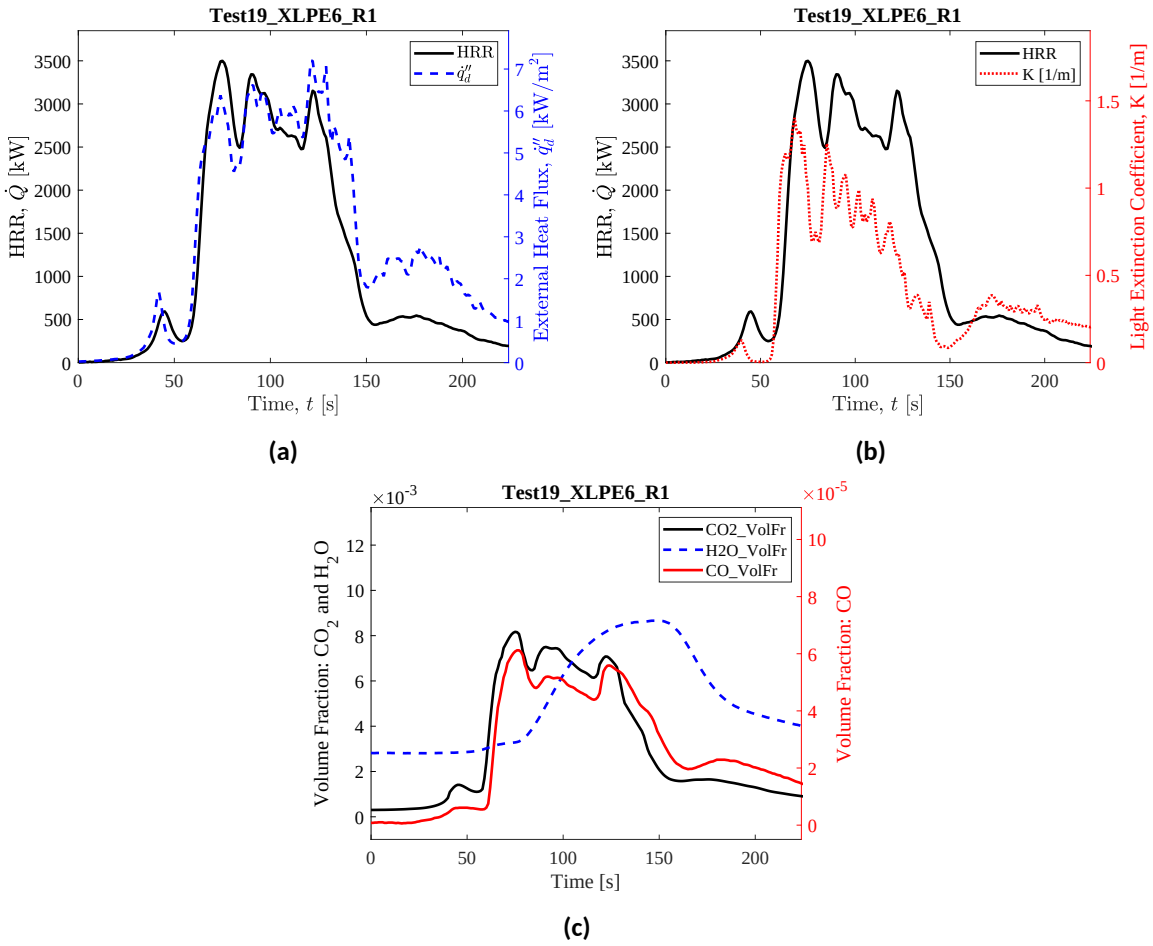

Fig. 258. Test 19 XLPE6 R1: (a) Heat release rate and heat flux at a distance, $\dot{q}''_{\mathrm{d}}$ (here, $\dot{q}''_{\mathrm{d}}$ is measured at x =-100 cm, y =-300 cm, z =90 cm); (b) Heat release rate and light extinction coefficient, K (smoke particulate in exhaust duct [111]); (c) Time-resolved volume fractions of CO_2, H_2O, and CO.

Test 38 XLPE6 R2

Test Description

1 in. thick, 24 in. wide, 96 in. tall panels (in two sections, each 24 in.x48in.) of XLPE Foam (6lb/ft3 density) backed by an alumninum foil layer and held by wire to 1 in. thick Marinite board. Panels were ignited using a rectangular propane burner (60 kW nominal heat release rate) filled with layers of Pea Gravel, Sand, and Kaowool Insulation (i.e., the 'Final Burner configuration'; see Fig. 12). The burner was shut off ($t = 41$ s) and shielded ($t = 50$ s) after sustained flaming of both walls was achieved. Flame to wall heat flux measurements were not recorded in this test.

(a) Pre-test

(b) Ignition

(c) Peak HRR

(d) End of Test

Fig. 259. Photographs of Test 38 XLPE6 R2.

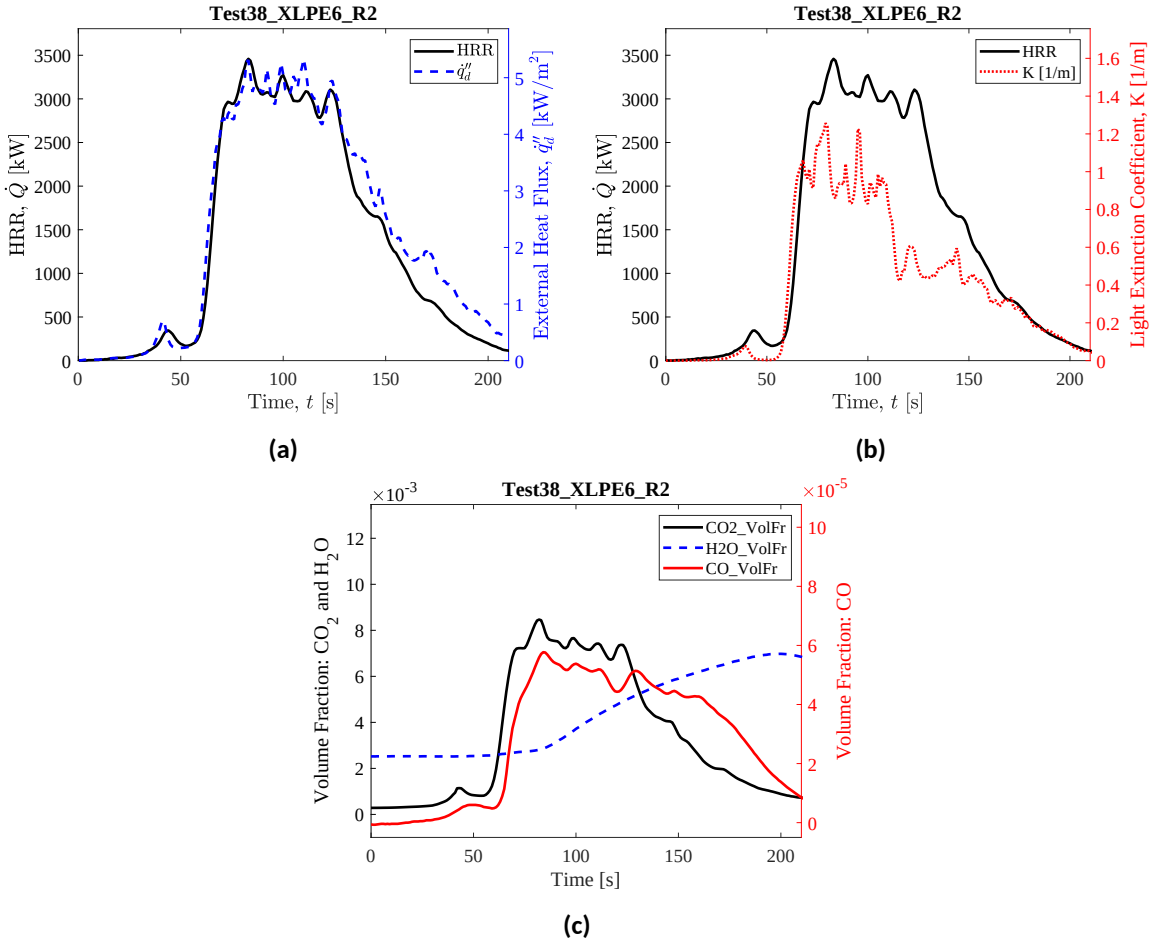

Fig. 260. Test 38 XLPE6 R2: (a) Heat release rate and heat flux at a distance, $\dot{q}''_{\mathrm{d}}$ (here, $\dot{q}''_{\mathrm{d}}$ is measured at x =-232 cm, y =-300 cm, z =90 cm); (b) Heat release rate and light extinction coefficient, K (smoke particulate in exhaust duct [111]); (c) Time-resolved volume fractions of CO_2, H_2O, and CO.

Test 39 XLPE6 R3

Test Description

1 in. thick, 24 in. wide, 96 in. tall panels (in two sections, each 24 in.x48in.) of XLPE Foam (6lb/ft3 density) backed by an aluminum foil layer (only at $z \leq 60$ cm) and held by wire to 1 in. thick Marinite board. Panels were ignited using a rectangular propane burner (60 kW nominal heat release rate) filled with layers of Pea Gravel, Sand, and Kaowool Insulation (i.e., the 'Final Burner configuration'; see Fig. 12). The burner was shut off ($t = 40$ s) and shielded ($t = 48$ s) after sustained flaming of both walls was achieved. Flame to wall heat flux measurements were not recorded in this test.

(a) Pre-test

(b) Ignition

(c) Peak HRR

(d) End of Test

Fig. 261. Photographs of Test 39 XLPE6 R3.

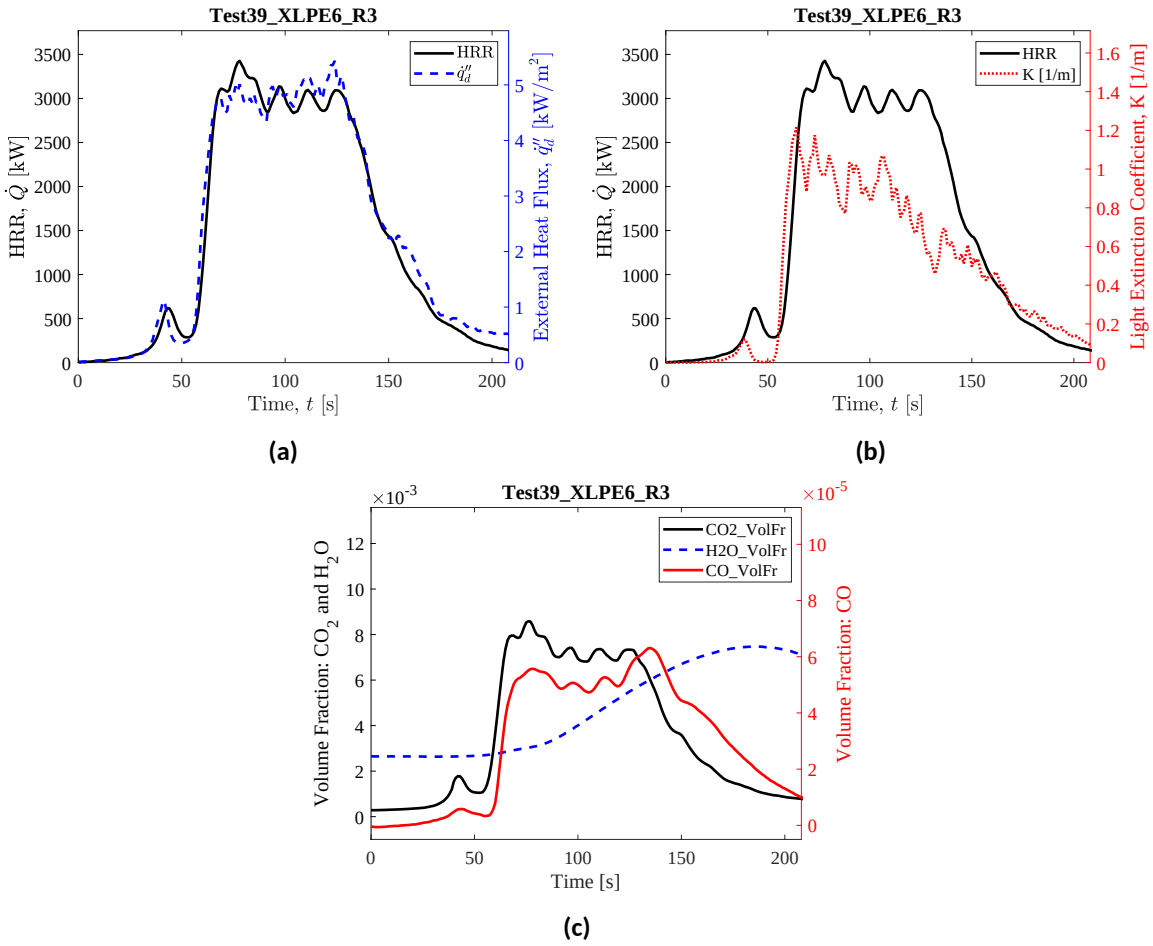

Fig. 262. Test 39 XLPE6 R3: (a) Heat release rate and heat flux at a distance, $\dot{q}''_{\mathrm{d}}$ (here, $\dot{q}''_{\mathrm{d}}$ is measured at x =-232 cm, y =-300 cm, z =90 cm); (b) Heat release rate and light extinction coefficient, K (smoke particulate in exhaust duct [111]); (c) Time-resolved volume fractions of CO_2, H_2O, and CO.

C.16. XPS Foam - Extruded Polystyrene Foam

Test 34 XPSgreen1 R1

Test Description

1 in. thick, 24 in. wide, 96 in. tall panels of Green XPS Foam held by wire to 1 in. thick Marinite board. Panels were ignited using a rectangular propane burner (60 kW nominal heat release rate) filled with layers of Pea Gravel, Sand, and Kaowool Insulation (i.e., the 'Final Burner configuration'; see Fig. 12). The burner was kept on throughout the experiment until samples self-extinguished. Flame to wall heat flux measurements were not recorded in this test.

(a) Pre-test

(b) Ignition

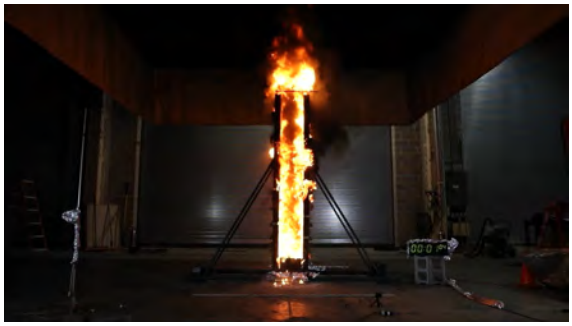

(c) Peak HRR

(d) End of Test

Fig. 263. Photographs of Test 34 XPSgreen1 R1.

Heat Release Rate, Heat Flux at a Distance, and Species Yields

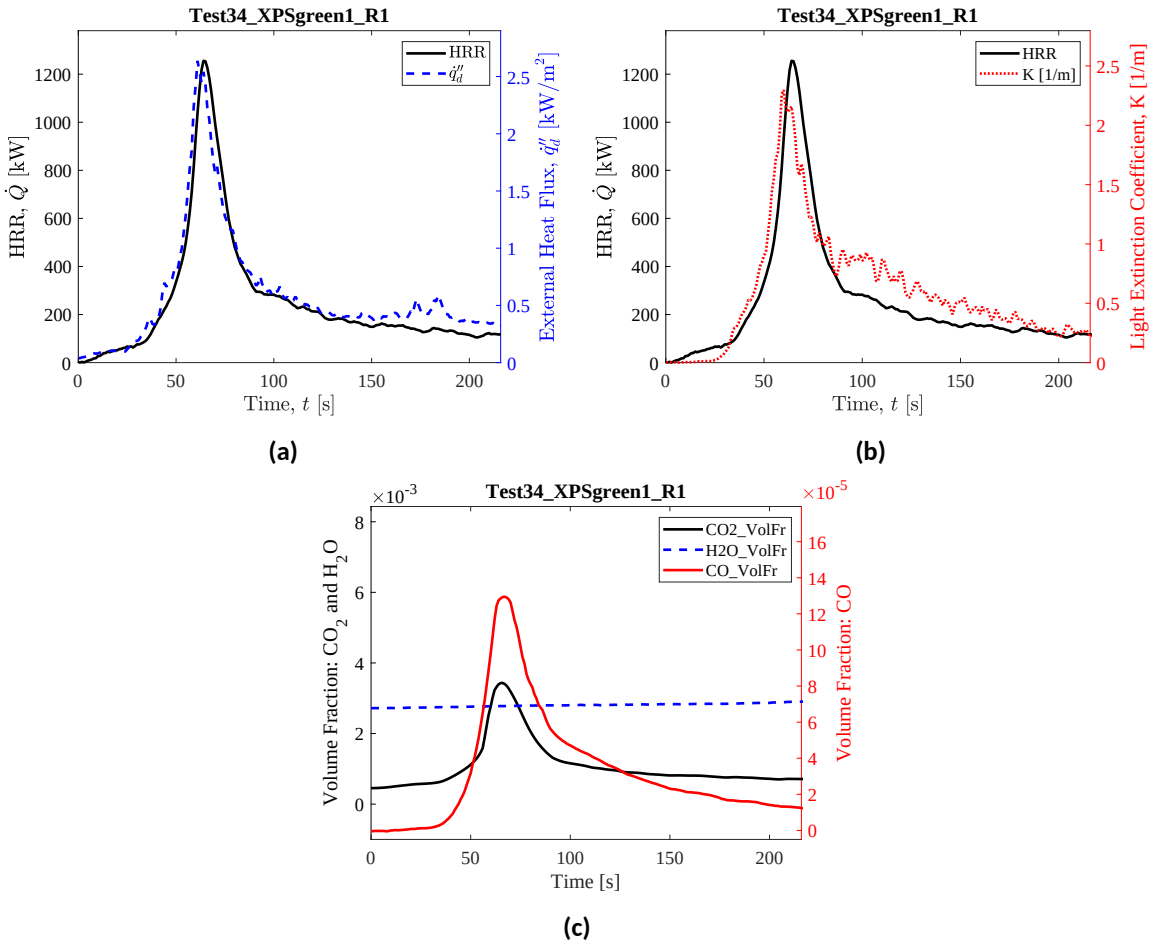

Fig. 264. Test 34 XPSgreen1 R1: (a) Heat release rate and heat flux at a distance, $\dot{q}''_{\mathrm{d}}$ (here, $\dot{q}''_{\mathrm{d}}$ is measured at x =-232 cm, y =-300 cm, z =90 cm); (b) Heat release rate and light extinction coefficient, K (smoke particulate in exhaust duct [111]); (c) Time-resolved volume fractions of CO_2, H_2O, and CO.

Test 36 XPSgreen1 R2

Test Description

1 in. thick, 24 in. wide, 96 in. tall panels of Green XPS Foam held by wire to 1 in. thick Marinite board. Panels were ignited using a rectangular propane burner (60 kW nominal heat release rate) filled with layers of Pea Gravel, Sand, and Kaowool Insulation (i.e., the 'Final Burner configuration'; see Fig. 12). The burner was kept on throughout the experiment until samples self-extinguished. Initially, upward flame spread was delayed because XPS foam samples shrank/collapsed away from the burner flame without fully igniting. Flame to wall heat flux measurements were not recorded in this test.

(a) Pre-test

(b) Ignition

(c) Peak HRR

(d) End of Test

Fig. 265. Photographs of Test 36 XPSgreen1 R2.

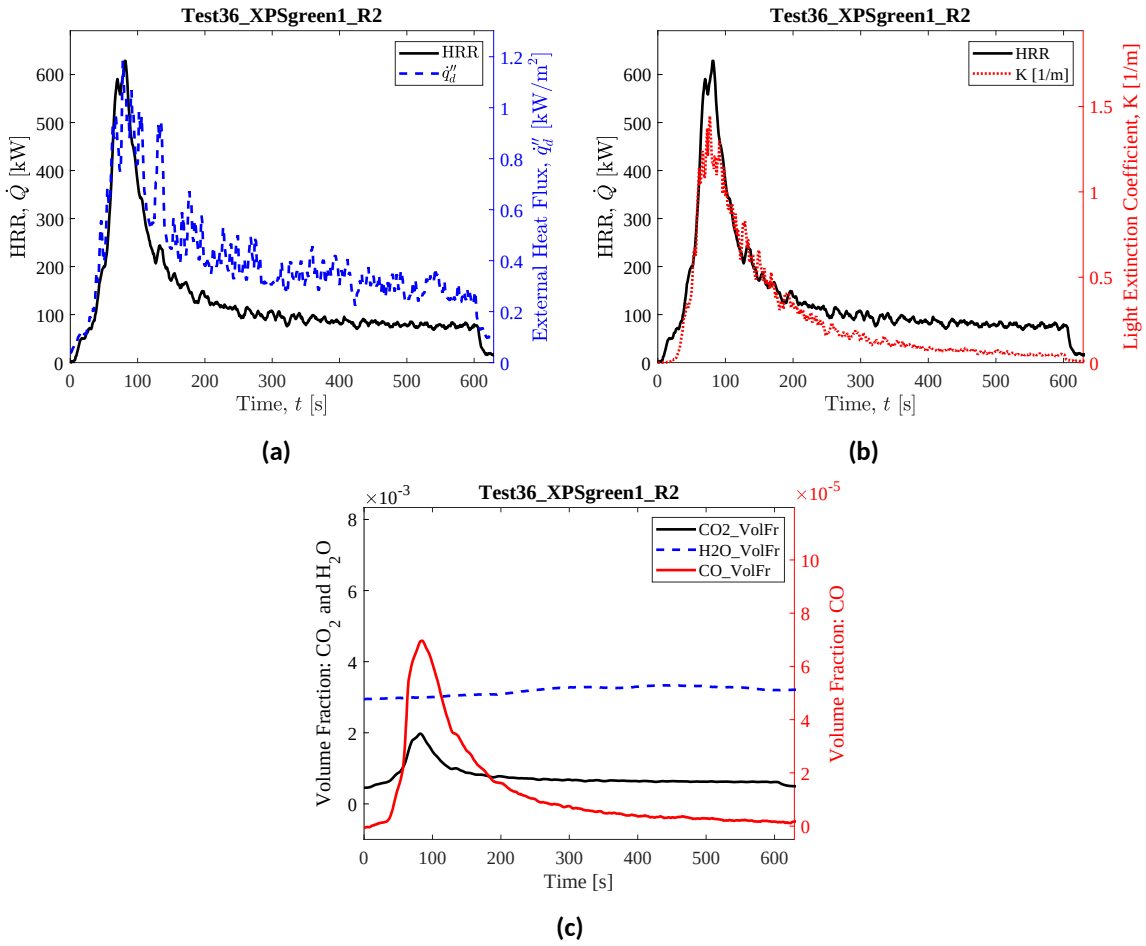

Fig. 266. Test 36 XPSgreen1 R2: (a) Heat release rate and heat flux at a distance, $\dot{q}''_{\mathrm{d}}$ (here, $\dot{q}''_{\mathrm{d}}$ is measured at x =-232 cm, y =-300 cm, z =90 cm); (b) Heat release rate and light extinction coefficient, K (smoke particulate in exhaust duct [111]); (c) Time-resolved volume fractions of CO_2, H_2O, and CO.

Test 62 XPSgreen1 R3

Test Description

3/4 in. thick, 24 in. wide, 96 in. tall panels of Green XPS Foam held by wire to 1 in. thick Marinite board. Panels were ignited using a rectangular propane burner (60 kW nominal heat release rate) filled with layers of Pea Gravel, Sand, and Kaowool Insulation (i.e., the 'Final Burner configuration'; see Fig. 12). The burner was kept on throughout the experiment until samples self-extinguished. Upward flame spread was not observed in this test due to complete sample collapse (melting/shrinking away of samples) near the burner flames without igniting. At the start of XPSgreen1 Test R3, it was observed that foam panels were notably thinner (18.3 mm to 18.6 mm) than the nominal, average thickness (25 mm) of panels used in Tests R1 and R2. Flame to wall heat flux measurements were not recorded in this test.

(a) Pre-test

(b) Ignition

(c) Peak HRR

(d) End of Test

Fig. 267. Photographs of Test 62 XPSgreen1 R3.

Heat Release Rate, Heat Flux at a Distance, and Species Yields

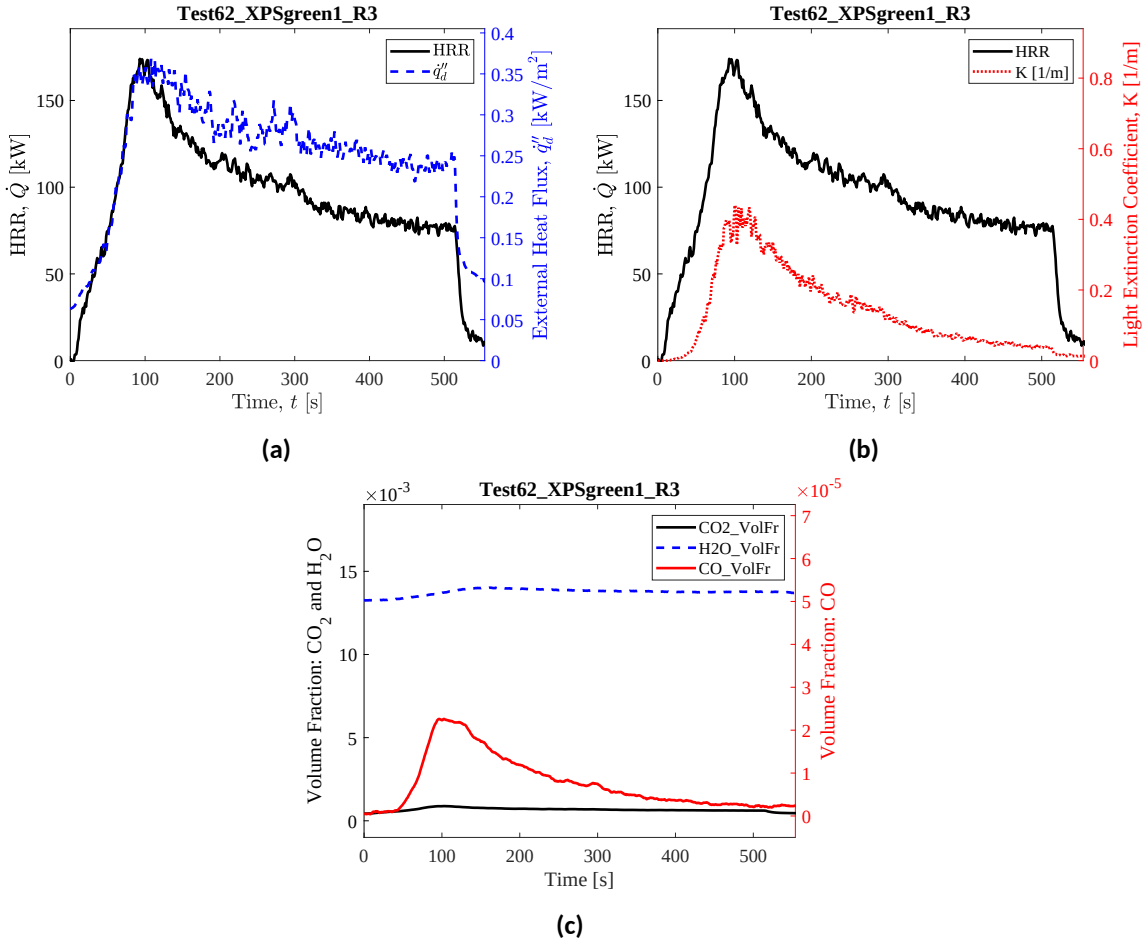

Fig. 268. Test 62 XPSgreen1 R3: (a) Heat release rate and heat flux at a distance, $\dot{q}''_{\mathrm{d}}$ (here, $\dot{q}''_{\mathrm{d}}$ is measured at x =300 cm, y =-305 cm, z =91 cm); (b) Heat release rate and light extinction coefficient, K (smoke particulate in exhaust duct [111]); (c) Time-resolved volume fractions of CO_2, H_2O, and CO.

Test 42 XPSgreen2 R1

Test Description
2 in. thick, 24 in. wide, 96 in. tall panels of Green XPS Foam held by wire to 1 in. thick Marinite board. Panels were ignited using a rectangular propane burner (60 kW nominal heat release rate) filled with layers of Pea Gravel, Sand, and Kaowool Insulation (i.e., the 'Final Burner configuration'; see Fig. 12). The burner was kept on throughout the experiment until samples self-extinguished. Flame to wall heat flux measurements were not recorded in this test.

(a) Pre-test

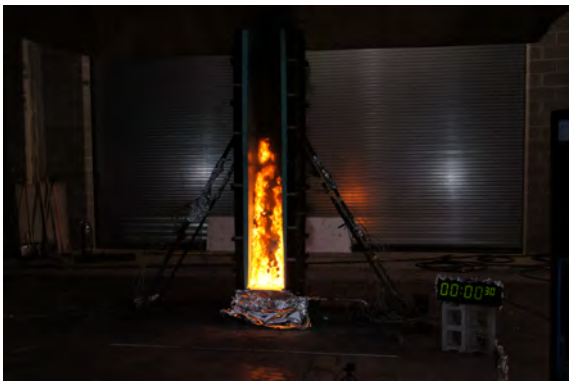

(b) Ignition

(c) Peak HRR

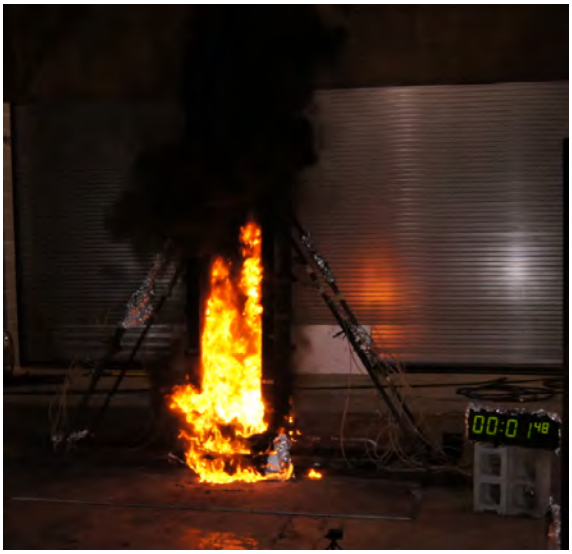

(d) End of Test

Fig. 269. Photographs of Test 42 XPSgreen2 R1.

Heat Release Rate, Heat Flux at a Distance, and Species Yields

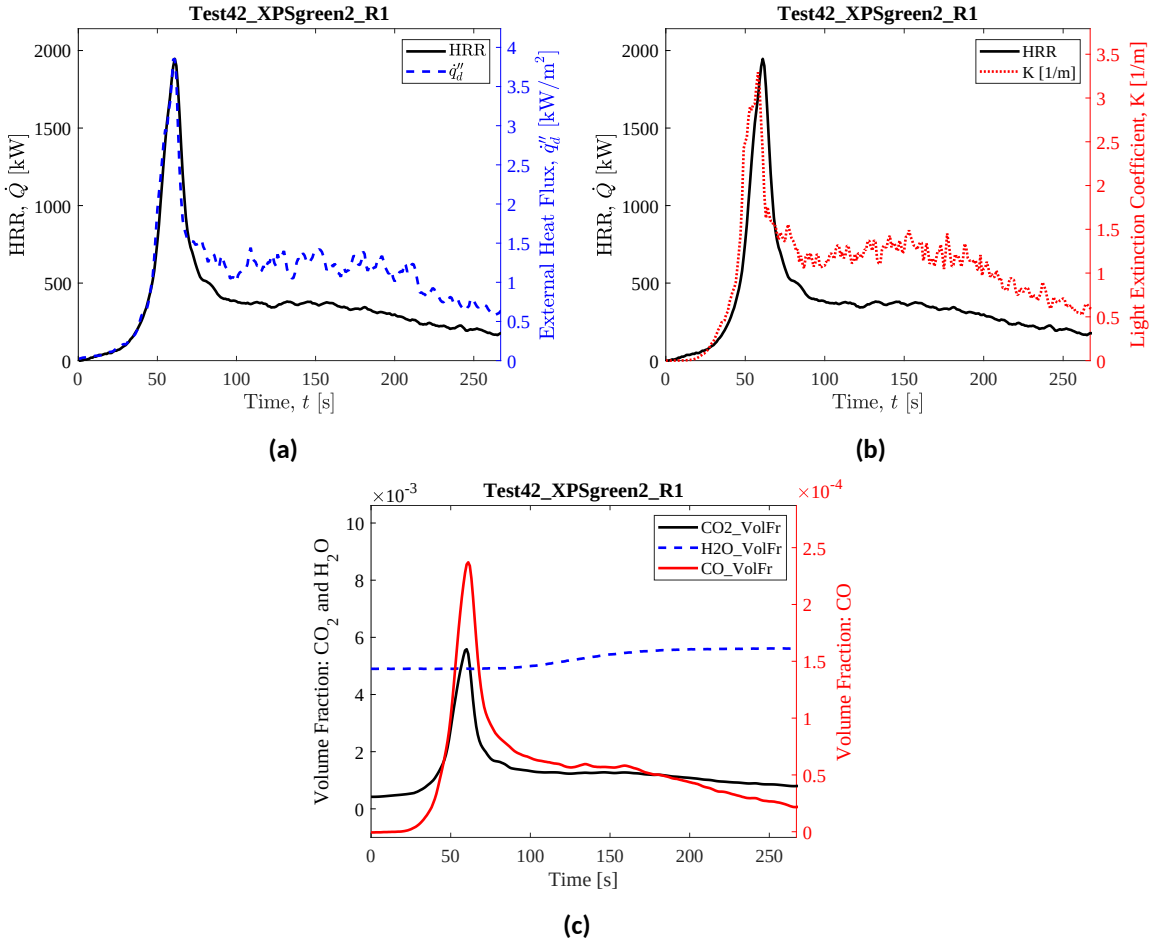

Fig. 270. Test 42 XPSgreen2 R1: (a) Heat release rate and heat flux at a distance, $\dot{q}''_{\mathrm{d}}$ (here, $\dot{q}''_{\mathrm{d}}$ is measured at x =-232 cm, y =-300 cm, z =90 cm); (b) Heat release rate and light extinction coefficient, K (smoke particulate in exhaust duct [111]); (c) Time-resolved volume fractions of CO_2, H_2O, and CO.

Test 55 XPSgreen2 R2

Test Description
2 in. thick, 24 in. wide, 96 in. tall panels of Green XPS Foam held by wire to 1 in. thick Marinite board. Panels were ignited using a rectangular propane burner (60 kW nominal heat release rate) filled with layers of Pea Gravel, Sand, and Kaowool Insulation (i.e., the 'Final Burner configuration'; see Fig. 12). The burner was kept on throughout the experiment until samples self-extinguished. Flame to wall heat flux measurements were not recorded in this test.

(a) Pre-test

(b) Ignition

(c) Peak HRR

(d) End of Test

Fig. 271. Photographs of Test 55 XPSgreen2 R2.

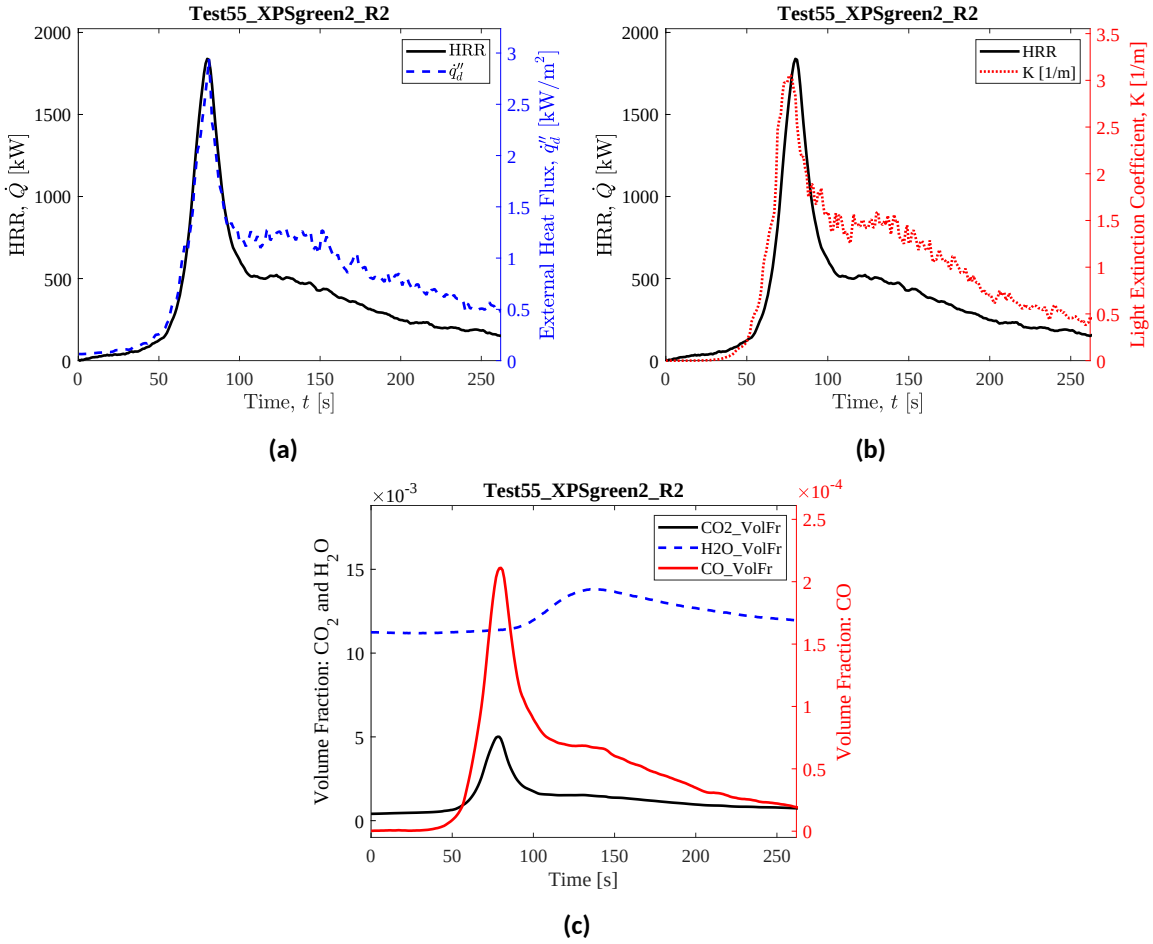

Fig. 272. Test 55 XPSgreen2 R2: (a) Heat release rate and heat flux at a distance, $\dot{q}''_{\mathrm{d}}$ (here, $\dot{q}''_{\mathrm{d}}$ is measured at x =300 cm, y =-305 cm, z =90 cm); (b) Heat release rate and light extinction coefficient, K (smoke particulate in exhaust duct [111]); (c) Time-resolved volume fractions of CO_2, H_2O, and CO.

Test 64 XPSgreen2 R3

Test Description
2 in. thick, 24 in. wide, 96 in. tall panels of Green XPS Foam held by wire to 1 in. thick Marinite board. Panels were ignited using a rectangular propane burner (60 kW nominal heat release rate) filled with layers of Pea Gravel, Sand, and Kaowool Insulation (i.e., the 'Final Burner configuration'; see Fig. 12). The burner was kept on throughout the experiment until samples self-extinguished. Flame to wall heat flux measurements were not recorded in this test.

(a) Pre-test

(b) Ignition

(c) Peak HRR

(d) End of Test

Fig. 273. Photographs of Test 64 XPSgreen2 R3.

Heat Release Rate, Heat Flux at a Distance, and Species Yields

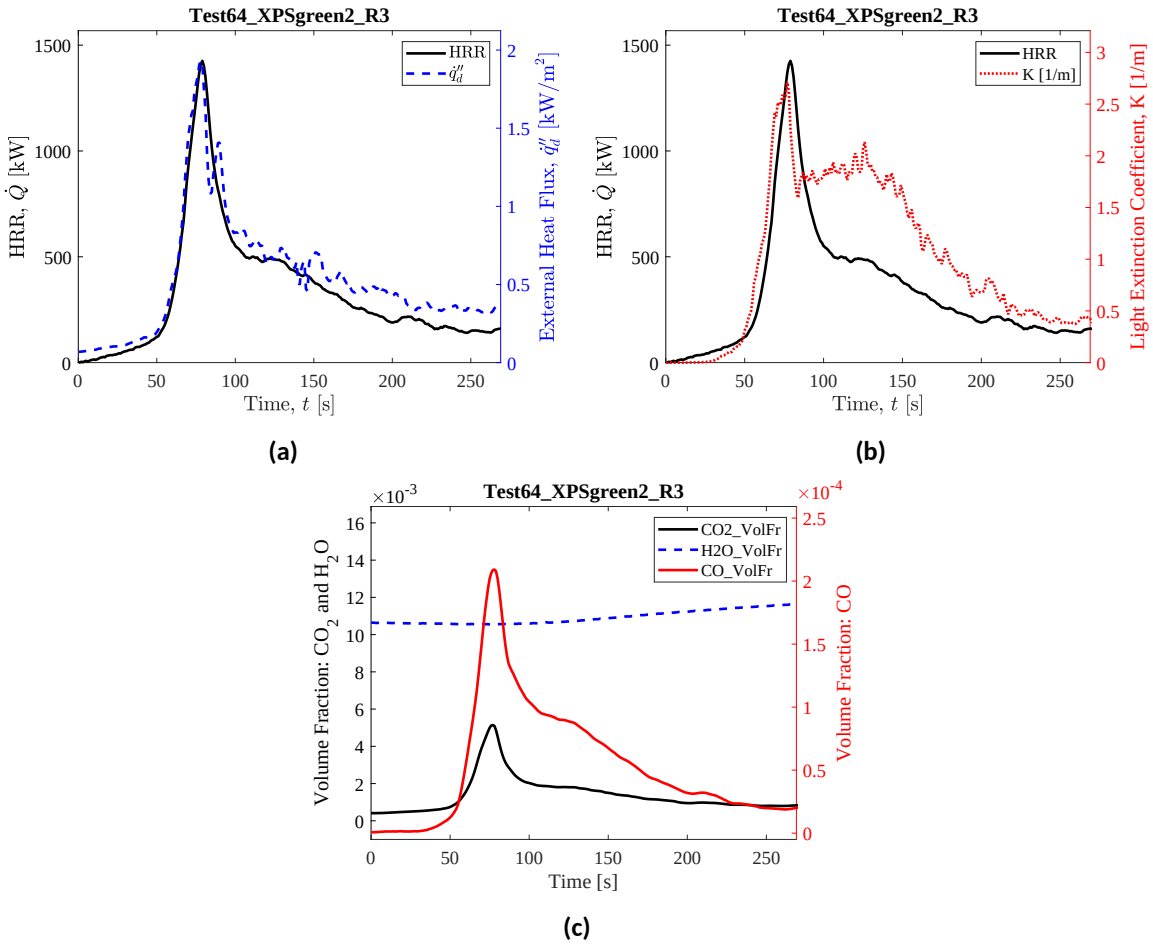

Fig. 274. Test 64 XPSgreen2 R3: (a) Heat release rate and heat flux at a distance, $\dot{q}''_{\mathrm{d}}$ (here, $\dot{q}''_{\mathrm{d}}$ is measured at x =300 cm, y =-305 cm, z =90 cm); (b) Heat release rate and light extinction coefficient, K (smoke particulate in exhaust duct [111]); (c) Time-resolved volume fractions of CO_2, H_2O, and CO.

Test 33 XPSpink1 R1

Test Description

1 in. thick, 24 in. wide, 96 in. tall panels of Pink XPS Foam held by wire to 1 in. thick Marinite board. Panels were ignited using a rectangular propane burner (60 kW nominal heat release rate) filled with layers of Pea Gravel, Sand, and Kaowool Insulation (i.e., the 'Final Burner configuration'; see Fig. 12). The burner was kept on throughout the experiment until samples self-extinguished. Flame to wall heat flux measurements were not recorded in this test.

(a) Pre-test

(b) Ignition

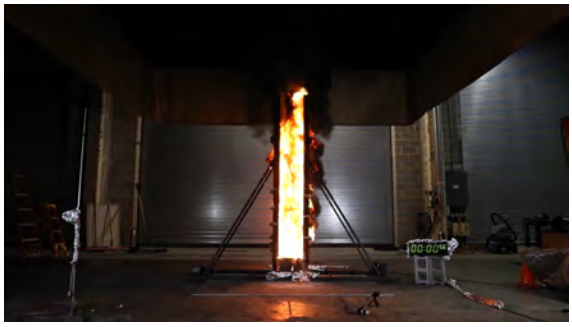

(c) Peak HRR

(d) End of Test

Fig. 275. Photographs of Test 33 XPSpink1 R1.

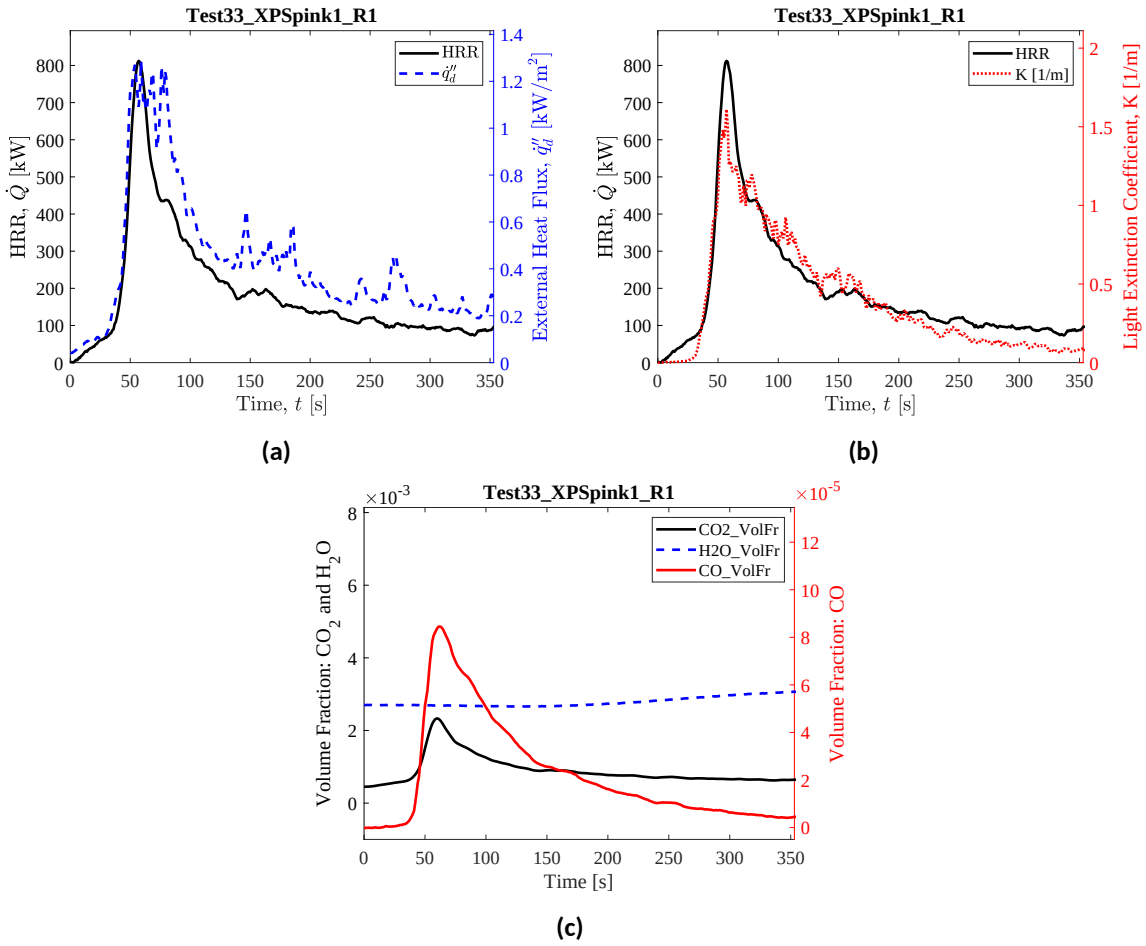

Fig. 276. Test 33 XPSpink1 R1: (a) Heat release rate and heat flux at a distance, $\dot{q}''_{\mathrm{d}}$ (here, $\dot{q}''_{\mathrm{d}}$ is measured at x =-232 cm, y =-300 cm, z =90 cm); (b) Heat release rate and light extinction coefficient, K (smoke particulate in exhaust duct [111]); (c) Time-resolved volume fractions of CO_2, H_2O, and CO.

Test 35 XPSpink1 R2

Test Description

1 in. thick, 24 in. wide, 96 in. tall panels of Pink XPS Foam held by wire to 1 in. thick Marinite board. Panels were ignited using a rectangular propane burner (60 kW nominal heat release rate) filled with layers of Pea Gravel, Sand, and Kaowool Insulation (i.e., the 'Final Burner configuration'; see Fig. 12). The burner was kept on throughout the experiment until samples self-extinguished. Flame to wall heat flux measurements were not recorded in this test.

(a) Pre-test

(b) Ignition

(c) Peak HRR

(d) End of Test

Fig. 277. Photographs of Test 35 XPSpink1 R2.

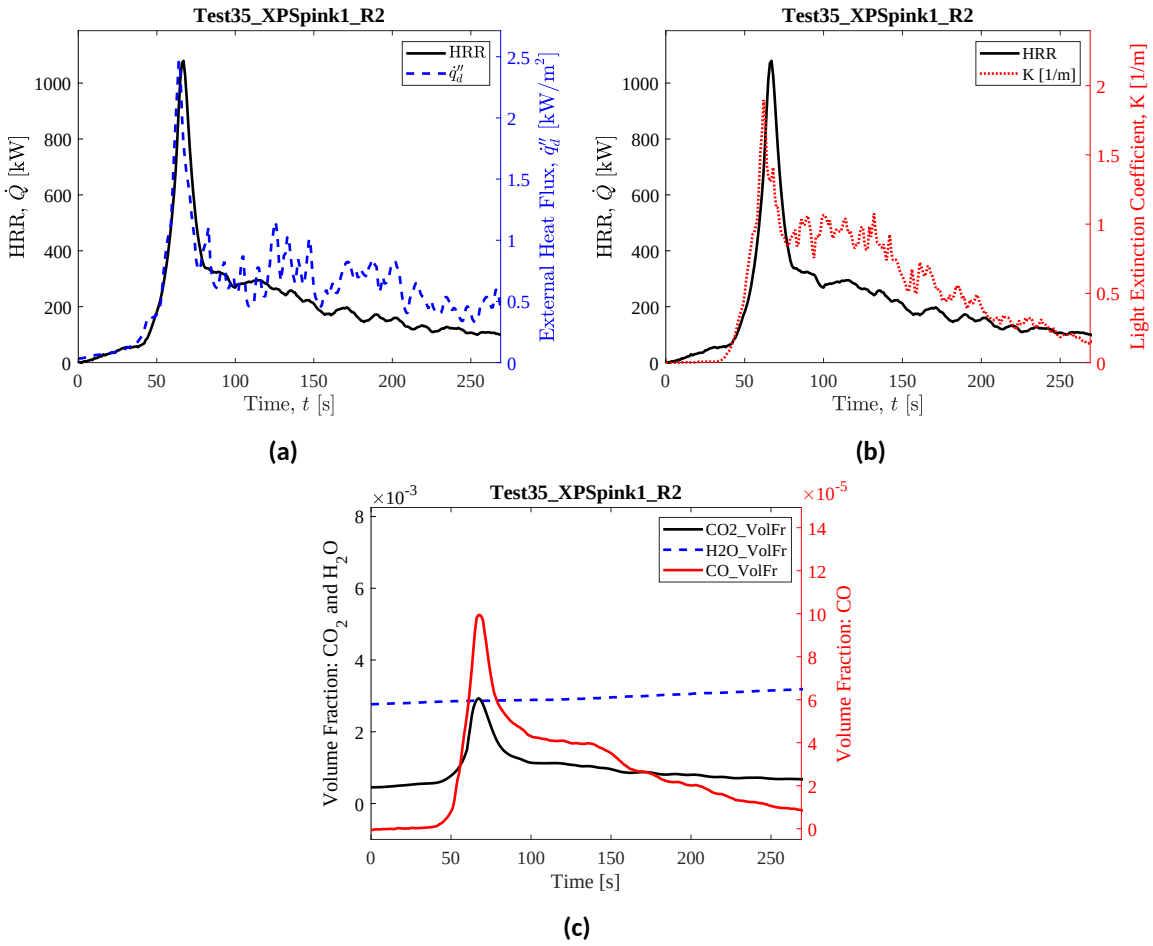

Fig. 278. Test 35 XPSpink1 R2: (a) Heat release rate and heat flux at a distance, $\dot{q}''_{\mathrm{d}}$ (here, $\dot{q}''_{\mathrm{d}}$ is measured at x =-232 cm, y =-300 cm, z =90 cm); (b) Heat release rate and light extinction coefficient, K (smoke particulate in exhaust duct [111]); (c) Time-resolved volume fractions of CO_2, H_2O, and CO.

Test 48 XPSpink1 R3

Test Description
1 in. thick, 24 in. wide, 96 in. tall panels of Pink XPS Foam held by wire to 1 in. thick Marinite board. Panels were ignited using a rectangular propane burner (60 kW nominal heat release rate) filled with layers of Pea Gravel, Sand, and Kaowool Insulation (i.e., the 'Final Burner configuration'; see Fig. 12). The burner was kept on throughout the experiment until samples self-extinguished. Flame to wall heat flux measurements were not recorded in this test.

(a) Pre-test

(b) Ignition

(c) Peak HRR

(d) End of Test

Fig. 279. Photographs of Test 48 XPSpink1 R3.

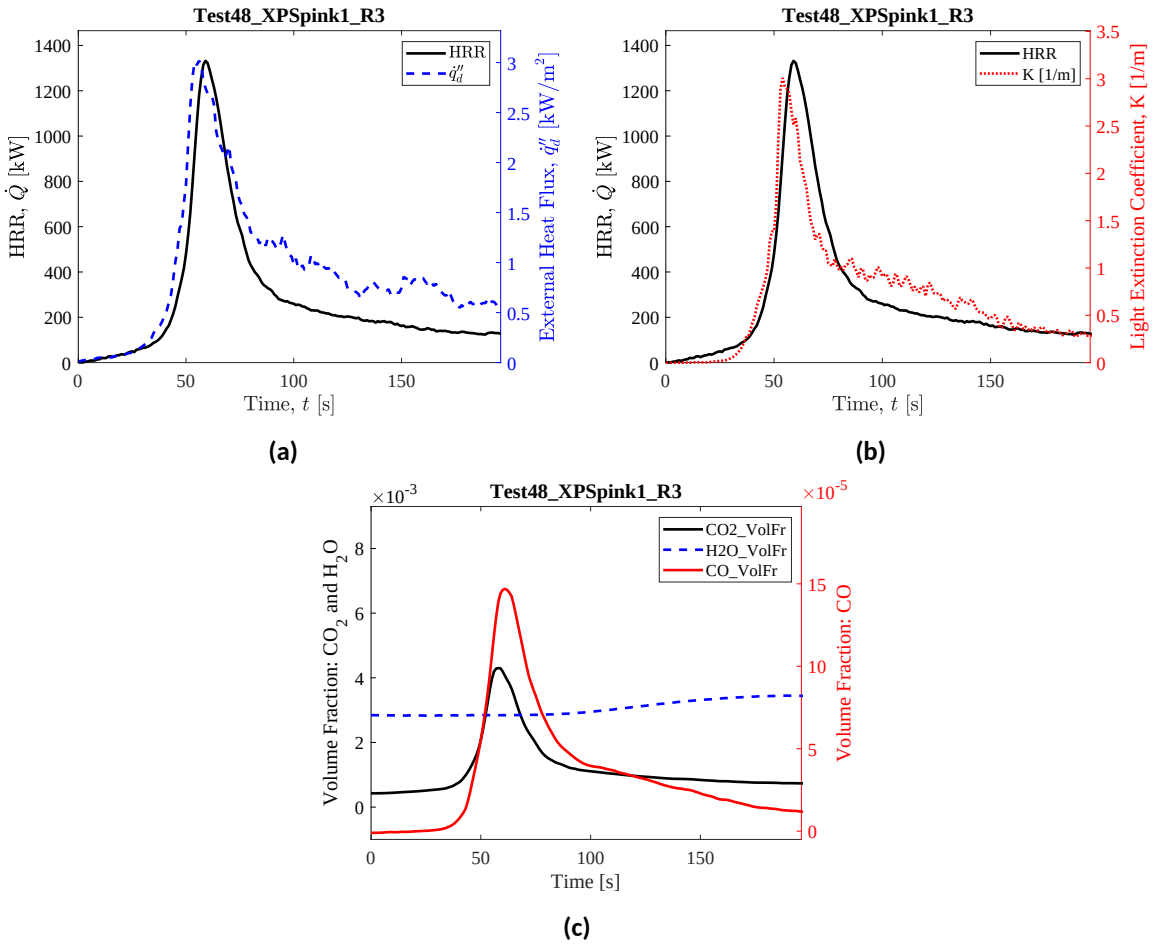

Fig. 280. Test 48 XPSpink1 R3: (a) Heat release rate and heat flux at a distance, $\dot{q}''_{\mathrm{d}}$ (here, $\dot{q}''_{\mathrm{d}}$ is measured at x =-220 cm, y =-310 cm, z =90 cm); (b) Heat release rate and light extinction coefficient, K (smoke particulate in exhaust duct [111]); (c) Time-resolved volume fractions of CO_2, H_2O, and CO.

Test 41 XPSpink2 R1

Test Description

2 in. thick, 24 in. wide, 96 in. tall panels of Pink XPS Foam held by wire to 1 in. thick Marinite board. Panels were ignited using a rectangular propane burner (60 kW nominal heat release rate) filled with layers of Pea Gravel, Sand, and Kaowool Insulation (i.e., the 'Final Burner configuration'; see Fig. 12). The burner was kept on throughout the experiment until samples self-extinguished. Flame to wall heat flux measurements were not recorded in this test.

(a) Pre-test

(b) Ignition

(c) Peak HRR

(d) End of Test

Fig. 281. Photographs of Test 41 XPSpink2 R1.

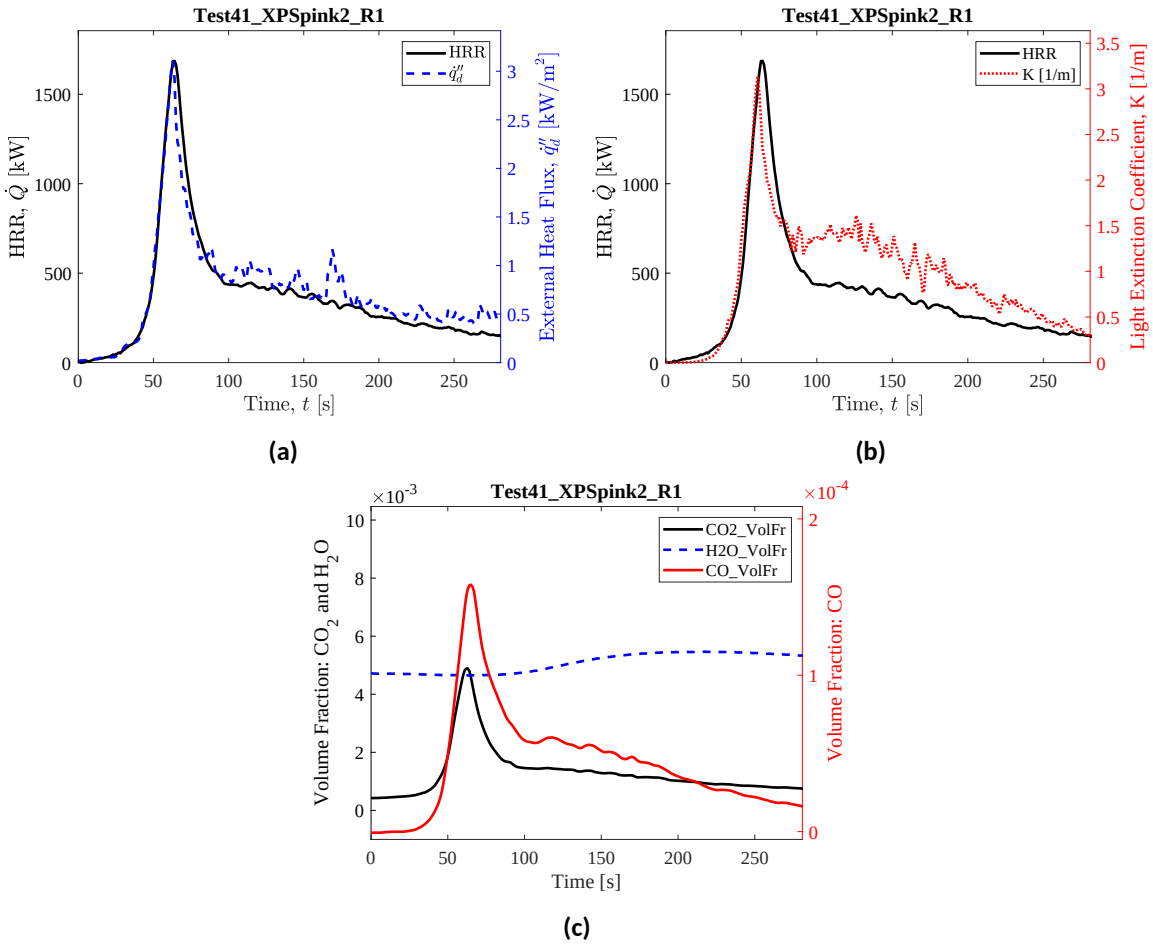

Fig. 282. Test 41 XPSpink2 R1: (a) Heat release rate and heat flux at a distance, $\dot{q}''_{\mathrm{d}}$ (here, $\dot{q}''_{\mathrm{d}}$ is measured at x =-232 cm, y =-300 cm, z =90 cm); (b) Heat release rate and light extinction coefficient, K (smoke particulate in exhaust duct [111]); (c) Time-resolved volume fractions of CO_2, H_2O, and CO.

Test 54 XPSpink2 R2

Test Description
2 in. thick, 24 in. wide, 96 in. tall panels of Pink XPS Foam held by wire to 1 in. thick Marinite board. Panels were ignited using a rectangular propane burner (60 kW nominal heat release rate) filled with layers of Pea Gravel, Sand, and Kaowool Insulation (i.e., the 'Final Burner configuration'; see Fig. 12). The burner was kept on throughout the experiment until samples self-extinguished. Flame to wall heat flux measurements were not recorded in this test.

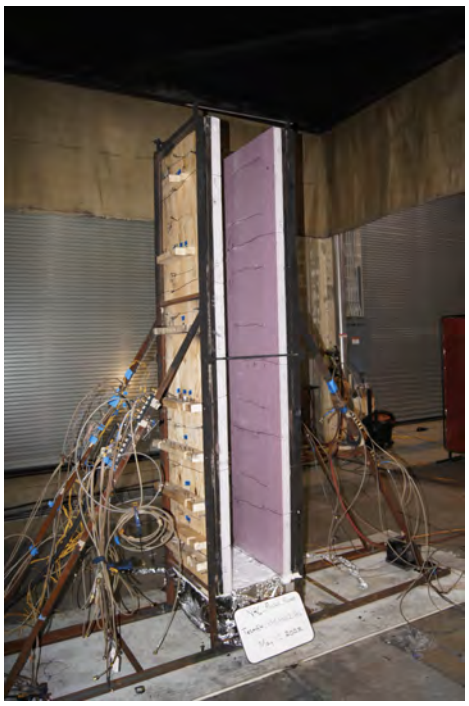

(a) Pre-test

(b) Ignition

(c) Peak HRR

(d) End of Test

Fig. 283. Photographs of Test 54 XPSpink2 R2.

Heat Release Rate, Heat Flux at a Distance, and Species Yields

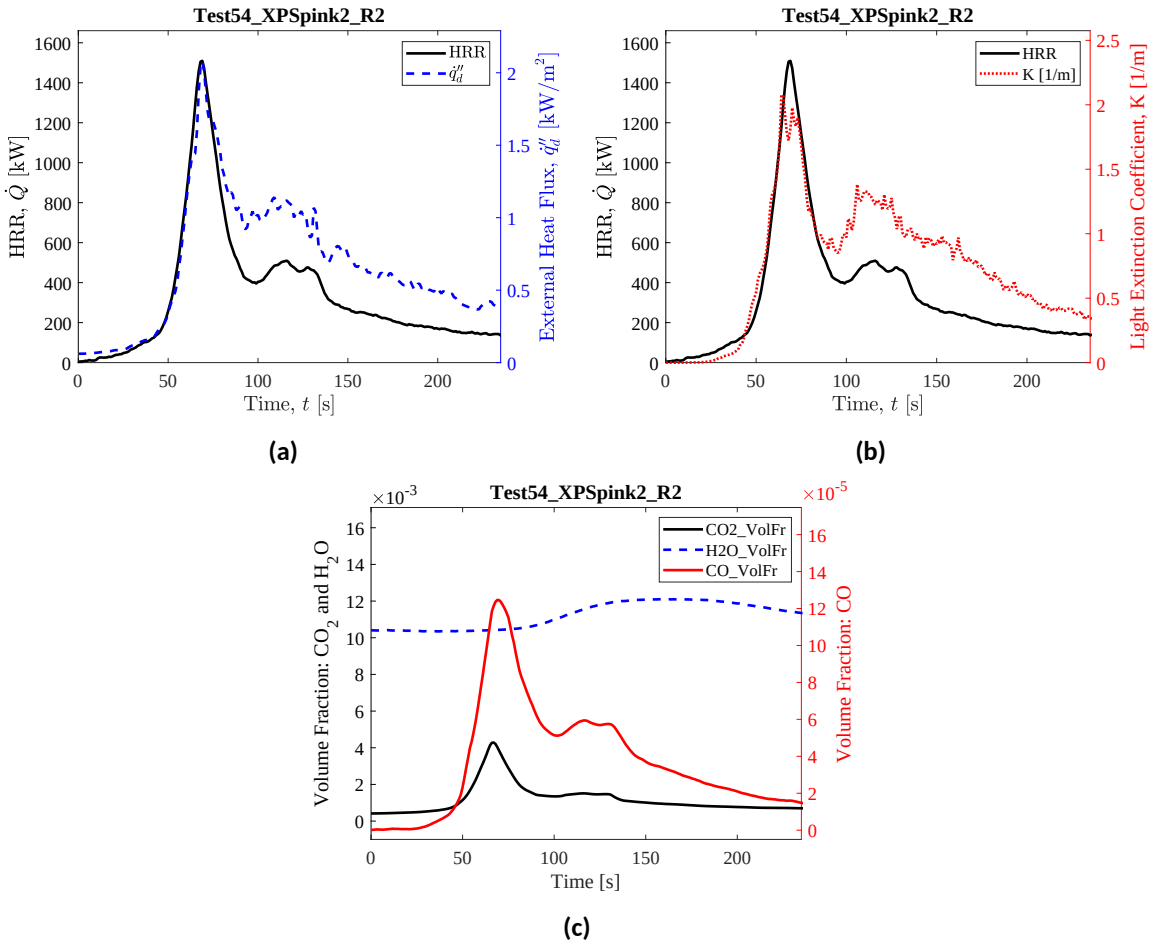

Fig. 284. Test 54 XPSpink2 R2: (a) Heat release rate and heat flux at a distance, $\dot{q}''_{\mathrm{d}}$ (here, $\dot{q}''_{\mathrm{d}}$ is measured at x =300 cm, y =-305 cm, z =90 cm); (b) Heat release rate and light extinction coefficient, K (smoke particulate in exhaust duct [111]); (c) Time-resolved volume fractions of CO_2, H_2O, and CO.

Test 63 XPSpink2 R3

Test Description
2 in. thick, 24 in. wide, 96 in. tall panels of Pink XPS Foam held by wire to 1 in. thick Marinite board. Panels were ignited using a rectangular propane burner (60 kW nominal heat release rate) filled with layers of Pea Gravel, Sand, and Kaowool Insulation (i.e., the 'Final Burner configuration'; see Fig. 12). The burner was kept on throughout the experiment until samples self-extinguished. Flame to wall heat flux measurements were not recorded in this test.

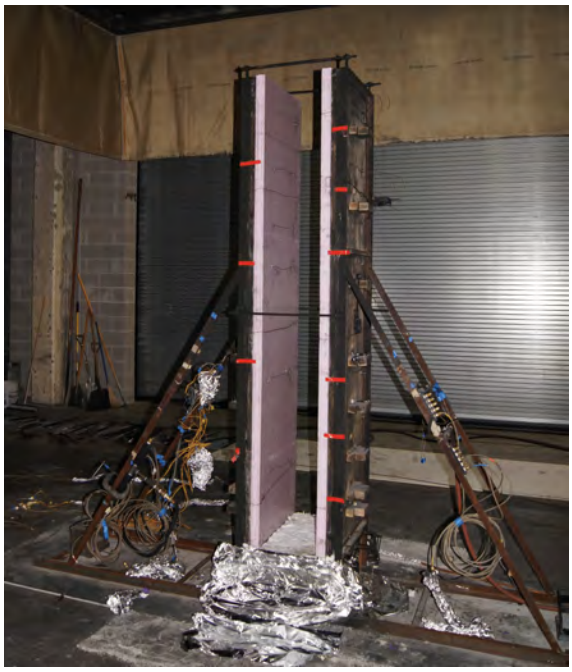

(a) Pre-test

(b) Ignition

(c) Peak HRR

(d) End of Test

Fig. 285. Photographs of Test 63 XPSpink2 R3.

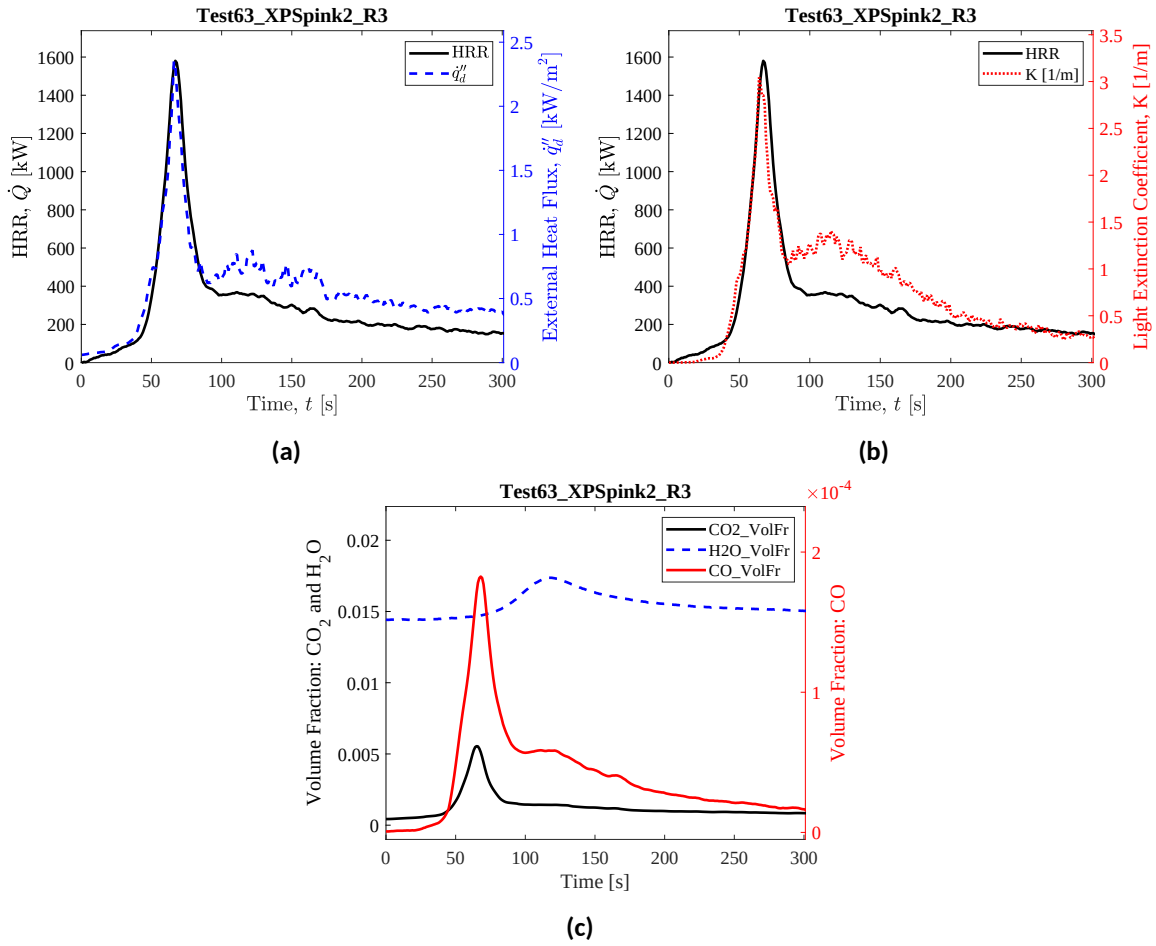

Fig. 286. Test 63 XPSpink2 R3: (a) Heat release rate and heat flux at a distance, $\dot{q}''_{\mathrm{d}}$ (here, $\dot{q}''_{\mathrm{d}}$ is measured at x =300 cm, y =-305 cm, z =92 cm); (b) Heat release rate and light extinction coefficient, K (smoke particulate in exhaust duct [111]); (c) Time-resolved volume fractions of CO_2, H_2O, and CO.